Investigation of Oxetane Reactive Intermediates for the Synthesis of 3,3-Disubstituted Oxetanes

A Thesis Submitted by

Juan José Rojas Muñoz

In partial fulfilment of the requirements for the degree of

DOCTOR OF PHILOSOPHY

Department of Chemistry

Imperial College London

Molecular Sciences Research Hub

White City Campus

London W12 0BZ

United Kingdom

2023

I confirm that the work presented within this document is my own. Clear acknowledgement has been made when referring to the work of others, or where help has been received.

The copyright of this thesis rests with the author. Unless otherwise indicated, its contents are licensed under a Creative Commons Attribution-Non Commercial-No Derivatives 4.0 International Licence (CC BY-NC-ND).

Under this licence, you may copy and redistribute the material in any medium or format on the condition that; you credit the author, do not use it for commercial purposes and do not distribute modified versions of the work.

When reusing or sharing this work, ensure you make the licence terms clear to others by naming the licence and linking to the licence text.

Please seek permission from the copyright holder for uses of this work that are not included in this licence or permitted under UK Copyright Law.

Acknowledgements

First of all, I would like to thank Dr James Bull for giving me the chance to work in his research group. His endless enthusiasm, motivation and passion for chemistry is contagious and his support and encouragement know no boundaries. I have yet to meet a more ethical, honest and thorough researcher and I could not have wished for a better doctoral advisor.

I would like to thank Pfizer and Imperial College London for funding, without which none of this would have been possible. Thank you to Dr James Mousseau and especially Charlie Choi at Pfizer for being great collaborators, for all the work conducted at Pfizer and for taking their time to meet regularly with me to discuss chemistry with such honest interest.

Thanks to past and present members of the Bull group who laughed with me all these years and put up with my nonsense. Without you, PhD life would have been slightly duller. Thanks for tolerating my questionable choice of French rap music and more seriously, for being so incredibly supportive, helpful and truly *good* people. I will miss you a little. Thanks to Steph, Hikaru, Oli, Hannah, Freeman, Hannan and Peerawat for proofreading my thesis.

Thank you to the Crimmin group (our inorganic neighbours that actually run anhydrous reactions) for being so cool and easy-going people. I really enjoyed your company and help with fancy set-ups. Thank you, Feriel and Marina for being such incredible friends – my only regret is not to have met you sooner.

I am grateful to have had the opportunity to work directly and indirectly with so many different people throughout my PhD, including Rosie, Ed, Dani, Luka, Maryne, Hannah, Elena, Riashat, Oli, Peerawat, Emma, Jianing, Joyce, Hikaru, Harry and Joe. I learned so much from all of you. You made me realise that diverse thinking leads to better research. Collaboration is always better.

Many thanks also to collaborators from other groups, Dr Anna Barnard, Dr Charles Romain, and especially to Alistair and Prof Fernanda Duarte from the University of Oxford. Working together with Alistair and Fernanda was a truly amazing experience, teaching me a lot along the way about fundamental chemistry and how honest symbiotic collaboration always leads to a better research output.

I am grateful for all the technical staff from Imperial College London and their passion to go beyond the requirements to help out colleagues. Special thanks to Pete Haycock from NMR for accepting repeatedly “my last sample”, for Dr Andrew White from crystallography for looking at all the “ugly crystals” I submitted that somehow refracted just fine, and to Dr Lisa

Haigh from mass spectrometry for treating my “urgent samples” quite literally. Thanks also to Stefanos Karapanagiotidis who works for three but was always happy to go out of his way to help me fix our machines, even if it meant having to spend the whole day with me.

Gracias a mis padres por siempre haber estado de mi lado y haberme apoyado en todo, sin importar que escogiera hacer. Sin su soporte y ayuda nunca hubiera llegado hasta este punto. Gracias por siempre preguntarme por mi trabajo y escucharme por horas con la mayor atención, aun sin entender una palabra de química.

Clara, my partner in crime, thank you eternally for your unconditional support in the good and bad times. You brighten up my life and fill it with joy and laughter. Without you, I am lost. Thank you for being you.

Abstract

Four-membered ring heterocycles are attractive motifs for drug discovery due to their low molecular weight, high polarity and marked 3-dimensionality. 3,3-Disubstituted oxetanes have gained further popularity as surrogates for carbonyl groups to improve their physicochemical properties. However, the dearth of synthetic methods to access substituted oxetane motifs has hampered their systematic evaluation as motifs in a pharmaceutical context. This thesis describes the development of methodologies to access new 3,3-disubstituted oxetanes through the generation of oxetane reactive intermediates: carbocations, radicals and carbanions.

Chapter **3** describes the generation of oxetane carbocations from oxetane sulfonyl fluoride precursors through an unprecedented defluorosulfonylation pathway. 3-Aryloxetane carbocations are coupled to nucleophiles to achieve varied substitution in the 3-position. Reaction with amines yields aryl amino-oxetanes as potential isosteres of benzamides and the physicochemical properties of selected amino-oxetane/benzamide pairs are compared. Applicability to drug discovery is shown through late-stage functionalisation and the synthesis of oxetane drug analogues. Defluorosulfonylation proceeds by an S_N1 mechanism with rate-determining formation of planar oxetane carbocations, whereby the oxetane structure provides the right balance of carbocation stability to achieve a useful reactivity window.

Oxetane radicals are examined in Chapter **4**. Oxetane-3-carboxylic acids are suitable radical precursors *via* photoredox-catalysed decarboxylation, demonstrated in Giese-type reactions. The influence of ring strain and heterosubstitution on radical reactivity is investigated, showing radical-destabilising and radical-delocalising effects of the oxetane structure as a consequence of ring strain and Bent's rule, resulting in an exergonic Giese addition. Oxetane benzoates are also shown to be suitable radical precursors in a radical recombination process with cyanopyridines to yield 4-pyridyl diaryl-oxetanes.

Chapter **5** investigates the sulfoxide–metal exchange of oxetane sulfoxides to generate oxetane carbanions. Protonation studies provide evidence for the formation of the unstable anionic intermediates. Reaction of oxetane sulfoxides with 2-pyridylmagnesium chloride favours a ligand-to-ligand coupling pathway to yield 2-pyridyl diaryl-oxetane products.

Table of Contents

1 Introduction 15

1.1 Importance of New Scaffolds in Drug Discovery 15

1.2 Oxetanes in Drug Discovery 18

1.2.1 Oxetanes in Natural Products 18

1.2.2 Oxetanes as Attractive Motifs in Drug Design 19

1.2.3 Oxetanes as Bioisosteres 24

1.2.4 Developments in the Application of Oxetanes in Drug Discovery Campaigns 31

1.3 Synthesis of Oxetanes 38

1.3.1 C–O Bond Formation 38

1.3.2 C–C Bond Formation 40

1.3.3 [2+2] Cycloadditions 40

1.3.3.1 Paternò-Büchi Reaction (Photochemical) 40

1.3.3.2 Non-Paternò-Büchi Cycloadditions 41

1.3.4 Ring Expansion/Ring Contraction 42

1.4 Functionalisation of the Intact Ring 43

1.4.1 α-Functionalisation 43

1.4.2 Reaction of 3-Halo-oxetanes 44

1.4.3 Functionalisation of Oxetan-3-one Derivatives 45

1.4.3.1 Oxetane-3-alkylidenes 45

1.4.3.2 Displacement of Oxetan-3-ols 47

2 Aims 50

3 Oxetane Carbocations: Synthesis of Amino-oxetanes Using Oxetane Sulfonyl Fluorides 52

3.1 Sulfonyl Fluorides 52

3.1.1 Alternative Reactivity of Sulfonyl Fluorides 53

3.2 Oxetane Sulfonyl Fluorides 56

3.2.1 Previous Work within the Group 56
3.2.2 Aims 61
3.2.3 Preparation of Oxetan-3-ol Starting Materials 62
3.2.4 Amination of Oxetanols 63
3.2.5 Synthesis of Oxetane Sulfonyl Fluorides 64
3.2.6 Optimisation and Robustness of Defluorosulfonylation Reaction 70
3.2.7 Scope of Defluorosulfonylation Reaction 75
3.2.8 Investigation of Selectivities 80
3.2.9 Other Nucleophiles 84
3.2.10 Synthesis of Amino-oxetane Drug Analogues 90
3.2.11 Assessment of Isosterism: Matched Molecular Pair Analysis (MMPA) 94
3.2.11.1 Structural Analysis 94
3.2.11.2 Physicochemical Properties 99
3.2.12 Mechanistic Investigations of Defluorosulfonylation 106
3.2.12.1 Kinetic Analysis 109
3.2.12.2 Computational Studies 121
3.2.13 Conclusion and Future Work 128
4 Oxetane Radicals 131
4.1 Strategies for Radical Generation and Photoredox Catalysis 131
4.2 Radicals on Oxetanes 133
4.2.1 Previous Work within the Group: Radicals from Oxetane Carboxylic Acids 136
4.2.1.1 Aims 138
4.2.1.2 Synthesis of Oxetane Acids 140
4.2.1.3 Scope of Giese Reaction 142
4.2.1.4 Conformational Analysis 145
4.2.1.5 Mechanistic Investigations 147
4.2.1.5.1 Trends in the Giese Reaction of Different Arylacetic Acids 147
4.2.1.5.2 Key Steps and Intermediates of the Giese Mechanism 152
4.2.1.5.3 Side Products of Reduction (**155**) and Di-Alkylation (**149'**) 159

4.2.1.5.4 Mechanistic Proposal 161
4.2.1.6 Application of Oxetane Radical to Further Transformations....162
4.2.1.7 Conclusions....164
4.2.2 Oxetane Radicals from Oxetanols 165
4.2.2.1 Synthesis of Precursors 166
4.2.2.2 Oxetane Radicals and Radical–Radical Coupling to Cyanopyridines....167
4.2.2.3 Application of Oxetane Radical to Further Transformations....168
4.2.2.4 Conclusions and Future Work 170
5 Oxetane Carbanions: Investigation of Ligand Exchange and Ligand Coupling Pathways of Oxetane Sulfoxides....171
5.1 Organometallic Reactions on Sulfoxide Centres 172
5.1.1 Sulfoxide–Metal Exchange....175
5.1.2 Ligand-to-Ligand Coupling 176
5.2 Aims....179
5.3 Sulfoxide–Metal Exchange of Oxetane Sulfoxides 180
5.4 Ligand-to-Ligand Coupling of Oxetane Sulfoxides....186
5.5 Conclusion and Future Work 187
6 Conclusion and Future Work....191
7 Experimental....195
7.1 General Experimental Considerations 195
7.2 Measurement of Physicochemical Properties....199
7.3 Kinetic Studies of Oxetane Sulfonyl Fluorides by ^{1}H NMR 201
7.4 Details to Cyclic Voltammetry Experiments 203
7.5 Reaction Profiles of the Giese Reaction of Oxetane Acids 204
7.6 Experimental Details and Characterisation Data....205
7.6.1 Oxetanols 205
7.6.2 Ring-opening of Oxetanol 22a by Morpholine....213
7.6.3 Oxetane Sulfonyl Fluorides and Precursors....214

7.6.4 Reactions of Oxetane Sulfonyl Fluorides and Related Compounds 233
7.6.4.1 Amino-oxetanes 234
7.6.4.2 Oxetane Products From Other Nucleophiles.....252
7.6.4.3 Oxetane Analogues of Drugs 264
7.6.4.4 Azetidine Sulfonyl Fluoride 131 and Amino-azetidine 132 277
7.6.5 Oxetane Carboxylic Acids and Precursors.....279
7.6.6 3-Aryl-3-alkyl-oxetanes and Related Compounds.....282
7.6.7 Redox-Active Oxetane Esters 297
7.6.8 4-Pyridyl Diaryl Oxetanes and Related Structures.....300
7.6.9 Oxetane Sulfoxides and Precursors.....304
7.6.10 Products of Ligand Exchange 310
7.6.11 2-Pyridyl Diaryl Oxetanes.....313
8 References.....315
9 Appendix.....354
9.1 Appearance of Thietane Rings in the Literature.....354
9.2 Complete List of References for the Application of Oxetanes in Medicinal Chemistry Campaigns.....354
9.3 Reactivity and Applications of Sulfonyl Fluorides.....370
9.4 Raw Cyclic Voltammograms 374
9.5 ^{1}H NMR Spectra of Deuteration Studies.....380
9.6 References Appendix.....382

Abbreviations

Acr	9-Mesitylacridine
ADMET	Absorption-Distribution-Metabolism-Excretion-Toxicity
AML	Acute Myeloid Leukaemia
APCI	Atmospheric Pressure Chemical Ionisation
API	Active Pharmaceutical Ingredient
App	Apparent
aq.	Aqueous
Ar	Aryl
as	Asymmetric
ASAP	Atmospheric Solids Analysis Probe
ASF	Azetidine Sulfonyl Fluoride
ATR	Attenuated Total Reflectance
BBB	Blood-Brain-Barrier
BCP	Bicyclo[1.1.1]pentane
BDE	Bond Dissociation Energy
BHT	Butylated Hydroxy Toluene
Bn	Benzyl
Boc	*tert*-Butyloxycarbonyl
br	Broad
BTMG	2-*tert*-Butyl-1,1,3,3-Tetramethylguanidine
cAMP	Catabolite Activator Protein
CAS	Chemical Abstracts Service
CFL	Compact Fluorescent Lamp
CI	Chemical Ionisation
Cl	Clearance
CNS	Central Nervous System
COSY	Correlated Spectroscopy
COX	Cyclooxygenase
Cp	Cyclopentadienyl
Cp*	1,2,3,4,5-Pentamethylcyclopentadienyl
CPME	Cyclopentane Methyl Ester
CSF	Cyclobutane Sulfonyl Fluoride
CYP	Cytochrome P450 Enzymes
CV	Cyclic Voltammetry OR Column Volume

DABCO	1,4-Diazabicyclo[2.2.2]octane
DABSO	1,4-Diazabicyclo[2.2.2]octane bis(sulfur dioxide) adduct
DAST	Diethylaminosulfur Trifluoride
dATP	Deoxyadenosine Triphosphate
DBU	1,8-Diazabicyclo[5.4.0]undec-7-ene
deFS	Defluorosulfonylation
DEL	DNA Encoded Library
DIC	*N*,*N*'-Diisopropylcarbodiimide.
DIPEA	*N*,*N*-Diisopropylethylamine
DMA	*N*,*N*-Dimethylacetamide
DMAP	4-Dimethylaminopyridine
DME	Dimethoxyethane
DMF	*N*,*N*-Dimethylformamide
DMSO	Dimethylsulfoxide
DNA	Deoxyribonucleic Acid
DOS	Diversity Oriented Synthesis
dppbz	1,2-bis(Diphenylphosphino)benzene
dppf	1,1'-bis(Diphenylphosphino)ferrocene
dtbbpy	4,4'-Di-*tert*-butyl-2,2'-dipyridyl
dtbpf	1,1'-bis(Di-*tert*-butylphosphino)ferrocene
EDO	2,2-Di-(*p*-ethoxyphenyl)-3,3-dimethyloxetane
ee	Enantiomeric excess
EI	Electron Ionisation
ESI	Electrospray Ionisation
ES-ToF	Electrospray Time of Flight
EWG	Electron-withdrawing Group
EZH2	Enhancer of Zeste Homolog 2
FBDD	Fragment Based Drug Discovery
Fc	Ferrocene
FGFR	Fibroblast Growth Factor Receptor
FGI	Functional Group Interconversion
FTIR	Fourier Transform Infrared Spectroscopy
GC	Gas Chromatography
gem	Geminal
GIST	Gastrointestinal Stromal Tumor
GLP-1R	Glucagon-Like Peptide Receptor 1
GSM	γ-Secretase Modulator

GST	Glutathione *S*-Transferase
HAT	Hydrogen Atom Transfer
HB	Hydrogen Bond
HE	Hantzsch Ester
hERG	human Ether-à-go-go Related Gene
HFIP	1,1,1,3,3,3-Hexafluoroisopropanol
HIV	Human Immunodeficiency Virus
HLM	Human Liver Microsomes
HMBC	Heteronuclear Multiple-Bond Coherence
HMDS	Hexamethyldisilazane
HMQC	Heteronuclear Multilple Quantum Coherence
HPLC	High-Performance Liquid Chromatography
HRMS	High Resolution Mass Spectrometry
HTS	High-Throughput Screening
IC_{50}	Half maximal Inhibitory Concentration
Int	Intrinsic
IP	Intellectual Property
IR	Infrared
iRAE	Inverted Redox-Active Ester
LCMS	Liquid Chromatography–Mass Spectrometry
LED	Light-Emitting Diode
Leu	Leucine
LG	Leaving Group
LiHMDS	Lithium bis(trimethylsilyl)amide
LipMetE	Lipophilic Metabolism Efficiency
LMN	Lupus Membranous Nephropathy
Log*D*	Logarithm of the water/octanol distribution
5-LOX	5-Lipooxygenase
LSF	Late-Stage Functionalisation
L2L	Ligand-to-Ligand
*m*CPBA	*meta*-Chloroperoxybenzoic Acid
mEH	microsomal Epoxide Hydrolase
Mes	Mesityl
MLCT	Metal-to-Ligand Charge-Transfer
MMP	Matched Molecular Pair
MMPA	Matched Molecular Pair Analysis
MO	Molecular Orbital

MOPS	Morpholine–Propane–Sulfonic Acid
MP	Melting Point (also abbreviated as mp)
mTOR	mammalian Target of Rapamycin
MS	Molecular Sieves OR Mass Spectrometry OR Multiple Sclerosis
MW	Molecular Weight
NA	Not Applicable
NADPH	Nicotinamide Adenine Dinucleotide Phosphate
NCS	*N*-Chlorosuccinimide
Neo	Neopentylglycol
NFSI	*N*-Fluorobenzenesulfonimide
NHC	N-Heterocyclic Carbene
NMPI	*N*-Methylphthalimide
NMR	Nuclear Magnetic Resonance
ns	Number of Scans
ORTEP	Oak Ridge Thermal-Ellipsoid Plot
OSF	Oxetane Sulfonyl Fluoride
PB	Paternò-Büchi
PC	Photocatalyst
PCET	Proton-Coupled Electron Transfer
PG	Protecting Group
PIFA	Phenyliodine bis(Trifluoroacetate)
PK	Pharmacokinetic
PKS	Polyketide Synthase
PMP	*p*-Methoxyphenyl
ppm	Parts Per Million
PrCP	Prolylcarboxypeptidase
PSA	Polar Surface Area
PTFE	Polytetrafluoroethylene
RAE	Redox Active Ester
rds	Rate Determining Step
R_f	Retention Factor
RPC	Radical-Polar Crossover
rpm	Revolutions Per Minute
RSM	Returned Starting Material
RSV	Respiratory Syncytial Virus
rt	Room Temperature
sat.	Saturated

SCE	Saturated Calomel Electrode
SCLC	Small Cell Lung Cancer
SET	Single Electron Transfer
SF	Shake-Flask
SMC	Suzuki–Miyaura Coupling
SPPS	Solid-Phase Peptide Synthesis
st	Stretch
SuFEx	Sulfur–Fluoride Exchange
sy	Symmetric
SYK	Tyrosine Protein Kinase
TBADT	Tetrabutylammonium Decatungstate
TBAF	Tetrabutylammonium Fluoride
TBS	*tert*-Butyl-dimethyl Silyl (also commonly abbreviated as TBDMS)
TEMPO	2,2,6,6-Tetramethylpiperidin-1-yl)oxyl
TES	Triethyl Silyl
TDAE	tetrakis-(*N*,*N*-Dimethylamino)ethylene
TFA	Trifluoroacetic Acid
THF	Tetrahydrofuran
THP	Tetrahydropyran
TI	Therapeutic Index
TIPS	Triisopropyl Silyl
TLC	Thin-Layer Chromatography
TMDS	1,1,3,3-Tetramethyldisiloxane
TMS	Trimethyl Silyl
Tol	*p*-Tolyl (4-MePh–)
TS	Transition State
UV	Ultraviolet
VTNA	Visual Time Normalisation Analysis
WHO	World Health Organisation

1 Introduction

1.1 Importance of New Scaffolds in Drug Discovery

Advances in synthetic chemistry have a direct impact on the discovery of new, life-changing medicines and have been central to the development of all marketed small molecule therapeutics.[1]

As programs in medicinal chemistry seek to focus on constantly more challenging biological targets, the molecular complexity of drug candidates has increased substantially in the last 50 years (Figure 1).[2] Although the quantification of 'complexity' is debated,[2,3] the general consensus is that complex molecular structures are 3-dimensional (*i.e.* not flat), often contain a high degree of tetrahedral, sp^3-hybridized carbon atoms, and span a very specific, often chiral, chemical space. There is a significantly lower attrition rate[a] of 'non-flat' clinical candidates,[4] which has been attributed to higher target selectivity[5] and more attractive pharmacokinetic (PK) and toxicity profiles.[6]

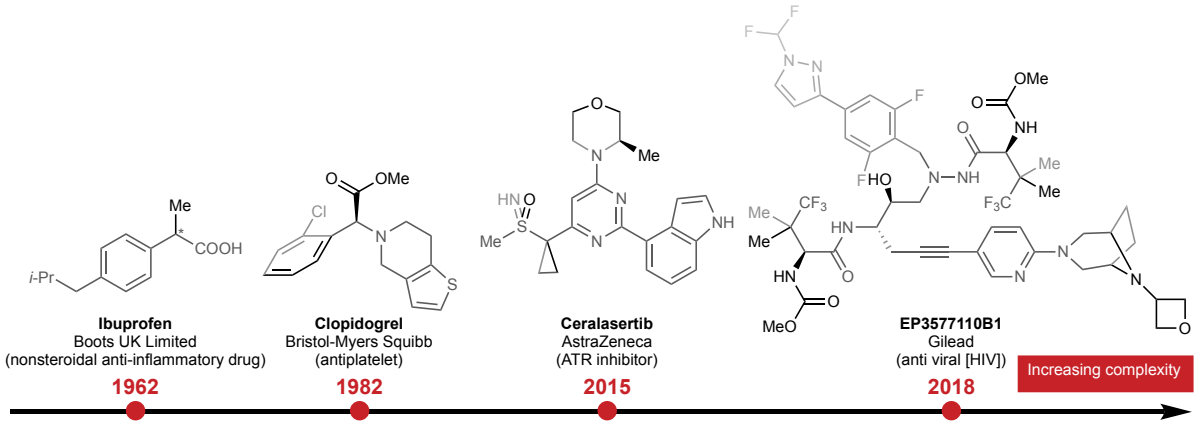


Figure 1. Increasing complexity in drugs.[7] 3-Dimensional representation of selected drug compounds. Black colour represents bonds pointing out of the plane and grey represents bonds pointing into the plane.

Despite the advantages of increasing the 3-dimensionality in drug candidates, hit identification and hit-to-lead optimisation campaigns still rely heavily on sp^2–sp^2 bond-forming reactions (*i.e.* flat-to-flat connections), such as metal-catalysed cross couplings and amide couplings.[8] This results in inefficient drug discovery programmes where most candidates are discarded due to poor selectivity and/or concerning safety profiles.[9] The reason for this over-usage of sp^2–sp^2 linkages is plain: their formations are reliable and robust, and so are amenable to high-throughput approaches to generate large libraries of potential hit compounds in the early

[a] The percentage of drug candidates that fail during pre-clinical or clinical development.

stages of drug discovery campaigns.[10] Such combinatorial approaches *require* robust reactions for successful and cost-efficient generation of libraries. Despite the copious libraries, most synthesised test compounds are biologically ineffective or unselective, resulting in unsustainably large and obsolete decks of legacy compounds being stored in the catacombs of pharmaceutical companies.[2,9]

The antithetical problem of the reliability on high throughput strategies and the need for higher complexity in drug-like compounds is at heart, a synthetic one.[1,11] There is an unmet need for new useful synthetic methodologies that allow the incorporation of complex, 3-dimensional scaffolds into active pharmaceutical ingredients (APIs).[b,8–12] This need spans throughout all areas and stages of drug discovery,[13] including new building blocks,[14] fragments for Fragment Based Drug Discovery (FBDD),[15] modern approaches like Late-Stage Functionalisation (LSF)[16] or DNA Encoded Libraries (DEL),[17] and new modalities such as protein degraders[18] or covalent inhibitors.[19] The requirement for new molecular architectures in medicinal chemistry has inspired new discoveries in synthetic chemistry and vice versa, new developments in synthesis have enabled the medication of challenging diseases, in what Grygorenko describes as a 'symbiotic relationship'.[1c]

The last two decades have seen exciting advances in organic chemistry being achieved at an unprecedented pace. Most notably, discoveries were made in 'click' chemistry—where reactions proceed with high fidelity and under non-stringent conditions[20]—and in 'one-electron' radical chemistry—which has unlocked reaction pathways unattainable by polar chemistry[21] and sparking important advances in technologies such as photoredox[22] and electrochemistry.[23] These advances have had enormous impact not on only on the chemical sciences, but also on drug discovery and chemical biology.[24,25] The mutual dependency of drug discovery (industry) and fundamental synthetic chemistry (academia) have ignited an increasing number of industrial–academic collaborations that have auto-catalysed the discovery of new synthetic methodologies and discovery of APIs.[26]

Drug discovery is in constant search for new molecular motifs that can modulate a compound's binding- and physicochemical properties. As such, four-membered heterocycles have emerged as promising scaffolds owing to their low molecular weight, high polarity and 3-dimensionality (see Figure 2 for examples in bioactive compounds).[27] These properties, which can have beneficial impacts on drug compounds such as higher target affinity and increased aqueous solubility, have led to an increase in popularity of heterocyclic four-membered rings

[b] API = The biologically active ingredient in an administered drug responsible for the observed therapeutic effect.

in the last 30 years, as is observed in the *relative* surge in publications since 1992 (Figure 3, right). Whilst publications that involve *N*- (azetidines) and *O*-systems (oxetanes) have been steadily increasing, the *S*-system (thietanes) has been lagging and with a less constant upward trend (see Appendix **9.1**), presumably due to its higher synthetic burden and low occurrence in natural products.[c]

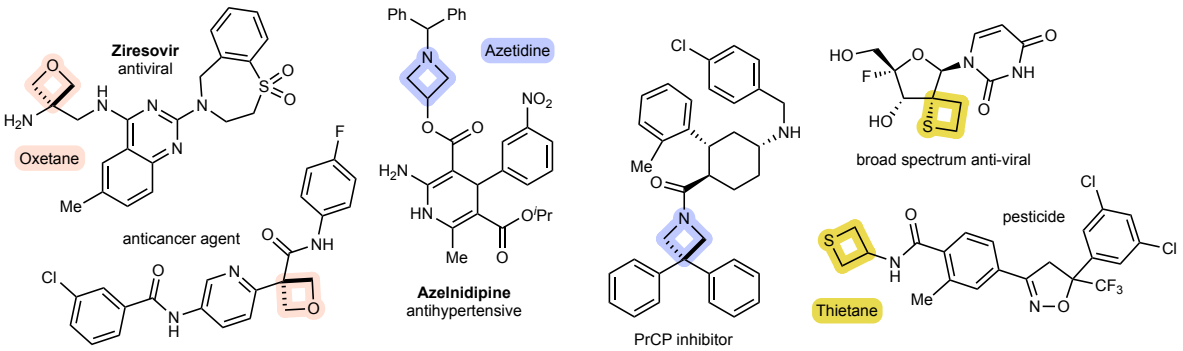


Figure 2. Examples of bioactive four-membered heterocycles.[28]

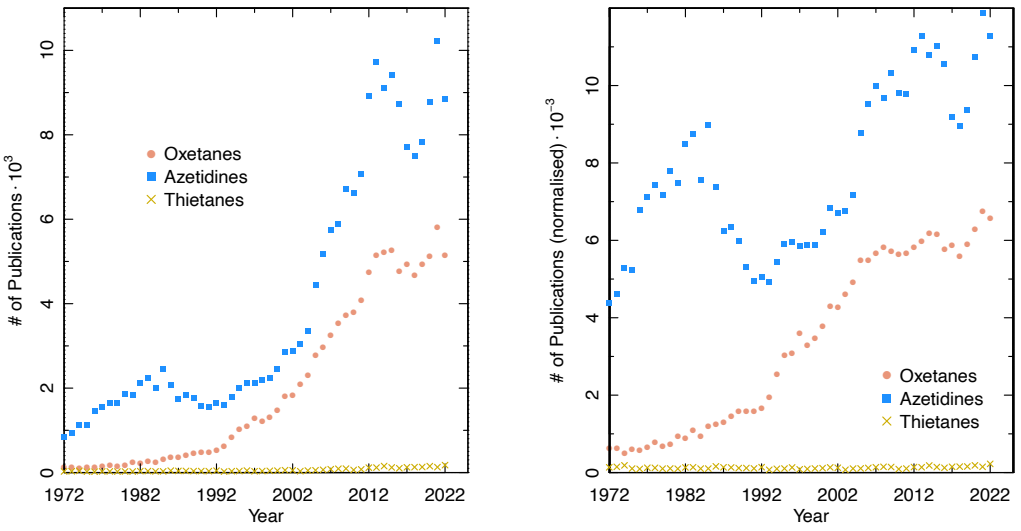


Figure 3. Appearance of four-membered heterocycles in the literature.[d] Left: Absolute number of publications. Right: normalised against the total number of publications recorded per year.

Despite the benefits, the uptake of four-membered heterocycles into medicinal chemistry campaigns has been relatively slow due to a lack of synthetic methods to access and incorporate such rings into drug-like compounds. This challenge has fuelled symbiotic efforts in academia and industry to enable their efficient inclusion into target compounds.[29]

---

[c] There have been 392 reports on oxetane natural products since 1972, 78 on azetidine natural products and only 3 reports on natural products that contain a thietane ring (Scifinder search 19.01.2023).

[d] Values obtained from a Scifinder search on 19.01.2023. Only publications included that report: biological study, therapeutic use, pharmacological activity, preparation, synthetic preparation, biological study (unclassified), pharmacokinetics, biological use (unclassified), agricultural use, biosynthetic preparation and natural product occurrence.

1.2 Oxetanes in Drug Discovery

Despite the higher occurrence of azetidines compared with oxetanes in the literature (Figure 3), which can be attributed to azetidine's additional dimension for functionalisation through nitrogen and their generally higher stability, oxetanes are anecdotally the most popular four-membered heterocycles in drug discovery and the synthetic community. This is in part due to historical reasons, since oxetanes occur more frequently in the structures of natural products (Section **1.2.1**), but also due to their unique properties (Section **1.2.2**) and application as bioisosteres (Section **1.2.3**). There have been many recent reviews on oxetanes which focus on their synthesis,[29a,30] Paternò-Büchi reactions,[31] ring openings, ring expansions and contractions,[32] general behaviour,[27,29b,33,34] and medicinal applications.[27,29b,33,34] Apart from applications to drug discovery, oxetanes are employed in polymer synthesis,[35] as propellants and energetic materials,[36] and as synthetic intermediates[37] (see ref. 34 for a comprehensive overview). This section will describe the occurrence of oxetanes in natural products, their desirable properties as medicinal motifs, the use of oxetanes as bioisosteres and will discuss recent tactical applications of oxetanes in drug discovery campaigns.

1.2.1 Oxetanes in Natural Products

By far the best-known oxetane-containing natural product is paclitaxel, commonly known by its brand name Taxol (Figure 4a). Isolated from the bark of the Pacific yew *Taxus brevifolia*, Taxol is an important chemotherapy agent part of the WHO List of Essential Medicines.[38,39] The synthetic burden of Taxol is considered too high to be commercially sustainable, with current production relying on a semi-synthetic approach from the European yew, *Taxus baccata*, from which 10-deacetylbaccatin is extracted, an oxetane-containing precursor to Taxol.[40] As such, the total synthesis of Taxol became a major endeavour amongst the synthetic community, considered especially challenging with its complex and unique structure, including an oxetane ring, which is rare in natural products. To date, twelve total syntheses of Taxol have been reported[41] and Taxol has become a benchmark for synthetic chemists to demonstrate ingenious disconnections and new methodologies.[42] In all examples the oxetane ring was constructed through intramolecular C–O bond formation and the oxetane motif was found not be crucial for bioactivity.[43]

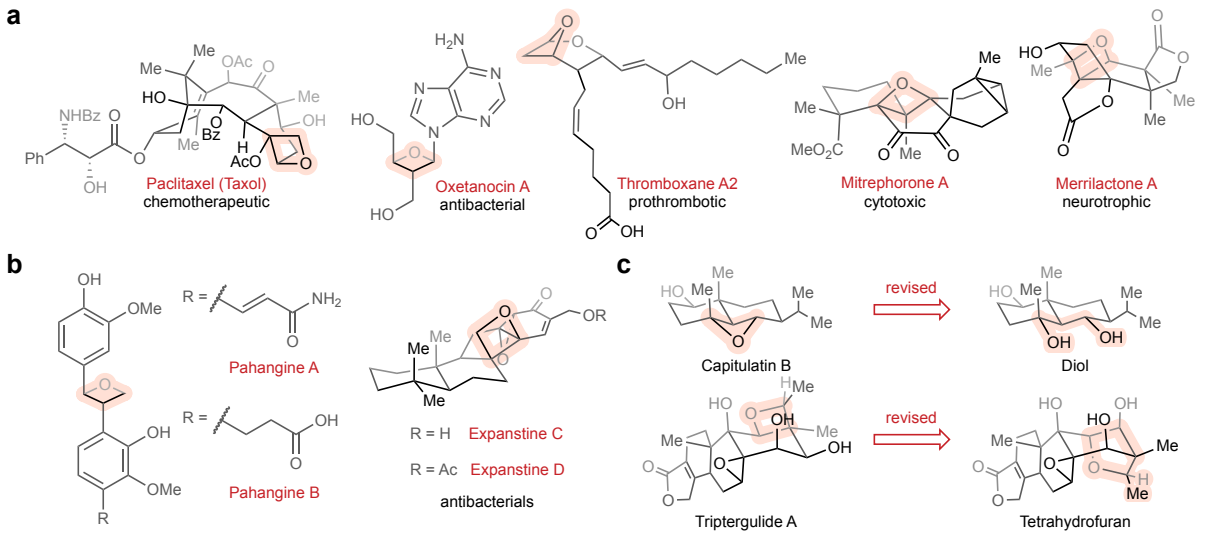


Figure 4. Oxetanes in natural products. a, Best-known oxetane-containing natural products. **b**, Newly discovered oxetanyl natural products. **c**, Revised structures of oxetanyl natural products (representative examples).

In addition to paclitaxel, oxetanes appear in an array of other bioactive natural products including oxetanocin A,[44] thromboxane A2,[45] mitrephorone A[46] and merrilactone A[47] (Figure 4a).[29b] Recent years have seen progress in the synthesis of mitrephorone A[48] and merrilactone A,[49] the biosynthetic pathway of albucidin[50] and the isolation of four new oxetane-containing natural products (pahangine A and B,[51] expanstine C and D; Figure 4b).[52] Further, a systematic computational and spectroscopical study of natural products containing the oxetane ring revised several oxetane structures to 1,3-diols or other ring systems (Figure 4c).[53]

1.2.2 Oxetanes as Attractive Motifs in Drug Design

Oxetanes have attracted increased attention in medicinal chemistry due to their combination of low molecular weight (MW), 3-dimensionality and high polarity.[54]

Controlling MW is important to keep a drug's lipophilicity levels within an acceptable range to maintain sufficient aqueous solubility and permeability.[55] High lipophilicity, most often measured by the water/octanol distribution coefficient Log*D*, has been associated with lower metabolic stability.[56,57] High aqueous solubility is important to increase a compound's bioavailability.[e] Sufficient permeability is needed for the API to cross cell membranes and this property is most relevant for neuroactive agents which must cross the lipophilic blood brain barrier (BBB).[58,59] In a broad sense, increasing the relative number of polar groups (*i.e.* H-bond donors and acceptors) within an organic molecule increases its aqueous solubility (through H-

[e] That is, how well the compound can travel through the human system and reach the site of action, measured as the fraction of administered API that ends up in the circulatory system.[55]

bonding with H_2O molecules), but decreases permeability, and the right balance needs to be found for each biological application. Similarly, a higher MW tends to decrease solubility and permeability, but might increase target affinity. 3-Dimensionality is a generally desirable property in drug candidates (see Section **1.1**) and has been shown to positively affect aqueous solubility.[60]

As such, the small ring size of oxetanes confers the motif with a low MW. The polar oxygen atom (H-bond acceptor) contributes to a beneficial reduction in lipophilicity and increase in aqueous solubility. The three tetrahedral, sp^3-hybridised carbons on oxetane increase the 3-dimensionality of the scaffold and could also lead to an increase in aqueous solubility. Indeed, Wipf developed an oxetane sulfoxide motif as an effective neutral solubilizing 'tag' that improved the solubility of selected poorly water-soluble drug compounds without impacting bioactivity.[61]

The four-membered oxetane ring is relatively flat compared to cyclobutane, typically exhibiting small puckering angles (<10 º) from the lower steric requirement of the lone pairs on oxygen compared to substituents on a carbon atom. A higher puckering angle reduces Pitzer strain (*i.e.* eclipsing interactions) but increases angle strain (*i.e.* the increase in energy due to acute bond angles). Puckering on oxetane is influenced by its substituents, with larger groups inducing a higher degree of puckering to relieve Pitzer strain (Figure 5a). For example, unsubstituted oxetane was shown to be close to planar by X-ray crystallography (puckering = 8.7 º at 140 K),[62] but when substituted with several alkyl and/or aryl groups, puckering is significantly increased (for example the puckering in 2,2,3,3-tetrasubstituted oxetanyl insecticide **EDO** is 16 º).[63] The degree of puckering in oxetane derivatives is important to consider for medicinal applications since it determines the position and direction of the oxygen lone pairs. In a planar oxetane conformation, the spatial orientation of the oxygen lone pairs would resemble that of a carbonyl group—relevant for applications as carbonyl isosteres (see Section **1.2.3**).

The small ring size of oxetanes imposes acute internal angles which have implications on structure, reactivity and its medicinal applications. For example, the lower-than-ideal endocyclic bond angles in four-membered rings of ~90 º (ideal bond angles for sp^3 hybridisation: 109.5 º) require the hybrid orbitals involved in the cyclic bonds to augment their p-character to accommodate the acute bond angles. This increased p-character means that hybrid orbitals involved in *exocyclic* bonds must have an increased s-character, which manifests as wider bond angles to exocyclic substituents. An alternative molecular orbital (MO) picture with the same ramifications is given by Walsh orbitals, which suggest sp^2-

hybridised atoms and an in-plane π-bonding framework.[64,65] The exocyclic bond angles in oxetanes are ~111 °, approaching typical carbonyl bond angles (~120 °) (Figure 5b).[62]

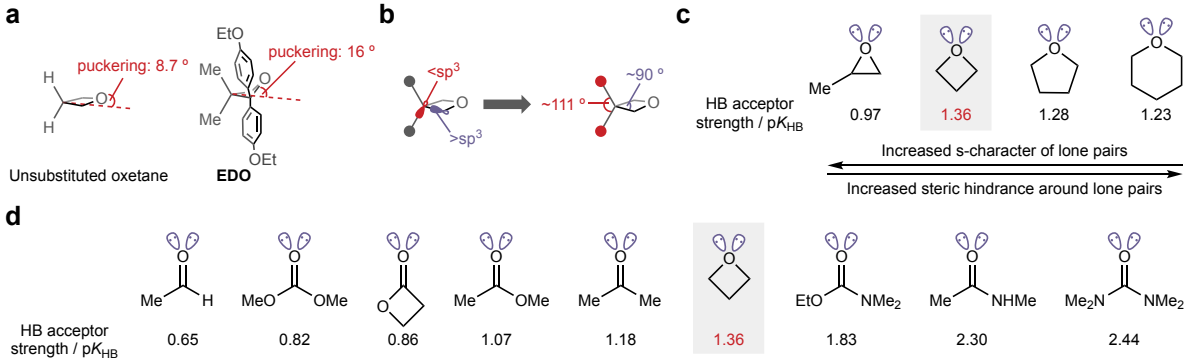


Figure 5. Medicinally relevant properties of oxetanes. a, Substitution-dependent puckering angle.[62,63] **b**, Hybridisation requirements and bond angles.[62] **c**, HB acceptor strength of cyclic ethers.[66] **d**, HB acceptor strength of oxetane in comparison to other carbonyl functionality.[69]

Another important consequence of the small ring angles in oxetanes is the Lewis basicity of the oxygen lone pairs. Oxetane shows the highest Lewis basicity amongst cyclic ethers as a consequence of two opposing effects (Figure 5c).[66] Firstly, as ring size decreases, substituents α to oxygen move away from the lone pairs and the lone pairs become more exposed.[67] On the other hand, as explained above, decreasing ring size increases the s-character of hybrid orbitals not involved in cyclic bonds.[68] Electron density in lone pairs with increased s-character is lower in energy, and hence they are less nucleophilic or Lewis basic. The latter effect is most pronounced in the three-membered ring (oxirane). The high Lewis basicity of oxetanes makes them good hydrogen bond (HB) acceptors, relevant for bioactivity to form strong HB interactions with polar groups in biomolecules. The HB acceptor strength of oxetanes was measured spectroscopically to be higher than aldehydes and ketones, but lower than *N*-functionalised carbonyls such as amides and carbamates (Figure 5d).[69]

A notable feature of oxetanes is their pronounced electron-withdrawing effect due the electronegative oxygen atom. This negative inductive effect is amplified in oxetanes compared to acyclic ethers or larger ring systems because it propagates simultaneously through two short σ frameworks to reach substituents in the 3-position. Carreira and coworkers demonstrated that an oxetane α to a tertiary amine reduces the pK_a of the amine by 2.7 units (that is, ca. 500 times less basic) from 9.9 to 7.2 by means of its negative inductive effect.[70] The same effect is observed at more distal positions, albeit to a lesser extent (pK_a: β: 8.0, γ: 9.2, δ: 9.6), as is typical for σ effects.

The unsubstituted oxetane ring has a ring strain of 106 kJ mol^{-1} (*c.f.* epoxide: 112 kJ mol^{-1} and tetrahydrofuran (THF): 25 kJ mol^{-1}),[71] rendering oxetanes both sufficiently stable but

potentially reactive, the extent of which is entirely dependent on molecular context and tuneable by the choice of substituents. This stability grey zone is unique, rendering *stable* oxetane-containing structures valuable for long-lasting medical applications, and *reactive* oxetane derivatives useful as synthetic intermediates.[29a,30] Oxetanes are anecdotally unstable to acidic conditions, which results in ring-opening and has been routinely exploited for the synthesis of polyoxetanes.[34,35] The categorical instability of oxetanes to acidic conditions is, however, a misconception. Oxetane stability is often dictated by its substitution pattern, whereby substituents that sterically block the path of external nucleophiles to the C–O σ* antibonding orbital confer the oxetane ring with increased stability (Figure 6a–b).[70] 2-Substituted oxetanes favour ring-opening reactions *via* S_N1-like formation of carbocations, while 3,3-disubstituted oxetanes are considered a privileged substitution-constellation for robustness to demanding chemical environments (see Sections **1.2.3**, **1.4** and **3.2**). Oxetane structures with *internal* nucleophiles (*e.g.* alcohols,[72,73] carboxylic acids,[74] etc.) in the right geometry, can position the nucleophile directly behind the C–O bond and easily undergo intramolecular ring-opening transformations under acidic conditions or by simple heating to generate a larger, usually 5- or 6-membered, (hetero)cycle (Figure 6c).

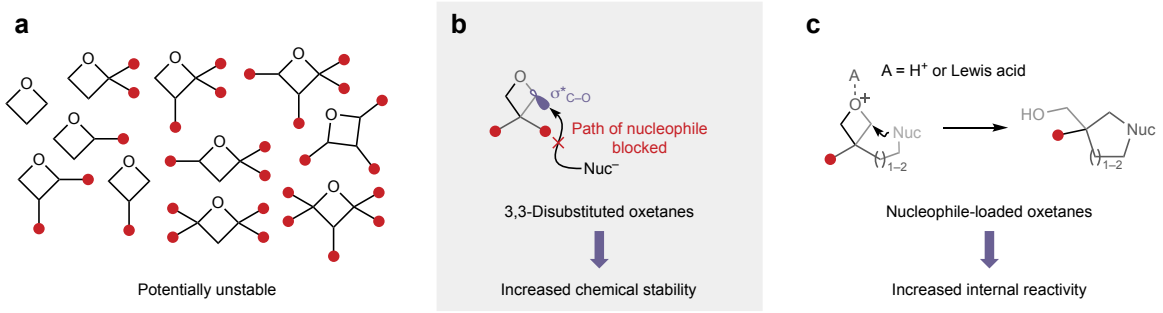


Figure 6. Oxetane stabilities. a, Substitution patterns with variable stabilities. **b**, Increased chemical stability in oxetanes with 3,3-substituents. **c**, Facile intramolecular ring-opening on mild activation.

Interest in the oxetane scaffold as beneficial substructures to incorporate into drugs has provoked several studies on their metabolic stability. Duncton and coworkers demonstrated that from a library of 3-aryloxetanes, around half of the compounds showed conjugates[f] upon incubation with glutathione, human liver microsomes and nicotinamide adenine dinucleotide phosphate (NADPH).[75] This was an important early report showing that the oxetane structure was not a categorical metabolic liability. Later, Stepan (Pfizer) reported 2- and 3-substituted oxetanes as less lipophilic analogues of tetrahydrofuran structures that led to a many-fold improvement in metabolic stability without compromising bioactivity (Figure 7a).[76] The

[f] *I.e.* reacted covalently with glutathione. Such an assay is often used in medicinal chemistry as an initial assessment to identify potential reactive metabolites within a library of compounds.

substitution pattern on oxetane was also found to impact metabolic clearance, with 2-substituted oxetanes shown to metabolically ring-open and form diol and hydroxy-acid metabolites. A systematic study from the same group on cyclic ethers revealed two important findings:[77] 1) reduction in ring size (from tetrahydropyran (THP) → tetrahydrofuran (THF) → oxetane) led to an improvement in metabolic stability due to reduction in lipophilicity, determined by a lipophilic metabolism efficiency analysis (LipMetE), 2) substitution in the 2-position of cyclic ethers was metabolically less tolerated than in the 3-position. Dowling (AstraZeneca) reported on oxetanyl-containing CK2 kinase inhibitors that showed reduced lipophilicity, higher selectivity and a lower metabolic clearance than cyclopropane and cyclobutane analogues (Figure 7b).[78]

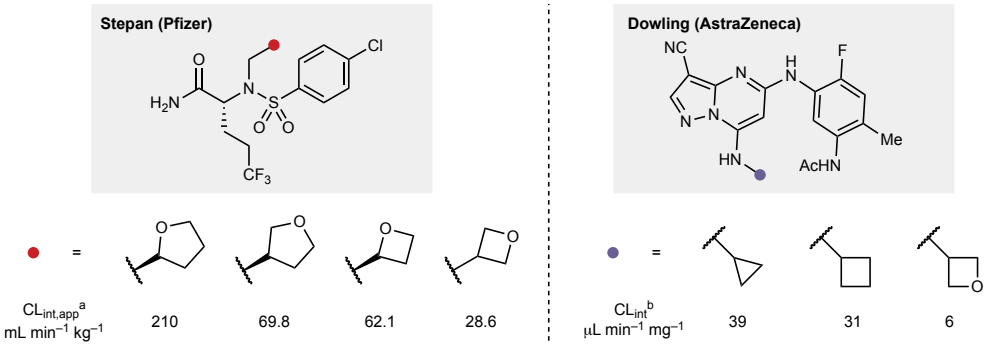


Figure 7. Examples of improved metabolic stability upon oxetanyl substitution. [a] $CL_{int,app}$ = total intrinsic clearance from scaling *in vitro* HLM (human liver microsomes) half-lives.[77] [b] CL_{int} = intrinsic clearance determined from rat liver microsome incubations.[78]

The apparent metabolic robustness of oxetane scaffolds prompted more in-depth mechanistic studies on their metabolic clearance pathways, spearheaded by Hayes (AstraZeneca). Oxetane-containing drug candidate AZD1979 was shown to be metabolised by either glutathione *S*-transferase (GST) through ring-opening of an azetidine functionality,[79] or by the human microsomal epoxide hydrolase (mEH) by ring-opening the oxetane ring (Figure 8a).[80] This study represented the first example of a non-epoxide substrate being hydrolysed by mEH. Subsequent systematic studies of oxetane-containing compound libraries revealed mEH metabolism not to be limited to AZD1979, but also applicable to other oxetanyl substrates (Figure 8b).[81] The analysis revealed that subtle structural modifications changed the preferred pathway of metabolic clearance without any statistically significant correlation to intrinsic properties such as pK_a or Log*D*, and also noting other reports of oxetane degradation by cytochrome P450 enzymes (CYPs).[82]

The majority of (drug) compounds are cleared by cytochrome P450 enzymes (CYPs), which can be problematic due to undesired and poorly predictable drug–drug interactions on comedication. It can be hence advantageous for medicinal chemists to deliberately add motifs

to a drug candidate that 'steer away' from CYPs towards metabolic clearance through alternative pathways. Oxetane structures, which were shown by Hayes to be potential substrates for mEH enzymes,[79–81] could be useful as such a metabolic tag,[83] with the added advantage of increased stability over *e.g.* epoxide substrates for the mEH metabolic pathway.[84]

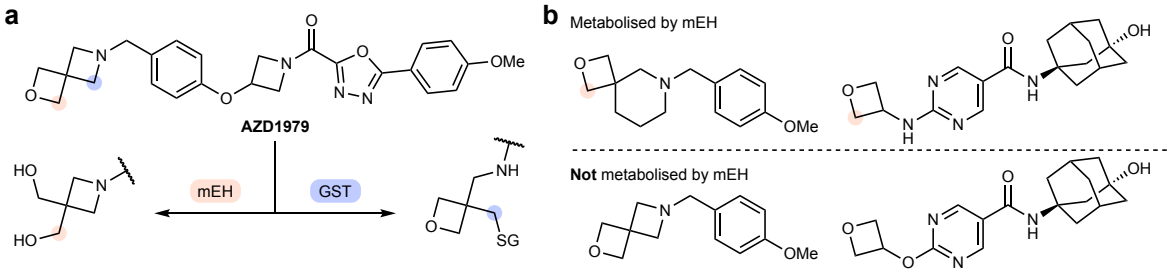


Figure 8. Metabolic clearance of oxetanyl substrates my mEH. a, Metabolic pathways of drug candidate AZD1979. **b**, Examples of oxetanes cleared, and not cleared, by mEH.

The oxetane ring has been shown to be an attractive motif for drug discovery. It introduces steric bulk without significantly increasing molecular weight or lipophilicity, is a strong hydrogen-bond acceptor, increases aqueous solubility, is stable (*e.g.* vis-à-vis epoxides), categorically not a metabolic liability, and has potential to influence clearance pathways (Figure 9).

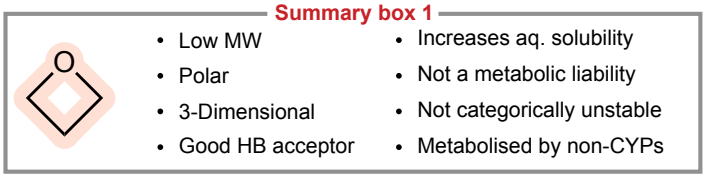


Figure 9. Summary of medicinally relevant properties of the oxetane motif.

1.2.3 Oxetanes as Bioisosteres

Bioisosteres are chemical groups with similar physical and chemical properties that show comparable biological activity against a given target.[85] In the context of drug discovery, bioisosteric replacement is routinely applied to optimise hit- or lead compounds by adjusting the compounds' pharmacological or toxicity profile and to access new intellectual property (IP) space, whilst maintaining, or improving, bioactivity.[86] Conceptually, bioisosterism is attractive for medicinal chemists because it allows the optimisation and fine-tuning of compound properties in a logical manner. A classic bioisosteric replacement (*i.e.* conserved valence electron structure as per Langmuir)[87] is to swap a hydrogen- for a fluoride atom to block a molecular position at risk of oxidative metabolism.[88] Non-classical bioisosterism (in the broadest sense) often finds application in mimicking common amide functionality.[89]

Amide bonds are ubiquitous in nature as the central building tool in proteins and are also key bonding units in drug compounds.[90] The popularity of amide motifs is further fuelled by the robustness and reliability of amide couplings[8] and the availability of the native functional groups that form the amide bond: carboxylic acids and amines.[g] Despite being excellent HB donors and acceptors and *relatively* stable carbonyl scaffolds,[90] amides may not always offer the required properties for the desired therapeutic effect. For example, a different conformation of the compound might be needed, or aqueous solubility is poor, or the amide functional group is quickly metabolised by amidases. Hence, the bioisosteric substitution of amide groups is an active field of research in medicinal chemistry. Amide mimics attempt to replicate the broad overall geometry of the amide unit with comparable pK_a and the correct orientation of HB donors and acceptors, whilst providing potentially advantageous subtle differences in conformation and physicochemical properties (Figure 10).[89]

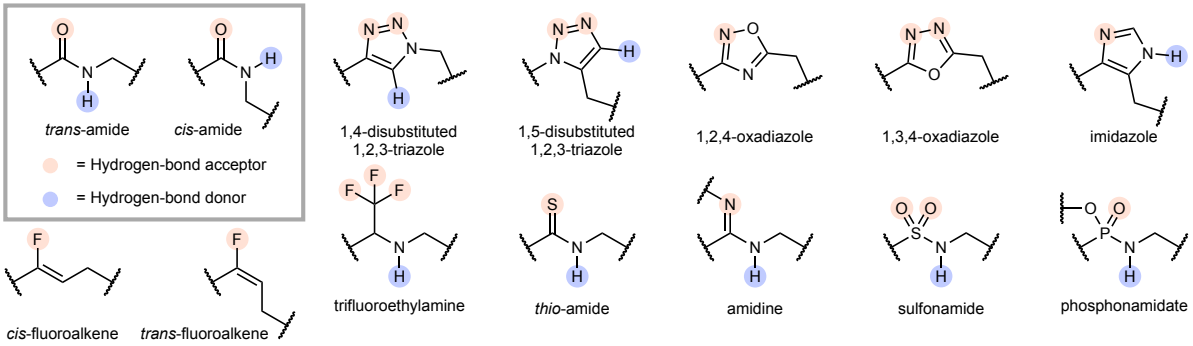


Figure 10. Examples of common amide isosteres.[89]

A considerable challenge for bioisostere-guided drug optimisation is the synthetic intractability of bioisosteric alternatives compared to the native functionality. Whilst powerful, well established and understood amidation methods exist,[91] accessing the corresponding target isostere (*e.g.* compounds in Figure 10) is often non-trivial and requires a distinct synthetic route for each isosteric analogue. It is hence valuable to develop methods that can assemble the desired bioisostere with equal ease, and ideally using the same building blocks (*i.e.* carboxylic acids/amines for amide isosteres) as the parent scaffold.

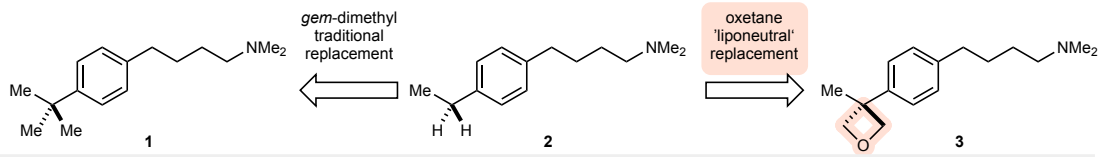
An influential communication by Carreira (ETH) and Roger-Evans (Hoffmann–La Roche) in 2006 awoke serious interest on oxetanes as bioisosteres of *gem*-dimethyl and carbonyl groups.[92] Strategic placement of *gem*-dimethyl groups is a common approach to protect metabolically labile sites such as benzylic C–H positions which are easily oxidised by CYPs.

---

[g] Representatively, the size of libraries of carboxylic acids and amines from the vendor Enamine, are >37'000 and >57'000, respectively. https://enamine.net/building-blocks/functional-classes. Retrieved: 24.01.2023.

However, the addition of two methyl groups is accompanied by a significant increase in lipophilicity (Log*D*) which often results in poor solubility and counterproductively, in lipophilicity-driven CYP degradation. Carreira and Roger-Evans showed that by adding an oxetane instead of a *gem*-dimethyl group, the labile site was still blocked but there was no unfavourable increase in lipophilicity, owing to the oxetane's polarity. Oxetane **3** was metabolically more stable than methylene **2** or *gem*-dimethyl **1**, more soluble, less lipophilic and safer *in-vitro* (measured by hERG inhibition;[93] not measured for methylene **2**) (Table 1).

Table 1. Pharmacokinetic properties of methylene–*gem*-dimethyl–oxetane analogues. Data from refs. 70 and 92. Note there is a discrepancy in the solubility data of compound **3**. Here the most recent dataset was taken.[70]



	1	2	3
CL_{int} / μL min^{-1} mg^{-1}	420	520	43
Log*D*	2.5	1.8	0.8
solubility / μmol L^{-1}	<4	250	18'000
hERG IC_{50} / μM	7.5	not determined	35

Oxetanes have also been proposed and evaluated as isosteres of *tert*-butyl groups. Whilst a structural change from *tert*-butyl **4** to 3-methyl-oxetane **5** had surprisingly no effect in microsomal stability (Figure 11a),[94] a trifluoromethyl oxetane GSM (γ-secretase modulator) analogue (**7**) reduced Log*D* and metabolic clearance compared to *tert*-butyl analogue **6** without significant compromise on affinity (Figure 11b).[95]

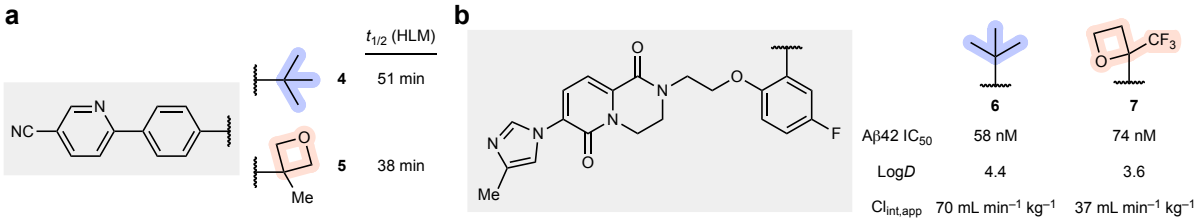


Figure 11. Evaluation of oxetanes as *tert*-butyl isosteres.[94,95] **a**, Effect of a change from *t*-Bu to 3-methyl-oxetane on microsomal stability.[94] **b**, Isosteric comparison of a *t*-Bu and a 3-(CF_3)-oxetane scaffold.[95]

Later, Carreira and scientists at Hoffmann–La Roche also demonstrated oxetanes to be suitable bioisosteric replacements for carbonyl groups, shown specifically on ketones and alkyl amides. Carbonyl derivatives, whilst synthetically useful and straight-forward binding structures, can suffer in biological environments from metabolic degradation and low 3-

dimensionality due to their electrophilic character and π-system, respectively.[96] 3,3-Dialkyl-spiro-oxetanes were shown to have similar dipole moments, geometry and HB properties (see Figure 5 and Figure 12), similar or slightly higher Log*D*, and a higher metabolic stability compared to analogous ketones (Figure 12a).[70,97]

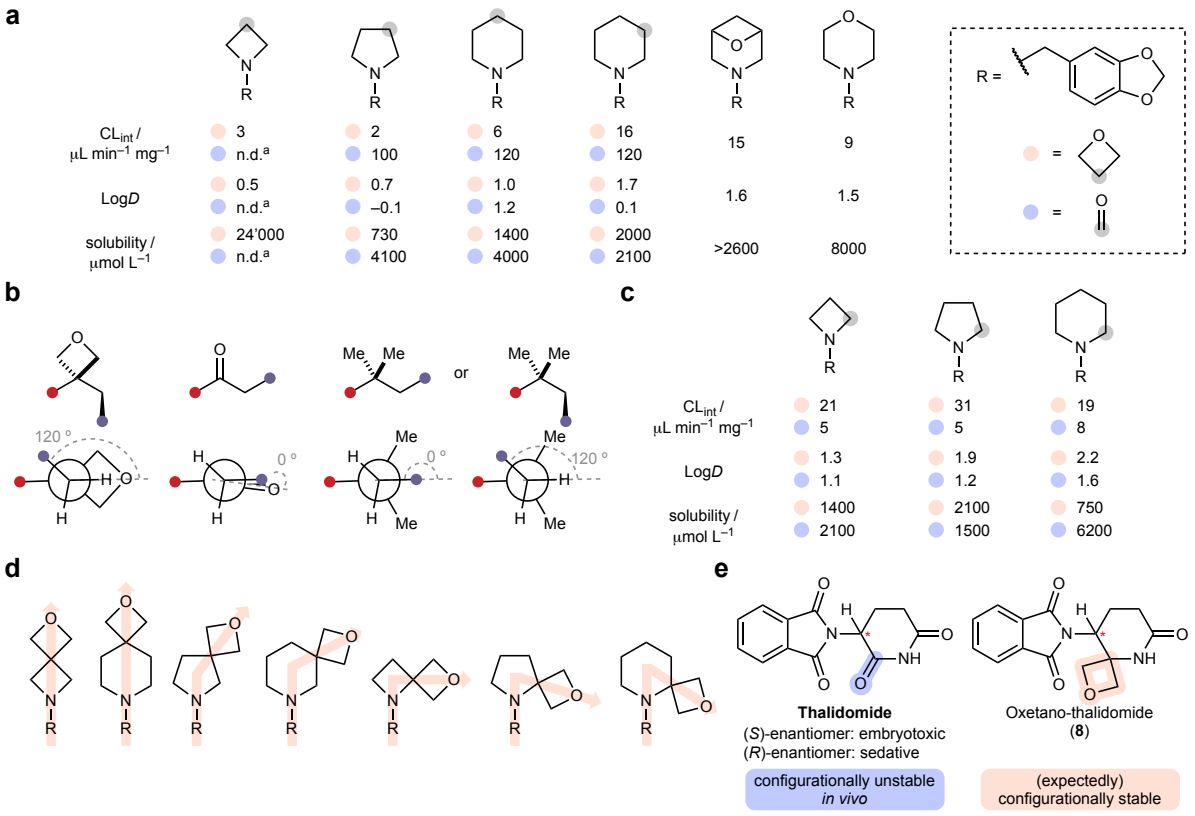


Figure 12. Early isosterism studies of spiro-oxetanes as surrogates of ketones and amides. **a**, Physicochemical comparison of spiro-oxetanes vs cyclic ketones.[70,97] **b**, Conformational differences between oxetanes, ketones and *gem*-dimethyl groups on alkyl chains.[70] **c**, Physicochemical comparison of spiro amino-oxetanes vs cyclic amides.[70,97] **d**, Directionality of aza-spiro-oxetanes.[97] **e**, Application of an oxetane analogue of thalidomide.[100] [a] Compound unstable.

The most striking differences between oxetanes and ketones were structural in nature (Figure 12b).[70] First, the C–O distance in oxetanes (across the ring) was on average 0.9 Å longer than in carbonyls (2.1 vs 1.2 Å), second, oxetanes introduced additional lateral bulk and third, there was a distinct change in conformational preference of the alkyl chain to which the carbonyl/oxetane is attached. Whilst the preferred conformation in carbonyl derivatives was antiperiplanar, oxetanes clearly favoured a gauche conformation. As a comparison, *gem*–dimethyls showed equal preference for all three staggered conformations. The acute angle fixed by the oxetane ring (~90 °) prohibited population of the antiperiplanar staggered conformation to avoid filled–filled non-covalent orbital interactions. The oxetane-induced gauche conformation was leveraged by scientists at Roche to obtain a compound with a

defined and restricted shape that fitted well into the protein pocket and improved affinity (and other physicochemical properties) compared to the *gem*-dimethyl predecessor.[27a]

In the limited set of spiro amino-oxetane/amide pairs evaluated, the amino-oxetanes showed minimally increased lipophilicity and metabolic clearance and a slight decrease in solubility vs the amides (Figure 12c).[70,97] Spiro-oxetane derivatives are intriguing scaffolds with physicochemical and structural similarities to morpholines, which are often used as solubility tags but which can suffer from oxidative metabolic clearance.[70,98,99] By changing the position of oxetane along the aza-cycle, a further dimension for tuning and optimisation was unlocked: the directionality of the oxygen lone pairs (Figure 12d). A noteworthy application of a spiro amino-oxetane was seen in an analogue of thalidomide, an anti-cancer and sedative medication (Figure 12e).[100] Thalidomide suffers from configurational instability *in vivo* by deprotonation of the acidic α-keto C–H bond.[101] The (–)-(*S*)-enantiomer is teratogenic and embryotoxic which led to a medical catastrophe in the 1950s with over 10,000 children born with birth defects.[102] The (+)-(*R*)-enantiomer has the desired sedative effect. Unlike parent thalidomide, the C–H bond at the stereogenic centre of 'oxetano-thalidomide' **8** is no longer acidic thanks to the absence of the carbonyl group and is hence likely to be configurationally stable, although this was not demonstrated explicitly.[100]

Bull and Mousseau (Pfizer) recently investigated the bioisosteric quality of 3,3-diaryl-oxetanes to replace benzophenones and diaryl-methanes (Figure 13a).[103] Both the diaryl-ketone and -methylene structures appear frequently in bioactive compounds,[104,105] but their use in medicinal chemistry programs has been hampered by their inherent *in vivo* nucleophilic- (ketone), photo- (ketone)[106] and oxidative (methylene) instability.[107] Diaryl-oxetanes were shown not to be a physicochemical liability, with comparable stability, metabolic, lipophilicity, permeability and solubility properties to benzophenones and generally improved properties vis-à-vis diaryl-methanes.

Oxetane bioisosteres of other carbonyl derivatives have been proposed and investigated, albeit to a lesser extent. In 2017, Brunden and Ballatore showed that oxetanols and other four-membered ring alcohols can act as surrogates of carboxylic acid derivatives.[108,109] Oxetanols were demonstrated to be more lipophilic and much less acidic than the carboxylic acids and consequently, also more permeable, an important property for drugs that target the central nervous system (CNS) and need to cross the BBB (Figure 13b). Further, an oxetane analogue of ibuprofen (**9**) was shown to retain most of the inhibitory effect of the cyclooxygenase (COX) pathway and additionally, in contrast to parent ibuprofen, also inhibited the 5-lipooxygenase (5-LOX) pathway. Later, Bull reported on the synthesis of oxetane sulfides and the physicochemical properties of selected examples[110] and Vanderwal showed that oxetane

sulfide **10** was a more stable analogue of substrates of polyketide synthases (PKSs) (Figure 13c).[111] The oxetane PKS substrate mimic allowed the structural investigation of acyl-enzyme intermediates and shed light on the biosynthetic pathway of PKSs. In a recent structure property relationship study by Ballatore, sulfonamido-oxetanes were shown to possess similar physicochemical properties as the corresponding *N*-acylsulfonamides, whilst reducing N–H acidity by ca. five units and increasing Log*D* by ca. two units.[112]

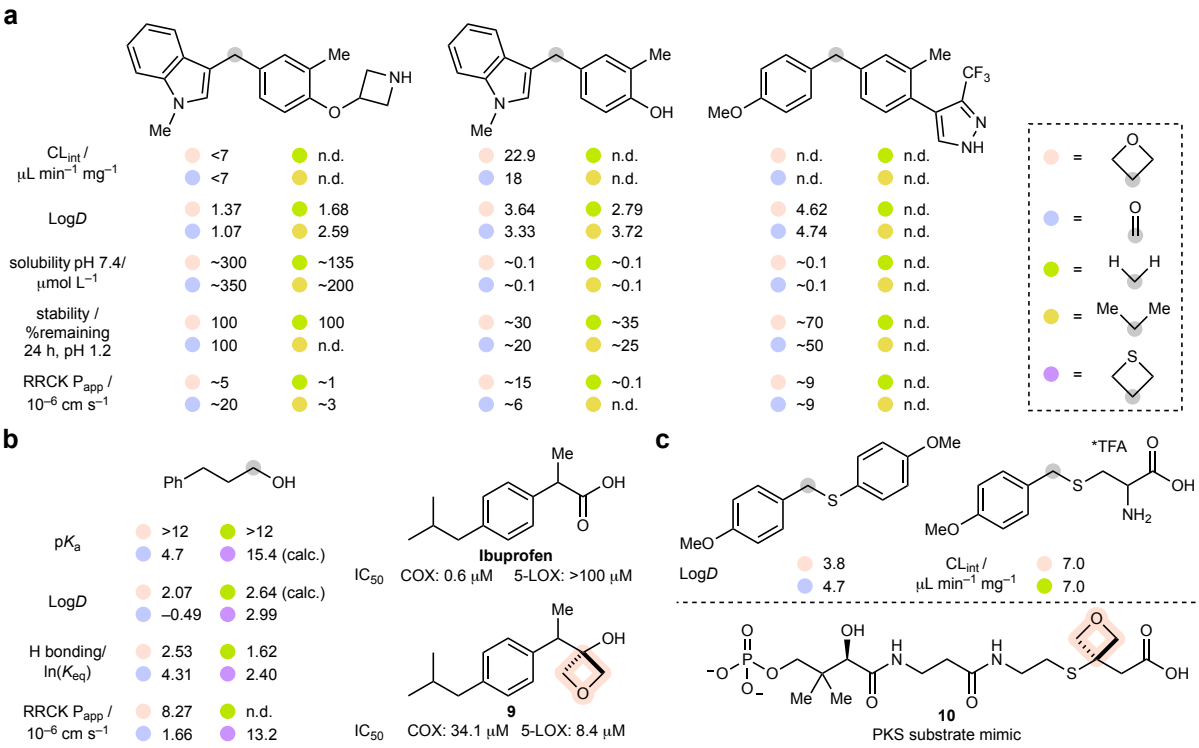


Figure 13. 3,3-Disubstituted-oxetanes as isosteres of ketones (a),[103] carboxylic acids (b)[108] and thioesters (c).[110,111]

Amino-oxetanes are most often used as peptidomimetics, whereby one or more carbonyl groups are substituted by an oxetane to impart the compounds with improved properties, most notably increased metabolic stability.[113] Designed peptide-based APIs can provide highly selective and potent ligands that are uniquely shaped for their destined target pockets. Nevertheless, therapeutic peptides often suffer from poor bioavailability due to metabolic degradation by amidases that specifically cleave the amide bond, and also from poor permeability. Amide bioisosteres are hence of considerable value in medicinal chemistry as peptidomimetics to replace the enzymatically labile peptide linkage.[89b] Amino-oxetanes offer an intriguing peptidomimetic strategy, emulating the carbonyl's HB accepting capacity and orientation, removing the liability towards protease-associated degradation, inducing a change in conformation (see Figure 12b) and increasing the basicity of the nitrogen atom (compared to amides). Despite the attractive properties, amino-oxetanes have been poorly studied due to the dearth of synthetic methods, as evidenced in a recent amide isosterism study.[114]

In 2014, Shipman and Carreira reported independently on the synthesis of amino-oxetanes as peptidomimetics by an aza-Michael addition into oxetane alkylidenes (Figure 14a).[115] This methodology was recently extended to N-heterocyclic nucleophiles.[116] Later, Carreira showed that oxetanyl analogues of the endogenous opioid peptide neurotransmitter Leu-enkephalin were more stable in blood serum without critically compromising activity (Figure 14b).[117] Shipman elegantly demonstrated the incorporation of oxetanyl-peptide building blocks into solid-phase peptide synthesis (SPPS) and the synthesis of an oxetane analogue of physiologically active peptide bradykinin, albeit without biological data (Figure 14c).[118] Further, oxetanes incorporated into peptide backbones enabled more facile macrocyclisation and the oxetane-modified macrocyclic peptide **11** fully retained the bioactivity of the parent amide inhibitor cCNGRC (Figure 14d).[119] Since these pioneering reports, there have been further advances in the synthesis of new oxetanyl-peptide building blocks,[120] the application of oxetane peptidomimetics in hydrogels,[121] and the conformational understanding of oxetane analogues of α-helical peptides, which lost helicity on oxetane incorporation.[122] A recent study looked at the differences in polar surface area (PSA) between amides and its isosteres, concluding that amino-oxetanes do not alter this property significantly compared to the amide. The sample set of amino-oxetanes was however very limited and the substitution pattern on oxetane and nitrogen not given.[114]

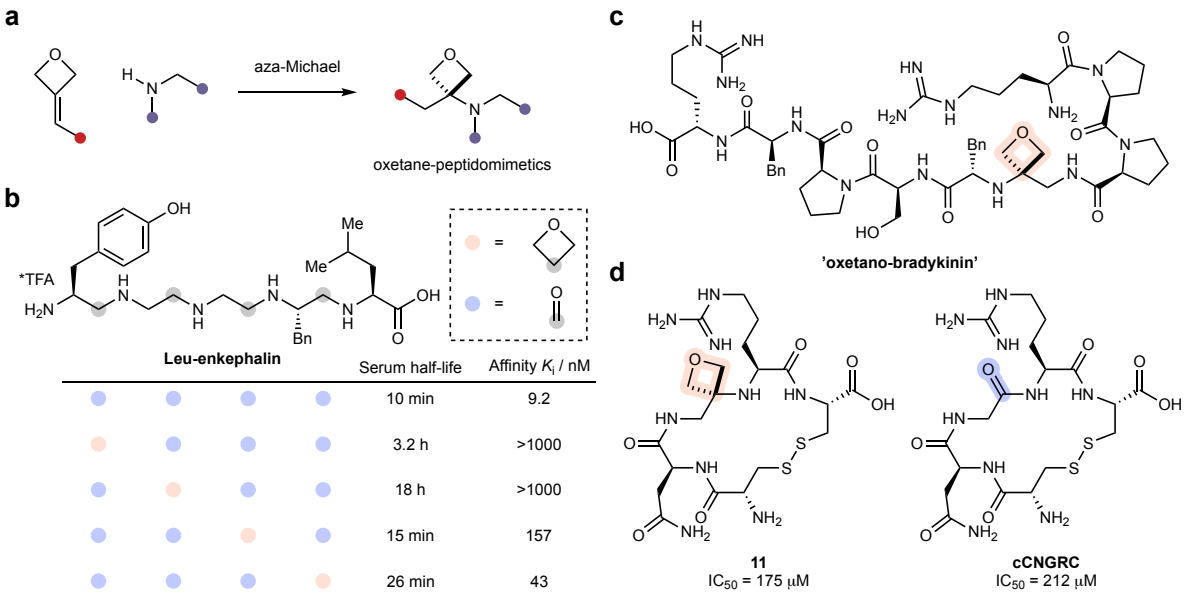


Figure 14. Application of amino-oxetanes as peptidomimetics. a, General synthetic logic *via* an aza-Michael addition.[115] **b**, Effect of oxetane substitution in Leu-enkephalin on serum stability and bioactivity.[117] **c**, Oxetane analogue of bradykinin synthesised on an SPPS system.[118] **d**, Oxetane enabled synthesis of macrocyclic peptides and comparison of biological activity to cCNGRC.[119]

Spirocyclic oxetanes have been used as bioisosteres in pharmaceutical campaigns, as analogues of 1,25-dihydroxyvitamin D_3 and *seco*-steroids.[123] 3,3-Disubstituted oxetanes have been demonstrated to be suitable isosteres of several alkyl and carbonyl derivatives, including

gem-dimethyl groups, methylenes, ketones, amides, carboxylic acids and thioesters (Figure 15). The oxetane motif was not a categorical liability in any of the investigated physicochemical properties (*e.g.* metabolism, stability, solubility, permeability) and performed equally well or, in many cases, better than the parent structures. The change to an oxetane ring induced conformational changes to the compounds' structures due to oxetane's unique geometry. The biological activity of oxetane isosteres was varied and dependent on structural subtleties but the oxetane ring did not fundamentally shut down inhibitory activity. These early studies highlight the potential of oxetanes as bioisosteres, but more work is needed to better the understanding of the substitutional effect of the oxetane ring on physicochemical and biological properties.

Summary box 2



- Polar isostere of *gem*-dimethyl groups
- No physicochemical liability vs ketones or alkyl amides
- Reduces pK_a of adjacent amines
- Potential as isostere of carboxylic acids and thioesters
- Validated peptidomimetics

Figure 15. Summary of 3,3-disubstituted oxetanes as bioisosteres.

1.2.4 Developments in the Application of Oxetanes in Drug Discovery Campaigns

The popularity of the oxetane ring for medicinal applications has increased dramatically since it's 'rediscovery' in 2006, fuelled by oxetane's attractive properties as designer motif and bioisostere of problematic functionality, as was highlighted in the last two sections (**1.2.2** and **1.2.3**). Applications as part of drug discovery campaigns, including the patent literature, have been comprehensively covered in reviews up to 2016 with instructive case studies.[27,29b,33,34] This section provides an update of such applications (2017–2022).

There are currently seven oxetane containing drug candidates undergoing clinical trials,[124] which will be discussed here with an emphasis on the role of the oxetane ring, where such information was available (Figure 16). In phase III are: crenolanib, developed by AROG Pharmaceuticals/Pfizer for treatment of various types of cancer (AML, GIST, glioma);[125] fenebrutinib, developed by Genentech as a treatment for multiple sclerosis (MS);[126] and ziresovir, developed by Hoffmann–La Roche/Ark Biosciences for treatment of respiratory syncytial virus (RSV).[28a,127] Lanraplenib (Gilead Sciences, treatment of Lupus Membranous Nephropathy (LMN))[128] and danuglipron (Pfizer, treatment of diabetes)[129] are in phase II, and GDC-0349 (developed by Genentech, treatment of Non-Hodgkin's lymphoma and solid tumours)[130] and PF-06821497 (Pfizer, treatment of relapsed/refractory SCLC (small cell lung cancer, prostate cancer and follicular lymphoma)[131] in phase I.

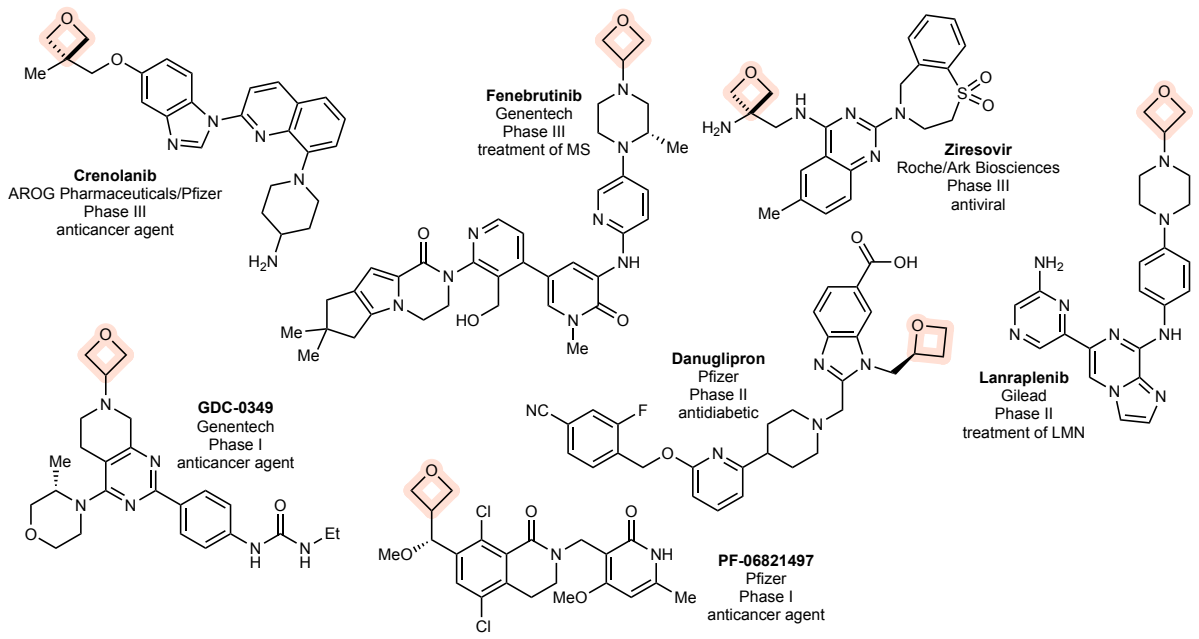


Figure 16. Fully synthetic drug candidates containing an oxetane scaffold.[125–131]

There are several apparent trends in the molecular structures in Figure 16. First, over 50% of the structures are amino-oxetanes (4/7), highlighting the important use of oxetanes to moderate amine basicity. Second, in six out of seven compounds the oxetane is substituted in the 3-position, likely due to superior stability and/or higher synthetic tractability (see **1.2.2**).

In fenebrutinib, the oxetane motif was an essential component of the drug, crucial to lower the pK_a of the piperazine ring from 7.8 (*N*-methyl predecessor) to 6.3 (*N*-oxetane; fenebrutinib; Figure 16).[126b]

The oxetane moiety in ziresovir, deemed the 'highlight of the discovery',[127b] was introduced to reduce the basicity of the terminal amine in amino-alcohol **12**, which was important to lessen the candidate's volume of distribution (V_{ss})[h] to avoid its undesired accumulation in tissue and minimise risks of toxicity (Figure 17a).[127] Ziresovir improved potency and selectivity, although the oxetane was found not to be involved in any interactions with protein residues. Instead, the oxetane ring served as a conformational and basicity control. The oxetane was crucial to achieve the desired properties, cyclobutyl, cyclopropyl and *gem*-dimethyl analogues had a clearly inferior therapeutic index (TI).[i]

[h] V_{ss} = Volume required to dissolve an API to the same concentration as that measured in blood plasma.
[i] TI = ratio of required dose for therapeutic effect vs toxic dose.

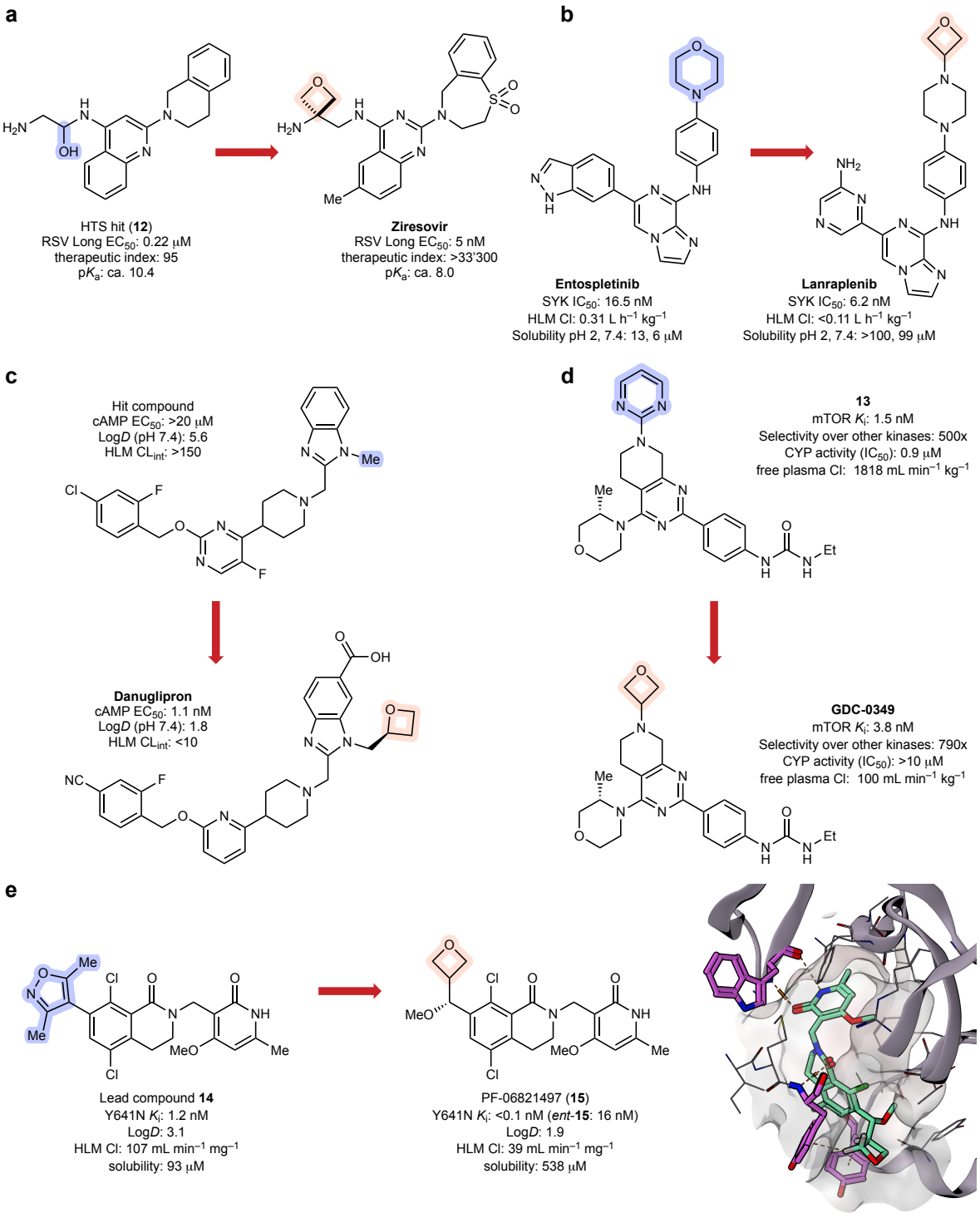


Figure 17. Introduction of oxetane ring in the campaigns of clinical candidates. a, Ziresovir;[127] **b**, lanraplenib;[128] **c**, danuglipron;[129] **d**, GDC-0349[130] and **e**, PF-06821497 (**15**). Cocrystal structure of oxetane **15** available under PDB code 4W2R (2.8 Å).[131]

In the last iterations of optimisation of lanraplenib, the morpholine structural motif in its predecessor (entospletinib) was substituted by an *N*-oxetanyl piperazine which maintained potency, improved metabolic stability and pH-independent solubility, attenuated piperazine basicity and regulated Log*D* (Figure 17b).[128a] In the final optimisation, the indazole ring in

entospletinib was exchanged for an amino-pyrazine to reduce aromatic count and increase 3-dimensionality. This change reduced Log*D* from 2.0 to an optimal value of 1.3 (lower was detrimental for permeability), whilst maintaining the rest of favourable physicochemical properties. Lanraplenib is the prime example of using a piperazine-oxetane as a more metabolically stable analogue of morpholine and of reducing planarity to improve drug-like properties.

The oxetane motif in danuglipron was introduced as a small polar head which increased potency without negatively impacting Log*D* and other physicochemical properties, essentially acting as a 'lipo-neutral' bulk increase[92] (Figure 17c).[129] Danuglipron mimics the binding mode of peptide agonists to GLP-1R (glucagon-like peptide receptor 1) but circumvents the metabolic instability associated with peptidic therapeutics (see **1.2.3**).

GDC-0349 was developed to improve its predecessor's (**13**) unfavourable CYP metabolic behaviour and poor free plasma clearance (Figure 17d).[130a] Introduction of the 3-amino-oxetane structure on the fused piperidine-pyrimidine core ring system showed attenuated basicity (pK_a 5.0), increasing safety *in vivo* (no detectable hERG inhibition). GDC-0349 was also highly selective against mTOR (mammalian target of rapamycin) over 266 other kinases and showed a ten-fold reduction in free plasma clearance compared to pyrimidine **13**.

In PF-06821497 (**15**), a dimethyl-isoxazole motif (**14**) was exchanged for a methoxy-methyl oxetanyl scaffold which significantly reduced Log*D* (3.1→1.9) and increased microsomal stability, thermodynamic solubility and potency (Figure 17e).[131a] The stereochemistry of the newly introduced stereogenic centre α to oxetane was important for binding, with the (+)-(*R*) enantiomer (**15**) showing a 16-fold increase in potency compared to *ent*-**15**. A cocrystal structure of oxetane **15** in complex with EZH2 (enhancer of zeste homolog 2) revealed the oxetane substituent to occupy a defined space in the protein cavity with two potential CH–π interactions between polarised oxetane CH groups and two tyrosine side chains (Figure 17e).

Between 2017–2022, 6007 patents were filed that included an oxetane compound with reported biological activity.[j] A considerable portion of this large number is due in part to the now frequent inclusion of oxetane substituents in claims to cover all the relevant IP space. Figure 18 shows selected examples from such patents that cover oxetane structures with varied substitution patterns. In general, the most common use of the oxetane scaffold in drug

[j] Values obtained from a Scifinder search on 26.01.2023. Only patents included that report: biological study, therapeutic use, pharmacological activity, biological study (unclassified), pharmacokinetics, biological use (unclassified) and agricultural use. Published in English between 2017 and 2022.

discovery continues to be as substituent on nitrogen functionality to attenuate basicity and add bulk without a lipophilic increase.

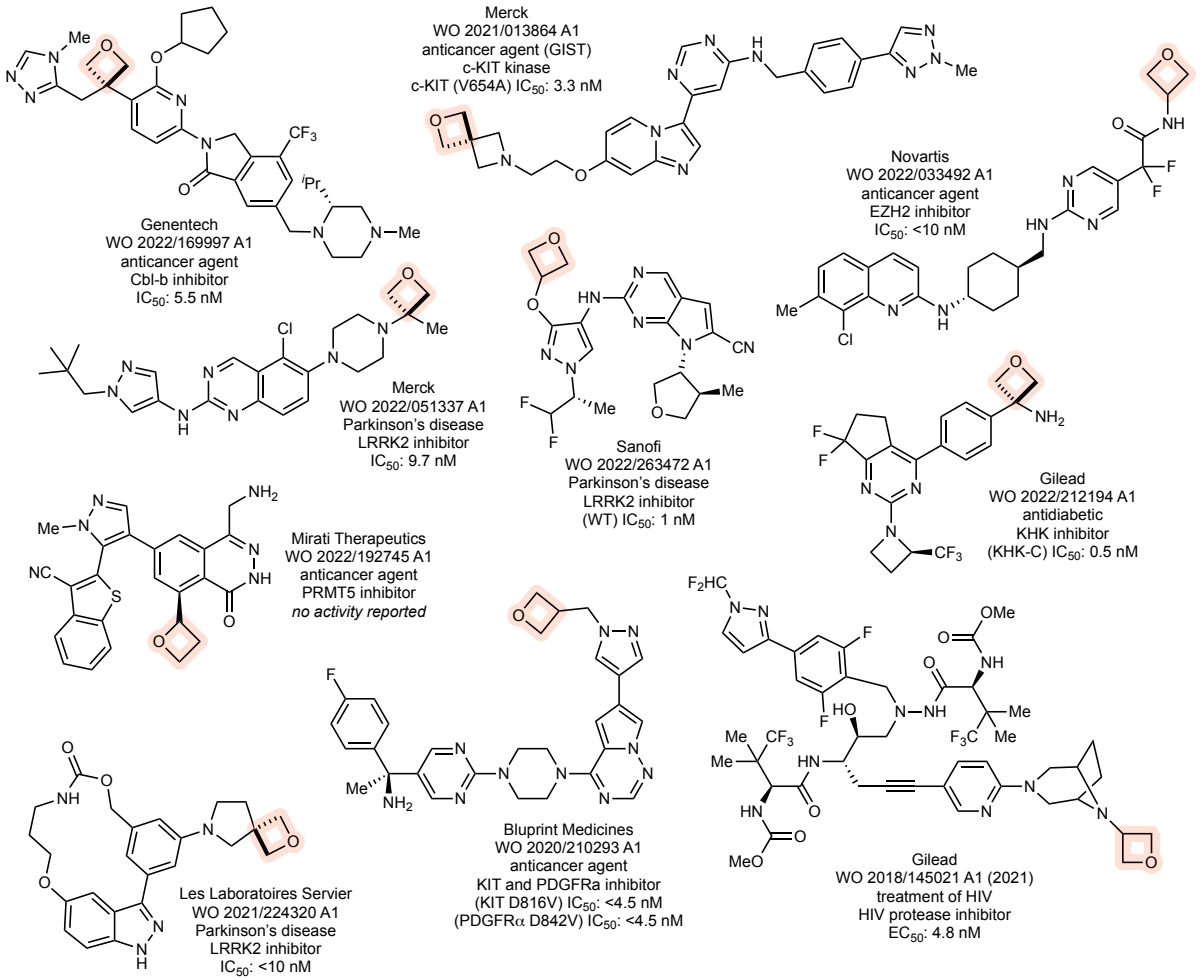


Figure 18. Oxetanes in the patent literature.[7d,132] Selected examples of oxetane-containing compounds in recently filed patents (2017–2022).

In addition to the patent literature, oxetanes have appeared in over 100 peer-reviewed publications on medicinal chemistry campaigns between 2017–2022 (Appendix **9.2**). A Scifinder search was conducted (19th of January 2023) with an oxetane ring as substructure, excluding heteroatomic substitution in the 2-position (*i.e.* also excluding β-lactones). Publications included that report: biological study, therapeutic use, pharmacological activity, biological study (unclassified), pharmacokinetics and biological use (unclassified). Results limited to those published in English, between 2017–2022 and in the following medicinal chemistry journals: *ACS Medicinal Chemistry Letters, Bioorganic and Medicinal Chemistry, Bioorganic and Medicinal Chemistry Letters, ChemMedChem, The European Journal of Medicinal Chemistry, The Journal of Medicinal Chemistry, Medicinal Chemistry Research, MedChemComm* and *RSC Medicinal Chemistry*. The results (449 articles) were then manually triaged to those that included a synthetic oxetane compound (*e.g.*, not taxol-related) in the

optimisation campaign (198 articles) and the effect of oxetane substitution, as well as the source of oxetane were analysed (where this information was available).

38 studies recognised an oxetane compound as the most promising structure, stating that the oxetane motif increased solubility,[133] metabolic stability,[133b,134] permeability,[135] reduced pK_a[136] or Log*D*,[28b,137] or simply provided a better conformational fit into the desired target pocket (Figure 19a).[138] Often, oxetane substitution was beneficial for several parameters simultaneously, as they can be intrinsically linked (*e.g.* Log*D* and metabolic stability or solubility). A popular approach was to adhere an oxetane ring to increase steric bulk in a desired direction to improve affinity without raising Log*D* values to unacceptable levels.

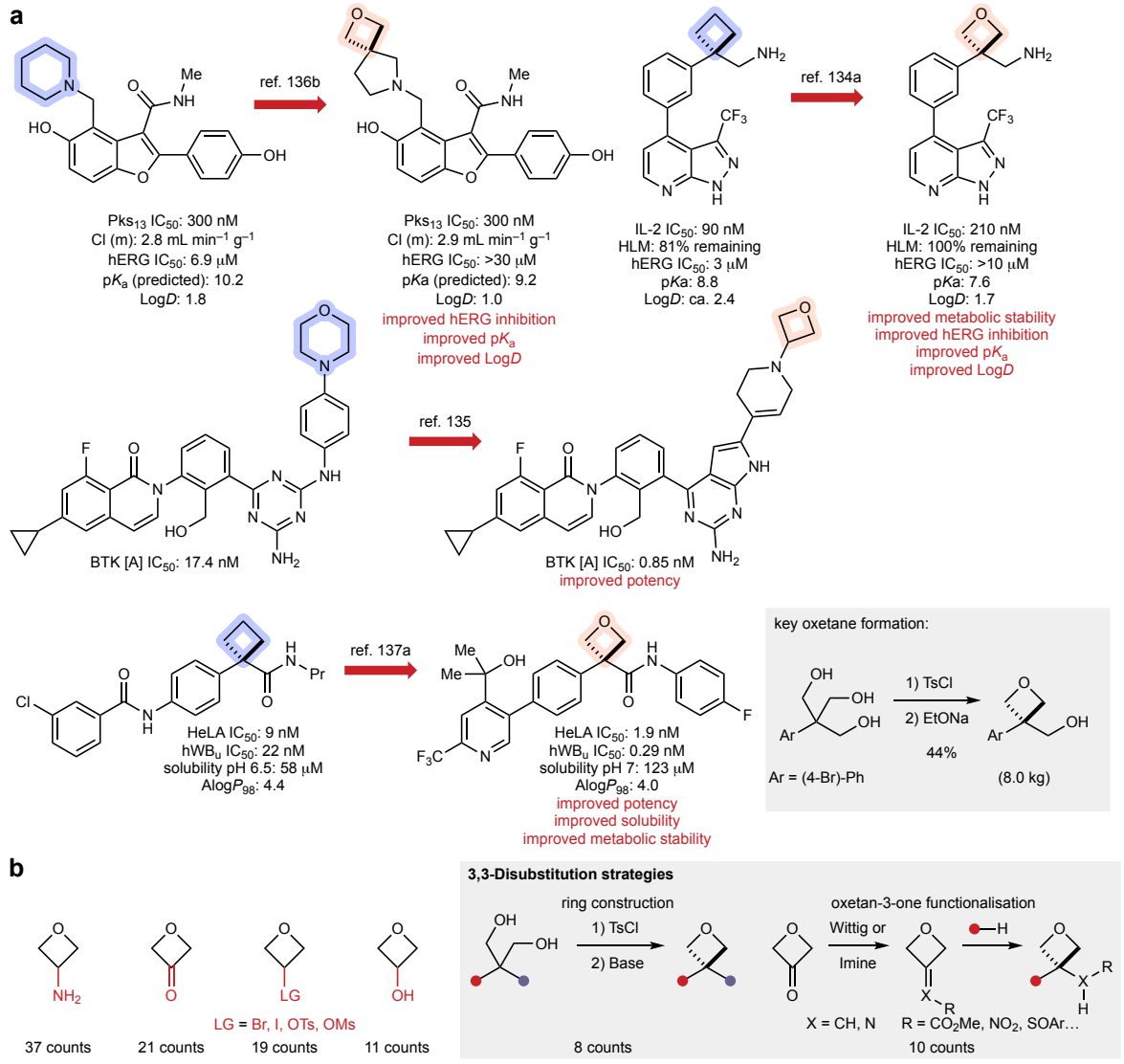


Figure 19. Oxetanes in drug discovery programs (2017–2022). a, Selected examples in scientific articles. **b**, Occurrence of most popular oxetane building blocks used (from references in Appendix **9.2**).

Naturally, the majority of campaigns that evaluated oxetanyl substituents, did not choose an oxetane compound as the lead structure, as was found in 160 studies between 2017–2022

(Appendix **9.2**). In most cases this was due to higher potency of another scaffold and not because of unfavourable physicochemical properties of oxetane substituents. In fact, frequently, oxetane introduction had the desired physicochemical effect (*e.g.* lower pK_a or Log*D*, increased stability, improved solubility) but did not provide sufficient affinity.[139] Only in scattered examples, was the oxetane analogue a chemical liability, and was subsequently eliminated due to insufficient chemical stability, despite high potency and favourable PK properties.[140]

The source of oxetanes in medicinal chemistry campaigns provided another interesting analysis (Figure 19b).[k] By far the most widely used oxetane building block is 3-amino-oxetane (37 counts), which served as substrate in amide couplings, reductive amination- and S_NAr reactions, amongst others. This is followed by oxetan-3-one (21 counts), which was similarly involved in reductive amination reactions and also in organometallic carbonyl additions to yield substituted oxetanols. Further popular building blocks were oxetanes with a leaving group (LG) in the 3-position, involved in nucleophilic substitution reactions, and oxetan-3-ols, often used as nucleophiles.

There were two main strategies to access 3,3-disubstitution patterns: oxetane ring formation by intramolecular etherification (8 counts) and nucleophilic additions into oxetane alkylidenes/imines followed by functional group interconversions (FGIs, 10 counts). The two main drawbacks of these strategies are the use of harsh reagents such as TsCl and strong bases (most often NaH) and the linear nature of the transformations: each analogue requires a distinct synthetic sequence. The commercial availability of 3-mono-substituted oxetane building blocks by far exceeds that of 2-substituted or 3,3-disubstituted examples, which is reflected in their increased appearance in medicinal chemistry programs (Figure 19b). The increased availability has influenced oxetane substitution patterns in APIs, which are majoritarily 3-mono substituted (see Figure 16). 3,3-Disubstituted oxetanes are potentially more attractive (*e.g.* as bioisosteres or more stable derivatives; see Sections **1.2.3** and **1.2.2**, respectively), but suffer from a higher synthetic burden and a lack of useful methods for their incorporation into drug-like molecules. It would hence be valuable to the drug discovery community to develop oxetane reagents that would allow for facile incorporation of 3,3-disubstituted functionality.

Despite the absence of a synthetic oxetane-containing drug on the market (not taking into account naturally occurring Taxol and its derivatives), the increased appearance of oxetanes

[k] Numbers taken from Appendix **9.2**.

in clinical candidates, investigational compounds and scientific reports, leaves no doubt that they may soon be a mainstay of commercial drugs. Research on general oxetane chemistry, synthetic advances, and behaviour in medicinal contexts have been instrumental to increase the community's awareness of this underinvestigated motif. Additionally, the over-reliance on a few well-explored oxetane substitution patterns makes it clear that more research is needed both in the synthesis of diversely substituted oxetanes, and to better understand the structural, physicochemical and biological behaviour of oxetane-containing drug molecules.

1.3 Synthesis of Oxetanes

Conceptually, there are five ways of constructing the oxetane ring: ring-closure through C–O or C–C bond formation, [2+2] cycloaddition, or ring contraction/ring expansion (Figure 20a). The commercial development of useful oxetane precursors such as oxetan-3-one, 3-oxetane carboxylic acid and 3-oxetane halides has prompted numerous synthetic efforts to functionalise the intact oxetane ring (Figure 20b). The unique fundamental properties of oxetane (Section **1.2.2**) coupled with the increased interest from the pharmaceutical sector (Section **1.2.4**) have made oxetanes attractive targets for academic and industrial research campaigns (synthetic and physical organic). Published reviews comprehensively cover the historic developments of oxetane synthesis.[27,29–34] Recent studies have been less fundamental in nature and have rather focused on the synthesis of cyclisation precursors[141] or the application to translationally valuable target structures. This chapter will focus on such recent advances and will highlight selected important contributions.

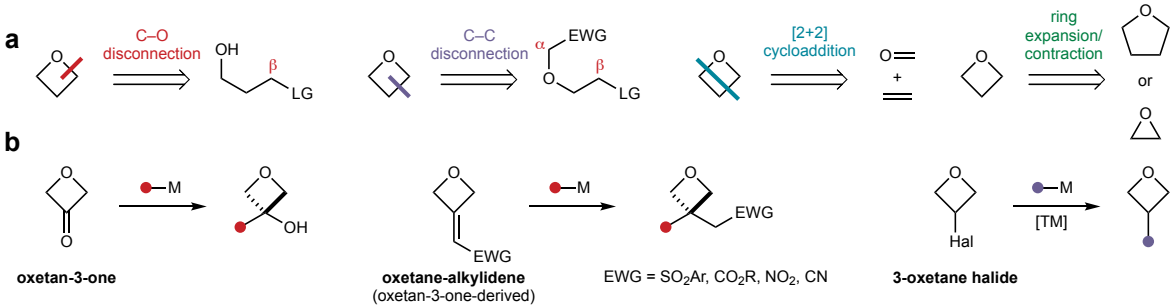
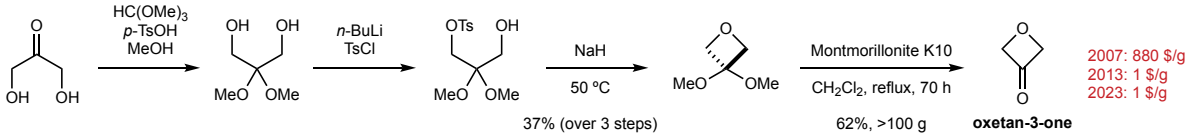


Figure 20. Synthesis of oxetanes. a, The five general tactics for oxetane ring synthesis. **b**, Examples of functionalisation on the intact oxetane ring. M = metal, TM = transition metal.

1.3.1 C–O Bond Formation

C–O bond formation is the oldest[142] and continues to be most popular way of constructing oxetanes. As shown in Figure 20a, the approach involves the intramolecular cyclisation of an alcohol bearing an internal leaving group on the β-carbon atom, most often mediated by a strong base. If the leaving group is a halide, *i.e.* the substrate is a 1,3-halohydrin, the reaction is an example of the Williamson etherification, used *e.g.* in some syntheses of Taxol

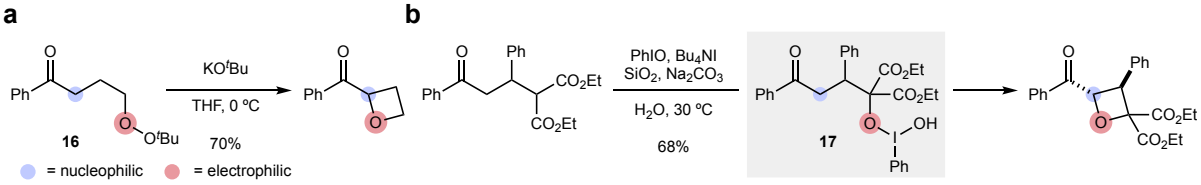
(see **1.2.1**).[42] The C–O disconnection suffers from several drawbacks including low yields due to side products of Grob fragmentation,[l,143] low functional group tolerance owing to the strong base required, and little scope for diversification. The use of 1,3-diol substrates followed by mono-tosylation and intramolecular cyclisation is a useful approach towards oxetanes from convenient starting materials (see for example Figure 19). One synthesis worthy of highlighting is Wuitschik and Carreira's 4-step synthesis of oxetan-3-one in over 100 g scale[144] which provided the foundation for commercialisation and democratisation of oxetan-3-one as an ubiquitous building block, dropping the price from 880 $/g in 2007 to 1 $/g in 2013 and still at 1 $/g in 2023[m] (Scheme 1).[27a]



Scheme 1. Wuitschik and Carreira's large scale synthesis of oxetan-3-one.[144]

Notable advances in oxetane synthesis *via* C–O bond formation included the synthesis of 3,3-disubstituted examples (precursors particularly susceptible to Grob fragmentation),[145] oxetanyl nucleoside analogues,[146] building blocks for medicinal chemistry[147] and oxetane nitroxide radicals as spin labels.[148] Other reports included a gold-catalysed cyclisation of propargylic alcohols,[149] an *in situ* formed organopalladium as leaving group (through C–H activation),[150] and a Heck/oxidative cyclisation cascade.[151]

Recently, polarity-inversed strategies, whereby an alcohol is activated towards intramolecular nucleophilic attack by enolates, have been achieved by using peroxides (**16**; Scheme 2a)[152] or *in situ* generated hypoiodites (**17**; Scheme 2b).[153] Mechanistically, the latter was also suggested to proceed *via* an α-iodo ketone intermediate, followed by C–O cyclisation in the normal-polarity regime.[153b]



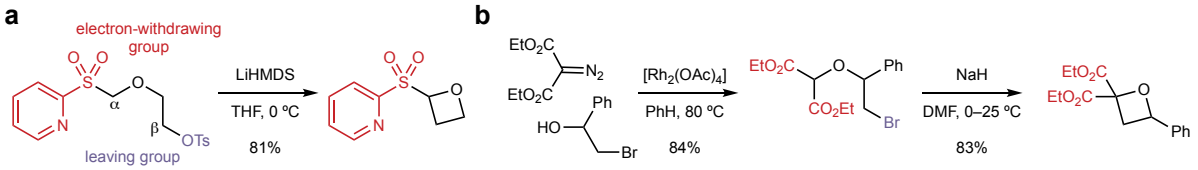
Scheme 2. Polarity-inversed oxetane synthesis by C–O bond formation. a, Peroxide as electrophilic oxygen.[152] **b**, Hypoiodite as electrophilic oxygen.[153a]

[l] An elimination reaction that results in three fragments. In the case of 1,3-bromohydrin, this would be methanal, ethylene and hydrogen bromide.
[m] Price obtained from a Reaxys search on oxetan-3-one, performed on 29.03.2023.

Oxetane formation has also seen applications en route towards complex natural products, either as isolated distinct intermediate, or formed and opened transiently. Examples include the synthesis of (–)-xishacorene B by Sarpong,[154] (–)-bilobalide by Shenvi,[155] Mycolactones A/B by Altmann[156] and Zincophorin by Yadav.[157]

1.3.2 C–C Bond Formation

C–C bond forming strategies are attractive alternatives to C–O bond formation but are much less developed. As shown in Figure 20a, cyclisation precursors require an electron-withdrawing group α, and a leaving group β to the oxygen atom. The Bull group have made significant contributions in this regard, reporting the synthesis 2-sulfonyl oxetanes (Scheme 3a)[158] and later an O–H insertion/cyclisation two-step protocol (Scheme 3b).[159] Using a similar logic to the latter, Moody and coworkers developed a synthesis of substituted β-lactones which were then reduced to the corresponding oxetane.[160] A drawback of C–C bond forming strategies is the imposition of specific substitution patterns on the cyclisation precursors, notably electron-withdrawing groups in the 2-position.



Scheme 3. Representative examples of oxetane synthesis by C–C bond formation. a, Towards 2-sulfonyl oxetanes.[158] **b**, O–H insertion/cyclisation two-step protocol.[159]

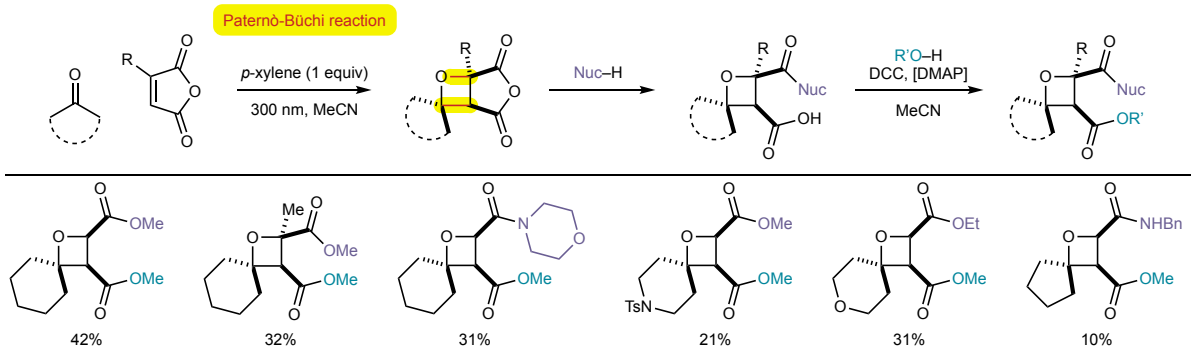
1.3.3 [2+2] Cycloadditions

Hetero-[2+2] cycloadditions between carbonyls and olefins are common strategies to access complex polysubstituted oxetane architectures. Most frequently, these transformations are photo-mediated, in a named process better known as the Paternò-Büchi (PB) reaction (**1.3.3.1**). Recently, contemporary, non-light mediated processes have been developed, whereby the carbonyl/olefin system is activated thermally or by Lewis acids or bases (**1.3.3.2**).

1.3.3.1 Paternò-Büchi Reaction (Photochemical)

PB reactions have been extensively studied since their discovery by Paternò in 1909.[161] Recently, several reviews have been published which focus on regio- and stereoselectivities,[31a] mechanism and synthetic applications[31c,e] and general developments.[31b,d] PB reactions have seen advances in their application to complex substrates,[162,163] synthesis of fluorinated oxetanes,[164] use of photocatalysts to mediate energy transfer under mild conditions,[165] and application to electron-deficient alkene-[166] and enamide

substrates.[167] Translation to a flow set-up significantly reduced irradiation times and improved reaction efficiency and selectivity.[168] The PB reaction has also emerged as powerful tool in biochemical analytics to investigate interactions and properties of lipids and membranes by identifying downstream PB products by mass spectrometry techniques.[169] Despite the vast mechanistic studies already performed on PB reactions, its mechanism has continued to intrigue researchers, with new insights reported that exploit modern spectroscopic techniques.[170] A recent report by Coote and coworkers epitomises synthetic advances of the PB reaction (Scheme 4). A highly functionalised library of spiro-oxetanes was built through a three-step protocol starting from cyclic ketones and maleic anhydrides involving a PB reaction, nucleophilic anhydride opening and esterification.[162b] The use of *p*-xylene supressed dimerisation of the olefin and was key to a successful PB reaction.



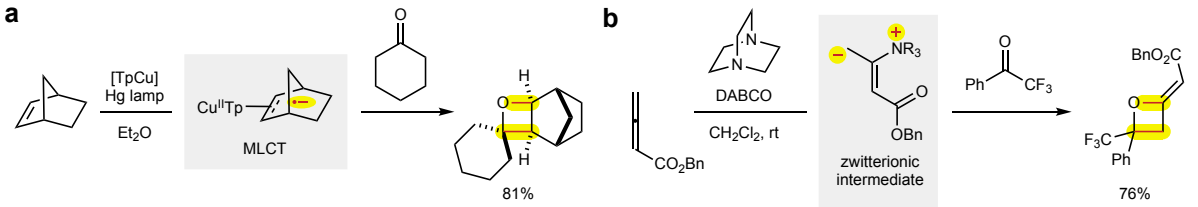
Scheme 4. Representative recent example of a Paternò-Büchi reaction.[162b]

A major drawback of PB reactions is their requirement of precise substitution patterns on olefin and carbonyl. For example, 2-unsubstituted (*e.g.* 3,3-disubstituted) oxetane motifs are inaccessible *via* Paternò-Büchi reactions, as aldehydes such as methanal are not supported.

1.3.3.2 Non-Paternò-Büchi Cycloadditions

The last decade has witnessed a newly awoken interest in 'non-PB' [2+2] hetero-cycloadditions. Here, instead of promoting carbonyls into an electronically excited state using high-energy irradiation (as in 'PB-like' transformations), Lewis acids and -bases are used to activate carbonyl substrates. The Schindler group has reported several studies on Lewis acid-catalysed [2+2] cycloadditions, albeit only seldomly stopping the synthetic sequence at the oxetane. In most cases, the [2+2] is followed by a retro [2+2] in an overall carbon–olefin metathesis process.[171] In 2019 Schmidt developed a Cu-catalysed [2+2] cycloaddition between aliphatic ketones and norbornene (Scheme 5a).[172] Distinct from PB reactions, this system relied on a metal-to-ligand charge transfer (MLCT) mechanism, whereby a norbornene-coordinated Cu^{I} complex was photochemically excited and an electron transferred from copper to norbornene, followed by trapping of the norbornene radical anion by the

carbonyl, leading to oxetane formation. Lewis base-mediated strategies have been developed, whereby formal [2+2] cycloadditions were achieved between allenoates and ketones to yield 2-alkylideneoxetanes (Scheme 5b).[173] Mechanistically, the Lewis base (here DABCO) is thought to add onto the orthogonal π system to generate a zwitterionic intermediate which attacked the ketone, followed by C–O bond forming cyclisation and expulsion of the Lewis base catalyst.



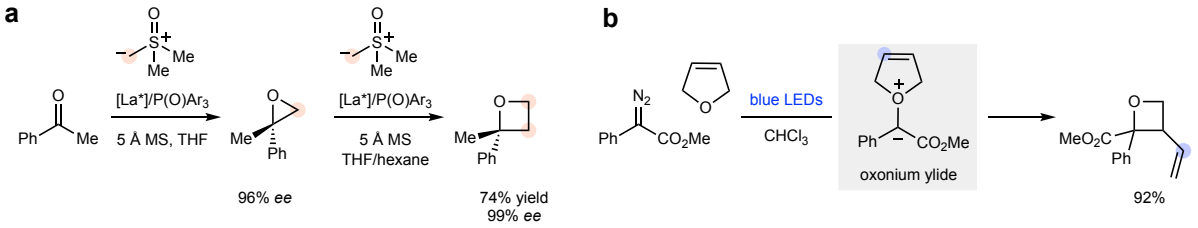
Scheme 5. Non-Paternò-Büchi [2+2] cycloadditions. a, Copper-catalysed reaction of norbornene and ketones *via* a MLCT mechanism.[172] **b**, Lewis base-catalysed formal [2+2] cycloaddition *via* a zwitterionic intermediate.[173a] NR_3 = DABCO.

The young field of Lewis acid/base-catalysed [2+2] hetero-cycloadditions has seen exciting developments in recent years and future endeavours will hopefully expand methodologies to tolerate additional substitution patterns on oxetane, for example 3,3-disubstitution.

1.3.4 Ring Expansion/Ring Contraction

The ring expansion of epoxides is a common strategy for the synthesis of oxetanes, often as part of a double Corey-Chaykovsky reaction process from ketone substrates.[174] Recent advances have mostly focused on enantioretentive[175] and enantioselective processes to access optically pure 2-substituted oxetanes (Scheme 6a).[176]

Less common are ring contraction methodologies. A biosynthetic investigation recently recognised enzyme OxsB to catalyse an unusual ring contraction of deoxyadenosine triphosphate (dATP) to an oxetane aldehyde en route to the natural product oxetanocin A.[177] Further developments included the Wolff rearrangement of diazotetrahydrofuranones under Hg lamp irradiation,[178] and the intermolecular reaction of 2,5-dihydrofurans with diazo compounds to yield poly-substituted oxetanes *via* an oxonium ylide (Scheme 6b).[179]



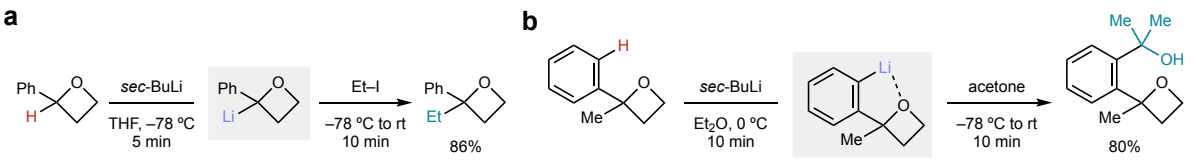
Scheme 6. Ring expansion/contraction strategies. **a**, Sequential enantioselective Corey Chaykovsky reaction.[176] **b**, Ring contraction of 2,5-dihydrofurans with stabilised carbenes.[179] LED = Light-emitting diode.

1.4 Functionalisation of the Intact Ring

The commercial rise of oxetane building blocks brought with it a surge in new methodologies to functionalise them. Most common were developments that involved 3-oxetane halides and derivatives of oxetan-3-one. This section will focus on such recent advances, as well as functionalisation of the activated 2-position α to the oxygen atom.

1.4.1 α-Functionalisation

The position α to oxygen on oxetanes (*i.e.* 2-position) is typically easier to functionalise than the 3-position due to the extra stabilisation of reactive intermediates provided by the oxygen atom (carbanions through inductive stabilisation, carbocations through oxocarbenium intermediates and radicals due to a lower C–H bond dissociation energy). Capriati reported the α-lithiation of 2-phenyl oxetanes with *sec*-BuLi and subsequent trapping with electrophiles such as silyl chlorides, alkyl halides, aldehydes and ketones (Scheme 7a).[180,181] The 2-lithio-2-phenyl-oxetane showed a remarkable lifetime of 30 minutes at –78 ºC. Following this, the Bull group then reported the deprotonation of 2-sulfone-oxetanes and trapping with various electrophiles.[158a] Relatedly, treatment of 2-aryl-2-methyl-oxetanes with organolithium bases led to regioselective *ortho*-lithiation of the aromatic, directed by coordination of the Lewis basic oxetane oxygen atom to lithium (Scheme 7b).[182] Direct trapping with electrophiles or transmetallation to an organoboron intermediate followed by Suzuki cross coupling yielded *ortho*-functionalised products. α-Oxygen radical generation was also achieved and will be discussed in Section **4.2**.

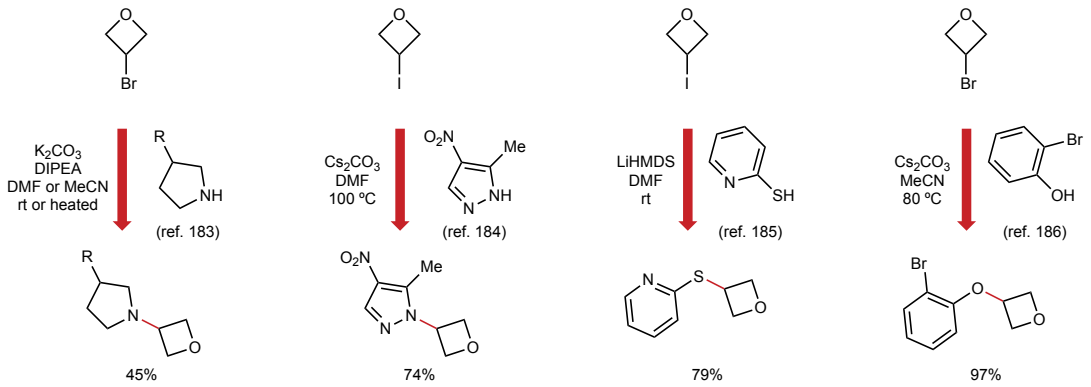


Scheme 7. Lithiation of 2-aryl-oxetanes. **a**, α-Functionalisation.[180a] **b**, Oxetane-directed *ortho*-lithiation.[182a]

1.4.2 Reaction of 3-Halo-oxetanes

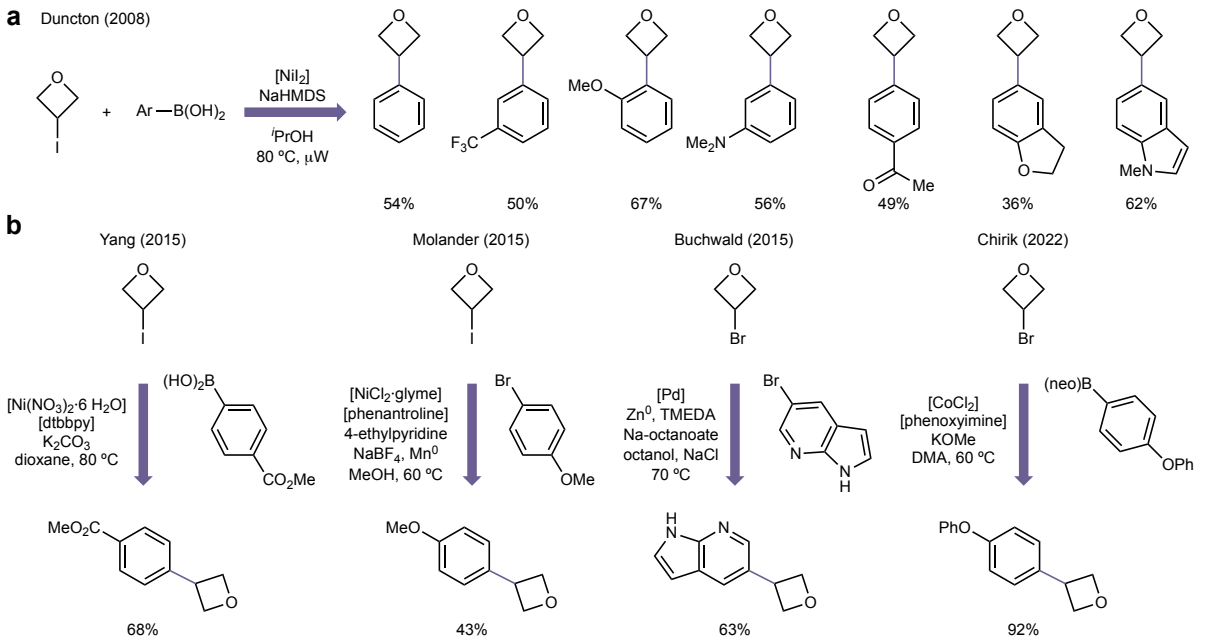
3-Bromo- and 3-iodo-oxetanes have been extensively used as electrophiles in nucleophilic substitutions, as coupling partners in cross coupling reactions, and as radical precursors. Driven by pharmaceutical and fundamental interest, oxetane halides are now routinely showcased in the reaction scope of new methodology as 'medicinally relevant functionality'. Recent examples of polar reactivity are discussed in this section and methods that involve radical processes will be presented in Section **4.2**.

S_N2 reactions of oxetane halides, tosylates or mesylates are frequently chosen to incorporate oxetane scaffolds to drug-like molecules (Figure 19b).[133–140] For example, amines,[183] N-heterocycles,[184] thiols[185] and phenols[186] have been shown to be suitable nucleophiles to react with oxetane halides (Scheme 8). Bernardes demonstrated that 3-bromo-oxetane (as well as 3-($BrCH_2$)-oxetane and 3,3-bis($BrCH_2$)-oxetane) could be reacted chemoselectively with cysteine residues of proteins, without compromising the integrity of the oxetane ring, which has potential applications in protein engineering.[187]



Scheme 8. Nucleophilic substitutions of 3-halo-oxetanes.[183–186]

3-Halo-oxetanes are now also considered standard substrates for transition metal-catalysed cross coupling reactions. The first systematic study on 3-iodo-oxetane was conducted by Duncton (Evotec) in 2008, who developed a nickel-catalysed sp^2–sp^3 Suzuki cross coupling reaction with aryl boronic acids (Scheme 9a).[75] Further occurrences of 3-halo-oxetanes involved in cross couplings processes, albeit only as isolated examples in scope tables, were reported for example by Yang,[188] Molander,[189] Buchwald[190] and Chirik (Scheme 9b).[191]



Scheme 9. Cross couplings of 3-halo-oxetanes. a, Systematic study by Duncton.[75] **b**, Other selected examples using Ni, Pd and Co catalysis.[188–191]

1.4.3 Functionalisation of Oxetan-3-one Derivatives

Oxetan-3-one is the central building block for derivatisation reactions on oxetane. In most chemical settings oxetan-3-one behaves as a 'typical ketone' and is routinely used in the pharmaceutical industry as a substrate for reductive aminations and oxetanol synthesis (see Section **1.2.4** and Figure 19b). There have also been reports on the generation of oxetane enolates for α-functionalisation with electrophiles.[192] Innovative methods have been reported to functionalise oxetan-3-one derivates, such as on oxetane-3-alkylidenes, attainable *via* a Wittig or Henry reaction,[70,92] and on 3-substituted-oxetan-3-ols.

1.4.3.1 Oxetane-3-alkylidenes

Several derivatives of oxetane-3-alkylidenes have been developed and used as Michael acceptors for the synthesis of 3,3-disubstituted derivatives, as highlighted in Figure 19b and Section **1.2.3** for oxetane peptidomimetics (Figure 21).[115] Successful Michael additions have been reported with amines,[92] boronic acids,[92] organocuprates,[92] fluoroenolates,[193] pyrazolones,[194] thiols[111] and thio-acids.[195] Spiro-oxetane structures were also accessed in this manner by employing the appropriate synthetic handles.[97,193] Nucleophilic addition into related oxetane-3-sulfinimines were developed independently by Ellman and Brubaker for the synthesis of amino-oxetanes and will be covered in Section **3.2.1**.

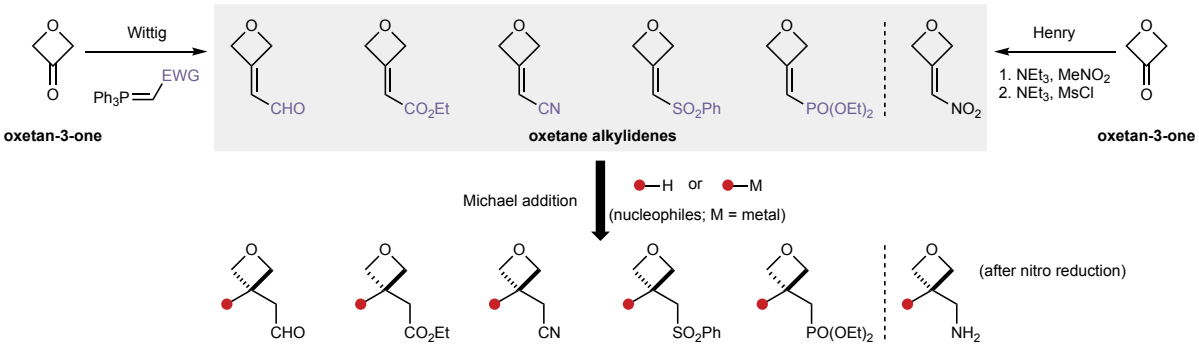
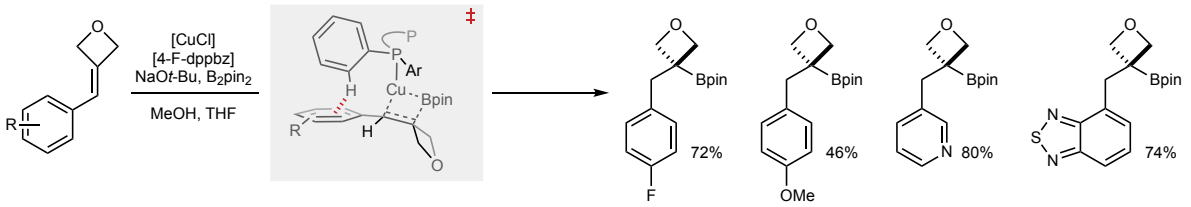


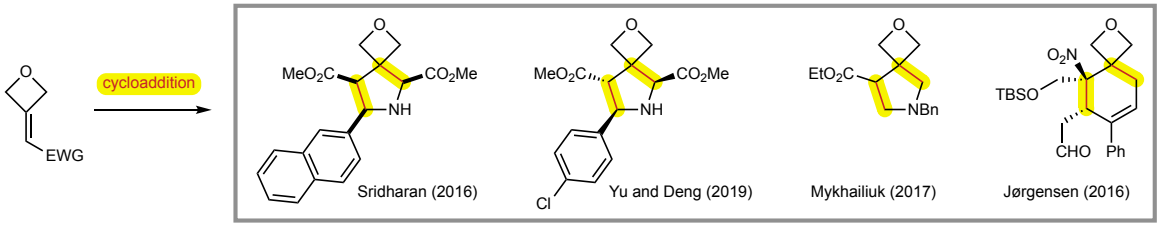
Figure 21. Synthesis and Michael reactivity of oxetane alkylidenes.

In 2020 Engle and coworkers disclosed a copper-catalysed hydroboration of 3-benzylidene four-membered rings, including oxetanes (Scheme 10).[196] Complete regioselectivity of the hydroboration was achieved with a 1,2-bis(diphenylphosphino)benzene (dppbz) ligand which exploited a T-shaped π–π interaction with the substrate in the transition state (TS) of the turnover-limiting migratory insertion step. Diversification of the tertiary boronic ester products was demonstrated on an azetidine substrate and included Zweifel–Aggarwal vinylation, Matteson homologation and Minisci and Giese radical reactions (after prior conversion to the corresponding potassium trifluoroborate salt).



Scheme 10. Markovnikov hydroboration of oxetane-3-alkylidenes.

Oxetane spirocycles were accessed through cycloadditions of oxetane alkylidenes with imines (Sridharan,[197] Yu and Deng[198]), azomethine ylides (Mykhailiuk)[199] and 2,4-dienals (Jørgensen)[200] (Scheme 11). Radical generation on the 3-position of oxetanes has also been achieved from oxetane alkylidenes and will be discussed in Section **4.2**.

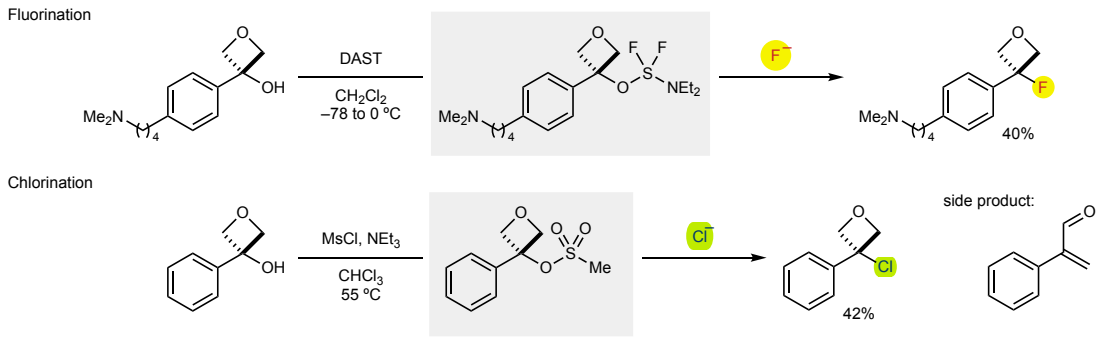


Scheme 11. Cycloaddition reactions of oxetane-3-alkylidenes.[197–200]

1.4.3.2 Displacement of Oxetan-3-ols

3-Substituted-oxetan-3-ols can be conveniently obtained in one step from oxetan-3-one by the addition of an organometallic reagent. The reaction usually proceeds in high yields (>90%) and is scalable (>20 g). The tertiary alcohols, particularly if benzylic, present exciting avenues for selective activation, yet have not been sufficiently exploited. However, harnessing the reactivity of the oxetane alcohols is a formidable challenge due to ring strain, as strongly basic and/or acidic conditions can lead to undesired polymerisation, or hydroxyl elimination to generate unstable oxetenes which rapidly degrade to ring-opened products (*e.g.* Scheme 12).

Isolated examples have been reported for the deoxy-fluorination and -chlorination of oxetan-3-ols (Scheme 12). Diethylaminosulfur trifluoride (DAST)[92] and other F^- sources such as Xtal-fluor or deoxofluor[201] have been used for the fluorination and methanesulfonyl chloride for chlorination.[144] Mechanistically, it was unclear whether the reaction proceeded *via* an oxetane carbocation (S_N1), or through an S_N2 pathway on a hindered quaternary carbon centre, although higher yields with electron-rich aromatics suggested S_N1.[144] Common synthetic sequences have also been demonstrated for the dehydroxylation of oxetanols. Either a three-step deprotonation/tosylation/reduction sequence[92] or a combination of trifluoroacetic acid (TFA) and triethylsilane (only on selected substrates)[144] were successful.

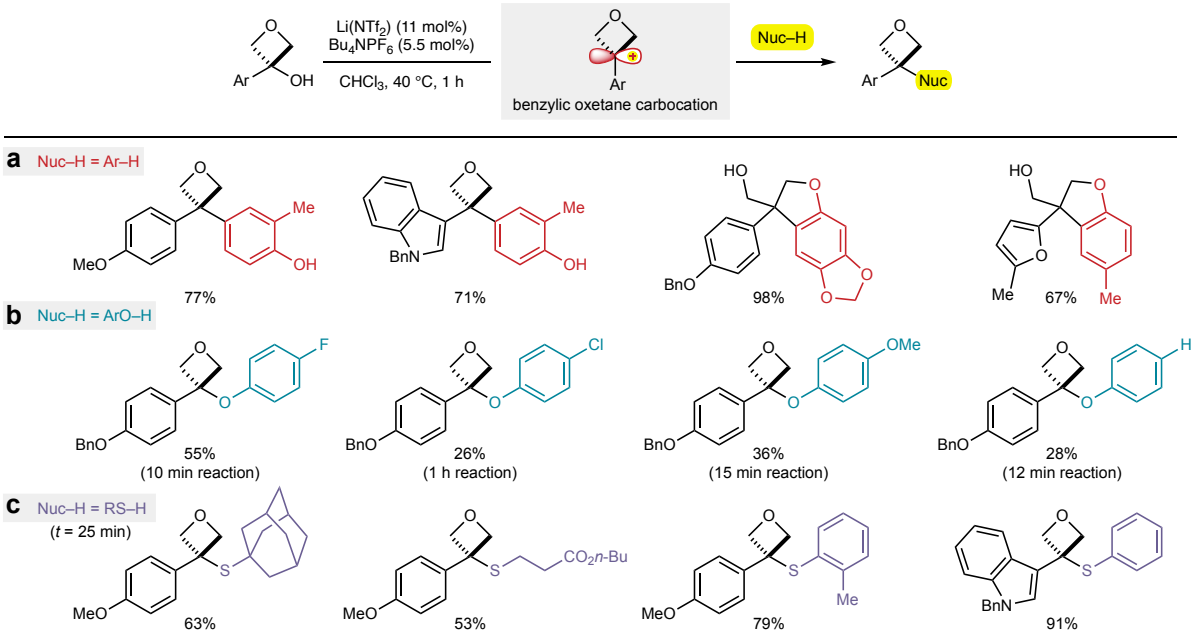


Scheme 12. Halogenations of 3-aryl-oxetan-3-ols.[92,144]

The dehydration of 3-aryl-oxetan-3-ols to generate benzylic oxetane carbocations followed by trapping with nucleophiles has been extensively studied by the Bull group and was shown to be a powerful strategy to access 3,3-disubstituted oxetane motifs.

A successful Friedel–Crafts alkylation with phenols and 3-aryl-oxetan-3-ols was developed in 2016 using Niggemann's Li(NTf_2) catalytic system (Scheme 13a).[202] Tuning the Lewis acidity of the catalyst was key: too weak catalysts were insufficient for the required dehydration and too strongly acidic catalysts led to oxetane ring opening with associated polymerisation processes. The transformation was tolerant to a wide range of electron-rich oxetanols and phenols, including medicinally relevant heteroaromatics such as indole or furan. Divergent

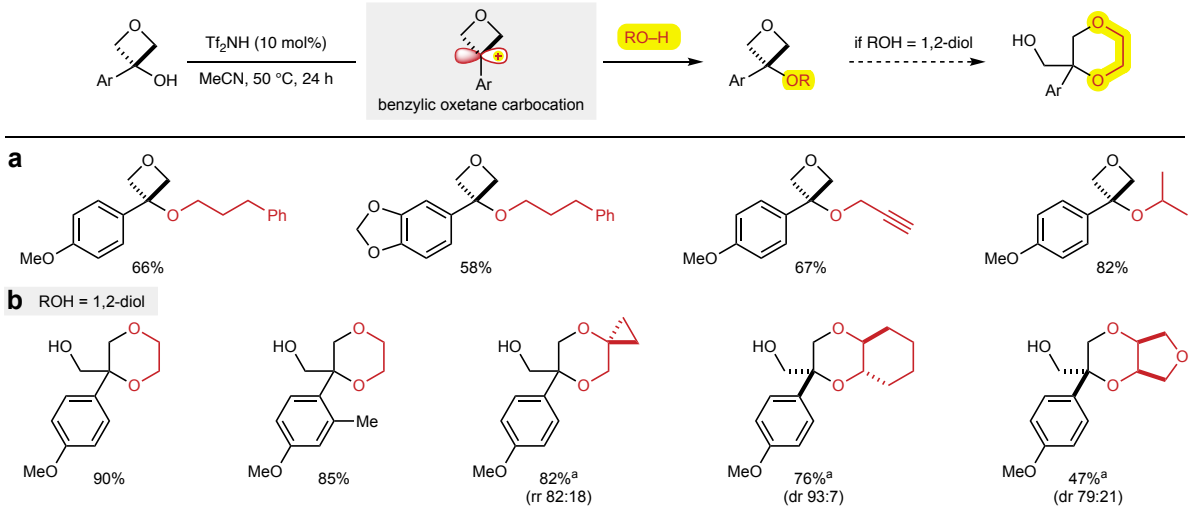
reactivity was observed with *para*-substituted phenol nucleophiles which underwent *ortho* Friedel–Crafts reaction, followed by rapid and *in situ* intramolecular oxetane ring opening promoted by the same Lewis acid catalyst to yield dihydrobenzofurans (Scheme 13a). Although the Friedel–Crafts reaction was limited to electron-rich aryl oxetanols, electron-poor functionality could be appended through cross couplings of phenol-derived triflates. Oxetane ethers were later shown to be formed and consumed as part of the reaction, essentially acting as a 'reservoir' of oxetane carbocations.[203] The oxetane ether products, potential isosteres of metabolically labile esters, were isolated at short reaction times (Scheme 13b). For an isosterism assessment of diaryl-oxetanes vs benzophenones and diaryl-methanes, see Section **1.2.3**, Figure 13a.[103] Oxetane sulfides, proposed isosteres of thioesters (Figure 12c), were accessed under the same Lewis acid-catalytic conditions using thiol nucleophiles and slightly adjusted continuous reaction variables (Scheme 13c).[110] Thiols were significantly more reactive than aromatic nucleophiles and required lower reaction times and equivalents of nucleophile to minimise unwanted oxetane ring opening. This thiol-alkylation represented a crucial step towards oxetane sulfonyl fluorides, key compounds in this thesis, and was further investigated for practical reproducibility and scale up procedures (Section **3.2.5**).



Scheme 13. Lewis acid-catalysed dehydration of 3-aryl-oxetan-3-ols for the generation of benzylic oxetane carbocations. a, Friedel–Crafts reactions.[202] **b**, Etherifications at short reaction times.[203] **c**, Thiol-alkylation.[110]

Notably, aliphatic alcohols were incompatible with Lewis acid systems, presumably due to catalyst coordination and poisoning. Later efforts by myself and others in the Bull group developed Brønsted acid-catalysed conditions for the synthesis of aliphatic oxetane ethers (Scheme 14a)[204,205] and 1,4-dioxanes (Scheme 14b).[72,204] The latter products were obtained

through an unusual annulation reaction between oxetanols as 1,2-bis-electrophiles and 1,2-diols as bis-nucleophiles. Related to the formation of dihydrobenzofurans (Scheme 13a), oxetane ethers were presumed to be intermediates of the reaction, which were internally ring opened *in situ* by the remaining free alcohol to yield 1,4-dioxane products.



Scheme 14. Brønsted acid-catalysed dehydration of 3-aryl-oxetan-3-ols for the generation of benzylic oxetane carbocations. a, Etherification reactions with aliphatic alcohols.[205] **b**, 1,4-Dioxanes by intramolecular oxetane ring opening.[72] [a] Reaction run at 30 °C.

The Lewis acid catalytic systems developed for oxetanes were extended towards the synthesis of 3,3-diaryl-azetidines[206] and 3-aryl-3-azetidine sulfides[207] and a systematic study revealed the best Lewis acid/benzylic alcohol combination for the synthesis of diaryl-methanes with different (hetero)-cyclic linkers.[208] Scientists at Genentech recently reported the generation of benzylic oxetane carbocations *via* an unusual radical-polar crossover mechanistic pathway from the decarboxylation of oxetane carboxylic acids under photoredox conditions.[209]

2 Aims

The goal of this thesis was to develop methodologies to transform an inexpensive oxetane source (oxetan-3-one) into medicinally valuable 3,3-disubstituted oxetane derivatives. The envisaged strategy was the generation of oxetane reactive intermediates (*i.e.* carbocations, radicals and carbanions) from oxetan-3-ols or derivatives followed by trapping with nucleophiles, radical acceptors or electrophiles, respectively (Figure 22). The intermediates would be complimentary and broaden the possibilities of achievable substitution patterns. Such strained reactive intermediates had been little-studied and the influence of ring strain on stability and reactivity was not well understood. The focus of this work was to investigate the effect of the oxetane scaffold and its substituents on the reactivity of carbocations, radicals and carbanions. The acquired fundamental knowledge would then aid the design of synthetic methods tailored to the properties of the oxetane reactive intermediates.

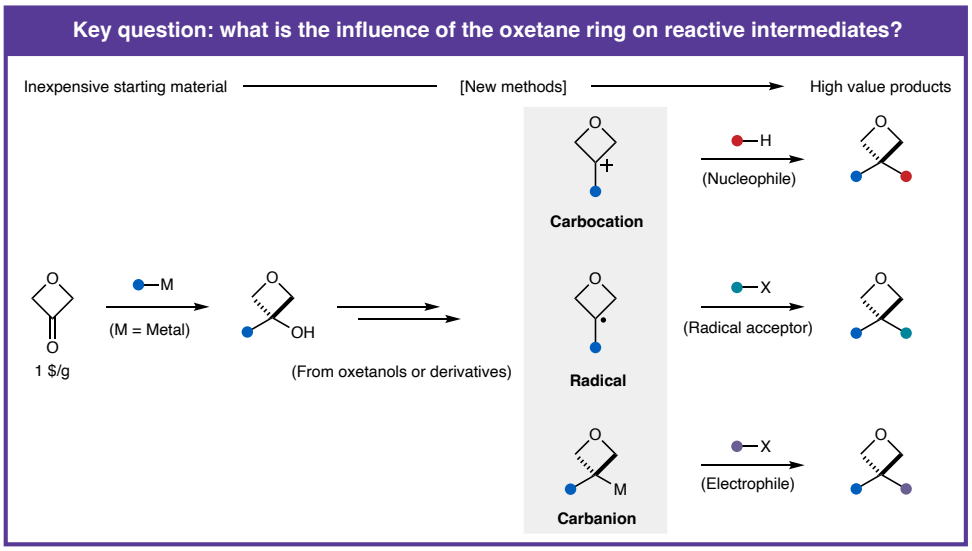


Figure 22. Aim of this thesis: oxetane reactive intermediates for the synthesis of 3,3-disubstituted oxetanes.

One main challenge was recognised and associated with the project: oxetanes are ambiphilic in nature, prone to nucleophilic attack due to their ring strain, but also abnormally Lewis basic on oxygen also due to the small ring size. This combination posed a challenge for the controlled activation of oxetane substrates: usual activators such as strong Lewis- or Brønsted acids would coordinate to the Lewis basic oxetane oxygen and activate the oxetane ring towards undesired ring-opening and cationic polymerisation reactions. Hence, the right balance was required, to provide sufficient activation for the generation of the desired (and expectedly unstable) reactive intermediate, but without degrading the sensitive oxetane ring.

Three primary aims were identified:

1. Investigate and develop the generation of oxetane carbocations from alternative precursors. The main goal of this programme was to establish a suitable chemical system to couple oxetane carbocations to amine nucleophiles, not achievable with previous methodologies. This first aim built on the initial discovery and preliminary investigations within the Bull group which had shown oxetane sulfonyl fluorides to be suitable oxetane carbocation precursors, generated on warming.[210] A focus here was to also understand the fundamentals of the transformation, through kinetic and computational investigations (in collaboration with the Duarte group at the University of Oxford), and show its applicability to drug discovery settings and other chemical systems.
2. Investigate the generation of oxetane radicals. As in point 1, the focus here was to understand the behaviour of little-studied oxetane radicals and of strained radicals in general, again in a collaborative effort with the Duarte group. The starting point was given by prior work within the Bull group, which had demonstrated the feasibility to generate oxetane radicals from carboxylic acids in a decarboxylative photoredox catalysed Giese-type process.[211] The goals were to better understand the mechanism of the process as a whole, expand the radical reactions beyond Giese reactivity, and investigate the generation of oxetane radicals from synthetically more tractable precursors, optimally from oxetan-3-ols or direct derivatives.
3. Study the feasibility of generation of unreported oxetane-3-carbanions. It was of fundamental interest to investigate whether such oxetane carbanions could be formed *at all*. The anionic intermediate would complement cationic systems and allow the incorporation of more electron-poor functionality and different substitution patterns.

The results of this thesis are organised in three chapters according to the primary aims and starting with the investigation of oxetane carbocations from sulfonyl fluoride precursors.

3 Oxetane Carbocations: Synthesis of Amino-oxetanes Using Oxetane Sulfonyl Fluorides

The bulk of the results presented in this section were published in *Nature Chemistry*[212] and *Encyclopaedia of Reagents for Organic Synthesis*.[213] An account of carbocations on four-membered heterocyclic rings was published in *CHIMIA*.[214]

3.1 Sulfonyl Fluorides

Although long known to the dye industry,[215] sulfonyl fluoride motifs have only recently gained popularity amongst the broad chemistry community, coined by Sharpless as click reagents in 2014.[216] Sulfonyl fluorides are best known for their combination of high stability, yet reliable reactivity with nucleophiles under precise activating conditions to yield S(VI) derivatives in a process termed Sulfur–Fluoride Exchange (SuFEx; Figure 23a). Sulfonyl fluorides are considerably more stable than related sulfonyl chlorides (and other halides) thanks to the highly polarised S–F bond, which confers sulfonyl fluorides with increased thermodynamic stability (S–F BDE: 81 ± 2 kcal mol^{-1}; S–Cl BDE: 46 ± 4 kcal mol^{-1}),[217] and in contrast to sulfonyl chlorides, complete inertness towards reductive processes (Figure 23b). Key to sulfonyl fluorides' 'click' behaviour is the activation of fluoride as a leaving group. Fluoride normally being a sluggish leaving group, sulfonyl fluorides are stable towards nucleophilic and hydrolytic conditions. However, specific fluoride activators (most notably protons, R_3Si^+ reagents and more recently Lewis acids[248]), transform the complexed fluoride into a good leaving group, potentially under defined kinetic and spatial constraints, and allow for clean redox-neutral substitution reactions at sulfur(VI).

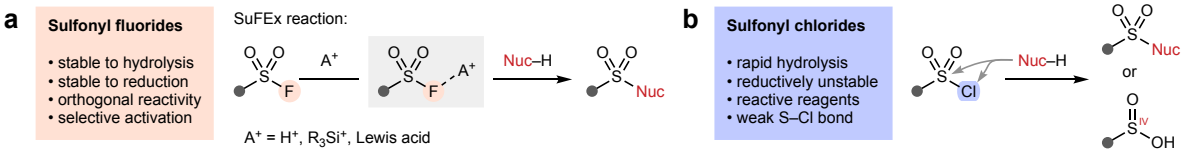


Figure 23. Properties of sulfonyl fluorides (a) vs sulfonyl chlorides (b).

The unique properties of sulfonyl fluorides have allowed their notable application as warheads in chemical biology and covalent inhibitors in drug discovery. Once attached to a selective ligand, the sulfonyl fluoride head can be spatially activated inside the target protein pocket through close-contact H–bonding interactions with protein residues and undergo irreversible SuFEx reaction with nucleophilic side chains such as lysine, serine or tyrosine. Further applications have been seen in materials and polymer science.[218] Many excellent reviews have been published on the general chemistry of sulfonyl fluorides,[216,219] applications to synthesis,[220] medicinal chemistry and chemical biology,[14,221] catalysis[222] and a review on their

early developments.[223] The next section will discuss applications of sulfonyl fluoride reagents reacting through non-SuFEx reaction pathways. For recent advances in the reactivity and applications of sulfonyl fluorides as part of SuFEx processes, see Appendix **9.3**.

3.1.1 Alternative Reactivity of Sulfonyl Fluorides

As highlighted in the last section, the value of the sulfonyl fluoride motif as a clickable SuFEx handle is beyond question. However, little is known about *alternative* non-SuFEx reactivity of sulfonyl fluorides. Examples of alternative reactivity are scarce, but nevertheless show promising potential for the use of sulfonyl fluoride functionality beyond click SuFEx chemistry. An overview of such examples will be presented in this section.

Sulfones and sulfinates have long been recognised as attractive reagents for cross coupling reactions.[224,225] However, the same cannot be said of related sulfonyl fluoride reagents, which have only received significant attention as part of SuFEx processes. A notable exception is the defluorosulfonylative Suzuki–Miyaura coupling (SMC) of aryl sulfonyl fluorides with boronic acids, developed independently by Moran[226] (Figure 24a) and Ding[227] (Figure 24b) in 2021 and 2022, respectively. In both cases, experimental and computational evidence suggested oxidative addition of the sulfonyl fluoride to be turnover limiting[228] and to proceed through the C–S instead of S–F bond. One difference between both reports is noticeable: whilst the base additive was indispensable in Ding's SMC, no base was required in Moran's conditions. This basic disparity is reflected on the transmetallation pathways proposed. Whilst experimental (inhibition by $LiBF_4$, gas evolution) and computational observations suggested F-transfer from sulfur to palladium to occur prior to transmetallation in Moran's work, Ding proposed a base-assisted transmetallation directly on the FO_2S–Pd species. These developments are particularly relevant in the context of the orthogonality of sulfonyl fluorides to cross coupling conditions.[216,219]

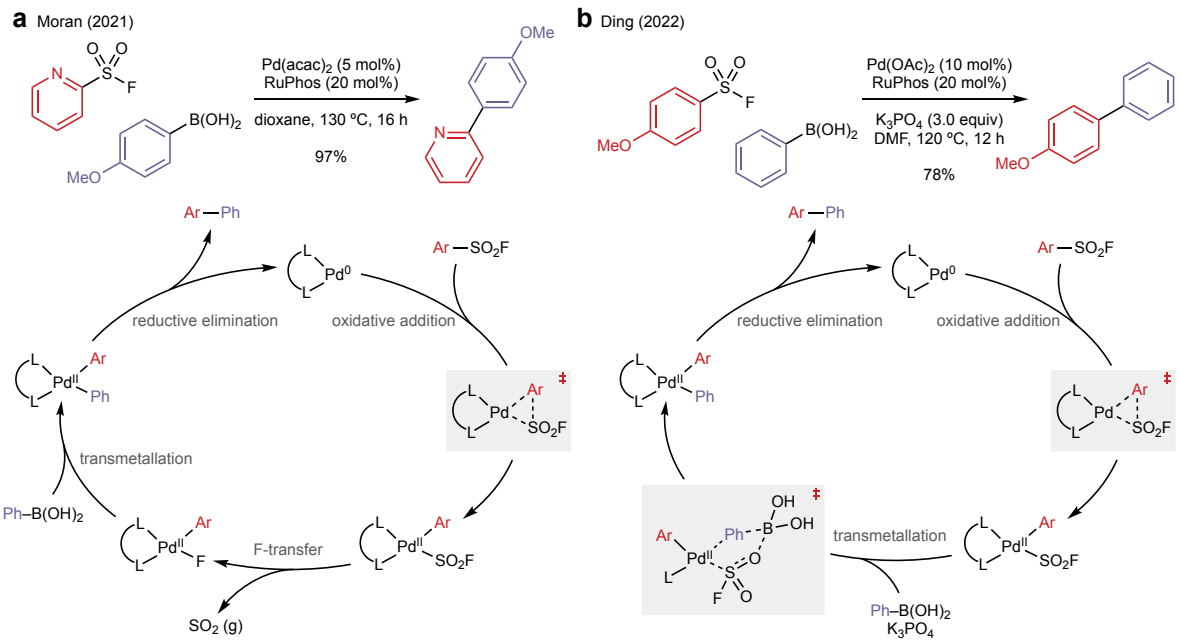
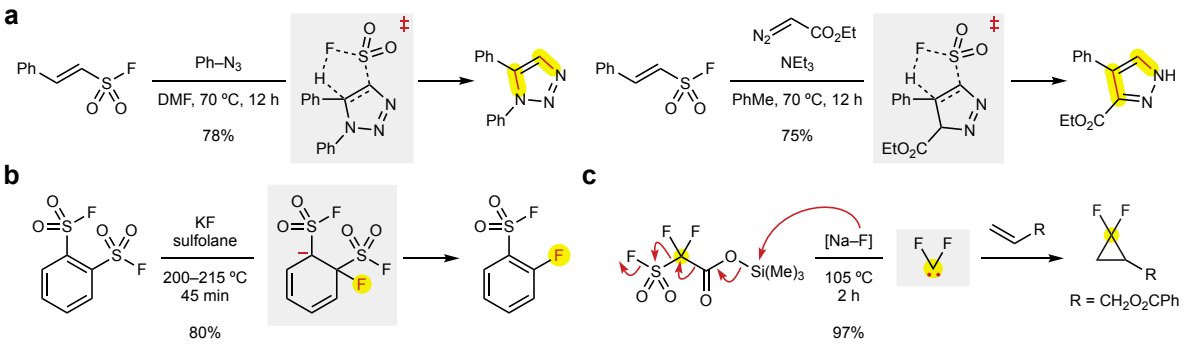


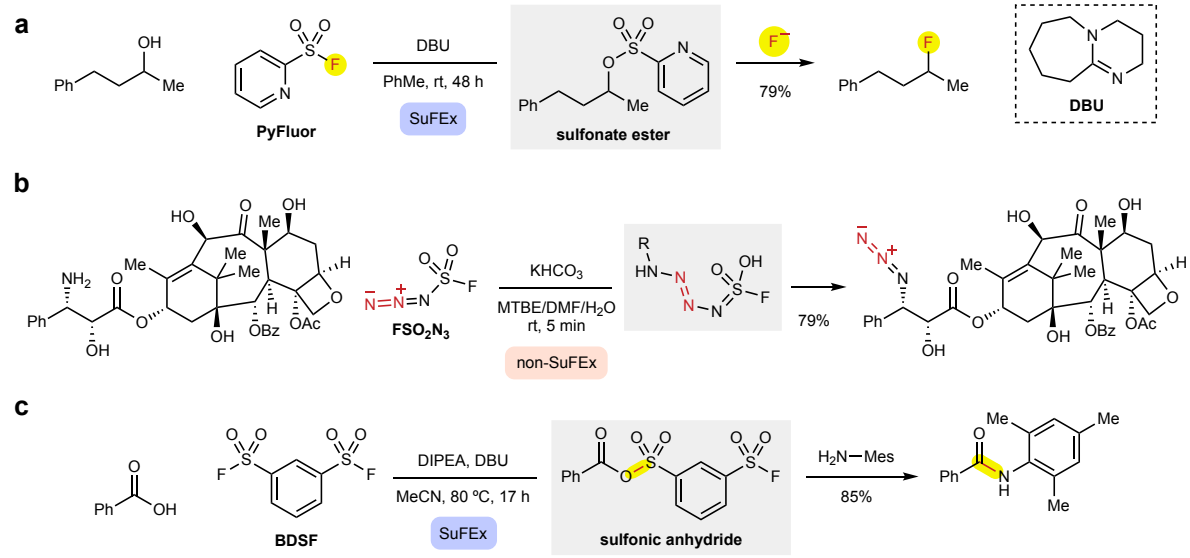
Figure 24. Suzuki–Miyaura coupling of aryl sulfonyl fluorides by Moran (a)[226] and Ding (b).[227]

The electron-poor nature of sulfonyl fluorides has also seen limited applications as leaving group for various processes. For example, ethanesulfonyl fluoride (ESF) derivatives have been employed as dipolarophiles in 1,3-dipolar cycloaddition reactions with diazonium betaines, whereby the sulfonyl fluoride group was eliminated to yield aromatic products (Scheme 15a).[229] The initial triazoline and pyrazoline intermediates were thereby not observed, but rather underwent *in situ* SO_2F elimination to yield triazoles and pyrazoles, proposedly *via* an E_i mechanism. Further elimination examples have been reported which proceeded through an intramolecular SuFEx reaction, followed by *syn* elimination.[230] At significantly elevated temperatures (>200 °C), sulfonyl fluoride substituents have served as stabilising groups for σ Meisenheimer complexes of S_NAr reactions using external fluoride nucleophiles (Scheme 15b).[221c,231] Fluorosulfonyldifluoroacetate derivatives have shown intriguing applications as difluorocarbene precursors (Scheme 15c).[232] Thermal activation triggered decarboxylation, which was followed by defluorosulfonylation to generate the carbene. Despite the robustness of sulfonyl fluorides towards reduction, scattered reductive processes have been disclosed with silyl iodides[233] or boron halides[234] to generate disulfides.



Scheme 15. Sulfonyl fluorides as leaving group. a, In 1,3-dipolar cycloadditions.[229] **b**, In S_NAr reactions.[231] **c**, As difluorocarbene reagent.[232]

There have been further notable non-SuFEx applications of sulfonyl fluoride reagents, albeit not as part of defluorosulfonylation processes. Doyle reported on the deoxyfluorination of alcohols with sulfonyl fluoride reagents, most notably **PyFluor** (Scheme 16a).[235] The alcohol was activated *via* SuFEx to a sulfonate ester leaving group, which was displaced by fluoride. Sharpless and Dong developed fluorosulfuryl azide (**FSO_2N_3**) as a diazotransfer reagent for the azidation of primary amines and as an alternative to the common-use diazotizing reagent triflyl azide ($CF_3SO_2N_3$) (Scheme 16b).[236,237] The diazotransfer was thought to proceed by an unusual pathway whereby the amine nucleophile attacked the terminal nitrogen on azide and released sulfamoyl fluoride as by-product.[238] Lastly, Moses demonstrated the clever use of benzene-1,3-disulfonyl fluoride (**BDSF**) as an amide-coupling reagent (Scheme 16c).[239,240] Fluoride substitution on sulfur by the carboxylic acid generated a sulfonic anhydride, which was transformed *in situ* to a reactive acyl fluoride that ultimately served as the substrate for amide coupling.



Scheme 16. Other alternative applications of sulfonyl fluorides. a, Deoxyfluorination.[235c] **b**, Azidation of amines.[236] **c**, Promoter of amide couplings.[239]

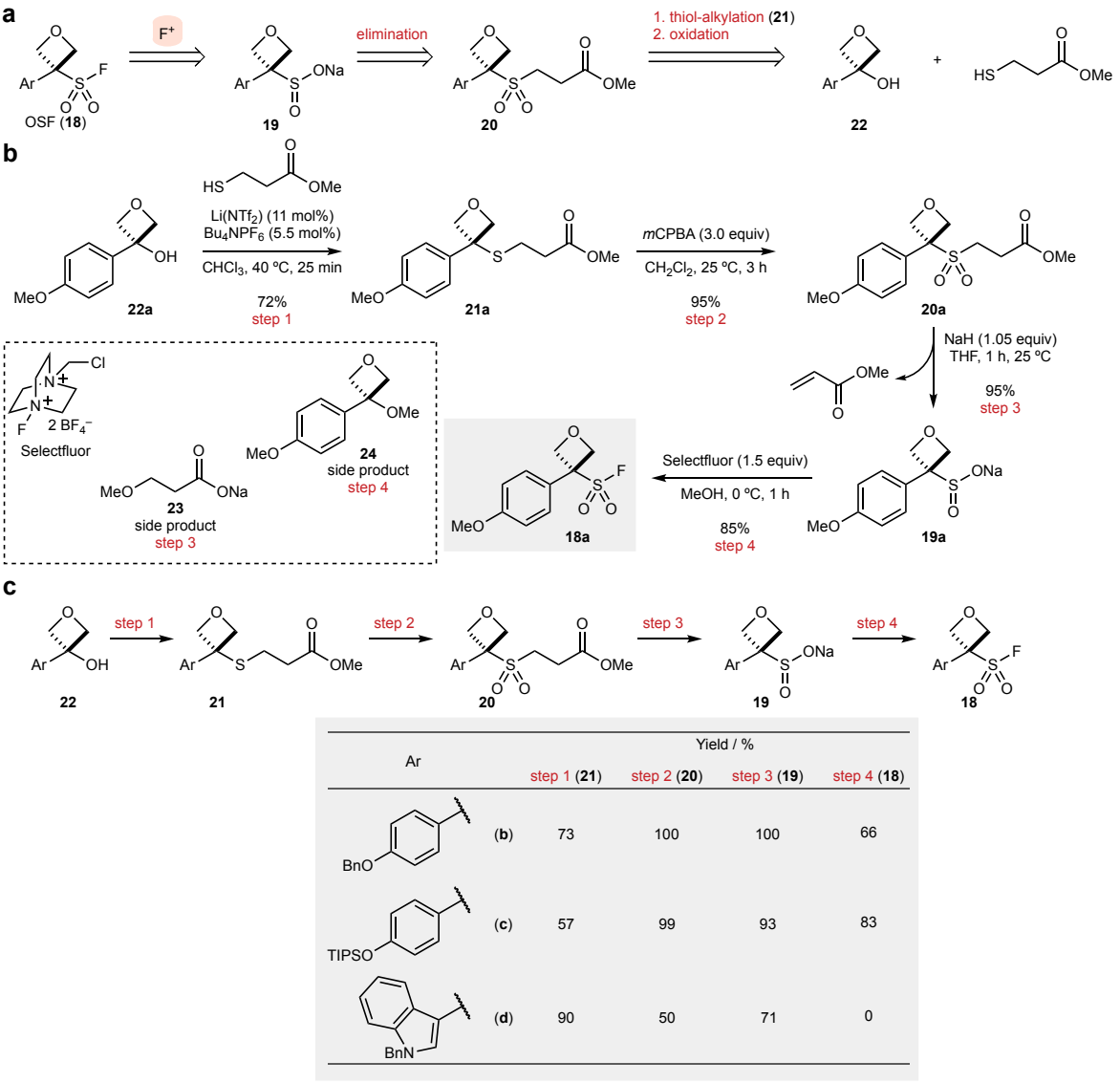
3.2 Oxetane Sulfonyl Fluorides

In 2017, 3-aryl-oxetane sulfonyl fluorides (OSFs) became a synthetic target in the Bull group, interesting as a small reactive oxetane building block with potential applications as chemical probe or useful intermediate. Such a reagent was envisaged to deliver polar sulfur^{VI}-containing oxetane scaffolds upon SuFEx reaction with nucleophiles (*e.g.* sulfonamides with amine nucleophiles). Synthetically, a route was devised from oxetane sulfides, recently having become accessible *via* a developed thiol-alkylation reaction (Scheme 13c).[110] The first OSF was synthesised by R. Croft, who also conducted key early studies on the synthesis and reactivity of OSFs.[210] Such efforts provided the foundation for this thesis and will be highlighted in the next section.

3.2.1 Previous Work within the Group[210]

Whilst attempts to synthesise oxetane sulfonyl chlorides were unsuccessful,[210] oxetane sulfonyl fluorides (OSFs; **18**) were envisaged as a more stable alternative, potentially accessible from a sulfinate intermediate (**19**) through electrophilic fluorination (Scheme 17a).[241] Sulfinate **19** could be obtained from sulfone **20** *via* base-mediated elimination, entropically driven by the release of methyl acrylate.[242] Sulfone **20** is the oxidation product of sulfide **21**, accessible from oxetanol **22** through the developed thiol-alkylation protocol (Scheme 17a).[110]

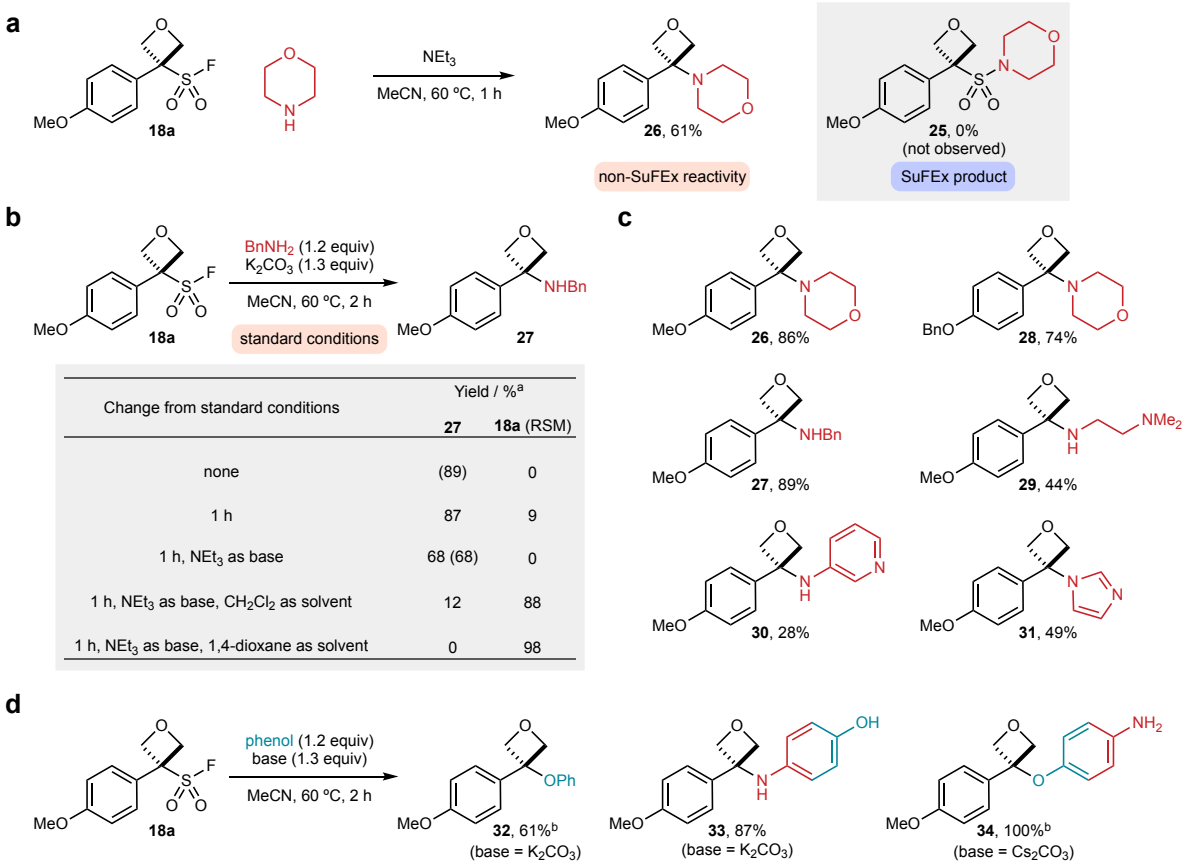
In a forward sense, reaction of oxetanol **22a** with methyl 3-mercaptopropanoate under Li(NTf_2)-catalysed conditions[110] yielded sulfide **21a** in 72%, followed by *m*CPBA oxidation to sulfone **20a** in 95% yield (Scheme 17b). Elimination to sulfinate **19a** required some optimisation to minimise the formation of sodium 3-methoxypropanoate (**23**) as inseparable side product. Sodium hydride in THF proved optimal and sulfinate **19a** was obtained in 95% yield (after simple filtration). Fluorination of sulfinate **19a** with electrophilic fluoride sources such as NFSI (*N*-fluorobenzenesulfonimide) or Selectfluor were successful. Optimal conditions conducted the fluorination at 0 ºC to avoid defluorosulfonylative etherification to oxetane ether **24**. Significant efforts were spent in the purification protocol to avoid degradation of OSF **18a** on silica. Celite filtration followed by a short silica plug proved optimal and yielded **18a** in 85% isolated yield. Two further OSFs (**18b**, **18c**) were synthesised with this sequence in similar yield (Scheme 17c). Fluorination of indole sulfinate **19d** led to degradation, presumably due to reaction of the electron-rich indole with Selectfluor.



Scheme 17. Previous work towards oxetane sulfonyl fluorides. a, Retrosynthetic strategy towards OSFs *via* oxetane sulfinate **19**. **b**, Synthesis of OSF **18a**. **c**, Synthesis of two further OSFs (**18b**, **18c**) and failed fluorination of indole oxetane **19d**.

As outlined above, OSF **18a** was envisaged as a precursor to novel oxetane sulfonamides upon reaction with amine nucleophiles. However, instead of undergoing the expected SuFEx click reaction to sulfonamide **25**, OSF **18a** *defluorosulfonylated*, *i.e.* lost SO_2 and F^-, and coupled to morpholine to yield amino-oxetane **26** (Scheme 18a). Such reactivity of sulfonyl fluorides with nucleophiles was unprecedented, represented an unusual non-SuFEx pathway and provided a direct oxetane–amine coupling. The initial 61% yield of amino-oxetane **26** was improved to 86% by changing the base from triethylamine to potassium carbonate, serving as fluoride scavenger by formation of insoluble KF (optimised with benzylamine to yield amino-oxetane **27**; Scheme 18b) and minimising the formation of an oxetane fluoride side product (**35**, see Scheme 19a). The stark solvent dependency of the defluorosulfonylation (deFS) was notable, proceeding rapidly in polar solvents like acetonitrile, but not at all in less polar media

such as dichloromethane or 1,4-dioxane. An initial scope of the reaction was investigated, showing reactivity with primary, secondary and heterocyclic amines, as well as with imidazole (**26**–**31**; Scheme 18c). The product of reaction with phenol was initially ascribed to oxetane ether **32** (*cf*. Section **3.2.8**) and interestingly, with 4-aminophenol, *N*-functionalisation was achieved under the standard conditions (**33**; base = K_2CO_3), but a complete switch in selectivity was observed towards *O*-functionalisation (**34**; see Section **3.2.8** for a structural revision) with Cs_2CO_3 as base (Scheme 18d).[210]

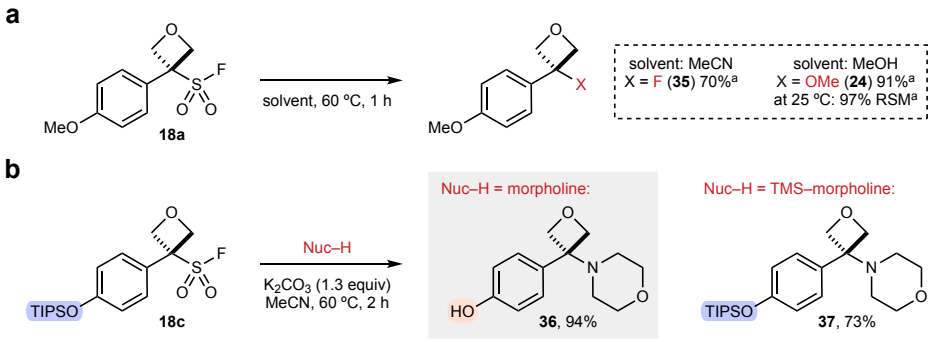


Change from standard conditions	Yield / %[a]	
	27	**18a** (RSM)
none	(89)	0
1 h	87	9
1 h, NEt_3 as base	68 (68)	0
1 h, NEt_3 as base, CH_2Cl_2 as solvent	12	88
1 h, NEt_3 as base, 1,4-dioxane as solvent	0	98

Scheme 18. Defluorosulfonylation of OSFs. a, Initial non-SuFEx reaction of OSF **18a** with morpholine. **b**, Selected optimisation of the deFS reaction. **c**, Preliminary scope of the deFS reaction under the standard conditions (**b**). **d**, Reactivity of OSF **18a** with phenol nucleophiles. [a] Yields calculated by analysis of the ^{1}H NMR spectrum of the crude mixture of the reaction using 1,3,5-trimethoxybenzene as internal standard. Isolated yields in parenthesis. [b] For revised structure, see Section **3.2.8**.

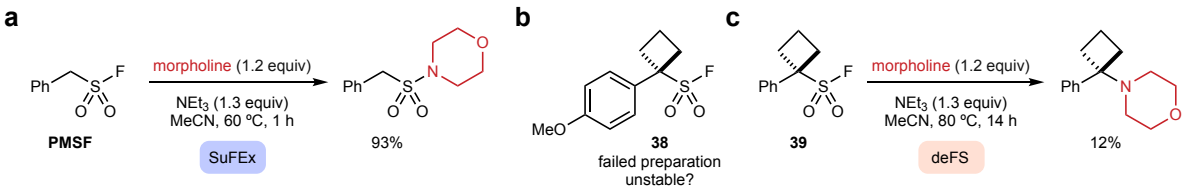
Heating OSF **18a** in MeCN in the absence of nucleophile and base yielded oxetane fluoride **35** in 70% yield by ^{1}H NMR, providing evidence for the release of fluoride ions throughout the reaction (Scheme 19a). Heating in MeOH had a similar effect, now obtaining solvolysis product oxetane ether **24** in 91% yield by ^{1}H NMR. On the other hand, OSF **18a** was stable in MeOH at 25 °C for 1 h (3% conversion to ether **24**). OTIPS OSF **18c** showed intriguing reactivity virtue of the silyl group (Scheme 19b). Under the standard conditions, deprotected aminophenol **36** was obtained in 94% yield, benefitting from *in situ* TIPS deprotection by the

released fluoride ions and irreversible fluoride trapping by the formation of a strong Si–F covalent bond. TIPS deprotection could also be entirely suppressed by using TMS–morpholine as nucleophile (**37**, 73%). The smaller trimethylsilyl group reacted faster with the released fluoride ions and prevented TIPS deprotection.



Scheme 19. On the reactivity of OSFs. a, Behaviour in MeCN and MeOH at different temperatures. **b**, Reactivity of OSF **18c**. [a] Yields calculated by analysis of the ^{1}H NMR spectrum of the crude mixture of the reaction using 1,3,5-trimethoxybenzene as internal standard.

The reactivity of oxetane sulfonyl fluorides was shown to stand in stark contrast to non-oxetanyl analogues. For example, related phenylmethane sulfonyl fluoride (**PMSF**), a serine protease inhibitor,[243] showed exclusive SuFEx reactivity with both morpholine and benzylamine (Scheme 20a; reaction with morpholine shown).[210] On the other hand, the cyclobutane analogue (**38**) of OSF **18a** could not be synthesised due to an unsuccessful fluorination step, presumably due to its decreased stability (Scheme 20b; also see Section **3.2.12.2**). Phenyl-cyclobutane sulfonyl fluoride **39** showed deFS reactivity, albeit more sluggishly and in low yields (Scheme 20c).

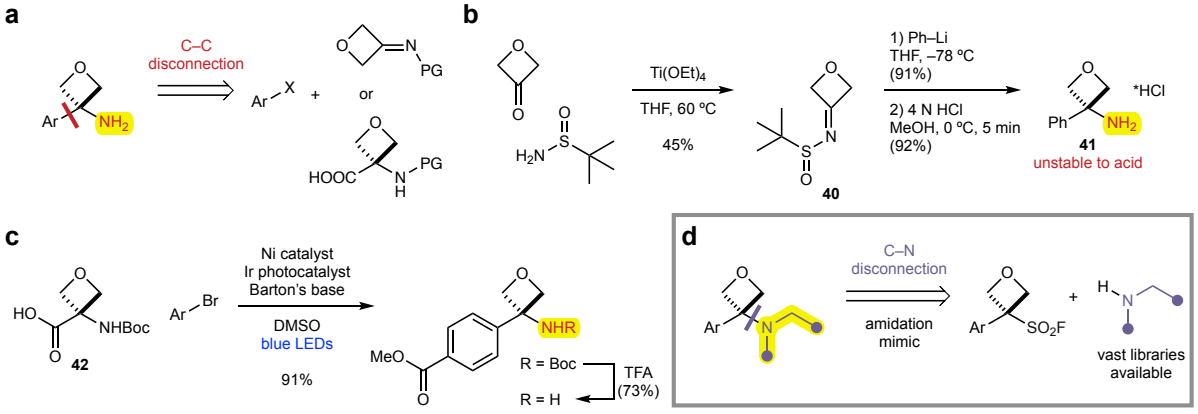


Scheme 20. Reactivity of other sulfonyl fluorides. a, SuFEx reactivity of **PMSF**. **b**, Failed synthesis of cyclobutane sulfonyl fluoride **38**. **c**, deFS reaction of phenyl-cyclobutane sulfonyl fluoride **39**.

The aryl amino-oxetane products shown in Scheme 18c are potential isosteres of benzamides. Benzamides are important pharmacophores, present in over 100 approved drugs,[244] but often suffer from poor pharmacokinetic properties such as low aqueous solubility owing to their planarity imposed by π-conjugation. Aryl amino-oxetanes present exciting opportunities as 3-dimensional isosteres of benzamides, with further potential for higher *in vivo* stability than benzamides due to inertness to enzymatic degradation by amidases. However, the dearth of

methods to access aryl amino-oxetanes (*vide infra*) has hampered their synthesis, inclusion into medicinal chemistry programmes and evaluation as isosteres of benzamides.

Previous literature methods towards 3-aryl-3-amino-oxetanes, which functionalised an amino-oxetane fragment with an aryl partner (C–C bond disconnection), could only access primary amino-oxetane products and were not able to directly use the large commercial libraries available for archetypical amide couplings (Scheme 21a). Access to functionalised target amino-oxetane structures required additional cumbersome functionalisation on nitrogen. The first reported synthesis of 3-aryl-3-amino-oxetanes by functionalisation of the intact ring was disclosed by Brubaker (Merck) in 2010 (Scheme 21b).[245] Addition of aryl lithium reagents into oxetane sulfinimine **40**, synthesised from oxetan-3-one, yielded aryl-oxetane sulfinamides (not shown). Acidic sulfinamide deprotection at 0 ºC gave access to primary amino-oxetane **41**, noting that oxetane **41** was unstable to HCl in MeOH at prolonged times at room temperature, leading to a ring-opened γ-chlorohydrin. A related effort was communicated by Ellman using arylboroxines.[246] Recently, Terrett and Huestis reported the photoredox-catalysed decarboxylation of Boc-protected amino-oxetane **42** with subsequent Ni-catalysed cross coupling to aryl halides (Scheme 21c).[247] Synthesising aryl amino-oxetanes by coupling an aryl-oxetane fragment with functionalised amines (C–N bond disconnection), as shown by the initial investigations by Croft, offers an advantage since it mimics the amidation reaction and allows the direct use of existing amine libraries (Scheme 21d).



Scheme 21. Strategies toward aryl amino-oxetanes. a, Previous approaches *via* a C–C bond disconnection. **b**, Aryl lithium addition into oxetane sulfinimines (Brubaker).[245] **c**, Metallophotoredox coupling of oxetane amino acids (Terrett and Huestis).[247] **d**, Alternative approach: C–N disconnecting logic to mimic amide couplings.

The previous results highlighted in this section represented the foundation of this thesis, which expanded and further developed this early work, as discussed in the next sections.

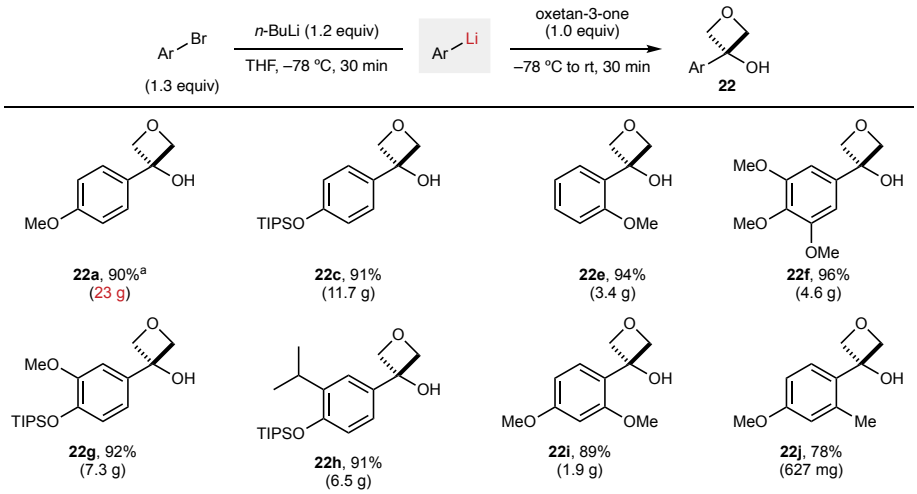
3.2.2 Aims

Seven aims were established at the outset of the investigation presented in this chapter:

1. Examine approaches to amino-oxetanes from simpler oxetane precursors.
2. Optimise and scale a robust and reproducible synthesis of oxetane sulfonyl fluoride reagents.
3. Optimise and investigate the robustness of the defluorosulfonylation reaction to changes in the reaction conditions.
4. Expand the scope of the defluorosulfonylation reaction, with an emphasis on functional group tolerance, chemoselectivities and applications to a drug discovery setting.
5. Investigate the general reactivity of oxetane sulfonyl fluorides to diverse nucleophiles.
6. Examine the structural and physicochemical properties of the amino-oxetane compounds and make comparisons to related benzamide structures.
7. Investigate the mechanism of the unprecedented defluorosulfonylation reaction pathway by means of kinetic and computational studies.

3.2.3 Preparation of Oxetan-3-ol Starting Materials

3-Aryl-oxetan-3-ols **22**, derived from commercial oxetan-3-one, were the starting point for all investigations described in this thesis. In a typical reaction, *n*-butyl lithium was added to the requisite aryl bromide at –78 ºC to effect lithium-halogen exchange and generate an aryl lithium organometallic *in situ*. Neat oxetan-3-one was then added dropwise to the aryl lithium at –78 ºC. Nucleophilic addition of aryl lithium into the ketone yielded the 3-aryl-oxetan-3-ol **22** (Scheme 22). The reactions generally proceeded cleanly, in high yields, were scalable (max scale performed: 143 mmol) and purification was uncomplicated. Typically, the oxetanol product only needed to be separated from unreacted aryl bromide (used in slight excess), and proto-dehalogenated aryl bromide (formed on quenching of unreacted aryl lithium with H_2O, also used in slight excess). Most aryl-oxetanols **22** were bench-stable crystalline solids, ideal starting materials for method development. Eight examples were synthesised and results summarised in Scheme 22.

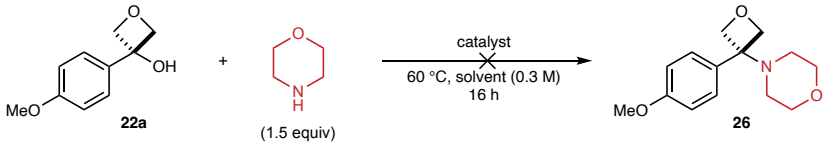


Scheme 22. Synthesis of aryl-oxetanol starting materials 22. All masses correspond to a single run. [a] Reaction run with 1.2 equiv aryl bromide, 1.1 equiv *n*-BuLi and lithium–halogen exchange and nucleophilic addition run for 1 h each.

3.2.4 Amination of Oxetanols

First, oxetanol structures were re-evaluated as simpler precursors than OSFs towards amino-oxetanes. The investigation commenced with *p*-methoxyphenyl (PMP) oxetanol **22a**, using morpholine as nucleophile, under previously developed acid-catalysed conditions known to generate oxetane and/or azetidine carbocations in the presence of phenols,[202,203,206,208] thiols[110,207] and alcohols (Table 2).[72,205] Unfortunately, all reactions returned starting material **22a**, notably also with $Bi(OTf)_3$, which had previously led to polymerisation reactions of oxetanols.[202] Most likely, the highly nucleophilic amine coordinated and poisoned both the Lewis- and Brønsted acid catalysts, shutting down reactivity.

Table 2. Unsuccessful direct amination of oxetanol **22a** under catalytic acidic conditions.

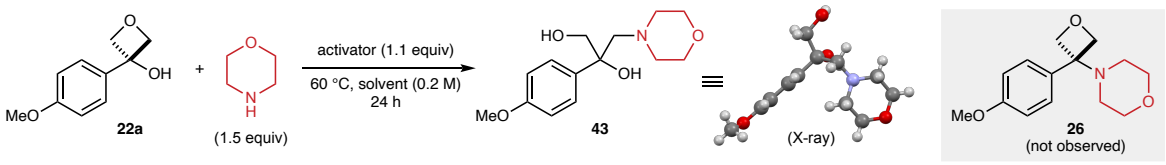


	Yield **22a** (RSM) / %[a]				
	$Li(NTf_2)$ (11 mol%) NBu_4PF_6 (5.5 mol%)	$Ca(NTf_2)_2$ (5 mol%) NBu_4PF_6 (5 mol%)	$FeCl_3$ (7.5 mol%)	TfOH (10 mol%)	$Bi(OTf)_3$ (10 mol%)
MeCN	87	100	90	98	100
PhMe	91	100	79	98	96
$CHCl_3$	97	100	88	96	95

[a] Reactions run on a 0.2 mmol scale and yields calculated by analysis of the ^1H NMR spectrum of the crude mixture of the reaction using 1,3,5-trimethoxybenzene as internal standard. RSM = recovered starting material.

With stoichiometric amounts of Lewis acids and different activators in alternative solvents, akin to the work of am Ende and Ball,[248] again starting material **22a** was recovered, but in some cases, diol **43** (characterised by X-ray crystallography), the product of oxetane ring-opening, was obtained in high yields (Table 3, entry 1). In contrast to previous works, the oxetane ring was activated selectively over the alcohol under these conditions and may provide a useful approach into the chemical space of amino-alcohols such as **43**.

Table 3. Unsuccessful direct amination of oxetanol **22a** under stoichiometric Lewis acidic conditions.



Entry	Activator	Solvent	Yield / %[a]		
			22a (RSM)	**43**	**26**
1	$Ca(NTf_2)_2$	THF	12	85 (79)	0
2	$Ca(NTf_2)_2$	*t*-amyl alcohol	40	52	0
3	$Ca(NTf_2)_2$	MeCN	63	24	0
4	$Ca(NTf_2)_2$ + Bu_4NPF_6 (1.1 equiv)	THF	68	0	0
5	$Ca(NTf_2)_2$ + Bu_4NPF_6 (1.1 equiv)	*t*-amyl alcohol	88	0	0
6	$Ca(NTf_2)_2$ + Bu_4NPF_6 (1.1 equiv)	MeCN	69	0	0
7	$Ca(NTf_2)_2$ + DABCO (1.5 equiv)	THF	26	60	0
8	$Ca(NTf_2)_2$ + DABCO (1.5 equiv)	*t*-amyl alcohol	60	34	0
9	$Ca(NTf_2)_2$ + DABCO (1.5 equiv)	MeCN	73	16	0
10	$FeCl_3$	THF	60	0	0
11	$FeCl_3$	*t*-amyl alcohol	84	0	0
12	$FeCl_3$	MeCN	83	0	0

[a] Reactions run on a 0.1 mmol scale and yields calculated by analysis of the ^{1}H NMR spectrum of the crude mixture of the reaction using 1,3,5-trimethoxybenzene as internal standard. Isolated yields in parenthesis.

Since none of the conditions to aminate oxetanols directly yielded the target amino-oxetane, oxetane sulfonyl fluoride reagents were further studied.

3.2.5 Synthesis of Oxetane Sulfonyl Fluorides

At the outset of the project, two hurdles were to be tackled: irreproducibility of the thiol-alkylation and sulfone elimination steps (steps 1 and 3 in Scheme 17). The initially reported 40 ºC, 25 min thiol-alkylation could not always be reproduced,[110,210] and it was discovered empirically that the reaction required an induction period before the reported 25 min reaction time. Keeping the 25 min reaction time was paramount to minimise overalkylation and ring opening of oxetane by the excess thiol. Initiation of the reaction was indicated by a change in colour (most often from clear to colourful), which could be triggered by physical disruption of the reaction (Figure 25). For example, slow increase of reaction temperature (5 ºC/10 min), briefly opening the reaction vessel to air or stopping the stirring, triggered the colour change.[212] Further, the thiol-alkylation was found to proceed better on large scales in a round bottom flask than on small scales in sealed reaction tubes. Presumably, the quality of the hygroscopic Lewis acid catalyst, $Li(NTf_2)$, in particular its hydration state, significantly impacted its activity

and/or solubilising properties. These reaction irregularities warrant further investigation of the catalytic process to homogenise reaction conditions across all substrates.

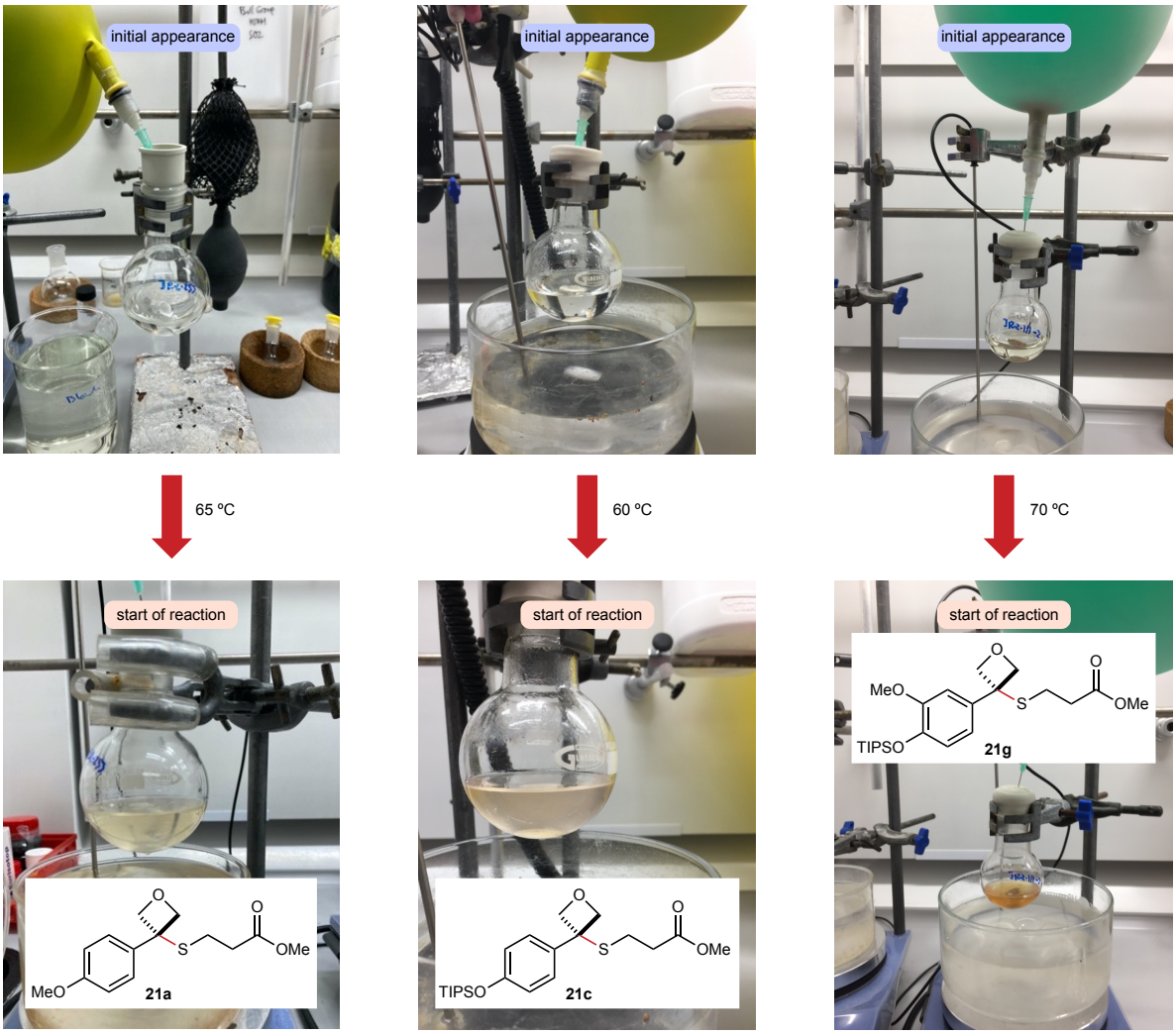


Figure 25. Representative examples of colour change in the thiol-alkylation reaction.

The next troublesome step was the sulfone elimination (step 3, Scheme 17). The initial conditions developed by R. Croft using NaH in THF were irreproducible by several group members (E. Briggs, D. Antermite, L. Blagojevic) for the elimination of OTIPS oxetane sulfone **20c** (Figure 26a). Hence, second-generation conditions using a milder base, NaOH in MeOH, were developed by E. Briggs, which were also irreproducible (Figure 26a). Ultimately, OTIPS oxetane sulfinate **19c** was found to be unstable in DMSO solution, as needed for solubility (Figure 26c). The higher lipophilicity of sulfinate **19c** (*e.g.* vs **19a**) may have increased its solubility in organic solvents and promoted solution-state degradation. Finally, third-generation telescoped conditions were developed based on literature precedent[249] using a commercially available NaOMe solution (5.4 M in MeOH) in THF (Figure 26b). After the elimination step, the solvent was removed *in vacuo* and crude sulfinate **19c** submitted directly to the fluorination conditions. This telescoped protocol was standardised and used for all further examples.

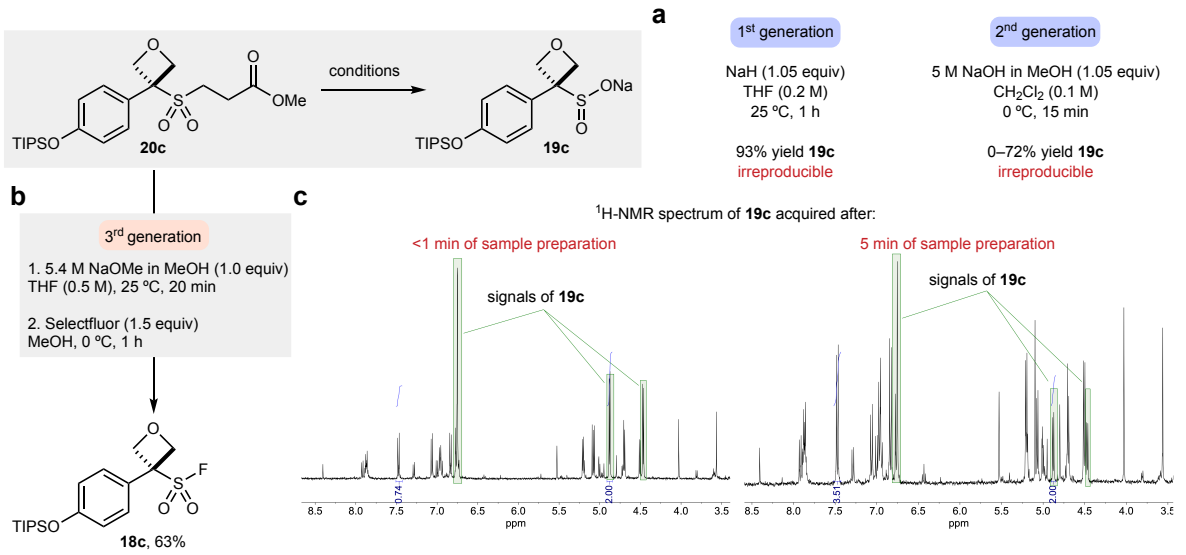
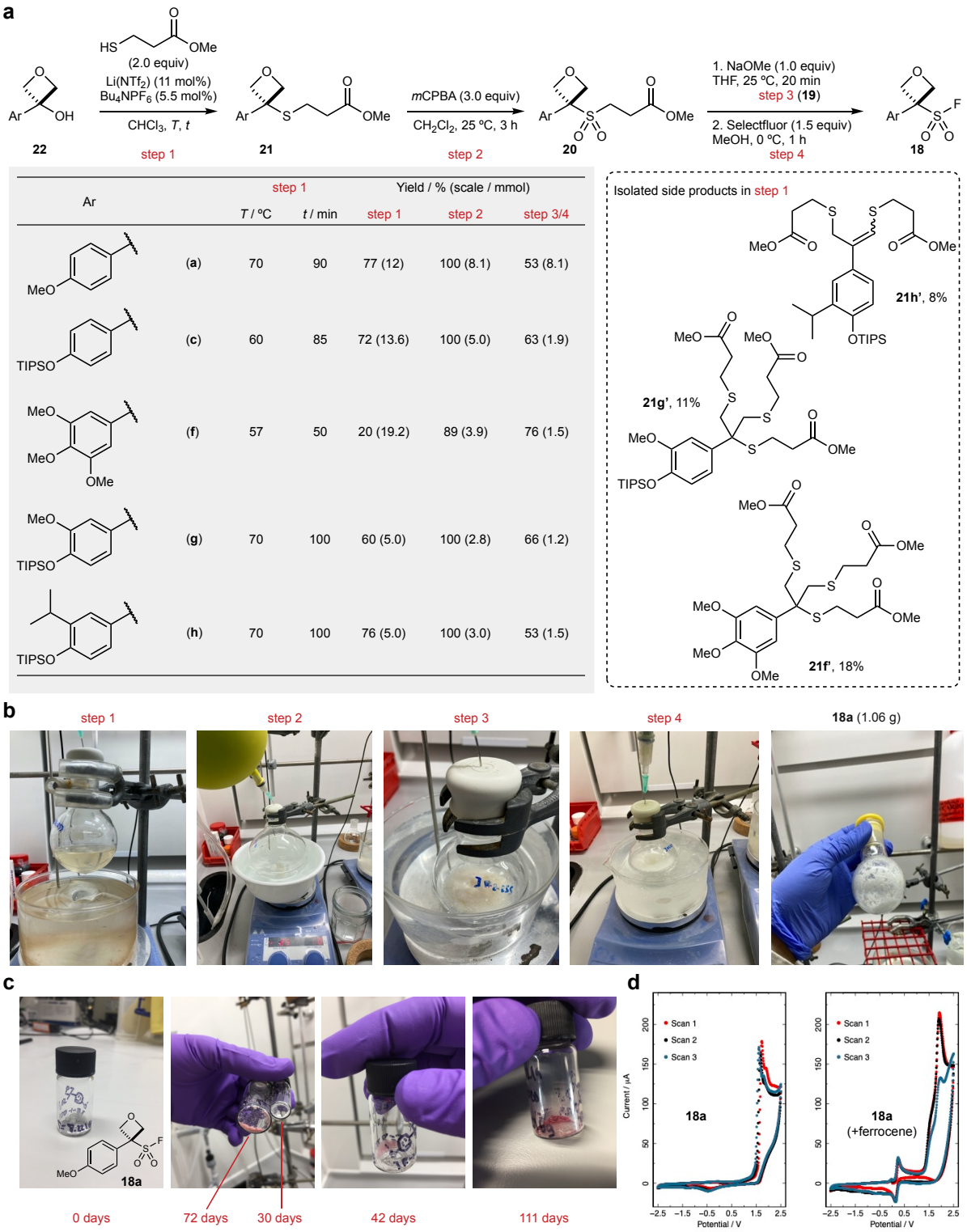


Figure 26. Optimisation of sulfone elimination. a, 1st and 2nd generation conditions previously developed by other members of the Bull group. **b**, Third-generation two-step protocol. **c**, Degradation of sulfinate **19c** in DMSO-d_6.

With a reproducible and convenient synthetic sequence towards OSFs in hand, five examples were synthesised with varying aryl substitution patterns (Figure 27a). All steps worked similarly well across the substrates with the exception of the thiol-alkylation of trimethoxy oxetanol **22f** (step 1). This compound showed increased amounts of over-alkylation products such as **21f'** (Figure 27a) and incomplete consumption of oxetanol **22f**. The 3,4,5-trimethoxy-phenyl group was shown to stabilise oxetane carbocations poorly compared to other methoxy aromatics (see Sections **3.2.12.1** and **3.2.12.2**). The ratio of the rate of formation of sulfide **21f** over the rate of ring-opening (of **21f**) was therefore likely to be less favourable in the less carbocation-stabilising trimethoxy compound compared to the other examples in Figure 27a. *para*-Methoxyphenyl OSF **18a** was synthesised on a gram-scale in two days from oxetanol **22a** (Figure 27b). The synthetic sequence was scalable, required one column chromatography (step 1) and all reaction times were short (longest: 3 h). Oxetane sulfonyl fluorides were bench-stable (room temperature {ca. 22 °C}, under air), but stability was substrate dependent. For example, on the bench, OSF **18a** turned from a white to a pink solid (Figure 27c). The ^{1}H and ^{19}F NMR spectra of **18a** freshly synthesised (white) or after 111 days on the bench (pink) were identical.[n] On the other hand, OTIPS OSF **18c** degraded entirely after 30 days on the bench. All oxetane sulfonyl fluorides have been indefinitely[o] stable in the freezer (–20 °C). OSF **18a** was shown to be stable to electrochemical reduction and oxidation between

[n] At Pfizer, the purity of **18a** after six months on the bench was determined to be 85%.
[o] Maximum time span assessed: 3 years.

–2.5 and +2.0 V vs SCE (Figure 27d). An oxidation at +2.11 V vs SCE was ascribed to oxidation of the electron-rich *para*-methoxyphenyl ring.

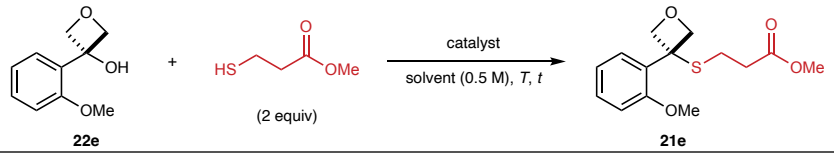


Ar		step 1 T / °C	step 1 t / min	Yield / % (scale / mmol) step 1	step 2	step 3/4
MeO	(**a**)	70	90	77 (12)	100 (8.1)	53 (8.1)
TIPSO	(**c**)	60	85	72 (13.6)	100 (5.0)	63 (1.9)
MeO, MeO, OMe	(**f**)	57	50	20 (19.2)	89 (3.9)	76 (1.5)
MeO, TIPSO	(**g**)	70	100	60 (5.0)	100 (2.8)	66 (1.2)
TIPSO	(**h**)	70	100	76 (5.0)	100 (3.0)	53 (1.5)

Figure 27. Oxetane sulfonyl fluorides. a, Synthesis. **b**, Gram-scale synthesis of **18a** (in pictures). **c**, Stability of **18a**. **d**, Cyclic voltammogram of **18a** (measured with a 100 mV s^{-1} scan rate, in a 0.1 M solution of NBu_4ClO_4 in MeCN and in a 2 mM analyte concentration). The oxidation potential of **18a**, reported as the anodic peak potential (E_{pa}),[250] was calculated using ferrocene as internal standard and converted to vs SCE using tabulated conversion values.[251,252] See Section **7.4** for further details.

Thiol-alkylation with *o*-methoxyphenyl-oxetanol (**22e**) was investigated (Table 4). This substrate has the added challenge of higher steric hindrance close to the reactive benzylic carbon centre, increasing the energy of corresponding transition states. As expected, under previously developed oxetanol dehydration conditions (see Section **1.4.3.2**)[72,110,202–208] oxetane sulfide **21e** was obtained in <15% yield (entries 1–4). Further optimisation on the $Ca(NTf_2)_2$ catalytic system (time and temperature), which had shown the most favourable mass balance, had no benefit on yield (entries 5–9). The highest yield of **21e** (20%) was observed with high catalytic loadings (20 mol%) of inexpensive $FeCl_3$ at 60 ºC (entry 10).

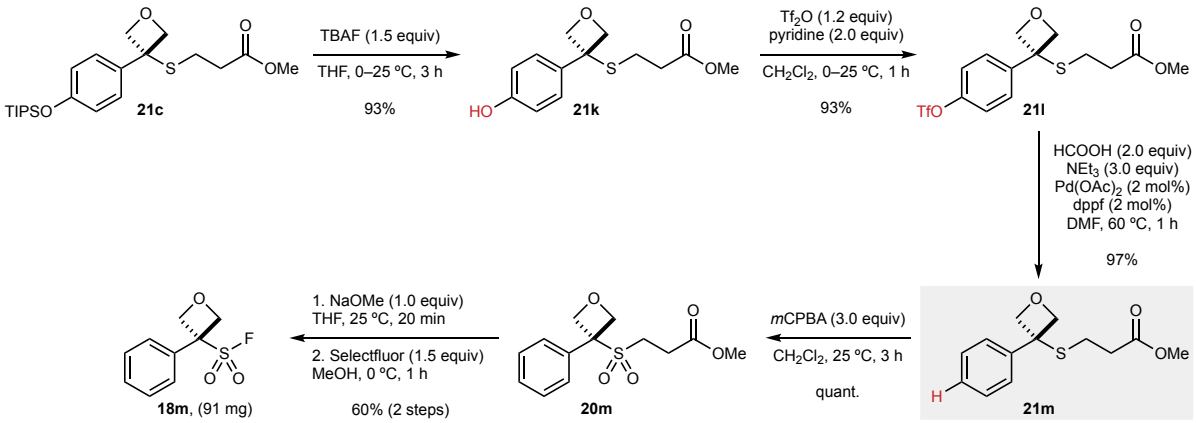
Table 4. Towards the thiol-alkylation of *ortho*-methoxy oxetanol **22e**.



Entry	Catalyst (loading / mol%)	Solvent	*T* / º C	*t* / h	Yield / %[a]	
					21e	**22e** (RSM)
1[b,c]	$Li(NTf_2)$ (11)	$CHCl_3$	40–100	5	13 (4)	33
2[d]	$Ca(NTf_2)_2$ (5)	$CHCl_3$	40	1	8	67
3	$FeCl_3$ (7.5)	$CHCl_3$	40	1	13	35
4	$HNTf_2$ (7.5)	MeCN	50	1	15	46
5[d]	$Ca(NTf_2)_2$	$CHCl_3$	40	3	10	61
6[d]	$Ca(NTf_2)_2$	$CHCl_3$	40	18	9	65
7[d]	$Ca(NTf_2)_2$	$CHCl_3$	60	1	16	70
8[d]	$Ca(NTf_2)_2$	PhMe	80	1	12	58
9[d]	$Ca(NTf_2)_2$	PhMe	100	1	10	52
10	$FeCl_3$ (20)	$CHCl_3$	60	1	20	30

[a] Reactions run on a 0.25 mmol scale and yields calculated by analysis of the ^1H NMR spectrum of the crude mixture of the reaction using 1,3,5-trimethoxybenzene as internal standard. Isolated yields in parenthesis. [b] 0.5 mmol scale. [c] With Bu_4NPF_6 as additive (5.5 mol%). [d] With Bu_4NPF_6 as additive (5.0 mol%).

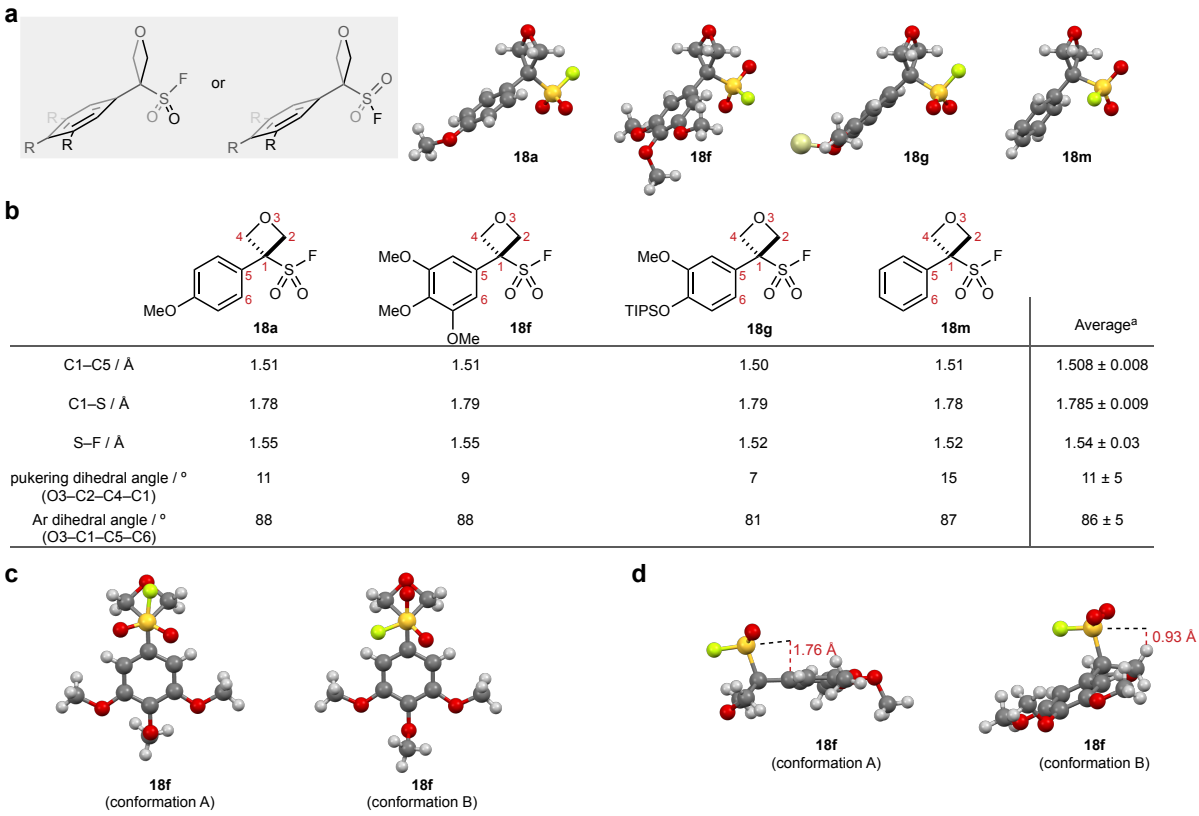
To probe the electronic requirement of the defluorosulfonylation reaction of OSFs, electron-neutral Ph OSF **18m** was prepared from OTIPS oxetane sulfide intermediate **21c** through traditional functional group interconversions (Scheme 23). At the outset, it was unclear whether the ester and sulfide functionalities would be tolerated under the required reaction conditions. **21c** was deprotected using TBAF to give phenol **21k** in 93% yield. Triflation (**21l**) followed by Pd-catalysed deoxygenation[253] yielded phenyl oxetane sulfide **21m** in 90% over two steps. OSF **18m** was finally obtained through the usual oxidation/elimination/fluorination sequence. Overall, the sequence of **18m** required nine synthetic steps from commercially available 4-bromophenol and oxetan-3-one with an overall yield of 33%.



Scheme 23. Synthesis of Ph OSF 18m.

Several OSFs (**18a**, **18f**, **18g**, **18m**) were further characterised by X-ray crystallography (Figure 28a).[p] Observed conformations were typical to that of 3,3-disubstituted oxetanes (Figure 12b, Section **1.2.3**), with a small puckering angle (11 ± 5 °) and a 'twisted' aromatic ring (Ar dihedral angle: 86 ± 5 °) (Figure 28b).[q] There were no significant correlations between bond lengths or dihedral angles and the aromatic substitution on OSFs (Figure 28b). Substituents on sulfur adopted a quasi-staggered conformation with either an oxygen or fluoride eclipsed to the C1–O3 oxetane coordinate (Figure 28c). The structural properties of OSFs give a clue to their inertness towards fluoride exchange reactions at sulfur (Figure 27d). In both *S*-conformations (A and B), there is significant steric hindrance along the S–F coordinate which would result in a high-energy early SuFEx TS with significant unfavourable filled–filled orbital interactions between an incoming nucleophile and the aromatic π system (conformation A) or an oxetane C–H (conformation B). These unfavourable interactions would increase the activation energy for SuFEx and decrease its rate of reaction. A considerably diminished SuFEx rate could render alternative non-SuFEx pathways competitive, or more favourable than SuFEx. Further structural characteristics also gave insights to explain the different rates of defluorosulfonylation of OSFs (see Sections **3.2.12.1** and **3.2.12.2**).

[p] Data collection by A. White from Imperial College's crystallography service.
[q] Dihedral angle calculated between O3–C1–C5–C6 and corresponds to the degree the aromatic ring is twisted away from the O3–C1–C5 plane, which corresponds to what would be the carbonyl plane.



	18a	18f	18g	18m	Average[a]
C1–C5 / Å	1.51	1.51	1.50	1.51	1.508 ± 0.008
C1–S / Å	1.78	1.79	1.79	1.78	1.785 ± 0.009
S–F / Å	1.55	1.55	1.52	1.52	1.54 ± 0.03
pukering dihedral angle / ° (O3–C2–C4–C1)	11	9	7	15	11 ± 5
Ar dihedral angle / ° (O3–C1–C5–C6)	88	88	81	87	86 ± 5

Figure 28. Structural features of oxetane sulfonyl fluorides. a, X-ray crystal structures of OSFs **18a**, **18f**, **18g** and **18m**. Tri(isopropyl) group on silicon in **18g** omitted for clarity. **b**, Pertinent bond lengths and dihedral angles. **c**, The two conformations observed at sulfur, here with **18f** as example which packed in both conformations. **d**, Theoretical SuFEx trajectory and closest contacts exemplified on both conformations of **18f**. Distances calculated using trigonometrical relationships assuming a planar trapezoidal geometry of the relevant coordinates. [a] Mean average given with a 95% confidence interval (CI), calculated using the formula: $\mathrm{CI} = t_{\mathrm{s}} \frac{s}{\sqrt{n}}$, whereby t_{s} corresponds to the 95th fractile with ν degrees of freedom ($\nu = n - 1$), s the sample standard deviation, and n the sample size (4).[254]

With an optimised route to OSFs in hand and significant amounts of six OSF substrates, their defluorosulfonylative reactivity was investigated, as discussed in the next sections.

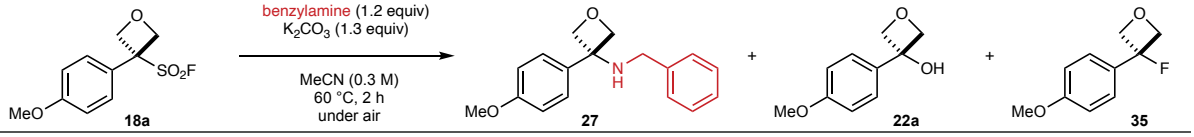
3.2.6 Optimisation and Robustness of Defluorosulfonylation Reaction

The defluorosulfonylative coupling of OSFs with amines had been initially optimised by R. Croft to high yields of amino-oxetanes (see Section **3.2.1**; *e.g.* 89% yield of amino-oxetane **27** with benzylamine as standard nucleophile).[210] Nevertheless, further investigations were conducted to better understand the robustness of the transformation to deviations in the conditions, especially with biocompatible applications in mind. To this end, different solvents, Lewis acid activators and the effect of water were investigated.

The deFS reaction was shown by D. Antermite to be insensitive to an atmosphere of air (vs Ar), high dilution or base loading, which was important to conduct array-type workflows.[212] deFS reactions were henceforth conducted under air unless otherwise stated.

The deFS coupling proceeded at physiological temperature (37 ºC) without a significant drop in yield (Table 5, entries 1–2). Previous work had shown the clear requirement of the deFS reaction for polar solvents (Scheme 18b). DMSO, DMF and their mixtures in MeCN were examined as alternative media that could dissolve MeCN-insoluble nucleophiles. Only minimal amounts of amino-oxetane **27** were observed in pure DMF and DMSO with high quantities of oxetanol **22a** (Table 5, entries 3–4). In 10% DMF/MeCN or 10% DMSO/MeCN a more favourable **27**:**22a** ratio was obtained but still with high amounts of oxetanol **22a** (entries 5–6). Very polar solvents such as DMF or DMSO seem to favour the attack of *O*- over *N*-nucleophiles, reflected by the change in product distributions based on water content alone (*cf.* Table 7). Then, the compatibility of silyl additives that may trap the released fluoride ions was examined (entries 7–12).[255,256,257] TMS_2O and TMS–OH were both compatible and even improved the yield marginally (entries 7–8). HMDS had a negative impact and reduced the yield of amino-oxetane **27** by ca. 30%, with many unidentifiable side products in trace amounts (entry 9). In the presence of Si-reagents but in the absence of base, the yield of amino-oxetane **27** was reduced in all cases to ≤ ca. 50% (entries 10–12). Comparing the yield of oxetane fluoride **35** between entries 10 and 11, it seems that TMS–OH is a better fluoride trapping agent than TMS_2O in this chemical system.

Table 5. Reaction of OSF **18a** with benzylamine under different conditions.

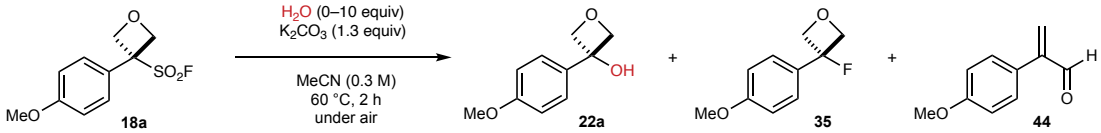


Entry	Change from standard conditions	Yield / %[a]			
		27	**22a**	**35**	**18a** (RSM)
1	none	94	2	0	0
2	37 ºC, 24 h	86	2	3	0
3	DMF as solvent, under Ar	6	80	3	0
4	DMSO solvent, under Ar	2	53	5	0
5	10% DMF in MeCN as solvent, under Ar	28	47	5	0
6	10% DMSO in MeCN as solvent, under Ar	32	63	3	0
7	+ TMS_2O (1.3 equiv)	97	0	0	3
8	+ TMS–OH (1.3 equiv)	97	0	0	3
9	+ HMDS (1.3 equiv)	66	0	0	5
10	+ TMS_2O (1.3 equiv), no K_2CO_3	51	12	17	2
11	+ TMS–OH (1.3 equiv), no K_2CO_3	50	5	4	2
12	+ HMDS (1.3 equiv), no K_2CO_3	38	0	5	5

[a] Reactions run on a 0.1 mmol scale and yields calculated by analysis of the ^{1}H NMR spectrum of the crude mixture of the reaction using 1,3,5-trimethoxybenzene as internal standard.

The high amounts of oxetanol **22a** observed in polar solvents such as DMF and DMSO (Table 5, entries 3–6), prompted an investigation on the effect of water on the deFS reaction. The general reactivity of OSF **18a** with water was initially assessed by using water as the only nucleophile, at different concentrations (Table 6). First, in the absence of water and base (K_2CO_3), *i.e.* only **18a** in MeCN, fluoride outcompeted traces of water in the solvent and only 6% of oxetanol **22a** was obtained, alongside 78% of fluoride **35** (entry 1). Adding K_2CO_3 reduced the amounts of fluoride **35**, presumably by trapping the fluoride as KF, and running the reaction under argon reduced the amount of oxetanol **22a** (entries 2–3). Under Ar, the basic conditions promoted formation of aldehyde **44**, the product of elimination/oxetene retro-electrocyclisation (entry 2, also see Section **3.2.12**). Unsurprisingly, the yield of oxetanol **22a** increased with increasing water content (entries 3–7 and Figure 29a).

Table 6. Reaction of OSF **18a** with increasing equivalents of water.



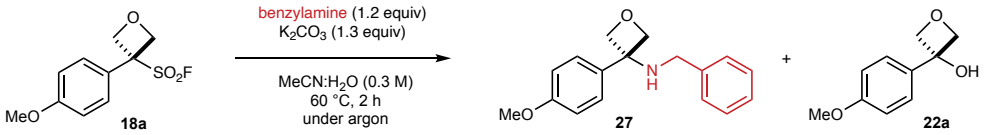
Entry	Equiv H_2O	Yield / %[a]			
		22a	**35**	**44**	Total
1	0[b]	6	78	1	85
2	0[c]	11	58	9	78
3	0	42	35	1	78
4	1	65	27	0	92
5	2	64	31	0	95
6	3	68	32	0	100
7	10	84	12	0	96

[a] Reactions run on a 0.1 mmol scale and yields calculated by analysis of the ^{1}H NMR spectrum of the crude mixture of the reaction using 1,3,5-trimethoxybenzene as internal standard. [b]In the absence of base. [c]Under Ar.

Then, the robustness of the deFS amination towards moisture was examined (Table 7). Using benzylamine as nucleophile, the amount of water was increased from 17 to 91 equivalents (10:1 to 1:1 MeCN:H_2O). A yield of 92% of amino-oxetane **27** was observed at 17 equivalents of water (amine: 1.2 equivalents; entry 2) and still 36% of amino-oxetane **27** (40% of oxetanol **22a**) was observed at 91 equivalents of H_2O (entry 5; corresponds to a 1:1 MeCN:H_2O volume ratio). With the product distributions and the equivalents of amine and water, a ratio was calculated that reflects the ratio of the rate of reaction of the proposed oxetane carbocation intermediate (see Section **3.2.12**) with each nucleophile (amine and water).[258] Taking out entry 1 and 2 (entry 1 is not applicable and entry 2 seems to be numerically and graphically

out of place; see Figure 29b), it can be estimated that reaction of the oxetane carbocation with benzylamine is ca. 65 ± 13 (95% CI, n = 3) times faster than with water. These results are important and relevant for future biocompatible applications such as functionalisation of macromolecules (*i.e.* peptides, proteins, antibodies), which only tolerate a certain degree of organic solvent (usually not more than 1:1 H_2O:organic solvent).

Table 7. Reaction of OSF **18a** with benzylamine and increasing equivalents of water. Concentration kept constant at 0.3 M (volume MeCN + H_2O = 0.33 mL).



Entry	Equiv H_2O (MeCN:H_2O)	Yield / %[a]		Ratio of rate ($\frac{r_{27}}{r_{22a}}$)[b]
		27	**22a**	
1	0 (NA)	94	0	NA
2	17 (10:1)	92	8	163
3	30 (5:1)	71	26	68
4	61 (2:1)	50	43	59
5	91 (1:1)	36	40	68

[a] Reactions run on a 0.1 mmol scale and yields calculated by analysis of the ^{1}H NMR spectrum of the crude mixture of the reaction using 1,3,5-trimethoxybenzene as internal standard. [b] Ratio of rate calculated by $\frac{r_{27}}{r_{22a}} = \frac{[27]}{[22a]} \cdot \frac{[H_2O]_0}{[amine]_0}$, whereby [**27**] and [**22a**] correspond to the final product concentrations and $[H_2O]_0$ and $[amine]_0$ to the initial concentrations of water and amine, respectively. NA = not applicable.

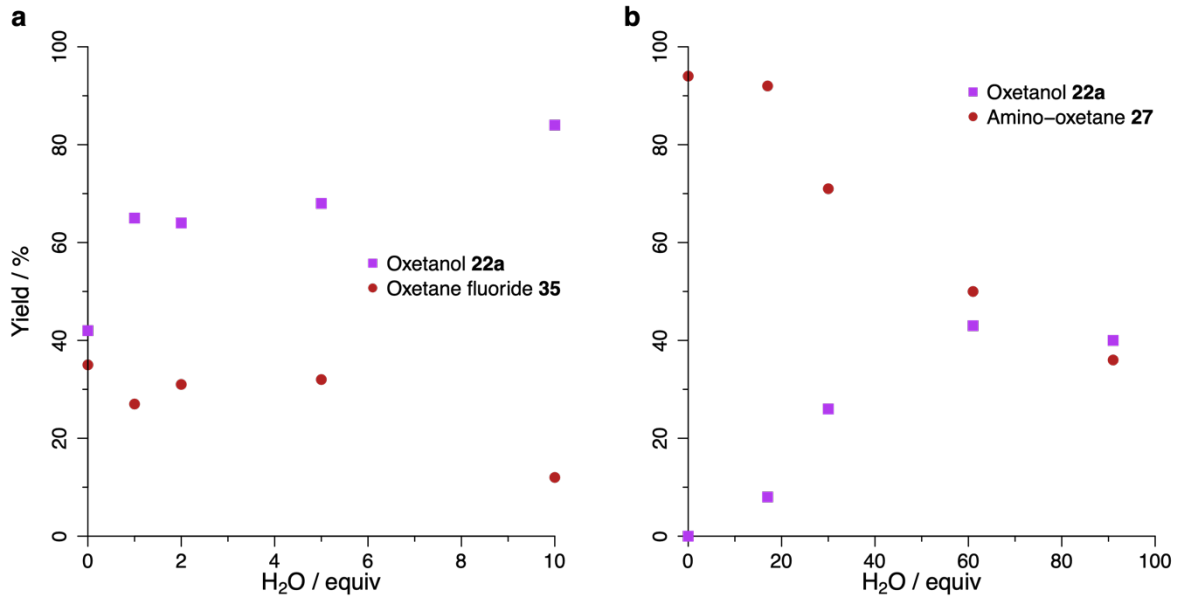
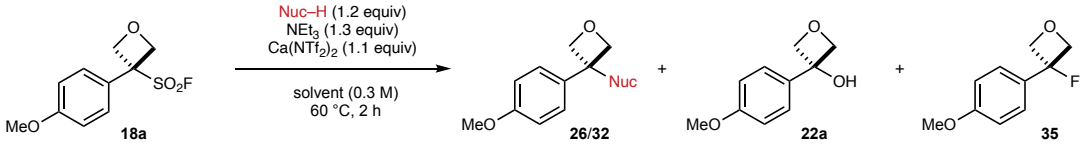


Figure 29. Influence of water on deFS reaction. a, H_2O as nucleophile (Table 6, entries 3–7). **b**, Competition between benzylamine and varying equivalents H_2O (Table 7).

Finally, the effect of Lewis acid additives on the deFS reaction, which have been shown to positively affect SuFEx processes, was investigated (Table 8).[248,255] Using both morpholine or phenol as nucleophile, a complex mixture was obtained in all cases with neither the SuFEx nor deFS products observed, only small amounts of oxetanol **22a** (entries 1–2).

Table 8. Reaction of OSF **18a** with morpholine or phenol under Lewis acidic conditions.



Entry	Nucleophile	Solvent	Yield / %[a]		
			26/32	**22a**	**35**
1[b]	morpholine	MeCN	0	27	0
2[b]	morpholine	*tert*-amyl alcohol	0	30	4
3	phenol	MeCN		complex mixture	
4	phenol	*tert*-amyl alcohol		complex mixture	

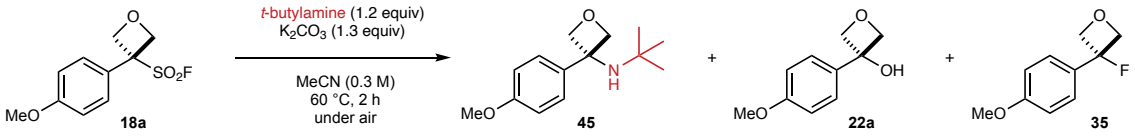
[a] Reactions run on a 0.025 mmol scale and yields calculated by analysis of the ^{1}H NMR spectrum of the crude mixture of the reaction using 1,3,5-trimethoxybenzene as internal standard. [b] A complex mixture of many species was obtained.

With a better understanding of the defluorosulfonylative process and its requirements in conditions, the scope of both OSF and nucleophile coupling partners was investigated and is described in the next section.

3.2.7 Scope of Defluorosulfonylation Reaction

Investigations started with the coupling of OSF **18a** with a challenging nucleophile, *t*-butylamine (Table 9). *t*-Butylamine is sterically very hindered and usually reacts sluggishly as a nucleophile due to high energy transition states. Under the standard conditions (1.2 equivalents of amine, under air), amino-oxetane **45** was isolated in a moderate 40% yield, accompanied by relatively high amounts of oxetanol **22a** and oxetane fluoride **35** (entry 1). Changing the reaction atmosphere from air to argon, previously shown to reduce the amounts of **22a** (see Table 6), the yield of amino-oxetane **45** was increased to 71% (entry 2). A further improvement in yield was seen by increasing the equivalents of amine from 1.2 to 2.0, which finally resulted in 82% isolated yield of amino-oxetane **45** (entries 3–4).

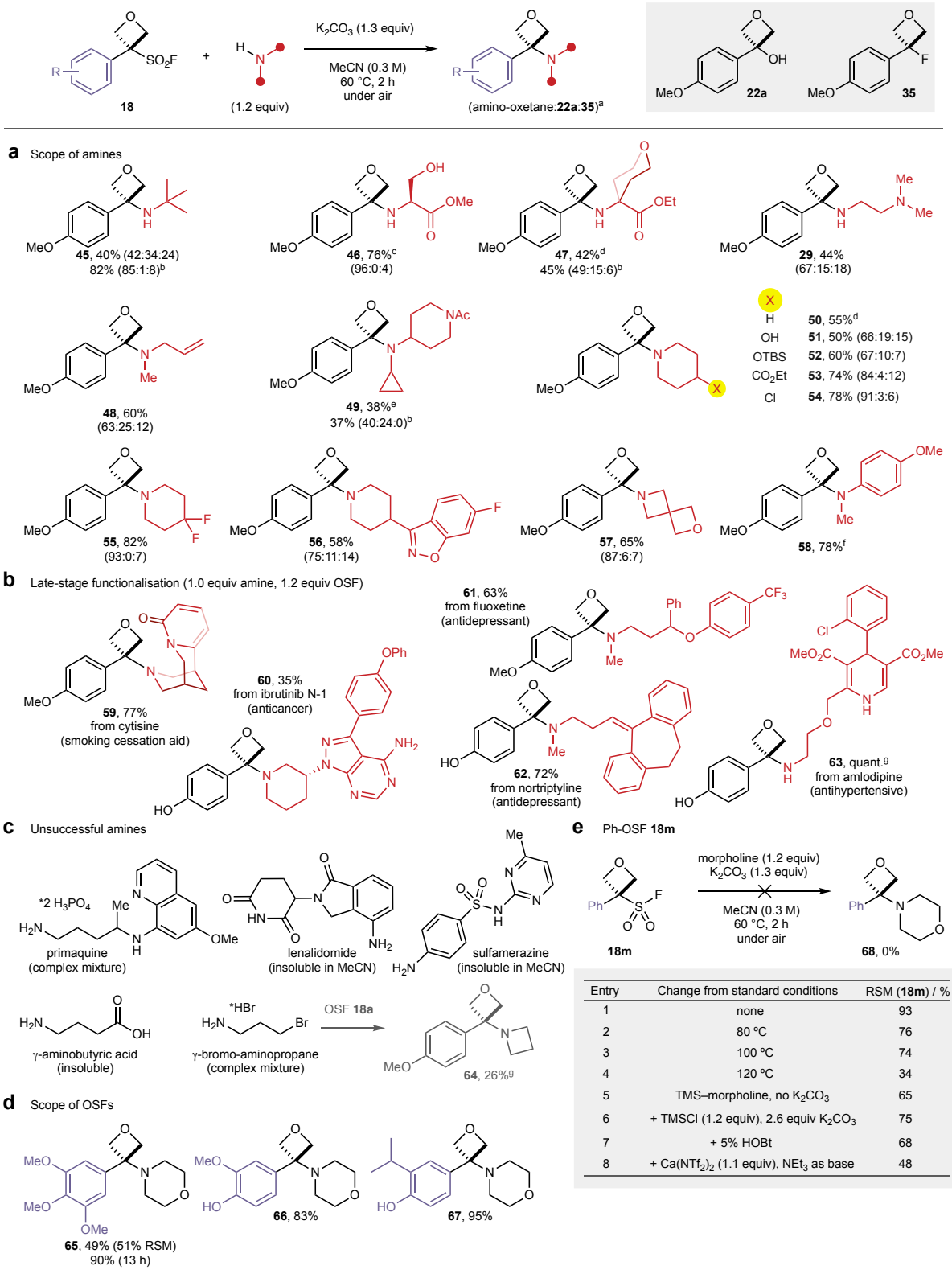
Table 9. Reaction of OSF **18a** with *t*-butylamine under different conditions.



Entry	Change from standard conditions	Yield / %[a]		
		45	**22a**	**35**
1[b]	none	42 (40)	34	24
2	under Ar	71 (69)	8	8
3	under Ar and 1.5 equiv *t*-$BuNH_2$	85 (75)	3	5
4	under Ar and 2.0 equiv *t*-$BuNH_2$	85 (82)	1	8

[a] Reactions run on a 0.1 mmol scale and yields calculated by analysis of the ^{1}H NMR spectrum of the crude mixture of the reaction using 1,3,5-trimethoxybenzene as internal standard. Isolated yields in parenthesis. [b] Yields represent ratios in the ^{1}H NMR spectrum of the crude mixture of the reaction without an internal standard.

With two sets of optimised conditions in hand, the scope of the defluorosulfonylative coupling was investigated (Scheme 24). A wide range of structural and electronic variations were tolerated, and functional groups such as free alcohols (**46**), esters (**47**), tertiary amines (**29**), terminal alkenes (**48**) and amides (**49**) were successfully incorporated. The second-generation conditions developed for *t*-butylamine (Table 9) did not improve the yield with other sterically hindered amines (**47**, **49**; previous syntheses by D. Antermite and L. Blagojevic shown for comparison). The reasons for the moderate yields seem to be poor solubility in MeCN (amino-tetrahydropyran) and high hygroscopicity and deliquescence (cyclopropylamine).



Entry	Change from standard conditions	RSM (**18m**) / %
1	none	93
2	80 °C	76
3	100 °C	74
4	120 °C	34
5	TMS–morpholine, no K_2CO_3	65
6	+ TMSCl (1.2 equiv), 2.6 equiv K_2CO_3	75
7	+ 5% HOBt	68
8	+ $Ca(NTf_2)_2$ (1.1 equiv), NEt_3 as base	48

Scheme 24. Scope of deFS reaction.[212] **a**, Varying the amine nucleophile. **b**, Late-stage functionalisation of amine-containing drugs. **c**, Unsuccessful amine nucleophiles. **d**, Varying the OSF reagent **18**. **e**, Reactivity of Ph OSF **18m**. [a] Ratios in the ^{1}H NMR spectrum of the crude mixture of the reaction. [b] Under Ar and using 2.0 equiv of amine. [c] Ammonium chloride salt with 2.6 equiv K_2CO_3 used. [d] Reaction performed by D. Antermite. [e] Reaction performed by L. Blagojevic. [f] Ratio could not be determined from the ^{1}H NMR spectrum of the crude mixture of the reaction. [g] As suggested by the ^{1}H NMR spectrum; not characterised further.

The piperidine series showed an interesting trend. Electron-poor piperidines, less nucleophilic and expected to show a slower rate of attack, showed unexpectedly higher yields (**53**–**55**) than electron-neutral (**50**, synthesised by D. Antermite) and electron-rich examples (**51**). This trend was further correlated to pK_a calculations (Figure 31) and investigated with competition experiments (Section **3.2.8**). A TBS group was tolerated and not deprotected under the reaction conditions, in contrast to TMS or TIPS groups (see *e.g.* Schemes 19 and 26). Further, the medicinally relevant 3-piperidino-6-fluoro-benzisoxazole (*e.g.* part of risperidone)[259] and oxazaspiro[3.3]heptane motifs were successfully installed (**56**, **57**), oxetane **57** representing a 'double isostere' of a morpholine benzamide. The deFS coupling tolerated many nucleophiles that would be challenging for traditional amide couplings, either due to their steric hindrance (**45**, **47**, **49**) or reduced nucleophilicity (**53**–**55**, **58**). Several amino-oxetanes were further characterised by X-ray crystallography and their structural characteristics will be discussed in Section **3.2.11.1**.

The potential of OSFs as useful reagents for drug discovery campaigns was showcased through the late-stage functionalisation of complex amine-containing drugs, an attractive modern strategy for the derivatisation of lead compounds (see Section **1.1**).[16] Five bioactive compounds were successfully appended with an aryl-oxetane functionality in good yields (**59**–**63**). Particularly, the chemoselective functionalisation of ibrutinib-N1 on piperidine and not amino-pyrimidine is worth highlighting (**60**; assigned by ^{1}H and ^{13}C NMR chemical shifts, see Section **7.6.4.1**).

Unsuccessful amines were those that were either insoluble in the solvent (MeCN), or those with more than one reactive site, which led to complex mixtures of products (Scheme 24c). Reaction of γ-bromo-aminopropane with OSF **18a** led to 26% of azetidine **64**, formed through base-mediated cyclisation either before or after coupling to oxetane.

Next, the reactivity of newly synthesised OSF reagents (Figure 27a) with morpholine was investigated (Scheme 24d). Trimethoxy OSF **18f** reacted significantly slower than all other examples and 51% of OSF **18f** was recovered after the standard 2 h reaction time. Leaving the defluorsulfonylation for 13 h showed complete consumption of starting material and amino-oxetane **65** was isolated in 90% yield. The two further OTIPS disubstituted OSF examples also reacted cleanly and in high yields, benefitting from fluoride trapping by the TIPS group (**66**, **67**).

Electron-neutral Ph-OSF **18m** did not react with amines in SuFEx or deFS pathways and was mostly stable to elevated temperatures up to 120 ºC (Scheme 24e, entries 1–4). Adding

fluoride-trapping agents such as TMS-morpholine or TMSCl, or SuFEx-accelerating additives like HOBt[256] or $Ca(NTf_2)_2$[248] also had little effect (entries 5–8).

Then, more forcing conditions were tested on OSF **18m** (Figure 30a). Conditions developed by Sharpless using a combination of MgO and H_2O to activate the S–F bond[216] saw for the first time complete consumption of **18m**, with 21% yield of oxetanol **22m** (by ^{1}H NMR), but no formation of desired amino-oxetane **68**. This result was encouraging since oxetanol formation likely occurred *via* the defluorosulfonylative pathway with coupling to H_2O as nucleophile. An anhydrous modification to supress oxetanol formation still did not yield amino-oxetane **68** and 44% of OSF **18m** was recovered, suggesting H_2O acted as an activator of sulfonyl fluorides. Finally, changing to 1,1,1,3,3,3-hexafluoroisopropanol (HFIP) as solvent, known to stabilise reactive cationic intermediates,[260,261] also fully consumed OSF **18m** without formation of amino-oxetane **68**. A potential HFIP-oxetane ether (**69**) was observed in the ^{1}H NMR spectrum of the crude mixture of the reaction (Figure 30b), but degraded on silica during purification. Overall, these preliminary results were promising to find suitable reaction conditions able to activate non-electron-rich OSFs in a controlled manner for the direct coupling to amines, a significant limitation of the developed methodology.[262]

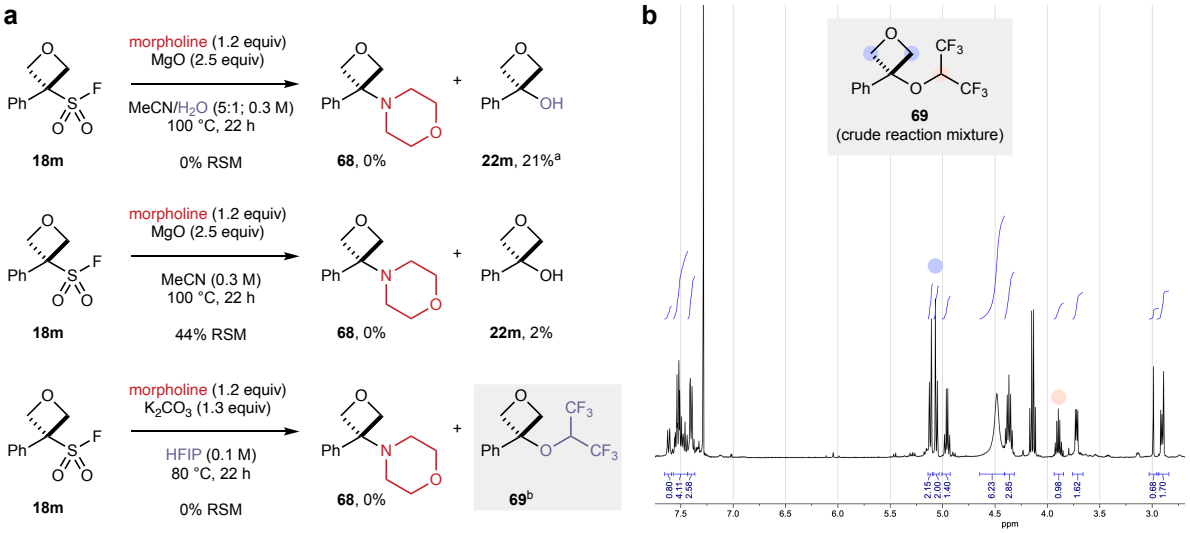


Figure 30. Further reactions of OSF 18m. a, Using MgO and H_2O as activators and in HFIP as solvent. **b**, ^{1}H NMR spectrum of the crude mixture of the reaction in HFIP ($CDCl_3$, 400 MHz). [a] Yield calculated by analysis of the ^{1}H NMR spectrum of the crude mixture of the reaction using 1,3,5-trimethoxybenzene as internal standard. [b] Tentatively assigned from the ^{1}H NMR spectrum of the crude mixture of the reaction (**b**).

Finally, the inverse trends in yields observed with electronically diverse amines (*i.e.* higher yield observed with less nucleophilic amines), prompted a correlation study with the corresponding pK_a values (Figure 31; pK_a values, which here refer to the pK_a of the corresponding conjugate ammonium acids, were calculated by C. Choi at Pfizer using in-

house software developed by ACDLabs).[r,263] Graphically, it was qualitatively clear that there is a correlation between yield of amino-oxetane and pK_a of the amine nucleophile (Figure 31a). This trend became evident when looking at the aniline series (green squares), through which a linear regression can be modelled (black line) with a good coefficient of determination (R^2 = 0.8697). Filtering to only piperidine structures to remove any steric factors that might have influenced yield, the correlation is still qualitatively clear, albeit with a smaller R^2 value (R^2 = 0.4324; Figure 31b). A potential explanation for the described trend is that the amine nucleophile is deprotonated synchronously to its attack into the proposed oxetane carbocation, so that more acidic amines are deprotonated more easily, hence have a lower-energy TS and react faster than more basic examples. Further competition experiments are described in the next section (**3.2.8**) and a full mechanistic discussion in Section **3.2.12**.

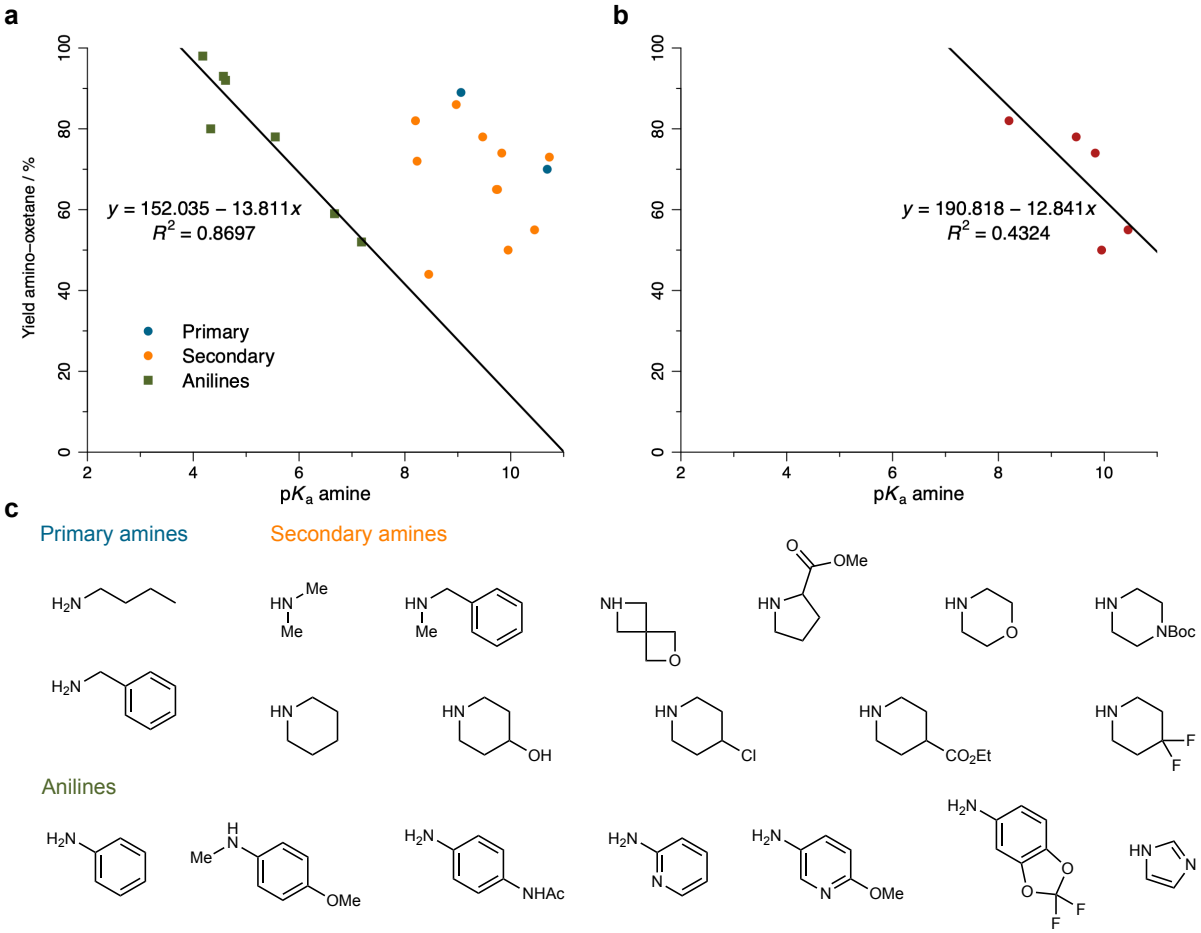


Figure 31. Correlation of yield of amino-oxetane with calculated pK_a of amine nucleophile. a, All values. **b**, Limited to piperidine structures. **c**, Structures of amines. pK_a values refer to the pK_a of the corresponding conjugate ammonium acids. Imidazole included in the aniline category.

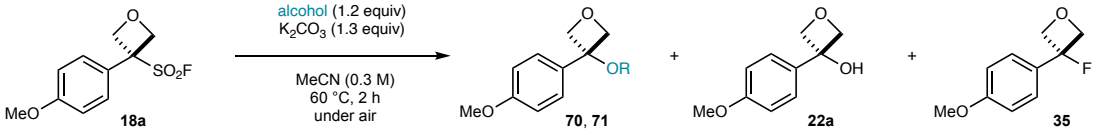
[r] Yields of amino-oxetanes not present in Scheme 24, were taken from ref. 212 and synthesised by other members of the group.

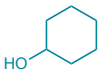
3.2.8 Investigation of Selectivities

Competition experiments were performed to better understand the chemoselectivity of the defluorosulfonylation, *e.g.* amines over alcohols (for example compounds **46** and **51**), and the apparent better reaction with electron-deficient amines vs electron-rich examples (for example compounds **55** and **50**).

First, OSF **18a** was reacted with alcohols to generate oxetane ethers **70** and **71** in moderate yields using only a slight excess of primary and secondary alcohols (Table 10; *cf.* refs. 72, 204–205). The higher amounts of oxetanol **22a** and fluoride **35** observed compared to the reaction with amines (*e.g.* Table 5), was indicative of the inferiority of alcohols compared to amines as nucleophiles. Both oxetane ether products were characterised by X-ray crystallography (Figure 32). As with OSFs (Figure 28), the aromatic ring was twisted by ca. 80 º out of the central O3-C1-C15 (O3-C1-C12 in **71**) plane, which corresponds to the carbonyl plane of benzoate analogues. As observed by Carreira, Roger-Evans and Müller,[70] oxetane ethers **70** and **71** adapted a synclinal gauche conformation with a dihedral angle of 50 and 61 º, respectively.

Table 10. Reaction of OSF **18a** with aliphatic alcohols.



Entry	Alcohol	Yield / %[a]			
		Oxetane ether **70/71**	**22a**	**35**	Total
1		**70**, 57 (50)	18	20	95
2		**71**, 64 (60)	14	16	94

[a] Reactions run on a 0.2 mmol scale and yields calculated by analysis of the ^{1}H NMR spectrum of the crude mixture of the reaction using 1,3,5-trimethoxybenzene as internal standard. Isolated yields in parenthesis.

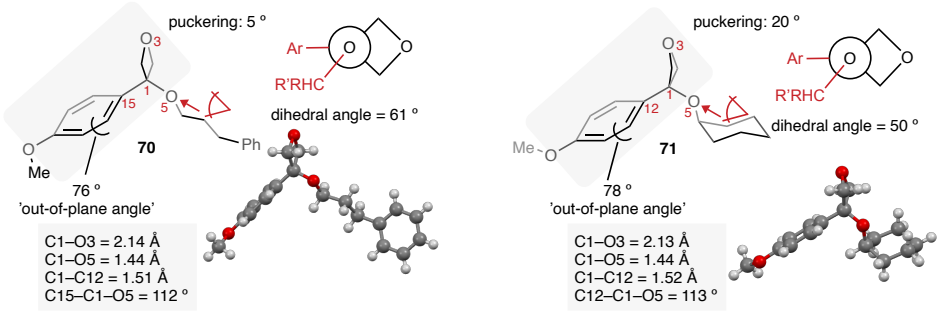
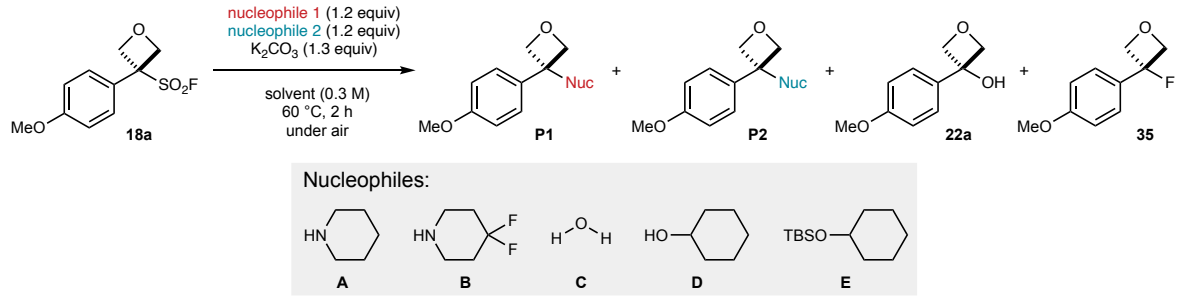


Figure 32. X-ray structures and analysis of oxetane ethers 70 and 71.

Next, competition reactions were performed with two sterically similar but electronically different amines, which had differed significantly in yield of amino-oxetane (piperidine: 50% **50**; 4,4-difluoropiperidine: 82% **55**). First, the increased amounts of side products **22a** and **35** suggested that piperidine reacted slower than difluoropiperidine, which was corroborated in a direct intermolecular competition experiment between both amines (Table 11, entries 1–3).

Table 11. Competition reactions of OSF **19a** with piperidines and other nucleophiles.



Entry	Nucleophile 1	Nucleophile 2	Change from standard conditions	Yield / %[a] P1	P2	22a	35
1	**A**	–	none	64 (**50**)	–	8	11
2	**B**	–	none	90 (**55**)	–	1	5
3	**A**	**B**	none	29 (**50**)	50 (**55**)	2	8
4	**A**	**B**	no base	20 (**50**)	59 (**55**)	12[b]	13
5	**A**	**B**	NEt_3 as base	22 (**50**)	55 (**55**)	10[b]	9
6	**A**	**B**	37 °C, 24 h	24 (**50**)	38 (**55**)	3	0
7	**A**	**C**	none	67 (**50**)	8 (**22a**)	**P2**	11
8	**B**	**C**	none	87 (**55**)	1 (**22a**)	**P2**	5
9	**A**	**D**	none	74 (**50**)	0 (**71**)	7	15
10	**B**	**D**	none	91 (**55**)	1 (**71**)	1	6
11[c]	**E**	–	none	0 (**71**)	–	36	23
12[d]	**B**	**E**	none	88 (**55**)	0 (**71**)	1	4

[a] Reactions run on a 0.1 mmol scale and yields calculated by analysis of the ^{1}H NMR spectrum of the crude mixture of the reaction using 1,3,5-trimethoxybenzene as internal standard. Compound numbers in parenthesis. [b] Approximate values, signals very obscured. [c] 85% nucleophile **E** (volatile) recovered. [d] 69% nucleophile **E** (volatile) recovered.

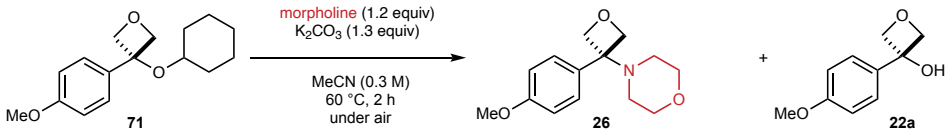
A lower total mass balance with piperidine (83%, entry 1) than with difluoropiperidine (96%, entry 2) was also suggestive of a higher degree of degradation with the former, speculatively *via* an elimination pathway promoted by the more basic nucleophile. A further hypothesis is that the concentration of free basic amine was reduced due to protonation during the course of the reaction, which is directly correlated with a reduction in rate of nucleophilic attack. A competition experiment in the absence of base supported the latter hypothesis, further increasing the ratio of **55**:**50** (entry 4). No significant change in selectivity was observed with

NEt_3 as base, indicating the non-participation of K^+ and CO_3^{2-} ions in the chemodetermining step of the reaction (entry 5). Finally, reducing the reaction temperature to 37 ºC reduced the yield of **22a** and the **55**:**50** ratio and the overall mass balance (entry 6).

As already seen with benzylamine as nucleophile (Table 7), water was not a competitive nucleophile for piperidine nor difluoropiperidine and the yields of all species remained virtually unaffected with H_2O as 'Nucleophile 2' (Table 11, entries 7–8, *cf.* entries 1–2). Alcohols, which can react with OSFs (Table 10) and were shown to be intramolecularly uncompetitive vs amines (**46** and **51**, Scheme 24), were also shown intermolecularly to leave the amination reaction unaffected (Table 11, entries 9–10). Lastly, the influence of the OTBS group, which was left untouched as part of a protected piperidinol (**52**, Scheme 24), was examined (entries 11–12). Alone, TBS-protected cyclohexanol did not yield oxetane ether **71** under the deFS reaction conditions (entry 11) and it also did not inhibit the reaction with difluoropiperidine (entry 12).

The formation of the ether bond in aliphatic oxetane ethers had been previously shown to be reversible.[204] Therefore, to show true *N*-over-*O* chemoselectivity instead of oxetane ether formation, followed by re-equilibration to an oxetane carbocation followed by attack of the amine, oxetane ether was resubmitted to the reaction conditions in the absence and presence of an amine nucleophile (Table 12). In both cases oxetane ether **71** was recovered to a high degree without formation of amino-oxetane **26** (entry 2), excluding a re-equilibrating scenario and base-mediated degradation of **71** *via* an E_1 or E_2 elimination pathway.

Table 12. Resubmission of oxetane ether **71** to the reaction conditions in the absence and presence of morpholine.



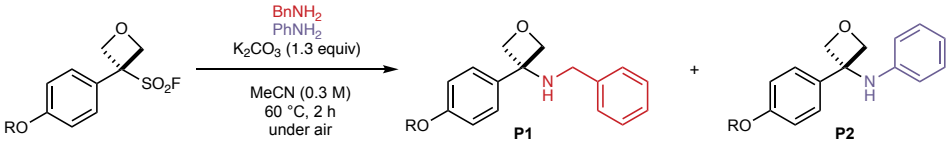
Entry	Change from standard conditions	Yield / %[a]		
		71 (RSM)	**26**	**22a**
1	Without morpholine	84	–	0
2	none	86	0	0

[a] Reactions run on a 0.1 mmol scale and yields calculated by analysis of the ^{1}H NMR spectrum of the crude mixture of the reaction using 1,3,5-trimethoxybenzene as internal standard.

Anilines were surprisingly effective nucleophiles in the defluorosulfonylation reaction with OSFs.[212] This behaviour is in accordance with the yield-pK_a trend observed and previously discussed (see Figure 31), whereby amines with *relatively* acidic N–H bonds led to high yields of amino-oxetanes. To investigate whether aniline would react faster than structurally related

and sterically unhindered benzylamine, competition experiments were conducted (Table 13). Indeed, in direct competition, the yield of aniline amino-oxetane **72** was double that of benzylamine (**27**) (entry 3), similar to the behaviour of piperidine vs difluoropiperidine (Table 11). The selectivity was hypothesised to be either a consequence of a positive acidity effect (aniline), or a negative basicity effect (benzylamine), although the former seemed more likely since a high yield was observed with benzylamine alone (entry 1). Released fluoride ions could interact strongly with the acidic aniline N–H proton *via* H-bonding to generate a quasi-deprotonated aniline nucleophile that would react faster than benzylamine. A competition experiment with OTIPS OSF **18c**, shown to irreversibly trap fluoride ions as TIPS–F, led to a switch in selectivity to support this hypothesis (entry 4). This result is in line with the selectivity observed with ibrutinib N-1 (Scheme 24b). On the other hand, increasing the equivalents of base, which should increase the concentration of free base benzylamine, had no impact on selectivity (entry 5).

Table 13. Competition reactions between aniline and benzylamine with OSFs.



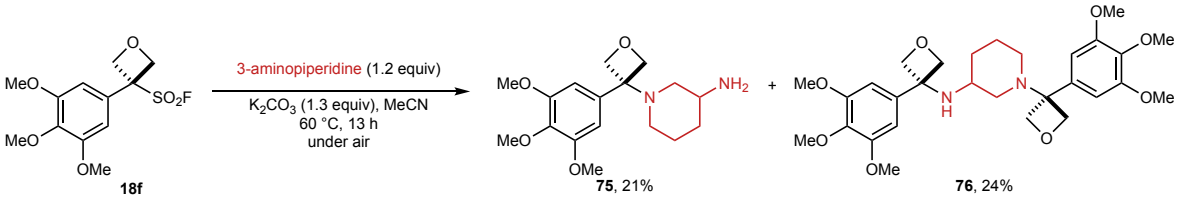
Entry	R	Equiv $BnNH_2$	Equiv $PhNH_2$	Change from standard conditions	Yield / %[a] P1	Yield / %[a] P2
1	Me	1.2	0	none	94 / **27**	–
2	Me	0	1.2	none	–	(92)[b] / **72**
3	Me	1.2	1.2	none	33 / **27**	67 / **72**
4	TIPS	1.2	1.2	none	67 (57) / **73**	33 (29) / **74**
5	Me	1.2	1.2	3.0 equiv K_2CO_3	34 / **27**	66 / **72**
6	Me	1.2	1.2	37 °C, 24 h	23 / **27**	65 / **72**
7	Me	1.2	1.2	+ TMS_2O (1.3 equiv), no K_2CO_3	36 / **27**	64 / **72**
8	Me	1.2	1.2	+ TMS_2O (1.3 equiv)	12 / **27**	90 / **72**

[a] Reactions run on a 0.1 mmol scale and yields calculated by analysis of the ^1H NMR spectrum of the crude mixture of the reaction using 1,3,5-trimethoxybenzene as internal standard. Isolated yields in parenthesis. [b] Synthesised by E. Briggs.

Finally, it was speculated that trapping the released fluoride ions with a silyl additive could display the same effect as OTIPS OSF **18c** and favour reaction of OSF **18a** with benzylamine over aniline. Decreasing the operating temperature (37 °C), or using TMS_2O instead of K_2CO_3 did not affect selectivity either (entries 6–7). However, using TMS_2O as additive, *i.e.* in conjunction with K_2CO_3, the inverse effect was observed and there was an increase in

selectivity for aniline over benzylamine (entry 8). The reason for the increase in selectivity is unclear but it was speculated that TMS_2O functioned as silylating agent, reacting *in situ* with benzylamine and reducing its free base concentration.

A preliminary intramolecular competition experiment between a primary and a secondary amine was conducted en route to an oxetane analogue of troxipide (see Section **3.2.10**). A complex mixture of products was obtained from which two species were isolated, including di-functionalisation product **76** (Scheme 25).

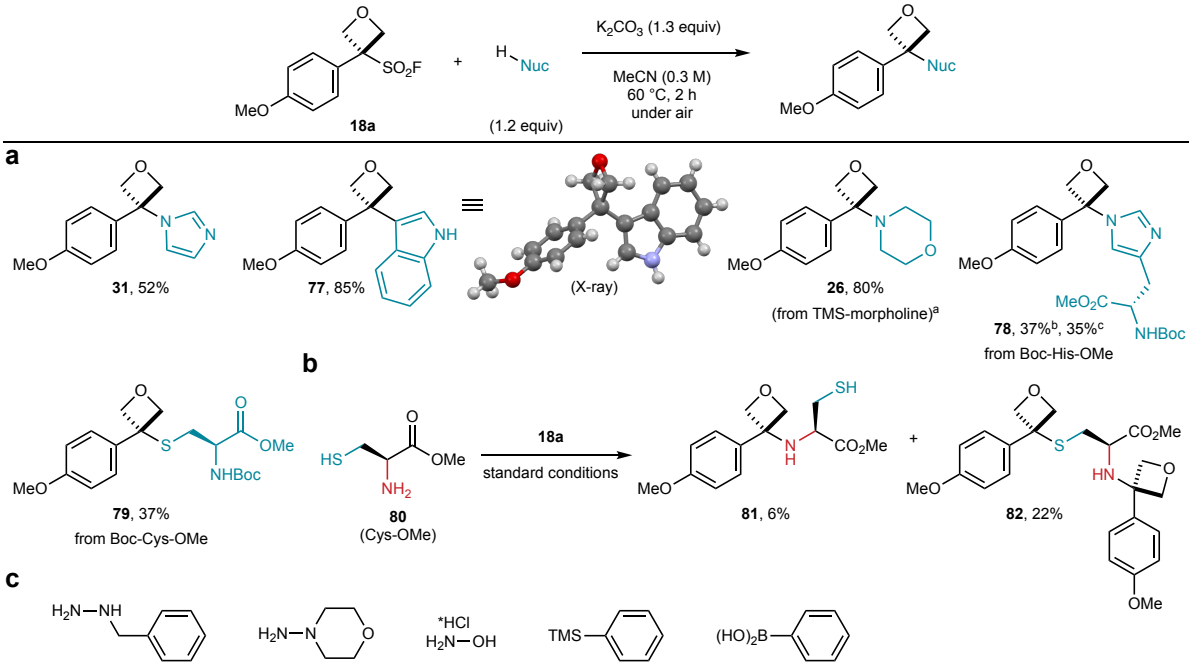


Scheme 25. Intramolecular competition experiment with 3-aminopiperidine.

In this section, the defluorosulfonylation of OSFs was demonstrated to be highly selective for amines over other nucleophiles such as alcohols. Electron-deficient amines were shown to be unusually more reactive than their electron-rich counterparts, both yield-wise and in competition experiments. Preliminary studies with chemical additives showed promising results to affect selectivities, for example between anilines and aliphatic amines.

3.2.9 Other Nucleophiles

The previous section saw the use of aliphatic alcohols as alternative nucleophiles for the deFS coupling. This section investigated whether the defluorosulfonylation of OSFs could be developed as a general method to couple an aryl-oxetane fragment to further nucleophiles (Scheme 26). N-Heterocycles such as imidazole and indole were successful, yielding amino-oxetane **31** and diaryl-oxetane **77**, respectively. Indole represented the first example of a *C*-nucleophile and the structure of diaryl-oxetane **77** was confirmed by X-ray crystallography. As previously shown with OSF **18c** (Scheme 19), TMS-morpholine also reacted successfully with OSF **18a** to yield morpholino-oxetane **26**. Relevant to biological applications, unnatural oxetane amino acids **78** and **79** were synthesised from protected histidine and cysteine (*S*-nucleophile), respectively. Reaction with *N*-unprotected cysteine **80** led to a complex mixture of polyfunctionalised products such as thiol **81** and bis-oxetane **82** (Scheme 26b). Further *N*-nucleophiles such as hydrazines and hydroxylamine, as well as organosilanes and boronic acids, potential *C*-nucleophiles upon fluoride-mediated desilylation/deborylation, were unsuccessful and led to a complex mixture of products, usually accompanied by small amounts of oxetanol **22a** and fluoride **35** side products (Scheme 26c).

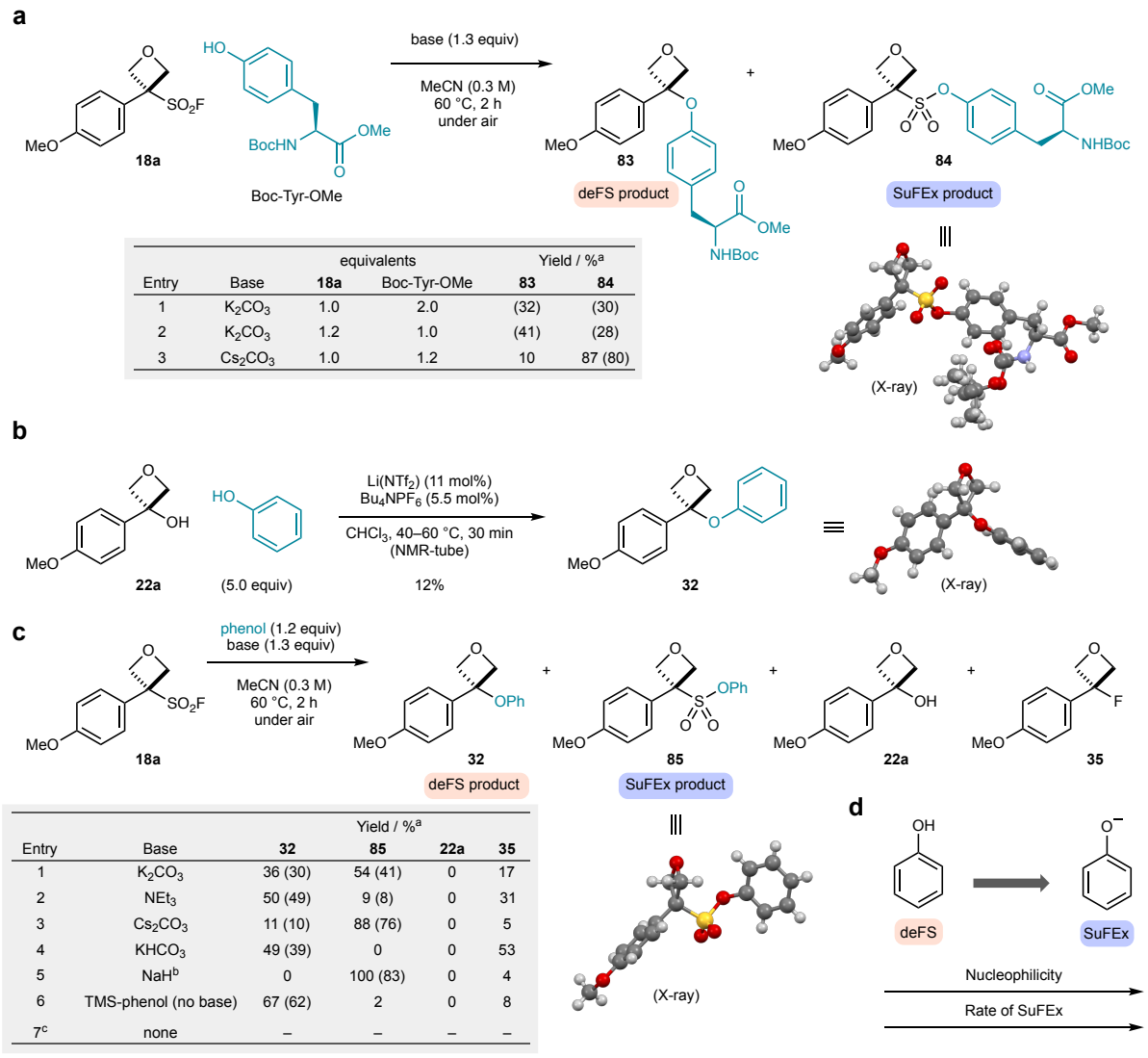


Scheme 26. Reaction of OSF 18a with other nucleophiles. a, Scope of oxetane derivatives. **b**, Reaction with Cys-OMe. **c**, Unsuccessful nucleophiles. [a] No K_2CO_3 added. [b] Using 2.0 equiv of amine. [c] Using 1.0 equiv of amine and 1.2 equiv **18a**.

The reaction with protected tyrosine (Boc-Tyr-OMe) proved to be more interesting than initially expected (Scheme 27a). Under the standard conditions, that is with K_2CO_3 as base, two oxetane products were isolated: expected oxetane ether **83**, but also sulfonate ester **84**, the product of fluoride exchange (structure confirmed by X-ray crystallography). Switching to Cs_2CO_3 as base clearly favoured the SuFEx reaction pathway and sulfonate ester **84** was obtained in 80% yield as an oxetanyl unnatural amino acid (entry 3, Scheme 27a).

This observation led to re-evaluation of the reaction of OSF **18a** with phenol, of which the product had been assigned as oxetane ether **32** (see Scheme 18d). First, an authentic sample of the oxetane ether (**32**) was synthesised from oxetanol **22a** using previously developed Lewis acid conditions[203] and the structure confirmed by X-ray crystallography (Scheme 27b). Repetition of the reaction between OSF **18a** and phenol (*cf.* Scheme 18d) using K_2CO_3 as base gave a mixture of oxetane ether **32** and sulfonate ester **85**, whose structure was also confirmed by X-ray crystallography (Scheme 27c, entry 1). From previous observations (*e.g.* Scheme 18d), it was clear that the basic additive would be crucial to control selectivity. Switching to NEt_3 as a soluble base yielded mostly ether **32** (entry 2). Cs_2CO_3, a base with a softer countercation (Cs^+), was highly selective for the sulfonate ester (entry 3), as observed with tyrosine (Scheme 27a). A weaker base unable to deprotonate phenol ($KHCO_3$) was completely selective for the oxetane ether (**32**; entry 4), and preformation of sodium phenolate with NaH formed sulfonate ester **85** exclusively in 83% isolated yield (entry 5). TMS-protected

phenol yielded ether **32** in full selectivity (entry 6) and a complex mixture of products was obtained in the absence of base (entry 7).



Entry	Base	equivalents 18a	equivalents Boc-Tyr-OMe	Yield / %[a] 83	Yield / %[a] 84
1	K_2CO_3	1.0	2.0	(32)	(30)
2	K_2CO_3	1.2	1.0	(41)	(28)
3	Cs_2CO_3	1.0	1.2	10	87 (80)

Entry	Base	Yield / %[a] 32	85	22a	35
1	K_2CO_3	36 (30)	54 (41)	0	17
2	NEt_3	50 (49)	9 (8)	0	31
3	Cs_2CO_3	11 (10)	88 (76)	0	5
4	$KHCO_3$	49 (39)	0	0	53
5	NaH[b]	0	100 (83)	0	4
6	TMS-phenol (no base)	67 (62)	2	0	8
7[c]	none	–	–	–	–

Scheme 27. Reactivity of OSFs with phenols. a, Boc-Tyr-OMe as nucleophile. **b**, Synthesis of oxetane ether **32** from oxetanol **22a**.[203] **c**, Investigation of bases for the reaction of OSF **18a** with phenol. **d**, Reactivity picture of phenols as a function of state of protonation. [a] Yields calculated by analysis of the ^{1}H NMR spectrum of the crude mixture of the reaction using 1,3,5-trimethoxybenzene as internal standard. Isolated yields in parenthesis. [b] 1.205 equiv NaH were used: NaH was added portionwise to a solution of phenol in MeCN at 0 °C. The reaction was warmed to 25 °C, OSF **18a** was added and the reaction vial was sealed. The reaction mixture was warmed up to 60 °C and stirred at this temperature for 2 h. [c] The ^{1}H NMR spectrum of the crude mixture of the reaction was too complex to determine *in situ* yields.

The experimental results in Scheme 27c suggested the following reactivity picture of OSFs with phenol nucleophiles (Scheme 27d): the rate of deFS with phenols is quicker than the corresponding SuFEx reaction. Deprotonated phenols, *i.e.* phenolates,[264] have a significantly higher nucleophilicity than phenols (and amines[265]). The rate of defluorosulfonylation is independent of the nucleophile (see Section **3.2.12.1**), but the rate of SuFEx, presumed to

proceed *via* a bimolecular process,[266] would be influenced by both sulfonyl fluoride and nucleophile. Hence, strong nucleophiles, like phenolates, could be expected to kinetically favour a SuFEx pathway, whereas weaker nucleophiles (phenols) would favour the defluorosulfonylation mechanistic path. The reason for the divergent outcomes between Cs_2CO_3 and K_2CO_3 was unclear, but a possible explanation is that CsOPh formed a soft/hard mismatched ion pair which made the phenolate more nucleophilic than the corresponding KOPh hard/hard ion pair and increased its selectivity for the SuFEx pathway (Scheme 27c, entry 3).

A comparison of the analytical data of ether **32** vs sulfonate ester **85** represented an educative exercise (Figure 33). First, the σ electron-withdrawing nature of the $S(VI)^{2+}$ group significantly deshielded the oxetane protons of **85**, expressed as a downfield shift of the signals in the ^1H NMR spectrum compared to the oxetane signals of ether **32** (Figure 33a). A similar indicative shift was observed in the chemical shift of the oxetane quaternary carbon in the ^{13}C NMR spectrum, which is characteristic of the substitution pattern on oxetane (Figure 33b).[203] Further, there were strong SO_2 asymmetric (1362 cm^{-1}) and symmetric (1142 cm^{-1}) stretches present in the IR spectrum of sulfonate ester **85** that were absent in the spectrum of ether **32** (Figure 33c). Finally, and previously misleading, the mass spectrum of sulfonate ester **85** (atmospheric pressure chemical ionisation, APCI) detected the mass of oxetane ether **32** ($[M–H^+]^-$ = 255.1027) with complete accuracy (0 ppm), formed in the ionisation chamber by desulfonylative radical recombination, a known fragmentation pathway for sulfonate esters (Figure 33d).[267] Closer inspection revealed further SO_2-containing fragments (Figure 33d).

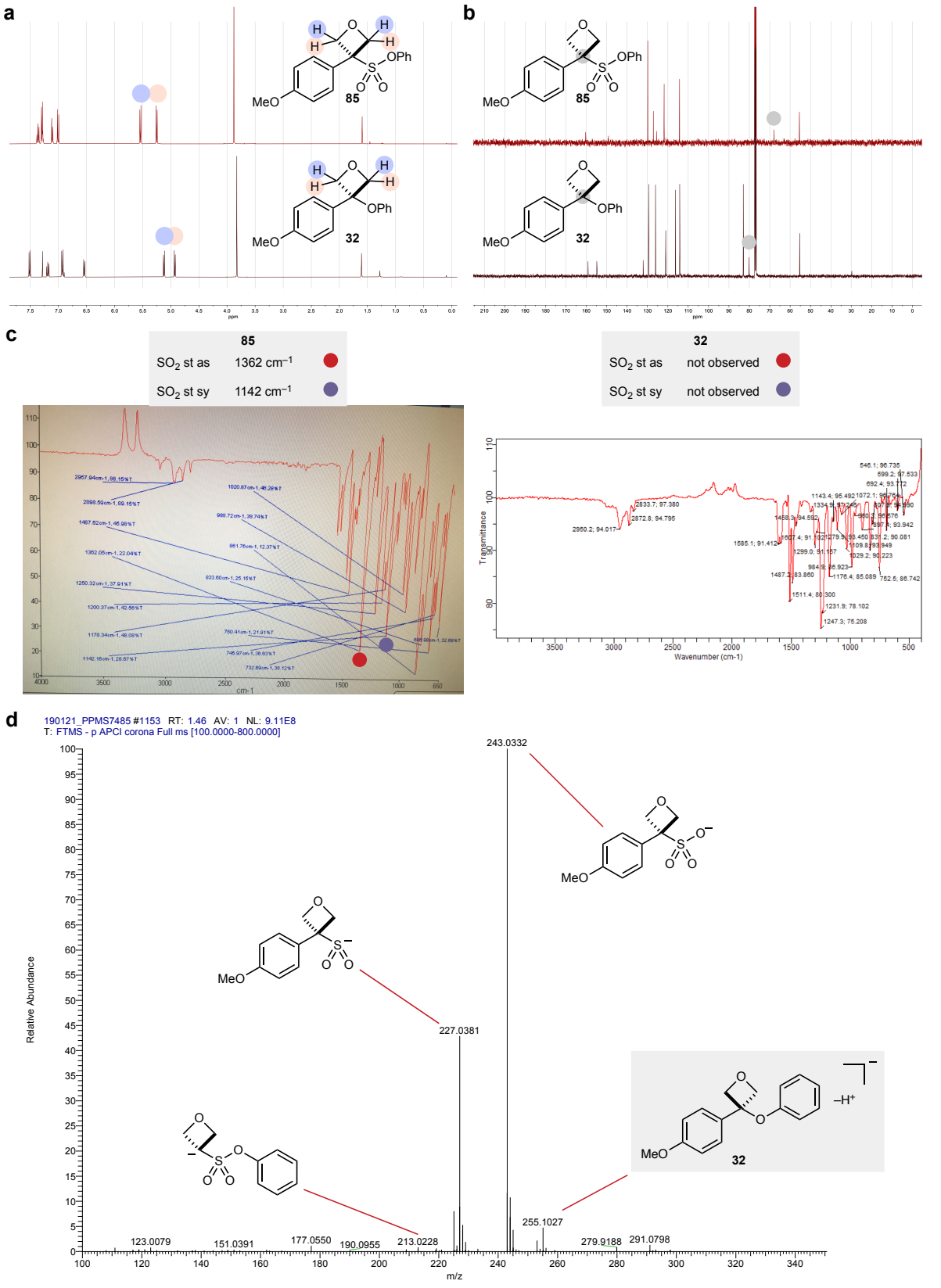
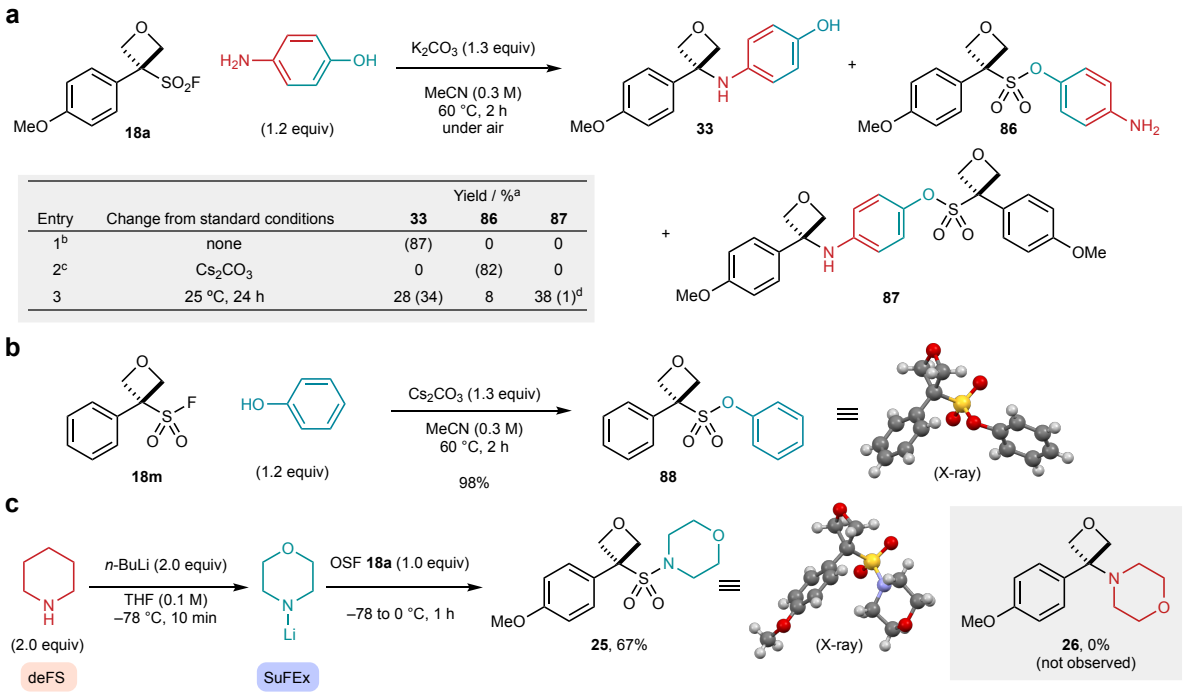


Figure 33. Comparison of analytical data between sulfonate ester 85 and ether 32. a, ^{1}H NMR spectra (both in $CDCl_3$, 400 MHz). **b**, ^{13}C NMR spectra (both in $CDCl_3$, 101 MHz). ^{13}C NMR spectrum of **85** recorded by R. Croft. **c**, IR spectra (spectrum of **85** recorded by R. Croft). **d**, Mass spectrum of sulfonate ester **85** (APCI in negative mode). st = stretch; as = asymmetric; sy = symmetric.

With a better understanding of the reactivity of OSFs with phenols and of the analytical data of their products, the structure of oxetane ether **34** (Scheme 18d) was also revised to sulfonate ester **86** (Scheme 28a; reactions performed by R. Croft, entry 1, and D. Antermite, entry 2).



Entry	Change from standard conditions	Yield / %[a] 33	86	87
1[b]	none	(87)	0	0
2[c]	Cs_2CO_3	0	(82)	0
3	25 °C, 24 h	28 (34)	8	38 (1)[d]

Scheme 28. Implications of SuFEx reactivity of OSFs with strong nucleophiles. a, Revised outcome with 4-aminophenol (*cf.* Scheme 18d). **b**, Reaction of OSF **18m** with phenol using Cs_2CO_3 as base. **c**, SuFEx reactivity of OSF **18a** with *N*-Li morpholine. [a] Yields calculated by analysis of the ^{1}H NMR spectrum of the crude mixture of the reaction using 1,3,5-trimethoxybenzene as internal standard. Isolated yields in parenthesis. [b] Reaction performed by R. Croft. [c] Reaction performed by D. Antermite. [d] Difference between isolated and *in situ* yield due to challenging separation from sulfonate ester **86**.

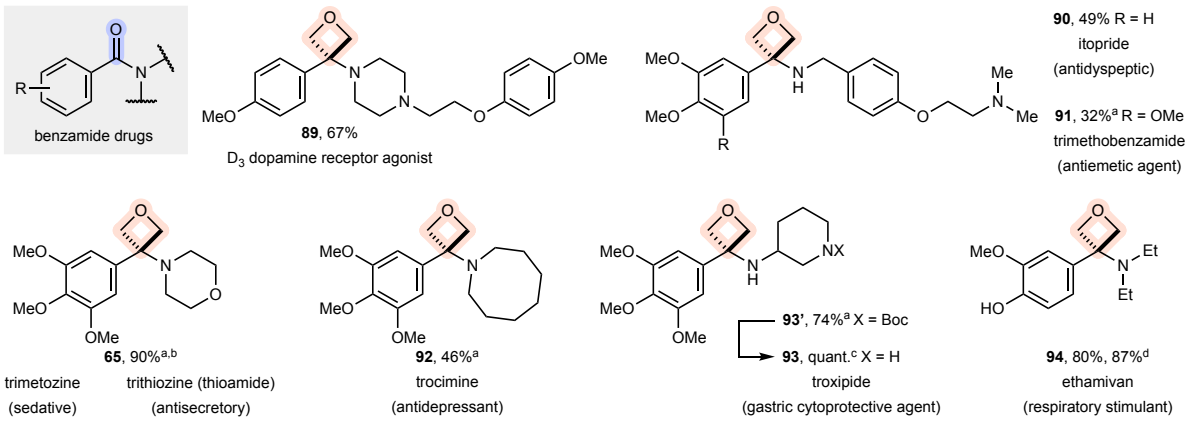
The control in chemoselectivity and preferred mechanistic pathway (deFS vs SuFEx) between *N* and *O* attack with 4-aminophenol by a simple change of base is remarkable. Conducting the reaction with 4-aminophenol at 25 ºC with K_2CO_3, hoping for insufficient activation energy for the desulfonylative pathway, led to a complex mixture of products, including amino-oxetane **33**, sulfonate ester **86** and bis-oxetane **87** (entry 3). Since the SuFEx pathway with phenolates should be fairly unaffected from the electronics of the aromatic on OSFs (in contrast to the oxetane-centred deFS pathway), it was hypothesised that non-electron-rich OSFs could undergo smooth fluoride–phenol exchange with phenolates. Indeed Ph-OSF **18m** reacted with phenol and Cs_2CO_3 to sulfonate ester **88** in 98% yield (Scheme 28b). The inertness of **18m** towards amines and general stability under a variety of chemical environments but facile reaction with phenols has promising potential for **18m** as bio-compatible and tyrosine-selective protein probe. Finally, with the knowledge that very strong nucleophiles favour a SuFEx pathway, morpholine was deprotonated using *n*-butyllithium in THF at –78 ºC, to which

OSF **18a** was added and allowed to warm to 0 ºC over 1 h, yielding oxetane sulfonamide **25** in 67% and without the formation of amino-oxetane **26** (Scheme 28c).

In this section OSF reagents were demonstrated to react with other nucleophiles apart from amines. Examples included N-heterocycles, alcohols, phenols, thiols and *N*-TMS- and *N*-lithiated amines. Reactions with amino acid derivatives in particular constitute an important foundation for biological applications such as peptide and protein functionalisation. Selectivity studies with phenols revealed a switch in the selectivity of the reaction pathway to favour either defluorosulfonylation (phenols) or SuFEx (phenolates) depending on the degree of protonation and countercation. This insight led to the initial design of a 'forced' SuFEx reaction of OSFs with amines by preformation of lithium amides. Further inter- and intramolecular selectivity studies between amino acid side chains must be conducted to understand the breadth of application of OSFs as bio-orthogonal functionalisation reagents and the reactivity of OSFs towards other nucleophiles should be explored to assess the application space of OSFs as reagents for organic synthesis (see Section **3.2.13**).

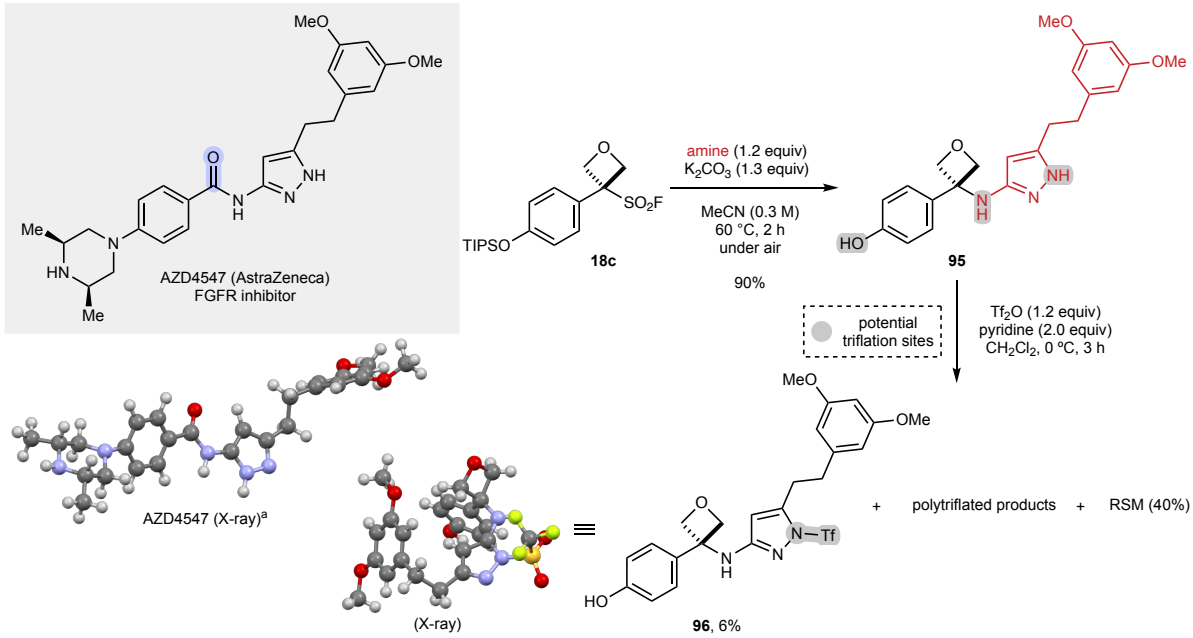
3.2.10 Synthesis of Amino-oxetane Drug Analogues

With OSFs **18a**, **18f** and **18g** in hand, a series of oxetane analogues of benzamide drugs were targeted to demonstrate the usefulness of these oxetane reagents for drug discovery settings. By simply coupling the appropriate aryl-oxetane fragment to the correct amine nucleophile, seven oxetane drug analogues were synthesised in one step (Scheme 29). All amino-oxetanes were obtained in good yields (**65**, **89**–**94**). OSF **18a** gave an analogue of a D3 dopamine receptor agonist (**89**)[268] and 3,4-dimethoxyphenyl OSF **18n** (synthesised by E. Briggs, not shown) generated oxetanyl-itopride **90**.[269] The 3,4,5-trimethoxyphenyl motif is a privileged pharmacophore present in numerous bioactive compounds,[270] most notably colchicine.[271] With this fragment (*i.e.* OSF **18f**) four drug analogues were synthesised (**65**, **91**–**93**).[272] Finally, coupling of **18g** with diethylamine took advantage of the *in situ* TIPS deprotection and gave ethamivan analogue **94** in 80% yield.[273]



Scheme 29. Synthesis of oxetane analogues of benzamide drugs. [a] Reaction time: 13 h. [b] Also reported in Scheme 24. [c] Conditions: TFA (10 equiv), CH_2Cl_2, 0–25 °C, 18 h. [d] Using 3.0 equivalents of amine.

OSF **18c** was identified as an ideal starting point en route to more complex drug analogues by functionalisation of the uncovered phenol handle. Chemoselective reaction with an aminopyrazole generated amino-phenol **95** in 90% yield, an oxetane analogue of the core of FGFR inhibitor AZD4547 (Scheme 30).[274] However, the subsequent phenol triflation was unselective and a mixture of poly-triflated products was obtained. Triflated pyrazole **96** was isolated in 6% from the mixture of compounds and its structure confirmed by X-ray crystallography. The solid-state conformation of triflate **96**, which folded back unto itself, differed starkly from that of AZD4547 (X-ray structure obtained in complex with FGFR1),[275] which is relatively flat and linear (Scheme 30).

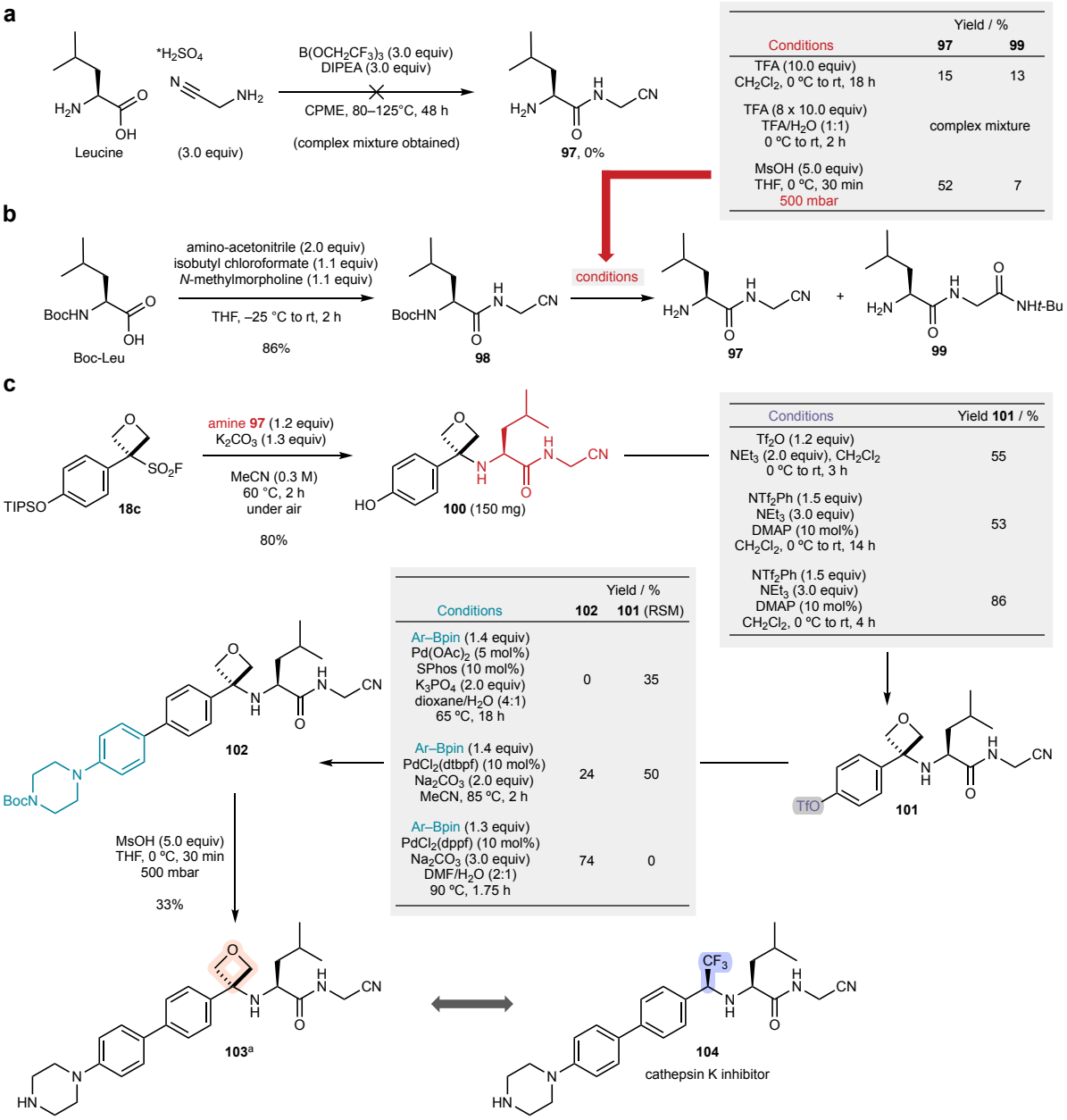


Scheme 30. Synthesis of oxetane analogue of AZD4547 core. [a] Crystallised in complex with FGFR1. Protein omitted for clarity. PDB code 4V05 (2.57 Å).

Next, an oxetane analogue of cathepsin K inhibitor **104** was targeted (Scheme 31).[276] The parent drug compound contains a chiral amino-CF_3 group as amide isostere, which generated two diastereomeric products that were separated by preparative HPLC. Commercially unavailable amine **97** was first synthesised.

Direct coupling of amino-acetonitrile with unprotected leucine using Sheppard amidation conditions was unsuccessful and led to a complex mixture of products (Scheme 31a).[277] Amide coupling conditions with Boc-Leu *via* an *in situ* generated mixed anhydride intermediate yielded amide **98** in 86% yield (Scheme 31b).[278] Boc deprotection gave product mixtures and increased amounts of *tert*-butyl amide **99** under standard TFA-mediated conditions.[279] Amide **99** was presumed to be formed by nitrile attack into the generated *tert*-butyl carbocation, followed by hydrolysis. Using methanesulfonic acid and application of a light vacuum (ca. 500 mbar) to remove gaseous isobutene (which could reform the *tert*-butyl carbocation under the acidic conditions) at 0 ºC yielded the desired product **97** in 52%.[280]

deFS coupling of amine **97** with OSF **18c** generated ca. 150 mg of amino-phenol **100** in 80% yield (Scheme 31c). Subsequent triflation proved best with the mild reagent NTf_2Ph and careful control of reaction time (4 h) to give triflate **101** in 86% yield. Suzuki–Miyaura coupling to an aryl-piperazine Bpin was first unsuccessful using previously developed coupling conditions for oxetane aryl triflates.[110] A literature survey revealed Pd-bis(phosphino)ferrocene complexes with Na_2CO_3 as base to be most promising for related systems.[276,281,282] Ultimately, a combination of three different sets of conditions yielded bi-aryl oxetane **102** in 74%.[103,276,282] The final, also difficult Boc-deprotection step gave oxetane drug analogue **103** in 33% yield using the previously employed vacuum conditions after a challenging purification (two silica normal-phase columns and one C18 reversed-phase column).



Scheme 31. Synthesis of an oxetane analogue (103) of cathepsin K inhibitor 104. a, Unsuccessful Sheppard amidation for the synthesis of amide **97**. **b**, Synthesis of amine **97** using a traditional amide coupling method and unusual Boc deprotection under reduced pressure. **c**, Synthesis of oxetane analogue **104**. [a] Isolated as the trifluoroacetic acid salt.

The chemical integrity of the oxetane ring under the variety of conditions including strong acids, reactive triflating agents, high temperatures and active Pd complexes is noteworthy. In no case were products of oxetane ring-opening observed. These synthetic case studies highlight the potential of the deFS coupling to access oxetane-containing drug-like compounds. Further targets could be potentially accessed through other cross coupling reactions of oxetane aryl triflates, for example AZD4547 (Scheme 30) by Buchwald–Hartwig amination, or moclobemide by deoxygenative chlorination.[283]

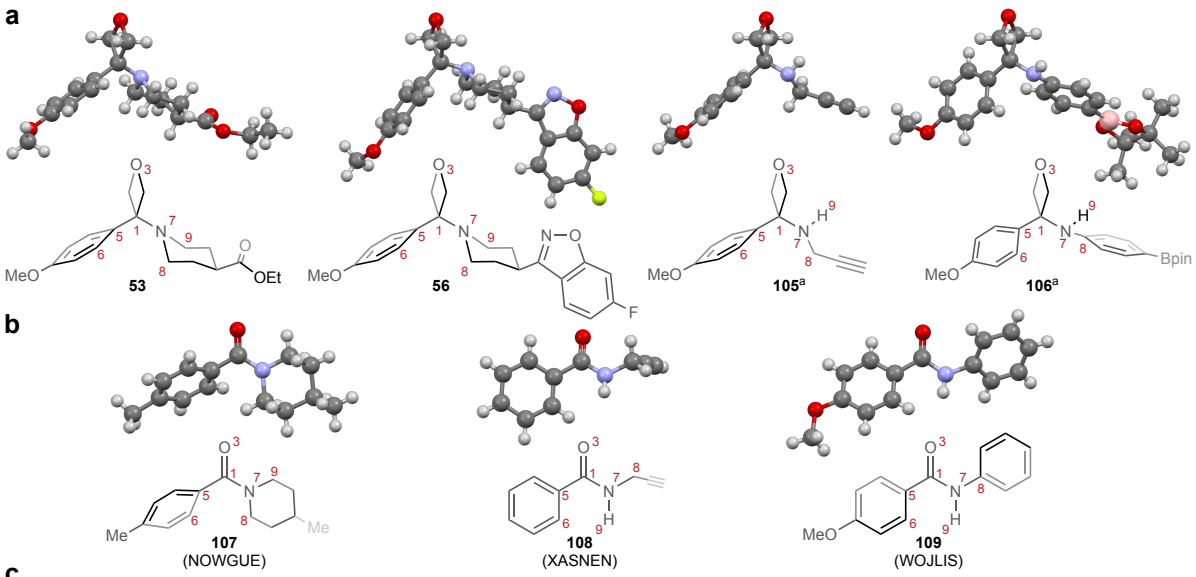
3.2.11 Assessment of Isosterism: Matched Molecular Pair Analysis (MMPA)

A high synthetic burden and little opportunity for diversity-oriented strategies have hampered the use and evaluation of the aryl amino-oxetane motif as a potential isosteric replacement of benzamides, and as attractive medicinal scaffold in its own right. Discovery and development of the defluorosulfonylative coupling of oxetane sulfonyl fluorides to amines discussed in the previous sections allowed a convenient route into aryl amino-oxetanes with options for facile diversification and analogue synthesis. To assess the isosterism of aryl amino-oxetanes vis-à-vis benzamides and to gain an initial general understanding of their ADMET properties, a matched molecular pair analysis (MMPA)[284] was performed and will be discussed in this section. Eight pairs were synthesised by L. Blagojevic as part of an MRes project (not discussed)[285] and selected ADMET properties were measured by Pfizer. Further, a conformational analysis was performed on the X-ray crystal structures (data from diffractometric measurements were collected and processed by A. White from Imperial College's crystallography service) of five amino-oxetane examples and compared to structurally related benzamides. The C–N rotational barrier of amino-oxetanes and benzamides, determined computationally by J. Luk as part of an MSci project,[286] will also be briefly discussed.

3.2.11.1 Structural Analysis

Suitable crystals for diffraction were grown by slow evaporation from $CDCl_3$ (**53**, **56**, **105**) or Et_2O (**106**). Other techniques such as vapour- or liquid-liquid diffusion were ineffective for amino-oxetanes. Figure 34a shows the X-ray crystal structure of four aryl amino-oxetanes (amino-pyrazole **96** not taken into this analysis).

An initial qualitative visual assessment showed amino-oxetanes to be rather 3-dimensional with defined molecular topologies (Figure 34a). The conformation of amino-oxetanes was defined by steric demands, locating substituents on oxetanes (*i.e.* C6, C8 and C9) almost perpendicular to the 'pseudocarbonyl-plane' (O3–C1–C5 and O3–C1–N7 planes, respectively) to avoid energetically unfavourable steric interactions.



c

	Oxetanes				Amides			Average[e]	
	53	**56**[b]	**105**[c]	**106**	**107**	**108**[d]	**109**	oxetanes	amides
C1–O3 / Å	2.15	2.15 ± 0	2.16 ± 0.06	2.17	1.23	1.24 ± 0	1.22	2.158 ± 0.015	1.23 ± 0.03
C1–C5 / Å	1.52	1.522 ± 0.014	1.51 ± 0	1.52	1.50	1.50 ± 0	1.49	1.518 ± 0.008	1.497 ± 0.014
C1–N7 / Å	1.47	1.47 ± 0.03	1.46 ± 0	1.46	1.35	1.34 ± 0	1.36	1.465 ± 0.009	1.35 ± 0.03
'carbonyl' bond angle / ° (C5–C1–N7)	115	115 ± 3	111 ± 0	113	118	117 ± 0	116	114 ± 3	117 ± 3
pukering dihedral angle / ° (O3–C2–C4–C1)	2	12 ± 9	12 ± 0	5	–	–	–	8 ± 8	–
Ar dihedral angle / ° (O3–C1–C5–C6)	86	86 ± 9	75 ± 6	31	56	16 ± 19	30	70 ± 42	(3 ± 5) • 10^1
dihedral angle on *N* / ° (C1–N7–C8–C9) or (C1–N7–C8–H9)	51	53 ± 3	(6 ± 4) • 10^1	40	8	6 ± 40	0	51 ± 12	5 ± 10

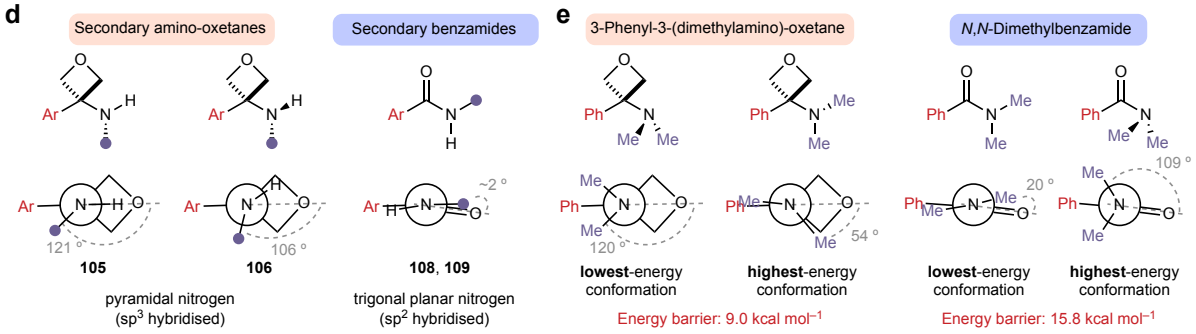


Figure 34. Structural analysis of aryl amino-oxetanes. a, Acquired X-ray crystal structures of amino-oxetanes. **b**, Related X-ray crystal structures of benzamides from the literature. Structure identifiers in parenthesis. Numbering kept the same as in **a** to facilitate comparison. **c**, Pertinent bond lengths, interatomic distances and dihedral angles. Errors represent the 95% CI. **d**, Analysis of dihedral angles along the C–N bond of amino-oxetanes and amides. **e**, Calculated minimum and maximum conformations of 3-phenyl-3-(dimethylamino)-oxetane and *N,N*-dimethylbenzamide using the B3LYP/6-31+G(d,p) basis set [keywords: solvent = water; dispersion]. Calculations performed by J. Luk.[286] [a] Amino-oxetanes **105** and **106** synthesised by E. Briggs. [b] Values are the average of three independent molecules of **56** that formed the unit cell. [c] Values are the average of two independently diffracted enantiomeric crystals of **105** (chiral at pyramidal *N*), formed by spontaneous resolution of the sample upon crystallisation. Uncertainty in Flack parameters was too high for definitive identification of absolute configuration. [d] Values are the average of two independent molecules of **108** that formed the unit cell. [e] For compounds with more than one structure (**56**, **105** and **108**), the mean value was taken without further treatment of error propagation.

Related benzamides on the other hand, are rather planar and linear (Figure 34b). Their conformation is strongly influenced by energetically favourable filled-unfilled orbital interactions, maximised by conjugation between the systems of π-electrons (aromatic ring–carbonyl–nitrogen lone pair), which is achieved by situating the aromatic ring, the carbonyl and the (sp^2 hybridised) nitrogen on the same plane. This electronically most favourable conformation is distorted to different extents depending on substitution to reduce unfavourable steric clashes with the overall lowest energy conformation resulting from a compromise between a maximisation of π-conjugation and minimisation of steric interactions.

The most relevant geometric properties of the analysed amino-oxetanes and amides are summarised in Figure 34c. First, the spatial C–O distance was (expectedly) much longer in amino-oxetanes (2.16 Å) than in amides (1.23 Å). Similarly, the C–N bond of amino-oxetanes (1.47 Å) was slightly longer than of benzamides (1.35 Å) due to the partial C–N double bond character of amides (due to π-conjugation). Also notable is the relatively large C5–C1–N7 bond angle in amino-oxetanes (114 º), which is imposed by the small internal angles of the oxetane ring (ca. 90 º). The bond angle of 114 º is close to that observed in benzamides (117 º, also see Figure 5).

The puckering angle of the oxetanyl structures was small but variable (2–12 º) with no immediately apparent trend. The aromatic substituent in amino-oxetanes was twisted largely out of the O3–C1–C5 plane, with the exception of **106**, which was sterically very crowded due to the two aromatic rings. The aromatic rings in **106** were positioned 89 º to each other, minimising steric interactions between the aromatic protons and potentially allowing for a weak T-shaped π–π interaction. The decreased O3–C1–C5–C6 dihedral angle in **106** also significantly reduced the distance between an *ortho* proton of the methoxyphenyl ring and an oxetane CH_2 (2.05 Å; *cf.* 2.30 Å in piperidine **53**). The O3–C1–C5–C6 dihedral angle in benzamides was generally smaller, *i.e.* aryl ring closer to the carbonyl plane, with some variations to reduce unfavourable steric clash (*e.g.* in amides **107** or **109**). Lastly, from the dihedral angle on nitrogen, it is evident that in amino-oxetanes the nitrogen atom is rather pyramidal with sp^3 hybridised orbitals, whilst in benzamides nitrogen is almost perfectly planar and sp^2 hybridised to improve conjugation of the lone pair with the rest of the π system.

Looking at the dihedral angle along the N7–C1 coordinate, several meaningful differences between secondary amino-oxetanes and -amides were recognised (Figure 34d). First, the steric demands on C1 were entirely opposite. In benzamides, the sterically most demanding side of C1 was on the side the aromatic ring, further increased due to the electronically favoured small dihedral angle of the arene which brought an *ortho* proton closer to nitrogen.

On the other hand, the methylene groups of the oxetane ring in amino-oxetanes added significant lateral bulk and rendered the oxetane side on C1 sterically most demanding. This steric difference on C1 placed the largest *N*-substituent on the carbonyl side in benzamides, but on the aromatic side in amino-oxetanes. Relevant to medicinal chemistry settings, *e.g.* for H-bonding with a protein target, an important consequence of this conformational difference is the direction of the N–H bond. In amino-oxetanes the N–H bond pointed towards the oxetane side,[s] reminiscent of the H–bond constellation observed with *cis*-amides. Secondary amides (like **108** and **109**) on the other hand, existed primarily in their more stable *trans* conformation. A more complex spatial setting was seen with aniline **106** compared to amine **105** (Figure 34d). The aromatic substituent on nitrogen is relatively large and was 'pushed' further away from the methoxyphenyl ring, thereby reducing the dihedral angle to the C1–O3 coordinate to 106 º (*cf.* 121 º in **105**) and placing the N–H in an unfavourable eclipsed conformation with the oxetane ring. *N*-substituents of secondary benzamides were perfectly antiperiplanar (~2 º dihedral angle) for maximal π–π conjugation.

Lastly, a brief computational analysis (performed by J. Luk)[286] of C–N bond rotation in 3-phenyl-3-(dimethylamino)-oxetane and *N*,*N*-dimethylbenzamide provided interesting insights (Figure 34e). The lowest-energy conformation of the amino-oxetane mapped well unto the highest-energy conformation of the benzamide. Also notable is the difference in energy barrier for C–N rotation, which was almost double in the benzamide vs amino-oxetane (15.8 vs 9.0 kcal mol^{-1}) due to a change in *N*-hybridisation and loss of π-conjugation during C–N bond rotation in the benzamide. This latter difference could be relevant for protein binding since it gives amino-oxetanes more flexibility for alignment inside a protein pocket.

The structural differences between aryl amino-oxetanes and benzamides described above were highlighted visually by structural overlays (Figure 35). One conformational difference was omnipresent: in all benzamide structures the largest *N*-substituent was on the side of the carbonyl group, whilst in oxetanes, this substituent was opposite the side of the oxetane motif. Conformational similarities were mostly dependent on the steric requirement of the substituents on nitrogen. If the steric requirement was large, for example in the case of anilines, molecular conformation was primarily defined to minimise unfavourable steric clashes, and the conformations of amino-oxetane and benzamide were similar (oxetane **106** and amide **109**; difference in Ar-dihedral angle: 1 º). If the steric requirement was small, like with alkynes **105** and **108**, the conformation of the amino-oxetane (**105**) was still dictated by

[s] Direction of N–H bond in amino-oxetanes determined unambiguously by intermolecular H-bonding to O3 of an adjacent molecule in the unit cell.

sterics, but benzamides were now able to optimally align to maximise π-conjugation without compromising energetically costly steric clashes, and the conformation of amino-oxetane and benzamide were completely opposite (oxetane **105** and amide **108**; difference in Ar-dihedral angle: 59 º). The piperidine examples (**53**, **56** and **107**) lay around halfway on the spectrum with a difference in Ar-dihedral angle of 30 º.

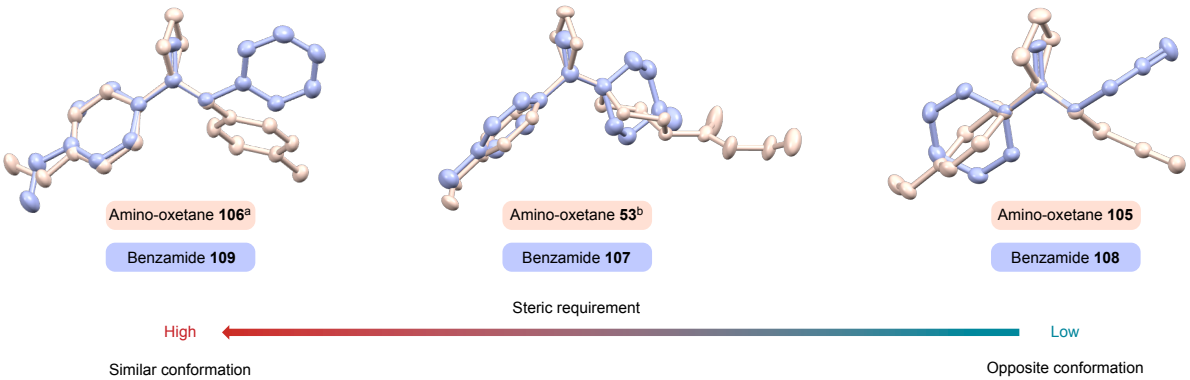


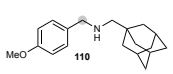
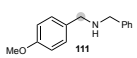
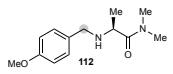
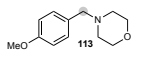
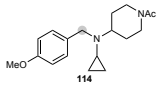
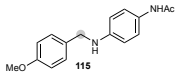
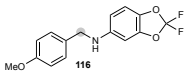
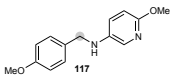
Figure 35. Overlay of X-ray crystal structures. Structures overlaid using Mercury, by overlaying C1, C5 and N7, shown in the ORTEP representation. [a] Pinacol group on boron omitted for clarity. [b] Same overlay was obtained with oxetanyl piperidine **56**.

This section presented the structural conformational differences between aryl amino-oxetanes and benzamides in the solid state by means of X-ray crystal structures. Most relevant for applications in drug design, *N*-substituents in secondary amino-oxetanes were shown to adopt the opposite conformation as in benzamides, resembling difficult to obtain, thermodynamically unfavourable *cis*-amides. The conformation of amino-oxetanes was shown to be predominately dominated by steric interactions, whilst the conformation of benzamides by a combination of sterics and π-conjugation, the degree of each contribution dependent on the steric requirements of *N*-substituents. Thus, the conformation of benzamides with a sterically complex chemical environment resembled that of comparable amino-oxetanes, but sterically unencumbered benzamide structures were entirely orthogonal to analogous amino-oxetanes.

3.2.11.2 Physicochemical Properties

Oxetanyl structures are often proposed as metabolically more stable or generally superior isosteres of carbonyl groups. However, such claims are seldomly backed up with experimental data, especially for difficult-to-access scaffolds such as amino-oxetanes, for which “little details on effect on physicochemical, biological or PK/PD properties [exist]” (Trippier).[89a] The goal of this part was hence, to broaden the physicochemical understanding of the (aryl) amino-oxetane motif for applications in drug design and to assess the scope of the comparison between amino-oxetanes and amides. To this end, a matched molecular pair analysis of eight aryl amino-oxetane–benzamide pairs was conducted. Specifically, stability at different pH’s, solubility, Log*D*, clearance, and DOF IC_{50} values were measured and are summarised in Table 14 (measurements performed by Pfizer).

Table 14. Measured physicochemical properties of amino-oxetane/benzamide pairs (performed by Pfizer). See Section **7.2** for experimental details. Values are the average of two independent measurements, unless otherwise specified.

Compound[a]		Stability / %[b]									Solubility / μM			eLog*D*	SF-Log*D*	$Cl^{c}_{int,app}$ HHEPG / mL min^{-1} million^{-1}	DOF IC_{50} / μM
		pH 1.2			pH 7.4			pH 10.0									
		1 h	4 h	24 h	1 h	4 h	24 h	1 h	4 h	24 h	pH 3.0	pH 7.4	pH 10.0	pH 7.4	pH 7.4		
 **110**		98	87	88	20	7	3	15	6	2	533	<9	<0.3	4.9	3.6	–	43
		91	68	46	72	60	36	77	67	36	<0.1	<0.1	<0.8	4.4	3.8	51	>150
 **111**		93	98	95	98	83	70	99	84	49	521	359	285	2.6	2.5	62	27
		96	88	94	100	97	94	96	94	99	104	91	76	2.5	2.7	30	>150
 **112**		82	89	92	98	94	95	99	100	97	464	472	458	–	0.4	2.5	>150
		100	100	98	100	93	91	95	93	100	405	440	420	–	1.0	1.9	>150
 **113**		94	86	82	90	93	88	99	100	95	486	556	492	1.0	1.2	4.1	>200[d]
		97	93	97	100	98	100	100	97	100	461	575	465	–	0.8	2.7	>150
 **114**		100[d]	100[d]	100[d]	95[d]	84[d]	79[d]	100[d]	100[d]	93[d]	299	223	195	1.8	1.7	38	>150
		81	93	100	98	100	96	100	100	99	465	467	480	1.2	1.2	3.6	>150
 **115**		98	91	74	98	95	92	100	99	97	509	505	500	1.7	–	–	>150
		100	100	87	100	100	97	100	98	96	13	10	8	1.9	1.9	20	>150
 **116**		90[d]	85[d]	16[d]	80[d]	57[d]	24[d]	86[d]	57[d]	26[d]	7	8	12	4.7	–	112	>150
		81	31	18	76	35	18	86	41	22	<0.1	<0.1	<0.1	4.5	3.8	57	>150
 **117**		100	100	86	100	98	96	98	97	92	441[d]	357[d]	306[d]	2.3	2.5	42	30
		79	78	94	97	94	95	95	92	92	50	31	24	2.2	2.5	13	>150

[a] Synthesised by L. Blagojevic. The following compounds are the same: **111a** and **27**, **113a** and **26**, **114a** and **49**. [b] Stability at 0 h was 100% for all compounds at all pH values. [c] Dose: 1 μM. [d] One measurement performed.

Chemical stabilities and aqueous solubilities were compared in colour-coded figures (Figures 36–37). First, amino-oxetanes showed high chemical stability, notably under acidic conditions. The 3,3-disubstitution pattern on amino-oxetanes seemed to account for much of the observed chemical stability, with a comparable behaviour to 3,3-diaryl-oxetanes at neutral and basic pH values.[103] Under acidic conditions however (pH = 1.2), the 3-aryl-3-amino-oxetane system appeared to be generally more stable than comparable 3,3-diaryl-oxetane structures. A possible reason is the basicity of the amine, which will be protonated at pH 1.2 and would disfavour a second protonation at the oxetane oxygen and prevent Brønsted acid-activation of the oxetane ring towards ring opening. Compared to benzamides, amino-oxetanes showed a similar stability behaviour and did not represent a categorical liability as isostere in this regard.

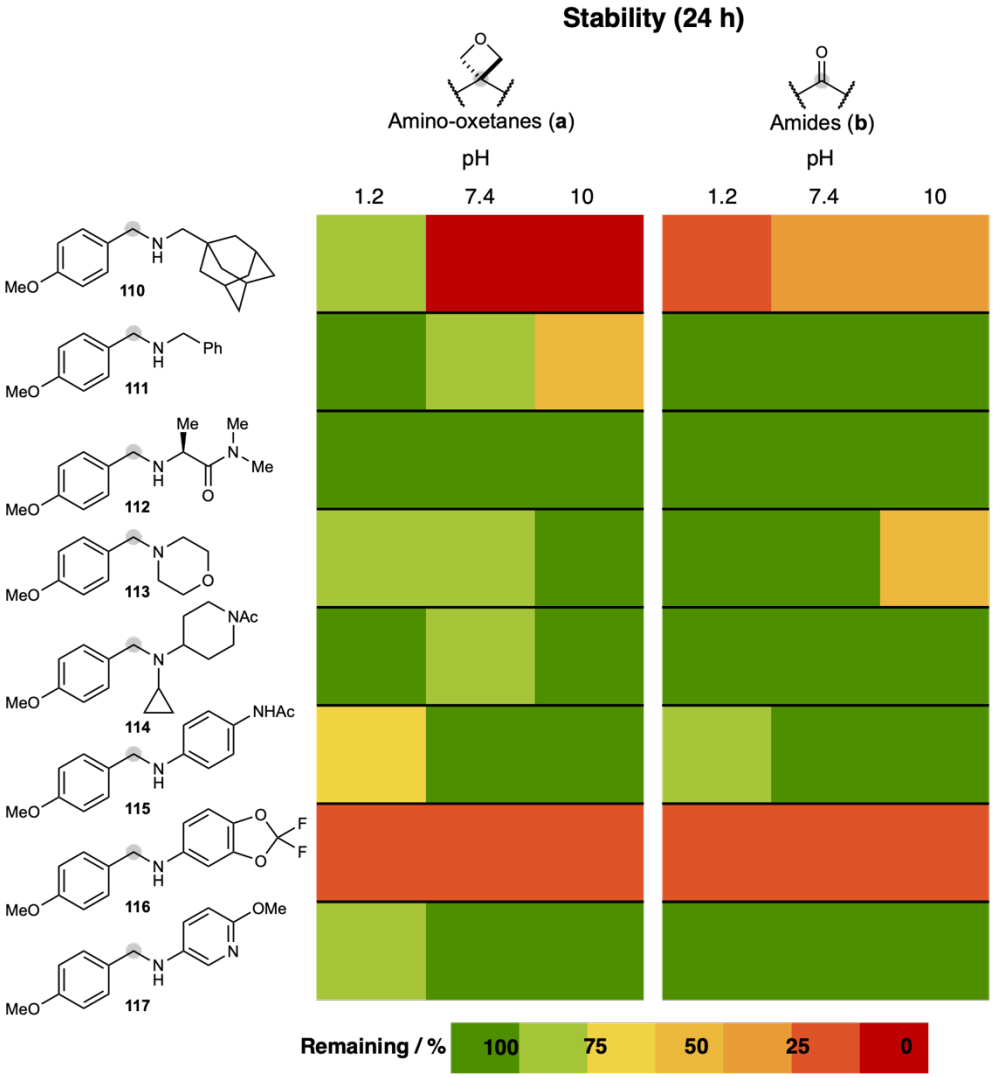
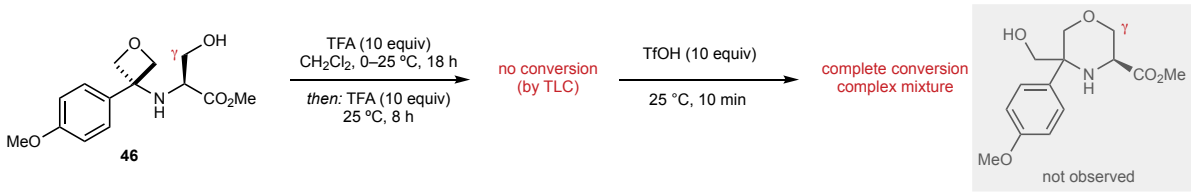


Figure 36. Colour-coded stability of aryl amino-oxetanes and benzamides at different pH values. See Table 14 for numerical values and Section **7.2** for experimental procedures.

Oxetanes with internal nucleophiles are known to degrade *via* intramolecular ring-opening, often exploited as an astute strategy to generate new heterocyclic scaffolds.[72,73] To probe this behaviour with amino-oxetanes, a preliminary experiment was conducted with oxetane-serine derivative **46**, which showed unexpected stability towards acidic conditions, being unreactive towards excess TFA (pK_a: 3.45 in DMSO)[287] after 26 h (Scheme 32; 10 equiv TFA, 18 h, then 20 equiv TFA, 8 h). Further addition of 10 equiv of highly acidic TfOH (pK_a: ca. –14 in DMSO)[288] led to complete degradation of amino-oxetane **46** to a complex product mixture. This preliminary result supports the hypothesis that the amine group serves as a proton sink and prevents acidic oxetane activation. By comparison, structurally related non-aminic γ-hydroxyl oxetane examples ring-opened quickly under catalytic amounts (5 mol%) of chiral phosphoric acids (pK_a: ca. 3.6 in DMSO).[73b,289]



Scheme 32. Preliminary investigation of the reactivity of amino-alcohol 46 under acidic conditions.

Increased 3-dimensionality is often associated with a higher aqueous solubility, important to ensure acceptable bioavailability of APIs.[60] In the last section, aryl amino-oxetanes were shown to adopt a more 3-dimensional conformation than related benzamides due to loss of π-conjugation, particularly evident in examples with low steric requirements.

Assessment of aqueous solubility of the eight MMPs showed an increase in solubility upon oxetane incorporation in almost every pair (Figure 37a). This trend was observed particularly at a low pH (3.0), likely owing to protonation of the amino-oxetane, see for example pair **110** which showed a solubility increase of +533 μM upon oxetane incorporation. The increase in solubility at neutral (7.4) and basic pH (10.0), although less pronounced, was still evident. It is notable that in pairs with two aromatic systems (*i.e.* **111**, **115**–**117**) the amino-oxetane scaffold always showed higher solubility and rescued the solubility of completely insoluble compounds such as **115b**–**117b**. Based on solid-state structures (Figures 34 and 35), this could be due to increased intermolecular π-interactions in benzamides (Ar rings 65 ° to each other in amide **109**) compared to amino-oxetanes (Ar rings 89 ° to each other in oxetane **106**).

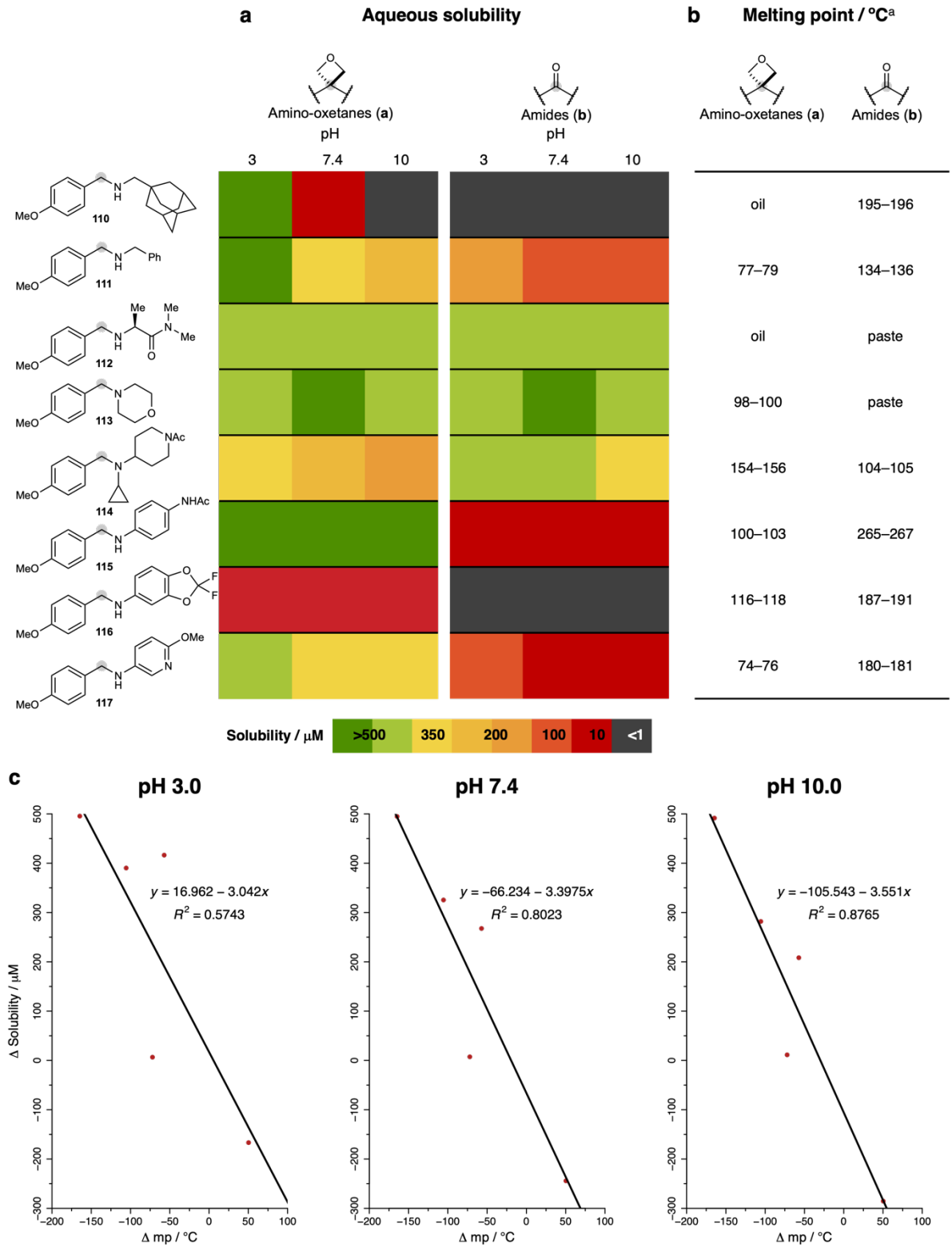


Figure 37. Aqueous solubility of MMPs. a, Colour-coded solubility of aryl amino-oxetanes and benzamides at different pH values. See Table 14 for numerical values and Section **7.2** for experimental procedures. **b**, Melting points of pairs. **c**, Correlation between difference in solubility (Δ Solubility) and difference in melting point (Δ mp) of relevant pairs at different pH values. [a] Melting points recorded by L. Blagojevic.

Further, there was good correlation between melting point and solubility (Figure 37b and c), a known behaviour to medicinal chemistry due to an increase in the energy required to overcome the enthalpy of fusion of higher-melting solids.[290] That is, within a pair, the compound with the lower melting point showed a higher solubility. The coefficient of determination R^2 increased with increasing pK_a due to influence of protonation at lower pH values, with a good R^2 of 0.8765 at pH 10. The increase in aqueous solubility of amino-oxetanes vs benzamides, despite the higher molecular weight and Log*D* (in most cases) of the former, may be ascribed to both the change in conformation and the marked polarity of oxetane scaffolds.

The eLog*D* of amino-oxetanes ranged between 1.0–4.9 (0.4–3.6 using the shake-flask {SF} method) with an average of 3.0 ± 1.5 (SF: 2.0 ± 1.2), lying under the Lipinski threshold (+5.0)[291] and the Ghose range (–0.4 to +5.6).[292] Compared to benzamides, amino-oxetanes were expected to show higher Log*D* values due to the two additional methylene groups (typically 0.3–0.5 increase in Log*D* upon introduction of a methyl group)[293] and the partial ionic character of benzamides conferred by resonance structures (N–C=O↔N^+=C–O^-). Previous work with 3,3-disubstituted oxetanes had shown a lipophilicity increase upon carbonyl-to-oxetane modification by +0.5 Log*D* units (spirocyclic amide–amino-oxetane)[97] and +0.2 Log*D* units (benzophenones–diaryl-oxetanes).[103] Here, the lipophilicity of the pairs showed a similar trend, with an ∆eLog*D* of –0.2 to +0.6 units (average ∆eLog*D* = +0.2 ± 0.3) upon oxetane introduction. Using the SF method, the difference in lipophilicity was more variable, with an ∆SFLog*D* of –0.6 to +0.5 units (average ∆SFLog*D* = 0.0 ± 0.4) upon oxetane introduction. Although somewhat pair- and method-specific, the general low magnitude of increase in Log*D* is notable, given the additional methylene groups and loss of resonance structures. It is likely that the pronounced polarity of the oxetane ring, conveyed by the small ring size (seen for example in HB acceptor strengths, see Figure 5), is responsible for the attenuated increase in lipophilicity. The assessed amino-oxetane scaffolds can be considered moderately lipophilic with Log*D* values that do not represent a systematic liability on their own, nor in comparison to benzamide analogues.

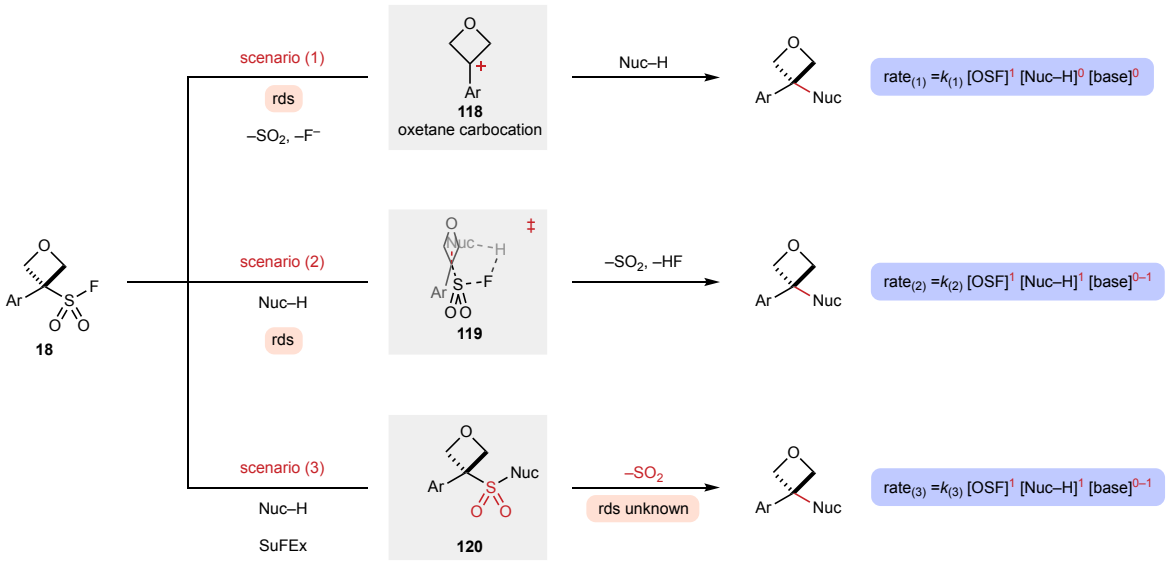
Lastly the metabolic clearance (HHEPG) of amino-oxetanes was similar to slightly higher than that of benzamides with some correlation to an associated increase in Log*D*, but no values were of significant concern (Table 14). Similarly, DOF IC_{50} inhibition[t] was within acceptable ranges (>5 μM) and posed no concern for cardiac toxicity.[294] Both of these values demonstrated that the amino-oxetane motif per se is neither a metabolic nor cardiotoxic liability.

The preliminary MMP study presented in this section is a promising start for the assessment of aryl amino-oxetanes as benzamide isosteres, and for the physicochemical evaluation of aryl amino-oxetanes as a new motif for drug discovery in their own right. The high polarity and 3-dimensionality of amino-oxetane scaffolds is pronounced in Log*D* values and particularly, in aqueous solubility, which was systematically higher than that of benzamides. The amino-oxetane motif was shown not to be a liability in regard to other relevant properties such as metabolic clearance, toxicity and most notably, chemical stability. Nevertheless, a larger dataset of pairs is needed to make statistically more relevant claims and recognise general trends. Further, comparing pK_a values of aryl amino-oxetane–benzylamine pairs would be of medicinal interest. According to previous measurements by Carreira and Roche, the oxetane should reduce the pK_a of adjacent amines by ca. two units.[70] Lastly, measuring the biological activity of oxetane drug analogues (*e.g.* Schemes 29–31) would be important to make a more meaningful statement on the *bio*isosterism of aryl amino-oxetanes.

[t] A competition binding assay between [^{3}H]dofetilide and the test compound in hERG-transfected cells as a measure of cardiac toxicity.

3.2.12 Mechanistic Investigations of Defluorosulfonylation

The defluorosulfonylative mode of reactivity of sulfonyl fluorides with nucleophiles was unprecedented, and it was hence of interest to investigate its mechanism. At the outset, three potential mechanistic scenarios for the defluorosulfonylation of oxetane sulfonyl fluorides were envisaged (Scheme 33): (1) an S_N1-type mechanism, with SO_2F^- as leaving group and the formation of an oxetane carbocation intermediate (**118**), which is then trapped by the nucleophile to generate the coupled oxetane products; (2) a concerted mechanism with the nucleophile involved in the TS of the defluorosulfonylation (**119**) and forming a partial bond with oxetane and an H–F bond with the sulfonyl fluoride part; (3) formation of an oxetane sulfonamide (**120**), followed by SO_2 extrusion to generate the SO_2-free coupled product.



Scheme 33. Potential mechanistic pathways of defluorosulfonylative coupling of OSFs (18).

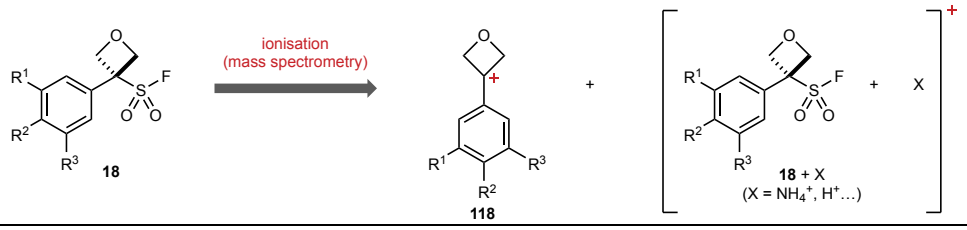
To discriminate between the three potential mechanistic pictures, focused control experiments were performed (*vide infra*), the kinetics of the reaction investigated (Section **3.2.12.1**) and a computational study was conducted in collaboration with the Duarte group at the University of Oxford (Section **3.2.12.2**). The kinetic data would generate information on the reaction rate and order of each component of the reaction, which would be different for each of the potential mechanistic pathways. For example, scenario (1) would show a reaction of order of 1 in OSF and 0 in all other components, scenario (2) an order of 1 in OSF, 1 in nucleophile and potentially 1 in base, and scenario (3) could show a positive reaction order in all components, depending on the slowest step of the process.

Several trends in reactivity already gave insight into the possible mechanistic scenario. The requirement of electron-rich aromatic functionality on oxetane for successful defluorosulfonylation (Scheme 24), formation of oxetane fluoride **35** in the absence of external

nucleophile (Table 6), observation of aldehyde **44** as side product (Table 6), and previous work on the dehydrative couplings of oxetane alcohols (Section **1.4.3.2**) hinted towards the involvement of an oxetane carbocation (scenario (1)). On the other hand, the superior yields observed with electron-poor amines over electron-rich examples (Section **3.2.8**) is rather suggestive of scenario (2), whereby more acidic NH protons could lower the energy of a concerted TS. Lastly, the detection of oxetane ether **32** in the mass spectrum of sulfonate ester **85** supported the possibility of an SO_2-extrusion pathway (scenario (3)).

The potential generation of mechanistically relevant intermediates upon ionisation, prompted an analysis of the mass spectra of OSFs (Table 15). Interestingly, all OSFs detected oxetane carbocation **118** in the mass spectrum and it was the base peak (*i.e.* the peak of highest intensity) in all examples that used a soft ionisation technique (APCI, CI, ESI; entries 1–7), suggestive of a relatively stable oxetane carbocation. Further, the mass spectrum of trimethoxy **18f** measured the highest relative intensity of the OSF molecular ion (**18f** + X; entry 7), in accordance with the lower reactivity of this OSF (see Scheme 24). This mass spectrometry study is an additional indication for the involvement of an oxetane carbocation and the S_N1 mechanistic pathway (scenario (1); Scheme 33).

Table 15. Ionisation products of OSFs **18**.

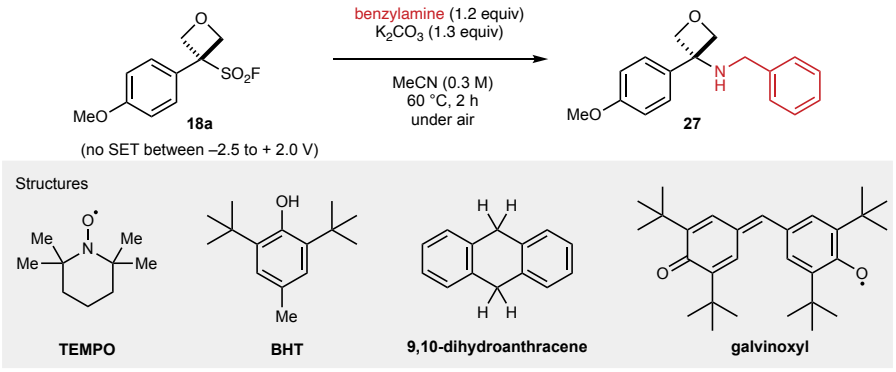


Entry	R^1	R^2	R^3	OSF (**18**)	Ionisation technique[a]	Ion intensity / %[b]	
						118	**18** + X
1	H	OMe	H	**a**	APCI	100	0
2	H	OTIPS	H	**c**	CI	100	1
3	H	O*i*Pr[c]	H	**o**	ESI	100	0
4	OMe	OMe[c]	H	**n**	APCI	100	0
5	OMe	OTIPS	H	**g**	APCI	100	0
6	*i*Pr	OTIPS	H	**h**	APCI	100	0
7	OMe	OMe	OMe	**f**	APCI	100	35
8	H	H	H	**m**	EI[d]	5[e]	1[f]

[a] APCI = Atmospheric Pressure Chemical Ionisation. CI = Chemical Ionisation. ESI = Electrospray Ionisation. EI = Electron Ionisation. [b] The peak with the highest intensity was normalised to 100%. [c] Synthesised by L. Briggs. [d] Hard ionisation technique. [e] Found with 10 ppm error. [f] Found with 17 ppm error.

The generation of oxetane carbocation **118** under radical ionisation conditions indicated the possibility of a fourth potential mechanistic scenario involving radical intermediates. Cyclic voltammetry (CV) measurements (Figure 27d) had shown OSF **18a** not to be ionisable within a synthetically useful potential range (–2.5 to + 2.0 V vs SCE), but control deFS reactions with radical trap additives were nevertheless carried out to unambiguously exclude the involvement of radical intermediates (Table 16). The reaction remained unaffected using TEMPO, BHT and 9,10-dihydroanthracene radical scavengers (entries 1–4). Solely with galvinoxyl, a reactive organic free radical, the yield of amino-oxetane **27** dropped to 40% (entry 5), but the reaction was not shut down entirely and OSF **18a** was consumed in all cases (<5%). Together with the CV measurements, these control experiments are a strong indication for the non-involvement of radical intermediates in the defluorosulfonylation of OSFs.

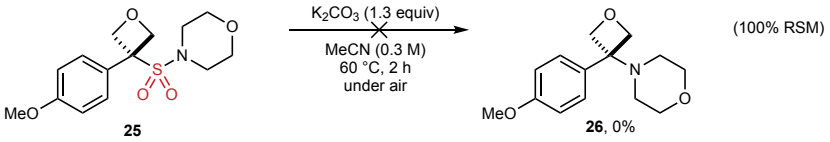
Table 16. Control experiments with radical scavenger additives.



Entry	Additive (1.0 equiv)	Yield / %[a]	
		27	**18a** (RSM)
1	none	94	0
2	TEMPO	87	3
3	BHT	98	3
4	9,10-dihydroanthracene	95	3
5	galvinoxyl	40	0

[a] Reactions run on a 0.1 mmol scale and yields calculated by analysis of the ^{1}H NMR spectrum of the crude mixture of the reaction using 1,3,5-trimethoxybenzene as internal standard. SET = Single Electron Transfer, TEMPO = 2,2,6,6-Tetramethylpiperidin-1-yl)oxyl, BHT = Butylated Hydroxy Toluene.

Lastly, oxetane sulfonamide **25** (see Section **3.2.9** for synthesis), the proposed intermediate of scenario (3), was subjected to the defluorosulfonylation conditions (Scheme 34; MeCN, 60 ºC, 2 h). Amino-oxetane **26** was not observed and 100% of sulfonamide **25** was recovered, ruling out scenario (3).



Scheme 34. Reactivity of sulfonamide 25 under the defluorosulfonylation conditions.

3.2.12.1 Kinetic Analysis

The defluorosulfonylative coupling of OSFs to amines was further investigated kinetically to gain a better understanding of the reaction and to determine the reaction order of each component. The reaction was conducted in a J. Young's NMR tube under Ar, with NEt_3 as a soluble base and in CD_3CN. The reaction mixture was heated inside the NMR probe and a ^1H NMR spectrum recorded every 30 s using mesitylene as internal standard (see Section **7.3** for experimental details). All operations associated with the NMR instrument (heating probe, locking, shimming…) were performed by P. Haycock from the NMR Spectroscopy Service from Imperial College London. The spectra were superimposed (see Figure 38 for an example), baseline and phase corrected, and the time-dependent integrals exported.

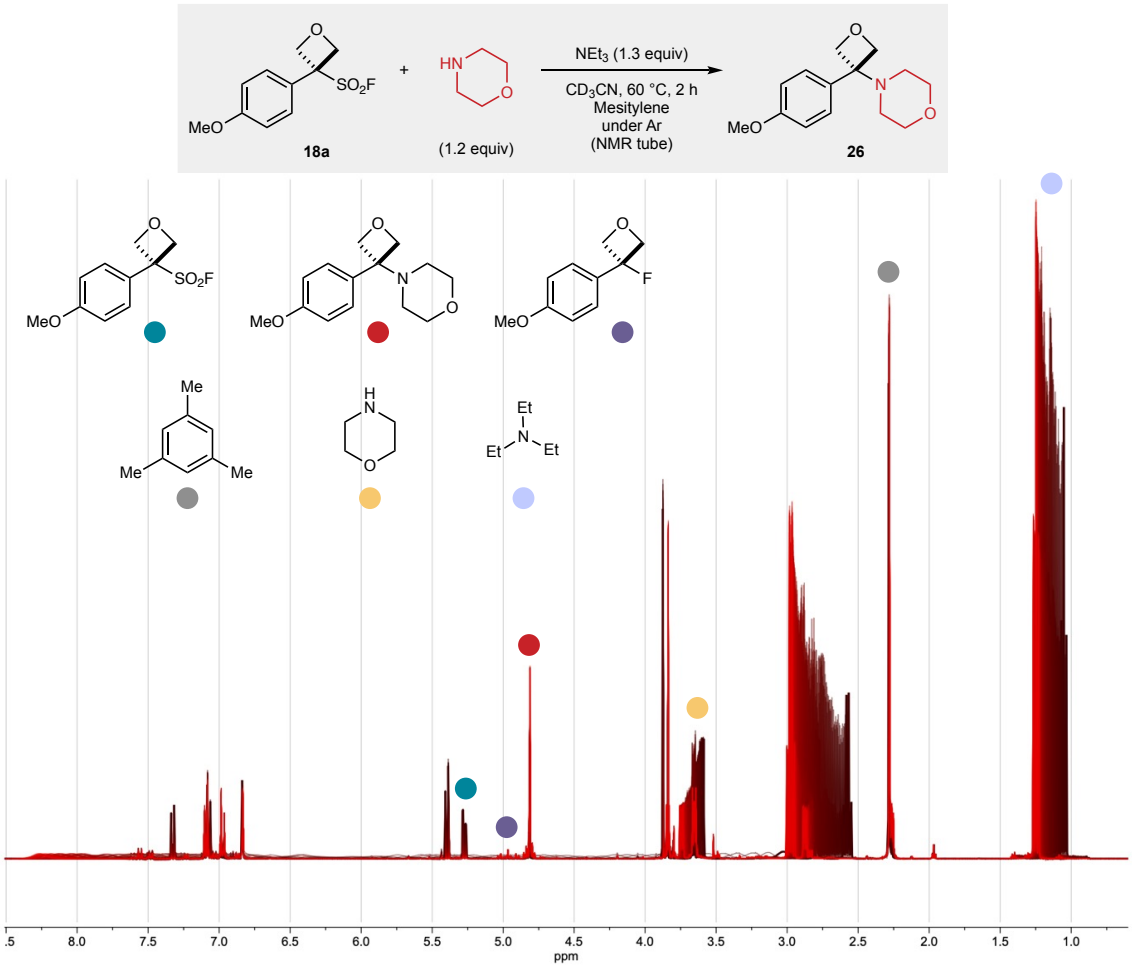


Figure 38. Time-dependent superimposed spectra in the reaction of OSF 18a with morpholine. The signals brighten as a function of time, *i.e.* early signals appear dark red (OSF **18a**) and late signals as bright red (amino-oxetane **26**).

The reaction profile for OSF **18a** + morpholine was recorded three times to ensure reproducibility (Figure 39). The rate of consumption of OSF (**18a**) was acceptably reproducible with a good overlay of the traces, but the rate of product (**26**) formation was somewhat variable. Hence, the rate of OSF consumption was used for quantitative analyses. Graphically, it can already be observed that the half-life $t_{1/2}$ of OSF **18a** remained unaffected throughout the progress of the reaction and was not influenced by the concentration of OSF, a strong indication for a first-order reaction, such as an S_N1-type mechanism (scenario (1)). $t_{1/2}$ of a first-order reaction is derived from the integrated rate-law to be:

$$t_{\frac{1}{2}} = \frac{\ln(2)}{k} ,$$

with k = the kinetic constant of the reaction.

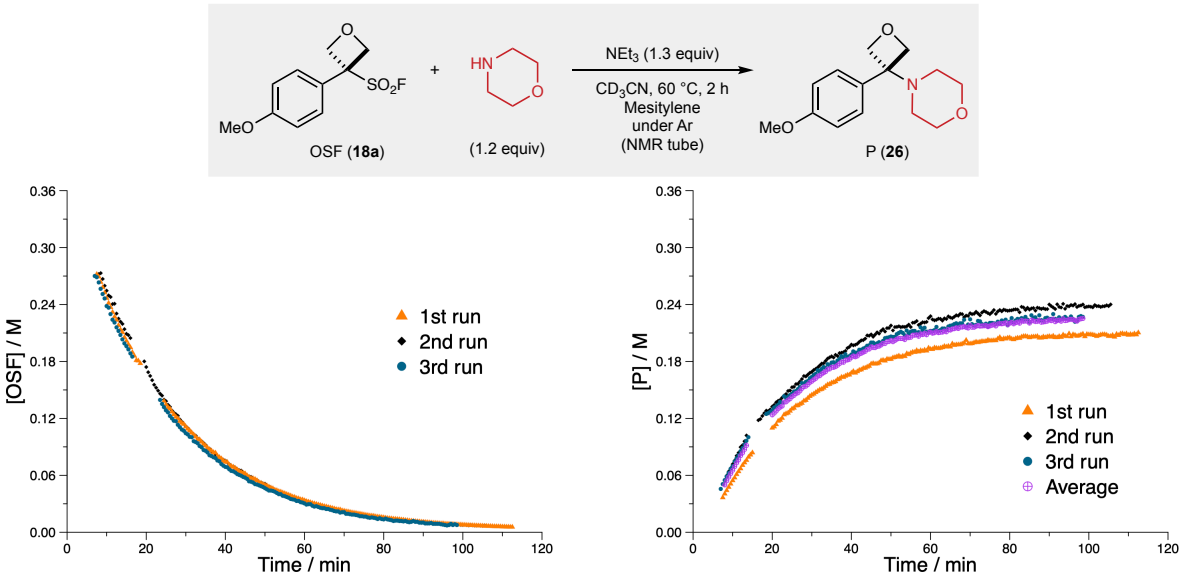


Figure 39. Monitoring of the reaction of OSF 18a with morpholine. *Left*: rate of consumption of OSF **18a**. *Right*: rate of product formation (**26**). The data of OSF consumption from the '1st run' were used for further quantitative analyses. The average of the three traces of product formation was taken for further qualitative illustrations.

Trimethoxy OSF **18f** had been shown in the previously described synthetic studies (Section **3.2.8**) to react much more slowly than the rest of OSFs. The reaction rates of monomethoxy OSF **18a**, dimethoxy OSF **18n** and trimethoxy OSF **18f** were measured by ^{1}H NMR and compared (Figure 40). As expected, the rate of consumption of trimethoxy OSF **18f** was slowest, but dimethoxy OSF **18n** reacted quicker than monomethoxy **18a**. This behaviour was rationalised with help of a conformational and computational analysis and will be discussed in the next section.

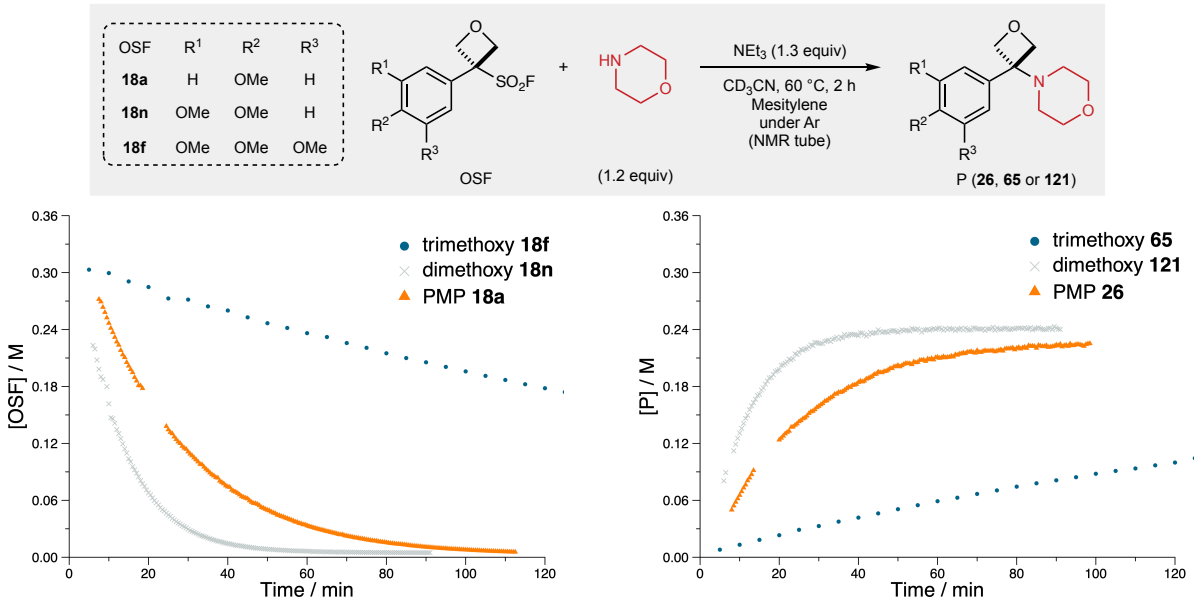


Figure 40. Monitoring of the reaction of OSF 18a, 18f and 18n with morpholine. *Left*: rate of consumption of OSF. *Right*: rate of product formation.

Then, the rate of reaction of OSF **18a** with different nucleophiles was compared (Figure 41). The first and most important observation is that the rate of OSF consumption stayed unaffected by the choice of nucleophile (Figure 41a), but the rate of product formation varied significantly across nucleophiles, even considering potential variability (Figure 41b). This qualitative evaluation is supportive of a two-step process, whereby the OSF is consumed in a rate-determining step, independent of the nucleophile, to an intermediate that then reacts in a second step with, and is influenced by, the nucleophile. Scenario (1) (Scheme 33) represents such a situation: the oxetane sulfonyl fluoride forms an oxetane carbocation in a rds, followed by trapping of the carbocation by the nucleophile in a rapid *chemo-determining* step.

Further, the difference in amounts of amino-oxetane formed with different nucleophiles was not reflected on the quantities of oxetane fluoride **35** (Figure 41b vs 41c). For example, amino-oxetane formation with aniline (yellow line, Figure 41b) was much higher than with methyl-benzylamine (green line, Figure 41b), but the amounts of oxetane fluoride **35** formed were comparable (yellow vs green line, Figure 41c). Such a discrepancy is indicative of a parallel, competitive degradation process, likely *via* elimination of the oxetane carbocation to an unstable oxetene (**123**), which can further degrade to a variety of species. One such compound was identified in the reaction without exogenous nucleophile, as aldehyde **44**, possibly formed by hetero-electrocyclic ring opening (Scheme 35). Supportive of this hypothesis was the higher amount of oxetane fluoride **35** formed in the absence of base compared to with base (blue vs black line, Figure 41b and 41c). Basic conditions can be prone to promote the elimination pathway and/or trap the fluoride ions as $HNEt_3F$.

Lastly, the base-controlled reactivity of OSFs with phenols to form either oxetane ethers or -sulfonate esters (Section 3.2.9) was also monitored by ^{1}H NMR with NEt_3 as base (Figure 41d). Unchanged from the outcome in-flask (Figure 28c), mostly oxetane ether **32** was formed with NEt_3 in the NMR tube. Sulfonate ester **85** formed rapidly early in the reaction and kept a constant concentration after ca. 10 minutes. Reduction in the total mass balance of the reaction (green line, Figure 41d) further supports the involvement of a degradative pathway.

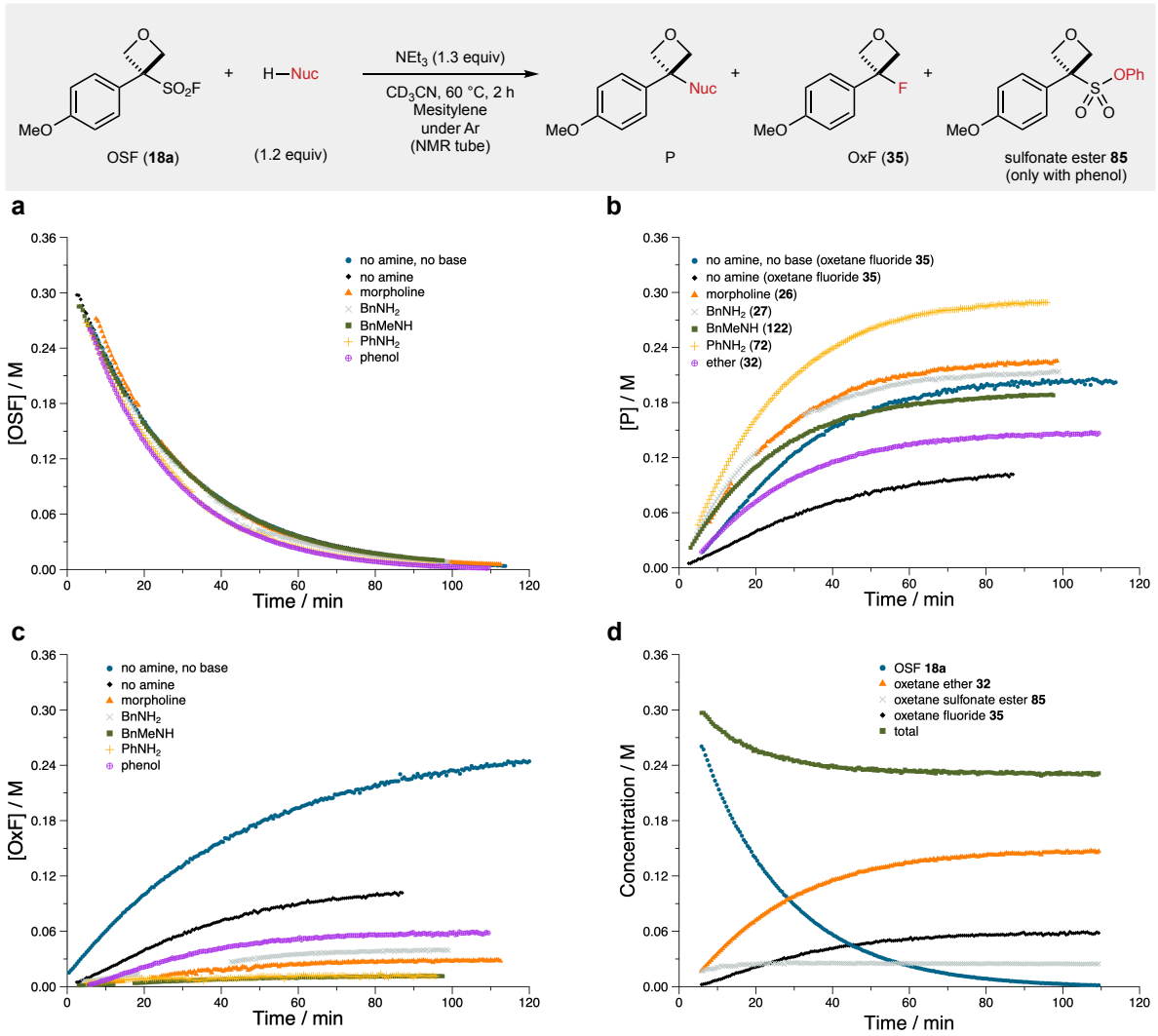
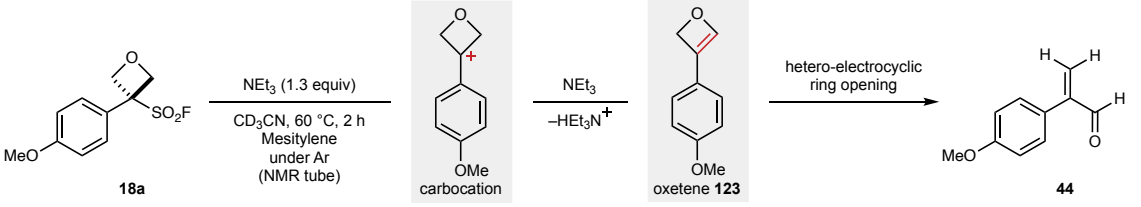
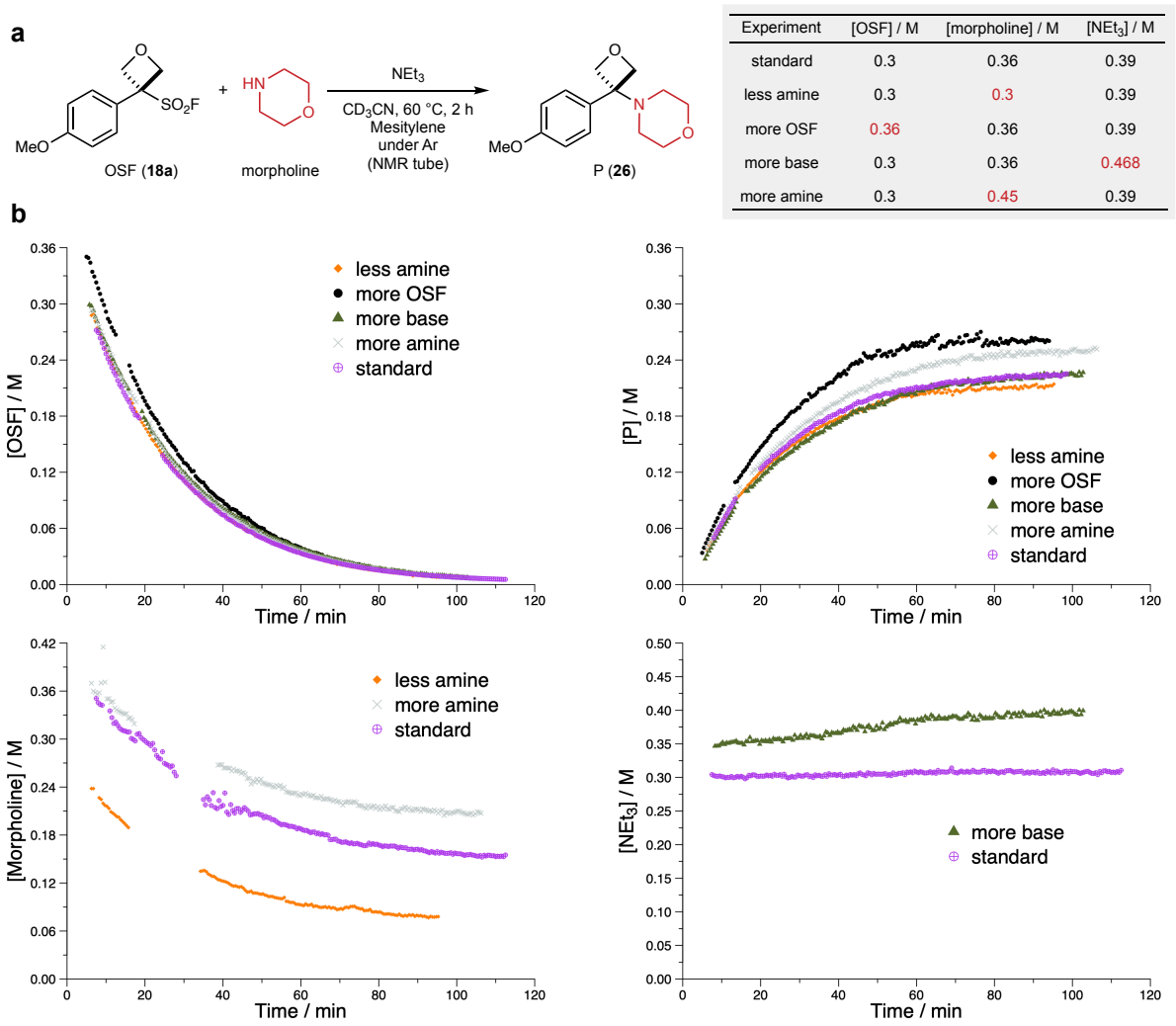


Figure 41. Rates of reaction of OSF 18a with different nucleophiles. a, Rate of consumption of OSF **18a**. **b**, Rate of product formation. **c**, Rate of formation of oxetane fluoride **35**. **d**, Reaction of OSF **18a** with phenol.



Scheme 35. Potential pathway for the formation of aldehyde 44 in the absence of nucleophile. Aldehyde **44** was identified by the diagnostic alkene and aldehyde signals in the ^{1}H NMR spectrum of the reaction mixture.[212,295] Aldehyde **44** could not be isolated due to its instability to silica.

Recent fundamental kinetic work by Burés has enabled the convenient determination of reaction orders by simple intuitive visual analysis of traces from reaction monitoring in a process termed Visual Time Normalisation Analysis (VTNA).[296] VTNA was performed on the defluorosulfonylation reaction using OSF **18a** and morpholine as nucleophile, and only required four (additional) reactions which varied the amount of each reaction component (see Figure 42 for unprocessed traces).



Experiment	[OSF] / M	[morpholine] / M	[NEt_3] / M
standard	0.3	0.36	0.39
less amine	0.3	0.3	0.39
more OSF	0.36	0.36	0.39
more base	0.3	0.36	0.468
more amine	0.3	0.45	0.39

Figure 42. Experiments performed for VTNA analysis. a, General reaction scheme and quantities used. **b**, Mathematically unprocessed traces. The traces of the 'standard' reaction represent the values of the 'first run' in Figure 38.

To determine the orders, following Burés' protocol,[296b] the following term was plotted in the *x*-axis:

$$\sum_{i=1}^{n}\left(\frac{[\mathrm{A}]_i + [\mathrm{A}]_{i-1}}{2}\right)^{\alpha}(t_i - t_{i-1}),$$

whereby *n* represents the number of collected data points, [A,B,C…] the concentration of the reaction component to be analysed (A,B,C…), α,β,γ… the reaction order of the corresponding

component, and t the time at which each measurement i was collected. The mathematically manipulated data were plotted for each component separately using the traces of the 'different excess' experiments (Figure 42). Plots for different reaction orders (α,β,γ…) were generated and compared visually, whereby the best overlay of the traces of 'different excesses' indicated the most probable reaction order.

The analysis was commenced with the different excesses of OSF **18a**, which was guaranteed to have a positive reaction order. Since the analysis was performed on the consumption of OSF **18a**, the values of the trace of 'more OSF' were modified artificially for the first value to match the 'standard' trace, as recommended by Burés (Figure 43a).[296c]

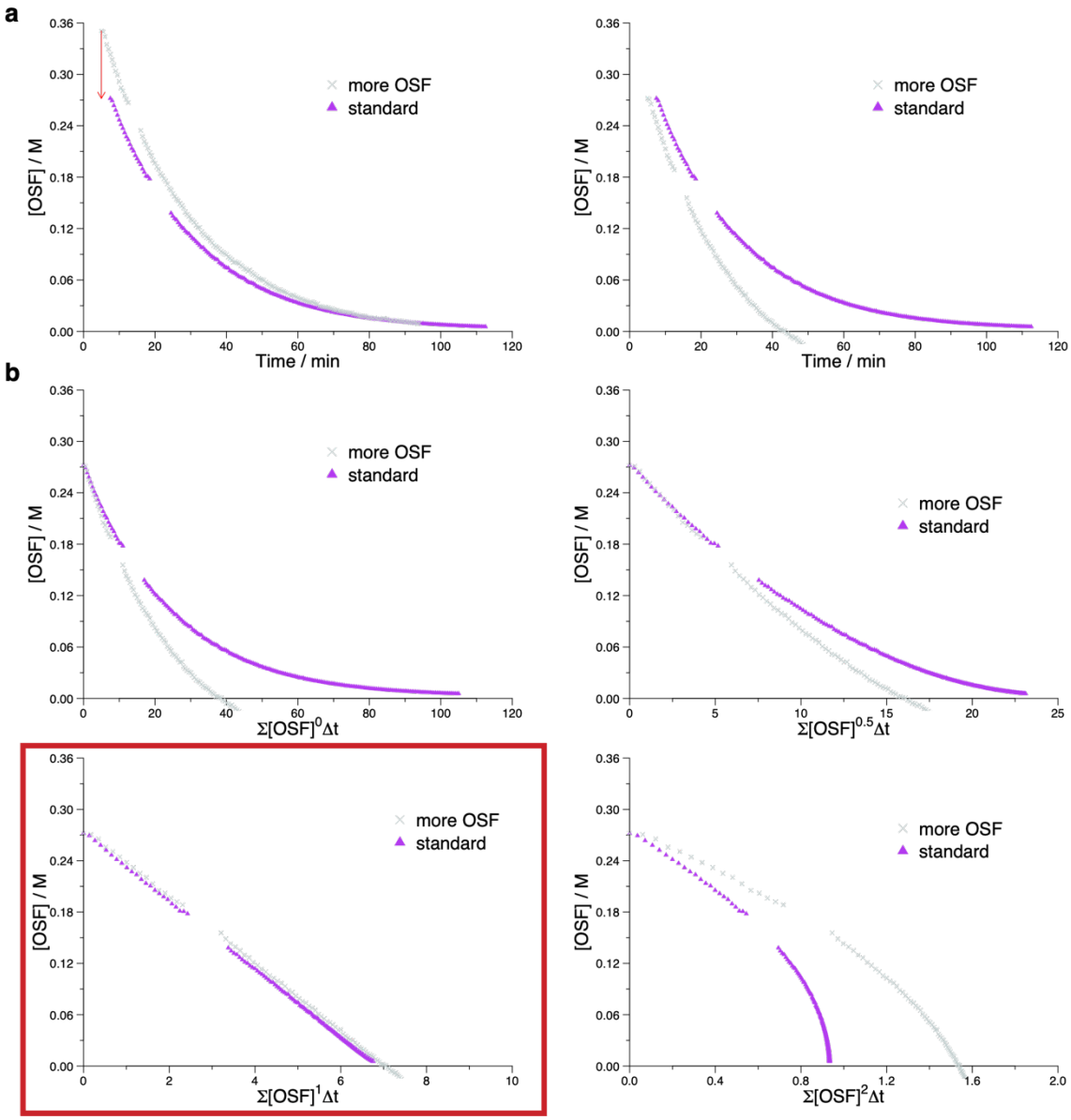


Figure 43. Determination of order in OSF by VTNA. a, Manipulation of the trace of 'more OSF' to match the standard value of the 'standard' trace. **b**, VTNA of different reaction orders in OSF. Orders shown in the exponent of the x-axis and best overlay shown in red box.

With this manipulation, overlaid curves, as opposed to parallel ones, were obtained using the right reaction order and facilitated visual analysis. VTNA clearly suggested a reaction order of 1 in OSF and the linearisation of the curve at this reaction order is indicative of a first-order reaction, dependent only on the concentration of OSF (Figure 43b).

As already implied by all previous observations, the reaction order was determined to be zero in both amine and base (Figures 44 and 45, respectively).

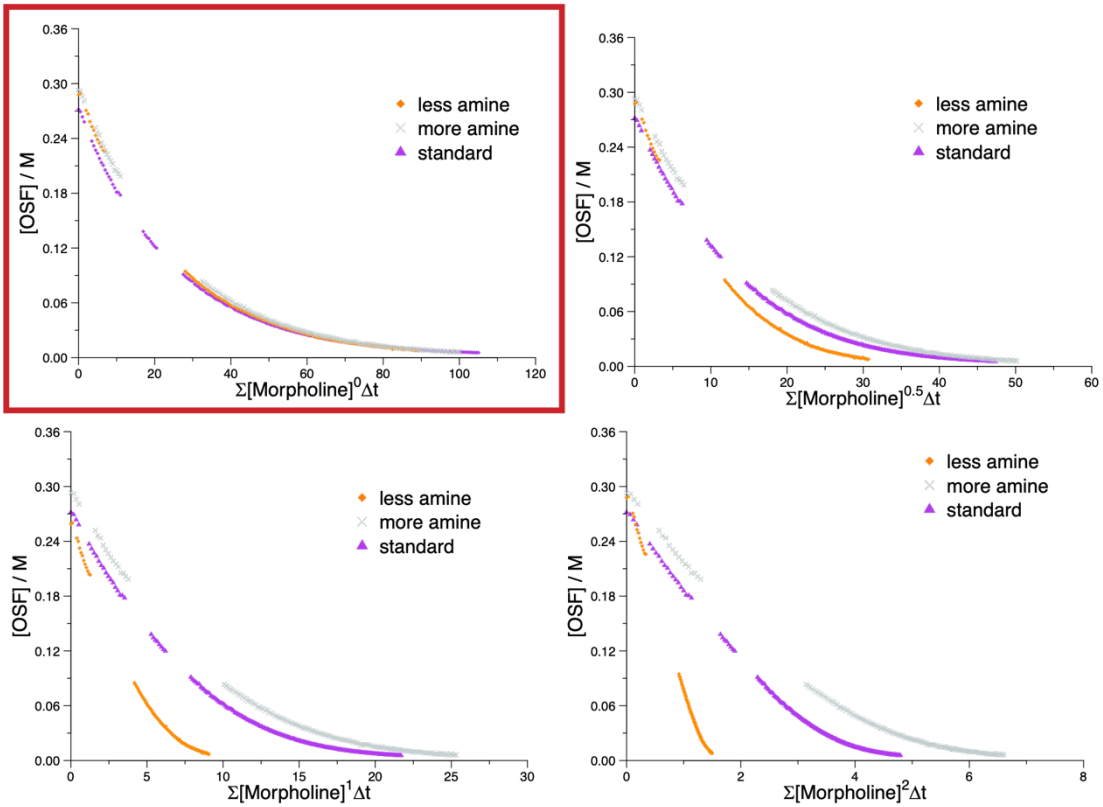


Figure 44. Determination of order in amine by VTNA. Orders shown in the exponent of the x-axis and best overlay shown in red box.

While with amines the best overlay was indisputably zero-order, the analysis in base was less clear-cut. Since the equilibrium between protonated and deprotonated forms of the base is quicker than the NMR time-scale, only an average of both species is seen in the ^{1}H NMR spectra, according to the regime of fast exchange given by the Bloch–McConnell equations.[297] Thus, the concentration of base by ^{1}H NMR ([NEt_3]) stayed quasiconstant throughout the reaction (Figure 42b) and the shape of the curve plotting the VTNA term on the *x*-axis was barely influenced by the reaction order (Figure 45). Nonetheless, the overlay worsened by deviating from a 0th order and all previous observations are supportive of a first-order reaction, *i.e.* 0-order in base.

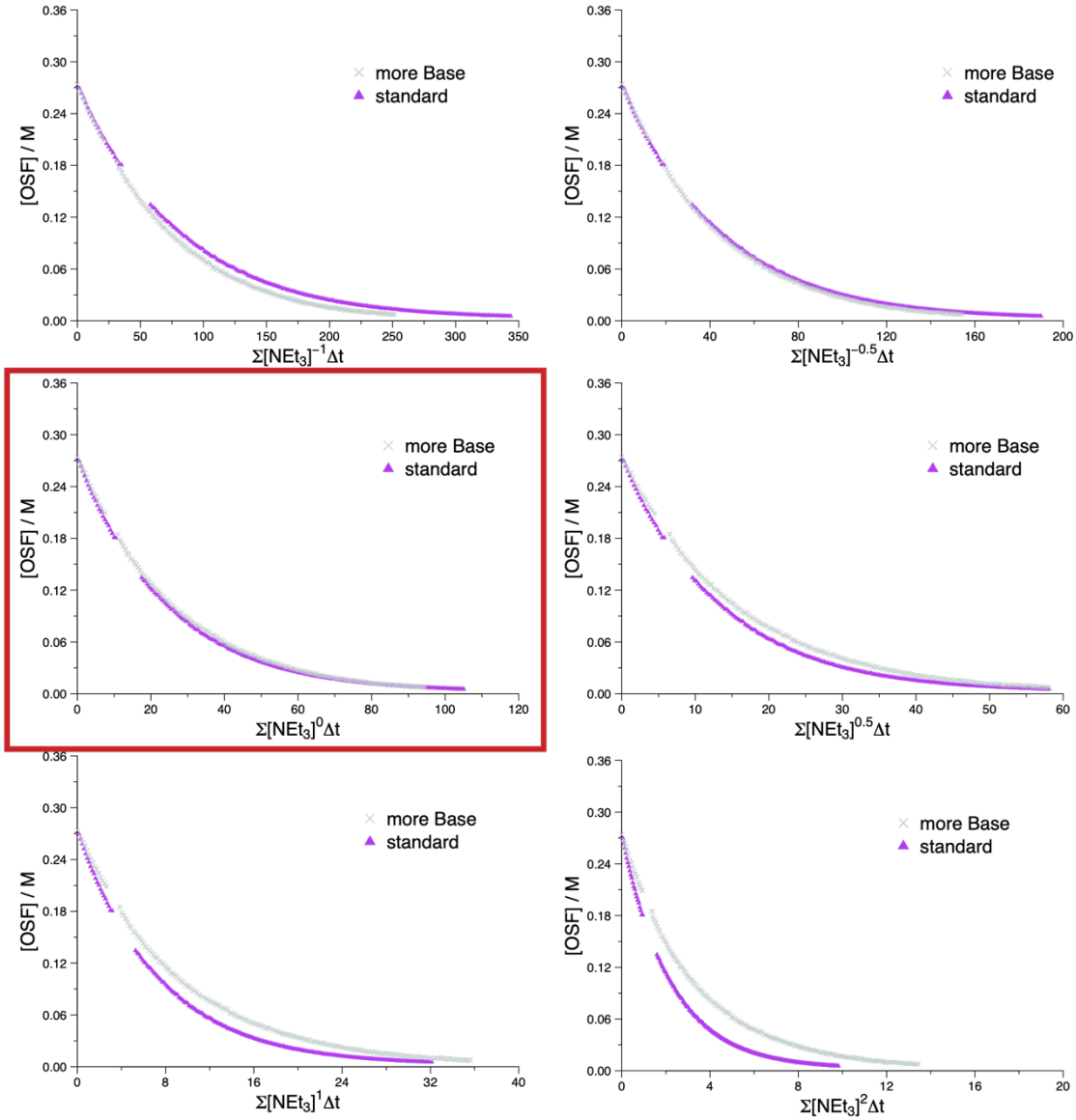


Figure 45. Determination of order in base by VTNA. Orders shown in the exponent of the x-axis and best overlay shown in red box.

VTNA determined the most likely reaction order in OSF (1), amine (0) and base (0) (Figures 43–45). The observed kinetic constant (k_{Obs}) of the rds of the defluorosulfonylation reaction was then calculated by including all components with their respective reaction orders into Burés' equation:

$$\sum_{i=1}^{n}\left(\frac{[\mathrm{OSF}]_i+[\mathrm{OSF}]_{i-1}}{2}\right)^{1}\left(\frac{[\mathrm{amine}]_i+[\mathrm{amine}]_{i-1}}{2}\right)^{0}\left(\frac{[\mathrm{NEt_3}]_i+[\mathrm{NEt_3}]_{i-1}}{2}\right)^{0}(t_i-t_{i-1}),$$

and plotting these against the consumption of OSF (Figure 46). Note that due to the 0th order in amine and base, the sum becomes identical to that used in the VTNA of OSF (Figure 43b):

$$\sum_{i=1}^{n}\left(\frac{[\mathrm{OSF}]_i + [\mathrm{OSF}]_{i-1}}{2}\right)^1 (t_i - t_{i-1})\,.$$

The absolute value of the slope of the curves, modelled by linear regression, equals k_{Obs}. Similar k_{Obs} values obtained from the different 'excesses' are indicative for a correctly derived rate law of the reaction (rate = k [OSF]^1 [amine]^0 [base]^0), which corresponds to the kinetics associated with an S_N1 mechanism (mechanistic scenario (1)). Non-perfect overlay of the curves is due to slight discrepancies in the starting value of [OSF], caused by slightly different time requirements of locking and shimming for each NMR experiment.

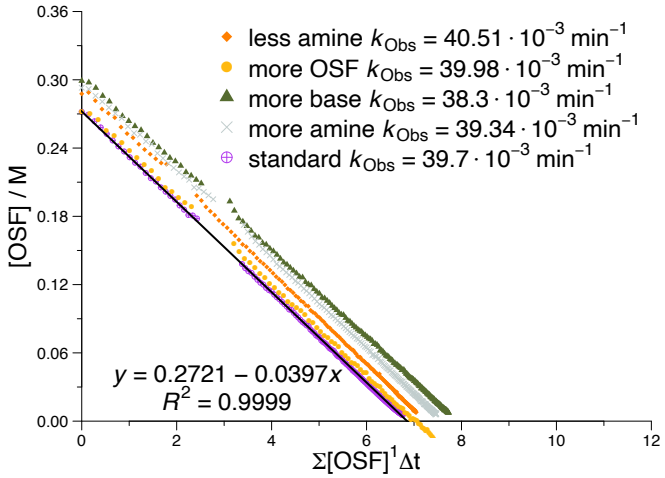


Figure 46. Determination of k_{Obs} by VTNA. Slope = $-k_{Obs}$. Equation for the modelled linear regression and the coefficient of determination R^2 are given for the 'standard' reaction conditions (purple line).

Next, the activation energy E_A of the defluorosulfonylation was determined through a standard Arrhenius approach. The kinetic constants k_{Obs} at two additional temperatures (40 and 70 °C) were calculated *via* VTNA using the derived rate law (Figure 48a), as described above. Unsurprisingly, the defluorosulfonylation was faster at 70 and slower at 40 °C (Figure 47).

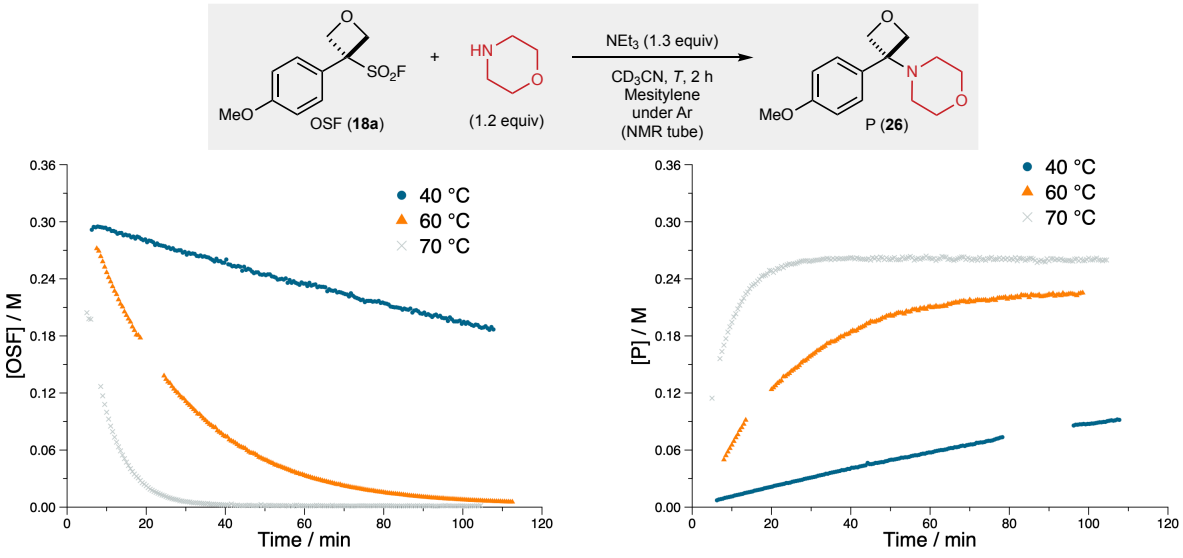


Figure 47. Rates of reaction of OSF 18a with morpholine at different temperatures (*T*).

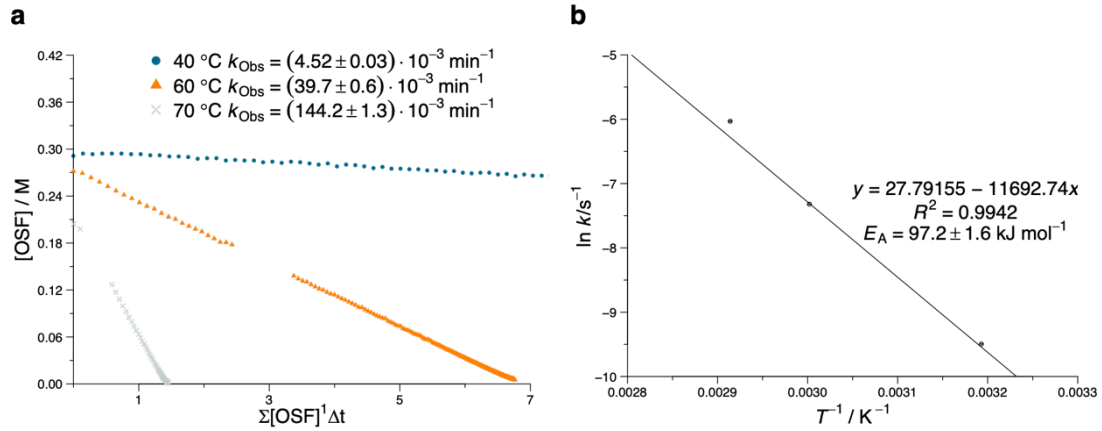


Figure 48. Determination of activation energy E_A. a, Calculation of k_{Obs} by VTNA. **b**, Arrhenius plot and modelled weighed linear regression with equation and R^2 given. E_A calculated from the slope of the linear regression and error corresponds to the 95% CI (n = 3).

The k_{Obs} values are given with their 95% CI (±), determined from the standard deviation of the modelled linear regression s and the student factor t_s at 95% confidence with ν degrees of freedom ($\nu = n–2$)[u]:

$$\mathrm{CI}_{0.95} = s \cdot t_s \,.$$

The ln(k_{Obs}) values were then plotted against T^{-1} and E_A calculated from the slope of a modelled linear regression on the datapoints (Figure 47b), according to Arrhenius[298]:

$$\textbf{Arrhenius equation: } \ln(k) = \ln(A) - \frac{E_A}{R}\left(\frac{1}{T}\right),$$

whereby A corresponds to a pre-exponential factor and R to the universal gas constant. Since the k_{Obs}, and by implication also the ln(k) values, have an associated uncertainty, a weighed linear regression was modelled on the Arrhenius plot to take errors into account and give more weight to ln(k) values with a lower uncertainty. The standard deviations of ln(k) values ($s_{\ln(k)}$) were calculated from the determined standard deviations of k_{Obs} data with the Gaussian formula for error propagation:

$$s_z^2 = \left(\frac{\partial f}{\partial a}\right)^2 s_a^2 + \left(\frac{\partial f}{\partial b}\right)^2 s_b^2 + \left(\frac{\partial f}{\partial c}\right)^2 s_c^2 + \cdots,$$

with s_z^2 being the squared standard deviation of the new function z ($f(a,b,c,\ldots)$), dependent from the variables a,b,c… and s_a^2, s_b^2, s_c^2 … the associated squared standard deviations. In this

[u] For a linear regression, only n–2 terms are independent (as opposed to the usual $\nu = n–1$) since both the intercept and the slope depend on the x and y values.[254]

case, there is only one variable ($a = k_{Obs}$), and the new function z corresponds to the natural logarithm of k_{Obs} ($z = \ln(k_{Obs})$), simplifying the standard deviation of $\ln(k)$ to:

$$s^2_{\ln(k)} = \left(\frac{\partial(\ln(k))}{\partial k}\right)^2 s_k^2 = \left(\frac{1}{k}\right)^2 s_k^2 = \frac{s_k^2}{k^2}$$

$$s_{\ln\,(k)} = \frac{s_k}{k}.$$

The intercept a and slope b of the weighed linear regression were calculated using the conventional Gaussian method of smallest squares, with the equations below:[v,254,299]

$$intercept\ a = \frac{\sum_{i=1}^{n} \frac{x_i^2}{s_i^2} \sum_{i=1}^{n} \frac{y_i}{s_i^2} - \sum_{i=1}^{n} \frac{x_i}{s_i^2} \sum_{i=1}^{n} \frac{x_i y_i}{s_i^2}}{\sum_{i=1}^{n} \frac{1}{s_i^2} \sum_{i=1}^{n} \frac{x_i^2}{s_i^2} - \left(\sum_{i=1}^{n} \frac{x_i}{s_i^2}\right)^2}$$

$$slope\ b = \frac{\sum_{i=1}^{n} \frac{1}{s_i^2} \sum_{i=1}^{n} \frac{x_i y_i}{s_i^2} - \sum_{i=1}^{n} \frac{x_i}{s_i^2} \sum_{i=1}^{n} \frac{y_i}{s_i^2}}{\sum_{i=1}^{n} \frac{1}{s_i^2} \sum_{i=1}^{n} \frac{x_i^2}{s_i^2} - \left(\sum_{i=1}^{n} \frac{x_i}{s_i^2}\right)^2}.$$

Note that the smallest square method is also the typical method used to model non-weighed linear regressions with unknown standard deviations ($s_i = 1$). In this case, s_i was known ($s_i = s_{\ln(k)}$), so it was imputed explicitly into the above equations. By means of the Gaussian formula for error propagation introduced above, the standard deviation for intercept and slope, and the related correlation coefficient R^2, were calculated:[v]

$$s_a^2 = \frac{\sum_{i=1}^{n} \frac{x_i^2}{s_i^2}}{\sum_{i=1}^{n} \frac{1}{s_i^2} \sum_{i=1}^{n} \frac{x_i^2}{s_i^2} - \left(\sum_{i=1}^{n} \frac{x_i}{s_i^2}\right)^2},$$

$$s_b^2 = \frac{\sum_{i=1}^{n} \frac{1}{s_i^2}}{\sum_{i=1}^{n} \frac{1}{s_i^2} \sum_{i=1}^{n} \frac{x_i^2}{s_i^2} - \left(\sum_{i=1}^{n} \frac{x_i}{s_i^2}\right)^2},$$

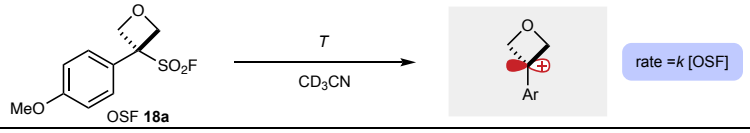
[v] Equations not derived here explicitly but used directly from known tabulated solutions.[254,299]

$$R^2 = \left(\frac{\sum_{i=1}^{n} \frac{1}{s_i^2} \sum_{i=1}^{n} \frac{x_i y_i}{s_i^2} - \sum_{i=1}^{n} \frac{x_i}{s_i^2} \sum_{i=1}^{n} \frac{y_i}{s_i^2}}{\sqrt{\sum_{i=1}^{n} \frac{1}{s_i^2} \sum_{i=1}^{n} \frac{x_i^2}{s_i^2} - \left(\sum_{i=1}^{n} \frac{x_i}{s_i^2} \right)^2} \sqrt{\sum_{i=1}^{n} \frac{1}{s_i^2} \sum_{i=1}^{n} \frac{y_i^2}{s_i^2} - \left(\sum_{i=1}^{n} \frac{y_i}{s_i^2} \right)^2}} \right)^2 .$$

The activation energy E_A of the reaction was then calculated from the slope of the linear regression (Figure 48b), as per the empirical Arrhenius relationship (*vide supra*). The calculated E_A of 97.2 ± 1.6 kJ mol^{-1} (23.2 ± 0.4 kcal mol^{-1}) correlated well with experimental reactivity (60 ºC, 2 h). Note the relatively large error of 1.6 kJ mol^{-1} due to the small sample size (n = 3, ν = 1).

With three experimentally determined k_{Obs} values (40, 60, 70 ºC) and the thereof derived Arrhenius terms (A and E_A), the half-life $t_{1/2}$ of OSF **18a** at different temperatures was calculated (Table 17). The small dataset used for the determination of $t_{1/2(25\,°C)}$ (n = 3) and the errors associated with the variables A and E_A led to the higher error of 30 days observed for $t_{1/2(25\,°C)}$. The reactivity window of OSF **18a** make it a convenient reagent for synthetic chemistry: bench-stable at 25 ºC ($t_{1/2}$ ≈ 40 days), but reactive upon mild thermal activation to 60 ºC ($t_{1/2}$ ≈ 18 min).

Table 17. Kinetically relevant values of the OSF defluorosulfonylation given with the 95% CI. Standard deviations were calculated with the Gaussian formula of error propagation.



T / ºC	A / s^{-1}	E_A / kJ mol^{-1}	k / 10^{-3} min^{-1}	$t_{1/2}$
independent	27.8 ± 0.6	–	–	–
independent	–	97.2 ± 1.6	–	–
70	–	–	144.2 ± 1.3	4.81 ± 0.04 min
60	–	–	39.7 ± 0.6	17.46 ± 0.03 min
40	–	–	4.52 ± 0.03	153.4 ± 0.9 min
25	–	–	0.011 ± 0.007[a]	(4 ± 3) × 10^1 days

[a] Derived from the Arrhenius equation (Figure 48b)

3.2.12.2 Computational Studies

The NMR experiments described in the previous section showed the defluorosulfonylation of OSFs to proceed under first-order kinetics, with a reaction order of one in OSF and zero in all other components. Further experimental evidence such as the requirement of electron-rich aromatics on oxetane, the reactivity with nucleophiles and the isolation of side products (*e.g.* aldehyde **44**) were indicative of an S_N1 mechanism with the rate-determining formation of an oxetane carbocation. Diverse product distributions with different nucleophiles were suggestive of a chemo-determining carbocation-trapping step by the nucleophile to form the coupled product. To gain a better fundamental understanding of the oxetane carbocation and to elucidate the driving force for the defluorosulfonylative reactivity and role of the oxetane structures, computational studies were performed in collaboration with the Duarte group (University of Oxford). Quantum mechanical calculations were performed on ORCA software (4.1.1)[300] and used variable levels of theory depending on the experiment (given separately in the caption of the relevant figures). The results of this study, which was conducted by A. Sterling and F. Duarte, will be analysed and presented in this section.[w] Details of the computation experiments, raw computational data and cartesian coordinates can be found in ref. 212 and at the Imperial College London Research Data Repository.[301]

First, the structure and conformation of the central oxetane carbocation were investigated. Two structures were considered: a planar geometry with the positive charge stabilised by aromatic resonance, and a bicyclic form stabilised by the oxygen lone pairs, akin to the related aza-analogue 1-azabicyclo[1.1.0]butane, an established strain-release reagent.[302] Interesting trends were observed on oxetane carbocations with different substitution patterns in the 3-position (Figure 49a).

[w] The computations were performed by A. Sterling and F. Duarte. The analysis of the results was conducted collaboratively between A. Sterling, F. Duarte, J. Bull and myself.

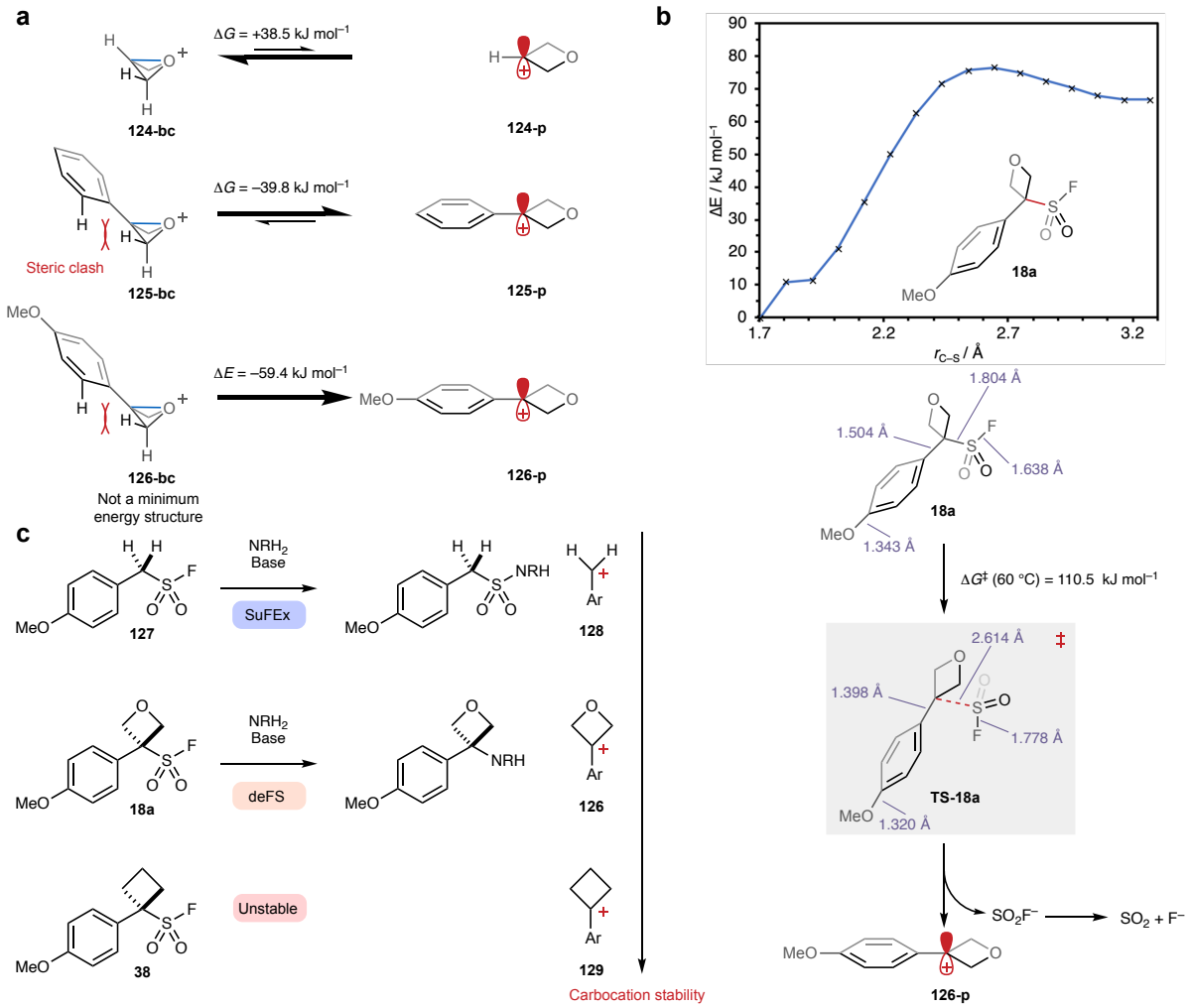


Figure 49. Computational study of oxetane defluorosulfonylation. a, Structure of oxetane carbocations. Optimisations and numerical frequency calculations of the planar and bicyclic forms of cations **124**, **125** and **126** were carried out at the SMD[303](MeCN)-RI-SCS-MP2[304]/def2-TZVP[305] level of theory (RI = resolution of identity approximation), followed by single-point energy corrections at the SMD(MeCN)-DLPNO-CCSD(T)[306]/def2-TZVPP (TightPNO) level of theory. **b**, Relaxed scan of the breaking of the C–S bond in **18a** and schematic representation of the ionisation process, including the geometry of **TS-18a**. Scan calculated at the [SMD(MeCN)-ωB97X-D3/def2-SVP (ma-def2-SVP on fluoride)] level of theory and graph generated by A. Sterling. Free energy evaluated at the [SMD(MeCN)-DLPNO-CCSD(T)/def2-TZVPP, (ma-def2-TZVPP on F)//SMD(MeCN)-ωB97X-D3[307]/def2-SVP (ma-def2-SVP on F)] level of theory. **c**, Schematic correlation between sulfonyl fluoride reactivity and carbocation stability.

Unsubstituted oxetane **124** (*i.e.* 3-H) preferred the bicyclic conformation over the planar one by 38.5 kJ mol^{-1} (at 25 ºC) with carbocation stabilisation through the transannular bond. 3-Phenyl carbocation **125** on the other hand, showed a stark preference for the planar conformation (**125-p**) due to unfavourable filled-filled orbital interactions in the bridged conformation **125-bc** between the *ortho* C–H bonds and the oxetane CH_2's ($\Delta G_{(25\,°C)}$ = 39.8 kJ mol^{-1}). The phenyl ring also provided additional resonance stabilisation of the carbocation in the planar conformation **125-p** by delocalisation of positive charge into the aromatic ring—not present in bicycle **125-bc** due to distortion of the aromatic

($\Delta E^{(2)}_{\pi(\text{planar})\rightarrow\pi(\text{bicyclic})}$ = –285 kJ mol^{-1}).[x] The more electron-rich and OSF-relevant 3-*p*-methoxyphenyl substituent showed an even higher preference for the planar- over the bicyclic conformation ((ΔG = 59.4 kJ mol^{-1}). In fact, the bicyclic conformation **126-bc** was not a minimum energy structure and its energy was determined by constraining the length of the C–O bond to that of **126-bc** (1.673 Å). An energetic comparison to phenyl carbocation **125** revealed the additional stabilisation by the *p*-OMe aromatic substituent to be worth ca. 25 kJ mol^{-1}, in accordance to the difference in resonance stabilisation ($\Delta\Delta E^{(2)}_{\pi(\text{planar})\rightarrow\pi(\text{bicyclic})}$ = +17 kJ mol^{-1}).

With an optimised geometry for carbocation **126** (**126-p**), the ionisation process was investigated. A scan of the elongation of the C–S bond in OSF **18a** revealed the TS structure **TS-18a** for the defluorosulfonylation at a C–S bond length of 2.614 Å (Figure 49b). Definitive breaking of the bond generated oxetane carbocation **126-p** and an SO_2F^- anion, which subsequently fragmented into SO_2 and F^- in a stepwise process. The S–F bond length also increased during the process (1.778 Å in **TS-18a**) but was not broken synchronously to the C–S bond. Partial double bond character between aromatic and carbocation was also observed in **TS-18a**, reflected on C–C and C–O bond lengths. Automatic location of a concerted TS using the *autodE* package[308] did not reveal any energetically favourable solutions. The rate of the ionisation was controlled by the stability of the carbocation and the $\Delta G^{\ddagger}$ (free energy barrier) of the defluorosulfonylation was calculated to be 110.5 kJ mol^{-1}.

The difference in reactivities observed between oxetane sulfonyl fluoride **18a**, cyclobutane sulfonyl fluoride (CSF) **38** and (*p*-methoxyphenyl)methanesulfonyl fluoride **127** suggested a potential correlation to the stability of the corresponding carbocations (Figure 49c). Primary sulfonyl fluoride **127** showed SuFEx reactivity,[309] OSF **18a** defluorosulfonylation, and CSF **38** could not be synthesised due to potential instability (Scheme 20b). The relative energies of the carbocations were thus calculated by SO_2F^- exchange equilibria between the sulfonyl fluoride–cation pairs.[212] Primary benzylic carbocation **128** was found to be 24.8 kJ mol^{-1} less stable than tertiary oxetane carbocation **126**, which was in turn 10.4 kJ mol^{-1} less stable than cyclobutane cation **129**, whose stability benefited from the absence of the electron-withdrawing oxygen atom of oxetane (Figure 49c). This trend in relative carbocation stabilities correlated well with the noted reactivities: primary benzylic carbocation **128** was too unstable to form and the corresponding sulfonyl fluoride (**127**) favoured a SuFEx pathway, further benefitting from lower steric hindrance around the reactive sulfur centre. Oxetane carbocation

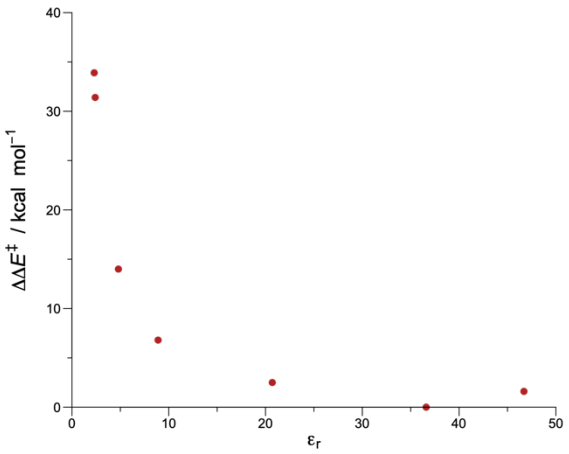
[x] $E^{(2)}_{\pi}$ = total perturbation energy that results from $\pi\longrightarrow\pi^*$ donation within the aromatic π-system + donation from the π-system into the empty p-orbital of the carbocation ($\pi\longrightarrow n^+$).

126 was more stable, and OSF **18a** favoured the defluorosulfonylative pathway. Cyclobutane cation **129** however, was too stable, leading to facile defluorosulfonylation of CSF **38** under ambient conditions and hence, instability under the fluorination conditions and/or subsequent isolation.

Oxetane sulfonyl fluorides seemed to occupy a privileged reactivity window (*cf.* $t_{1/2}$ values, Table 17), sufficiently stable under ambient conditions allowing convenient on-the-bench handling, but selectively reactive on mild thermal activation (60 ºC). The defluorosulfonylative pathway might be a general explanation for the anecdotal instability of alkyl sulfonyl fluoride systems and could be expandable to non-oxetanyl scaffolds with the right balance of electronic (and presumably also steric) properties.

Next, since an S_N1-type ionisation process was proposed, polar solvents were expected to stabilise the carbocation intermediate and S_N1-TS and lower the overall activation energy of the ionisation. This trend was observed experimentally with the defluorosulfonylation not proceeding at all in apolar solvents such as CH_2Cl_2 or dioxane (Scheme 18b). The energies of the S_N1-TS were hence determined computationally for solvents with a wide range of dielectric constants ε_r (Figure 50). In accordance with the S_N1 mechanistic model and experimental observations, the TS-energy increased with decreasing ε_r.

a



b

Solvent	ε_r	$\Delta E^{\ddagger}$ / kJ mol^{-1}	$\Delta\Delta E^{\ddagger}$ / kJ mol^{-1}
1,4-dioxane	2.3	119.5	33.9
PhMe	2.4	117.0	31.4
$CHCl_3$	4.8	99.6	14.0
CH_2Cl_2	8.9	92.4	6.8
acetone	20.7	88.1	2.5
MeCN	36.6	85.6	0
DMSO	46.7	87.2	1.6

Figure 50. Correlation between dielectric constant ε_r and activation energy of the ionisation. **a**, Plotted values. **b**, Tabulated values and solvents considered. TS energies were obtained at the [SMD(*solvent*)-ωB97X-D3/def2-SVP (ma-def2-SVP on F)//SMD(MeCN)-ωB97X-D3/def2-SVP (ma-def2-SVP on F)] level of theory.

Finally, the reaction rates of mono-, di-, and trimethoxy OSFs **18a**, **18n** and **18f** were rationalised kinetically, computationally and structurally. Monomethoxy OSF **18a** was shown to defluorosulfonylate quicker then trimethoxy OSF **18f** but surprisingly, more slowly than dimethoxy **18n** (Figure 40). Computed energy barriers of the S_N1-type defluorosulfonylation

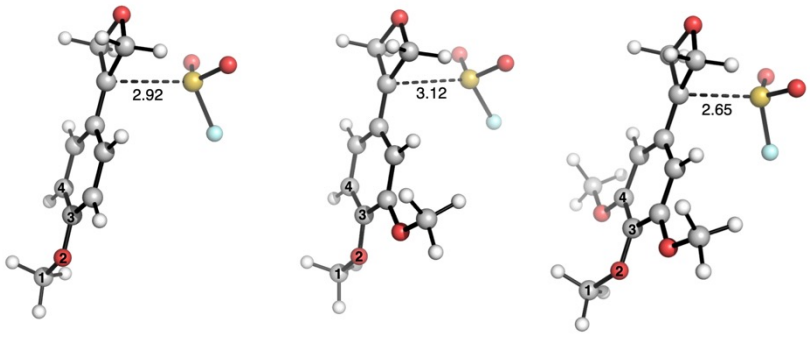
were in accordance with the experimental reaction rates (Figure 40 vs 51a). A rationalisation of the differences is provided below:

In trimethoxy OSF **18f**, the central methoxy substituent in the *para* position, responsible for resonance stabilisation of the oxetane carbocation, cannot adopt a coplanar conformation with the arene for optimal conjugation of its lone pair with the π-system, due to significant steric clash with the flanking *meta*-substituents (Figure 51b). Because of these unfavourable steric interactions, the TS of the S_N1 ionisation of trimethoxy OSF **18f** appears early on the reaction coordinate and is mostly dominated by the geometric distortion. The early TS of **18f** results in a shorter C–S bond, less developed positive charge on the benzylic carbon and hence, less stabilisation of the TS by the electron-rich aromatic ring compared to OSF **18a** (see Figure 51a). Note the increased C1–O2–C3 bond angle in **TS-18f** to decrease steric repulsion (Figure 51a). The structural differences of **18a** and **18f** in the conformation of the *para*-methoxy substituent were seen in the solid-state structure of the OSFs (Figure 51c). The para-methoxy methyl group in **18f** is perpendicular to the arene plane, disallowing efficient conjugation of the oxygen lone pair with the aromatic ring. The C1–O2–C3 bond angle in **18f** (113 º) also suggests a hybridisation of the oxygen atom close to sp^3, compared to **18a** (C1–O2–C3 bond angle = 118 º), indicative of little conjugation of the oxygen lone pair with the aromatic ring in **18f**.

The higher rate of reaction of OSF **18n** compared to **18a** was surprising, since the *meta*-methoxy group would contribute to steric hindrance in the TS and, is known to have a slightly electron-withdrawing effect ($\sigma^+_{(m-\mathrm{OMe})}$ = +0.05).[310] Two potential explanations are provided below (Figure 51d):

In the TS of dimethoxy OSF **18n**, the methoxy substituents are coplanar with the aromatic ring (Figure 51a). Repulsion between the coplanar lone pairs on the oxygen atoms could be reduced by increasing the π-electron donation of the orthogonal lone pair on *para*-methoxy into the arene, since this decreases the overall electron density around the nucleus of the *para*-oxygen atom and could lead to a contraction of the coplanar lone pair (Figure 51d). Note the decreased O2–C3–C4 bond angle in **TS-18n** to reduce steric repulsion between the *O*-lone pairs (Figure 51a). A second explanation is that the coplanar lone pair of the *meta*-methoxy substituent stabilises the positive charge developed on the *para*-oxygen atom during the TS through an electrostatic partial-ion pairing interaction (Figure 51d).

a



	TS-18a	TS-18n	TS-18f
$\Delta G^{\ddagger}$ / kJ mol^{-1}	110.2	101.4	127.7
$q^{\ddagger}_{cation}$ / *e*	+0.81	+0.88	+0.68
C1–O2–C3 bond angle / °	120.6	120.6	126.0
O2–C3–C4 bond angle / °	123.6	115.2	126.4

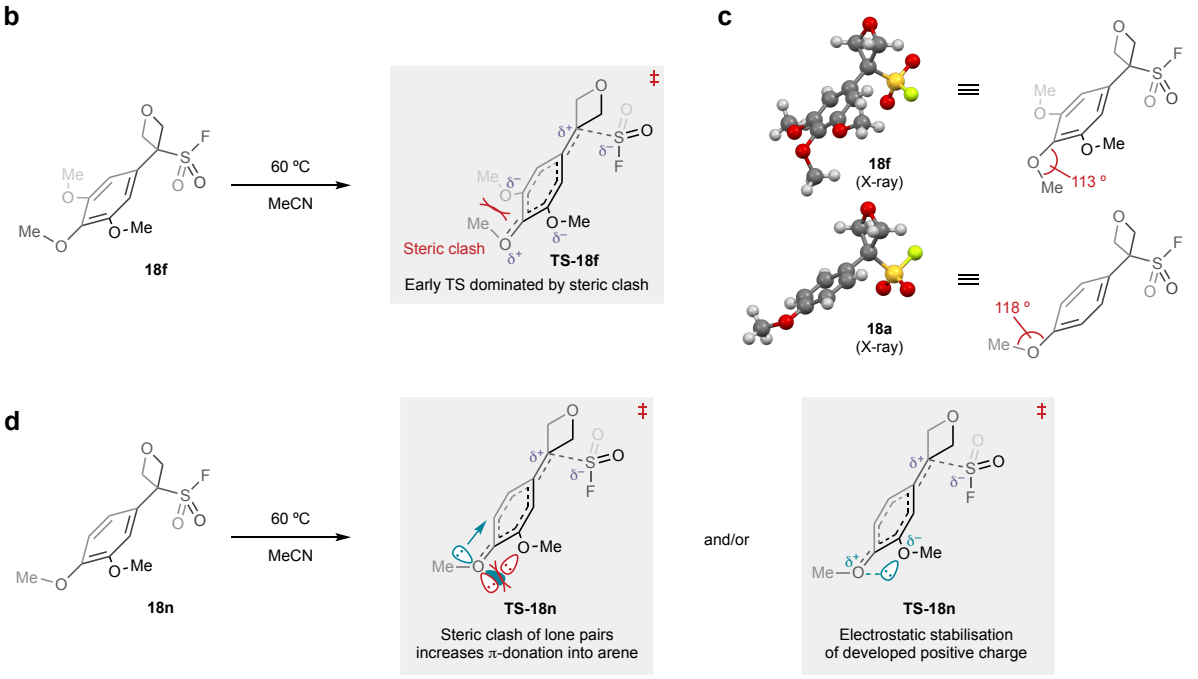


Figure 51. Rationalisation for the different reactivities observed with OSFs 18a, 18n and 18f. **a**, Computed TS structures (generated by A. Sterling) with relevant energetic and structural properties. Calculated at the [SMD(MeCN)-DLPNO-CCSD(T)/def2-TZVPP, ma-def2-TZVPP on F//SMD(MeCN)-PBE0-D3BJ/def2-SVP, ma-def2-SVP on F] level of theory. Partial charges (*e*) calculated with the Hirshfeld method. Distances shown in Å. **b**, Proposed sterics-dominated early TS of **18f**. **c**, X-ray structures of OSF **18a** and **18f** highlighting relevant structural features of the *para*-methoxy substituent. **d**, Proposed rationalisation of TS-stabilising interactions in **TS-18n** that could account for the increased reactivity. Analysis performed in collaboration with A. Sterling.

Taken together, the computational, kinetic and synthetic investigations are supportive of the following full mechanistic picture (Figure 52): oxetane sulfonyl fluorides defluorosulfonylate under thermal activation (60 ºC) to generate oxetane carbocation **118**. The defluorosulfonylative process is akin to typical S_N1-ionisation, proceeding by elongation of the

C–S bond to generate an SO_2F^- anion and cation **118**. The rate-determining step of the reaction was elucidated by kinetic experiments to be loss of SO_2F^-, dependent only on the concentration of OSF, in accordance with S_N1 kinetics. The fate of the generated oxetane carbocation intermediate (**118**) is determined by the nucleophile in a chemodetermining step, leading in the normal case to the coupled product. In the absence of external nucleophile, oxetane cation **118** is either trapped by the released fluoride ions to generate an oxetane fluoride, or degrades to ring-opened species (*e.g.* aldehyde **44**) likely *via* elimination pathways and an oxetene intermediate. The oxetane ring is responsible for the unique reactivity, providing just enough carbocation stabilisation (*i.e.* more than primary benzylic examples but less than tertiary carbocycles such as cyclobutane) to favour the defluorosulfonylation- over the SuFEx pathway (further benefitting from increased sterics around sulfur), but preventing defluorosulfonylation under ambient conditions, which leads to bench-instability. Fluoride-exchange at sulfur towards S^{VI}-species (*e.g.* **25** or **85**) can nevertheless be unlocked by using more reactive, anionic nucleophiles such as phenolates and lithium amides which lower the SuFEx activation barrier owing to an increase in the ground state energy of educts, but leave the nucleophile-independent rate of the deFS pathway unaffected.

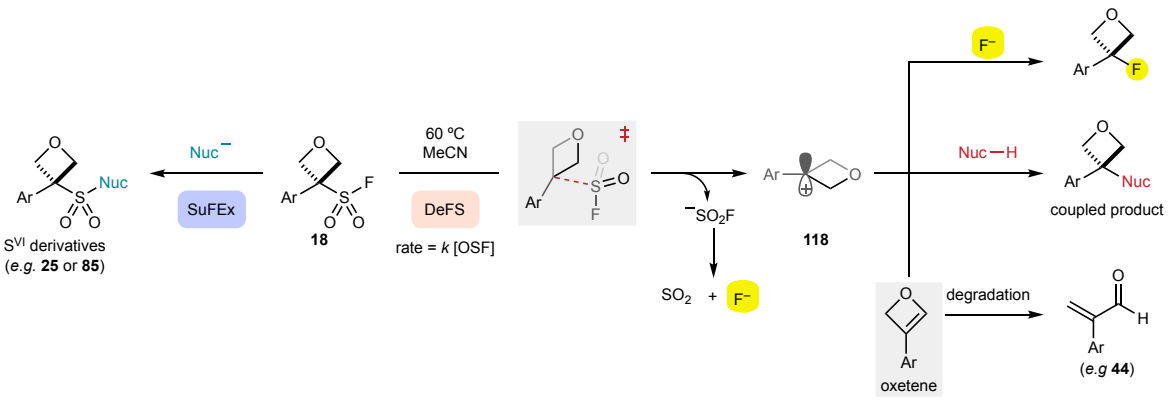


Figure 52. Mechanistic picture of the reactivity of oxetane sulfonyl fluorides.

3.2.13 Conclusion and Future Work

In this chapter, the defluorosulfonylative coupling of oxetane sulfonyl fluorides to various nucleophiles was described, most notably amines, to yield 3-aryl-3-amino-oxetanes as promising isosteres of benzamides. Oxetane sulfonyl fluorides did not display the usual click SuFEx reactivity associated with sulfonyl fluorides, but instead defluorosulfonylated upon warming in an unprecedented type of reaction pathway. The transformation was showcased through a focused scope, the late-stage functionalisation of complex amine-containing drugs and the synthesis of eight oxetane analogues of benzamide drugs. Tolerance to sensitive unprotected functionality such as alcohols, esters, terminal olefins, nitriles and pyrazoles was demonstrated. Coupling to anionic nucleophiles was shown to favour the SuFEx pathway to generate new oxetane S^{VI} scaffolds.

Relevant to applications in drug design, a preliminary isosteric evaluation revealed aryl amino-oxetanes to be promising surrogates for benzamide structures. The amino-oxetane motif was shown not to be a liability in regard to chemical stability, lipophilicity, metabolic clearance and cardiac toxicity. Notably, amino-oxetanes showed a general higher aqueous solubility than their benzamide pairs, potentially due to the higher 3-dimensionality of the oxetanyl scaffolds, demonstrated by a structural analysis.

A kinetic and computational investigation supported an S_N1-type mechanism with the rate-determining formation of an oxetane carbocation *via* defluorosulfonylation, followed by chemodetermining trapping by the nucleophile. The oxetane structure was shown to be crucial to tune reactivity/stability of the sulfonyl fluoride to favour the defluorosulfonylative pathway but providing sufficient stability for handling on the bench.

Oxetane sulfonyl fluorides offer exciting avenues for future research programmes. Some potential future directions are outlined below.

1) Defluorosulfonylative reactivity of other sulfonyl fluorides ‘XSF’ reagents (Figure 53):

Extension of the defluorosulfonylation pathway to other chemical systems is attractive as a new general way of achieving C–X bond formation from sulfonyl fluoride precursors. Based on the electronic and structural requirements of the deFS reaction outlined in this chapter, related small-ring benzylic sulfonyl fluorides could be expected to show similar reactivity (Figure 53a). The overall stabilisation of the resulting benzylic cyclic carbocation could be tuned by the substituents on the aromatic ring to favour defluorosulfonylation without compromising the stability of the reagent, as was for example demonstrated on the cyclobutane system (Scheme 20). Acyclic or larger-ring systems are expected to be prone to

degradation *via* elimination pathways, as was observed on dehydrative processes.[208] Preliminary work on azetidine sulfonyl fluorides (ASFs; **131**) demonstrated the deFS pathway also to be available to this ring system, and amino-azetidine **132** was isolated in 65% yield on a 0.1 mmol test scale (Figure 53b).

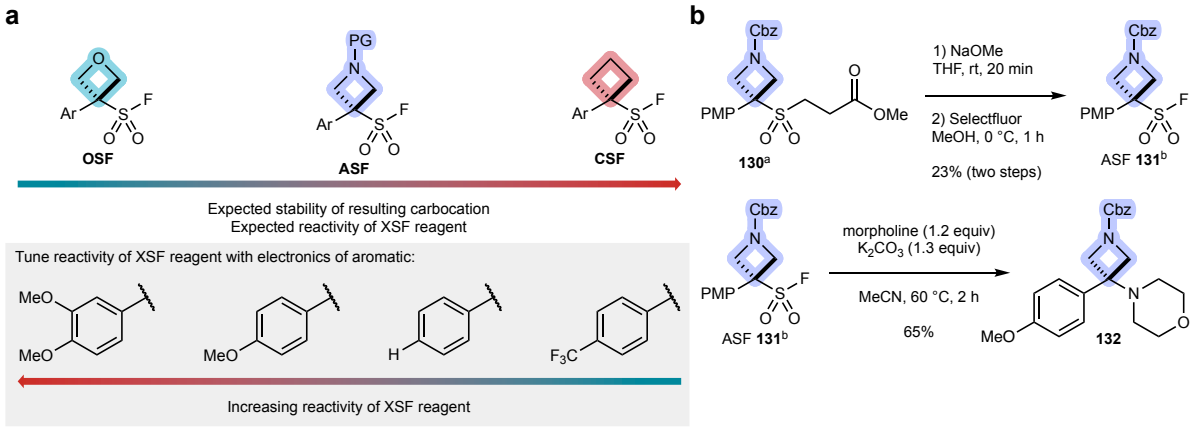


Figure 53. Expansion to further XSF reagents. a, Expected reactivity of XSF reagents and possibility for tuning with arene substituent. **b**, Proof-of-principle deFS reactivity of azetidine sulfonyl fluoride **131**. [a] Synthesised by A. Lazaridou.[207] [b] Isolated in a 9:1 mixture with the corresponding 3-aryl-azetidine 3-fluoride **131'**.

2) deFS coupling of oxetane sulfonyl fluorides with other nucleophiles (Figure 54)

This chapter demonstrated the successful defluorosulfonylative coupling of OSFs with amines, alcohols, phenols, thiols, azoles and indole. Other nucleophiles were not successful, such as hydrazines, hydroxylamine, aryl silanes and -boronic acids, all of which led to complex mixtures of compounds. Nevertheless, the breadth of potential nucleophiles is large and would expand the substitution patterns attainable on oxetane (Figure 54). For example, further azoles and related heterocycles would generate interesting new molecular systems, not available by other approaches. Reaction with diones, azides or cyanides would give access to oxetane building blocks with the potential for diversification towards heterocycles. Lastly, soft organometallics such as organozinc, -copper or -lanthanum reagents could be envisaged to be unreactive enough to avoid both SuFEx and degradative reactivity but undergo defluorosulfonylative C–C coupling with OSFs.

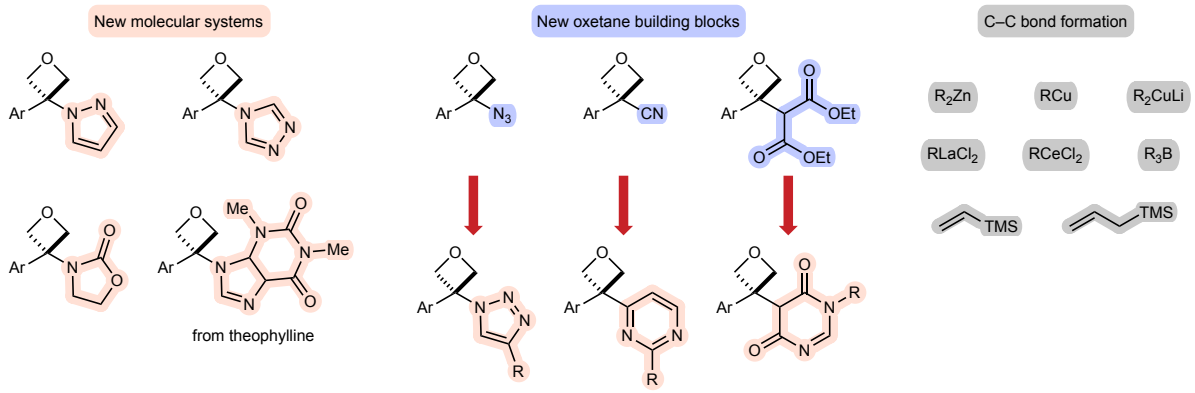


Figure 54. Potential reactions of OSFs with other nucleophiles.

3) Validation of aryl amino-oxetanes in medicinal chemistry

Section **3.2.11** described a preliminary matched-molecular pair analysis of a limited set of eight amino-oxetane/benzamide pairs with encouraging initial results, most notably in solubility properties. The dataset should be expanded to make more meaningful correlations between chemical structure and molecular properties. In particular, variation of the aromatic functionality was unilateral. Further medicinally relevant values such as pK_a, permeability, H-bonding capability and thermal stability should also be assessed.

4) Functionalisation of biologically relevant macromolecules

The covalent functionalisation of bioactive macromolecules such as peptides, proteins, antibodies, or oligonucleotides with small molecule fragments are of topical interest as molecular tools for fundamental chemical biology and as potential therapeutics or imaging probes. Sulfonyl fluoride inhibitors have been investigated and developed, which react covalently and selectively with protein residues upon spatial-chemical activation inside protein cavities.[221] It would be of biological relevance and interest to develop methods to functionalise such bio-macromolecules with OSF reagents. This chapter showed OSFs to undergo defluorosulfonylation under biocompatible conditions such as H_2O:MeCN solvent mixtures (up to 1:1 showed; Section **3.2.6**) and physiological temperatures (37 ºC). Irreversible covalent reactivity was also demonstrated between OSFs and amino acids such as Tyr, Ser, His and Cys, and selectivities between different nucleophiles were investigated. Systematic competition studies between amino acids could give an initial indication of amino acid compatibility for peptide functionalisation, *e.g.* on a lysine residue. Also promising is the selectivity of OSF reagents with phenol derivatives towards sulfur–fluoride exchange-type reactivity, especially with Ph OSF **18m** which is completely unreactive towards amines. This reaction pathway could be used for the selective functionalisation of Tyr residues on peptides or proteins.

4 Oxetane Radicals

The main parts of the results presented in this chapter were published as an article in *J. Org. Chem.*, in collaboration with other members of the Bull group (M. Dubois, H Broderick) and the Duarte group from the University of Oxford.[311] The main goals of this chapter were to better understand the reactivity of radical intermediates on strained rings, and to develop synthetic methods using oxetane radicals to expand the scope of 3,3-disubstitution patterns beyond those achievable with oxetane carbocations, which were described in the last chapter.

4.1 Strategies for Radical Generation and Photoredox Catalysis

One-electron retrosynthetic logic has received relatively little attention compared to polar, 2-electron disconnection strategies. This is likely to have been due to the belief that radical species cannot be controlled and require harsh conditions and toxic reagents for their formation.

The last 20 years have seen a 're-renaissance' of radical organic chemistry and an increase in research groups active in this area.[312] Concomitant fundamental advances in various areas of chemistry have led to the development of mild and selective methods for the formation of radicals in a *controlled* manner. Most notable have been developments in electrochemistry[313] and photoredox catalysis,[314] both of which rely on single-electron processes. Synthetic applications of these mild methods demonstrated the potential of one-electron radical reactivity to unlock reaction pathways not available to 2-electron chemistry[21] and have been employed, for example, for tactical disconnections in the synthesis of complex natural products[315] and in industrial settings.[22c,d,316]

Key to the mildness (no requirement for high temperatures, far UV light or toxic reagents) and success of photoredox chemistry is the use of photocatalysts (PCs), metal-based or extended organic π-conjugated entities capable of absorbing visible light (see Figure 55a for selected examples).[314a,317] Typical organic molecules (*i.e.* molecules that lack an extended π-system) do not absorb, *i.e.* are not excited by, irradiation in this region of the electromagnetic spectrum and hence are not degraded by the photoexcitation. Upon irradiation, an electron of the PC is promoted to an excited energy state (often metal-to-ligand charge-transfer [MLCT] or $\pi \rightarrow \pi^*$ processes in metal and organic PCs, respectively), able to selectively reduce or oxidise specific functional groups of a substrate. The RedOx-activated substrate may then undergo fragmentation, or another related process, to generate a free alkyl radical that is trapped by a suitable radical acceptor. Oxidation of the substrate, *i.e.* reduction of the PC, is termed *reductive quenching* and the opposite process is termed *oxidative quenching* (Figure 55b).

Turnover of the PC is achieved by single electron transfer (SET) from an electron acceptor or -donor, respectively (external or the substrate itself). Chemoselective activation of the desired functionality is achieved by closely matching the RedOx potentials of substrate and the excited state of the photocatalyst (PC*) to avoid undesired quenching.

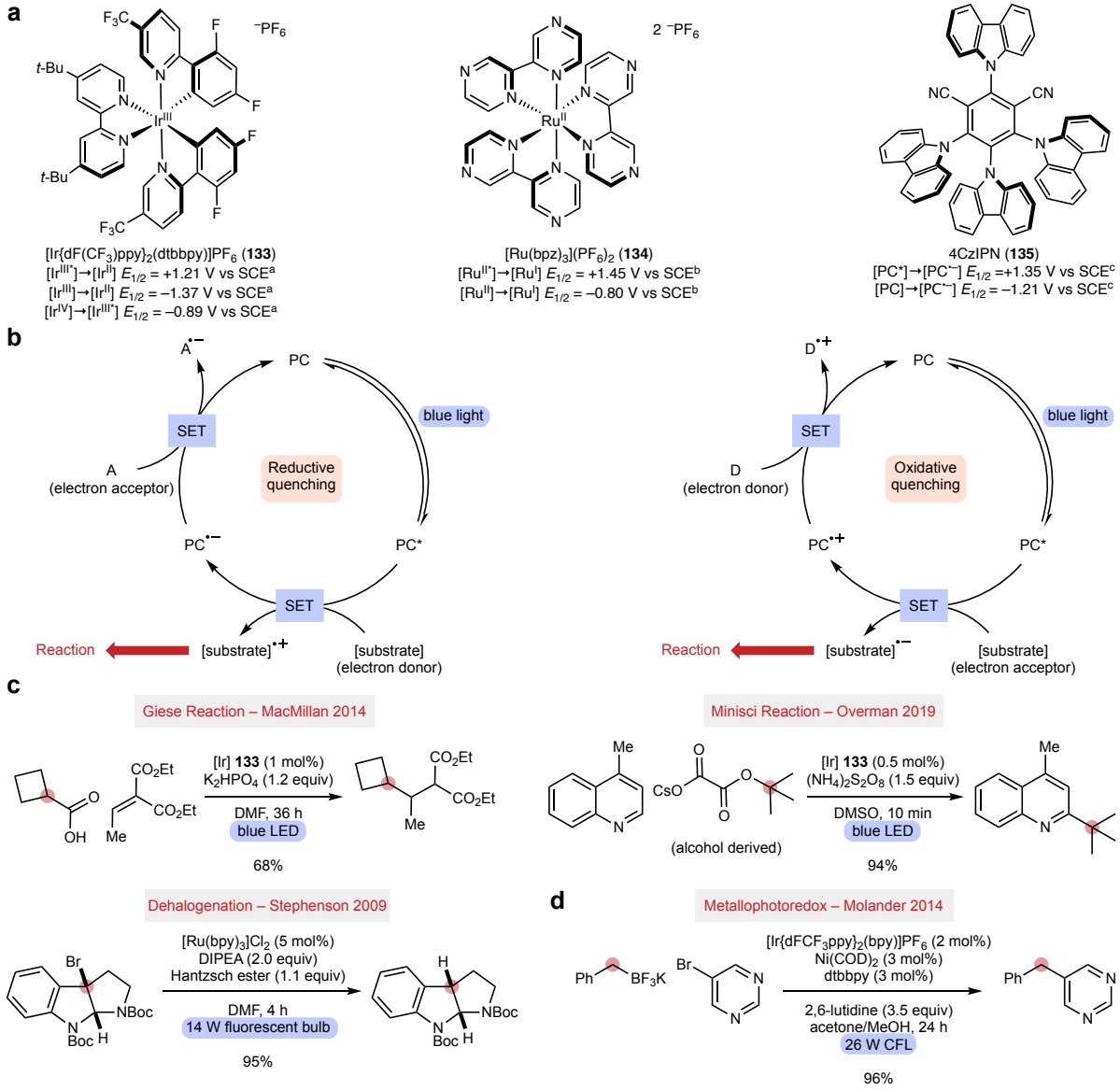


Figure 55. Introduction to photoredox catalysis. a, Three widely used photoredox catalysts (PCs). **b**, Schematic representation of reductive and oxidative quenching reactivity modes. **c**, Selected examples of typical photoredox-catalysed transformations.[318,319,322a] **d**, One of the seminal examples of metallophotoredox chemistry.[327a] CFL = compact fluorescent lamp.

It is worth noting that many of the archetypical transformations associated with photoredox catalysis, for example Giese,[320] Minisci[321] or dehalogenation reactions[322] (Figure 55c), are conceptually not new chemical processes.[323,324,325] The novelty lies in the mildness of the methods to generate the requisite alkyl radicals, which significantly expanded the synthetic scope and brought the transformations to a higher tier of translational applications. A

remarkable development in photoredox catalysis has been the merger of photoredox radical generation with transition metal catalysis.[326,327] In this mechanistic scenario, the generated radical is fed into a second, non-light mediated catalytic cycle, most often using nickel catalysts, forming previously unconceivable bonds between chemical matter (Figure 55d).

Photoredox catalysis has expanded the scope of radical precursors, enabling conceptually new disconnections and the use of feedstock chemicals and non-toxic starting materials. Most impactful has been the usage of carboxylic acids,[328] alcohols,[329,330] and trifluoroborates as radical precursors,[327a,331] and radical generation α to heteroatoms such as amines,[332] or ethers[333] (Figure 56).

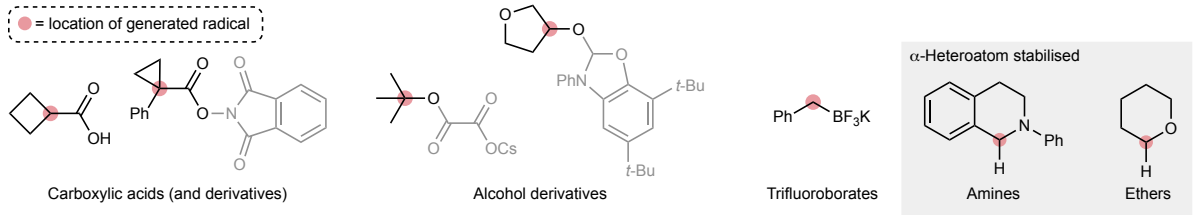
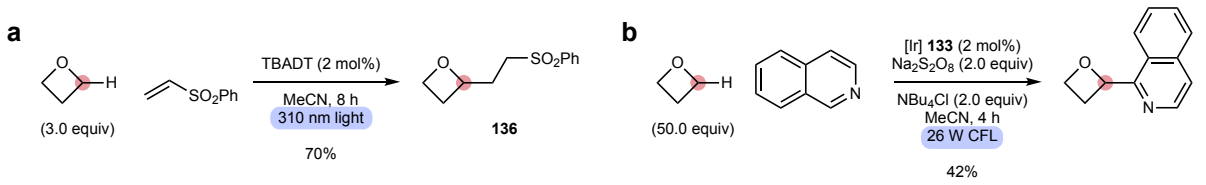


Figure 56. Examples of radial precursors. See Figure 55c and d for selected synthetic applications.

4.2 Radicals on Oxetanes

The increasing fundamental and medicinal interest in the oxetane scaffold has fuelled the development of synthetic methods that involve oxetanyl substrates, also including one-electron strategies. This section will highlight and discuss the generation of radicals on oxetane and selected synthetic applications.

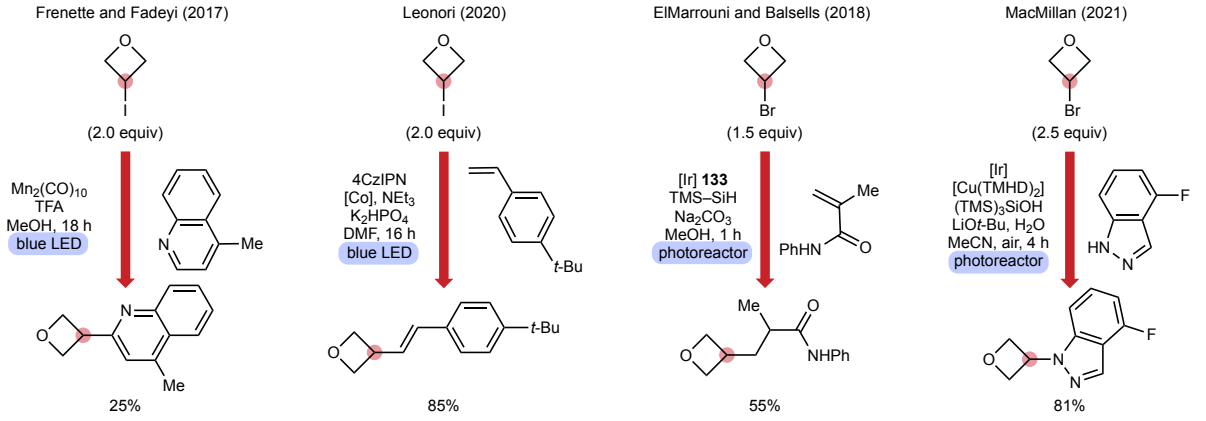
The bond dissociation energy (BDE) of C–H bonds α to heteroatoms (*e.g.*, C–H BDE in trimethylamine[334]: 84 ± 2 kcal mol^{-1}; C–H BDE in methanol[335]: 96.1 ± 0.2 kcal mol^{-1}) is lower than the BDE of inert C–H bonds (C–H BDE in methane[335]: 104.99 ± 0.03 kcal mol^{-1}). The weaker C–H bonds mean radical generation α to heteroatoms is more facile than at other sites on a molecule and can be achieved selectively with appropriate H-atom abstraction reagents. As such, Ravelli reported in 2014 an early example of light-mediated α-functionalisation of unsubstituted and substituted oxetane examples by H-atom abstraction using tetrabutylammonium decatungstate (TBADT) as photocatalyst.[336] The generated α-stabilised 2-oxetane radicals were trapped by electron-deficient alkenes in a Giese-type process to yield 2-alkylated oxetanes such as **136** (Scheme 36a). Further examples of functionalisation of 2-oxetane radicals have been reported, including Minisci reactions (Scheme 36b)[333a] and metallophotoredox couplings.[332c,337] The high excesses of oxetane normally required are notable.



Scheme 36. Radical α-functionalisation of oxetanes. a, As part of a Giese reaction.[336] **b**, As part of a Minisci reaction.[333a]

Selective H-atom abstraction at the 3-position of oxetanes is more challenging due to competition with heteroatom-driven radical generation at the 2-position. Hence, radical precursor groups are required to generate oxetane β radicals. Most popular is the use of commercially available 3-bromo- and 3-iodo-oxetane as precursors of the 3-oxetane radical, which are often demonstrated as part of scope tables (Scheme 37).

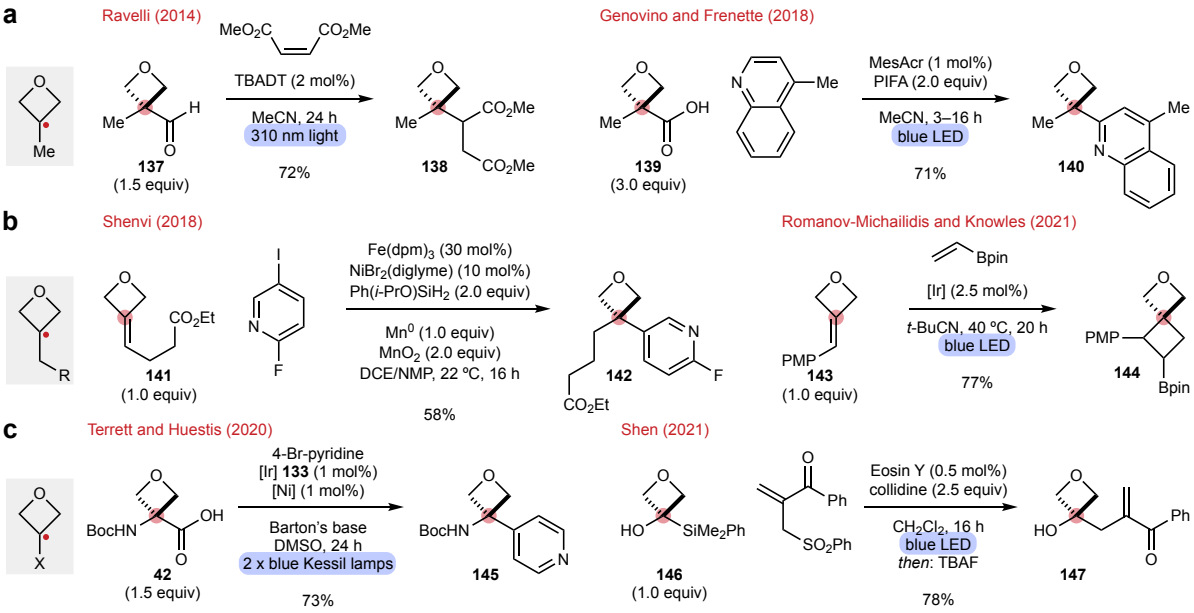
In 2009, Duncton (Evotec) conducted a systematic study on Minisci reactions employing 3-iodo-oxetane as coupling partner,[338] albeit not as part of a photolytic process but using the classic Fe^{2+}/H_2O_2/DMSO chemical system developed by Minisci to generate alkyl radicals from alkyl iodides.[339] In Duncton's study, 3-iodo-oxetane was used in two-fold excess and product yields ranged from 5–46%. Radical generation from 3-iodo- and 3-bromo-oxetane were further reported as single entries in scope tables, for example by Frenette and Fadeyi (Pfizer) in a Minisci reaction,[340] Leonori (several transformations),[341] ElMarrouni and Balsells (Merck) in a Giese reaction[342] and MacMillan in heterocyclic *N*-alkylation (26 oxetane examples) (Scheme 37).[343] Again notably, the oxetane reagent was always used in excess.



Scheme 37. Radical reactions of 3-halo-oxetanes.[340–343]

Examples that generate 3-oxetane radicals from non-halogenated precursors are scarce, and examples of 3-oxetane *tertiary* radicals, *i.e.* formation of quaternary carbon centres, even scarcer (Scheme 38). As part of the same 2014 publication by Ravelli (Scheme 36), 3-methyl-oxetane tertiary radicals were generated by formyl-H abstraction from oxetane aldehyde **137** by TBADT, followed by decarbonylation.[336] Giese reaction yielded 3,3-dialkylated oxetane

products such as **138** (Scheme 38a). In another collaboration between Pfizer and the Frenette group, Minisci reaction was achieved with 3-methyl-oxetane radicals, generated by reductive-decarboxylative radical anion collapse from methyl-oxetane carboxylic acid **139** (Scheme 38a).[344]



Scheme 38. Transformations that involve tertiary oxetane radicals. a, 3-Methyloxetane radicals.[336,344] **b**, 3-Alkyloxetane radicals from oxetane alkylidenes.[345,346] **c**, α-Heteroatom stabilised 3-oxetane radicals.[247,347] PIFA = Phenyliodine bis(trifluoroacetate).

Oxetane-3-alkylidenes, shown to be useful entities for polar oxetane functionalisation (Section **1.4.3.1**), have also been used for the generation of 3-alkyl oxetane radicals (Scheme 38b). In 2018, Shenvi reported a HAT/Ni dual catalytic strategy (non-photolytic) for the construction of 3-aryl-3-alkyl oxetane quaternary centres.[345] HAT from a catalytic iron–hydride species into alkylidene **141** was proposed to generate the tertiary oxetane radical which was fed into a nickel catalytic cycle resulting in oxetane arylation (**142**). In a 2021 report, Romanov-Michailidis (Bristol Myers Squibb) and Knowles demonstrated a [2+2] cycloaddition between oxetane alkylidenes and electron-poor olefins for the synthesis of spirocyclic oxetanes.[346] Formation of the oxetane radical was achieved by sensitisation of oxetane alkylidene **143** by the excited PC to a triplet species which added into the olefin and ring-closed to form the final spirocyclic product **144**.

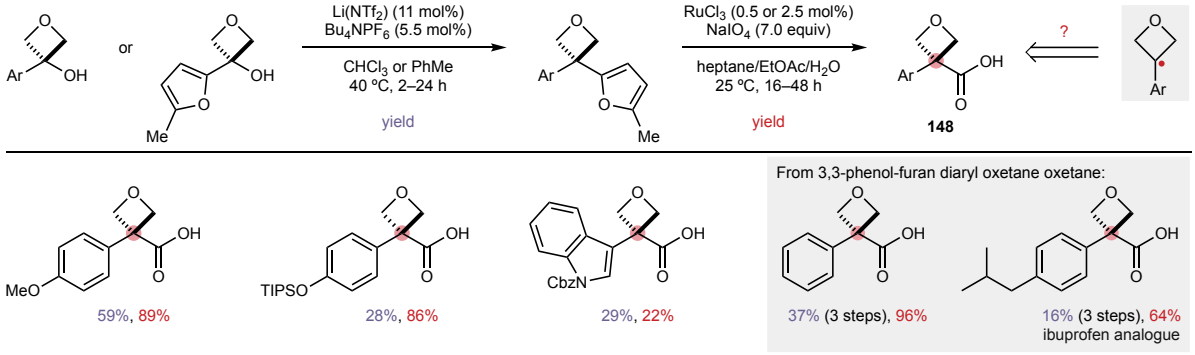
Lastly, there have been two recent reports of tertiary, α-heteroatom-stabilised oxetane radicals (Scheme 38c). Terret and Huestis (Genentech) reported decarboxylation from oxetane amino acid **42** using Barton's base and [Ir] **133** as photocatalyst (see also Section **3.2.1**, Scheme 21).[247] The amino-oxetane radical was then coupled to aryl halides in an overall metallophotoredox process (**145**). Recently, Shen and coworkers reported the generation of

3-silyloxy oxetane radicals followed by Giese addition to yield 3-alkyl oxetanols such as **147**.[347] The oxetane radical was formed by Lewis base-mediated single-electron oxidation of oxetanol **146** by the excited catalyst PC* which formed an alkoxide radical that underwent rapid Brook rearrangement to access the alkyl radical on oxetane.

4.2.1 Previous Work within the Group: Radicals from Oxetane Carboxylic Acids

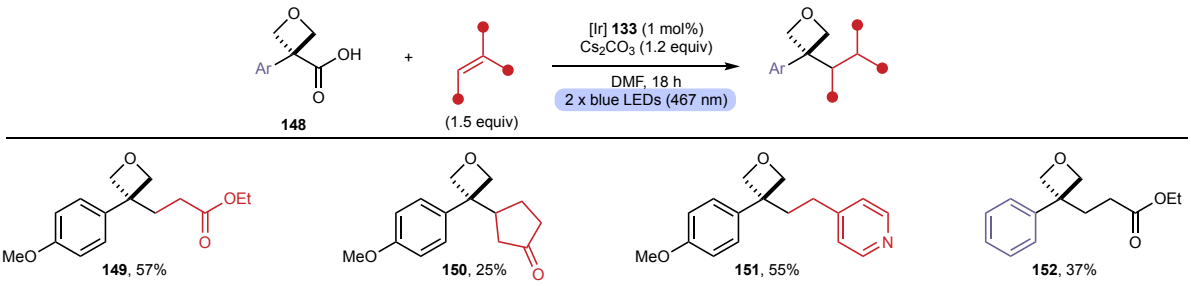
There have been notably few examples that utilise 3-oxetane carboxylic acids as radical precursors[247,344,348] and no examples that generate 3-aryloxetane radicals. As tertiary benzylic structures, 3-aryloxetane radicals were expected to provide a challenge due to their stabilised nature and steric demands around the reactive centre, which often lead to homo-coupling and reduced rates in addition reactions.[349,350] Benzylic radical intermediates have also shown preference for radical-polar crossover (RPC) reaction pathways towards benzylic carbocations.[209,351]

A two-step protocol was developed by M. Dubois to prepare 3-aryl oxetane 3-carboxylic acids **148** (Scheme 39).[352,353] The process involved a Friedel–Crafts reaction of oxetanol followed by oxidative furan ring cleavage with a mix of ruthenium trichloride and sodium periodate. M. Dubois also developed a protocol for the generation of 3-aryl oxetane radicals and implementation as part of a Giese-type reaction, noting that other radical precursors such as oxetane oxalates, were unsuccessful.[211]



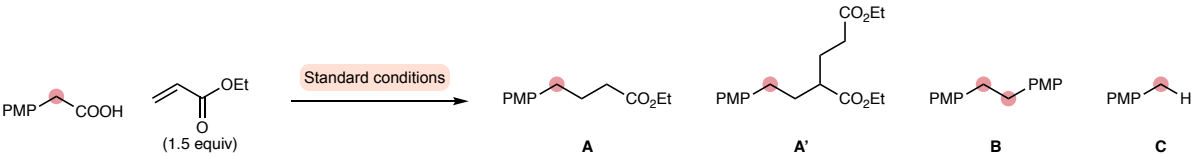
Scheme 39. 2-Step synthesis of 3-aryl oxetane 3-carboxylic acids.[352]

Initial conditions were based on previous work by MacMillan using [Ir] **133** as photocatalyst, blue Kessil lamps, Cs_2CO_3 as base and ethyl acrylate as radical acceptor.[318] Most deviations from these conditions had little, or no impact on the yield of the reaction.[211] The initial scope of the Giese reaction was investigated, with representative examples shown in Scheme 40.



Scheme 40. Selected scope of the aryloxetane Giese reaction.[211,311]

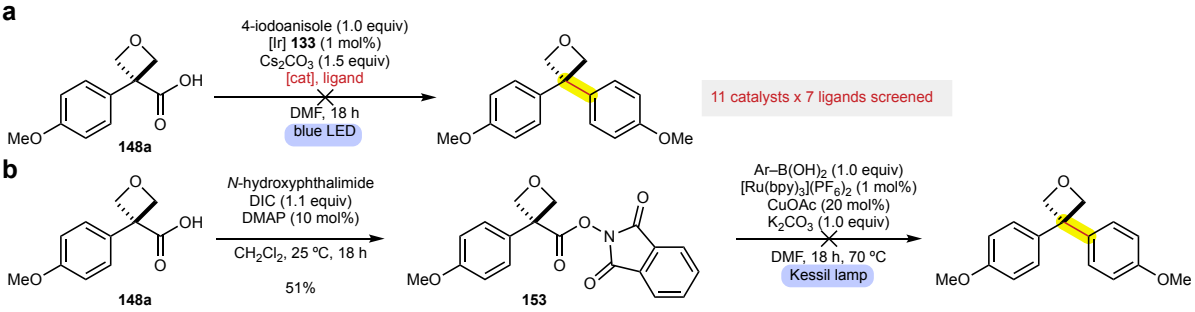
Further, to better understand the effect of ring strain and heteroatom substitution on radical reactivity, a series or arylacetic acids with varying benzylic linkers was investigated (Scheme 41). The benzylic linker (*i.e.* oxetane, cyclobutane, methylene, etc.) had a strong influence on the reaction outcome and product distributions, with only oxetane and azetidine showing a strong preference for the productive pathway.



Yields / %		Cbz			Me Me	H H
A	58	53	36	33	32	38
A'	0	12	7	12	10	9
B	0	0	6	23	38	11
C	0	0	0	0	0	0

Scheme 41. Radical reactivity of different arylacetic acids.[211,311] Isolated yields reported.

Finally, radical arylation strategies of oxetane substrates were examined to circumvent the required electron-rich functionality of the carbocation chemistry. Typical coupling conditions were screened at Pfizer but did not show any arylated product (Scheme 42a). An attempted photocatalysed cross-coupling of oxetane redox-active ester **153** with an aryl boronic acid based on conditions by Sanford was also not successful (Scheme 42b).[354]



Scheme 42. Attempted radical arylations of oxetane acid 148a.[211] **a**, Metallophotoredox screen (conducted at Pfizer). **b**, Arylation of redox active ester **153**. DIC = *N*,*N*'-Diisopropylcarbodiimide.

4.2.1.1 Aims

Two general aims were established at the outset of this chapter: 1) gain a better understanding of the benzylic oxetane radical derived from carboxylic acids, both structurally and in its application to radical coupling reactions; and 2) develop alternative precursors to oxetane radicals which are of higher synthetic tractability than oxetane carboxylic acids.

Concerning the 1st aim, the scope of the decarboxylative Giese reaction of oxetane carboxylic acids initially investigated by M. Dubois (Section **4.2.1**) was first to be expanded to include medicinally more relevant scaffolds and to better understand the reactivity of the benzylic oxetane radical. The aim was to investigate varied electronic and steric requirements on both the oxetane acid starting material and alkene acceptor.

Then, the aim was to investigate the structure and reactivity of the oxetane radical and the influence of ring strain and heterosubstitution on radical reactivity. This investigation was envisaged to be conducted through focused experimental and computational mechanistic studies (in collaboration with the Duarte group). In particular, the goal was to rationalise the trends in yields and product distributions of the Giese reaction involving different arylacetic acids and ethyl acrylate observed by M. Dubois (Scheme 41). Further, the mechanism of the Giese reaction of benzylic oxetane radicals was to be elucidated, with an emphasis on providing evidence (experimental and/or computational) for key elementary steps and for the formation of side products. The specific questions to be investigated are outlined below.

Based on previous literature,[318,355] an initial outline of the broad mechanistic picture of the aryloxetane Giese reaction was sketched (Figure 57). Nevertheless, several experimental observations raised mechanistic questions, which are graphically highlighted in Figure 56.

1) How are the observed side products formed (*e.g.* of the type **149'**, **154** or **155**)? These species have not been generally observed/characterised in the literature of photoredox Giese reactions, and little is known on their mechanism of formation. Although formation of dimer **154** is likely to proceed *via* radical recombination, the source of 'H' to form reduced product **155** was unknown (proton, HAT or hydride?), as well as the pathway by which **149'** is formed (radical or polar Michael addition?).
2) How and why is the Giese reaction impacted by the benzylic substituent of arylacetic acids (see Scheme 41)? Substrates differed significantly in the distribution of products (*e.g.* **149**, **149'**, **154** and **155**) with a potential correlation to ring strain and/or radical stability. Particularly, little was known on the effect of ring strain on the reactivity of radical intermediates.

3) Can some of the fundamental steps of the proposed catalytic cycle be corroborated by quantitative measurements? Specifically, it was not clear whether the final Giese product **149** was formed by protonation of enolate intermediate **149**$^{-}$ (catalytically most sensible) or HAT to Giese adduct **149**$^{\bullet}$. Cyclic voltammetry experiments would back up key RedOx steps in the cycle with thermodynamic data.

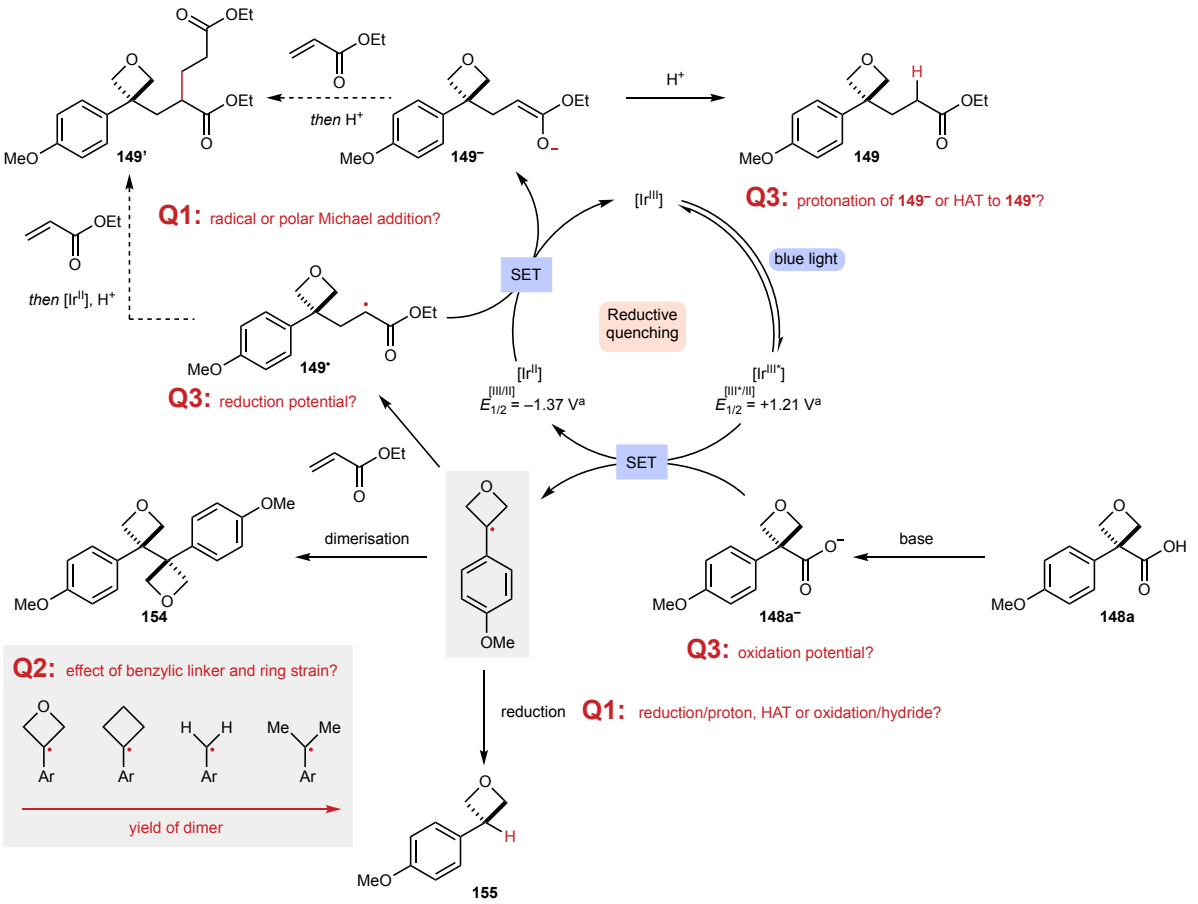
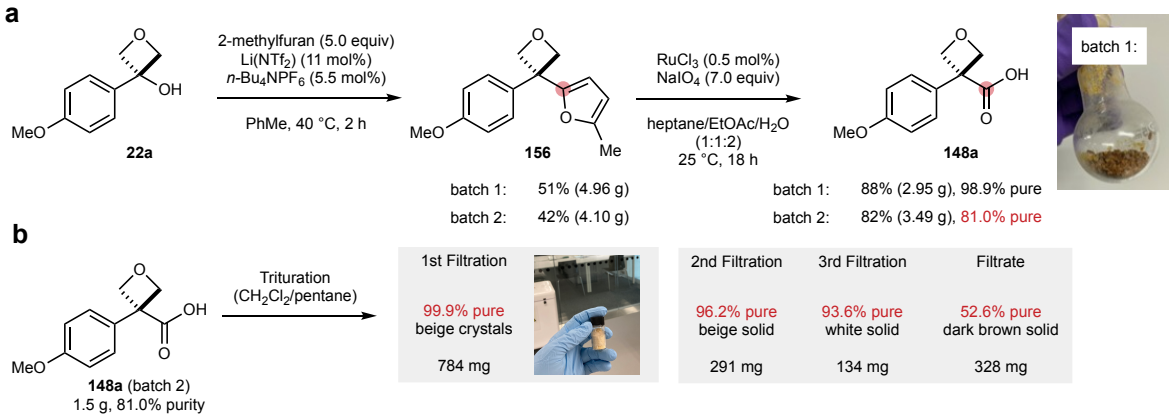


Figure 57. Initial mechanistic sketch of the oxetane Giese reaction based on literature precedent and questions to be answered. [Ir^{III}] = [Ir] **133**. [a] Literature values vs SCE in MeCN.[355a]

4.2.1.2 Synthesis of Oxetane Acids

First, *p*-methoxyphenyl oxetane carboxylic acid **148a** was synthesised on a large scale from oxetanol **22a** and was obtained in a similar yield over two steps as previously reported,[352] noting a discrepancy in appearance (dark brown vs off-white[352]) (Scheme 43a). The purity of the synthesised acid **148a** was assessed to be 98.9% by a quantitative ^{1}H NMR assay using 1,3,5-trimethoxybenzene as internal standard.[y] However, a repeat of the synthetic sequence yielded oxetane acid **148a** in only 81% purity, despite qualitatively pure ^{1}H and ^{13}C NMR spectra and comparable physical appearance. The NMR-silent impurities are likely to contain inorganic iodine-containing by-products from the oxidative cleavage step, further noting that solvent removal of oxetane acid **148a** by concentration *in vacuo* after the oxidation step released a red volatile impurity, likewise likely to contain strongly coloured iodine species.[352] To further purify oxetane acid **148a** from the second batch and to completely remove electron-rich iodine species that could potentially disrupt following reactions, acid **148a** (batch 2) was dissolved in CH_2Cl_2, triturated with pentane and filtered (Scheme 43b) to obtain oxetane acid **148a** as a beige crystalline solid in 99.9% purity (by quantitative ^{1}H NMR), as well as samples of lesser purity after subsequent filtrations (see Section **7.6.5** for procedural details).

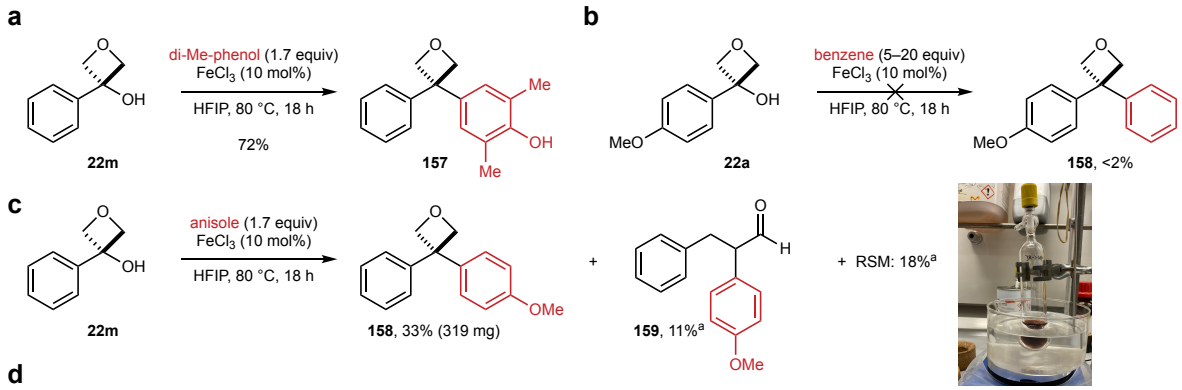


Scheme 43. Synthesis of oxetane acid 148a. a, Two synthesised batches of acid **148a** obtained in different purities. **b**, Purification of acid **148a** (second batch) by trituration from CH_2Cl_2/pentane.

Next, a more direct route into non-electron-rich oxetane acids was examined, since current strategies required five steps from commercially available oxetan-3-one (see Scheme 39).[352] Oxidative cleavage of the most electron-rich arene of diaryl-oxetanes **157** and **158** was investigated (Scheme 44).[356] Diaryl oxetanes **157** and **158** were accessible in one step from oxetanols **22a** or **22m** through an HFIP-promoted Friedel–Crafts reaction, noting that furan rings were not tolerated under these conditions (unpublished; Scheme 44a–c).[211]

[y] Note that unless otherwise stated, all further reactions were conducted with oxetane acid **148a** from 'batch 1'.

Ph-phenol diaryl-oxetane **157** was obtained in 72% yield from phenyl-oxetanol **22m** by M. Dubois (Scheme 44a). Ph-PMP diaryl-oxetane **158** was harder to access. Reaction of PMP-oxetanol **22a** with benzene yielded only trace amounts of diaryl-oxetane **158** (Scheme 44b) and reaction of phenyl-oxetanol **22m** with anisole gave diaryl-oxetane **158** in 33% yield, alongside 11% of aldehyde **159** on a 4.0 mmol scale using a J Young's ampoule as reaction vessel (Scheme 44c).



Entry	Substrate	Conditions	Scale / mmol	yield **148m** / %[b]
1	**157**	Sharpless	0.1	83 (65% pure)
2	**157**	Vasconcellos	0.1	0 (complex mixture)
3	**157**	Maulide	0.1	traces
4	**158**	Sharpless	0.1	0 (no reaction)
5	**158**	Vasconcellos	0.1	39 (55% pure)[c]
6	**158**	Maulide	0.07	51
7	**158**	Bull	0.1	0 (no reaction)
8	**158**	Maulide[d]	0.1	77
9	**158**	Maulide[d]	1.4	100 (85% pure) → 26%[e]

Scheme 44. Alternative synthetic route into oxetane acid 148m. a, HFIP-mediated Friedel–Crafts reaction of Ph oxetanol **22m** to dimethyl phenol **157** (reaction performed by M. Dubois).[211] **b**, Unsuccessful coupling of PMP oxetanol **22a** to benzene. **c**, Large scale (4.0 mmol) Friedel–Crafts reaction of oxetanol **22m** to anisole in a J Young's ampoule. **d**, Preliminary investigation of oxidative ring cleavage of **157** or **158** towards Ph oxetane acid **148m**. [a] Yields calculated by analysis of the ^{1}H NMR spectrum of the crude mixture of the reaction using 1,3,5-trimethoxybenzene as internal standard. [b] Isolated yields after acid/base workup. [c] No reaction after 4 days. H_2O added after 4 days and stirred for further 18 h. [d] Using 10 mol% $RuCl_3$. [e] Yield after purification by column chromatography.

Four sets of conditions for the phenol/PMP oxidative ring cleavage of **157**/**158** were tested (Scheme 44d). Generally, reactions of phenol substrate **157** were less selective and often led to mixtures of products (entries 1–3). PMP cleavage from oxetane **158** was broadly cleaner and Ph oxetane acid **148m** was obtained in 51% yield under the conditions developed by Maulide (entry 6).[356c] Reduction of ruthenium loading from 40 to 10 mol% further increased the yield of acid **148m** to 77%. Scale-up of the cleavage to 1.4 mmol yielded acid **148m** as a brown solid in 100% but only in ca. 85% purity after purification by an acid/base workup (entry 9; estimated by relative integrals in the ^{1}H NMR spectrum). However, further purification

by column chromatography isolated acid **148m** as colourless crystals in only 26% yield. Based on the physical appearance of acid **148m** after the acid/base workup (dark brown) and previous observations with PMP acid **148a** (see Scheme 43), it is presumed that the purity of **148m** after workup was much less than 85%, containing NMR-silent impurities.

These preliminary studies demonstrated that PMP rings can be oxidatively cleaved selectively in the presence of an oxetane ring to unmask free carboxylic acid functionality, but further optimisation should be performed to improve reaction efficiency. The protocol has promising potential for application to further PMP-containing oxetanyl compounds, for example on PMP amino-oxetanes (Section **3.2**), to generate unnatural oxetane amino acids.

With sufficient quantities of PMP and Ph oxetane acid in hand, the Giese reaction of 3-aryloxetane radicals was investigated and expanded and will be presented in the next section.

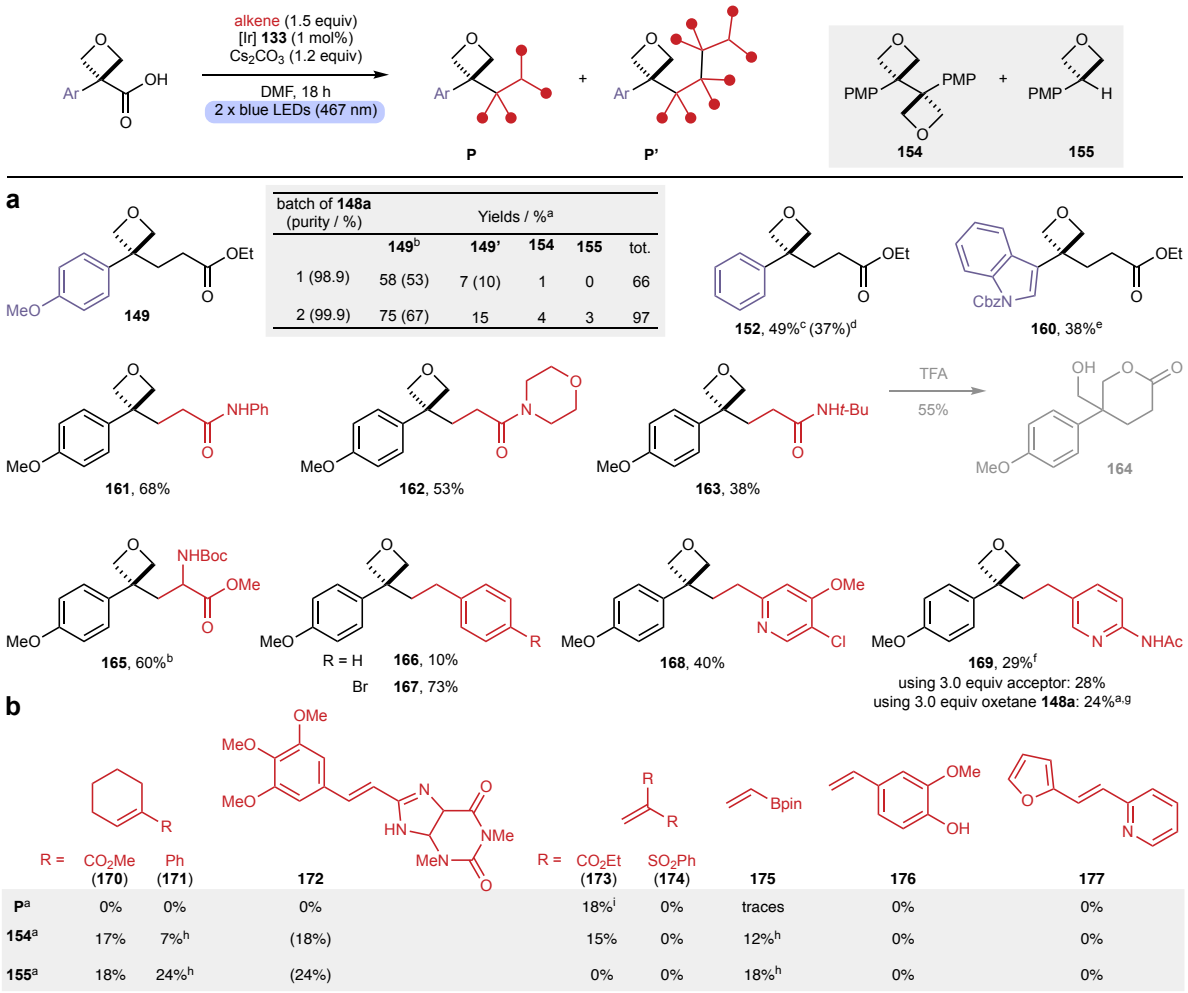
4.2.1.3 Scope of Giese Reaction

First, reproduction of the coupling of oxetane acid **148a** with ethyl acrylate showed a comparable yield of alkylated product **149** to that previously reported within the group (Section **4.2.1**) and side products of over-alkylation (**149'**), dimerisation (**154**) and reduction (**155**) were quantified and characterised (**149'**) (Scheme 45a).

Surprisingly, conducting the same Giese reaction with repurified oxetane acid **148a** (99.9% pure {repurified batch 2} instead of 98.9% pure {batch 1}, see Scheme 43) significantly increased the yield of oxetane **149** (53→67%) and the overall mass balance of the reaction (66→97%). The high impact of an impurity present in 1% relative quantity in the reaction is notable and was presumably due to an interaction of the impurity, likely to contain electron-rich iodine species, with the catalyst (1 mol% loading) or other catalytically formed intermediates (1% maximal relative amount). Ph oxetane acid **148m** purified by column chromatography (Scheme 44d) saw a similar jump in yield of Giese product **152** (37→49%), supporting the hypothesis of a catalytically inhibitory impurity. Lastly, on the aryl-oxetane side, an indole heterocycle was tolerated in moderate yield (**160**).

Then, further alkene acceptors were assessed (Scheme 45a). Acrylamides were successful and yielded medicinally relevant amide examples in moderate yields (38–68%; **161**–**163**). Acidic deprotection of the *tert*-butyl group in **163** led to oxetane ring-opening and formation of lactone **164** in 55% yield, likely *via* hydrolysis of a cyclic carboximidate intermediate. Di-acceptor Boc-protected dehydroalanine was also tolerated and yielded unnatural oxetane amino acid **165** in 60% yield. Reaction with styrene was reproducible (**166**), albeit in lower yield as previously reported (10%, *cf.* 35%),[211] and this yield increased remarkably with more

electron-poor *para*-bromostyrene to 73% of oxetane **167**. This trend is in line with a better polarity-matched coupling of a nucleophilic oxetane radical and an electrophilic radical acceptor. Giese reaction with functionalised 2- and 3-vinylpyridines was successful in moderate yields (**168**–**169**) and the yield of acetamide **169** was not improved by increasing the equivalents of vinylpyridine nor by using oxetane acid **148a** in excess.



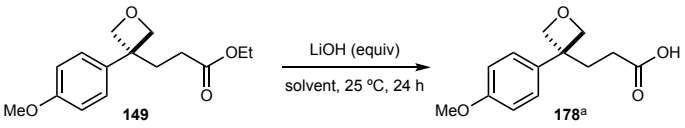
Scheme 45. Expanded scope of Giese reaction of oxetane carboxylic acids. a, Variation of oxetane acids and alkenes. Reactions run on a 0.2 mmol scale. **b**, Alkenes that did not yield the desired Giese product (**P**) with oxetane acid **148a**. [a] Yields calculated by analysis of the ^{1}H NMR spectrum of the crude mixture of the reaction using 1,3,5-trimethoxybenzene as internal standard and a 30 s relaxation delay (d1). Isolated yields in parenthesis. [b] Characterised by X-ray crystallography. [c] Using Ph oxetane acid **148m** purified by column chromatography, on a 0.1 mmol scale and for 14 h (isolated from time point for reaction profile, see Figure 63. [d] Reaction performed by M. Dubois (see Scheme 40).[211] [e] Reaction run on a 0.1 mmol scale. [f] Reaction performed by H. Broderick. [g] Yield based on alkene. [h] Estimated based on the mass of the crude reaction mixture and the ratio of oxetanes **154** and **155** in the ^{1}H NMR spectrum of the crude mixture. [i] Obtained as a mixture with dimer **154** and oligomers of varying length (not characterised).

More demanding alkene radical acceptors were also evaluated, and examples of unproductive Giese reactions are summarised in Scheme 45b. β-Substituted alkenes (**170**–**172**, **177**), in particular as part of cyclic structures, were ineffective and led to significantly higher amounts

of side products of homocoupling (**154**) and reduction (**155**). The higher steric requirement of the alkene presumably increased the energy of the TS of the radical Giese addition step, leading to an unfavourable relative rate of reaction compared to other deleterious pathways. Double acceptors such as methylene diester **173** (synthesised by Knoevenagel condensation) or -disulfone **174** were too reactive and led to mixtures of oligomerisation products of varying lengths. Other functionality such as caffeine derivative **172**, boronic acid pinacol esters (**175**), phenols (**176**) or furans (**177**) were not tolerated.

Unmasking of free carboxylic acid functionality in the ester-containing Giese products was of pharmaceutical interest to form a polar fragment and/or reactive synthetic handle. Acidic removal of a *tert*-butyl group had been shown to ring-open the oxetane ring by the internal nucleophile, promoted by the acidic conditions.[311] Under basic conditions on the other hand, oxetane ethyl ester **149** converted smoothly to the free carboxylic acid (**178**) with excess lithium hydroxide in an H_2O/THF/MeOH solvent mixture (Table 18, entry 3). In contrast to the recent report by Mykhailiuk (Enamine),[74] oxetane acid **178** was found to be stable to typical laboratory conditions such as handling at room temperature, concentration *in vacuo* at 40 ºC, aq. HCl (pH 1) or storage in a $CDCl_3$ solution.

Table 18. Saponification of oxetane ester **149**.



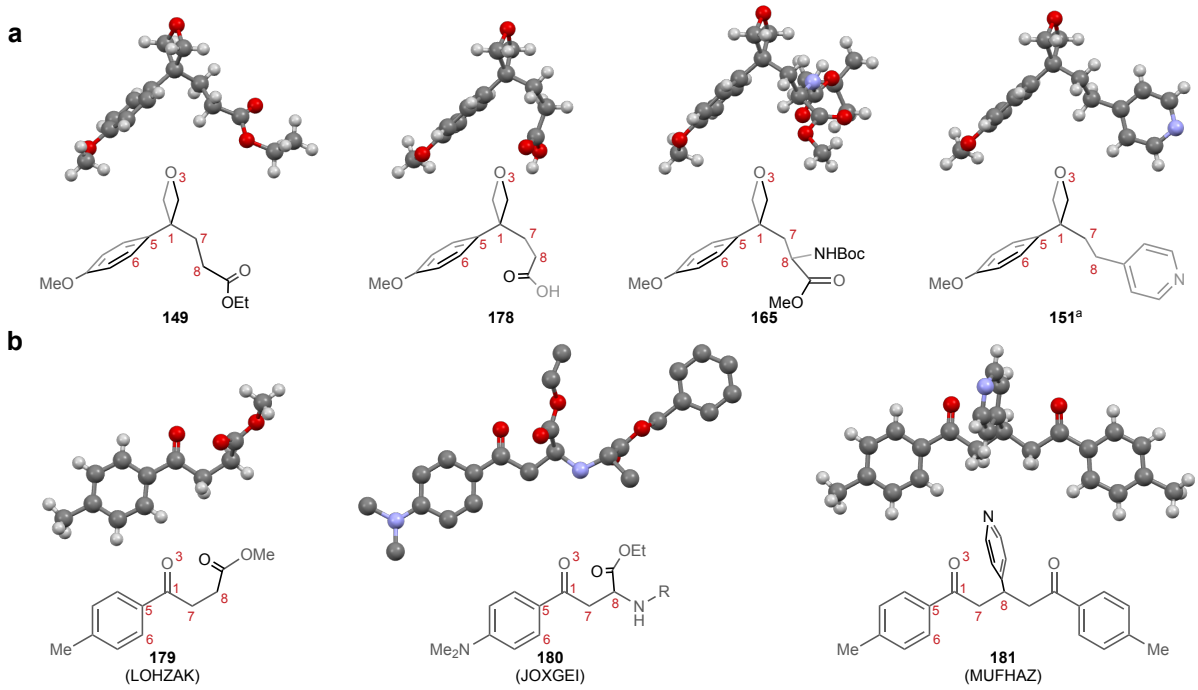
Entry	equiv	Solvent	Yield[b] **178** / %
1[c]	2	THF/H_2O (2:1)	low conversion
2	3	THF/H_2O (2:1)	94 (80% pure)
3	3	H_2O/THF/MeOH (3:1:1)	99 (>99% pure)

[a] Characterised by X-ray crystallography. [b] Reactions run on a 0.1 mmol scale and isolated yields after acid/base workup are reported. [c] Reaction run for 6 h.

4.2.1.4 Conformational Analysis

Suitable crystals for diffraction were grown by slow evaporation from $CDCl_3$ (**149**, **178**) or acetone (**165**, **151**), displayed on Figure 58a. Other techniques such as vapour- or liquid-liquid diffusion were ineffective for the 3-aryl-3-alkyl-oxetane products.

The conformation of the aryl-alkyl oxetane products showed many parallels to that of amino-oxetanes discussed in Section **3.2.11.1** (Figure 34a vs Figure 58a). Oxetanes showed generally more 3-dimensional character than ketones, with their conformation minimising unfavourable interactions (Figure 58a). The conformation in phenones maximised favourable π-conjugation (Figure 58b). Quantitatively, similar trends to the amino-oxetane/benzamides were observed (Figure 58c). The C–O interatomic distance was longer in oxetanes (2.15 Å) than in phenones (1.23 Å), the C5-C1-C7 bond angle was slightly more acute in oxetanes (112 º) than in phenones (119 º) and the Ar dihedral angle of oxetanes (82 º) was orthogonal to that of phenones (3 º), which showed a coplanar Ar-carbonyl conformation. The latter difference in Ar dihedral angle is responsible for the increased 3-dimensionality observed in the oxetane structures. The puckering angle of the oxetane ring was small (on average 10 ± 4º) but significantly non-planar, suggesting perhaps a high steric demand of the 3-substituents. As observed for amino-oxetanes (Section **3.2.11.1**) and also by Carreira and Roche for 3,3-dialkyl oxetanes,[70] the bulky oxetane ring induced a switch in the preferred conformation of the large substituent on C7 (*i.e.* C8), best seen in Newman projections (Figure 58d). In oxetanes, the aliphatic backbone chain clearly preferred a synclinal gauche conformation with the C8 substituent ca. 124 º degrees to oxetane (C1–O3 coordinate), whereas the backbone chain of phenones adopted preferably an antiperiplanar conformation with C8 on the side of the carbonyl (dihedral angle ca. 6 º). The high planarity of phenones and the contrasting increased 3-dimensionality of 3-aryl-3-alkyl-oxetanes is best appreciated by overlaid structures, exemplified with **149** and **179** (Figure 58e).



c

	Oxetanes				Ketone			Average	
	149	**178**	**165**	**151**[a]	**179**[b]	**180**	**181**	oxetanes	ketones
C1–O3 / Å	2.14	2.15	2.15	2.15	1.22	1.24	1.22	2.148 ± 0.008	1.23 ± 0.03
C1–C5 / Å	1.51	1.51	1.51	1.50	1.49	1.47	1.49	1.508 ± 0.008	1.48 ± 0.03
C1–C7 / Å	1.53	1.53	1.53	1.54	1.50	1.51	1.52	1.533 ± 0.008	1.51 ± 0.03
'carbonyl' bond angle / ° (C5–C1–C7)	112	113	110	112	119	119	118	111.8 ± 2.0	118.7 ± 1.4
pukering dihedral angle / ° (O3–C2–C4–C1)	8	14	8	10	–	–	–	10 ± 4	–
Ar dihedral angle / ° (O3–C1–C5–C6)	81	83	83	80	1	4	5	81.8 ± 2.4	3 ± 5

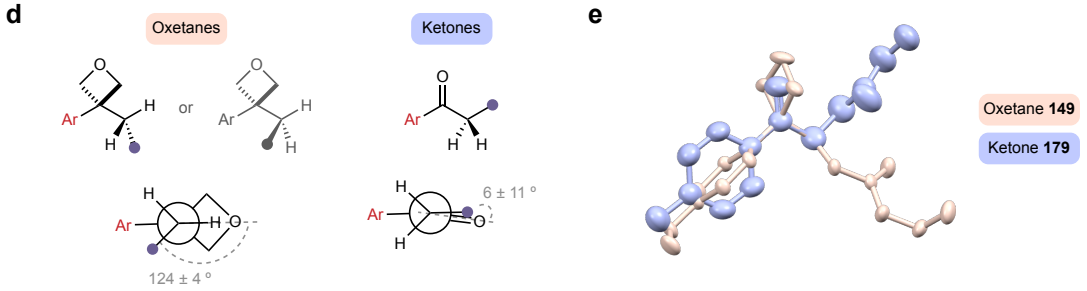


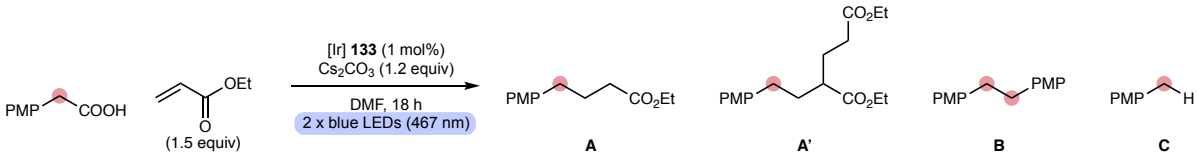
Figure 58. Structural analysis of 3-aryl-3-alkyl-oxetanes. a, Acquired X-ray crystal structures of 3-aryl-3-alkyl-oxetanes. **b**, Related X-ray crystal structures of phenones from the literature. Structure identifiers in parenthesis. Numbering kept the same as in **a** to facilitate comparison. **c**, Pertinent bond lengths, interatomic distances and dihedral angles. Errors represent the 95% CI. **d**, Analysis of dihedral angles along the C7–C1 bond of oxetanes and ketones. **e**, Overlay of representative oxetane (**149**) and ketone (**179**) X-ray structures. Structures overlaid using Mercury, by overlaying C1, C5 and C7, shown in the ORTEP representation. [a] **151** synthesised by M. Dubois. [b] Values are the average of two independent molecules of phenone **179** that formed the unit cell.

4.2.1.5 Mechanistic Investigations

In this section, the mechanistic questions outlined in Section **4.2.1.1** were investigated through experimental and computational studies. The computational study was undertaken in collaboration with the Duarte group (University of Oxford). Quantum mechanical calculations were performed on ORCA software (4.1.1)[300] and used variable levels of theory depending on the experiment (given separately in the caption of the relevant figures). The computational experiments were conducted by A. Sterling and F. Duarte and were analysed collaboratively with input from A. Sterling, F. Duarte, J. Bull and myself. Details of the computational experiments, raw computational data and cartesian coordinates can be found in ref. 311 and at the Imperial College London Research Data Repository.[357]

4.2.1.5.1 Trends in the Giese Reaction of Different Arylacetic Acids

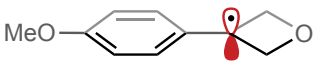
First, the product distribution of arylacetic acids was expanded to comprise a highly strained cyclopropane linker, which showed the lowest yield of the Giese product (**II-A**) and no side products (Scheme 46).



Yields / %	I[a]	II	III	IV[a]	V[a]	VI[a]	VII
A	38	19	53 (**149**)	53	36	33	45
A'	9	0	7 (**149'**)	12	7	12	12
B	11	0	1 (**154**)	0	6	23	40[b]
C	0	0	0 (**155**)	0	0	0	0

Scheme 46. Divergent radical reactivity of different arylacetic acids. [a] Compounds synthesised by M. Dubois.[211] [b] Characterised by X-ray crystallography (see Figure 59d).[311]

Then, fundamental properties of a series of benzylic radicals, and their correlation towards the observed experimental reactivity (Scheme 46), were studied computationally. First, all of the investigated benzylic radicals, strained and unstrained, were shown to adopt a planar conformation, with the free electron occupying a pure p-orbital on the benzylic carbon in conjugation with the arene (see Figure 59 with oxetane radical **III** as example).



III

Figure 59. Structure of benzylic oxetane radical III. Geometries calculated at the CPCM[358](DMF)-ωB97X-D3[359]/def2-TZVP//ωB97X-D3/def2-SVP[360] level.

Relative radical stabilities of the series of benzylic radicals were calculated (by H-atom exchange equilibria with cyclopropyl radical **II**),[311] as well as the Gibbs free energies (ΔG) and activation barriers ($\Delta G^{\ddagger}$) of the Giese addition of each radical into methyl acrylate (Figure 60a).[z] Radical stabilities followed a rough trend: highly strained radical (**II**) < primary radical (**I**) < tertiary heterocyclic radicals (**III**, **IV**), < tertiary carbocyclic and acyclic radicals (**V**, **VII**), and correlated well with Giese ΔG values, whereby less stable benzylic radicals showed a thermodynamically more favourable Giese addition (Figure 60b). Notably, only a slightly exergonic to endergonic process was observed for the most stable radicals (**V**–**VII**), rendering their Giese addition reversible. The Giese addition of the remaining radicals (**I**–**III**) was exergonic enough to be considered to be irreversible.

From the data available on product distributions (Scheme 46), it was clear that yield of the desired Giese product (**A**) was maximised when formation of the dimer homocoupling side product (**B**) was supressed. This apparent correlation prompted an in-depth computational study into the factors that favoured/disfavoured dimerisation. The driving force of the Giese addition (ΔG) was found to influence formation of dimer, whereby more stable radicals led to a more positive Giese ΔG which resulted in higher amounts of dimer (Figure 60b–c). The correlation was assessed quantitatively through a linearisation of the seemingly exponential dependency of yield of dimer to ΔG, and the logarithmic yield values showed a linear dependency, with a high adjusted R^2 value of 0.96 (Figure 60c, bottom graph).[aa]

The correlation is best explained with cyclopropane (**II**) and *gem*-dimethyl radicals (**VII**) as the most extreme examples. The instability of the cyclopropane radical (**II**) results in an exergonic Giese addition (ΔG = –11.7 kcal mol^{-1}), leading to rapid quenching and low concentration of radical **II** and suppression of dimer formation (0% **II-B**). Cyclopropyl radicals are notably prone to degradation, which explains the low yield of Giese product obtained with this example (19% **II-A**; Scheme 46).[361] On the other side of the stability spectrum, *gem*-dimethyl radical **VII** is so

---

[z] The relative stabilities ($\Delta\Delta G$) and Giese ΔG of the 3-Ph-oxetane and 3-($^{4\text{-CF}_3}$Ph)-oxetane radicals were also calculated: $\Delta\Delta G$: Ph: –8.2 kcal mol^{-1}; $^{4\text{-CF}_3}$Ph: –8.9 kcal mol^{-1}.ΔG: Ph: –2.6 kcal mol^{-1}; $^{4\text{-CF}_3}$Ph: –3.7 kcal mol^{-1}.

[aa] Cyclopropyl radical **II**, which has an undefined value of ln(yield), and methylene radical **I**, which was a clear outlier, were not taken into account for the modelled linear regression in Figure 60c.

stabilised, that Giese addition is endergonic (ΔG = +0.6 kcal mol^{-1}) and hence reversible according to the principle of microscopic reversibility.[362] Reversible Giese addition increases the concentration of benzylic radical **VII** and directly also the rate of dimerisation, which is dependent on the squared concentration of radical **VII** (rate ∝ [**VII**]^2). Such a scenario would be predicted to result in increased yield of dimer **VII-B** and reduced formation of Giese product **VII-A**, which was confirmed experimentally (Figure 60d).

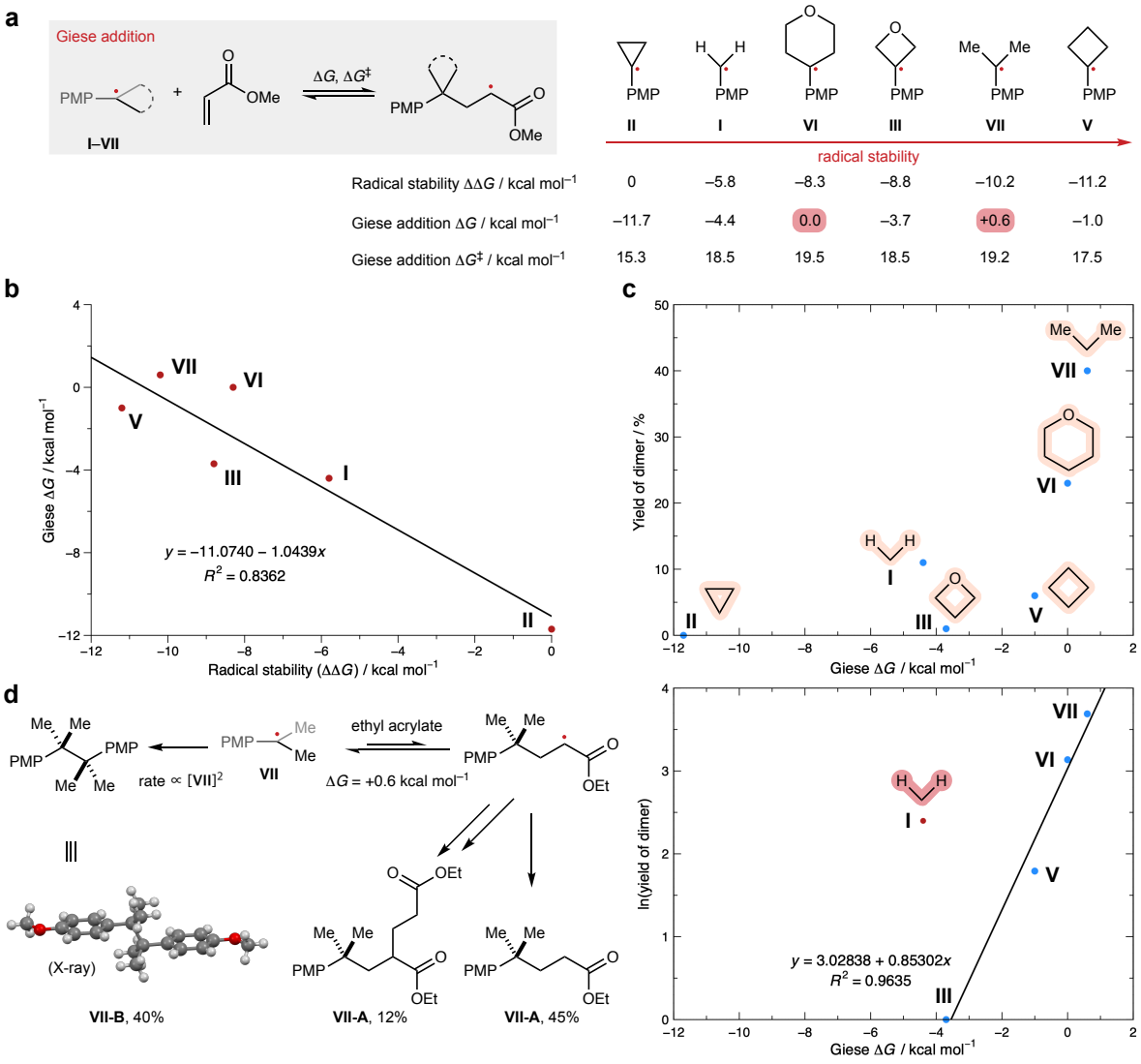


Figure 60. Correlation between radical stability and Giese addition. a, Calculated relative radical stabilities and ΔG and $\Delta G^{\ddagger}$ of the Giese addition. Relative stabilities ($\Delta\Delta G$) determined by H-atom exchange equilibria with cyclopropyl radical **II**.[311] All Calculations at the CPCM[358](DMF)-ωB97X-D3[359]/def2-TZVP//ωB97X-D3/def2-SVP[360] level. Free energies calculated at 298.15 K and 1 M standard state. **b**, Correlation between Giese ΔG with methyl acrylate and radical stabilities ($\Delta\Delta G$ vs cyclopropane radical **II**). **c**, ΔG vs. Yield of dimer (**B**) and correlation between ΔG and the natural logarithm of the yield of dimer (ln(yield of dimer)). The outlier methylene radical **I** and the undefined value for cyclopropyl radical **II** (ln(0) = undefined) were not taken into the model for linear regression. **d**, Reactivity of *gem*-dimethyl benzylic radical. Experimental isolated yields given (Scheme 46) and ΔG calculated for methyl acrylate (see part **a**).

There was one obvious outlier in the Giese ΔG–yield of dimer correlation: methylene radical **I** (Figure 60c). Based on radical stabilities and Giese driving force alone (Figure 60a), this species would be expected to show no formation of dimer. However, despite these indications, 11% of dimer **I-B** were observed experimentally (third highest value), suggestive of another factor(s) influencing dimer formation. In radical chemistry, radical localisation, or spin density (ρ_s), is often computed to predict reactivity, akin to calculations of charge distribution in pendant polar chemistry. In this regard, theoretical work by Savéant suggested a higher spin density of benzylic radicals to decrease the activation barrier to dimerisation due to a lower energetic penalty for localisation of the radical on the bond-forming carbon atom during the transition state.[363] Calculation and analysis of spin densities on radicals **I**–**VII** (except **IV**) showed the spin density on methylene radical **I** to be significantly higher than in all other analogues (Figure 61a), providing a plausible explanation for the unexpected high yield of dimer observed with this substrate.

The trend of increasing spin density from cyclopropane radical **II** to *gem*-dimethyl radical **VII** seemed to be roughly correlated to decreasing ring strain. An analysis of bonding orbitals in the radical species showed that, as the p-character of the hybrid orbital of the benzylic carbon atom (C1) involved in the σ bond with the arene (C1–C2) increases, spin density increases (Figure 61b). The decrease in s-character lengthens the C1–C2 bond, which reduces the extent of delocalisation of the radical into the aromatic π-system ($\Delta E^{(2)}(p \rightarrow \pi^*)$).

The key orbital hybridisation of C1 in the C1–C2 bond is dictated by the hybridisation of the remaining C1 orbitals, that is, those involved in the residual benzylic C–C bonds (C1–C3 and C1–C4) (Figure 61c). The acute internal bond angles imposed by the geometry of small rings must assign a higher p-orbital contribution on the hybrid orbitals that make up the endocyclic bonds to achieve the small bond angles. In turn, the high p-character of hybrid orbitals involved in the cyclic bonds of small rings, directly result in the assignment of greater s-character (*i.e.* lower p-character) on the hybrid orbitals that form the exocyclic bonds, which is the central C1–C2 bond in radicals **I**–**VII**. This effect of redistribution of hybridisation is greater in the cyclopropane system **II** (bond angles ~60 º, $sp^{3.75}$ in-ring hybridisation), than in the four-membered rings **III** and **V** (bond angles ~90 º, $sp^{3.40}$ (oxetane) and $sp^{3.15}$ (cyclobutane) in-ring hybridisations), and not present at all in larger rings (THP **VI**) or acyclic structures (**VII**). Figure 60d summarises the proposed model.

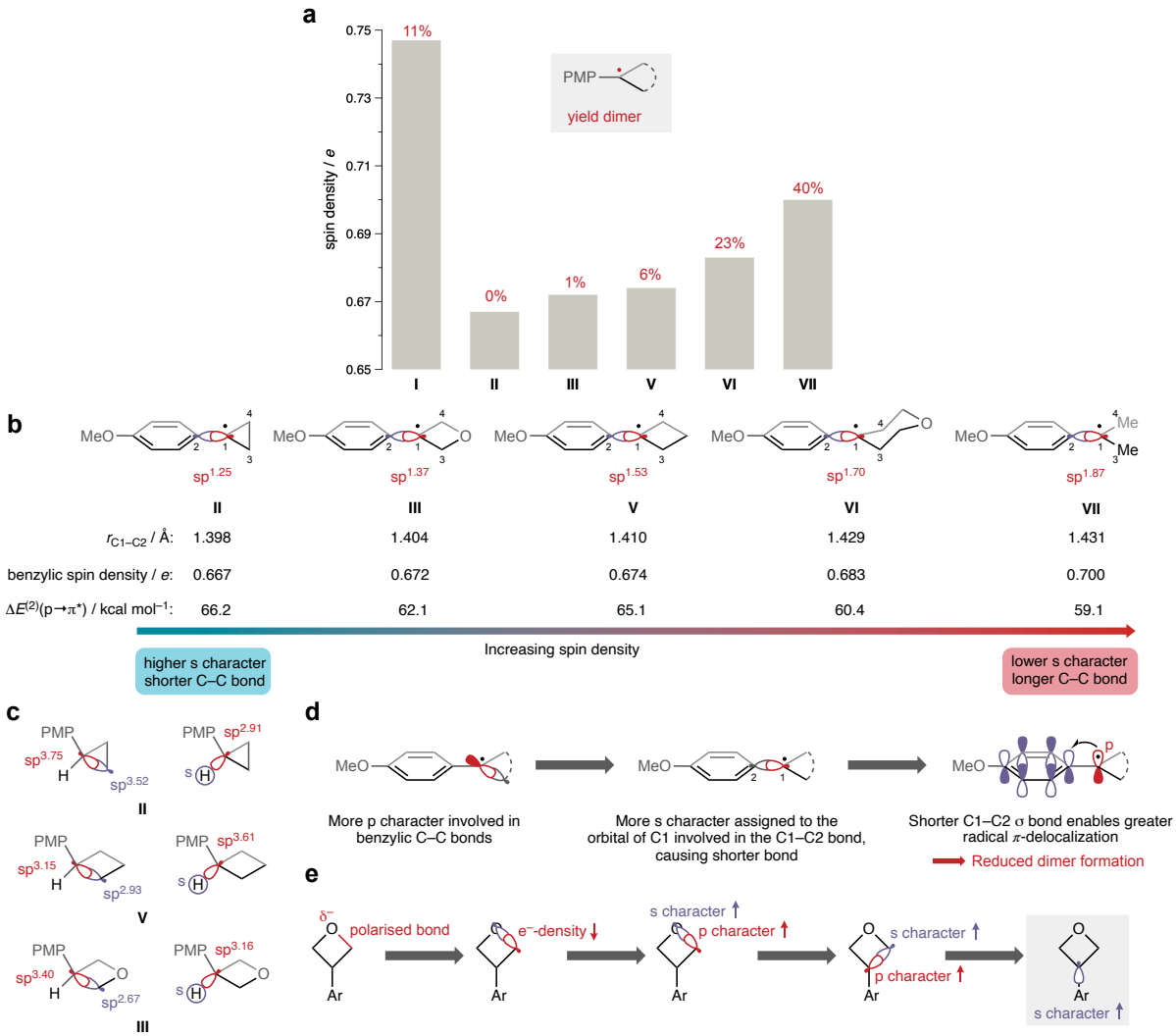


Figure 61. Influence of benzylic spin density on Giese addition. a, Calculated spin densities on the benzylic position. **b**, Hybridisation of atomic orbital on benzylic carbon involved in C1–C2 bond. **c**, Hybridisation of atomic orbitals on benzylic carbon involved in other bonds. **d**, Model for variation in benzylic spin density. **e**, Bent's rule to explain higher s-character of orbital of C1 involved in C1–C2 bond of radical **III** vs radical **V**. All Calculations at the CPCM[358](DMF)-wB97X-D3[359]/def2-TZVP//wB97X-D3/def2-SVP[360] level. Hybridisations calculated using Natural Bond Orbital (NBO) theory.[364] $\Delta E^{(2)}(p \rightarrow \pi^*)$ denotes the degree of radical delocalisation into aromatic ring and was calculated using NBO second order perturbation theory.

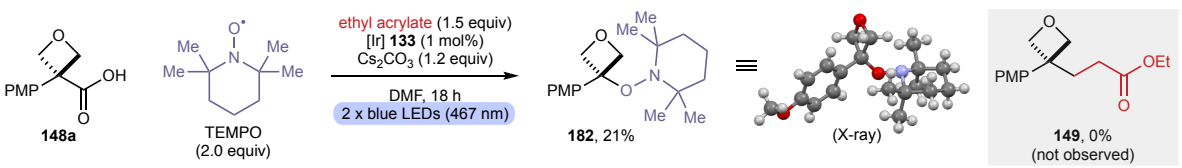
Lastly, the differences in hybridisation, and hence reactivity, between the cyclobutane and oxetane molecular systems were striking, since, solely based on geometrical considerations, both ring systems should show comparable hybridisation properties. The discrepancy, caused by the oxygen atom on oxetane, is explained by Bent's rule (Figure 61e).[365] The higher electronegativity of the oxygen atom compared to the carbon atom polarises the C–O σ bond and localises the electron-density forming this bond closer to the oxygen nucleus to provide better stabilisation of the negative charge. The electron-density on the hybrid bonding orbital of the carbon (C2/C3) that forms the C–O σ bond is hence reduced. Bent's rule implies that assigning greater p-character to this 'electron-poor' hybrid orbital incurs only a small energetic

penalty (since there is little negative charge on this orbital), and more s-character can be assigned to the hybrid orbitals with higher electron-density that form the remaining bonds. A higher s-character draws the electron-density closer to the carbon nucleus and provides an overall stabilisation of the system. The effect of Bent's rule propagates with decreasing intensity through the σ framework and is responsible for the often-invoked 'inductive effect'. In oxetane radical **III**, the abnormally high s-character of the hybrid orbital of the C3/C4 atoms involved in the C–C bonds (C3–C1 and C4–C1) now in turn withdraws electron-density from this bond (since the high s-character associated with this hybrid orbital better stabilises negative charge) and a higher p-character is assigned to the hybrid orbitals on C1 that form these C–C bonds, in analogy to the polarisation of the C–O bonds. The final repercussion of Bent's rule on oxetane radical **III** is the assignment of high s-character to the hybrid orbital on C1 that forms the key C–C bond to the arene (C1–C2), which significantly impacts radical reactivity and causes differentiation to cyclobutane radical **V**.

Based on considerations of radical stability and hybridisation, a rationalisation was provided for the superior Giese reactivity of oxetane (and by analogy azetidine) benzylic radicals compared to other cyclic and acyclic analogues. The computational study presented in this section shed light on the influence of ring strain and heterosubstitution on radical reactivity and improved the understanding of benzylic radicals. The enhanced stability of benzylic radicals and considerations of radical spin delocalisation might be a general explanation for the anecdotal inertness and sluggish reactivity of benzylic radicals.

4.2.1.5.2 Key Steps and Intermediates of the Giese Mechanism

First, adding TEMPO as a radical trap to the Giese reaction conditions provided evidence for an oxetane radical intermediate (Scheme 47). TEMPO supressed Giese reactivity and oxetane–TEMPO adduct **182** was isolated in 21% yield and characterised by X-ray crystallography.



Scheme 47. Addition of TEMPO to the Giese conditions.

Then, the cyclic voltammograms of several substrates were measured and compared (Table 19). Cyclic voltammetry (CV) is a powerful analytical tool in physical organic chemistry to assess the thermodynamic feasibility of reduction/oxidation-coupled chemical reactions.[250,366] Potentials were measured between –2.2 and +2.2 V, in a 0.1 M solution of

NBu_4ClO_4 (supporting electrolyte) in MeCN at room temperature (ca. 22 ºC) with a scan rate of 100 mV s^{-1}. A glassy carbon disc was used as working electrode, a Pt-coated copper block as counter electrode and a Pt-wire as quasi-reference electrode. Ferrocene (Fc) was used as an internal standard to convert the measured potentials against the Fc/Fc^+ redox couple to the standardised saturated calomel electrode (SCE).[367,368] The potentials of compounds with irreversible oxidation waves (common for organic compounds) are reported as the anodic peak potentials (E_{pa}) for better reproducibility.[366b] See Section **7.4** for further experimental details on the conducted CV measurements.

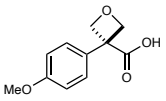
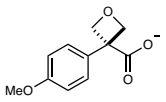
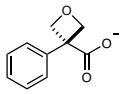
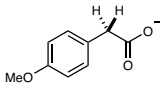
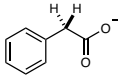
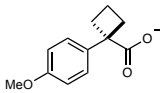
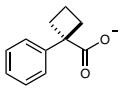
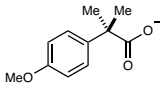
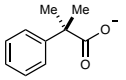
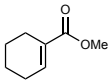
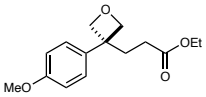
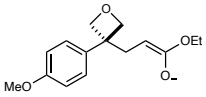
All measured potentials are summarised in Table 19 and the raw voltammograms can be found in Appendix **9.4**. First, the oxidation potential of neutral PMP oxetane carboxylic acid **148a** was measured to be much higher (≥2.01 V vs SCE) than that of its carboxylate form **148a**$^-$ (+0.89 V vs SCE) (Entries 1–2). Hence, carboxylate **148a**$^-$ can be oxidised by the excited photocatalyst [Ir^{III*}] **133*** ($E_{1/2}^{[III^*/II]}$ = +1.21 V vs SCE),[355a,bb] but direct oxidation of acid **148a** is thermodynamically outside the range of [Ir^{III*}], in line with the requirement of the Giese reaction for base.[211,311]

A qualitative correlation between oxidation potential and electronics of the carboxylate was observed, in accordance with an earlier report by Ravelli (entries 2–9).[349a] In general, the more electron-rich the carboxylate, the easier to oxidise (lower oxidation potential), which is intuitively sensible. The trend was observed both in the electronics of the aromatic, that is, E^{ox}(PMP) < E^{ox}(Ph) (entries 2/3, 4/5, 6/7, 8/9), and in the electronics of the benzylic linker, that is, E^{ox}(cyclobutane) ~ E^{ox}(*gem*-dimethyl) < E^{ox}(oxetane) ~ E^{ox}(methylene) (entries 2–9). The proposed correlation could, in principle, be extended to expected pK_a values of the carboxylic acids and radical philicities of the corresponding benzylic radicals (Figure 62). Specifically, higher benzylic electron density → higher pK_a of carboxylic acid → higher nucleophilicity of radical[cc] → lower oxidation potential. Such a correlation should be general and could be a practical way to compare relative pK_a values and radical philicity by means of CV measurements.

[bb] Compounds with an oxidation potential higher than +1.21 V vs SCE are thermodynamically unfavoured to be oxidised by [Ir*] **133***.

[cc] The nucleophilicity of a radical increases with its capability to stabilise positive charge (*i.e.* the radical can more easily 'give' its electron since it can better stabilise the developing positive charge).

Table 19. Measured oxidation potentials by CV of relevant species.

Entry	Substrate[a]	*E* / V			
		E_{pa} (Obs)	$E_{1/2}$ (Fc^+/Fc)	E_{pa} (vs Fc^+/Fc)	E_{pa} (vs SCE)
1[b]		≥2.08[c]	+0.45	≥1.63[c]	≥2.01[c]
2		+1.31	+0.80	+0.51	+0.89
3		+1.79	+1.09	+0.70	+1.08
4		+1.51	+1.07	+0.44	+0.82[d]
5		+1.81	+1.13	+0.68	+1.06[e]
6[f]		+1.48	+1.14	+0.34	+0.72
7[f]		+1.61	+1.11	+0.50	+0.88
8		+1.50	+1.15	+0.35	+0.73
9		+1.63	+1.09	+0.54	+0.92
10[b]		+1.91	+0.17	+1.74	+2.12
11[b]		≥2.14[c]	+0.47	≥1.66[b]	≥2.04[c]
12		+1.21	+0.99	+0.22	+0.60

[a] Anions generated by adding 1.0 equiv NBu_4OH (1 M solution in MeOH). [b] Run in the absence of NBu_4OH. [c] Estimated based on shoulder peak. No oxidation peaks between 0 and +2.0 V. [d] Literature value: +0.99 V vs SCE.[349a] [e] Literature value: +1.27 V vs SCE.[349a] [f] Substrate synthesised by M. Dubois.

Cyclohexene methyl carboxylate had shown significantly increased formation of dimer (**154**) and reduced side products (**155**) in the Giese reaction (Scheme 45b), so its CV was measured (Table 19, entry 10). No reduction waves were observed up to –2.2 V, suggesting this alkene cannot be reduced directly by the reduced form of the catalyst, [Ir^{II}] **133** ($E_{1/2}^{[II/III]}$ = –1.37 V vs SCE).[355a] See Table 22 and the associated discussion for more details.

Lastly, the oxidation potential of enolate **149**$^{-}$ (+0.60 V vs SCE), but not that of ester **149** (≥2.04 V vs SCE), was shown to be in the range of [Ir^{III*}] ($E_{1/2}^{[III^*/II]}$ = +1.21 V vs SCE), suggesting enolate **149**$^{-}$ can be oxidised back to Giese adduct **149**$^{\bullet}$, rendering product formation potentially reversible (Table 19, entries 11–12; see also Table 23 and Figure 66). The measured oxidation potential of oxetane **149**$^{-}$ is in accordance with literature values of related enolates.[369]

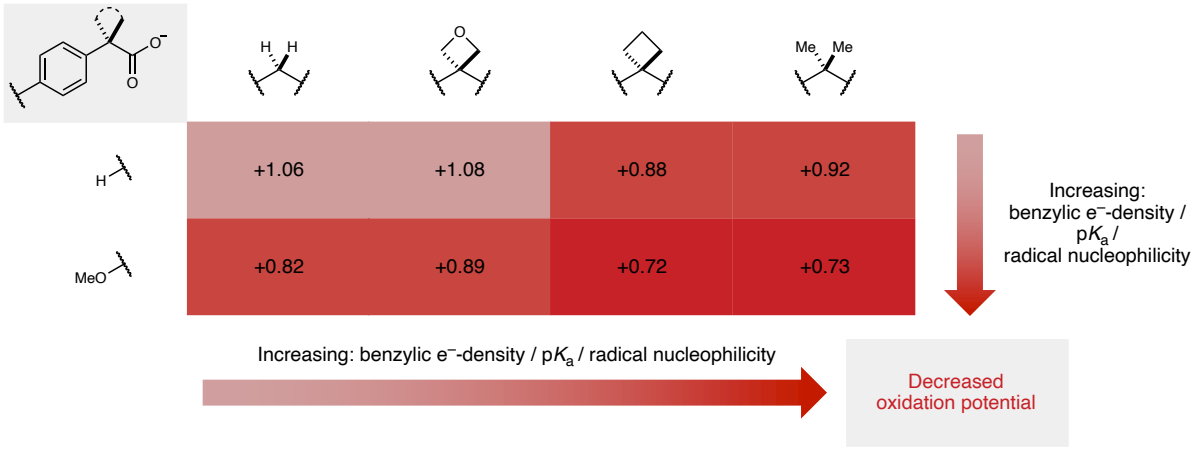


Figure 62. Correlation of oxidation potentials of arylacetic acids with electron density at benzylic position. Potentials given as E_{pa} in V vs SCE (Table 19, entries 2–9).

The reduction potentials of two key catalytic intermediates, which cannot be determined by cyclic voltammetry, were calculated (by A. Sterling; Figure 63). The potential required to reduce oxetane radical **III** was computed to be –1.67 V vs SCE; 0.33 V outside the range of [Ir^{II}] and therefore thermodynamically unfavourable to occur (cell potential of –0.33 V corresponds to a Gibbs free energy of ΔG = +7.6 kcal mol^{-1} for the electron transfer, using Faradays constant F) (Figure 63a). The calculated reduction potential of radical **III** suggests oxetane carbanion **III**$^{-}$ is not an intermediate in the reaction, for example, en route to reduced oxetane side product **155** (see Figure 57). Second, the reduction potential of Giese adduct **149**$^{\bullet}$ was calculated to be –0.80 V vs SCE (Figure 63b), well in the range of [Ir^{II}] (Gibbs free energy for reduction: ΔG = –12.4 kcal mol^{-1}), and supports this RedOx step that forms the Giese product and regenerates the iridium photocatalyst ([Ir^{III}] **133**).

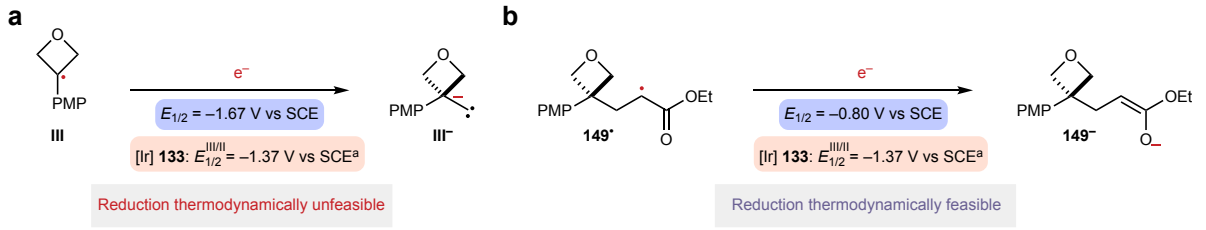
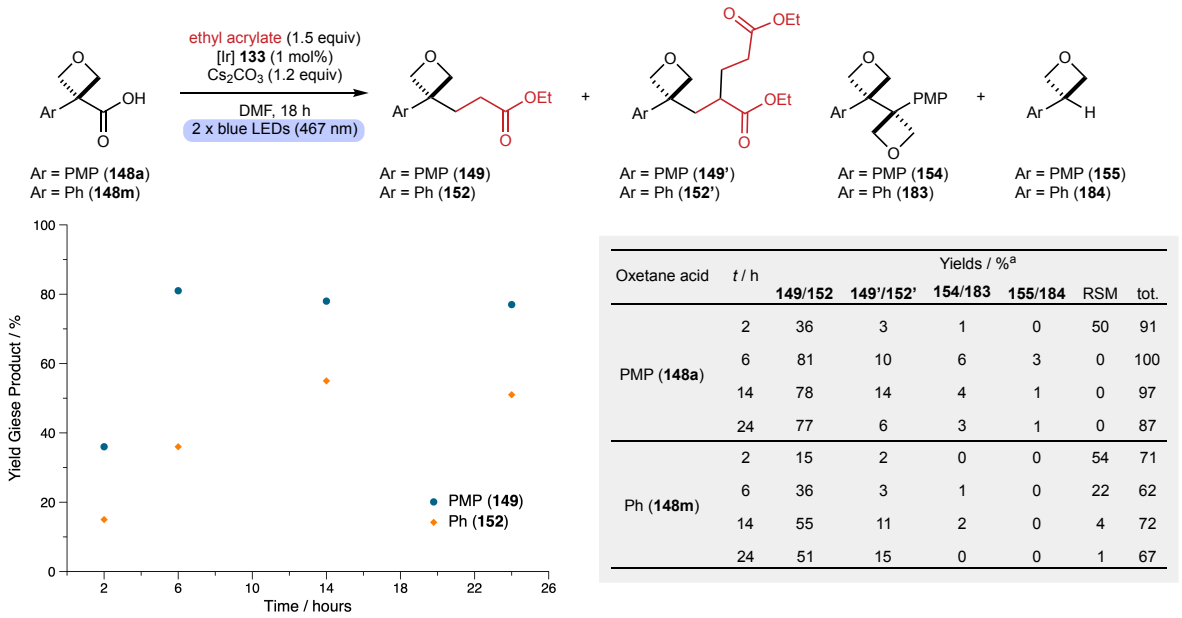


Figure 63. Calculated reduction potentials. a, 1-e^{-} reduction of oxetane radical **III** to carbanion **III**$^{-}$. **b**, Reduction of Giese adduct **149**$^{\bullet}$ to enolate **149**$^{-}$. Potentials calculated at the SMD(DMF)-M06-2X/ma-def2-TZVP level of theory. [a] Literature value.[355a]

The difference in yield between PMP and Ph oxetane acids **148a** and **148m** was investigated (Scheme 45a). Whilst it could be argued that the PMP oxetane radical is more nucleophilic than its Ph counterpart and would thus allow for a more favourable Giese addition with electrophilic alkenes, such a difference was not reflected in calculated Giese ΔG (ΔG (PMP) = –3.7 kcal mol^{-1}; ΔG (Ph) = –2.6 kcal mol^{-1}; see Figure 60 for details on calculations) nor relative radical stabilities ($\Delta\Delta G$ (PMP) = –8.8 kcal mol^{-1}; $\Delta\Delta G$ (Ph) = –8.2 kcal mol^{-1}; see Figure 60 for details on calculations). The relative rate of Giese reaction of PMP acid **148a** was however higher than that of Ph acid **148m**, seen in their measured reaction profiles (Figure 64). This discrepancy could be due to a lower oxidation potential of the carboxylate derived from PMP carboxylic acid **148a**$^-$ (Table 19), suggestive of oxidation being rate-influencing.



Oxetane acid	*t* / h	Yields / %[a]					
		149/152	**149'/152'**	**154/183**	**155/184**	RSM	tot.
PMP (**148a**)	2	36	3	1	0	50	91
	6	81	10	6	3	0	100
	14	78	14	4	1	0	97
	24	77	6	3	1	0	87
Ph (**148m**)	2	15	2	0	0	54	71
	6	36	3	1	0	22	62
	14	55	11	2	0	4	72
	24	51	15	0	0	1	67

Figure 64. Reaction profiles and corresponding yields of the Giese reaction of oxetane PMP acid 148a and Ph acid 148m with ethyl acrylate. Repurified starting materials (**148a**, **148m**) used, see Section **7.5** for experimental procedures. [a] Reactions run on a 0.1 mmol scale and yields calculated by analysis of the ^{1}H NMR spectrum of the crude mixture of the reaction using 1,3,5-trimethoxybenzene as internal standard and a 30 s relaxation delay (d1).

Lastly, a series of deuteration experiments were conducted to study the formation of the final ester Giese product **149**. Oxetane acid **148a** was deuterated by dissolution in CD_3OD (ca. 100 mg in 1 mL), followed by solvent removal *in vacuo*. Deuteration was confirmed by IR spectroscopy, seen as a hypsochromic shift (blue-shift) of the O–H stretch from 3444 cm^{-1} (ref. 352) to 2228 cm^{-1} (O–D stretch), caused by a significant increase (ca. two-fold) in reduced mass μ from proton to deuterium (Figure 65). From the difference in μ, a 0.728 fold decrease in stretching frequency would be expected from O–H to O–D (*i.e.* 2507 cm^{-1}). The

observed frequency of 2228 cm^{-1} is in good accordance, given the broadness of the O–H stretch (stretched ca. between 3500–2500 cm^{-1}).[352]

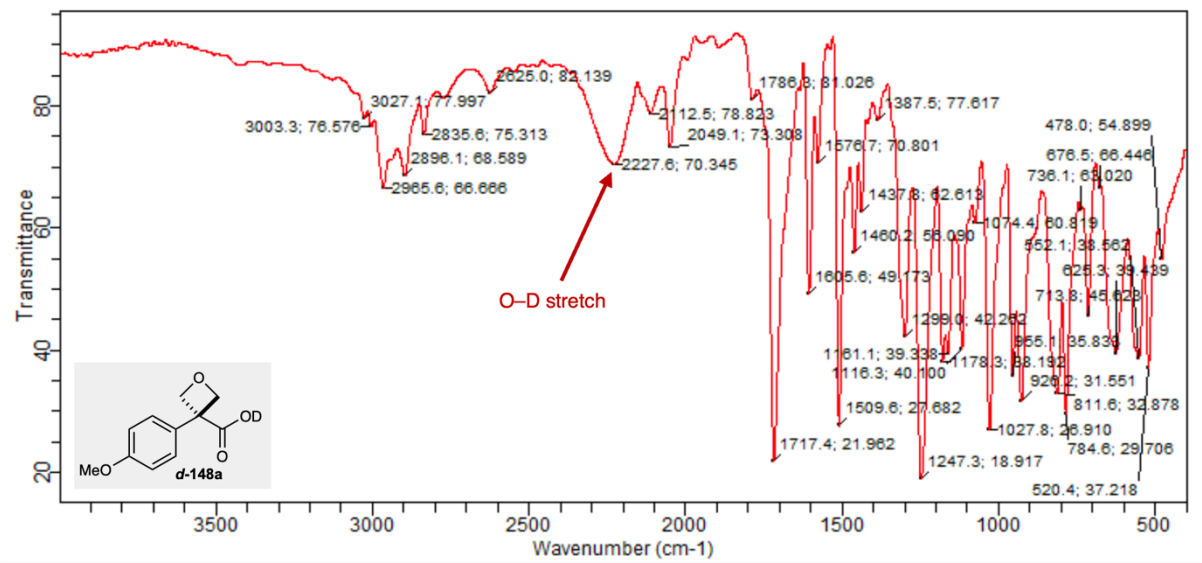
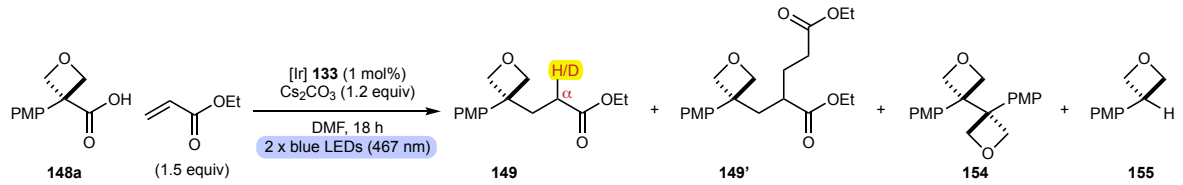


Figure 65. IR spectrum of *d*-148a.

The final step towards formation of ester **149** is believed to be protonation of an enolate intermediate **149**$^{-}$ (see Figure 57). To study this chemical step, the Giese reaction of oxetane acid **148a** with ethyl acrylate was conducted in the presence of potential deuterium donors (Table 20). Incorporation of deuterium was only observed with D_2O as additive (entries 5 and 6), but not with deuterated oxetane acid ***d*-148a** or deuterated DMF, a potential HAT donor (entries 2–4).[370] No deuterium incorporation with a D_2O quench (entry 7) suggested protonation of enolate **149**$^{-}$ during the course of the reaction and not upon quench. Figure 108 in Appendix **9.5** shows the ^{1}H NMR spectra for all entries of Table 20.

Incorporation of deuterium with D_2O as additive suggested the potential involvement of water as proton-mediator (Table 20, entries 5–6). To further investigate the possible role of H_2O in the reaction, various experiments under rigorously anhydrous conditions were performed (Table 21). The Giese reaction stayed unaffected by exclusion of water (entries 1–2; and also by deliberate addition of water; *cf.* Table 20, entries 5–6) and no deuterium was incorporated with ***d*-148a** nor a D_2O quench (entries 3–4). While the results in Tables 20 and 21 are suggestive of the involvement of a protonation step to yield the final ester product **149**, the source of protons could not be unambiguously determined.

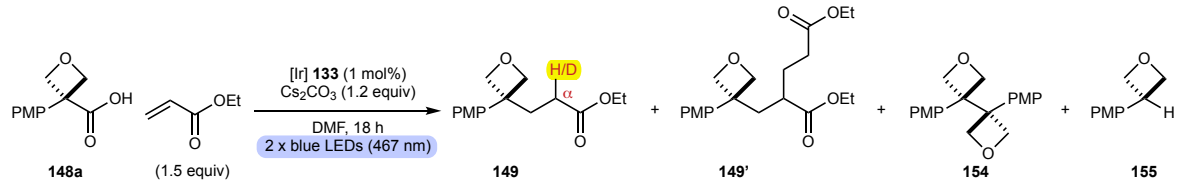
Table 20. Incorporation of deuterium α to the ester in Giese product **149**.



Entry	Change from standard conditions	Yield / %[a]			
		149 / D-incorporation (%)	**149'**	**154**	**155**
1	none	58 / NA	7	1	0
2	***d*-148a** (COOD)	57 / 0	13	2	2
3	using DMF-d_7[b]	67 / 0	8	2	0
4	using DMF-d_7 + ***d*-148a** (COOD)[b]	63 / 0	11	3	0
5	+ 2.77 equiv D_2O[c]	64 / 58[d]	8	2	0
6	+ 10.0 equiv D_2O	56 / 71[d] (78)[e]	10	1	0
7	D_2O quench[f]	60 / 0	8	3	0

[a] Reactions run on a 0.2 mmol scale and yields and percentage of deuteration calculated by analysis of the ^{1}H NMR spectrum of the crude mixture of the reaction using 1,3,5-trimethoxybenzene as internal standard and a 30 s relaxation delay (d1). [b] Run on a 0.14 mmol scale. [c] Corresponds to 10 μL (1% *v*/*v*). [d] Relevant signals in the ^{1}H NMR spectrum of the crude reaction mixture obscured by other species. Approximate value given. [e] Measured after purification by column chromatography. [f] 1.0 mL D_2O was added to the reaction mixture, stirred for 5 minutes, and followed by the standard workup (see Section **7.6.6**).

Table 21. Influence of water on the Giese reaction of oxetane acid **148a**.



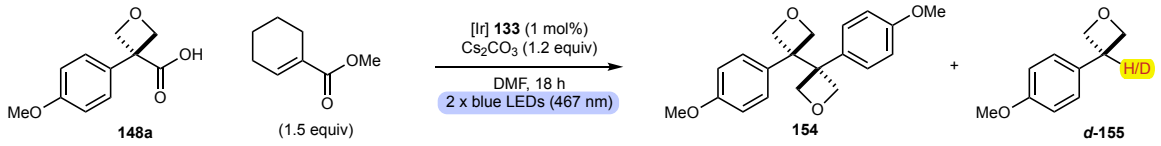
Entry	Change from standard conditions	Yield / %[a]			
		149 / D-incorporation	**149'**	**154**	**155**
1	none[b]	63 / NA	7	1	0
2	extra dry DMF[c]	68 / NA	9	1	0
3	extra dry DMF[c] + ***d*-148a** (COOD)	72 / 0	9	1	0
4	extra dry DMF[c] + D_2O quench[d]	60 / 0	5	1	0

[a] Reactions run on a 0.2 mmol scale and yields and percentage of deuteration calculated by analysis of the ^{1}H NMR spectrum of the crude mixture of the reaction using 1,3,5-trimethoxybenzene as internal standard and a 30 s relaxation delay (d1). [b] Repeat of the standard conditions, run in parallel. [c] Cs_2CO_3 dried overnight at 200 °C under high vacuum, acid **148a** and [Ir] **133** dried overnight at 25 °C under high vacuum, DMF dried by filtration through a drying column, then over activated molecular sieves for 48 h (water-content: 21 ppm by Karl-Fischer Titration [≙ 0.5 mol% H_2O]) in a J Young ampoule, solids of reaction mixture evacuated and refilled with Ar (3x) before addition of DMF. [d] 1.0 mL D_2O was added to the reaction mixture, stirred for 5 minutes and followed by the standard workup (see Section **7.6.6**).

4.2.1.5.3 Side Products of Reduction (**155**) and Di-Alkylation (**149'**)

The formation of reduced oxetane **155** was investigated by deuteration studies (Table 22). Cyclohexene methyl carboxylate, which had shown increased amounts of **155** (Scheme 45b), was chosen as alkene. In particular, the source of 'H' in reduced product **155** was unclear since no obvious reductants or HAT reagents were included in the reaction conditions. Surprisingly, significant deuteration was observed only with ***d*-148a** or D_2O as sources of H^+ (*i.e.* D^+), but not with DMF-d_7, a potential HAT donor (entries 2–6).[370] However, reduction of the oxetane radical followed by protonation seemed improbable based on the observed instability of 3-aryloxetane carbanions (see Section **5.3**) and the computed reduction potential of the oxetane radical **III** ($E_{1/2}^{[\mathbf{III}/\mathbf{III}^-]}$ = –1.67 V vs SCE; see Figure 62), which lay well outside the range of [Ir^{II}] ($E_{1/2}^{[II/III]}$ = –1.37 V vs SCE).[355a]

Table 22. Incorporation of deuterium in reduced oxetane **155**.



Entry	Change from standard conditions	Yield / %[a]		D-incorporation / %[a]
		154	**155**	
1	none	16	16	NA
2	using DMF-d_7	18	21	7
3	***d*-148a** (COOD)	14	10	33
4	using DMF-d_7 + ***d*-148a** (COOD)	6	13	37
5	+ 2.77 equiv D_2O[b]	4	8	75
6	+ 10.0 equiv D_2O	10	11	85
7	no acceptor	3	4	NA

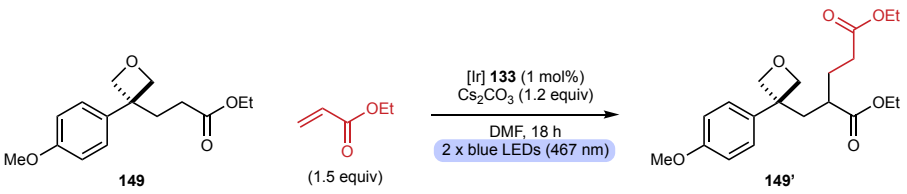
[a] Reactions run on a 0.14 mmol scale and yields and percentage of deuteration calculated by analysis of the ^{1}H NMR spectrum of the crude mixture of the reaction using 1,3,5-trimethoxybenzene as internal standard and a 30 s relaxation delay (d1). [b] Run on a 0.14 mmol scale. [b] Corresponds to 10 μL (1% *v*/*v*).

Concerted multisite proton-coupled electron transfer (PCET), an elementary concerted chemical process known to facilitate single electron-/proton transfers that would not be thermodynamically favourable in a sequential manner,[371] could explain the formation of oxetane **155**. The small amounts of side products **154** and **155** formed in the absence of alkene suggested the requirement of the alkene to regenerate the photocatalyst (Table 22, entry 7). However, CV measurements ruled out reduction of the alkene (*e.g.* cyclohexene methyl carboxylate: ≤ –2.12 V vs SCE, Table 19, or methyl acrylate: –2.10 V[372]/–2.60 V[373] vs

SCE) directly by [Ir^{II}] ($E_{1/2}^{[II/III]}$ = –1.37 V vs SCE) as thermodynamically unfeasible.[355a] A possible explanation is that oxetane radical **III** degrades into sterically less hindered ring-opened radical structures that undergo Giese reaction with the alkene to generate α-ester radicals that can be reduced by [Ir^{II}] to regenerate the photocatalyst. Note that the Giese products of such ring-opened radicals were neither isolated nor observed, but the feasibility of the proposed pathway is supported by the recent report by Chaładaj and Gryko on the Giese reaction of *C*-centred, ring-opened oxetane radicals.[374] Figure 109 in Appendix **9.5** shows the ^{1}H NMR spectra for all entries of Table 22.

Then, the formation of di-alkylation product **149'** was examined (Table 23). Resubjecting single-addition Giese product **149** to the reaction conditions formed di-alkylated **149'** in 18% yield (entry 1), which was reduced to 2–3% in the absence of photocatalyst and light (entries 2–3). These results support the formation of **149'** to be primarily by polarity mismatched radical Michael addition of Giese adduct **149•** into ethyl acrylate instead of polar Michael addition of enolate **149**$^-$. From the relative yields in entries 1–3, it can be estimated that the polar pathway contributes to ca. 14% towards formation of di-alkylated **149'**. Importantly, Giese-product **149** was not converted into di-alkylated **149'** in the absence of base (entry 4), supporting the involvement of enolate **149**$^-$ in both the radical and polar pathways. Radical addition of intermediate **149•** into ethyl acrylate can either occur as it is formed, or, as evidenced by CV experiments, enolate **149**$^-$ (E_{pa} = +0.60 V vs SCE) can be oxidised back to radical **149•** by [Ir^{III*}] ($E_{1/2}^{[III^*/II]}$ = +1.21 V vs SCE),[355a] rendering product formation (**149**) reversible and yielding increased amounts of di-alkylation product **149'** at long reaction times (Figure 64).

Table 23. Formation of di-addition product **149'**.



Entry	Change from standard conditions	Yield / %[a]	
		149 (RSM)	**149'**
1	none	79	18
2	no [Ir] **133**, no light	93	2
3	no [Ir] **133**	92	3
4	no base	88	0

[a] Reactions run on a 0.1 mmol scale and yields calculated by analysis of the ^{1}H NMR spectrum of the crude mixture of the reaction using 1,3,5-trimethoxybenzene as internal standard and a 30 s relaxation delay (d1).

4.2.1.5.4 Mechanistic Proposal

The focused experimental and computational mechanistic studies presented in the last three sections supported the initial mechanistic sketch based on literature precedent (Figure 57), whilst providing further detail on some of the constituent elementary steps of the catalytic cycle (Figure 66). Specifically, measured and calculated RedOx potentials were in accordance with the range of the [Ir] photocatalyst **133**. Deuteration studies supported formation of Giese product **149** by protonation and formation of reduced side product **155** *via* a PCET mechanism. Di-alkylation product **149'** was shown to be formed primarily by a radical Michael addition. The computational study determined the relative stability of the benzylic radical to influence the driving force for the Giese addition step and therewith the propensity towards dimerisation, the latter further affected by the spin density on the benzylic carbon, which is controlled by hybridisation. The oxetane radical was shown to be the only of the analysed structures to lie in the sweet spot between enough instability for an exergonic Giese process, but enough stability to supress degradative ring-opening pathways.

Briefly described, the transformation starts with the visible light excitation of the [Ir^{III}] photocatalyst to [Ir^{III*}], which oxidises oxetane carboxylate **148a**$^-$ to a carboxylate radical (not shown) that rapidly decarboxylates ($k \approx 10^{10}$ s^{-1})[375] to key aryloxetane radical **III**. Radical **III** undergoes preferential, exergonic and practically irreversible Giese addition into ethyl acrylate to generate adduct **149**$^\bullet$, which is reduced by [Ir^{II}] to regenerate the photocatalyst in the required +III oxidation state ([Ir^{III}]) and form enolate **149**$^-$, followed by a final proton transfer step to yield Giese product **149**.

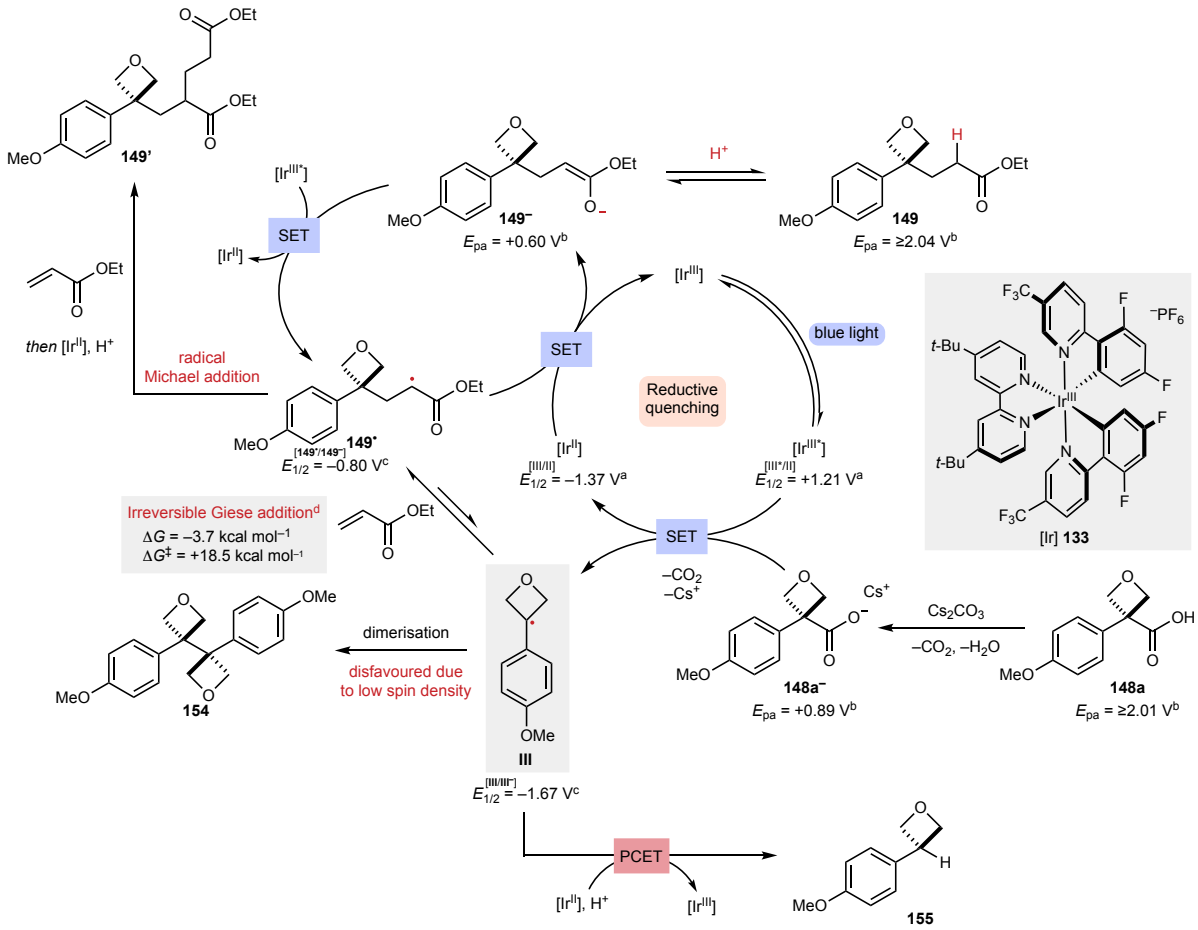


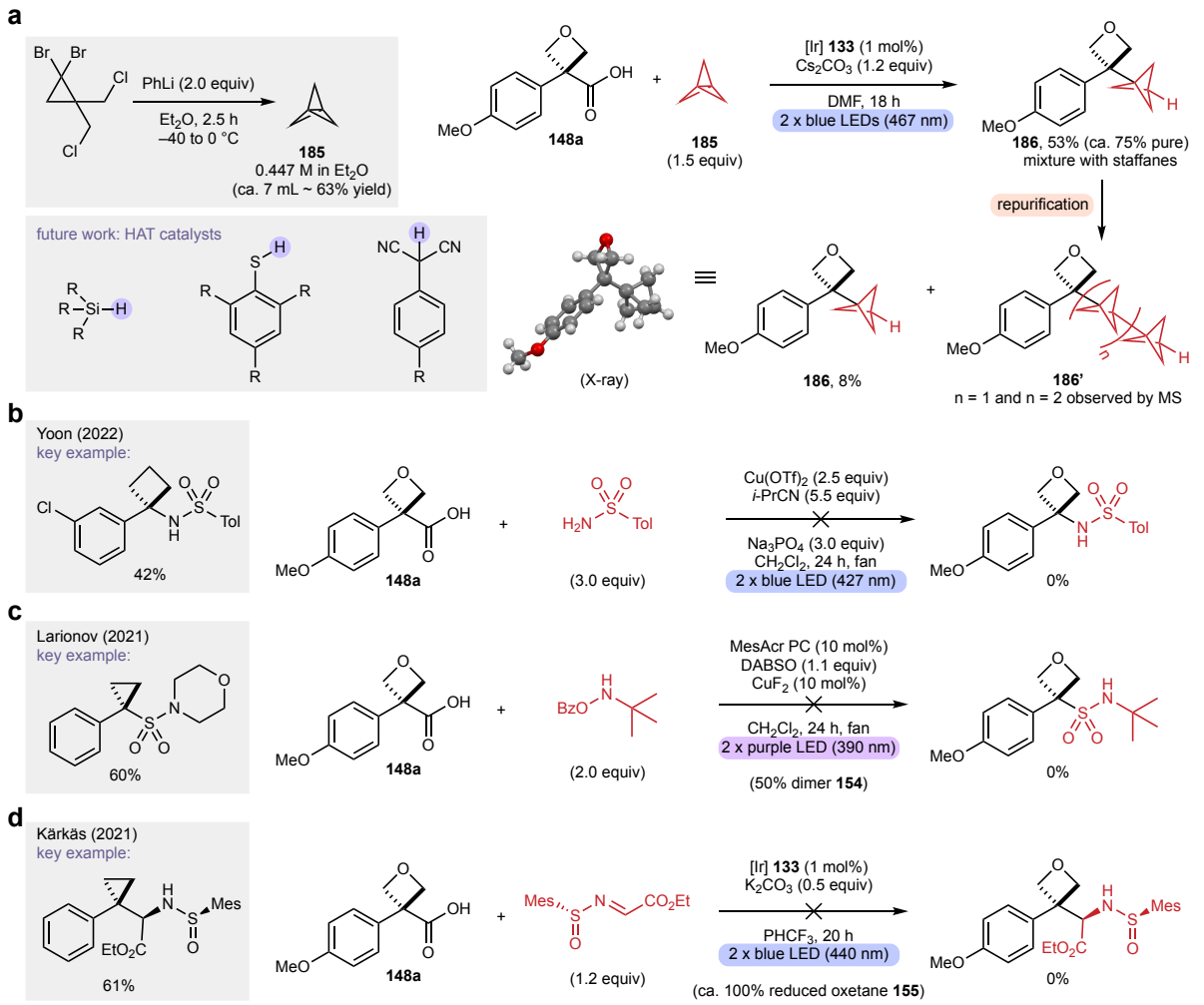
Figure 66. Proposed mechanistic picture of the Giese addition of aryloxetane radicals. [a] Literature values vs SCE in MeCN.[355a] [b] Measured value in MeCN, given vs SCE (see Table 19 for details). [c] Calculated value vs SCE (see Figure 63 for details). [d] Values calculated with methyl acrylate as acceptor (see Figure 60).

4.2.1.6 Application of Oxetane Radical to Further Transformations

The expansion of potential applications of aryloxetane radicals towards further oxetane derivatives was of interest, noting however, the considerable challenge associated with this radical species due to its relatively high thermodynamic (stabilisation by radical delocalisation into arene) and kinetic (significant steric crowding around reactive radical centre) stability. Nevertheless, recent years have seen the development of many decarboxylative radical coupling methods for carboxylic acid substrates and hence, preliminary studies were conducted, with a focus on reports with relevant related examples.

First, [1.1.1]propellane, a known strain-release reagent,[302,376] was used as radical acceptor for the oxetane radical, under the Giese conditions described in the last sections (Scheme 48a). Significant amounts of the coupled oxetane–bicyclo[1.1.1]pentane (BCP) product **186** were isolated, albeit as a mixture of the desired monomer (**186**) with oligomers of varying lengths (staffanes). Tedious purification by column chromatography yielded analytically pure oxetane–

BCP **186** in 8%, which was further characterised by X-ray crystallography. The mass of two staffane products (**186'**; n=1 and n=2) was identified by mass spectrometry in the remaining mixture of products. BCPs have gained recent popularity in drug discovery as isosteres of phenyl groups[377] and BCP **186** would represent an intriguing 'double-isostere' of a benzophenone with the carbonyl group exchanged for an oxetane and an arene for a BCP.



Scheme 48. Application of aryloxetane radical to other couplings. a, Reaction with propellane. **b**, Yoon's oxidative cross-coupling to sulfonamides.[379] **c**, Amidosulfonation by Larionov.[380] **d**, Addition into sulfinimines as reported by Kärkäs.[381]

This is an encouraging preliminary result. Future work would aim to minimise the formation of staffane side products, caused by a faster reaction of the generated BCP radical intermediate with another molecule of propellane than reduction.[376] Suppression of formation of staffanes has often been achieved by the addition of HAT catalysts, or other trapping agents such as *N*-chlorosuccinimide.[376a,c,e] The direct coupling of unactivated carboxylic acids is unprecedented in the literature (examples always from activated substrates)[378] and would be of interest for medicinal chemistry for the generation of BCPs directly from propellane and carboxylic acid feedstocks, not necessarily limited to oxetane-containing substrates.

Further decarboxylative protocols for coupling to sulfonamides,[379] amidosulfonation,[380] or addition into sulfinimines,[381] were unsuccessful on oxetane carboxylic acid **148a**, often leading to increased amounts of oxetane side products such as dimer **154** and reduced oxetane **155** (Scheme 48b–d).

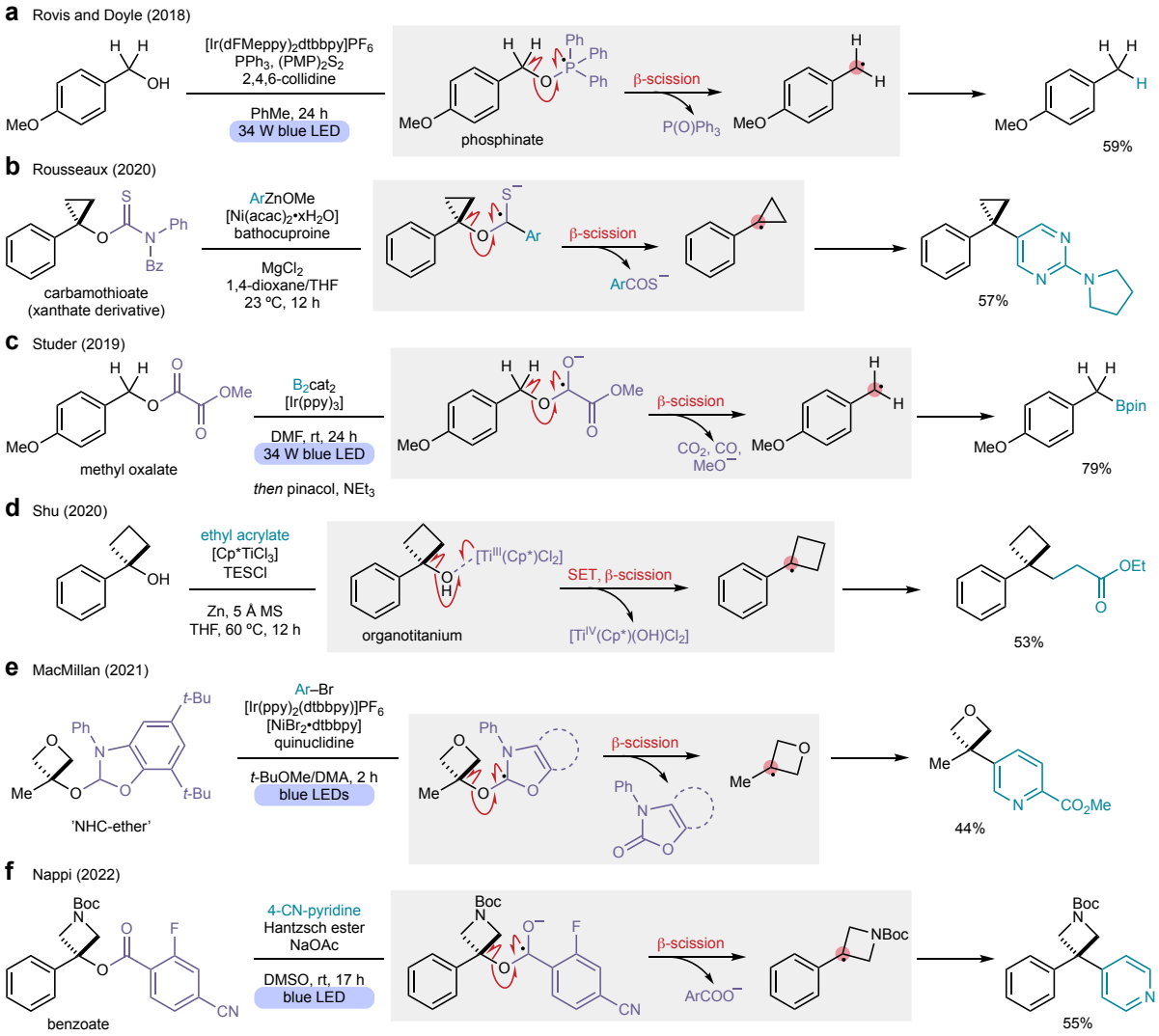
4.2.1.7 Conclusions

Tertiary benzylic oxetane radicals were shown to be generated from aryloxetane carboxylic acids and trapped with electron-deficient alkenes in a Giese-type reaction. The breadth of the scope of alkenes was expanded and the limitations in this regard indicated. Key mechanistic elementary steps were elucidated, and the effect of ring strain and benzylic radical stability was investigated computationally, demonstrating an interesting implication of Bent's rule.

Aryloxetane radicals in a broad global sense, were found to be too stable to favour intermolecular reaction pathways. Intermolecular reactivity was further hampered by steric shielding of the radical centre by the oxetane ring and reactions with radical acceptors (*e.g.* alkenes, imines, protonated N-heterocycles {Minisci}, etc.) were concluded to be too unfavourable for further investigation. Alternative processes which rely on radical recombination as the key bond-forming step were thus envisaged. The next section will describe such efforts as part of a preliminary investigation using 3-aryloxetanols as radical precursors.

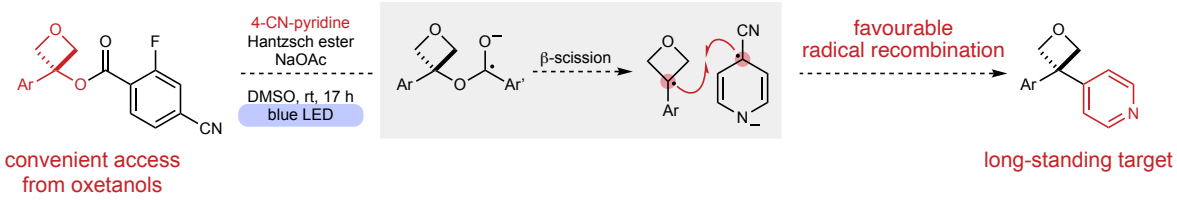
4.2.2 Oxetane Radicals from Oxetanols

The deoxygenative generation of carbon-centred radicals from alcohol feedstocks has garnered considerable interest amongst the synthetic and medicinal chemistry community. However, direct formation of the alkyl radical from free aliphatic alcohols is thermodynamically unfavourable due to the high bond strength[382] and RedOx potentials of the C–O bond,[383] which often results in alternative fragmentation pathways, such as C–C or C–H bond cleavage.[384,385] Activated alcohol derivatives, generated *in situ* or by facile pre-functionalisation, have hence emerged as an attractive alternative approach for the *quasi*-direct usage of alcohols as radical precursors.[330] Examples include phosphinates,[386] xanthate derivatives,[329c,387] oxalates,[329a,388] organotitanium species,[389] NHC-ethers[329d,390] and benzoates,[329e,391] and often involve the reduction of a redox-active alcohol derivative which subsequently undergoes β-scission to generate the requisite alkyl radical (Scheme 49).



Scheme 49. Recent and most relevant deoxygenative radical coupling strategies from alcohol derivatives. a, Phosphinate intermediate.[386b] **b**, Carbamothioate derivative.[387c] **c**, Methyl oxalate.[388d] **d**, Organotitanium intermediate.[389b] **e**, 'NHC-ether'.[329e] **f**, Redox-active benzoate.[391e]

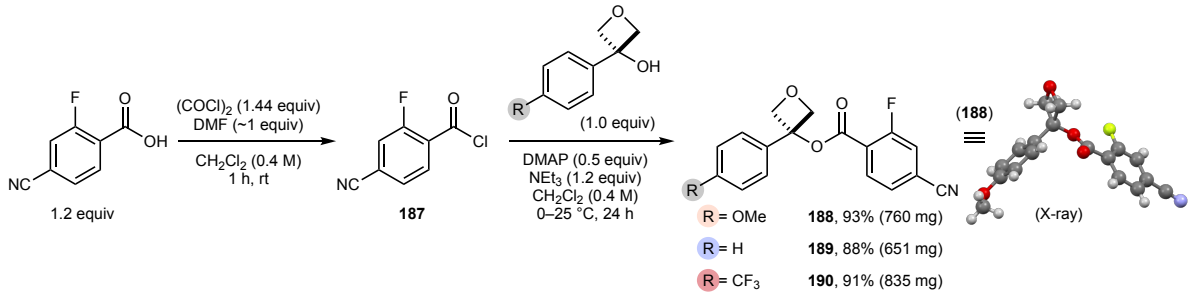
The recent example by Nappi (Scheme 49f)[391e] was particularly relevant: 1) the transformation was developed for benzylic substrates and tolerated relevant tertiary cyclic functionality, including an azetidine (Scheme 49f); 2) it utilised alcohol starting materials, convenient for the application to easily accessible 3-aryloxetanols; 3) the key C–C bond forming step relied on a radical-radical recombination process, which could be favourable for sterically hindered tertiary benzylic radicals; 4) the phenyl-pyridine di-aromatic substitution pattern of the products would be valuable to achieve on oxetanes and has been a key synthetic target. As such, it was envisaged to apply and further develop a related protocol on 3-aryloxetanol substrates (Scheme 50). Preliminary efforts in this regard will be presented in the next sections.



Scheme 50. Proposed radical recombination strategy of aryloxetane radicals with pyridines.

4.2.2.1 Synthesis of Precursors

To test the proposed oxetane arylation, three initial, electronically diverse oxetane benzoates (**188**–**190**) were synthesised in good yields and scales by DMAP-catalysed esterification of oxetanols with freshly prepared acyl chloride **187**, following Nappi's procedure with small modifications (Scheme 51). The oxetane benzoates were stable, crystalline solids, ideal for usage as starting materials for subsequent method development.

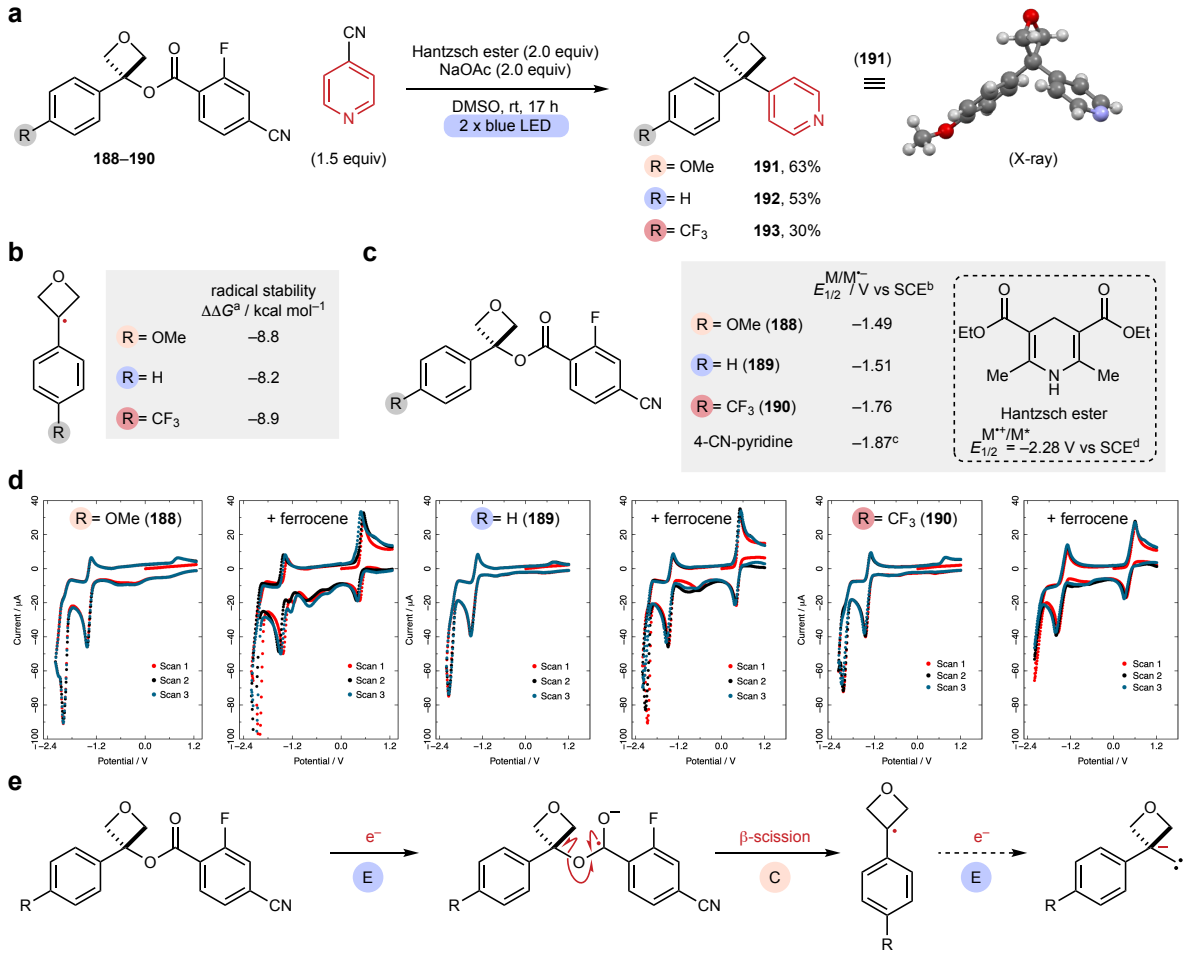


Scheme 51. Synthesis of oxetane benzoates 188–190.

With sufficient quantities of benzoates **188**–**190** in hand, the deoxygenative arylation to 4-cyanopyridine was tested.

4.2.2.2 Oxetane Radicals and Radical–Radical Coupling to Cyanopyridines

Initial test reactions were performed with benzoates **188**–**190** and 4-cyanopyridine under the reported conditions and protocol by Nappi, with slight modifications. The reactions were conducted in sealed microwave vials, oxygen excluded by purging with argon (10 min) and irradiated with two Kessil LED lamps (broad wavelength 'blue'). Under this rudimentary set-up and unoptimised conditions, pyridine diaryl-oxetanes **191**–**193** were obtained in 30–63% yield, with a strong positive correlation between yield and electron-rich character of the aromatic ring (Scheme 52a). This trend, which seems to be unrelated to radical stabilities (Scheme 52b), is intriguing since more electron-poor radicals (*e.g.* from **190**) would be expected to be more electrophilic and hence better polarity-matched with the nucleophilic cyanopyridine radical anion (see Scheme 50).



Scheme 52. Deoxygenative arylation of oxetanol derivatives 188–190. a, Coupling to 4-cyanopyridine. **b**, Calculated relative radical stabilities. **c**, Experimental reduction potentials. **d**, Cyclic voltammograms with and without ferrocene (internal standard) of benzoates **188**–**190**. **e**, Proposed ECE mechanism of electrolysis. [a] Relative stabilities ($\Delta\Delta G$) calculated by A. Sterling and determined by H-atom exchange equilibria with cyclopropyl radical **II** (see Section **4.2.1.5.1** and ref. 311). All Calculations at the CPCM[358](DMF)-wB97X-D3[359]/def2-TZVP//wB97X-D3/def2-SVP[360] level. Free energies calculated at 298.15 K and 1 M standard state. [b] CV measurements performed in a 0.1 M solution of NBu_4ClO_4 in MeCN, at room temperature (ca. 22 °C), between –2.4 and +2.2 V and with a scan rate of 100 mV s^{-1}. [c] Literature value measured in MeCN.[392] [d] Literature value measured in DMF.[393]

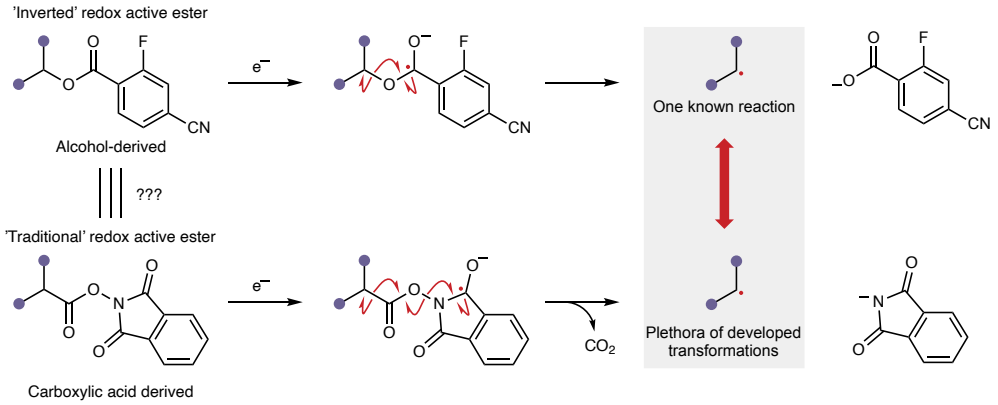
CV measurements saw a related counterintuitive trend in the reduction potentials of benzoates **188**–**190**, with electron-rich PMP-benzoate **188** being easiest to reduce, followed by Ph **189** and $^{4\text{-}CF_3}$Ph **190** (Scheme 52c–d). No oxidation waves were observed, apart from the oxidation of the PMP ring at high currents (>2.2 V). It is remarkable that the electronics of the arene, which is not conjugated to and relatively far from the presumed site of reduction (carbonyl), would impact the reduction potential of the substrates so starkly. All reductions were reversible or *quasi*-reversible and thus allowed for an accurate determination of the half wave potential ($E_{1/2}$). The current of the oxidation back peak was, however, significantly smaller than that of the reduction forward peak (see for example the CV of **190** where the reduction showed a current of ca. –40 μA and oxidation of ca. + 10 μA; Scheme 52d), suggestive of a chemical reaction succeeding electrochemical single-electron reduction in the time-scale of the voltammetric measurement, likely representing β-scission (Scheme 52e). There seems to be a second reductive wave occurring at ca. –2.35 V, which could correspond to further reduction of the oxetane radical to an unstable oxetane carbanion, but the peak was obscured by reduction of the solvent and the measurement constraints. The shape of the wave is in accordance with an ECE (electrochemical-chemical-electrochemical) mechanism of electrolysis, as just described (Scheme 52e). Further clarification of the electrochemical processes could be gained from additional CV measurements, including variable scan rates, which could be used to determine the kinetic constant of β-scission (potentially the rate-determining step),[394] and different electrolyte/solvent/range combinations to improve the observation of the second irreversible reduction.

The results shown in Scheme 52 are important preliminary data that demonstrate effective installation of pyridine functionality unto aryl-oxetane fragments conveniently derived from aryl-oxetanols. This strategy represents a valuable alternative to install electron-poor functionality such as pyridine and *p*-CF_3-phenyl, not tolerated in oxetane carbocation chemistry (Section **3.2**). To become of practical use, the protocol should be further optimised, and the fundamental understanding of the transformation improved. Potential approaches are discussed in Section **4.2.2.4**.

4.2.2.3 Application of Oxetane Radical to Further Transformations

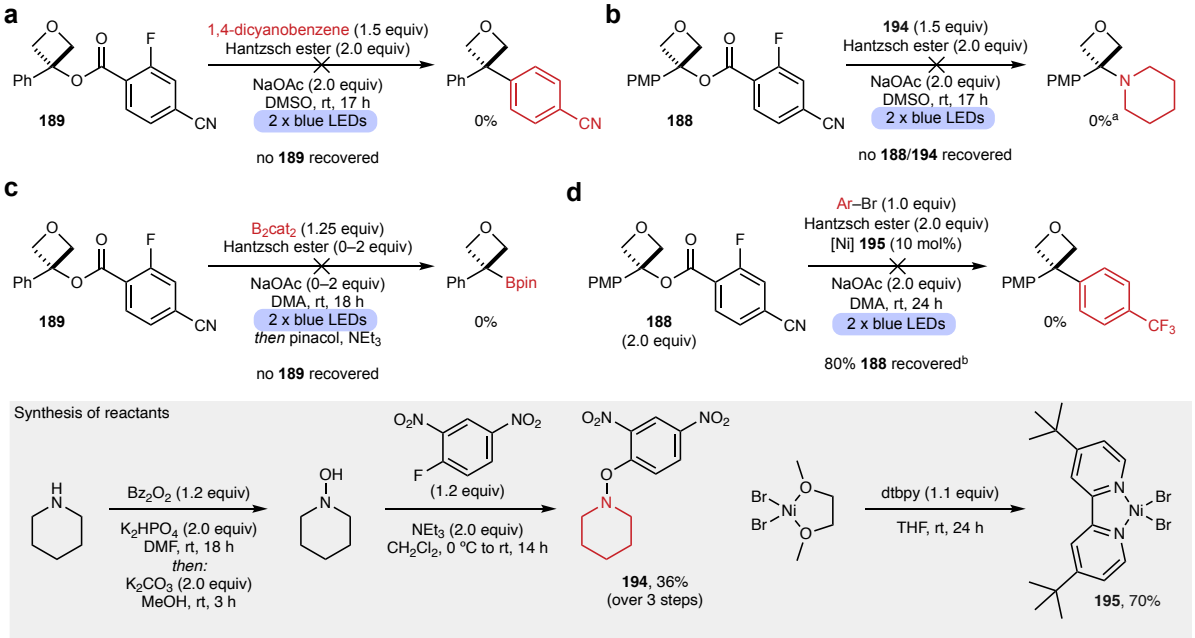
Benzoates are conceptually reminiscent of redox-active esters ('RAEs'), which have been extensively developed in the last ten years for the functionalisation of carboxylic acid derivatives.[395] As such, the development of synthetic methodology on alcohol-derived, redox active benzoates ('inverted' RAEs, iRAEs) based on the plethora of known chemical

transformations of RAEs would be valuable on oxetanols and on native alcohol substrates in general (Scheme 53).



Scheme 53. Redox active benzoates as potential hubs for general deoxygenative functionalisation of alcohols.

In this regard, four further transformations were tested, but none yielded the desired oxetane product (Scheme 54). Neither alternative radical-radical coupling to 1,4-dicyanobenzene[328a] nor substituted hydroxylamine **194** (*N*-centred radical precursor)[396] were successful (Scheme 54a–b). Similarly, borylation using a procedure developed by Aggarwal[397] and Ni-catalysed arylation were both unsuccessful (Scheme 54c–d).[398]



Scheme 54. Attempted further couplings of oxetane benzoates. a, Alternative C–centred radical coupling partner. **b**, Alternative N–centred radical coupling partner. **c**, Borylation.[397] **d**, Ni-catalysed metallophotoredox coupling to an aryl bromide.[398] [a] 84% of Hantzsch pyridine **196** were isolated. [b] Determined by analysis of the ^{1}H NMR spectrum of the crude mixture of the reaction using 1,3,5-trimethoxybenzene as internal standard.

4.2.2.4 Conclusions and Future Work

In conclusion, a proof-of-principle preliminary study was conducted to demonstrate that oxetanol-derived oxetane benzoates **188**–**190** are suitable precursors to aryl-oxetane radicals, which were coupled to 4-cyanopyridine radical anions to generate valuable pyridyl oxetane motifs not accessible by previous methodology. Electron-rich and electron-deficient arenes were tolerated on oxetanes, albeit with a reduction in yield with the electron-poor substrates. Further radical reactions of the oxetane benzoates were attempted with no productive species observed.

Future work should first focus on improving the current radical recombination process with cyanopyridines (Figure 67a). Potential possibilities to optimise the transformation could involve: 1) adjusting the equivalents of Hantzsch ester (HE) and pyridine; 2) tuning the redox active benzoic substituent on oxetane and 3) optimising the setup and reaction (temperature, solvent, wavelength, light intensity…). In particular, the original conditions used 1.5 equiv 4-cyanopyridine but only 2.0 equiv HE, meaning that, depending on the rates of reduction of 4-cyanopyridine and the benzoate substrates, only 0.5 equiv HE are available for benzoate reduction in the worst-case scenario. Then, the scope of the coupling should be investigated, with an emphasis on the introduction of medicinally valuable heterocycles both on the side of the oxetane and of the persistent radical.[399] The introduction of alkyl-oxetane fragments, not achievable under the previously developed radical[311] or carbocation[212] conditions, would be valuable to investigate (Figure 67b).

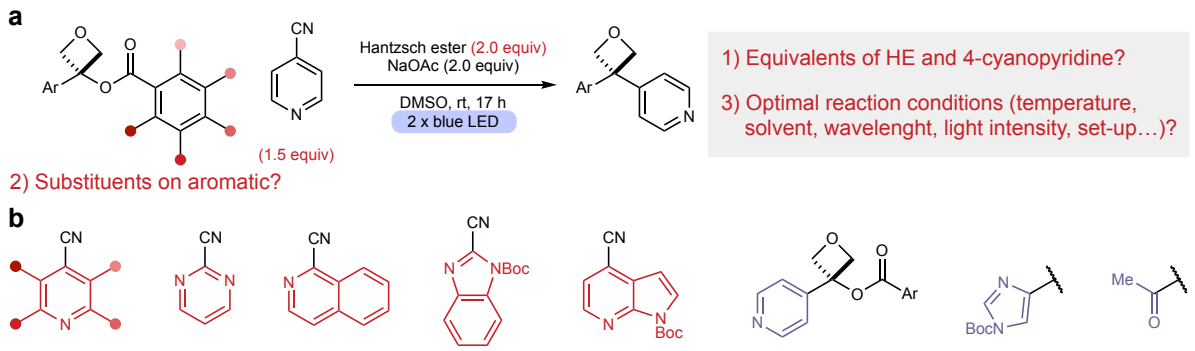


Figure 67. Future work of the oxetane deoxygenative arylation. a, Potential avenues for optimisation. **b**, Representative examples of potential substrates to investigate.

The generality and applicability of the reductively generated oxetane radicals should be further investigated. As highlighted in Scheme 53, the oxetane 'inverted' redox active esters (iRAEs) show similarities to the ubiquitous carboxylic acid-derived redox active esters (RAEs), and it would be valuable to examine whether oxetane iRAEs could be applied to reactions developed for RAE substrates.

5 Oxetane Carbanions: Investigation of Ligand Exchange and Ligand Coupling Pathways of Oxetane Sulfoxides

The last two chapters described efforts to functionalise 3-substituted oxetanes *via* carbocation- and radical intermediates. The 3,3-disubstitution patterns achieved were broad, but electron-poor functionality was generally not well tolerated. 3-Oxetane carbanions were therefore investigated as a potentially complimentary type of reactive intermediate to broaden the achievable substitution patterns on oxetane. 2-Oxetane carbanion species were precedented, achieved by α-lithiation with strong organolithium bases and stabilised as a carbenoid-type intermediate by the adjacent heteroatom (see Section **1.4.1**).[180–182] 3-Oxetane carbanion reactive intermediates were unreported and presented intriguing research targets of practical and fundamental interest.

Several challenges were associated with the proposed negatively charged oxetane intermediate: 1) generation of a carbanion at the oxetane 3-position will always compete with α-metalation at the 2-position and will hence require an exchangeable group at the 3-position to favour formation of the requisite carbanion intermediate; 2) the envisaged 3-oxetane carbanion was anticipated to be very unstable and to quickly degrade through intramolecular ring-opening processes, requiring cryogenic temperatures and rapid electrophilic trapping; 3) the high steric requirement of the 3-aryloxetane structural motif, demonstrated in the last two chapters, was anticipated to negatively impact both the rate of carbanion formation in the 3-position and also of intermolecular reactions of the 3-oxetane carbanion (Figure 68a). The expected fast kinetics of oxetane ring-opening of the key 3-aryloxetane carbanion, coupled with the anticipated slow intermolecular reactivity, promised to present considerable challenges.

Oxetane 3-sulfoxides **197** were identified as promising precursors to carbanions by known sulfoxide–metal exchange (Figure 68b). Oxetane 3-sulfoxides **197** have been previously synthesised in two-steps from oxetanols by thiol-alkylation, followed by selective oxidation.[110] This synthetic sequence was anticipated to be a further challenge (4), since the initial thiol-alkylation step proceeds *via* an oxetane carbocation, requiring electron-*rich* aromatic functionality, but the oxetane carbanion might need electron-*poor* functional groups for sufficient stabilisation.

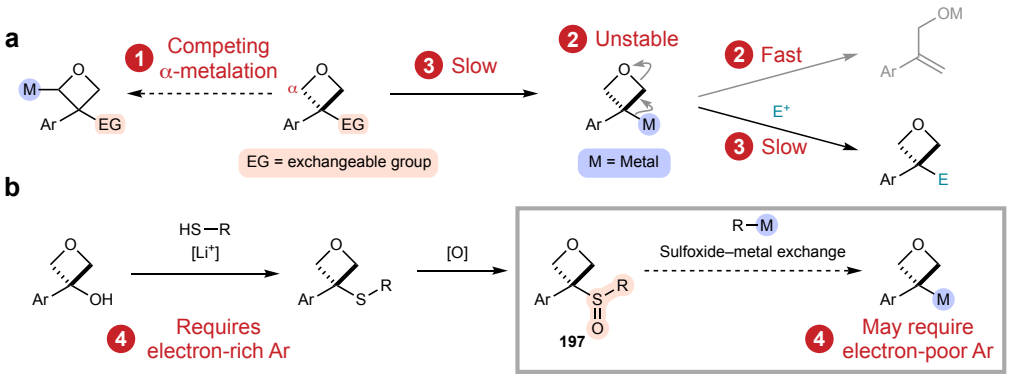


Figure 68. Proposed oxetane 3-carbanions and anticipated challenges. a, Proposed general entry into oxetane 3-carbanions. **b**, Synthetic sequence into oxetane sulfoxides **197** as potential precursors to oxetane 3-carbanions.

Efforts for the generation of 3-oxetane carbanions, as well as the investigation of general reactivity of oxetane sulfoxide substrates will be described in this chapter. The next section (**5.1**) will briefly introduce the organometallic chemistry of sulfoxides.

5.1 Organometallic Reactions on Sulfoxide Centres

The large atomic size of third- and higher-row p-block elements such as sulfur, phosphorus and selenium, allow for the formation of hypervalent structures[dd] with an expanded octet valence shell, energetically not available to lower-row p-block elements such as oxygen or carbon.[400] Hypervalent structures result in ligand-localised molecular orbitals which are non-bonding in large atoms but become anti-bonding in small atoms due to the short interatomic distances, and are hence, energetically forbidden. The addition of organometallic reagents to sulfoxides (**198**; S^{IV} oxidation state) results in such a hypervalent intermediate, termed σ-sulfurane (**199**; Figure 69). σ-Sulfuranes are short-lived, high-energy intermediates that rapidly collapse to reform stable entities. Common reorganisation pathways for hypervalent p-block structures include self-decomposition (as seen in *e.g.* the Wittig reaction), ligand exchange and ligand-to-ligand (L2L) coupling (Figure 69). The latter two pathways are most relevant for sulfoxide compounds and have been the subject of mechanistic- and practical synthetic investigations.

[dd] Hypervalent in the sense of more than four bonds of electron pairs (including lone pairs), not implying more than eight electrons assigned to the atom.

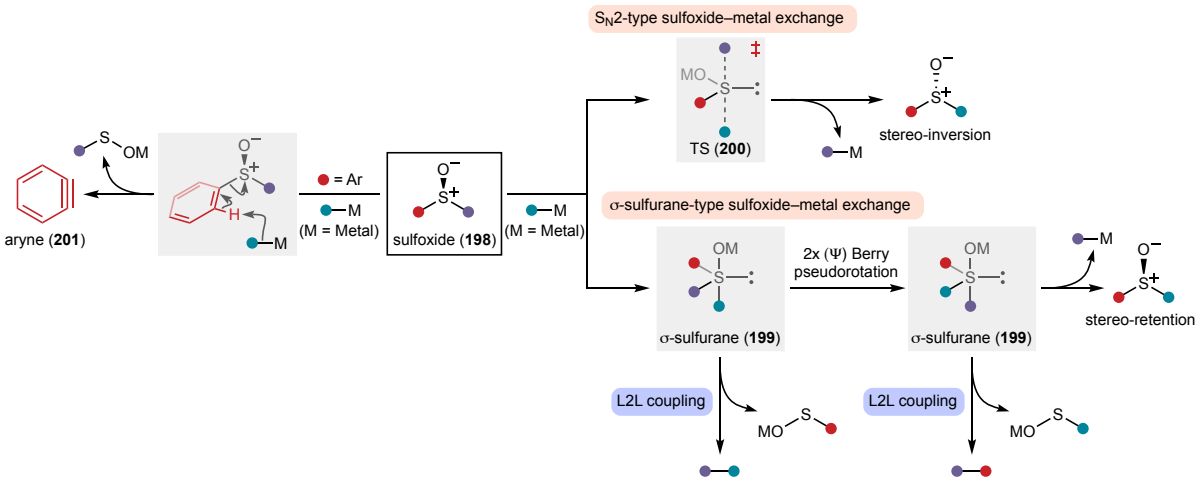


Figure 69. General reactivity of sulfoxides with organometallic reagents.

The sulfoxide–metal exchange pathway (ligand exchange) generates the lowest energy carbanionic species based on pK_a and has been employed extensively for the formation of complex organometallic reagents and/or sulfoxides, especially in enantioenriched formed (see Section **5.1.1**). The L2L coupling, which reductively couples two ligands on sulfur, is less widespread and until recently, had been considered a mechanistic curiosity (see Section **5.1.2**). Few reviews have been published on the chemistry of hypervalent sulfoxide intermediates, including one on general S(IV) chemistry by Maulide in 2019[401] and instructive accounts by Oae on L2L couplings.[402] An excellent chronicle on the historical developments of S-mediated couplings was written by Qin.[403]

There is no generally accepted consensus on the mechanism of addition and ligand exchange of organometallic reagents into sulfoxides, with the most favourable operating mechanism also being potentially substrate dependant. Evidence has been provided for the σ-sulfurane structure being a TS (**200**) of an S_N2-type process[404] or a formal reaction intermediate (**199**; Figure 69; see also Section **5.1.2**).[402] Ill-defined radical processes have also been considered.[401] Arguments for a σ-sulfurane intermediate (**199**) appear to be sounder than for the TS model (**200**) and include: isolation of two stabilised sulfurane-like compounds[405] and the observation of both ligand exchange- and L2L coupling products from the same reaction.[406] Calculations showed L2L coupling to occur preferably between an apical and a basal ligand.[407]

Reasoning for a TS structure has been based on competition experiments between leaving groups on sulfur and seem to have made unfounded assumptions on relative energy barriers and not considered the possibility of reversible exchange reactions.[404] Nevertheless, sulfoxide–metal exchange has been observed to occur both with retention- and inversion of configuration at sulfur, on a case-by-case basis.[402,404a] Such divergent outcome can be explained with a scenario dictated by the relative stability of the σ-sulfurane structure:

(relatively) stable σ-sulfuranes are long-lived enough to undergo double Berry pseudorotation,[408] followed by elimination to yield the new organometallic and sulfoxide with retained configuration (Figure 69). In such cases, the nucleophile is considered to attack the sulfur centre by an apical insertion anti to the oxygen atom,[ee] placing the incoming nucleophile in an apical position of the σ-sulfurane.[409] High-energy σ-sulfuranes are so short-lived that elimination occurs immediately without pseudorotation and with Walden inversion in the sulfoxide product, and could be in fact, considered to be a TS structure. Aryne intermediates (**201**), potentially formed by deprotonation *ortho* to an aryl sulfoxide have also been confirmed as intermediates in some cases (Figure 68).[410]

It is not entirely clear what factors favour the sulfoxide–metal exchange or the L2L pathway.[411] It is nevertheless useful for reaction design to consider a qualitative picture of the most relevant atomic/molecular orbitals. σ-Sulfuranes are generally accepted to be trigonal bipyramidal with sp^2-hybrid orbitals forming the basal bonds and a p-orbital 'shared' between the apical ligands in a three-centre-four-electron bonding arrangement (Figure 70a).

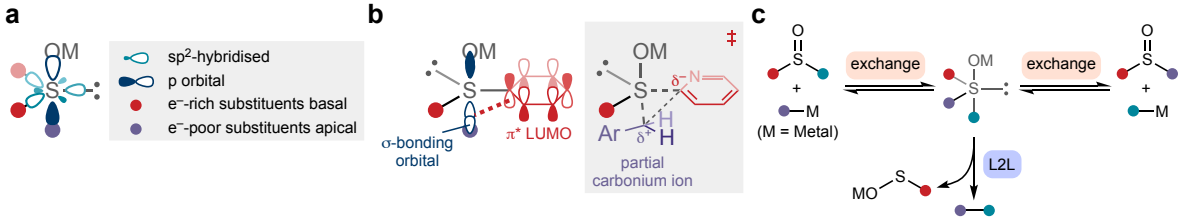


Figure 70. L2L coupling vs sulfoxide–metal exchange. a, Proposed atomic orbitals on sulfur in σ-sulfurane intermediates. **b**, Orbital interaction and TS of L2L coupling between a benzylic- and a 2-pyridyl substituent. **c**, Reversibility of sulfoxide–metal exchange and irreversible L2L coupling.

Thus, there is little stabilisation of negative charge provided by the sulfur centre in the apical positions and electron-rich substituents (including the lone pair) usually occupy basal sites and substituents that best stabilise negative charge are placed apically. Oae concluded that L2L coupling is preferred over sulfoxide–metal exchange when there are no ligands sufficiently capable of stabilising negative charge and when there is a favourable orbital interaction between an apical and basal ligand in the σ-sulfurane intermediate.[402] It was proposed that such an interaction could be donation of electron-density from the σ-bonding orbital of an apical ligand into the π* antibonding molecular orbital of a basal aryl substituent (Figure 70b). Hence, electron-poor aryl substituents tend to favour L2L coupling, most pronounced with 2-pyridyl owing to increased destabilisation of negative charge in the 2-position caused by repulsion of the negative charge with the nitrogen lone pair.[411] The inability of 2-pyridyl to

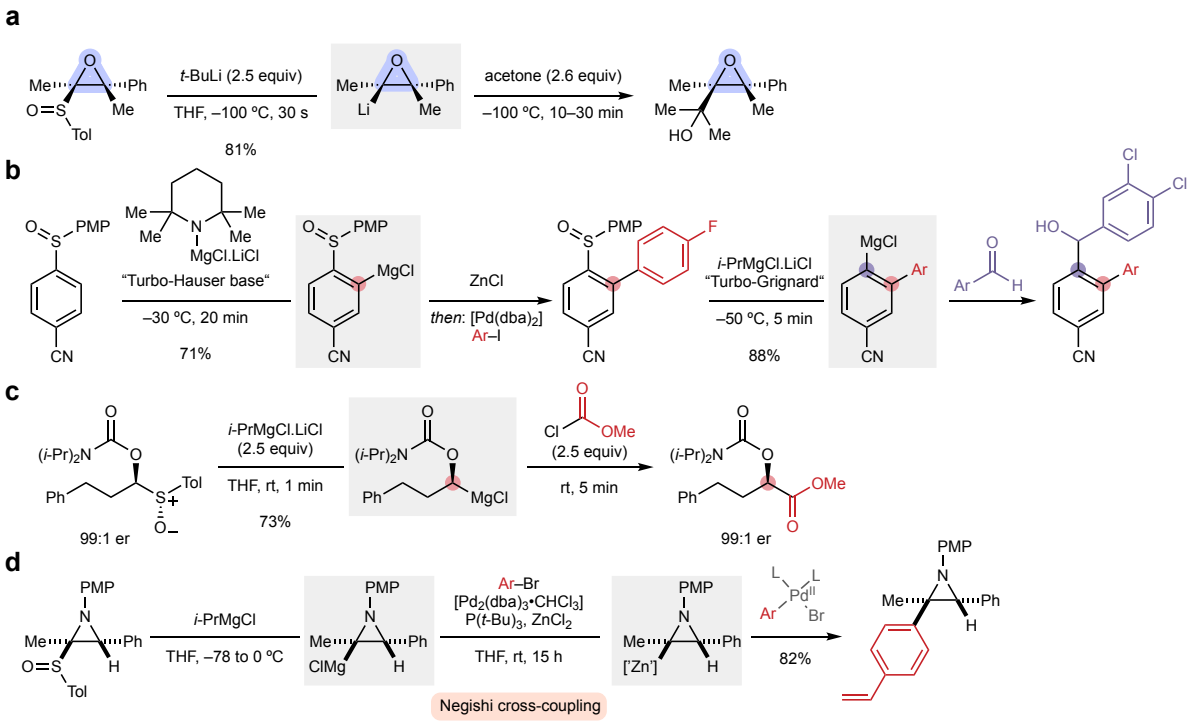
[ee] Although nucleophilic attack anti to oxygen is considered the norm for σ-sulfuranes, alternative approaches have been suggested in some cases.[406]

stabilise negative charge leads to a preference for a basal site for this substituent, situating the electron-deficient aromatic π-system optimally for interaction with the apical σ-bond (Figure 70b). It was further noted that benzylic substituents also seem to favour L2L coupling to aromatic substituents, especially 2-pyridyl. This was reasoned to be due to a stabilised benzylic partial carbonium ion formed by the developing positive charge on the benzylic carbon during the TS of the reductive coupling (Figure 70b).[411a] Lastly, owing to the reversible nature of sulfoxide–metal exchange but irreversibility of the L2L coupling, increasing the reaction temperature often led to a preference for the thermodynamic L2L coupled product, also noting that temperature had an uneven impact on the relative rates of ligand exchange, pseudorotation and L2L coupling (Figure 70c).[409,411]

5.1.1 Sulfoxide–Metal Exchange

The first example of sulfoxide–metal exchange was reported by Fuchs in 1929[412] and has since then seen many applications for the generation of designer organometallic reagents and synthesis of enantioenriched sulfoxides.[413] The latter application is useful due to the chiral nature of sulfoxide centres, which allows for the facile synthesis of diastereomeric sulfoxides from the natural chiral pool, which can be obtained as single diastereomers by conventional chromatographic methods. Stereospecific sulfoxide–metal exchange with an achiral organometallic then generates an enantiopure sulfoxide with a single stereogenic centre without the need of enantioselective methods throughout the process.

More widespread are applications of the sulfoxide–metal exchange to access bespoke organometallic reagents that would be unattainable by traditional methods from halides (*e.g.* metal–halogen exchange). Sulfoxide–metal exchange is regarded as a gentler approach that can achieve higher functional group tolerance and selectivity compared to metal–halogen exchange and avoids the use of reactive Mg^0 or Li^0 metals. Most relevant have been the contributions by Satoh and others, who showed the generation of organometallics on strained rings from the corresponding sulfoxides (Scheme 55a).[414] Knochel also reported valuable di-functionalisation approaches of aryl sulfoxides, which first directed selective *ortho*-lithiation with 'Turbo-Hauser base', followed by sulfoxide–metal exchange with 'Turbo-Grignard' to achieve di-functionalisation with electrophiles (Scheme 55b).[415] Enantio- and diastereomerically pure sulfoxides also generate an equivalent of an enantioenriched organometallic upon stereospecific sulfoxide–metal exchange, which can be trapped with electrophiles to access new enantioenriched chemical matter (Scheme 55c).[416] Further notable are examples where the generated organometallic was transmetallated to an organozinc reagent, which was intercepted by an aryl-palladium(II) species to yield arylated products in Negishi-type cross couplings (Scheme 55d).[417]



Scheme 55. Examples of sulfoxide–metal exchange. a, Satoh's generation of epoxide organolithiums.[414c] **b**, Knochel's di-functionalisation of aryl sulfoxides.[415a] **c**, Enantioenriched organometallics by O'Brien.[416] **d**, Bull's example of an azetidine organomagnesium and usage in a Negishi-type protocol.[417]

5.1.2 Ligand-to-Ligand Coupling

Synthetically less investigated is the reductive coupling between two ligands on the σ-sulfurane intermediate (L2L coupling, Figures 69–70).[418] Nevertheless, the concept is appealing because it allows transition metal-free cross-couplings akin to ubiquitous palladium catalysed reactions such as Suzuki–Miyaura or Negishi couplings. Transition metal-free disconnecting strategies are particularly attractive for basic heteroarene structures, which are privileged motifs in drug discovery, but are often incompatible with transition metals due to strong coordination of the heterocycle to the metal. Mechanistically, in addition to the scenario described in Figures 69–70, it is relevant to note that the L2L coupling generally occurs preferentially between the two ligands best predisposed for the coupling regardless of the kinetically favoured geometry of the σ-sulfurane, with some temperature-dependency.[409] For example, addition of benzylmagnesium bromide to phenyl-(2-pyridyl)-sulfoxide **203** generated σ-sulfurane **205**, which placed the introduced benzyl ligand in the apical position, optimally positioned for reductive coupling with 2-pyridyl to yield diaryl-methane **206** (Figure 71).[419] Interestingly, addition of phenylmagnesium bromide to benzyl-(2-pyridyl)-sulfoxide **202** also generated diaryl-methane **206**, meaning that initially formed σ-sulfurane **204** preferentially pseudorotated (twice) to the same predisposed σ-sulfurane **205** with the benzyl ligand in the apical position (Figure 71). The electronics of the ligands on sulfur were also shown to have

an irregular effect on the relative rates of pseudorotation, ligand exchange and L2L coupling pathways, with electron-withdrawing substituents accelerating pseudorotation.[420]

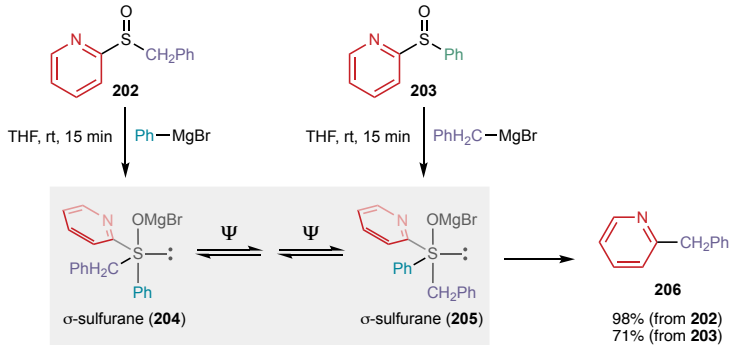
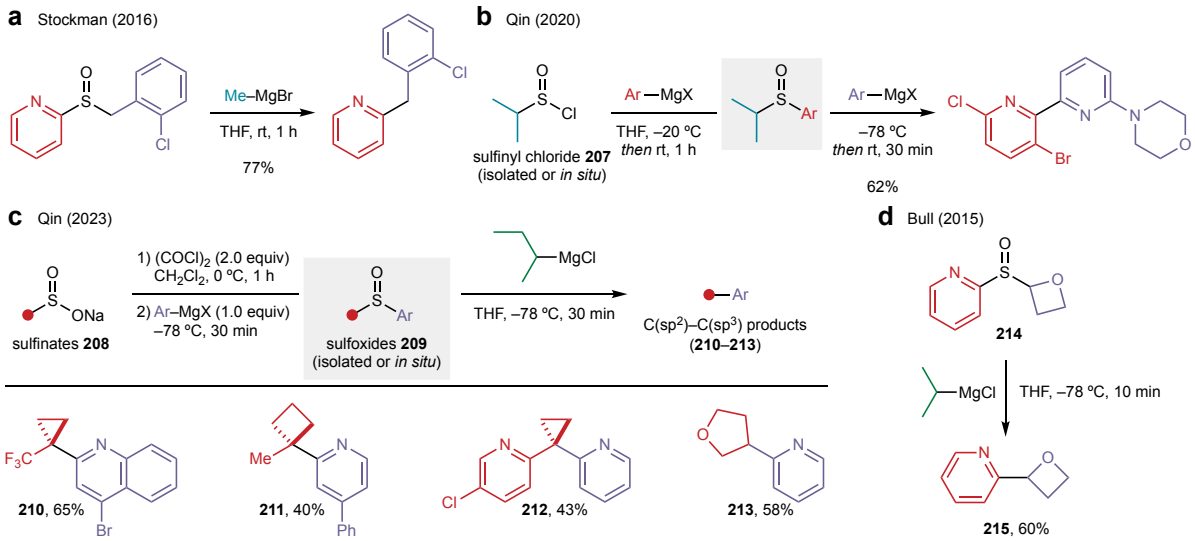


Figure 71. Benzyl–(2-pyridyl) L2L coupling from different sulfoxide substrates.[419]

Oae and Furukawa investigated L2L couplings extensively in the 1980's, focusing mostly on mechanistic and proof-of-principle studies, with at the time, little practical consequence (see *e.g.* Figure 71).[406,409–411,419–421] Recently however, this chemistry has experienced a small renaissance, sparked in part, by a report from Stockman in 2016 which coupled electron-deficient arenes to benzylic substituents in a stereospecific manner (Scheme 56a).[422]



Scheme 56. Examples of L2L couplings. a, Aryl–benzyl coupling by Stockman.[422] **b**, Aryl–aryl coupling by Qin.[403] **c**, Aryl–alkyl coupling by Qin.[423] **d**, (2-Pyridyl)–(2-oxetane) coupling by Bull.[158c]

Later, Qin developed a useful sulfinyl chloride reagent **207** as a hub for the coupling of organometallic heteroarenes *via* an L2L coupling pathway (Scheme 56b).[403] The same group very recently reported an C(sp^2)–C(sp^3) coupling between (hetero)-arenes and alkyl fragments, including strained rings, fluorinated compounds and unbiased substrates (Scheme 56c).[423] Alkyl sulfinates (**208**) were used as precursors which generated an aryl–alkyl sulfoxide intermediate (**209**) either isolated or *in situ*, which was activated to a σ-sulfurane

high-energy intermediate, followed by reductive coupling to the C(sp^2)–C(sp^3)-linked products (**210**–**213**). An interesting preference for coupling of the alkyl group pre-attached to the sulfoxide was noted, rationalised by the kinetically preferred formation of the requisite σ-sulfurane (*i.e.* with the pre-attached alkyl group in the apical position). This argumentation is however in discord with all previous mechanistic work by Oae and others, which suggested an apical attack of the incoming nucleophile to place the *exogenous alkyl group* in apical position and kinetically predisposed for reductive coupling (see *e.g.* Figure 70).[419] One isolated example of an L2L coupling on an oxetane was reported by the Bull group in 2015 with similarities to the later work of Qin (Scheme 56d).[158c] 2-Oxetane-(2-pyridyl)-sulfoxide **214** reacted with *i*-PrMgCl exclusively *via* the L2L coupling pathway to yield 2-(2-pyridyl)-oxetane **215**. Further notable is the activation of sulfoxides with benzyne reported by Peng[424] and the productive usage of the L2L by-product (a sulfenate anion) for the synthesis of complex sulfoxide- and sulfinamide compounds reported by Saito.[425]

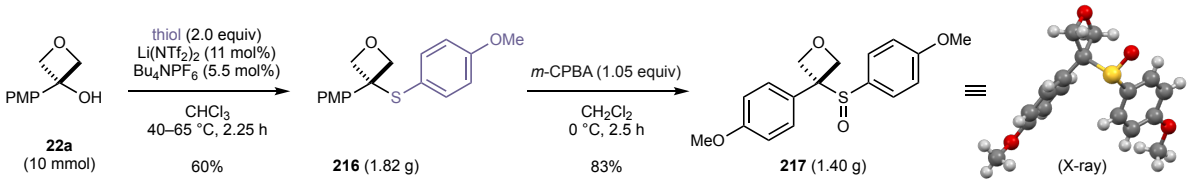
5.2 Aims

The specific aims of this chapter were:

1. Investigate the generation and stability of 3-oxetane carbanions by a sulfoxide–metal exchange from 3-aryloxetane sulfoxides.
2. Examine the reactivity of 3-oxetane carbanions towards several electrophiles and the effect of the aryl group on oxetane and the countercation of the oxetane organometallic.
3. Probe the reactivity of oxetane sulfoxides towards other pathways such as ligand-to-ligand coupling.

5.3 Sulfoxide–Metal Exchange of Oxetane Sulfoxides

The investigation of 3-oxetane carbanions commenced with oxetane–sulfoxide starting material **217**, synthesised in two steps from oxetanol **22a** (thiol-alkylation/oxidation; Scheme 57). Conveniently for downstream reactions, the sulfoxide product **217** was isolated as a crystalline solid, which was also further characterised by X-ray crystallography. The *para*-methoxyphenyl substituent on sulfur was chosen as an electron-rich aryl group which would poorly stabilise negative charge, disfavour its ligand exchange with an organometallic nucleophile in the requisite σ-sulfurane intermediate and thus increase the driving force for the generation of the targeted oxetane carbanion.

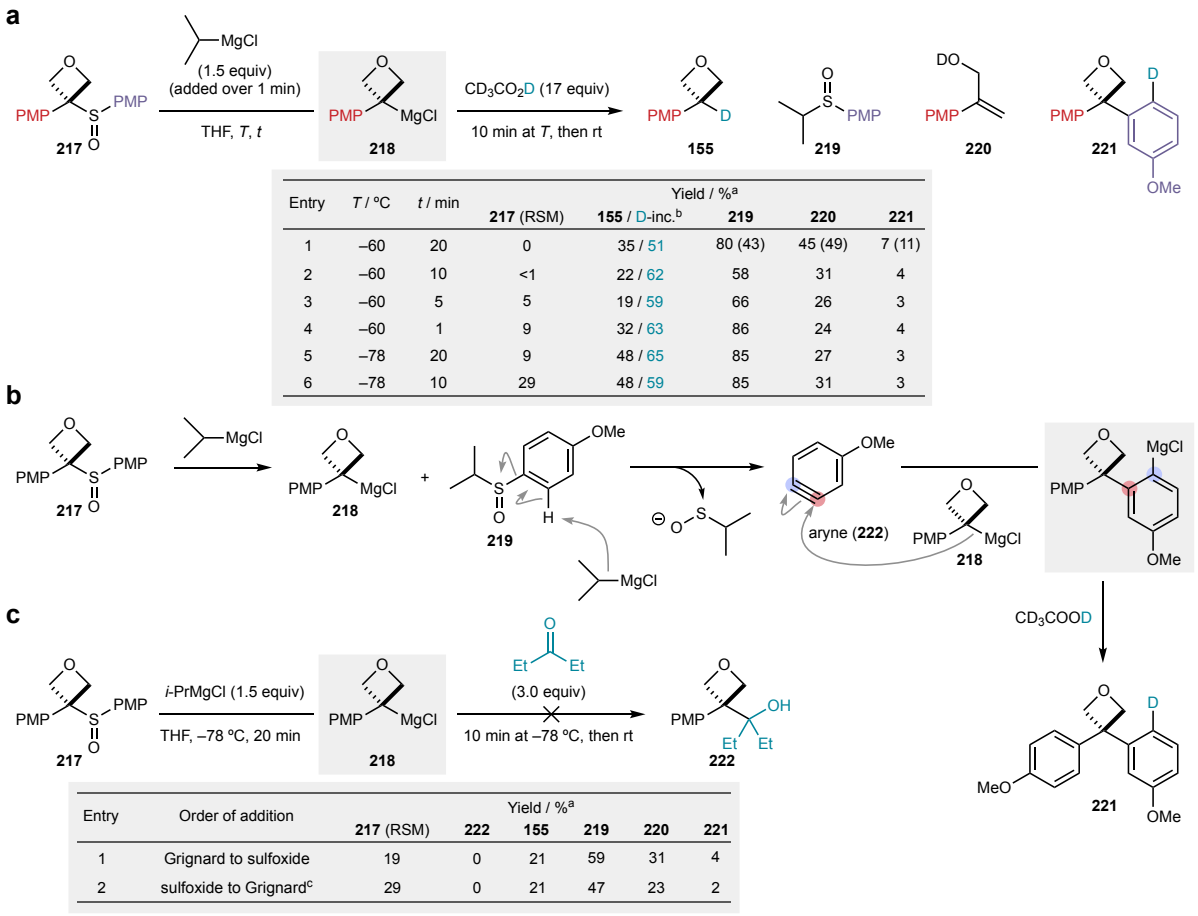


Scheme 57. Synthesis and crystal structure of oxetane sulfoxide 217.

Initial test reactions were performed with sulfoxide **217** as substrate, isopropylmagnesium chloride as organometallic, and deuterated acetic acid as quencher to gain a better understanding on the stability and lifetime of potential 3-oxetane carbanion **218** (Figure 72a). At –60 ºC, complete consumption of sulfoxide **217** was observed after 10 minutes induction time (time between addition of organometallic and quench) and already 91% consumption was observed after 1 minute (entries 1–4). Encouraging amounts of oxetane **155** (slightly volatile) were observed by ^{1}H NMR (19–35%) with moderate degrees of deuteration (51–63%), providing proof of principle that the target 3-oxetane carbanion intermediate **218** was generated and quenched by the deuterated acid. The remaining ca. 40% undeuterated **155** could have been formed by quenching with adventitious traces of water present in the solvent or by deprotonation of the expected sulfoxide by-product **219**, which was observed in varying, but relatively high amounts (58–86%), further indicating the occurrence of the desired sulfoxide–metal exchange. The differences in yields between **155** and **219** suggested that oxetane organometallic **218** also underwent significant degradation before the quench with the proton source. One such side product of degradation was identified as allylic alcohol **220** (observed to be unstable in $CDCl_3$ solution), which was obtained in higher amounts with increasing induction time and was presumably formed by rapid intramolecular ring opening of carbanion **218**, indicating its instability. A final species was separated from the complex mixture of products and identified as diaryl-oxetane **221**, which was proposed to be formed *via* aryne intermediate **222**, followed by attack of oxetane carbanion **218** (Figure 72b; *cf.*

Figure 69). A slight increase in the yield of oxetane **155** was observed at lower temperatures (–78 ºC) but still accompanied by significant degradation (Figure 72a, entries 5–6).

Nevertheless, trapping oxetane carbanion **218** with a synthetically more useful electrophiles such as pentan-3-one was attempted using two different orders of addition, but desired alcohol **222** was not observed in either case (Figure 72c).



Entry	*T* / ºC	*t* / min	Yield / %[a]				
			217 (RSM)	**155** / D-inc.[b]	**219**	**220**	**221**
1	–60	20	0	35 / 51	80 (43)	45 (49)	7 (11)
2	–60	10	<1	22 / 62	58	31	4
3	–60	5	5	19 / 59	66	26	3
4	–60	1	9	32 / 63	86	24	4
5	–78	20	9	48 / 65	85	27	3
6	–78	10	29	48 / 59	85	31	3

Entry	Order of addition	Yield / %[a]					
		217 (RSM)	**222**	**155**	**219**	**220**	**221**
1	Grignard to sulfoxide	19	0	21	59	31	4
2	sulfoxide to Grignard[c]	29	0	21	47	23	2

Figure 72. Preliminary investigation of sulfoxide–metal exchange with oxetane 217. **a**, Protonation studies with deuterated acetic acid. **b**, Proposed mechanism for the formation of diaryl-oxetane **221**. **c**, Unsuccessful quenching with pentan-3-one as electrophile. [a] Reactions run on a 0.2 mmol scale and 0.1 M concentration and yields and percentage of deuteration calculated by analysis of the ^{1}H NMR spectrum of the crude mixture of the reaction using 1,3,5-trimethoxybenzene as internal standard and a 20 s relaxation delay (d1). Isolated yields in parenthesis. [b] D-inc. = incorporation of deuterium (in %) in oxetane **155**. [c] Sulfoxide dissolved in 0.5 mL THF and added over 1 min to a solution of *i*-PrMgCl in 1.5 mL THF (end concentration of sulfoxide: 0.1 M).

As outlined at the start of this chapter (Figure 68), the rate of sulfoxide–metal exchange on hindered oxetane sulfoxide **217** and following intermolecular attack to electrophiles seems to be relatively slow compared to the rate of intramolecular ring opening to alcohol **220** (Figure 73). Presumably, the steric hindrance around sulfur incurred a relatively high energy barrier to Ψ pseudorotation, which is an elementary step required for the ligand exchange. This led to a

scenario where significant amounts of carbanion **218** had degraded before all sulfoxide **217** was consumed, *e.g.* Figure 72a, entry 6.

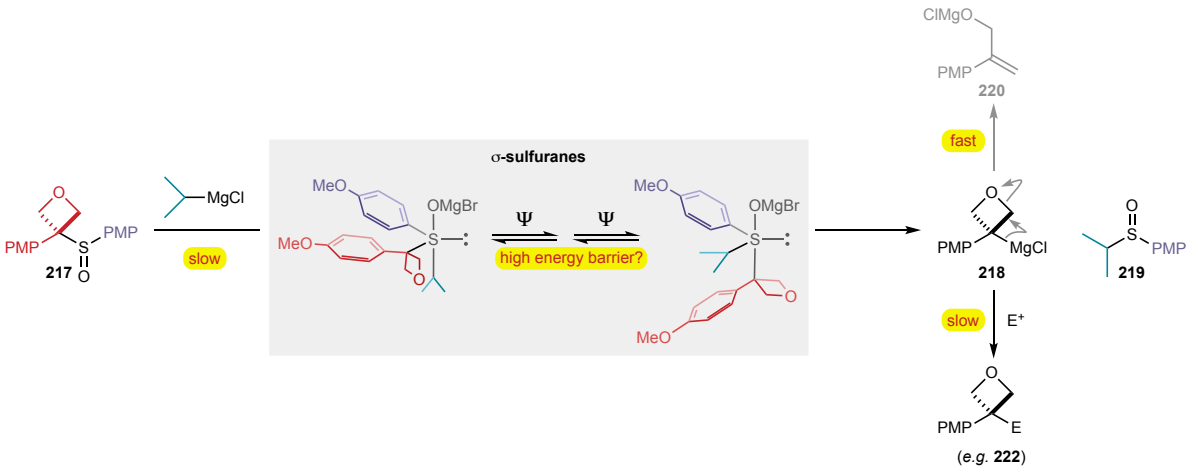
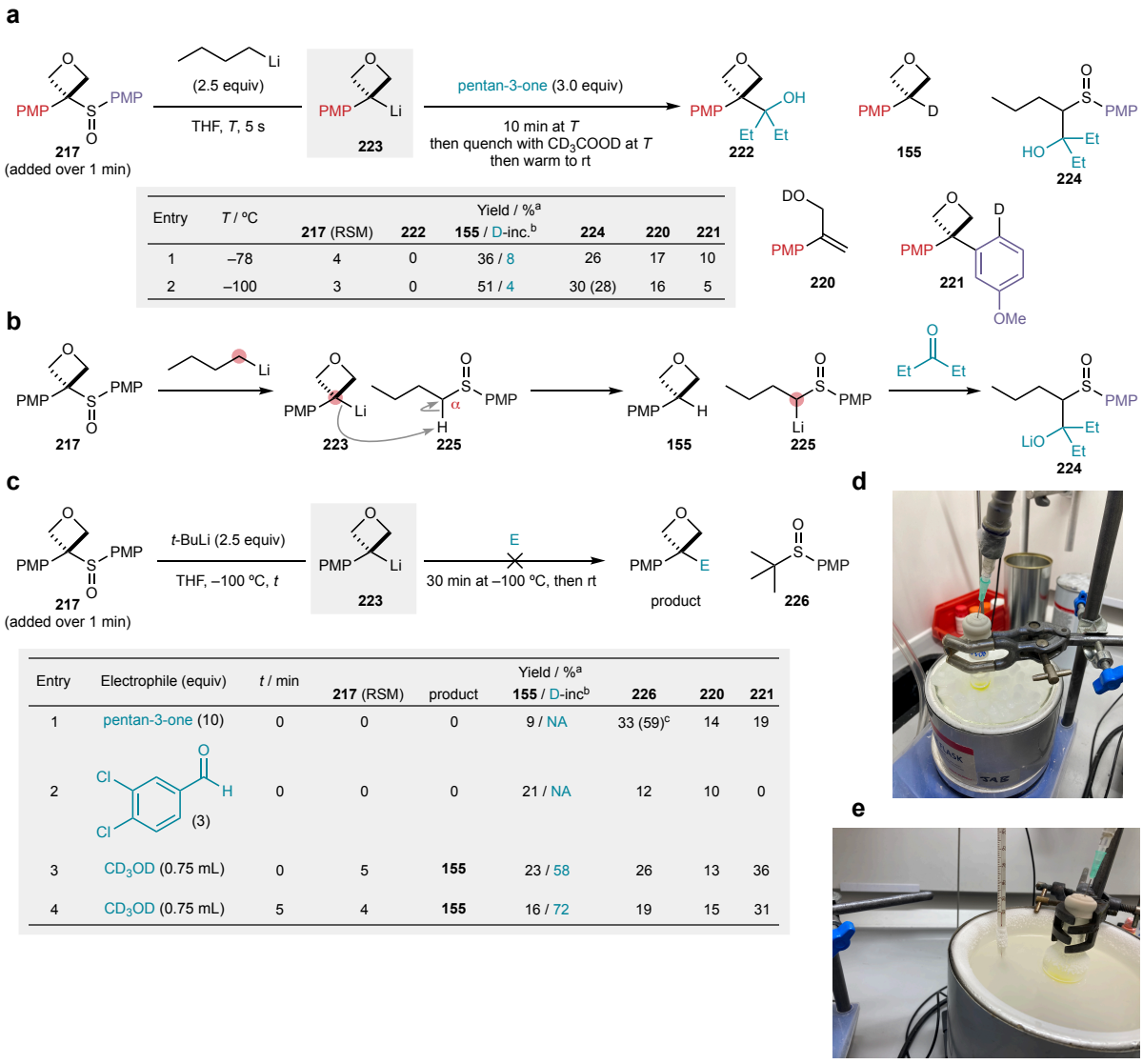


Figure 73. Proposed mechanistic scenario and mismatched relative rates in the sulfoxide–metal exchange of oxetane 217.

Consequently, to accelerate the initial sulfoxide–metal exchange, stronger organolithium bases were investigated (Figure 74). *n*-Butyl lithium successfully triggered the sulfoxide–metal exchange, consuming all oxetane sulfoxide **217** after 5 s induction time at –78 and –100 ºC (Figure 74a). Still, desired oxetane alcohol **222** was not observed upon quenching with pentan-3-one, but instead, sulfoxide alcohol **224** was isolated in increased amounts, as well as protonated oxetane **155**. Alcohol **224** was presumably formed by deprotonation of the acidic sulfoxide α-proton of the *n*-butyl sulfoxide by-product **225** by oxetane carbanion **218**, followed by attack of deprotonated **225** into the ketone electrophile (Figure 74b).

Then, the base was changed to *tert*-butyl lithium to exclude α-protons from the sulfoxide by-product and prevent quenching of oxetane carbanion **223** by undesired protonation (Figure 74c). Still, the desired reaction with carbon electrophiles was not successful with pentan-3-one (entry 1), nor with non-enolisable *m*,*p*-dichloro-benzaldehyde (entry 2), obtaining complex product mixtures in both cases. Finally, the sulfoxide–metal exchange with *t*-BuLi was tested with CD_3OD as quencher at –100 ºC (entries 3 and 4). Similar results after both 0 s and 5 min induction times indicated immediate reactivity and the low amounts of protonated oxetane **155** and particularly of sulfoxide by-product **226** suggested degradation of the oxetane ring *via* non-exchange pathways, potentially by α-lithiation at the oxetane 2-position. It is worth noting that there was a sharp change in colour from colourless to bright yellow upon addition of an organomagnesium- (Figure 74d) or organolithium reagents (Figure 74e) to a solution of oxetane sulfoxide **217** in THF, further indicative of the formation of a new organometallic species.



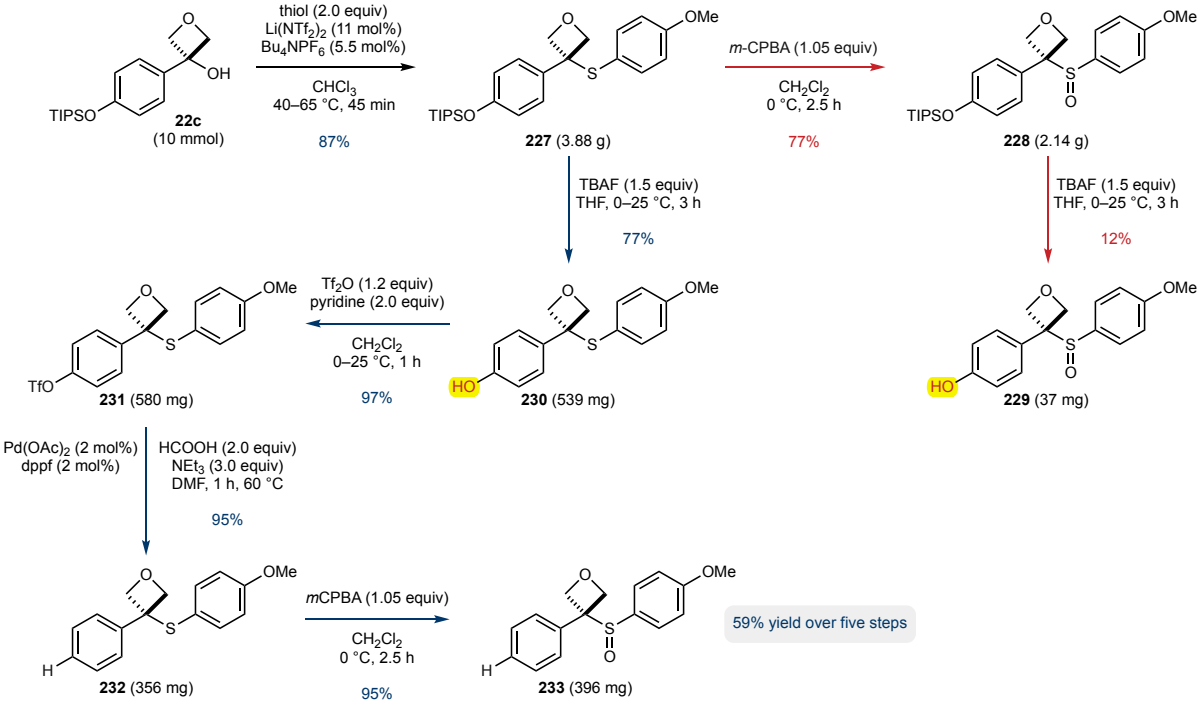
Entry	T / °C	Yield / %[a] 217 (RSM)	222	155 / D-inc.[b]	224	220	221
1	–78	4	0	36 / 8	26	17	10
2	–100	3	0	51 / 4	30 (28)	16	5

Entry	Electrophile (equiv)	t / min	Yield / %[a] 217 (RSM)	product	155 / D-inc[b]	226	220	221
1	pentan-3-one (10)	0	0	0	9 / NA	33 (59)[c]	14	19
2	(3)	0	0	0	21 / NA	12	10	0
3	CD_3OD (0.75 mL)	0	5	**155**	23 / 58	26	13	36
4	CD_3OD (0.75 mL)	5	4	**155**	16 / 72	19	15	31

Figure 74. Sulfoxide–metal exchange of oxetane 217 with organolithium bases. a, Using *n*-BuLi. **b**, Proposed mechanism for the formation of sulfoxide **224**. **c**, Using *t*-BuLi. **d**, Colour change of reaction after addition of *i*-PrMgCl at –78 °C (Figure 72a, entry 5). **e**, Colour change of reaction after addition of oxetane **217** to a solution of *t*-BuLi in THF at –100 °C (**c**, entry 1). [a] Reactions run on a 0.2 mmol scale and 0.1 M concentration and yields and percentage of deuteration calculated by analysis of the ^{1}H NMR spectrum of the crude mixture of the reaction using 1,3,5-trimethoxybenzene as internal standard and a 20 s relaxation delay (d1). Isolated yields in parenthesis. [b] D-inc. = incorporation of deuterium (in %) in **155**. [c] Isolated with impurities.

The high instability of oxetane carbanion **218**/**223** coupled with its sluggish intermolecular reactivity due to a high degree of sterics near the reactive centre, represented a considerable challenge. Next, a less electron-rich oxetane sulfoxide substrate was prepared to provide more efficient resonance stabilisation of the negative charge on oxetane and potentially increase its lifetime (Scheme 58). A free phenol group was envisaged to serve as a synthetic handle for convenient downstream functionalisation. OTIPS oxetane sulfide **227** was obtained from oxetanol **22c** in 87% yield using the previously developed lithium-catalysed thiol-alkylation conditions.[110] Oxidation to sulfoxide **228** (77%), followed by TIPS deprotection was an

unsuccessful route due to undesired reactivity with the sulfoxide functionality (*e.g. S*-fluorination followed by degradation) which led to a complex mixture of products during the deprotection with TBAF and only 12% of desired phenol **229**. Instead, the TIPS group was removed at the S^{II} oxidation state to yield sulfide **230** with the unmasked phenol functionality in 77% yield. Triflation with triflic anhydride (**231**; 97%), followed by Pd-catalysed deoxygenation (**232**; 95%) and sulfide oxidation yielded requisite electron-neutral 3-phenyl-oxetane sulfoxide **233** in 95% yield (59% over five steps).

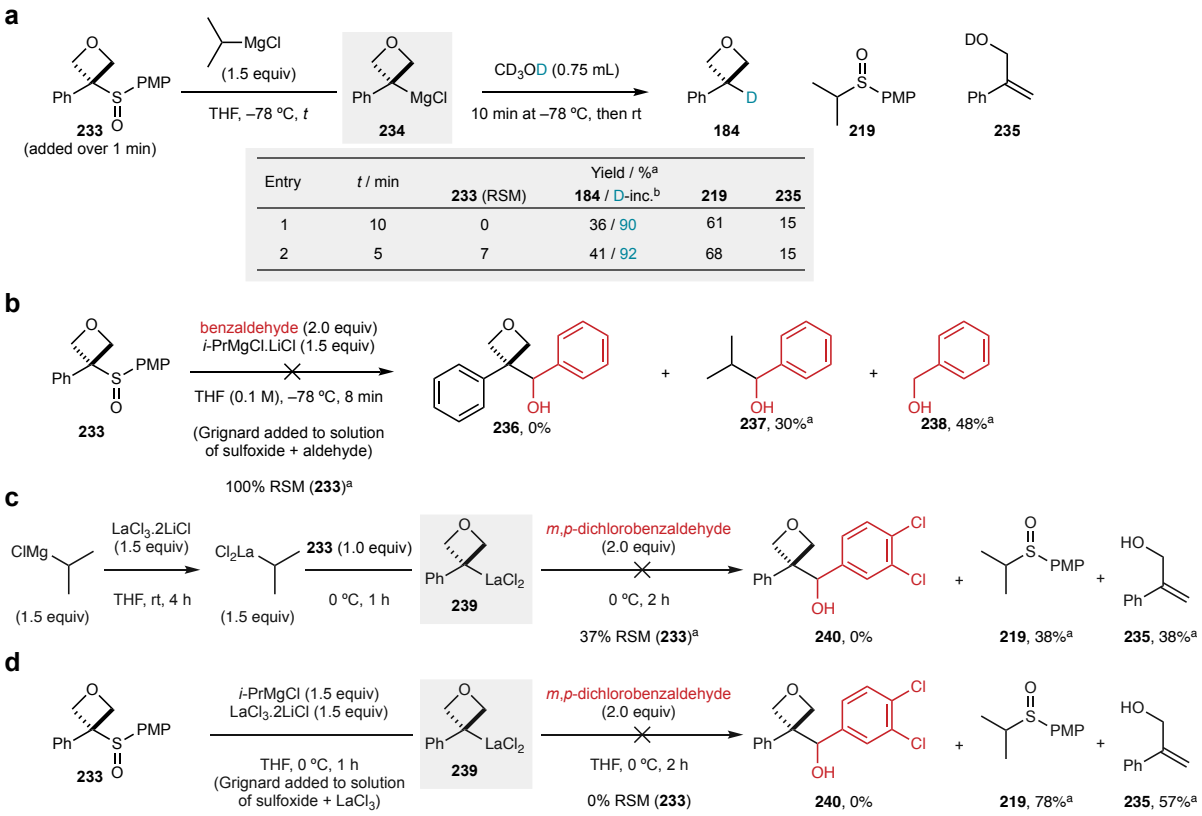


Scheme 58. Synthesis of oxetane sulfoxide 233.

Sulfoxide–metal exchange with phenyloxetane sulfoxide **233** was first tested with deuterated methanol as a proton quench at –78 ºC and with isopropylmagnesium chloride as nucleophile (Figure 75a). The outcomes after 5 and 10 minutes induction time were comparable, with moderate yield of protonated oxetane **184** (36–41%)[ff] but a high degree of deuteration (90–92% D-incorporation), and low amounts of ring-opened product **235** (15%). Especially the high degree of deuteration was encouraging. Three final attempts were made to trap 3-phenyloxetane carbanion **234** with carbonyl electrophiles (Figure 75b–d). First, Turbo Grignard (*i*-PrMgCl.LiCl) was added to a solution of sulfoxide **233** and benzaldehyde in THF in the hope of a fast exchange to generate the oxetane carbanion, followed by immediate quenching with benzaldehyde already present in the reaction mixture (Figure 75b). However, attack of isopropylmagnesium chloride into benzaldehyde was quicker than sulfoxide–metal

[ff] Noting that 3-phenyl oxetane **184** is even more volatile than 3-*p*-methoxyphenyl oxetane **155**.

exchange and isopropyl alcohol **237** was observed in 30% yield, alongside benzyl alcohol **238** in 48%, the product of reduction by hydride donation from *i*-PrMgCl.LiCl, and 100% recovered sulfoxide **233**. Attempts to generate a more stable oxetane organometallic such as organolanthanum **237** followed by trapping with dichloro-benzaldehyde were unsuccessful (Figure 75c–d). Neither sulfoxide–metal exchange with isopropyllanthanum trichloride (Figure 75c), nor transmetallation of oxetane organomagnesium **234** with $LaCl_3$.2LiCl were successful (Figure 75d).[426]



Entry	*t* / min	Yield / %[a]			
		233 (RSM)	**184** / D-inc.[b]	**219**	**235**
1	10	0	36 / 90	61	15
2	5	7	41 / 92	68	15

Figure 75. Sulfoxide–metal exchange of phenyl oxetane 233. a, Protonation studies. **b**, Reaction with benzaldehyde and Turbo Grignard. **c**, Sulfoxide–metal exchange with an organolanthanum. **d**, Transmetallation of Ph oxetane organomagnesium to organolanthanum **239**. [a] Reactions run on a 0.1 mmol scale and 0.1 M concentration and yields and percentage of deuteration calculated by analysis of the ^{1}H NMR spectrum of the crude mixture of the reaction using 1,3,5-trimethoxybenzene as internal standard and a 20 s relaxation delay (d1). [b] D-inc. = incorporation of deuterium (in %) in **184**.

The preliminary investigations presented in this section represent an important foundation for the future development of oxetane carbanions. Proof-of-principle studies by protonation/deuteration were supportive of the targeted oxetane carbanion, but its combination of instability and slow intermolecular reactivity rendered it a challenging intermediate to harness. Potential future work, which is described in Section **5.5**, could focus on more electron-poor oxetane sulfoxide substrates and/or the use of contemporary techniques for highly reactive intermediates such as ‘flash-chemistry’ using a flow system.

5.4 Ligand-to-Ligand Coupling of Oxetane Sulfoxides

Next, the potential for oxetane sulfoxides to react productively in a ligand-to-ligand coupling pathway was investigated (Section **5.1.2**).[422]

Several substantial challenges were also associated with this reaction pathway (Figure 76): 1) Previous literature reports have usually involved the coupling of electron-poor aromatics (such as heteroarenes) with *primary* benzylic substituents. It was anticipated that L2L coupling with *tertiary* benzylic oxetane structures would involve sterically challenging Ψ pseudorotations that might disfavour the productive pathway. 2) In all previous reports of L2L couplings, the coupled electron-poor (hetero)arene was already preinstalled on the sulfoxide and either a benzylic-, alkyl- or aryl organometallic was added to the (hetero)aryl-sulfoxide. An oxetane-heteroaromatic sulfoxide is however not accessible using the previously developed Li^+-catalysed conditions for sulfide synthesis,[110] because heteroarenes poisoned the Lewis acid catalyst. 3) Hence, successful L2L coupling of benzylic oxetane fragments to heteroarenes (*e.g.* 2-pyridyl as the most studied example) would require addition of a heteroaryl organometallic to the sulfoxides, which is unprecedented in the context of L2L couplings, and would generate an unfavourable σ-sulfurane intermediate (**241**) with the 2-pyridyl substituent in the apical position in the first instance.

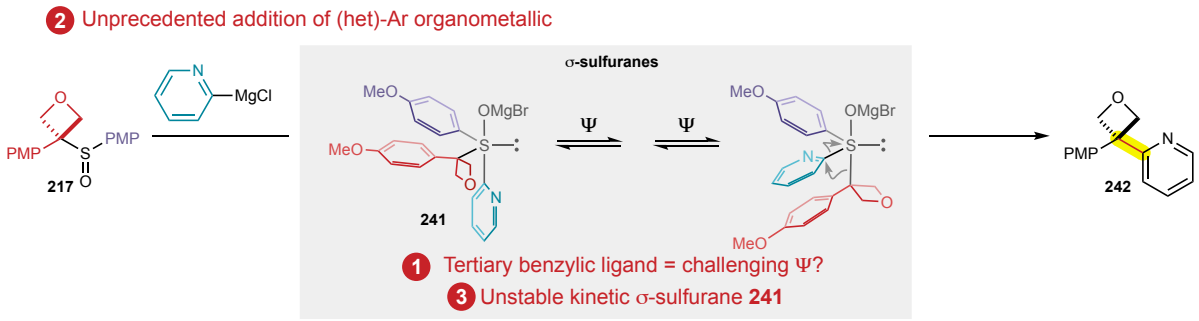
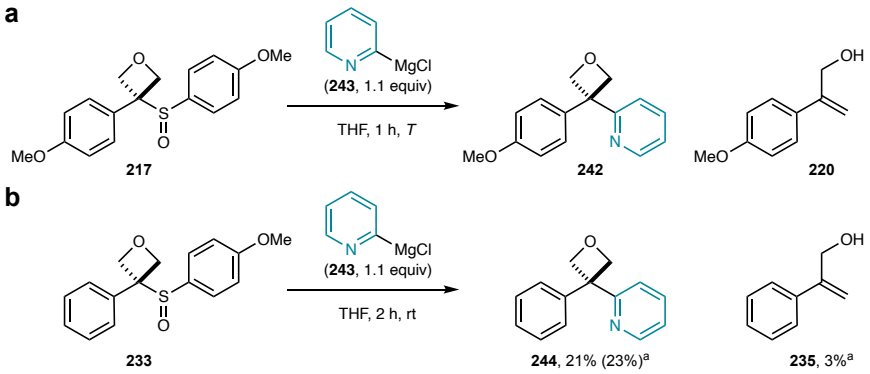


Figure 76. Challenges associated with the L2L coupling of oxetane sulfoxides.

The addition of 2-pyridylmagnesium chloride **243** (generated *in situ* from the corresponding bromide and Turbo Grignard)[403a] to PMP-oxetane sulfoxide **217** was attempted (Scheme 59a). At –78 ºC there was no reaction and 94% starting material was recovered. At room temperature however, 24% of desired 2-pyridyl diaryl-oxetane **242** was isolated, alongside 7% allylic alcohol **220** and 25% returned starting material. Importantly, electron-neutral Ph oxetane sulfoxide **233** reacted in a similar manner and phenyl-(2-pyridyl) diaryl-oxetane **244** was obtained in 23% yield (Scheme 59b).



T / °C	Yield / %[a]		
	242	**220**	**217** (RSM)
–78[b]	0	0	94
rt	36 (24)	7	25

Scheme 59. L2L coupling between oxetane sulfoxides and 2-pyridylmagnesium chloride. a, With PMP oxetane **217**. **b**, With Ph oxetane **233**. [a] Reactions run on a 0.2 mmol scale and 0.1 M concentration and yields calculated by analysis of the ^{1}H NMR spectrum of the crude mixture of the reaction using 1,3,5-trimethoxybenzene as internal standard. Isolated yields in parenthesis. [b] 30 min at –78 °C, then allowed to warm to rt (ca. 30 min).

Although preliminary, the results shown in Scheme 59 are encouraging for the L2L coupling of oxetane sulfoxides to install electron-poor heteroarenes, not possible *via* oxetane carbocations.

5.5 Conclusion and Future Work

This chapter demonstrated the formation of 3-oxetane carbanion intermediates from oxetane sulfoxides *via* a sulfoxide–metal exchange pathway. Trapping of the anionic intermediates with proton sources and the observation of the expected sulfoxide by-product were evidence of the targeted oxetane carbanion. However, trapping of the carbanion with larger electrophiles of higher synthetic value, *e.g.* aldehydes or ketones, was unsuccessful and led to high degrees of oxetane degradation *via* ring-opening. The oxetane carbanion intermediate appeared to be highly unstable even at cryogenic temperatures (–100 °C), likely due to ring strain and the non-stabilising aromatic ring on oxetane. The high steric hindrance around the reactive centre imposed by the oxetane ring also seems to have hampered the sulfoxide–metal exchange and electrophile trapping steps, which, coupled with the instability of the oxetane carbanion, led to an unfavourable kinetic situation of slow exchange and attack unto nucleophiles, but rapid degradation.

Nonetheless, there is still ample opportunity to improve the overall sulfoxide–metal exchange process with oxetanes. The central problem to solve are the unfavourable relative rates of each required step and involve: increase rate of ligand exchange, decrease rate of degradation (*i.e.* stabilise oxetane carbanion) and increase the rate of intermolecular reaction with electrophiles (Figure 77a). First, the rate of ligand exchange could be increased by using less hindered organomagnesium reagents such as EtMgCl and/or LiCl complexes

(*e.g.* Turbo Grignard reagent).[427] Organolithium reagents could also be an option, but initial investigations with *t*-BuLi showed significant degradation of oxetane.

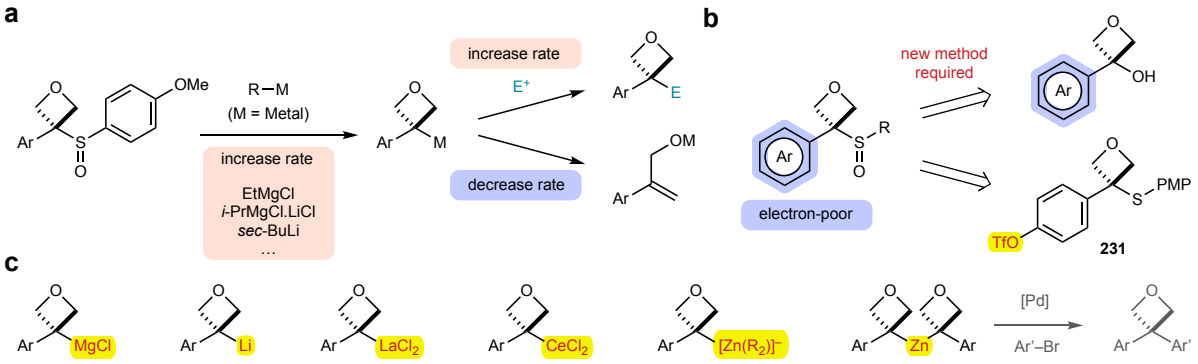


Figure 77. Potential future work for the generation of 3-aryloxetane carbanions. a, Increase rate of ligand exchange and reaction with electrophile, decrease rate of degradation. **b**, Access electron-poor 3-aryloxetane sulfoxides. **c**, Examine a range of oxetane organometallics.

Stabilisation could be achieved by several means. Introducing an electron-poor aromatic ring on oxetane would significantly stabilise the negative charge and could be crucial to favour the desired pathway of reaction (*e.g.* like the oxetane carbocation was only formed with electron-rich aromatics on oxetane). However, accessing electron-deficient oxetane sulfoxides is not possible by the previously developed thiol alkylation reaction of oxetanols, since the transformation involves an oxetane carbocation intermediate.[110] Access to the requisite electron-poor oxetane sulfoxides could be enabled by either developing new methodology for the thiol alkylation to tolerate electron-poor functionality, perhaps in HFIP solvent, as was shown for electron-poor Friedel–Crafts reactions of oxetanols,[211] or, triflate oxetane sulfide **231** could be developed as a cross-coupling hub to access the electron-deficient functional groups (Figure 77b). Other parameters that could improve stability are stabilising additives (*e.g.* LiCl, HMPA, TMEDA) or different solvent mixtures (for example, ether/pentane as shown by Knochel).[428]

The countercationic metal of the oxetane carbanion could have a significant impact on its stability and nucleophilicity (Figure 77c). For example, organolanthanum[426,429] and organocerium[430] species are generally more stable than their organomagnesium counterparts and usually show improved reactivity towards carbonyl electrophiles due to carbonyl activation by the oxophilic lanthanide cations. '-ate' type organometallics, most notably organozincates, are also known for their increased nucleophilicity.[431] Softer organometallics such as organozinc reagents, although much less nucleophilic, may be more stable and could be functionalised as part of cross-coupling processes such as Negishi couplings.[417]

Lastly, flow techniques could be exploited for a better time control between sulfoxide–metal exchange and trapping of the oxetane organometallic. Also known as 'flash chemistry', flow reaction set-ups allow for the continuous generation and quenching of reactive intermediates with reaction times of under 1 s achievable, by shortening the retention time. Flow circumvents the batch-requirement to turn all the starting material into the reactive intermediate before the quenching agent can be added and allows for higher working temperatures which could improve intermolecular reactivity without compromising on stability. There are sufficient examples of flash flow chemistry enabling 'ultra-fast' reactions that had been unsuccessful in batch to occur productively.[180b,432,433,434]

Oxetane sulfoxides were also shown to embark in ligand-to-ligand couplings with 2-pyridylmagnesium chloride as organometallic reagent to yield medicinally valuable 2-pyridyl diaryl-oxetanes for the first time. Particularly Ph-pyridyl oxetane **244** is notable, which now contains electron-neutral and electron-deficient arenes on oxetane. These results are promising to expand the substitution patterns that can be installed on oxetane motifs and represent an unusual L2L coupling of heteroaryl organometallics with a tertiary benzylic fragment on sulfoxide. Future work to improve the reaction could focus on the following: 1) non-participating group on sulfoxide, 2) type of heteroaryl organometallic and 3) conventional reaction variables such as solvent, concentration, temperature and time (Figure 78a).

Although the investigated *para*-methoxyphenyl substituent (electron-rich and sp^2-hybridised = basal position favoured) on sulfur should already favour the L2L coupling of the benzylic oxetane fragment, alternative groups could further improve the reaction. Primary alkyl groups would probably favour ligand exchange, tertiary alkyl might be too hindered for favourable Ψ pseudorotation, but secondary alkyl substituents, such as *sec*-butyl, could disfavour ligand exchange whilst kinetically allowing the necessary Ψ pseudorotations, as shown by Qin.[423] Then, different 2-pyridyl organometallics (*e.g.* R–MgCl, R–MgCl.LiCl, R–MgBr, R–Li, R–$LaCl_2$, R–$CeCl_2$, etc.) could be tested, as well as the remaining reaction variables (solvent, concentration, temperature, time).

Lastly, although less versatile, an alkyl Grignard (*e.g. sec*-BuMgCl) could be added to a (hetero)aryl-containing oxetane sulfoxide (Figure 78b). Non-heterocyclic electron-deficient benzene derivatives can be installed on the sulfur side of oxetane sulfoxides with existing methodology, but heteroaryl examples would need the development of an alternative thiol-alkylation procedure.

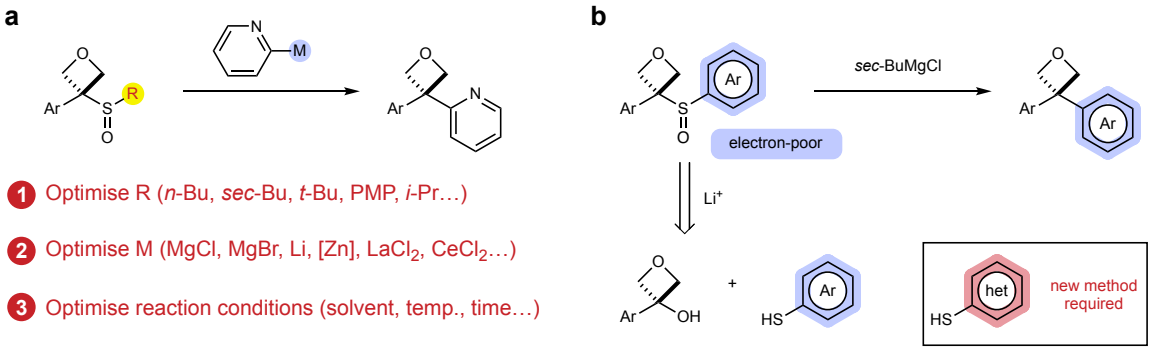


Figure 78. Potential future work for the L2L coupling of oxetane sulfoxides. a, Optimisation of R group, metal (M) and reaction variables. **b**, Addition of *sec*-BuMgCl to oxetane sulfoxides with an electron-poor (hetero)cycle on sulfur.

6 Conclusion and Future Work

This thesis investigated three types of oxetane reactive intermediates: carbocations, radicals and carbanions, to expand the palette of substitution patterns on oxetanes as valuable scaffolds for drug discovery. Oxetane sulfonyl fluorides were developed as precursors to oxetane carbocations,[212] oxetane carboxylic acids[311] and oxetane benzoates (oxetanol-derived) as precursors to oxetane radicals and oxetane sulfoxides were demonstrated to be potential precursors of oxetane carbanions (Figure 79).

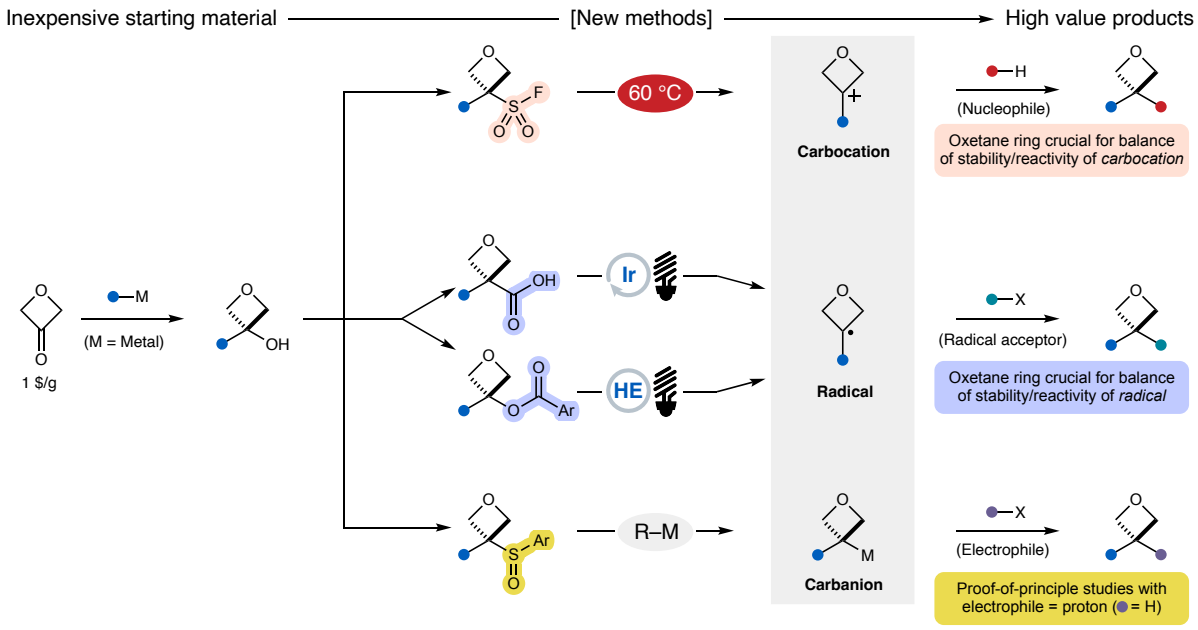


Figure 79. Overview of investigated approaches to generate oxetane reactive intermediates.

Oxetane sulfonyl fluorides (OSFs) were developed as useful reagents which served as precursors to oxetane carbocations on mild warming (60 ºC), followed by coupling to nucleophiles. A general and reliable 4-step synthetic sequence towards OSFs from readily accessible oxetanols was established and scaled up to 1 g of OSF. OSF reagents were shown to be bench-stable crystalline solids, convenient to handle in the laboratory. Oxetane sulfonyl fluorides underwent *defluorosulfonylation* to generate relatively stable benzylic oxetane carbocations upon loss of sulfur dioxide and fluoride, in an unprecedented type of reactivity that contrasted the typical behaviour of sulfonyl fluoride compounds, known to react with nucleophiles in a click Sulfur–Fluoride Exchange (SuFEx) process. The *in situ*-generated oxetane carbocations were trapped with various nucleophiles including amines, alcohols, N-heterocycles, phenols and thiols in generally high yields. The defluorosulfonylative coupling to amines was shown to be robust, insensitive to air and water, and tolerant to common sensitive functionality such as free alcohols, esters, terminal alkenes, alkyl halides and heterocycles. The protocol was showcased in the late-stage functionalisation of complex amines and the

synthesis of oxetane analogues of benzamide drugs, including multi-step processes which did not compromise the integrity of the oxetane ring.

The aryl amino-oxetane products occupied unexplored chemical space of value for drug discovery and as potential isosteres of benzamides. The structural and physicochemical properties of selected amino-oxetanes were investigated and compared to related benzamides. The amino-oxetane motif was demonstrated by an X-ray crystallographic study to adopt a more 3-dimensional structure than the corresponding benzamide due to a loss of π-conjugation. Amino-oxetanes were generally more water soluble than their benzamide analogues, showed high chemical stability at different pHs, and were neither a Log*D*, metabolic, nor toxicity liability.

Mechanistically, the defluorosulfonylation pathway was shown by kinetic and computational studies (in collaboration with the Duarte group) to proceed through an S_N1-type mechanism with the rate-determining formation of a planar benzylic oxetane carbocation, followed by chemodetermining trapping with nucleophiles. Defluorosulfonylation was computed to proceed by elongation of the C–S bond, and the tertiary benzylic aryl-oxetane structure was shown to be crucial to achieve the required stability/reactivity balance of the carbocation and the corresponding sulfonyl fluoride reagent.

Aryl-oxetane carboxylic acids were shown to be suitable precursors to oxetane radicals by a photoredox-catalysed decarboxylative strategy using an iridium photocatalyst and visible light. The benzylic oxetane radicals were trapped productively in a Giese-type process and coupled to a wide range of Michael acceptors including acrylates, acrylamides and styrenes in moderate to high yields. Importantly, electron-neutral functionality on oxetane, not tolerated on oxetane carbocation intermediates, could be incorporated. A computational study (in collaboration with the Duarte group) revealed the Giese addition of benzylic radicals to be generally reversible due to the increased stability of these radicals, leading often to low yields of Giese products and high amounts of side products of dimerisation. The strained oxetane structure, however, sufficiently destabilised the benzylic radical to render Giese addition exergonic and irreversible. Additionally, the oxetane oxygen heteroatom led to an increase in s-character of the hybrid orbital of the benzylic carbon involved in the bond with the arene as a manifestation of Bent's rule, which shortened this bond, increased π-delocalisation of the radical into the aromatic ring and minimised formation of the dimer side product. Nevertheless, the globally high stability of benzylic oxetane radicals (*e.g.* compared to non-benzylic alkyl radicals), coupled with the high steric requirements imposed by the oxetanyl structure, were too unreactive to achieve further productive reactions with radical acceptors.

Oxetanol-derived aryl-oxetane benzoates were also shown to be precursors to benzylic oxetane radicals, through single-electron reduction followed by β-scission. Instead of trapping the oxetane radicals with neutral radical acceptors, persistent 4-cyanopyridine radical anions, also generated by single-electron reduction, were reacted with the oxetane radicals in a recombination-type process with a high driving force. 4-Pyridine diaryl-oxetanes were generated, including an example with an electron-poor *p*-CF_3-phenyl group on oxetane.

3-Aryloxetane carbanions were generated for the first time, demonstrated by trapping with proton sources. Oxetane sulfoxides were used as precursors which underwent sulfoxide–metal exchange upon addition of organometallic reagents to release an oxetane organometallic. Trapping of the oxetane carbanions with other electrophiles such as ketones or aldehydes was unsuccessful, likely due to the high instability of, and steric crowding around the 3-aryloxetane carbanion intermediate. On the other hand, preliminary studies with 2-pyridylmagneisum chloride as organometallic reagent favoured a ligand-to-ligand coupling pathway which attached the 2-pyridyl fragment unto oxetane to generate 2-pyridine diaryl-oxetanes in an initial ca. 25% yield.

Specific suggestions for future developments on each oxetane reactive intermediate were proposed at the end the relevant section. Potential future directions of the field, in a broader sense, are presented below (Figure 80).

Concerning oxetane carbocations, methodologies should be developed to encompass and tolerate electron-poor functionality on oxetane, not supported by current methods (Figure 80a). This is important to incorporate privileged heteroaromatic functionality on oxetanes, typically electron-deficient but of valuable for medicinal chemistry. An interesting approach was proposed by M. Dubois using HFIP as solvent to stabilise unstable electron-deficient oxetane carbocations (see *e.g.* Scheme 44).[211] Further, future research should examine alternative precursors to oxetane carbocations which are of more general application than dehydrative processes from oxetanols (which *e.g.* do not tolerate amine nucleophiles) but of lower synthetic burden than oxetane sulfonyl fluorides (5 steps from commercial oxetan-3-one). The key will lie in finding a good enough leaving group that can generate the requisite oxetane carbocation but that does not compromise the stability of the oxetane precursor. Oxetanol-derived esters, for example benzoates, could be such promising candidates. Oxetane benzoates are accessible from oxetanols and acyl chlorides, and their electronic properties can be tuned by varying the substitution patterns on the acyl chloride precursor (Figure 80b).

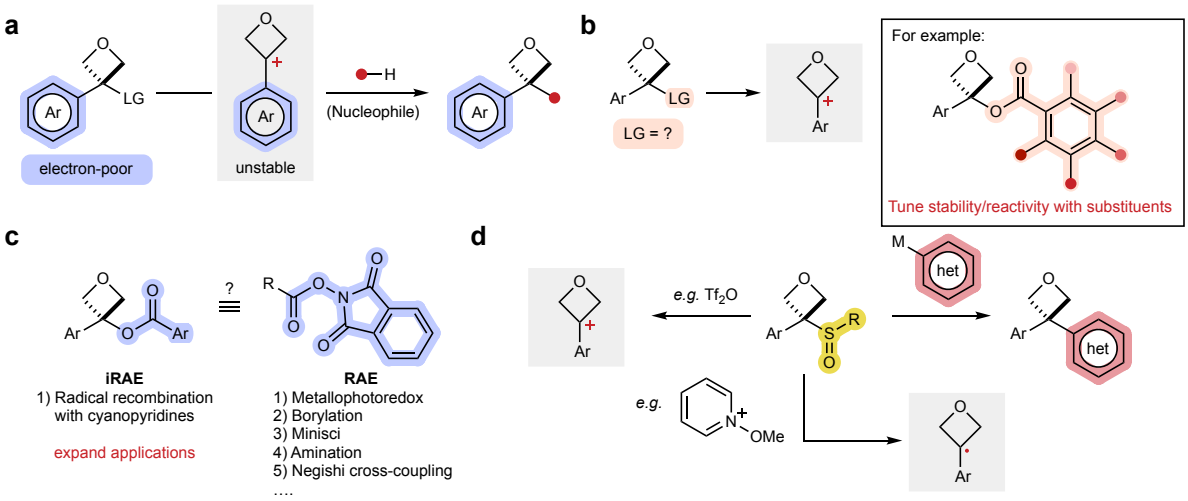


Figure 80. Potential future directions to investigate oxetane reactive intermediates. **a**, Tolerance of electron-poor aryloxetane carbocations. **b**, Alternative precursors to oxetane carbocations. **c**, Development of oxetane **iRAE**s as general precursors to oxetane radicals. **d**, Oxetane sulfoxides as useful precursors to oxetane reactive intermediates.

Concerning oxetane radicals, the chemistry of the convenient oxetane benzoate precursors should be further examined, as highlighted in Section **4.2.2**. These radical precursors show parallels with the well-investigated redox active esters derived from carboxylic acids and have promising potential to become new hubs for the generation of substituted oxetanes (Figure 80c).

Oxetane carbanions proved to be challenging due to their high instability. Although approaches to harness their reactivity were proposed (see Section **5.5**), investigating the alternative reactivity of oxetane sulfoxides seems more promising, for example the ligand-to-ligand coupling to heteroaromatic organometallics, carbocation generation through activation on oxygen akin to carbohydrate chemistry, or radical generation (Figure 80d).

7 Experimental

7.1 General Experimental Considerations

All non-aqueous reactions were carried out under an inert atmosphere (argon) with flame-dried glassware using standard techniques, unless otherwise specified. Anhydrous solvents were obtained by filtration through drying columns (CH_2Cl_2, THF, DMF, Et_2O) or used as supplied (MeCN, MeOH, DMSO). Reactions in sealed tubes were run using Biotage microwave vials (2–5 mL) and aluminium caps with molded butyl septa.

Reactions that required thermal activation were heated using a water bath (for temperatures up to 25 °C) or a silicon oil bath (for temperatures >25 °C).

Flash chromatography was performed using 230–400 mesh silica from Sigma Aldrich, with the indicated solvent system according to standard techniques. Analytical thin-layer chromatography (TLC) was performed on precoated glass-backed silica gel plates. Visualisation of the developed chromatogram was performed by UV absorbance (254 nm) and stained with a ninhydrin, *p*-anisaldehyde or phosphomolybdic acid solution in ethanol, followed by heating.

Infrared spectra (ν_{max}, FTIR ATR) were obtained using an Agilent Technologies Cary 630 FTIR Spectrometer and recorded in reciprocal centimeters (cm^{-1}) (br = broad, st = stretch, as = asymmetric, sy = symmetric).

Nuclear magnetic resonance spectra were recorded on 400 or 500 MHz spectrometers. The frequency used to record the NMR spectra is given in each assignment and spectrum (^{1}H NMR at 400 or 500 MHz; ^{13}C NMR at 101 MHz or 126 MHz; ^{19}F NMR at 377 MHz). Chemical shifts for ^{1}H NMR spectra were recorded in parts per million (ppm) from tetramethylsilane with the residual protic solvent resonance as the internal standard ($CHCl_3$: δ = 7.27 ppm, DMSO: δ = 2.50 ppm, CH_3OD: δ = 3.31 ppm, CH_3CN: δ = 1.97 ppm). Data is reported as follows: chemical shift (multiplicity [s = singlet, d = doublet, t = triplet, q = quartet, p = pentet, hept = heptet, m = multiplet and br = broad], coupling constant (in Hz), integration of equivalent nuclei and assignment). ^{13}C NMR spectra were recorded with complete proton decoupling. Chemical shifts are reported in parts per million (ppm) from tetramethylsilane with the solvent resonance as the internal standard ($^{13}CDCl_3$: δ = 77.0 ppm, $(^{13}CD_3)_2SO$: δ = 39.5 ppm, $^{13}CD_3OD$: δ = 49.0 ppm). *J* values are reported in Hz. Assignments of ^{1}H and ^{13}C spectra were based upon the analysis of δ and *J* values, as well as COSY, HMQC and HMBC experiments where appropriate. ^{19}F NMR spectra were recorded with

complete proton decoupling. Chemical shifts are reported in parts per million (ppm). ^{19}F NMR spectra were indirectly referenced to $CFCl_3$ automatically by direct measurement of the absolute frequency of the deuterium lock signal by the spectrometer hardware.

Melting points were obtained using an Optimelt MPA100 melting point apparatus and are uncorrected.

High-resolution mass spectra (HRMS) were obtained through the Imperial College mass spectrometry service. HRMS analyses were performed using an electrospray ion source (ESI), electron ionisation (EI) or atmospheric pressure chemical ionisation (APCI) using an atmospheric solids analysis probe (ASAP). ESI was performed using a Waters LCT Premier (ES-ToF) equipped with an ESI source operated in positive ion mode. EI was performed using a Micromass Autospec Premier/Agilent HP6890 GC. APCI was performed using a Thermo Scientific Q-Extractive/Dionex Ultimate 3000 using an ASAP to insert samples into the APCI source operated in positive or negative mode. The sample was introduced at ambient temperature and the temperature increased until the sample vapourised. The software used was either MassLynx 4.1 or Bruker Daltonics DataAnalysis 4.0. Please note: MassLynx 4.1 software does not account for the electron and all the calibrations/references were calculated accordingly, *i.e.* $[M+H]^+$ was detected and the mass was calibrated to output [M+H]. In the cases where this software was used, HRMS was reported as [M+H].

Observed optical rotations (α') were measured at the indicated temperature (T °C) and converted to the corresponding specific rotations $[\alpha]_D^T$ in deg cm^2 g^{-1}, concentration (c) in g per 100 mL.

Raw and processed data for published compounds[212,311] can be found at the Imperial College London Data Repository:

https://doi.org/10.14469/hpc/8380 and https://doi.org/10.14469/hpc/10668.

Generally, the identity of compounds previously synthesised and characterised within the group was confirmed by R_f and ^1H NMR data and no further characterisation data were collected. Complete characterisation data for literature compounds were collected, excluding HRMS data, unless such information was missing from the literature report.

Reagents

Where the synthesis of a reagent is not stated, the reagent was commercially available. Commercial reagents were used as supplied or purified by standard techniques where necessary. All volatile amines were distilled over $MgSO_4$ or KOH pellets before use.

- Anhydrous potassium carbonate (≥98%; powder, –325 mesh, CAS: 584-08-7) was purchased from Sigma-Aldrich and flame-dried as part of the reaction set-up.
- Bis(trifluoromethane)sulfonimide lithium salt (>99%, CAS: 90076-65-6) was purchased from Sigma-Aldrich and stored under an argon atmosphere in a desiccator.
- Sodium methoxide (pure, 5.4 M (30 wt %) solution in MeOH, CAS: 124-41-4, 67-56-1) was purchased from Acros Organics and stored under an argon atmosphere.
- The exact concentration of commercial (*n*-BuLi, PhLi, *i*-PrMgCl, *i*-PrMgCl.LiCl) and prepared organometallics (2-pyridyl-magnesium chloride) was determined by titration with salicylaldehyde phenylhydrazone as indicator before each reaction using a literature procedure.[435] The average of three titrations was taken.
- *m*CPBA was pre-washed before use. Procedure: dissolved commercial *m*CPBA (15 g, purity ≤77%, purchased from Sigma-Aldrich) in CH_2Cl_2 (300 mL), washed with a phosphate buffer (pH = 7.5, 3 × 300 mL), dried over Na_2SO_4, filtered and concentrated *in vacuo* using a rotatory evaporator to obtain pure *m*CPBA (free of benzoic acid and water). Special attention should be paid when handling pure *m*CPBA since it is shock-sensitive and potentially explosive. Do not heat on rotatory evaporator, do not scratch with a metal spatula when removing from round bottom flask (use for example a plastic spatula) and store at <4 °C.
- $[Ir\{dF(CF_3)ppy\}_2(dtbbpy)]PF_6$ ([Ir] **133**) was purchased from Sigma-Aldrich (CAS: 870987-63-6, product code: 747793-100MG, purity not given) or Strem Chemicals (CAS: 870987-63-6, product code: 77-0425, purity: 99%). Used without further purification.
- Alkenes were commercially available or obtained from the Pfizer in-house library. Liquid alkenes were distilled in the dark under vacuum and stored in a round bottom flask sealed with a septum, under argon and in the dark at –20 °C.
- NBu_4OH (1 M in MeOH) was purchased from Sigma-Aldrich (CAS: 2052-49-5, product code: 230189-100ML).
- NBu_4ClO_4 was purchased from TCI (CAS: 1923-70-2, product code: T0836-25G, purity ≥ 98%).

- Basic alumina grade IV for flash column chromatography was prepared from commercial basic alumina Brockmann I from Acros Organics (CAS: 1344-28-1, product code: 189990010) by adding 10% of water. For example: 10 mL of water were added to 100 g of basic alumina and shaken vigorously for 5 min until the mixture was powdery and free of lumps. Caution: basic alumina becomes warm upon mixture with water.[311]

7.2 Measurement of Physicochemical Properties[gg]

Chemical Stability Assay was performed in a 384 well plate format (volume = 450 μL). Plates were prefilled with 70 μL of the appropriate buffer (pH 1.2, 7.4, 10) after which the wells were spiked with 5 μL of test compounds (1 mM). Samples were incubated for their timepoint of interest (1 h, 4 h, 24 h) at 37 °C after which the samples were diluted in MeCN (and pH 12.8 buffer for experiment at pH 1.2), mixed with an internal standard and analysed by LCMS.

Aqueous buffer preparation: pH 3: 50 μL of 1 N hydrochloric acid was added to 500 mL of deionised water. The solution was titrated with 1 N hydrochloric acid to pH 3, and back titrated with 1 N sodium hydroxide.

pH 7.4: 100 mM sodium phosphate buffer was made by adding 56.4 g of dibasic sodium phosphate and 10.3 g of monobasic sodium phosphate to 4 L of deionised water. 250 μL of 100 mM sodium phosphate buffer was diluted with 250 μL of deionised water. The solution was titrated with 1 N hydrochloric acid to pH 7.4, and back titrated with 1 N sodium hydroxide.

pH 10: Fisher Scientific pH 10 buffer (SB116-500) containing potassium hydroxide, potassium carbonate, and potassium borate. pH 12.8: 30 mL of 1 N NaOH was added to 200 mL of deionised water. The solution was titrated with 1 N sodium hydroxide to pH 12.8, and back titrated with 1 N hydrochloric acid.

Kinetic solubility: Samples and controls were loaded onto an appropriate assay ready plated and centrifuged at 3000 rpm for 1 min. The samples were then diluted to 600 μM with the appropriate buffers (pH 3, 7.4, 10), shaken and incubated at 37 °C for 24 h. After this time the plates were shaken again, then centrifuged at 3000 rpm for 2 min. The supernatant was filtered through a 22 micron filter, diluted in MeCN and analysed by LCMS in the presence of an internal standard.

Assay ready plated: Plate containing 6 μL at 30 mM of test compounds in a 96 deep well plate (volume = 600 μL). Or: containing 50 nL at 30 mM of test compound in a 96 well plate (volume = 500 μL).

Aqueous buffer preparation: pH 3: 50 μL of 1 N hydrochloric acid was added to 500 mL of deionised water. The solution was titrated with 1 N hydrochloric acid to pH 3, and back titrated with 1 N sodium hydroxide.

[gg] Performed at Pfizer. Procedures given as provided by Pfizer.

pH 7.4: 100 mM sodium phosphate buffer was made by adding 56.4 g of dibasic sodium phosphate and 10.3 g of monobasic sodium phosphate to 4 L of deionised water. 250 μL of 100 mM sodium phosphate buffer was diluted with 250 μL of deionised water. The solution was titrated with 1 N hydrochloric acid to pH 7.4, and back titrated with 1 N sodium hydroxide.

pH 10: Fisher Scientific pH 10 buffer (SB116-500) containing potassium hydroxide, potassium carbonate, and potassium borate.

eLog*D*: An automated reversed phase-HPLC method developed by Lombardo was used for logD (pH 7.4) measurements.[436] All the chromatographic runs were performed on a HP-1100 HPLC ChemStation at ambient temperature. The HPLC columns used were Supelcosil LC-ABZ, 5 μm, 4.6 mm × 50 mm. A diode array detector was used to monitor signals at 210, 225, 245, and 310 nm. The mobile phase consisted of 15−75% of *A* and 85−25% of *B*.

Mobile phase A: methanol with addition of 0.25% 1-octanol.

Mobile phase B: 20 mM of MOPS (morpholine−propane−sulfonic acid) buffer prepared in octanol saturated water and 0.25% of *n*-decylamine. Samples were prepared in a 1:1 mixture of methanol/water at 100 μg/mL concentration. The retention of each compound was obtained at three different concentrations of methanol in the mobile phase and extrapolated to 0% methanol (100% water).

Toxicity assay: [^{3}H] Dofetilide (DOF) binding assay was performed as described by Finlayson[437] and Diaz.[294]

7.3 Kinetic Studies of Oxetane Sulfonyl Fluorides by ^{1}H NMR

The procedure below describes the reaction profiles for the defluorosulfonylation reaction of oxetane sulfonyl fluorides (Section **3.2.12.1**). Manipulations on the NMR instrument were performed by P. Haycock from the NMR Spectroscopy Service from Imperial College London.

Mesitylene (ca. 13 mg, 0.1 mmol, 0.66 equiv) was added by syringe to a tared oven-dried vial, followed by triethylamine (27 μL, 0.195 mmol, 1.3 equiv; added by a Gilson micropipette), amine nucleophile (0.18 mmol, 1.2 equiv; added by a Gilson micropipette) and oxetane sulfonyl fluoride (0.15 mmol, 1.0 equiv). CD_3CN (0.5 mL, 0.5 M) was added to the vial by syringe and after solvation of all the contents in the vial, the mixture was transferred using a glass pipette to an oven-dried J. Young's NMR tube under Ar and the tube was sealed using the J. Young's valve. The sealed J. Young's NMR tube was inserted into a 400 MHz Bruker NMR instrument with the probe pre-heated at 60 °C. The sample was locked to CD_3CN, shimmed, and a spectrum was acquired every 30 s until all the starting material had been consumed (~2 h, except for OSF **18f**, which was less reactive). The start of the reaction was taken as the time point when the sample was inserted into the pre-heated probe. The time point of the first measurement was taken as the time-interval between insertion of the sample into the probe and acquisition of the first spectrum. The ^{1}H NMR spectra were acquired with 8 number of scans (ns) and 1 s relaxation delay (d1) and processed using MestReNova (Version 12.0.4-22023). All the spectra of each reaction were superimposed and phase and baseline corrected using MestReNova. Then, the relevant signals for each species (Table 24) were integrated on the superimposed spectra. The absolute integral values were exported as a .txt file (Script: 1D Integral Series) and converted to the plotted concentrations by using the internal standard. For an example of the superimposed spectra of the standard reaction see Figure 37. All statistical analyses and graphical representations were performed with the open-source statistical program 'R', version 3.2.2 (April 08, 2015 – 'Fire Safety').[438]

Notes:

The exact amount of mesitylene added was measured by mass and it varied slightly between each experiment. The amounts of triethylamine and amine nucleophile added were measured by volume using a Gilson micropipette.

Triethylamine was used as base instead of K_2CO_3 to allow for a homogeneous reaction in the NMR tube. Optimisation of the reaction had shown that using NEt_3 as base was successful and gave only a slightly lower yield, with increased formation of the oxetane fluoride.[210]

*Trimethoxy OSF **18f** needed ns = 16, d1 = 18 s to yield high-quality spectra. Thus, with this example, a spectrum was measured every 5 min.*

*A broad signal (assigned as **H**Et_3N^+) appeared in almost all reactions and was shifted downfield over the course of the reaction, presumably due to changes in its concentration (i.e. changes in the equilibrium between protonated and neutral species) and pH of the reaction mixture (see e.g. Figure 38). This led in many cases to an overlap with the investigated signals during several minutes. These values were omitted from the analyses since they showed an artificial sharp increase (and later decrease) in concentration. Similarly, the signals of morpholine and triethylamine (see Table 24 and Figure 38) were also shifted downfield through the reaction. Accurate integration values were obtained by superimposing 10–20 spectra at a time and integrating the relevant signals over a small range.*

Table 24. ^{1}H NMR signals analysed.

Species	Chemical shift / ppm	Multiplicity	*J* / Hz	No. of H's	Assignment
OSFs					
18a	5.27	dd	8.5, 1.9	2	C*H*HOC*H*H
18n	5.30	dd	8.5, 1.9	2	C*H*HOC*H*H
18f	6.66	s	–	2	2 × Ar-CH
Amino-oxetanes					
26	4.81	d	0.9	4	$CH_2O_{(oxetane)}CH_2$
121	4.84–4.80[a]	2 × d	6.2	2 × 2	$CH_2O_{(oxetane)}CH_2$
65	6.38	s	–	2	2 × Ar-CH
72	4.93–4.87[a]	2 × d	6.2	2 × 2	CH_2OCH_2
27	4.75	dd	6.1, 0.6	2	C*H*HOC*H*H
122	4.91–4.81[a]	2 × d	6.2	2 × 2	CH_2OCH_2
Other					
35	5.03	dd	7.9, 1.3	1	C*H*HOCH_2
85	5.46	d	7.9	2	C*H*HOC*H*H
32	5.04	d	7.6	2	C*H*HOC*H*H
morpholine	3.60–3.75[b]	m	–	4	CH_2OCH_2
NEt_3	1.05–1.25[c]	t	7.2	9	$N(CH_2C\mathit{H_3})_3$
mesitylene	2.28[d]	d	0.7	9	3 × CH_3

[a] This signal is composed of two adjacent doublets which were integrated together as 4 protons. [b] The approximate range over which the multiplet shifted throughout progression of the reaction, not the range of the multiplet. [c] The approximate range over which the triplet shifted throughout progression of the reaction. [d] For the reaction with OSF **18f** as substrate, the mesitylene signal at 6.83 ppm (d, *J* = 0.7 Hz, 3 H, 3 × Ar-CH) was used.

7.4 Details to Cyclic Voltammetry Experiments

Cyclic voltammetry (CV) measurements were performed on an Autolab PGSTAT204 potentiostat from Metrohm using Nova 2.1 as software. A glassy carbon disc from Metrohm was used as working electrode (3 mm surface area and circular disk geometry), a Pt-plated copper block from IKA (part number: 0040002852) as counter electrode and a Pt-wire as quasi-reference electrode.

Cyclic voltammograms were measured at room temperature (ca. 22 °C), with a 100 mV s^{-1} scan rate, between –2.2 and +2.2 V, starting at 0 V in the positive scan direction, in 10 mV steps and with 1 mA current range.[hh] A quasi-Faraday cage was achieved by wrapping the electrochemical cell in Al-foil. The glassy carbon electrode was polished mechanically in a figure-of-eight motion using an aqueous suspension of nanometric alumina on a polishing pad, between each set of experiments (1 set = CV of analyte (3 scans) + CV of analyte with ferrocene (3 scans)).

Cyclic voltammograms were obtained using a 0.1 M solution of NBu_4ClO_4 in MeCN as supporting electrolyte. Oxygen-free conditions were achieved by purging the electrochemical cell with a balloon filled with argon for 5 minutes before each measurement. Three scans were performed per measurement and numerical values were extracted from the third scan. The analyte was measured in 2 mM concentration. Ferrocene (Fc) was added as an internal standard after each measurement (in 1 mM concentration) and the voltammogram was recorded again.[439] Potentials are reported vs the Fc^+/Fc couple and converted to vs SCE by adding 380 mV (see Table 19).[440] Carboxylates and enolates were generated *in situ* through the addition of 1.0 equiv NBu_4OH (1 M in MeOH) to the carboxylic acid/ester substrates.

Oxidation potentials of irreversible oxidations are reported as the anodic peak potentials (E_{pa}) instead of the potentials at half the peak ($E_{p/2}$) for better reproducibility, as suggested by Lam.[250]

Reduction potentials of reversible reductions (esters **188**–**190**) are reported as $E_{1/2}$, taken as the average potential of the anodic- (E_{pa}) and cathodic (E_{pc}) peak potentials of the reversible reduction.

Values were exported from the Nova software as Excel files. Data were analysed and plotted with the open-source statistical program 'R', version 3.2.2 (April 08, 2015 – 'Fire Safety').[438]

[hh] Range changed for selected examples when required.

7.5 Reaction Profiles of the Giese Reaction of Oxetane Acids

The reaction profiles for the formation of alkylated oxetanes **149** and **152** were conducted with PMP-oxetane acid **148a** and Ph-oxetane acid **148m** using the **Procedure** below for different durations. Each time point represents an independent reaction. Recovery of starting material was assessed by acidifying the basic aq. phase to pH 1 and re-extracting with EtOAc (see **Procedure**). 96% starting material **148a** was recovered when performing the workup at *t* = 0 min. The reaction profiles were conducted with repurified oxetane carboxylic acids. For repurification of PMP-acid **148a**, see Sections **4.2.1.2** and **7.6.5**. Ph-acid **148m** was repurified by column chromatography (30% EtOAc/pentane + 0.5% AcOH).

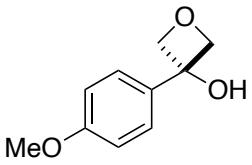
Procedure

An oven-dried 4 mL vial was charged with carboxylic acid (0.10 mmol, 1.0 equiv), oven-dried Cs_2CO_3 (39.1 mg, 0.12 mmol, 1.2 equiv) and $[Ir\{dF(CF_3)ppy\}_2(dtbbpy)]PF_6$ ([Ir] **133**, 1.1 mg, 0.001 mmol, 1.0 mol%). The vial was sealed with a screwcap equipped with a PTFE/silicon septum and anhydrous DMF (0.5 mL, 0.2 M) was added by syringe. Argon was bubbled through the mixture for 5 min and ethyl acrylate (18 μL, 0.15 mmol, 1.5 equiv) was added by syringe under argon. After sealing the cap with parafilm on top, the reaction mixture was stirred at 1000 rpm using the set-up shown in Figure 89 and irradiated with two 467 nm Kessel lamps at 36 °C (heat generated by the lamps).[211] After *t* the lights were switched off and the reaction mixture was transferred into a separating funnel. Distilled water (10 mL) and Et_2O (10 mL) were added, the layers were separated and the aqueous portion was extracted with Et_2O (2 × 10 mL). The aqueous phase was acidified to pH 1 and extracted with EtOAc (3 × 10 mL). The Et_2O and EtOAc extracts were combined separately, dried over Na_2SO_4, filtered and concentrated *in vacuo* using a rotatory evaporator. Yields were calculated by analysis of the ^1H NMR spectrum of the crude mixtures of the reaction (Et_2O and EtOAc extracts separately) using 1,3,5-trimethoxybenzene as internal standard and a 30 s relaxation delay (d1).

7.6 Experimental Details and Characterisation Data

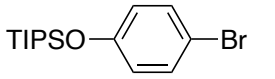
7.6.1 Oxetanols

3-(4-Methoxyphenyl)oxetan-3-ol (22a)



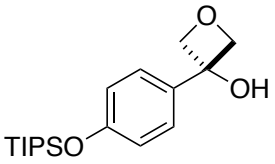
n-BuLi (1.59 M in hexanes, 98 mL, 155.8 mmol, 1.1 equiv) was added dropwise using a canula over 20 min to a solution of *p*-bromoanisole (21.3 mL, 170.0 mmol, 1.2 equiv) in anhydrous THF (650 mL, 0.22 M) at –78 °C in a 2000 mL 2-neck round bottom flask. The rate of the dropwise addition of *n*-BuLi was controlled by employing a positive pressure on the bottle of *n*-BuLi with a balloon filled with argon. One 100 mL bottle of *n*-BuLi was added to the reaction. 98 mL are an estimated volume based on losses during the preceding titration of *n*-BuLi and leftover liquid in the bottle and canula. After stirring for 1 h, oxetan-3-one (9.10 mL, 141.65 mmol, 1.0 equiv) was added dropwise to the reaction mixture. After further 1 h of stirring at –78 °C, the reaction mixture was warmed up slowly to 25 °C, stirred for 2 h and quenched with distilled water (200 mL). The aqueous layer was extracted with Et_2O (3 × 200 mL). The combined organic extracts were washed with brine (200 mL), dried over Na_2SO_4, filtered and concentrated *in vacuo* using a rotatory evaporator. Purification by flash column chromatography (45% EtOAc/hexane; ca. 500 g of silica were used) afforded oxetanol **22a** as a white solid (23.03 g, 90%). R_f = 0.20 (45% EtOAc/hexane); ^{1}H NMR (400 MHz, $CDCl_3$) δ 7.49–7.45 (m, 2 H, 2 × Ar-CH), 6.95–6.91 (m, 2 H, 2 × Ar-CH), 4.88 (d, *J* = 7.0 Hz, 2 H, C*H*HOC*H*H), 4.85 (d, *J* = 7.0 Hz, 2 H, CH*H*OCH*H*), 3.82 (s, 3 H, OCH_3), 3.32 (br s, 1 H, OH); ^{13}C NMR (101 MHz, $CDCl_3$) δ 159.2 (Ar-C_qOMe), 134.5 (Ar-C_qC_q), 125.9 (2 × Ar-CH), 114.0 (2 × Ar-CH), 85.6 (CH_2OCH_2), 75.6 (C_q), 55.3 (OCH_3). The observed characterisation data (R_f, ^{1}H, ^{13}C) were consistent with that previously reported in the group.[202]

(4-Bromophenoxy)triisopropylsilane (S1)



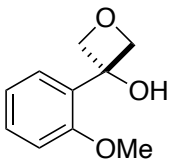
Triisopropylsilyl trifluoromethanesulfonate (5.9 mL, 22.0 mmol, 1.1 equiv) was added dropwise to a solution of 4-bromophenol (3.46 g, 20.0 mmol, 1.0 equiv) and 2,6-lutidine (2.8 mL, 24.0 mmol, 1.2 equiv) in anhydrous CH_2Cl_2 (27 mL, 0.75 M) in a 100 mL round bottom flask at 0 °C. The reaction mixture was stirred at 0 °C for 4 h and then quenched with distilled water (33 mL). The aqueous layer was extracted with CH_2Cl_2 (3 × 33 mL). The organic extracts were combined, dried over Na_2SO_4, filtered and concentrated *in vacuo* using a rotatory evaporator. Purification by filtration through a silica plug (100% pentane) afforded aryl bromide **S1** as a colourless oil (6.18 g, 94%). R_f = 0.68 (100% pentane); ^{1}H NMR (400 MHz, $CDCl_3$) δ 7.33–7.29 (m, 2 H, 2 × Ar-CH), 6.78–6.74 (m, 2 H, 2 × Ar-CH), 1.29–1.20 (m, 3 H, 3 × SiCH), 1.10 (d, *J* = 7.3 Hz, 18 H, 6 × SiCHC*H*$_3$). The observed characterisation data (R_f, ^{1}H) were consistent with that observed previously in the group.[202]

3-(4-((Triisopropylsilyl)oxy)phenyl)oxetan-3-ol (22c)



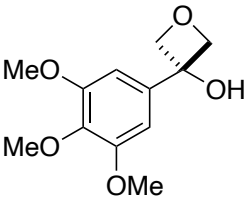
n-BuLi (1.60 M in hexanes, 27.5 mL, 44 mmol, 1.1 equiv) was added dropwise over 5 min to a solution of aryl bromide **S1** (13.64 mL, 48 mmol, 1.2 equiv) in anhydrous THF (182 mL, 0.22 M) at –78 °C in a 1000 mL round bottom flask. After stirring for 30 min, oxetan-3-one (2.56 mL, 40 mmol, 1.0 equiv) was added dropwise to the reaction mixture. After further 30 min of stirring at –78 °C, the reaction mixture was warmed to 25 °C and quenched with distilled water (90 mL). The aqueous layer was extracted with Et_2O (3 × 90 mL). The combined organic extracts were washed with brine (90 mL), dried over Na_2SO_4, filtered and concentrated *in vacuo* using a rotatory evaporator. Purification by flash column chromatography (10–40% EtOAc/pentane) afforded oxetanol **22c** as a white solid (11.72 g, 91%). R_f = 0.20 (20% EtOAc/pentane); ^{1}H NMR (400 MHz, $CDCl_3$) δ 7.43–7.40 (m, 2 H, 2 × Ar-CH), 6.94–6.90 (m, 2 H, 2 × Ar-CH), 4.93 (d, 2 H, *J* = 6.9 Hz, C*H*HOC*H*H), 4.89 (d, 2 H, *J* = 6.9 Hz, CH*H*OCH*H*), 2.50 (s, 1 H, OH), 1.31–1.22 (m, 3 H, 3 × SiCH), 1.11 (d, *J* = 7.3 Hz, 18 H, 6 × SiCHC*H*$_3$); ^{13}C NMR (101 MHz, $CDCl_3$) δ 155.8 (Ar-C_qOTIPS), 134.7 (Ar-C_qC_q), 125.8 (2 × Ar-CH), 119.9 (2 × Ar-CH), 85.5 (CH_2OCH_2), 75.7 (C_q), 17.9 (6 × SiCH*C*H$_3$), 12.6 (3 × SiCH). The observed characterisation data (R_f, ^{1}H, ^{13}C) were consistent with that observed previously in the group.[202]

3-(2-Methoxyphenyl)oxetan-3-ol (22e)



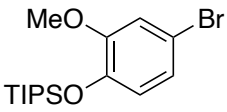
n-BuLi (1.54 M in hexanes, 15.9 mL, 24.0 mmol, 1.2 equiv) was added dropwise over 5 min to a solution of 1-bromo-2-methoxybenzene (3.24 mL, 26.0 mmol, 1.3 equiv) in anhydrous THF (91 mL, 0.22 M) at –78 °C in a 250 mL round bottom flask. After stirring for 30 min, oxetan-3-one (1.28 mL, 20.0 mmol, 1.0 equiv) was added dropwise to the reaction mixture. After further 30 min of stirring at –78 °C, the reaction mixture was warmed to 25 °C and quenched with distilled water (60 mL). The aqueous layer was extracted with Et_2O (3 × 60 mL). The combined organic extracts were washed with brine (60 mL), dried over Na_2SO_4, filtered and concentrated *in vacuo* using a rotatory evaporator. Purification by flash column chromatography (30–50% EtOAc/hexane) afforded oxetanol **22e** as a white solid (3.37 g, 94%). R_f = 0.29 (50% EtOAc/hexane); ^{1}H NMR (400 MHz, $CDCl_3$) δ 7.34 (ddd, ^3J = 8.2, 8.2 Hz, ^4J = 1.7 Hz, 1 H, Ar-CH), 7.29 (dd, ^3J = 7.6 Hz, ^4J = 1.7 Hz, 1 H, Ar-CH), 7.02 (ddd, ^3J = 7.6, 7.6 Hz, ^4J = 1.1 Hz, 1 H, Ar-CH), 6.95 (d, ^3J = 8.2 Hz, 1 H, Ar-CH), 5.05 (d, J = 7.1 Hz, 2 H, C*H*HOC*H*H), 4.88 (dd, ^2J = 7.1 Hz, J = 1.0 Hz, 1 H, CH*H*OCH*H*), 3.88 (s, 3 H, OCH_3), 3.35 (br s, 1 H, OH). The observed characterisation data (R_f, ^{1}H) were consistent with that observed previously in the group.[210]

3-(3,4,5-Trimethoxyphenyl)oxetan-3-ol (22f)



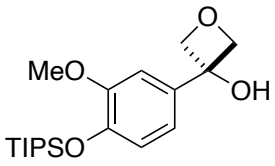
n-BuLi (1.54 M in hexanes, 15.9 mL, 24.0 mmol, 1.2 equiv) was added dropwise over 5 min to a solution of 5-bromo-1,2,3-trimethoxybenzene (6.42 g, 26.0 mmol, 1.3 equiv) in anhydrous THF (91 mL, 0.22 M) at –78 °C in a 250 mL round bottom flask. After stirring for 30 min, oxetan-3-one (1.28 mL, 20.0 mmol, 1.0 equiv) was added dropwise to the reaction mixture. After further 30 min of stirring at –78 °C, the reaction mixture was warmed to 25 °C and quenched with distilled water (60 mL). The aqueous layer was extracted with Et_2O (3 × 60 mL). The combined organic extracts were washed with brine (60 mL), dried over Na_2SO_4, filtered and concentrated *in vacuo* using a rotatory evaporator. Purification by flash column chromatography (30–70% EtOAc/hexane) afforded oxetanol **22f** as a light-yellow solid (4.62 g, 96%). R_f = 0.16 (50% EtOAc/hexane); ^{1}H NMR (400 MHz, $CDCl_3$) δ 6.83 (s, 2 H, 2 × Ar-CH), 4.92 (s, 4 H, CH_2OCH_2), 3.91 (s, 6 H, 2 × OCH_3), 3.87 (s, 3 H, OCH_3), 2.57–2.53 (m, 1 H, OH). The observed characterisation data (R_f, ^{1}H) were consistent with that observed previously in the group.[110]

(4-Bromo-2-methoxyphenoxy)triisopropylsilane (S2)



4-Bromo-2-methoxyphenol (6.09 g, 30.0 mmol, 1.0 equiv) was added dropwise to a solution of 1*H*-imidazole (5.11 g, 75.0 mmol, 2.5 equiv) in anhydrous CH_2Cl_2 (60 mL, 0.5 M) in a 250 mL round bottom flask at 0 °C. After stirring for 5 min, chlorotriisopropylsilane (7.7 mL, 36.0 mmol, 1.2 equiv) was added dropwise at 0 °C. The reaction mixture was warmed to 25 °C, stirred for 21 h and then quenched with distilled water (100 mL). The aqueous layer was extracted with CH_2Cl_2 (3 × 70 mL). The combined organic extracts were dried over Na_2SO_4, filtered and concentrated *in vacuo* using a rotatory evaporator. Purification by filtration through a plug of silica (0–15% pentane) afforded a mixture of **S2** with triisopropyl silanol which was purified by flash column chromatography (0–2% EtOAc/pentane) to afford TIPS-protected aryl bromide **S2** as a colourless oil (10.42 g, 97%). R_f = 0.83 (10% EtOAc/pentane); IR (film)/cm^{-1} 2945, 2866, 1584, 1498, 1465, 1398, 1301, 1267, 1226, 1182, 1126, 1074, 1033, 910, 883, 835, 809, 734, 682; ^{1}H NMR (400 MHz, $CDCl_3$) δ 6.95 (d, J = 2.4 Hz, 1 H, Ar-C_qAr-CHCBr), 6.92 (dd, ^3J = 8.3 Hz, ^4J = 2.4 Hz, 1 H, Ar-CHAr-C*H*CBr), 6.74 (d, J = 8.3 Hz, 1 H, Ar-CH), 3.80 (s, 3 H, OCH_3), 1.23 (hept, J = 7.3 Hz, 3 H, 3 × SiCH), 1.09 (d, J = 7.3 Hz, 18 H, 6 × SiCHC*H*$_3$); ^{13}C NMR (101 MHz, $CDCl_3$) δ 151.7 (Ar-C_qOMe), 144.8 (Ar-C_q(OTIPS)), 123.4 (Ar-CH), 121.5 (Ar-CH), 115.4 (Ar-C_qAr-*C*HCBr), 113.0 (Ar-C_qBr), 55.6 (OCH_3), 17.8 (6 × SiCH*C*H$_3$), 12.8 (3 × SiCH). The observed characterisation data (IR, ^{1}H, ^{13}C) were consistent with that previously reported.[441]

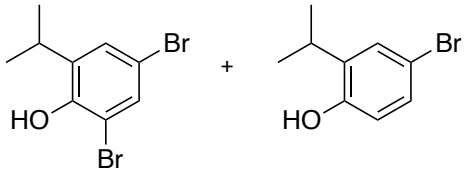
3-(3-Methoxy-4-((triisopropylsilyl)oxy)phenyl)oxetan-3-ol (22g)



n-BuLi (1.51 M in hexanes, 17.7 mL, 26.8 mmol, 1.2 equiv) was added dropwise over 5 min to a solution of aryl bromide **S2** (10.42 g, 29.0 mmol, 1.3 equiv) in anhydrous THF (100 mL, 0.22 M) at –78 °C in a 250 mL round bottom flask. After stirring for 30 min, oxetan-3-one (1.43 mL, 22.3 mmol, 1.0 equiv) was added dropwise to the reaction mixture. After further 30 min of stirring at –78 °C, the reaction mixture was warmed to 25 °C and quenched with distilled water (65 mL). The aqueous layer was extracted with Et_2O (3 × 65 mL). The combined organic extracts were washed with brine (65 mL), dried over Na_2SO_4, filtered and concentrated *in vacuo* using a rotatory evaporator. Purification by flash column chromatography (50–60% Et_2O/pentane) afforded oxetanol **22g** as a colourless oil which crystallised in the freezer (7.26 g, 92%). R_f = 0.28 (60% Et_2O/pentane); mp = 60 °C; IR (film)/cm^{-1} 3392 (OH st, br), 2945, 2866, 1603, 1517, 1465, 1413, 1308, 1274, 1219, 1167, 1129, 1036, 969, 928, 883, 850, 712, 682; ^{1}H NMR (400 MHz, $CDCl_3$) δ 7.04 (d, J = 2.2 Hz, 1 H, Ar-C_qAr-CHAr-C_q), 7.00 (dd, ^3J = 8.3 Hz, ^4J = 2.2 Hz, 1 H, Ar-CH), 6.90 (d, ^3J = 8.3 Hz, 1 H, Ar-C_q(OTIPS)Ar-CH), 4.92

(d, *J* = 6.8 Hz, 2 H, C*H*HOC*H*H), 4.88 (d, *J* = 6.8 Hz, 2 H, CH*H*OCH*H*), 3.84 (s, 3 H, OCH_3), 2.68 (br s, 1 H, OH), 1.32–1.30 (m, 3 H, 3 × SiCH), 1.10 (d, *J* = 7.4 Hz, 18 H, 6 × SiCHC*H*$_3$); ^{13}C NMR (101 MHz, $CDCl_3$) δ 151.0 (Ar-C_qOMe), 145.3 (Ar-C_q(OTIPS)), 135.4 (Ar-*C*$_q$C$_q$), 120.3 (Ar-CH), 116.8 (Ar-CH), 108.7 (Ar-C_qAr-*C*HAr-C_q), 85.6 (CH_2OCH_2), 75.9 (C_q), 55.6 (OCH_3), 17.9 (6 × SiCH*C*H$_3$), 12.9 (3 × SiCH); HRMS (ESI) *m/z* calcd for $C_{19}H_{31}O_3Si$ [M–OH]: 335.2042, found: 335.2034.

2,4-Dibromo-6-isopropylphenol (S3') and 4-bromo-2-isopropylphenol (S3)[442]



S3' **S3**

N-Bromosuccinimide (6.85 g, 38.5 mmol, 1.1 equiv) was added slowly and in portions to a solution of 2-isopropylphenol (4.7 mL, 34.9 mmol, 1.0 equiv) in anhydrous MeCN (50 mL, 0.7 M) in a 100 mL round bottom flask at 0 °C. After stirring for 5 h at 25 °C, the reaction mixture was concentrated *in vacuo* using a rotatory evaporator. Hexane was added to the residue and the formed suspension was filtered to remove any insoluble impurities. The filtrate was washed with distilled water (100 mL) and brine (100 mL). The organic layer was dried over Na_2SO_4, filtered and concentrated *in vacuo* using a rotatory evaporator. Purification by automated column chromatography afforded dibromophenol **S3'** as a light-yellow liquid (235 mg, 2%) followed by bromophenol **S3** as an orange liquid (6.05 g, 81%).

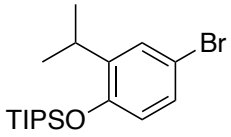
Column Conditions: Column Type: Biotage® Sfär HC 100 g. Flow rate: 120 mL/min. 1 column volume (CV) 2% EtOAc/pentane, 12 CV 2–30% EtOAc/pentane, 3 CV 30–100% EtOAc/pentane, 3 CV 0–100% MeOH/EtOAc, 2 CV 100% MeOH. Fractions 1–43: mixture of **S3'** + 2-bromo-6-isopropylphenol, fractions 44–79: **S3'**, fractions 94–143: **S3**.

Dibromophenol **S3'**: R_f = 0.55 (10% EtOAc/pentane); IR (film)/cm^{-1} 3507 (OH st, br), 3079, 2963, 2870, 1565, 1439, 1402, 1320, 1264, 1226, 1159, 958, 906, 854, 783, 738, 686; ^{1}H NMR (400 MHz, $CDCl_3$) δ 7.44 (d, *J* = 2.3 Hz, 1 H, CBrAr-CHCBr), 7.25 (*J* = 2.3 Hz, 1 H, Ar-C_qAr-CHCBr), 5.57 (s, 1 H, OH), 3.29 (hept, *J* = 6.9 Hz, 1 H, CH), 1.23 (d, *J* = 6.9 Hz, 6 H, 2 × CH_3); ^{13}C NMR (101 MHz, $CDCl_3$) δ 148.7 (Ar-C_qOH), 138.0 (Ar-*C*$_q$CH), 131.0 (C_qAr-*C*HCBr), 129.1 (CBrAr-*C*HCBr), 112.6 (CHAr-*C*$_q$BrCH), 110.9 (Ar-*C*$_q$BrCOH), 28.1 (CH), 22.2 (2 × CH_3). The observed characterisation data (^{1}H, ^{13}C) were consistent with that previously reported.[443]

Bromophenol **S3**: R_f = 0.18 (10% EtOAc/pentane); IR (film)/cm^{-1} 3548 (OH st, br), 2967, 2870, 1603, 1491, 1413, 1320, 1267, 1200, 1170, 1096, 880, 809, 746; ^{1}H NMR (400 MHz, $CDCl_3$) δ 7.29 (d, *J* = 2.4 Hz, 1 H, Ar-C_qAr-CHCBr), 7.17 (dd, ^{3}*J* = 8.5 Hz, ^{4}*J* = 2.4 Hz, 1 H, Ar-CHAr-

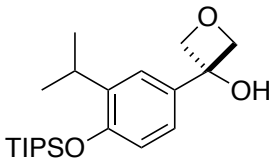
C*H*CBr), 6.64 (d, ^{3}J = 8.5 Hz, 1 H, Ar-C_qOHAr-C*H*), 4.75 (s, 1 H, OH), 3.18 (hept, *J* = 6.9 Hz, 1 H, CH), 1.26 (d, *J* = 6.9 Hz, 6 H, 2 × CH_3); ^{13}C NMR (101 MHz, $CDCl_3$) δ 151.8 (Ar-C_qOH), 136.8 (Ar-*C*$_q$CH), 129.4 (Ar-CH), 129.3 (Ar-CH), 116.9 (Ar-CHAr-*C*HCBr), 113.2 (Ar-C_qBr), 27.1 (CH), 22.4 (2 × CH_3). The observed characterisation data (^{1}H, ^{13}C) were consistent with that previously reported.[444]

(4-Bromo-2-isopropylphenoxy)triisopropylsilane (S4)



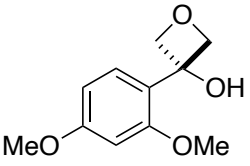
4-Bromo-2-isopropylphenol **S3** (6.04 g, 28.1 mmol, 1.0 equiv) was added dropwise to a solution of 1*H*-imidazole (4.78 g, 70.2 mmol, 2.5 equiv) in anhydrous CH_2Cl_2 (56 mL, 0.5 M) in a 250 mL round bottom flask at 0 °C. After stirring for 5 min, chlorotriisopropylsilane (7.21 mL, 33.7 mmol, 1.2 equiv) was added dropwise at 0 °C. The reaction mixture was warmed to 25 °C, stirred for 30 h and then additional chlorotriisopropylsilane (1.2 mL, 5.61 mmol, 0.2 equiv) and 1*H*-imidazole (764.7 mg, 11.2 mmol, 0.4 equiv) were added. The reaction was monitored by ^{1}H NMR of aliquots, since starting material and product showed the same R_f values and stain colour by TLC. After stirring for additional 20 h (50 h in total) at 25 °C, the reaction mixture was quenched with distilled water (90 mL). The aqueous layer was extracted with CH_2Cl_2 (3 × 50 mL). The combined organic extracts were dried over Na_2SO_4, filtered and concentrated *in vacuo* using a rotatory evaporator. Purification by filtration through a plug of silica (100% pentane) afforded aryl bromide **S4** as a white solid (9.50 g, 91%). R_f = 0.70 (100% pentane); mp = 55–59 °C; IR (film)/cm^{-1} 2945, 2870, 1484, 1402, 1338, 1275, 1189, 1100, 921, 883, 794, 686; ^{1}H NMR (400 MHz, $CDCl_3$) δ 7.28 (d, *J* = 2.6 Hz, 1 H, Ar-C_qAr-CHCBr), 7.12 (dd, ^{3}J = 8.6 Hz, ^{4}J = 2.6 Hz, 1 H, Ar-CHAr-C*H*CBr), 6.65 (d, ^{3}J = 8.6 Hz, 1 H, Ar-C_q(OTIPS)Ar-CH), 3.33 (hept, *J* = 6.9 Hz, 1 H, Ar-C_qCH), 1.35–1.26 (m, 3 H, 3 × SiCH), 1.20 (d, *J* = 6.9 Hz, 6 H, 2 × Ar-C_qCHC*H*$_3$), 1.11 (d, *J* = 7.4 Hz, 18 H, 6 × SiCHC*H*$_3$); ^{13}C NMR (101 MHz, $CDCl_3$) δ 152.3 (Ar-C_qOTIPS), 141.0 (Ar-*C*$_q$CH), 129.3 (Ar-CH), 128.9 (Ar-CH), 119.4 (Ar-CHAr-*C*HCBr), 113.1 (Ar-C_qBr), 26.9 (Ar-C_q*C*H), 22.6 (2 × Ar-C_qCH*C*H$_3$), 18.0 (6 × SiCH*C*H$_3$), 13.0 (3 × SiCH). The observed characterisation data (^{1}H, ^{13}C) were consistent with that previously reported.[445]

3-(3-Isopropyl-4-((triisopropylsilyl)oxy)phenyl)oxetan-3-ol (22h)



n-BuLi (1.41 M in hexanes, 16.7 mL, 23.5 mmol, 1.2 equiv) was added dropwise over 5 min to a solution of aryl bromide **S4** (9.48 g, 25.5 mmol, 1.3 equiv) in anhydrous THF (89 mL, 0.22 M) at –78 °C in a 250 mL round bottom flask. After stirring for 30 min, oxetan-3-one (1.26 mL, 19.7 mmol, 1.0 equiv) was added dropwise to the reaction mixture. After further 30 min of stirring at –78 °C, the reaction mixture was warmed to 25 °C and quenched with distilled water (60 mL). The aqueous layer was extracted with Et_2O (3 × 60 mL). The combined organic extracts were washed with brine (60 mL), dried over Na_2SO_4, filtered and concentrated *in vacuo* using a rotatory evaporator. Purification by flash column chromatography (10–20% EtOAc/pentane) afforded a mixture of oxetanol **22h** with ethyl acetate. Et_2O (10 mL) was added and the solvent was removed *in vacuo* using a rotatory evaporator to afford oxetanol **22h** as a colourless oil which crystallised after several weeks in the freezer (6.51 g, 91%). R_f = 0.19 (15% EtOAc/pentane); mp = 51 °C; IR (film)/cm^{-1} 3392 (OH st, br), 2948, 2870, 1610, 1498, 1465, 1387, 1267, 1193, 1081, 973, 936, 834, 820; ^{1}H NMR (400 MHz, $CDCl_3$) δ 7.36 (d, *J* = 2.5 Hz, 1 H, Ar-C_qAr-CHAr-C_q), 7.21 (dd, ^3J = 8.4 Hz, ^4J = 2.5 Hz, 1 H, Ar-CH), 6.81 (d, *J* = 8.4 Hz, 1 H, (TIPSO)C_qAr-CH), 4.96 (d, *J* = 7.2 Hz, 2 H, C*H*HOC*H*H), 4.90 (d, *J* = 7.2 Hz, 2 H, CH*H*OCH*H*), 3.40 (hept, *J* = 6.9 Hz, 1 H, Ar-C_qCH), 2.35 (br s, 1 H, OH), 1.40–1.32 (m, 3 H, 3 × SiCH), 1.23 (d, *J* = 6.9 Hz, 6 H, 2 × Ar-C_qCHC*H*$_3$), 1.13 (d, *J* = 7.4 Hz, 18 H, 6 × SiCHC*H*$_3$); ^{13}C NMR (101 MHz, $CDCl_3$) δ 152.9 (Ar-C_qOTIPS), 138.8 (Ar-*C*$_q$C$_q$), 134.3 (Ar-*C*$_q$CH), 122.6 (Ar-CH), 122.5 (Ar-CH), 117.7 (Ar-C_q(OTIPS)Ar-*C*H), 85.5 (CH_2OCH_2), 76.0 (Ar-C_q*C*$_q$), 26.9 (Ar-C_q*C*H), 22.8 (2 × Ar-C_qCH*C*H$_3$), 18.1 (6 × SiCH*C*H$_3$), 13.1 (3 × SiCH); HRMS (ESI) *m/z* calcd for $C_{21}H_{35}O_2Si$ [M–OH]: 347.2406, found: 347.2397.

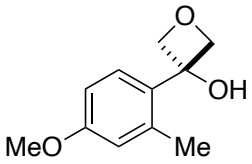
3-(2,4-Dimethoxyphenyl)oxetan-3-ol (22i)



n-BuLi (1.48 M in hexanes, 8.1 mL, 12 mmol, 1.2 equiv) was added dropwise over 5 min to a solution of 1-bromo-2,4-dimethoxybenzene (1.87 mL, 13 mmol, 1.3 equiv) in anhydrous THF (45 mL, 0.22 M) at –78 °C in a 250 mL round bottom flask. After stirring for 20 min, oxetan-3-one (0.64 mL, 10 mmol, 1.0 equiv) was added dropwise to the reaction mixture. After further 25 min of stirring at –78 °C, the reaction mixture was warmed to 25 °C and quenched with distilled water (30 mL). The aqueous layer was extracted with Et_2O (3 × 30 mL). The combined organic extracts were washed with brine (30 mL), dried over Na_2SO_4, filtered and concentrated *in vacuo* using a rotatory evaporator. Purification by flash column chromatography (30–70% EtOAc/pentane) afforded oxetanol **22i** as a white solid (1.86 g, 89%). R_f = 0.19 (50% EtOAc/pentane); mp = 65 °C; IR (film)/cm^{-1} 3338 (OH st, br), 2974, 1618, 1581, 1511, 1461,

1416, 1261, 1205, 1142, 1047, 1020, 950, 800; ^{1}H NMR (400 MHz, $CDCl_3$) δ 7.17 (d, *J* = 9.0 Hz, 1 H, Ar-CH), 6.52–6.49 (m, 2 H, 2 × Ar-CH), 5.02 (d, *J* = 7.0 Hz, 2 H, C*H*HOC*H*H), 4.86 (dd, *J* = 7.0, 0.9 Hz, 2 H, CH*H*OCH*H*), 3.84 (s, 3 H, OCH_3), 3.83 (s, 3 H, OCH_3), 3.23 (s, 1 H, OH); ^{13}C NMR (101 MHz, $CDCl_3$) δ 160.9 (Ar-C_qOMe), 157.9 (Ar-C_qOMe), 126.8 (Ar-C_qOMeAr-CHAr-*C*H), 122.5 (Ar-*C*$_q$C$_q$), 103.9 (Ar-CH), 99.2 (Ar-CH), 83.1 (CH_2OCH_2), 75.3 (C_q), 55.5 (OCH_3), 55.4 (OCH_3); HRMS (ESI) *m/z* calcd for $C_{11}H_{13}O_2^+$ [M–OH]$^+$: 193.0859, found: 193.0857.

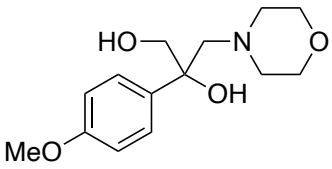
3-(4-Methoxy-2-methylphenyl)oxetan-3-ol (22j)



n-BuLi (1.53 M in hexanes, 3.0 mL, 4.59 mmol, 1.1 equiv) was added dropwise over 5 min to a solution of 1-bromo-4-methoxy-2-methylbenzene (1.0 g, 4.97 mmol, 1.2 equiv) in anhydrous THF (20 mL, 0.21 M) at –78 °C in a 100 mL round bottom flask. After stirring for 20 min, oxetan-3-one (0.27 mL, 4.14 mmol, 1.0 equiv) was added dropwise to the reaction mixture. After further 25 min of stirring at –78 °C, the reaction mixture was warmed to 25 °C, stirred for 1 h and quenched with distilled water (15 mL). The aqueous layer was extracted with Et_2O (3 × 20 mL). The combined organic extracts were washed with brine (25 mL), dried over Na_2SO_4, filtered and concentrated *in vacuo* using a rotatory evaporator. Purification by flash column chromatography (50% EtOAc/pentane) afforded oxetanol **22j** as a white solid (627 mg, 78%). R_f = 0.37 (50% EtOAc/pentane); mp = 73–76 °C; IR (film)/cm^{-1} 3369 (OH st, br), 2946, 1609, 1503, 1247, 1129, 977, 867; ^{1}H NMR (400 MHz, $CDCl_3$) δ 7.07 (d, *J* = 8.4 Hz, 1 H, Ar-CH), 6.76–6.70 (m, 2 H, 2 × Ar-CH), 5.18 (d, *J* = 6.9 Hz, 2 H, C*H*HOC*H*H), 4.86 (d, *J* = 6.9 Hz, 2 H, CH*H*OCH*H*), 3.80 (s, 3 H, OCH_3), 2.54 (s, 1 H, OH), 2.23 (s, 3 H, CH_3); ^{13}C NMR (101 MHz, $CDCl_3$) δ 159.5 (Ar-C_qOMe), 138.1 (Ar-C_q), 131.8 (Ar-C_q), 126.9 (Ar-CH), 117.3 (Ar-CH), 110.6 (Ar-CH), 83.6 (CH_2OCH_2), 77.4 (C_q), 55.2 (OCH_3), 19.4 (CH_3); HRMS (ESI) *m/z* calcd for $C_{11}H_{13}O_2$ [M–OH]: 177.0916, found: 177.0912.

7.6.2 Ring-opening of Oxetanol 22a by Morpholine

2-(4-Methoxyphenyl)-3-morpholinopropane-1,2-diol (43)



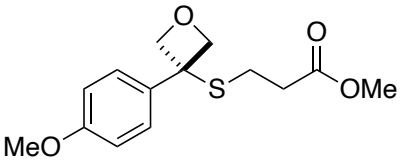
A flame-dried reaction tube was charged sequentially with oxetanol **22a** (18.0 mg, 0.10 mmol, 1.0 equiv), $Ca(NTf_2)_2$ (66.0 mg, 0.11 mmol, 1.1 equiv) and morpholine (17.5 μL, 0.20 mmol, 2.0 equiv). The tube was sealed, anhydrous THF (0.5 mL, 0.2 M) was added by syringe and the reaction mixture was stirred at 60 ºC for 24 h. After allowing the tube cool to room temperature (ca. 22 ºC), sat. aq. $NaHCO_3$ (10 mL) was added and the aqueous layer was extracted with CH_2Cl_2 (3 × 10 mL). The combined organic extracts were dried over Na_2SO_4, filtered and concentrated *in vacuo* using a rotatory evaporator. Purification by flash column chromatography (50–100% EtOAc/pentane, then 8% MeOH/EtOAc) afforded diol **43** as a white solid (21.2 mg, 79%). R_f = 0.09 (70% EtOAc/pentane); mp = 102 °C; IR (film)/cm^{-1} 3416 (OH st, br), 2954, 2850, 1610, 1511, 1247, 1115, 1034; ^{1}H NMR (400 MHz, $CDCl_3$) δ 7.35 (d, *J* = 8.3 Hz, 2 H, 2 × Ar-CH), 6.88 (d, *J* = 8.3 Hz, 2 H, 2 × Ar-CH), 4.00–3.20 (br s, 2 H, 2 × OH), 3.81 (s, 3 H, OCH_3), 3.64–3.61 (m, 5 H, CH_2OCH_2 + C*H*HOH), 3.52 (d, *J* = 11.5 Hz, 1 H, CH*H*OH), 3.01 (d, *J* = 13.1 Hz, 1 H, C_qCHHN), 2.79 (d, *J* = 13.1 Hz, 1 H, C_qCHHN), 2.51–2.45 (m, 2 H, C*H*HNC*H*H), 2.40–2.37 (m, 2 H, CH*H*NCH*H*); ^{13}C NMR (101 MHz, $CDCl_3$) δ 158.6 (Ar-C_qOMe), 136.3 (Ar-C_qC_q), 126.0 (2 × Ar-CH), 113.7 (2 × Ar-CH), 73.6 (C_q), 69.1 (CH_2OH), 67.0 (CH_2OCH_2), 64.6 (CH_2C_q), 55.2 (OCH_3), 54.9 (CH_2NCH_2); HRMS (ESI) *m/z* calcd for $C_{14}H_{22}NO_{24}^+$ $[M+H]^+$: 268.1543, found: 268.1543.

Notes:

***43** was further characterised by X-ray crystallography (see Table 3).*

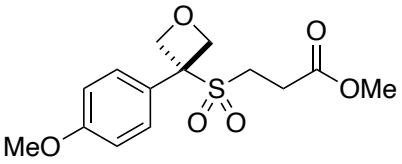
7.6.3 Oxetane Sulfonyl Fluorides and Precursors

Methyl 3-((3-(4-methoxyphenyl)oxetan-3-yl)thio)propanoate (21a)



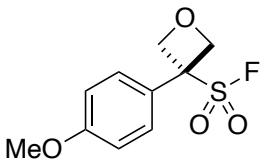
Lithium bis(trifluoromethanesulfonimide) (380 mg, 1.32 mmol, 0.11 equiv) and tetrabutylammonium hexafluorophosphate (255.9 mg, 0.66 mmol, 0.055 equiv) were added sequentially to a solution of oxetanol **22a** (2.16 g, 12.0 mmol, 1.0 equiv) and methyl 3-mercaptopropionate (2.6 mL, 24.0 mmol, 2.0 equiv) in non-anhydrous chloroform (25 mL, 0.5 M) in a 100 mL round bottom flask. The reaction flask was placed into a preheated oil bath at 40 °C. The reaction was stirred for 15 min and then heated up to 70 °C in 1 h. At 70 °C there was a change in colour from colourless to yellow. From the moment of the colour change, the reaction was stirred for further 25 min and quenched with sat. aq. $NaHCO_3$ (25 mL). The aqueous layer was extracted with CH_2Cl_2 (3 × 25 mL). The combined organic extracts were washed with aq. NaOH (1 M, 35 mL), dried over Na_2SO_4, filtered and concentrated *in vacuo* using a rotatory evaporator. Purification by flash column chromatography (50% Et_2O/pentane) afforded oxetane sulfide **21a** as a white solid (2.61 g, 77%). R_f = 0.26 (50% Et_2O/pentane); ^1H NMR (400 MHz, $CDCl_3$) δ 7.16–7.12 (m, 2 H, 2 × Ar-CH), 6.92–6.89 (m, 2 H, 2 × Ar-CH), 5.19 (d, *J* = 6.5 Hz, 2 H, C*H*HOC*H*H), 4.90 (d, *J* = 6.5 Hz, 2 H, CH*H*OCH*H*), 3.83 (s, 3 H, Ar-$C_q$$OCH_3$), 3.68 (s, 3 H, CO_2CH_3), 2.67 (t, *J* = 7.4 Hz, 2 H, SCH_2), 2.42 (t, *J* = 7.4 Hz, 2 H, CH_2CO_2Me). The observed characterisation data (R_f, ^1H) were consistent with that observed previously in the group.[210]

Methyl 3-((3-(4-methoxyphenyl)oxetan-3-yl)sulfonyl)propanoate (20a)[210]



*m*CPBA (4.20 g, 24.3 mmol, 3.0 equiv) was added to a solution of oxetane sulfide **21a** (2.29 g, 8.11 mmol, 1.0 equiv) in anhydrous CH_2Cl_2 (400 mL, 0.02 M) in a 1000 mL round bottom flask. The reaction mixture was stirred at 25 °C for 3 h then aq. KOH (3 M, 50 mL) was added and the phases were separated. The aqueous portion was extracted with CH_2Cl_2 (4 × 50 mL). The combined organic extracts were dried over Na_2SO_4, filtered and concentrated *in vacuo* using a rotatory evaporator to afford sulfone **20a** as a white solid (2.60 g, quant.); R_f = 0.59 (75% EtOAc/hexane); ^1H NMR (400 MHz, $CDCl_3$) δ 7.24–7.21 (m, 2 H, 2 × Ar-CH), 6.99–6.95 (m, 2 H, 2 × Ar-CH), 5.40 (d, *J* = 7.2 Hz, 2 H, C*H*HOC*H*H), 5.12 (d, *J* = 7.2 Hz, 2 H, CH*H*OCH*H*), 3.84 (s, 3 H, Ar-$C_q$$OCH_3$), 3.70 (s, 3 H, CO_2CH_3), 3.08 (dd, *J* = 8.2, 7.1 Hz, 2 H, SO_2CH_2), 2.71 (t, *J* = 8.2, 7.1 Hz, 2 H, CH_2CO_2Me). The observed characterisation data (R_f, ^1H) were consistent with that observed previously in the group.[210]

3-(4-Methoxyphenyl)oxetane-3-sulfonyl fluoride (18a)

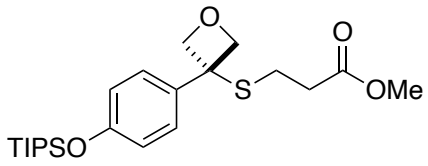


Sodium methoxide (5.4 M solution in MeOH, 1.5 mL, 8.11 mmol, 1.0 equiv) was added dropwise to a solution of oxetane sulfone **20a** (2.55 g, 8.11 mmol, 1.0 equiv) in anhydrous THF (16.2 mL, 0.5 M) in a 100 mL round bottom flask. Oxetane sulfinate salt **19a** precipitated after 2 min of the start of addition of base to form a light-yellow paste (Figure 27). The reaction mixture was stirred at 25 °C for 20 min, then concentrated *in vacuo* using a rotatory evaporator to afford oxetane sulfinate **19a** as a light-yellow solid, which was subjected directly to the next step without spectroscopical analysis. For the fluorination step, Selectfluor (4.31 g, 12.17 mmol, 1.5 equiv) was added to anhydrous MeOH (40 mL, 0.2 M) at 0 ºC in a 100 mL round bottom flask, then stirred for 5 min. Sulfinate salt **19a** was added portionwise. The reaction mixture was stirred at 0 ºC for 1 h then concentrated *in vacuo* using a rotatory evaporator. The residue was diluted with CH_2Cl_2 (30 mL) and filtered through a plug of Celite, eluting with further CH_2Cl_2. After concentration *in vacuo* using a rotatory evaporator, purification by flash column chromatography through a very short column (80% CH_2Cl_2/pentane) afforded oxetane sulfonyl fluoride **18a** as a white solid (1.06 g, 53% over 2 steps). R_f = 0.47 (80% CH_2Cl_2/pentane); R_f = 0.60 (100% CH_2Cl_2); ^{1}H NMR (400 MHz, $CDCl_3$) δ 7.23–7.19 (m, 2 H, 2 × Ar-CH), 7.01–6.97 (m, 2 H, 2 × Ar-CH), 5.44 (d, J = 7.9 Hz, 2 H, C*H*HOC*H*H), 5.24 (dd, ^2J = 7.9 Hz, J_{HF} = 1.5 Hz, 2 H, CH*H*OCH*H*), 3.86 (s, 3 H, OCH_3); ^{19}F NMR (377 MHz, $CDCl_3$) δ 34.4. The observed characterisation data (R_f, ^{1}H, ^{19}F) were consistent with that observed previously in the group.[210]

Notes:

***18a** was further characterised by X-ray crystallography (see Figure 27).*

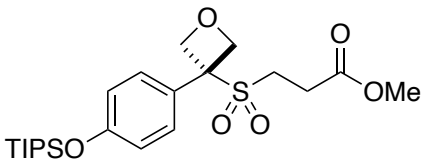
Methyl 3-((3-(4-((triisopropylsilyl)oxy)phenyl)oxetan-3-yl)thio)propanoate (21c)



Lithium bis(trifluoromethanesulfonimide) (429 mg, 1.50 mmol, 0.11 equiv) and tetrabutylammonium hexafluorophosphate (290.7 mg, 0.75 mmol, 0.055 equiv) were added sequentially to a solution of oxetanol **22c** (4.386 g, 13.6 mmol, 1.0 equiv) and methyl 3-mercaptopropionate (3.0 mL, 27.2 mmol, 2.0 equiv) in non-anhydrous chloroform (27 mL, 0.5 M) in a 100 mL round bottom flask. The reaction flask was placed into a preheated oil bath at 40 °C. The reaction was heated up to 60 °C in 1 h. At 60 °C there was a change in colour from clear and colourless to yellow and cloudy. From the moment of the colour change, the reaction was stirred for further 25 min and quenched with sat. aq. $NaHCO_3$ (25 mL). The aqueous layer was extracted with CH_2Cl_2

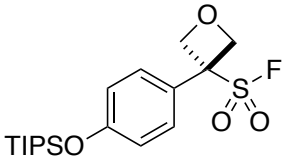
(3 × 25 mL). The combined organic extracts were washed with aq. NaOH (1 M, 35 mL), dried over Na_2SO_4, filtered and concentrated *in vacuo* using a rotatory evaporator. Purification by flash column chromatography (20% Et_2O/pentane) afforded oxetane sulfide **21c** as a colourless oil (4.13 g, 72%). R_f = 0.25 (20% Et_2O/pentane); ^{1}H NMR (400 MHz, $CDCl_3$) δ 7.08–7.04 (m, 2 H, 2 × Ar-CH), 6.89–6.86 (m, 2 H, 2 × Ar-CH), 5.20 (d, *J* = 6.4 Hz, 2 H, C*H*HOC*H*H), 4.89 (d, *J* = 6.4 Hz, 2 H, CH*H*OCH*H*), 3.67 (s, 3 H, CO_2CH_3), 2.65 (t, *J* = 7.4 Hz, 2 H, SCH_2), 2.42 (t, *J* = 7.4 Hz, 2 H, CH_2CO$_2$Me) 1.30–1.21 (m, 3 H, 3 × SiCH), 1.11 (d, *J* = 7.4 Hz, 18 H, 6 × SiCHCH_3). The observed characterisation data (R_f, ^{1}H) were consistent with that observed previously in the group.[210]

Methyl 3-((3-(4-((triisopropylsilyl)oxy)phenyl)oxetan-3-yl)sulfonyl)propanoate (20c)[210]



*m*CPBA (2.60 g, 15.0 mmol, 3.0 equiv) was added to a solution of oxetane sulfide **21c** (2.12 g, 5.0 mmol, 1.0 equiv) in anhydrous CH_2Cl_2 (250 mL, 0.02 M) in a 500 mL round bottom flask. The reaction mixture was stirred at 25 °C for 3 h then aq. KOH (3 M, 200 mL) was added and the phases were separated. The aqueous portion was extracted with CH_2Cl_2 (3 × 100 mL). The combined organic extracts were dried over Na_2SO_4, filtered and concentrated *in vacuo* using a rotatory evaporator to afford oxetane sulfone **20c** as a white solid (2.28 g, quant.). R_f = 0.36 (30% EtOAc/pentane); ^{1}H NMR (400 MHz, $CDCl_3$) δ 7.18–7.14 (m, 2 H, 2 × Ar-CH), 6.96–6.93 (m, 2 H, 2 × Ar-CH), 5.40 (d, *J* = 7.2 Hz, 2 H, C*H*HOC*H*H), 5.12 (d, *J* = 7.2 Hz, 2 H, CH*H*OCH*H*), 3.70 (s, 3 H, CO_2CH_3), 3.06 (dd, *J* = 8.3 Hz, *J* = 7.0 Hz, 2 H, SCH_2), 2.67 (dd, *J* = 8.3 Hz, *J* = 7.0 Hz, 2 H, CH_2CO$_2$Me), 1.32–1.23 (m, 3 H, 3 × SiCH), 1.11 (d, *J* = 7.3 Hz, 18 H, 6 × SiCHCH_3). The observed characterisation data (R_f, ^{1}H) were consistent with that observed previously in the group.[210]

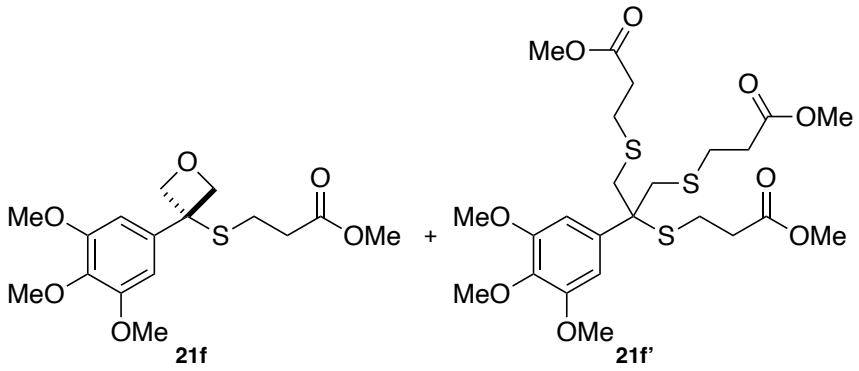
3-(4-((Triisopropylsilyl)oxy)phenyl)oxetane-3-sulfonyl fluoride (18c)



Sodium methoxide (5.4 M solution in MeOH, 0.36 mL, 1.90 mmol, 1.0 equiv) was added dropwise to a solution of oxetane sulfone **20c** (884 mg, 1.90 mmol, 1.0 equiv) in anhydrous THF (3.9 mL, 0.5 M) in a 10 mL round bottom flask. Oxetane sulfinate salt **19c** did not precipitate after addition of base and there was no change in colour. The reaction mixture was stirred at 25 °C for 20 min, then concentrated *in vacuo* using a rotatory evaporator to afford oxetane sulfinate **19c** as a light-yellow solid, which was subjected directly to the next step without spectroscopical analysis. For the fluorination step, Selectfluor (1.031 g, 2.91 mmol, 1.5 equiv) was added to anhydrous MeOH (9.8 mL, 0.2 M) at 0 °C in a 25 mL round bottom

flask, then stirred for 5 min. Sulfinate salt **19c** was added portionwise. The reaction mixture was stirred for at 0 °C for 1 h, then concentrated *in vacuo* using a rotatory evaporator. The residue was diluted with CH_2Cl_2 (15 mL) and filtered through a plug of Celite, eluting with further CH_2Cl_2. After concentration *in vacuo* using a rotatory evaporator, purification by flash column chromatography through a very short column (80% CH_2Cl_2/pentane) afforded oxetane sulfonyl fluoride **18c** as a white solid (478 mg, 63% over two steps). R_f = 0.71 (100% CH_2Cl_2); R_f = 0.60 (100% CH_2Cl_2); ^{1}H NMR (400 MHz, $CDCl_3$) δ 7.15–7.11 (m, 2 H, 2 × Ar-CH), 6.97–6.93 (m, 2 H, 2 × Ar-CH), 5.42 (d, J = 7.7 Hz, 2 H, C*H*HOC*H*H), 5.23 (dd, ^2J = 7.7 Hz, J_{HF} = 1.5 Hz, 2 H, CH*H*OCH*H*), 1.32–1.23 (m, 3 H, 3 × SiCH), 1.11 (d, J = 7.4 Hz, 18 H, 6 × SiCHC*H*$_3$); ^{19}F NMR (377 MHz, $CDCl_3$) δ 34.3. The observed characterisation data (R_f, ^{1}H, ^{19}F) were consistent with that observed previously in the group.[210]

Methyl 3-((3-(3,4,5-trimethoxyphenyl)oxetan-3-yl)thio)propanoate (21f) and trimethyl 3,3',3''-((2-(3,4,5-trimethoxyphenyl)propane-1,2,3-triyl)tris(sulfanediyl))tripropionate (21f')



Lithium bis(trifluoromethanesulfonimide) (607 mg, 2.11 mmol, 0.11 equiv) and tetrabutylammonium hexafluorophosphate (407 mg, 1.05 mmol, 0.055 equiv) were added sequentially to a solution of oxetanol **22f** (4.609 g, 19.2 mmol, 1.0 equiv) and methyl 3-mercaptopro-pionate (4.15 mL, 38.4 mmol, 2.0 equiv) in non-anhydrous chloroform (38 mL, 0.5 M) in a 100 mL round bottom flask. The reaction flask was placed into a preheated oil bath at 40 °C. The reaction was stirred for 15 min and then heated up to 57 °C in 10 min. At 57 °C there was a change in colour from light-yellow to dark purple (Figure 81). From the moment of the colour change, the reaction was stirred for further 25 min and quenched with sat. aq. $NaHCO_3$ (25 mL). The aqueous layer was extracted with CH_2Cl_2 (3 × 25 mL). The combined organic extracts were washed with aq. NaOH (1 M, 35 mL), dried over Na_2SO_4, filtered and concentrated *in vacuo* using a rotatory evaporator. Purification by flash column chromatography (60–100% Et_2O/pentane) afforded oxetane sulfide **21f** as a light-yellow oil (1.34 g, 20%) followed by trisulfide **21f'** as a light-yellow oil (1.99 g, 18%).

Oxetane sulfide **21f**: R_f = 0.19 (60% Et_2O/pentane); ^1H NMR (400 MHz, $CDCl_3$) δ 6.42 (s, 2 H, 2 × Ar-CH), 5.20 (d, *J* = 6.5 Hz, 2 H, C*H*HOC*H*H), 4.89 (d, *J* = 6.5 Hz, 2 H, CH*H*OCH*H*), 3.87 (s, 6 H, 2 × Ar-OCH_3), 3.86 (s, 3 H, Ar-OCH_3), 3.68 (s, 3 H, CO_2CH_3), 2.72 (t, *J* = 7.4 Hz, 2 H, SCH_2), 2.44 (t, *J* = 7.4 Hz, 2 H, CH_2CO_2Me). The observed characterisation data (R_f, ^1H) were consistent with that observed previously in the group.[210]

Trisulfide **21f'**: R_f = 0.12 (60% Et_2O/pentane); IR (film)/cm^{-1} 2948, 2866, 2255, 1737 (C=O st), 1603, 1513, 1465, 1413, 1357, 1275, 1245, 1178, 1141, 1036, 910, 816, 731, 686; ^1H NMR (400 MHz, $CDCl_3$) δ 6.78 (s, 2 H, 2 × Ar-CH), 3.89 (s, 6 H, 2 × Ar-OCH_3), 3.85 (s, 3 H, Ar-OCH_3), 3.68 (s, 6 H, 2 × CO_2CH_3), 3.64 (s, 3 H, CO_2CH_3), 3.38 (d, *J* = 12.7 Hz, 2 H, 2 × C_qC*H*HS), 3.33 (d, *J* = 12.7 Hz, 2 H, 2 × C_qCH*H*S), 2.73–2.69 (m, 4 H, 2 × SCH_2), 2.59–2.55 (m, 4 H, 2 × CH_2CO_2Me), 2.52–2.48 (m, 2 H, SCH_2), 2.41–2.37 (m, 2 H, CH_2CO_2Me); ^{13}C NMR (101 MHz, $CDCl_3$) δ 172.2 (2 × C_q=O), 172.0 (C_q=O), 152.8 (2 × Ar-C_qOMe), 137.4 (Ar-C_qOMe), 137.1 (Ar-C_qC_q), 105.2 (2 × Ar-CH), 60.9 (Ar-OCH_3), 56.8 (Ar-C_qC_q), 56.3 (2 × Ar-OCH_3), 51.8 (3 × CO_2CH_3), 41.0 (2 × C_qCH_2S), 34.8 (2 × CH_2CO_2Me), 33.5 (CH_2CO_2Me), 28.5 (2 × SCH_2CH_2), 24.4 (SCH_2CH_2); HRMS (ESI) *m/z* calcd for $C_{24}H_{36}O_9S_3Na$ [M+Na]: 587.1419; found: 587.1417.

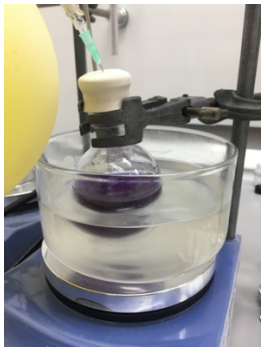
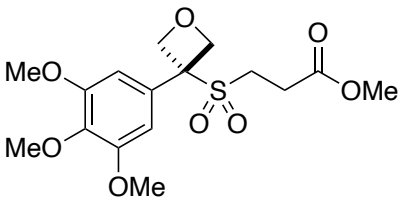


Fig. 80. Colour change of reaction mixture to dark purple after heating up to 57 °C.

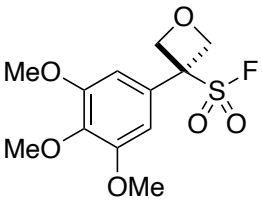
Methyl 3-((3-(3,4,5-trimethoxyphenyl)oxetan-3-yl)sulfonyl)propanoate (20f)



*m*CPBA (2.03 g, 11.8 mmol, 3.0 equiv) was added to a solution of oxetane sulfide **21f** (1.34 g, 3.90 mmol, 1.0 equiv) in anhydrous CH_2Cl_2 (196 mL, 0.02 M) in a 500 mL round bottom flask. The reaction mixture was stirred at 25 °C for 3 h then aq. KOH (3 M, 110 mL) was added and the phases were separated. The aqueous portion was extracted with CH_2Cl_2 (4 × 55 mL). The combined organic extracts were dried over Na_2SO_4, filtered and concentrated *in vacuo* using a rotatory evaporator to afford oxetane sulfone **20f** as a light-yellow solid (1.31 g, 89%). R_f = 0.27 (50% EtOAc/pentane); mp = 85–88 °C; IR (film)/cm^{-1} 2995, 2948, 2888, 2831, 1732 (C=O st), 1588, 1509, 1456,

1417, 1367, 1351, 1340, 1304 (SO_2 st as), 1267, 1257, 1200, 1183, 1088, 1059, 1034, 1001, 959, 917, 900, 837, 814, 779, 764, 744, 716, 673; ^{1}H NMR (400 MHz, $CDCl_3$) δ 6.49 (s, 2 H, 2 × Ar-CH), 5.38 (d, *J* = 7.3 Hz, 2 H, C*H*HOC*H*H), 5.14 (d, *J* = 7.3 Hz, 2 H, CH*H*OCH*H*), 3.881 (s, 3 H, Ar-C_qOCH_3), 3.876 (s, 6 H, 2 × Ar-C_qOCH_3), 3.71 (s, 3 H, CO_2CH_3), 3.15 (t, *J* = 7.5 Hz, 2 H, SO_2CH_2), 2.72 (t, *J* = 7.5 Hz, 2 H, CH_2CO_2Me); ^{13}C NMR (101 MHz, $CDCl_3$) δ 170.8 (C_q=O), 153.6 (2 × Ar-C_qOMe), 139.0 (Ar-C_qOMe), 129.0 (Ar-C_qC_q), 105.6 (2 × Ar-CH), 76.3 (CH_2OCH_2), 69.0 (C_q), 60.9 (Ar-C_qOCH$_3$), 56.4 (2 × Ar-C_qOCH$_3$), 52.4 (CO_2CH_3), 43.6 (CH_2CO_2Me), 26.1 (SO_2CH_2); HRMS (ESI) *m/z* calcd for $C_{18}H_{25}NO_8SNa$ [M+MeCN+Na]: 438.1199, found: 438.1195.

3-(3,4,5-Trimethoxyphenyl)oxetane-3-sulfonyl fluoride (18f)



Sodium methoxide (5.4 M solution in MeOH, 0.28 mL, 1.50 mmol, 1.0 equiv) was added dropwise to a solution of oxetane sulfone **20f** (562 mg, 1.50 mmol, 1.0 equiv) in anhydrous THF (3.0 mL, 0.5 M) in a 10 mL round bottom flask. Oxetane sulfinate salt **19f** precipitated immediately after the start of addition of base to form a light-yellow paste (Figure 82). The reaction mixture was stirred at 25 °C for 20 min, then concentrated *in vacuo* using a rotatory evaporator to afford oxetane sulfinate **19f**, which was subjected directly to the next step without spectroscopical analysis. For the fluorination step, Selectfluor (797.1 mg, 2.25 mmol, 1.5 equiv) was added to anhydrous MeOH (7.5 mL, 0.2 M) at 0 °C in a 25 mL round bottom flask, then stirred for 5 min. Sulfinate salt **19f** was added portionwise. The reaction mixture was stirred for at 0 °C for 1 h, then concentrated *in vacuo* using a rotatory evaporator. The residue was diluted with CH_2Cl_2 (15 mL) and filtered through a plug of Celite, eluting with further CH_2Cl_2. After concentration *in vacuo* using a rotatory evaporator, purification by flash column chromatography through a very short column (100% CH_2Cl_2) afforded oxetane sulfonyl fluoride **18f** as a white solid (348 mg, 76%). R_f = 0.14 (100% CH_2Cl_2); mp = 113 °C; IR (film)/cm^{-1} 2963, 2947, 2894, 2841, 1590, 1510, 1459, 1420, 1400 (SO_2 st as), 1351, 1338, 1249, 1208, 1177, 1130, 1002, 960, 913, 886, 837, 814, 789, 736, 687; ^{1}H NMR (400 MHz, $CDCl_3$) δ 6.44 (s, 2 H, 2 × Ar-CH), 5.42 (d, *J* = 7.9 Hz, 2 H, C*H*HOC*H*H), 5.27 (dd, ^2J = 7.9 Hz, J_{HF} = 1.4 Hz, 2 H, CH*H*OCH*H*), 3.89 (s, 3 H, OCH_3), 3.88 (s, 6 H, 2 × OCH_3); ^{13}C NMR (101 MHz, $CDCl_3$) δ 153.7 (2 × Ar-C_qOMe), 139.6 (Ar-C_qOMe), 126.6 (Ar-C_qC_q), 105.6 (2 × Ar-CH), 77.0 (CH_2OCH_2), 68.7 (d, $^2J_{CF}$ = 14.8 Hz, C_q), 60.9 (OCH_3), 56.4 (2 × OCH_3); ^{19}F NMR (377 MHz, $CDCl_3$) δ 35.1; HRMS (APCI) *m/z* calcd for $C_{12}H_{15}FO_6S^{\bullet+}$ $[M]^{\bullet+}$: 306.0568, found: 306.0565.

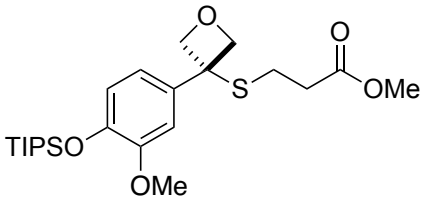
Notes:

***18f** was further characterised by X-ray crystallography (see Figure 28).*



Figure 82. Solidification of reaction mixture after addition of NaOMe. Picture was taken from a 0.5 mmol scale reaction.

Methyl 3-((3-(3-methoxy-4-((triisopropylsilyl)oxy)phenyl)oxetan-3-yl)thio)propanoate (21g)



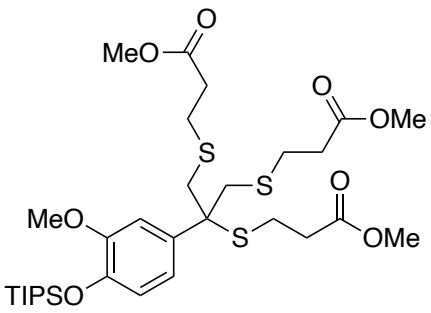
Lithium bis(trifluoromethanesulfonimide) (157.9 mg, 0.55 mmol, 0.11 equiv) and tetrabutylammonium hexafluorophosphate (106.5 mg, 0.275 mmol, 0.055 equiv) were added sequentially to a solution of oxetanol **22g** (1.76 g, 5.0 mmol, 1.0 equiv) and methyl 3-mercaptopropionate (1.08 mL, 10.0 mmol, 2.0 equiv) in non-anhydrous chloroform (10 mL, 0.5 M) in a 50 mL round bottom flask. The reaction flask was placed into a preheated oil bath at 40 °C. The reaction was stirred for 15 min and then heated up to 70 °C in 1 h. At 70 °C there was a change in colour from clear and colourless to dark orange (Figure 25). From the moment of the colour change, the reaction was stirred for further 25 min and quenched with sat. aq. $NaHCO_3$ (10 mL). The aqueous layer was extracted with CH_2Cl_2 (3 × 10 mL). The combined organic extracts were washed with aq. NaOH (1 M, 10 mL), dried over Na_2SO_4, filtered and concentrated *in vacuo* using a rotatory evaporator. Purification by flash column chromatography (30% Et_2O/pentane) afforded oxetane sulfide **21g** as a colourless oil which crystallised in the freezer to a white solid (1.36 g, 60%). R_f = 0.25 (30% Et_2O/pentane); mp = 49 °C; IR (film)/cm^{-1} 2945, 2866, 1737 (C=O st), 1513, 1465, 1308, 1275, 1249, 1215, 1133, 1036, 988, 913, 883, 813, 734, 682; ^{1}H NMR (400 MHz, $CDCl_3$) δ 6.85 (d, *J* = 8.1 Hz, 1 H, (TIPSO)C_qAr-CH), 6.67 (d, *J* = 2.2 Hz, 1 H, Ar-C_qAr-CHAr-C_q), 6.64 (dd, ^{3}*J* = 8.1 Hz, ^{4}*J* = 2.2 Hz, 1 H, Ar-CH), 5.20 (d, *J* = 6.3 Hz, 2 H, C*H*HOC*H*H), 4.88 (d, *J* = 6.3 Hz, 2 H, CH*H*OCH*H*), 3.81 (s, 3 H, Ar-$C_q$$OCH_3$), 3.66 (s, 3 H, CO_2CH_3), 2.64 (t, *J* = 7.4 Hz, 2 H, SCH_2), 2.36 (t, *J* = 7.4 Hz, 2 H, CH_2CO_2Me), 1.30–1.20 (m, 3 H, 3 × SiCH), 1.10 (d, *J* = 7.3 Hz, 18 H, 6 × SiCHCH_3); ^{13}C NMR (101 MHz, $CDCl_3$) δ 172.1 (C_q=O), 151.1 (Ar-C_qOMe), 144.8 (Ar-C_q(OTIPS)), 135.1 (Ar-$C_q$$C_q$), 120.0 (Ar-CH), 118.6 (Ar-CH), 110.3 (Ar-C_qAr-*C*HAr-C_q), 83.3 (CH_2OCH_2), 55.5 (Ar-C_qO*C*H_3), 52.5 (Ar-

C_qC_q), 51.8 (CO_2CH_3), 34.2 (CH_2CO_2Me), 25.2 (SCH_2), 17.9 (6 × SiCHCH_3), 12.8 (3 × SiCH); HRMS (APCI) *m/z* calcd for $C_{23}H_{38}O_5SSiNa^+$ $[M+Na]^+$: 477.2101, found: 477.2080; also: *m/z* calcd for $C_{19}H_{31}O_3Si^+$ $[M–SCH_2CH_2CO_2Me]^+$: 335.2037, found: 335.2024.

Notes:

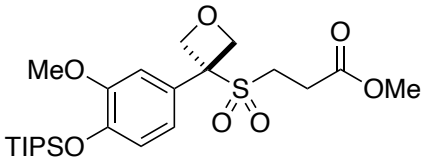
*On a 0.25 mmol scale, a trisulfide side product (**21g'**) was isolated in 11% yield (18.2 mg, colourless oil):*

Trimethyl 3,3',3''-((2-(3-methoxy-4-((triisopropylsilyl)oxy)phenyl)propane-1,2,3-triyl)tris(sulfa-nediyl))tripropionate (21g')



R_f = 0.11 (30% Et_2O/pentane); IR (film)/cm^{-1} 2948, 2866, 2255, 1737 (C=O st), 1603, 1513, 1465, 1413, 1357, 1275, 1245, 1178, 1141, 1036, 910, 816, 731, 686; ^{1}H NMR (400 MHz, $CDCl_3$) δ 7.11 (d, *J* = 2.3 Hz, 1 H, Ar-C_qAr-CHAr-C_q), 6.89 (dd, ^3J = 8.3 Hz, ^4J = 2.3 Hz, 1 H, Ar-CH), 6.81 (d, *J* = 8.3 Hz, 1 H, (TIPSO)C_qAr-CH), 3.83 (s, 3 H, Ar-$C_q$$OCH_3$), 3.69 (s, 6 H, 2 × CO_2CH_3), 3.62 (s, 3 H, CO_2CH_3), 3.39 (d, *J* = 12.8 Hz, 2 H, 2 × C_qC*H*HS), 3.33 (d, *J* = 12.8 Hz, 2 H, 2 × C_qCH*H*S), 2.71–2.66 (m, 4 H, 2 × SCH_2), 2.58–2.55 (m, 4 H, 2 × CH_2CO_2Me), 2.46–2.42 (m, 2 H, SCH_2), 2.35–2.31 (m, 2 H, CH_2CO_2Me), 1.30–1.19 (m, 3 H, 3 × SiCH), 1.08 (d, *J* = 7.4 Hz, 18 H, 6 × SiCHCH_3); ^{13}C NMR (101 MHz, $CDCl_3$) δ 172.2 (2 × C_q=O), 172.0 (C_q=O), 150.9 (Ar-C_qOMe), 144.9 (Ar-C_q(OTIPS)), 134.6 (Ar-$C_q$$C_q$), 119.8 (Ar-CH), 119.7 (Ar-CH), 111.9 (Ar-C_qAr-CHAr-C_q), 56.4 (C_q), 55.6 (Ar-C_qOCH_3), 51.8 (2 × CO_2CH_3), 51.7 (CO_2CH_3), 40.8 (2 × C_qCH_2S), 34.8 (2 × CH_2CO_2Me), 33.7 (CH_2CO_2Me), 28.4 (2 × SCH_2CH_2), 24.4 (SCH_2CH_2), 17.8 (6 × SiCHCH_3), 12.8 (3 × SiCH); HRMS (APCI) *m/z* calcd for $C_{31}H_{52}O_8S_3Si^{35}Cl^-$ $[M+^{35}Cl]^-$: 711.2288, found: 711.2286.

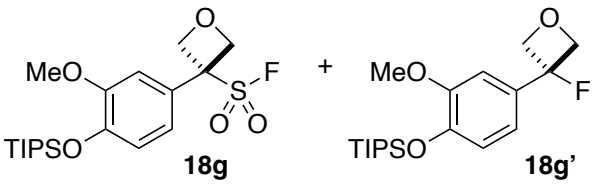
Methyl 3-((3-(3-methoxy-4-((triisopropylsilyl)oxy)phenyl)oxetan-3-yl)sulfonyl)propanoate (20g)



*m*CPBA (1.45 g, 8.4 mmol, 3.0 equiv) was added to a solution of oxetane sulfide **21g** (1.27 g, 2.8 mmol, 1.0 equiv) in anhydrous CH_2Cl_2 (140 mL, 0.02 M) in a 250 mL round bottom flask. The reaction mixture was stirred at 25 °C for 3 h then aq. KOH (3 M, 70 mL) was added and the phases were separated. The aqueous portion was extracted with CH_2Cl_2 (4 × 40 mL). The combined organic extracts were dried over Na_2SO_4, filtered and concentrated *in vacuo* using a rotatory evaporator to

afford oxetane sulfone **20g** as a white solid (1.36 g, quant.). R_f = 0.21 (50% Et_2O/pentane); mp = 153 °C; IR (film)/cm^{-1} 2945, 2866, 1741 (C=O st), 1603, 1512, 1465, 1364, 1312 (SO_2 st as), 1282 (SO_2 st sy), 1219, 1174, 1133, 1100, 1066, 1033, 917, 883, 813, 734, 682; ^{1}H NMR (400 MHz, $CDCl_3$) δ 6.93–6.90 (m, 1 H, (TIPSO)C_qAr-CH), 6.76–6.73 (m, 2 H, 2 × Ar-CH), 5.40 (d, *J* = 7.1 Hz, 2 H, C*H*HOC*H*H), 5.13 (d, *J* = 7.1 Hz, 2 H, CH*H*OCH*H*), 3.82 (s, 3 H, Ar-C_qOCH_3), 3.69 (s, 3 H, CO_2CH_3), 3.04 (t, *J* = 7.6 Hz, 2 H, SCH_2), 2.64 (t, *J* = 7.6 Hz, 2 H, C*H*$_2$$CO_2$Me), 1.31–1.21 (m, 3 H, 3 × SiCH), 1.10 (d, *J* = 7.3 Hz, 18 H, 6 × SiCHC*H*$_3$); ^{13}C NMR (101 MHz, $CDCl_3$) δ 170.7 (C_q=O), 151.3 (Ar-C_qOMe), 146.7 (Ar-C_q(OTIPS)), 126.4 (Ar-*C*$_q$$C_q$), 120.5 (Ar-CH), 120.4 (Ar-CH), 111.9 (Ar-C_qAr-*C*HAr-C_q), 76.3 (CH_2OCH_2), 68.6 (C_q), 55.7 (Ar-C_qO*C*H_3), 52.4 (CO_2*C*H_3), 43.6 (*C*H_2CO_2Me), 26.1 (SO_2CH_2), 17.8 (6 × SiCH*C*H_3), 12.8 (3 × SiCH); HRMS (ESI) *m/z* calcd for $C_{23}H_{42}NO_7SSi$ [M+NH_4]: 504.2451, found: 504.2437.

3-(3-Methoxy-4-((triisopropylsilyl)oxy)phenyl)oxetane-3-sulfonyl fluoride (18g) and (4-(3-fluorooxetan-3-yl)-2-methoxyphenoxy)triisopropylsilane (18g')



Sodium methoxide (5.4 M solution in MeOH, 0.22 mL, 1.20 mmol, 1.0 equiv) was added dropwise to a suspension of oxetane sulfone **20g** (583 mg, 1.20 mmol, 1.0 equiv) in anhydrous THF (2.4 mL, 0.5 M) in a 10 mL round bottom flask. The reaction mixture turns from colourless cloudy to dark orange and clear upon addition of base (Figure 83). The reaction mixture was stirred at 25 °C for 20 min, then concentrated *in vacuo* using a rotatory evaporator to afford oxetane sulfinate **19g** as a white solid, which was subjected directly to the next step without spectroscopical analysis. For the fluorination step, Selectfluor (637.6 mg, 1.8 mmol, 1.5 equiv) was added to anhydrous MeOH (6.0 mL, 0.2 M) at 0 °C in a 25 mL round bottom flask, then stirred for 5 min. Sulfinate salt **19g** was added portionwise. The reaction mixture was stirred for at 0 °C for 1 h, then concentrated *in vacuo* using a rotatory evaporator. The residue was diluted with CH_2Cl_2 (15 mL) and filtered through a plug of Celite, eluting with further CH_2Cl_2. After concentration *in vacuo* using a rotatory evaporator, purification by flash column chromatography through a very short column (50% CH_2Cl_2/pentane) afforded a 95:5 mixture of oxetane sulfonyl fluoride **18g** and oxetane fluoride **18g'** as a white solid (337 mg, 66%). The R_f values of **18g** and **18g'** were very similar and attempts to further purify the obtained mixture by flash column chromatography led to significant loss in mass of sulfonyl fluoride **18g** due to degradation on silica without improvement in purity. All following oxetane amination reactions were carried out successfully with this mixture showing that the presence of oxetane fluoride in the reaction mixture did not interfere with the oxetane amination. R_f = 0.31 (50% CH_2Cl_2/pentane); mp = 57-60 °C; IR (film)/cm^{-1} 2945, 2892, 2870, 1603, 1517,

1465, 1402 (SO_2 st as), 1320, 1282, 1260, 1208, 1182, 1133, 1070, 1036, 999, 917, 883, 824, 787, 686; ^{1}H NMR (400 MHz, $CDCl_3$) δ 6.93 (d, *J* = 8.2 Hz, 1 H, (TIPSO)C_qAr-CH), 6.73 (dd, ^3J = 8.2 Hz, ^4J = 2.3 Hz, 1 H, Ar-CH), 6.68 (d, *J* = 2.3 Hz, 1 H, Ar-C_qAr-CHAr-C_q), 5.42 (d, *J* = 7.7 Hz, 2 H, C*H*HOC*H*H), 5.25 (dd, ^2J = 7.1 Hz, J_{HF} = 1.4 Hz, 2 H, CH*H*OCH*H*), 5.11 (dd, ^2J = 7.7 Hz, J_{HF} = 1.4 Hz, 0.05 H, C*H*HO, **18g'**), 5.06 (dd, ^2J = 7.7 Hz, J_{HF} = 1.1 Hz, 0.05 H, C*H*HO, **18g'**), 4.92 (dd, ^2J = 7.7 Hz, J_{HF} = 1.2 Hz, 0.05 H, CH*H*O, **18g'**), 4.87 (dd, ^2J = 7.7 Hz, J_{HF} = 1.2 Hz, 0.05 H, CH*H*O, **18g'**), 3.82 (s, 3 H, Ar-$C_q$$OCH_3$), 1.31–1.21 (m, 3.29 H, 3 × SiCH, **18g** + **18g'**), 1.10 (d, *J* = 7.4 Hz, 19.1 H, 6 × SiCHC*H*$_3$, **18g** + **18g'**); ^{13}C NMR (101 MHz, $CDCl_3$) δ 151.3 (Ar-C_qOMe), 147.4 (Ar-C_q(OTIPS)), 123.8 (Ar-*C*$_q$$C_q$), 121.1 (Ar-CH), 120.5 (Ar-CH), 111.8 (Ar-C_qAr-*C*HAr-C_q), 77.1 (CH_2OCH_2), 68.5 (d, $^2J_{CF}$ = 14.6 Hz, C_q), 55.7 (OCH_3), 17.8 (6 × SiCH*C*H_3), 12.9 (3 × SiCH); ^{19}F NMR (377 MHz, $CDCl_3$) δ 34.5 (**18g**), –146.1 (**18g'**); HRMS (APCI) *m/z* calcd for $C_{19}H_{31}O_3Si^+$ [$M_{\mathbf{18g}}$–SO_2F or $M_{\mathbf{18g'}}$–F]$^+$: 335.2037, found: 335.2037.

Notes:

18g *was further characterised by X-ray crystallography (see Figure 28).*

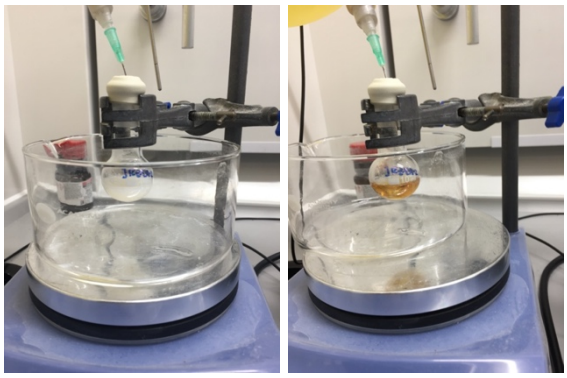
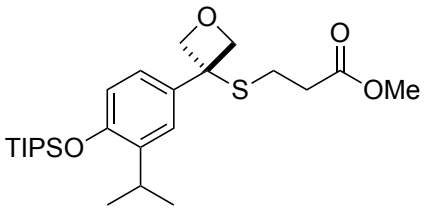


Figure 83. Appearance of reaction mixture before (left) and after (right) addition of base, including change in solubility properties.

Methyl 3-((3-(3-isopropyl-4-((triisopropylsilyl)oxy)phenyl)oxetan-3-yl)thio)propanoate (21h)



Lithium bis(trifluoromethanesulfonimide) (158.0 mg, 0.55 mmol, 0.11 equiv) and tetrabutylammonium hexafluorophosphate (106.8 mg, 0.276 mmol, 0.055 equiv) were added sequentially to a solution of oxetanol **22h** (1.82 g, 5.0 mmol, 1.0 equiv) and methyl 3-mercaptopropionate (1.08 mL, 10.0 mmol, 2.0 equiv) in non-anhydrous chloroform (10 mL, 0.5 M) in a 50 mL round bottom flask. The reaction flask was placed into a preheated oil bath at 40 °C. The reaction was stirred for 15 min and then heated up to 70 °C in 1 h. At 70 °C there was a change in colour from clear and colourless to light-pink and cloudy (Figure 84).

From the moment of the colour change, the reaction was stirred for further 25 min and quenched with sat. aq. $NaHCO_3$ (10 mL). The aqueous layer was extracted with CH_2Cl_2 (3 × 10 mL). The combined organic extracts were washed with aq. NaOH (1 M, 10 mL), dried over Na_2SO_4, filtered and concentrated *in vacuo* using a rotatory evaporator. Purification by flash column chromatography (5% acetone/pentane) afforded oxetane sulfide **21h** as a white solid (1.77 g, 76%). R_f = 0.19 (5% acetone/pentane); mp = 53 °C; IR (film)/cm^{-1} 2948, 2870, 1737 (C=O st), 1607, 1495, 1461, 1342, 1275, 1189, 1081, 988, 910, 820, 790, 731, 686; ^{1}H NMR (400 MHz, $CDCl_3$) δ 6.99 (d, *J* = 2.5 Hz, 1 H, Ar-C_qAr-CHAr-C_q), 6.85 (dd, ^{3}*J* = 8.3 Hz, ^{4}*J* = 2.5 Hz, 1 H, Ar-CH), 6.75 (d, *J* = 8.3 Hz, 1 H, (TIPSO)C_qAr-CH), 5.21 (d, *J* = 6.5 Hz, 2 H, C*H*HOC*H*H), 4.90 (d, *J* = 6.5 Hz, 2 H, CH*H*OCH*H*), 3.65 (s, 3 H, OCH_3), 3.37 (hept, *J* = 6.9 Hz, 1 H, Ar-C_qCH), 2.67 (t, *J* = 7.4 Hz, 2 H, SCH_2), 2.32 (t, *J* = 7.4 Hz, 2 H, C*H*$_2$$CO_2$Me), 1.38–1.27 (m, 3 H, 3 × SiCH), 1.20 (d, *J* = 6.9 Hz, 6 H, 2 × Ar-C_qCHC*H*$_3$), 1.12 (d, *J* = 7.4 Hz, 18 H, 6 × SiCHC*H*$_3$); ^{13}C NMR (101 MHz, $CDCl_3$) δ 172.1 (C_q=O), 152.3 (Ar-C_qOTIPS), 138.8 (Ar-C_q), 134.1 (Ar-C_q), 124.1 (Ar-*C*HAr-C_qAr-*C*H), 117.7 (Ar-CH), 83.4 (CH_2OCH_2), 52.5 (C_q), 51.7 (OCH_3), 34.2 (*C*H_2CO_2Me), 26.7 (Ar-C_q*C*H), 25.2 (SCH_2), 22.7 (2 × Ar-C_qCH*C*H_3), 18.1 (6 × SiCH*C*H_3), 13.0 (3 × SiCH); HRMS (APCI) *m/z* calcd for $C_{25}H_{42}O_4SSiNa^+$ $[M+H]^+$: 489.2465, found: 489.2446.

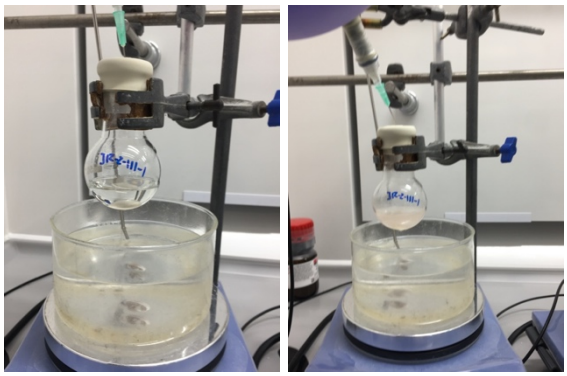
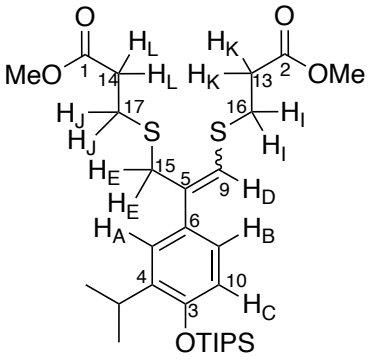


Figure 84. Reaction mixture before (left) and after (right) heating to 70 ºC. Start of reaction is marked by a sharp change in colour. Here from clear and colourless to cloudy and light-pink.

Notes:

*On a 0.25 mmol scale, an alkene side product (**21h'**) was isolated in 8% yield (11.0 mg, colourless oil):*

Dimethyl 3,3'-((2-(3-isopropyl-4-((triisopropylsilyl)oxy)phenyl)prop-1-ene-1,3-diyl)bis-(sulfanediyl))dipropionate (21h')

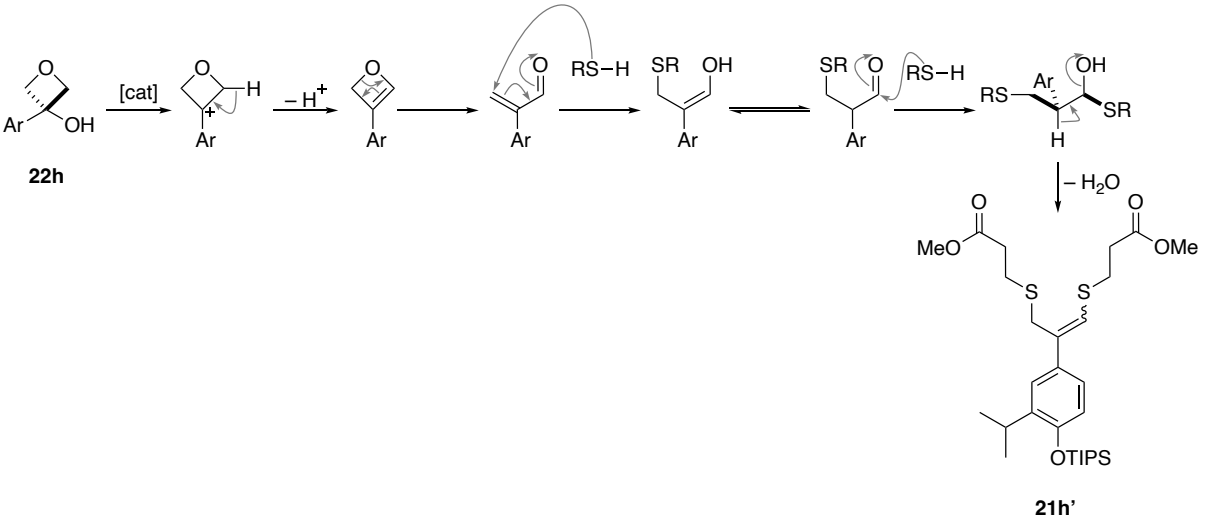


R_f = 0.13 (5% acetone/pentane); IR (film)/cm^{-1} 2948, 2866, 1737 (C=O st), 1603, 1495, 1461, 1439, 1357, 1271, 1077, 1018, 984, 932, 887, 813, 686; ^{1}H NMR (400 MHz, $CDCl_3$) δ 7.22 (d, J = 2.5 Hz, 1 H, H_A), 7.07 (dd, ^3J = 8.4 Hz, ^4J = 2.5 Hz, 1 H, H_B), 6.72 (d, J = 8.4 Hz, 1 H, H_C), 6.30 (s, 1 H, H_D), 3.73 (s, 2 H, H_E), 3.70 (s, 3 H,CO_2CH_3), 3.68 (s, 3 H, CO_2CH_3), 3.36 (hept, J = 6.9 Hz, 1 H, Ar-C_qCH), 3.04 (t, J = 7.3 Hz, 2 H, H_I), 2.80–2.76 (m, 2 H, H_J), 2.70 (t, J = 7.3 Hz, 2 H, H_K), 2.65–2.62 (m, 2 H, H_L), 1.36–1.29 (m, 3 H, 3 × SiCH), 1.22 (d, J = 6.9 Hz, 6 H, 2 × Ar-C_qCHCH_3), 1.12 (d, J = 7.4 Hz, 18 H, 6 × SiCHCH_3); ^{13}C NMR (101 MHz, $CDCl_3$) δ 172.4 (C1), 172.1 (C2), 152.8 (C3), 138.4 (C4), 136.6 (C5), 132.3 (C6), 123.61 (Ar-CH), 123.57 (Ar-CH), 117.6 (C10), 51.9 (OCH_3), 51.7 (OCH_3), 35.3 (C13), 34.8 (C14), 32.5 (C15), 29.4 (C16), 26.9 (C17), 26.8 (Ar-C_qCH), 22.8 (2 × Ar-C_qCHCH_3), 18.1 (6 × SiCHCH_3), 13.1 (3 × SiCH). HRMS (ESI) *m/z* calcd for $C_{29}H_{48}O_5S_2SiNa^+$ $[M+H]^+$: 591.2605, found: 591.2593.

Notes:

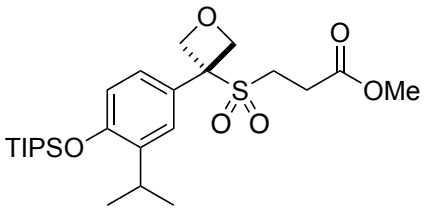
C9 is under the signals at 123.61 & 123.57 ppm. This was confirmed by HSQC and HMBC 2D correlation spectra.

The unexpected alkene side product was potentially formed through a series of eliminations and nucleophilic additions (Scheme 60).



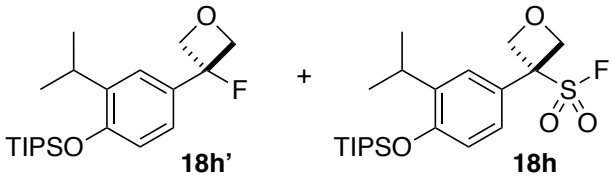
Scheme 60. Proposed mechanism for the formation of alkene 21h'.

Methyl 3-((3-(3-isopropyl-4-((triisopropylsilyl)oxy)phenyl)oxetan-3-yl)sulfonyl)propanoate (20h)



*m*CPBA (1.52 g, 8.8 mmol, 2.9 equiv) was added to a solution of oxetane sulfide **21h** (1.40 g, 3.0 mmol, 1.0 equiv) in anhydrous CH_2Cl_2 (150 mL, 0.02 M) in a 250 mL round bottom flask. The reaction mixture was stirred at 25 °C for 3 h then aq. KOH (3 M, 70 mL) was added and the phases were separated. The aqueous portion was extracted with CH_2Cl_2 (4 × 40 mL). The combined organic extracts were combined, dried over Na_2SO_4, filtered and concentrated *in vacuo* using a rotatory evaporator to afford oxetane sulfone **20h** as a white solid (1.50 g, quant.). R_f = 0.43 (50% Et_2O/pentane); mp = 125 °C; IR (film)/cm^{-1} 2948, 2866, 1741 (C=O st), 1607, 1495, 1461, 1309 (SO_2 st as), 1275, 1178, 1133, 1100, 999, 921, 887, 828, 794, 731, 686; ^{1}H NMR (400 MHz, $CDCl_3$) δ 7.07 (d, *J* = 2.5 Hz, 1 H, Ar-C_qAr-CHAr-C_q), 6.96 (dd, ^3J = 8.4 Hz, ^4J = 2.5 Hz, 1 H, Ar-CH), 6.82 (d, *J* = 8.4 Hz, 1 H, (TIPSO)C_qAr-CH), 5.41 (d, *J* = 7.1 Hz, 2 H, C*H*HOC*H*H), 5.13 (d, *J* = 7.1 Hz, 2 H, CH*H*OCH*H*), 3.67 (s, 3 H, OCH_3), 3.39 (hept, *J* = 6.9 Hz, 1 H, Ar-C_qCH), 3.05 (t, *J* = 7.7 Hz, 2 H, SO_2CH_2), 2.58 (t, *J* = 7.7 Hz, 2 H, CH_2CO_2Me), 1.39–1.28 (m, 3 H, 3 × SiCH), 1.20 (d, *J* = 6.9 Hz, 6 H, 2 × Ar-C_qCHCH_3), 1.13 (d, *J* = 7.5 Hz, 18 H, 6 × SiCHCH_3); ^{13}C NMR (101 MHz, $CDCl_3$) δ 170.7 (C_q=O), 154.1 (Ar-C_qOTIPS), 139.6 (Ar-C_q), 126.2 (Ar-CH), 126.0 (Ar-CH), 125.4 (Ar-C_q), 118.2 (Ar-CH), 76.4 (CH_2OCH_2), 68.5 (C_q), 52.3 (OCH_3), 43.6 (*C*H_2CO_2Me), 26.7 (Ar-C_q*C*H), 26.2 (SO_2CH_2), 22.7 (2 × Ar-C_qCH*C*H_3), 18.0 (6 × SiCH*C*H_3), 13.0 (3 × SiCH); HRMS (ESI) *m/z* calcd for $C_{25}H_{46}NO_6SSi$ [M+NH_4]: 516.2815, found: 516.2812.

(4-(3-Fluorooxetan-3-yl)-2-isopropylphenoxy)triisopropylsilane (18h') and 3-(3-isopropyl-4-((triisopropylsilyl)oxy)phenyl)oxetane-3-sulfonyl fluoride (18h)



Sodium methoxide (5.4 M solution in MeOH, 0.28 mL, 1.50 mmol, 1.0 equiv) was added dropwise to a solution of oxetane sulfone **20h** (748 mg, 1.50 mmol, 1.0 equiv) in anhydrous THF (3.0 mL, 0.5 M) in a 10 mL round bottom flask. The reaction mixture turns from colourless to yellow upon addition of base (Figure 85). The reaction mixture was stirred at 25 °C for 20 min, then concentrated *in vacuo* using a rotatory evaporator to afford oxetane sulfinate **19h** as a light-yellow solid, which was subjected directly to the next step without spectroscopical analysis. For the fluorination step, Selectfluor (797.2 mg, 2.25 mmol, 1.5 equiv) was added to anhydrous MeOH (7.5 mL, 0.2 M) at 0 °C in a 25 mL round bottom flask, then stirred for 5 min. Sulfinate salt **19h** was added portionwise. The reaction mixture

was stirred for at 0 °C for 1 h, then concentrated *in vacuo* using a rotatory evaporator. The residue was diluted with CH_2Cl_2 (15 mL) and filtered through a plug of Celite, eluting with further CH_2Cl_2. After concentration *in vacuo* using a rotatory evaporator, purification by flash column chromatography through a very short column (60% CH_2Cl_2/pentane) afforded a 9:1 mixture of oxetane sulfonyl fluoride **18h** and oxetane fluoride **18h'** as a colourless gum (461 mg, 72%). Repurification of the mixture by flash column chromatography (3% Et_2O/pentane) afforded oxetane fluoride **18h'** as a colourless gum (38.8 mg, 7%) followed by oxetane sulfonyl fluoride **18h** as a colourless gum which crystallised in the freezer to a white solid (342 mg, 53%).

Oxetane fluoride **18h'**: R_f = 0.37 (3% EtOAc/pentane); IR (film)/cm^{-1} 2945, 2870, 1610, 1498, 1465, 1346, 1308, 1271, 1192, 1081, 984, 932, 883, 820, 768, 686; ^{1}H NMR (400 MHz, $CDCl_3$) δ 7.33 (d, J = 2.4 Hz 1 H, Ar-C_qAr-CHAr-C_q), 7.19 (ddd, ^3J = 8.4 Hz, ^4J = 2.4 Hz, $^5J_{HF}$ = 0.9 Hz, 1 H, Ar-CH), 6.82 (dd, ^3J = 8.4 Hz, J = 0.9 Hz, 1 H, (TIPSO)C_qAr-CH), 5.11 (dd, ^2J = 7.7 Hz, J_{HF} = 1.2 Hz, 1 H, C*H*HO), 5.06 (dd, ^2J = 7.7 Hz, J_{HF} = 1.2 Hz, 1 H, C*H*HO), 4.95 (dd, ^2J = 7.7 Hz, J_{HF} = 1.2 Hz, 1 H, CH*H*O), 4.90 (dd, ^2J = 7.7 Hz, J_{HF} = 1.2 Hz, 1 H, CH*H*O), 3.41 (hept, J = 6.9 Hz, 1 H, Ar-C_qCH), 1.38–1.29 (m, 3 H, 3 × SiCH), 1.23 (d, J = 6.9 Hz, 6 H, 2 × Ar-C_qCHC*H*$_3$), 1.13 (d, J = 7.5 Hz, 18 H, 6 × SiCHC*H*$_3$); ^{13}C NMR (101 MHz, $CDCl_3$) δ 153.4 (Ar-C_qOTIPS), 138.9 (Ar-*C*$_q$CH), 130.1 (d, $^2J_{CF}$ = 23.7 Hz, Ar-*C*$_q$C$_q$), 122.3 (d, $^3J_{CF}$ = 8.8 Hz, Ar-CH), 122.2 (d, $^3J_{CF}$ = 8.6 Hz, Ar-CH), 95.7 (d, $^1J_{CF}$ = 205.4 Hz, C_q) 83.1 (d, $^2J_{CF}$ = 26.0 Hz, CH_2OCH_2), 26.8 (Ar-C_q*C*H), 22.7 (2 × Ar-C_qCH*C*H$_3$), 18.1 (6 × SiCH*C*H$_3$), 13.1 (3 × SiCH); ^{19}F NMR (377 MHz, $CDCl_3$) δ 34.2; HRMS (APCI) *m/z* calcd for $C_{21}H_{35}O_2Si^+$ [M–F]$^+$: 347.2401, found: 347.2403.

Oxetane sulfonyl fluoride **18h**: R_f = 0.23 (3% EtOAc/pentane); mp = 57-64 °C; IR (film)/cm^{-1} 2948, 2892, 2870, 1607, 1495, 1465, 1402 (SO_2 st as), 1342, 1279, 1215 (SO_2 st sy), 1193, 1111, 1003, 925, 887, 824, 783, 686; ^{1}H NMR (400 MHz, $CDCl_3$) δ 7.05 (d, J = 2.5 Hz 1 H, Ar-C_qAr-CHAr-C_q), 6.94 (dd, ^3J = 8.4 Hz, ^4J = 2.5 Hz, 1 H, Ar-CH), 6.83 (d, J = 8.4 Hz, 1 H, (TIPSO)C_qAr-CH), 5.43 (d, J = 7.6 Hz, 2 H, C*H*HOC*H*H), 5.24 (dd, ^2J = 7.6 Hz, J_{HF} = 1.4 Hz, 2 H, CH*H*OCH*H*), 3.38 (hept, J = 7.0 Hz, 1 H, Ar-C_qCH), 1.38–1.29 (m, 3 H, 3 × SiCH), 1.21 (d, J = 7.0 Hz, 6 H, 2 × Ar-C_qCHC*H*$_3$), 1.13 (d, J = 7.4 Hz, 18 H, 6 × SiCHC*H*$_3$); ^{13}C NMR (101 MHz, $CDCl_3$) δ 154.7 (Ar-C_qOTIPS), 139.7 (Ar-C_q), 126.3 (Ar-CH), 126.1 (Ar-CH), 123.1 (Ar-C_q), 118.1 (Ar-CH), 77.3 (CH_2OCH_2), 68.4 (d, $^2J_{CF}$ = 14.2 Hz, C_q), 26.8 (Ar-C_q*C*H), 22.6 (2 × Ar-C_qCH*C*H$_3$), 18.0 (6 × SiCH*C*H$_3$), 13.0 (3 × SiCH); ^{19}F NMR (377 MHz, $CDCl_3$) δ –145.0; HRMS (APCI) *m/z* calcd for $C_{21}H_{35}O_2Si^+$ [M–SO_2F]$^+$: 347.2401, found: 347.2401.

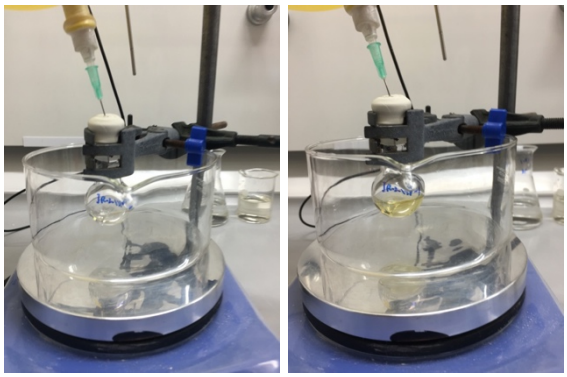
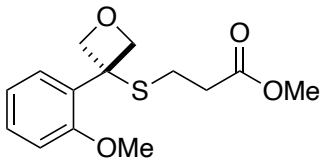


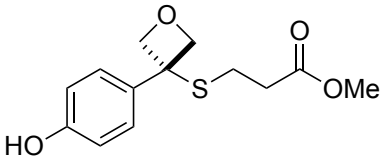
Figure 85. Appearance of reaction mixture before (left) and after (right) addition of base.

Methyl 3-((3-(2-methoxyphenyl)oxetan-3-yl)thio)propanoate (21e)



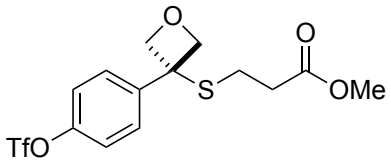
Lithium bis(trifluorometha-nesulfonimide) (16.0 mg, 0.055 mmol, 0.11 equiv) and tetrabutylammonium hexafluorophosphate (10.8 mg, 0.0275 mmol, 0.055 equiv) were added sequentially to a solution of oxetanol **22e** (90.2 mg, 0.5 mmol, 1.0 equiv) and methyl 3-mercaptopropionate (0.11 mL, 1.0 mmol, 2.0 equiv) in non-anhydrous chloroform (1.0 mL, 0.5 M) in a reaction tube. The reaction vessel was sealed, purged with argon and placed into a preheated oil bath at 40 °C. The reaction was stirred for 15 min and then heated up to 100 °C in 3.75 h. There was no colour change during the reaction. After stirring for 1 h at 100 °C, the reaction was allowed to cool to room temperature (ca. 22 ºC) and quenched with sat. aq. $NaHCO_3$ (5 mL). The aqueous layer was extracted with CH_2Cl_2 (3 × 10 mL). The combined organic extracts were washed with aq. NaOH (1 M, 15 mL), dried over Na_2SO_4, filtered and concentrated *in vacuo* using a rotatory evaporator. Purification by flash column chromatography (30–50% Et_2O/pentane) afforded oxetane sulfide **21e** as a colourless oil (5.8 mg, 4%). R_f = 0.45 (60% Et_2O/pentane); IR (film)/cm^{-1} 2952, 2874, 1737 (C=O st), 1599, 1490, 1461, 1439, 1357, 1293, 1245, 1178, 1129, 1096, 1062, 1025, 980, 932, 846, 790, 757, 708; ^{1}H NMR (400 MHz, $CDCl_3$) δ 7.28 (ddd, ^3J = 8.3, 7.3 Hz, ^4J = 1.9 Hz, 1 H, Ar-CH), 6.96 (ddd, ^3J = 7.3, 7.3 Hz, ^4J = 1.0 Hz, 1 H, Ar-CH), 6.91–6.89 (m, 2 H, 2 × Ar-CH), 5.23 (d, J = 7.3 Hz, 2 H, C*H*HOC*H*H), 4.80 (d, J = 7.3 Hz, 2 H, CH*H*OCH*H*), 3.82 (s, 3 H, Ar-C_qOCH_3), 3.66 (s, 3 H, CO_2CH_3), 2.74 (t, J = 7.6 Hz, 2 H, SCH_2), 2.42 (t, J = 7.6 Hz, 2 H, CH_2CO_2Me); ^{13}C NMR (101 MHz, $CDCl_3$) δ 172.2 (C_q=O), 156.3 (Ar-C_qOMe), 130.0 (Ar-C_qC_q), 128.9 (Ar-CH), 127.1 (Ar-CH), 120.5 (Ar-CH), 111.4 (Ar-CH), 82.6 (CH_2OCH_2), 55.4 (Ar-C_qOCH_3), 51.7 (CO_2CH_3), 51.6 (Ar-C_qC_q) 34.2 (CH_2CO_2Me), 25.0 (SCH_2); HRMS (ESI) *m/z* calcd for $C_{14}H_{19}O_4S$ [M+H]: 283.1004; found: 283.1006.

Methyl 3-((3-(4-hydroxyphenyl)oxetan-3-yl)thio)propanoate (21k)



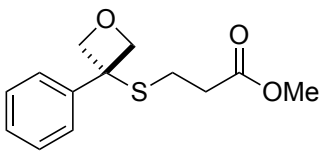
TBAF (1.0 M in THF, 3.0 mL, 3.0 mmol, 1.5 equiv) was added dropwise to a solution of OTIPS oxetane sulfide **21c** (854 mg, 2.0 mmol, 1.0 equiv) in anhydrous THF (6.7 mL, 0.3 M) at 0 °C in a 50 mL round bottom flask. The reaction mixture was warmed to 25 °C and stirred for further 3 h. The reaction was then quenched with sat. aq. NH_4Cl (30 mL). The aqueous layer was extracted with EtOAc (3 × 30 mL). The combined organic extracts were dried over Na_2SO_4, filtered and concentrated *in vacuo* using a rotatory evaporator. Purification by flash chromatography (60–75% EtOAc/pentane) afforded phenol oxetane sulfide **21k** as colourless crystals (497 mg, 93%). R_f = 0.30 (70% EtOAc/pentane); mp = 79 °C; IR (film)/cm^{-1} 3305 (OH st, br), 3018, 2947, 2871, 1730 (C=O st), 1610, 1591, 1512, 1435, 1358, 1218, 1173, 1111, 1039, 1013, 976, 923, 833, 732, 703, 579, 541; ^{1}H NMR (400 MHz, $CDCl_3$) δ 7.08–7.04 (m, 2 H, 2 × Ar-CH), 6.83–6.79 (m, 2 H, 2 × Ar-CH), 5.20 (d, *J* = 6.5 Hz, 2 H, C*H*HOC*H*H), 4.91 (d, *J* = 6.5 Hz, 2 H, CH*H*OCH*H*), 3.68 (s, 3 H, CH_3), 2.67 (t, *J* = 7.4 Hz, 2 H, SCH_2), 2.43 (t, *J* = 7.4 Hz, 2 H, CH_2CO_2Me); ^{13}C NMR (101 MHz, $CDCl_3$) δ 172.4 (C_q=O), 155.1 (Ar-C_qOH), 133.9 (Ar-C_qC_q), 127.6 (2 × Ar-CH), 115.5 (2 × Ar-CH), 83.3 (CH_2OCH_2), 52.1 (C_q), 52.0 (CO_2CH_3), 34.0 (CH_2CO_2Me), 25.1 (SCH_2); HRMS (APCI) *m/z* calcd for $C_{13}H_{15}SO_4^-$ $[M–H]^-$: 267.0697; found: 267.0694.

Methyl 3-((3-(4-(((trifluoromethyl)sulfonyl)oxy)phenyl)oxetan-3-yl)thio)propanoate (21l)



Pyridine (0.25 mL, 3.12 mmol, 2.0 equiv) and triflic anhydride (0.32 mL, 1.87 mmol, 1.2 equiv) were added sequentially to a solution of phenol oxetane sulfide **21k** (418 mg, 1.56 mmol, 1.0 equiv) in anhydrous CH_2Cl_2 (20 mL, 0.08 M) at 0 °C in a 50 mL round bottom flask. The reaction mixture was warmed to 25 °C and stirred for 1 h. The reaction was then quenched with distilled water (45 mL). The aqueous layer was extracted with CH_2Cl_2 (3 × 90 mL). The combined organic extracts were dried over Na_2SO_4, filtered and concentrated *in vacuo* using a rotatory evaporator. Purification by flash column chromatography (50% Et_2O/pentane) afforded oxetane triflate **21l** as a colourless gum which solidified in the freezer (578 mg, 93%). R_f = 0.26 (50% Et_2O/pentane); mp = 35–38 °C; IR (film)/cm^{-1} 2952, 2878, 1737 (C=O st), 1506, 1424, 1208, 1141, 984, 887, 760, 611; ^{1}H NMR (400 MHz, $CDCl_3$) δ 7.35–7.29 (m, 4 H, 4 × Ar-CH), 5.18 (d, *J* = 6.6 Hz, 2 H, C*H*HOC*H*H), 4.93 (d, *J* = 6.6 Hz, 2 H, CH*H*OCH*H*), 3.69 (s, 3 H, CH_3), 2.69 (t, *J* = 7.3 Hz, 2 H, SCH_2), 2.45 (t, *J* = 7.3 Hz, 2 H, CH_2CO_2Me); ^{13}C NMR (101 MHz, $CDCl_3$) δ 171.8 (C_q=O), 148.4 (Ar-C_qOTf), 143.0 (Ar-C_qC_q), 128.3 (2 × Ar-CH), 121.6 (2 × Ar-CH), 118.7 (q, J_{CF} = 321.1 Hz, CF_3), 82.6 (CH_2OCH_2), 51.9 (CO_2CH_3), 51.8 (C_q), 33.8 (CH_2CO_2Me), 25.0 (SCH_2); ^{19}F NMR (377 MHz, $CDCl_3$) δ –72.8; HRMS (APCI) *m/z* calcd for $C_{14}H_{16}F_3S_2O_6^+$ $[M+H]^+$: 401.0335; found: 401.0337.

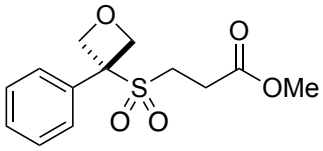
Methyl 3-((3-phenyloxetan-3-yl)thio)propanoate (21m)



Following adapted conditions developed by Ortar,[253] triethyl amine (0.50 mL, 3.6 mmol, 3.0 equiv) and formic acid (90.6 μL, 2.4 mmol, 2.0 equiv) were added sequentially to a solution of oxetane triflate **21l** (480.5 mg, 1.2 mmol, 1.0 equiv), $Pd(OAc)_2$ (5.4 mg, 0.024 mmol, 0.02 equiv) and (ferrocene-1,1′-diyl) bis(diphenylphosphane) (dppf; 13.3 mg, 0.024 mmol, 0.02 equiv) in anhydrous DMF (12 mL, 0.1 M) in a 50 mL round bottom flask. The reaction mixture was warmed to 60 °C and stirred for 1 h. The reaction was cooled down to 25 °C, then brine was added (50 mL). The aqueous layer was extracted with EtOAc (4 × 50 mL). The combined organic extracts were washed with brine (2 × 50 mL), dried over Na_2SO_4, filtered and concentrated *in vacuo* using a rotatory evaporator. Purification by flash column chromatography (50% Et_2O/pentane) afforded phenyl oxetane sulfide **21m** as a colourless gum (294 mg, 97%). R_f = 0.44 (50% Et_2O/pentane); IR (film)/cm^{-1} 2951, 2873, 1737 (C=O st), 1599, 1497, 1437, 1358, 1244, 1088, 986, 932, 835, 763, 529; ^{1}H NMR (400 MHz, $CDCl_3$) δ 7.41–7.36 (m, 2 H, 2 × Ph-CH), 7.31–7.28 (m, 1 H, Ph-CH), 7.21–7.18 (m, 2 H, 2 × Ph-CH), 5.24 (d, *J* = 6.5 Hz, 2 H, C*H*HOC*H*H), 4.92 (d, *J* = 6.5 Hz, 2 H, CH*H*OCH*H*), 3.67 (s, 3 H, CH_3),

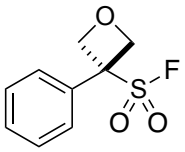
2.67 (t, *J* = 7.4 Hz, 2 H, SCH_2), 2.40 (t, *J* = 7.4 Hz, 2 H, CH_2CO_2Me); ^{13}C NMR (101 MHz, $CDCl_3$) δ 172.0 (C_q=O), 142.2 (Ph-C_qC_q), 128.6 (2 × Ph-CH), 127.3 (Ph-CH), 126.2 (2 × Ph-CH), 82.9 (CH_2OCH_2), 52.4 (C_q), 51.8 (OCH_3), 33.9 (CH_2CO_2Me), 25.1 (SCH_2); HRMS (APCI) *m/z* calcd for $C_{13}H_{17}SO_3^+$ $[M+H]^+$: 253.0893; found: 253.0893.

Methyl 3-((3-phenyloxetan-3-yl)sulfonyl)propanoate (20m)



*m*CPBA (683 mg, 3.96 mmol, 3.0 equiv) was added to a solution of oxetane sulfide **21m** (333 mg, 1.32 mmol, 1.0 equiv) in anhydrous CH_2Cl_2 (70 mL, 0.02 M) in a 250 mL round bottom flask. The reaction mixture was stirred at 25 °C for 3 h then aq. KOH (3 M, 30 mL) was added and the phases were separated. The aqueous portion was extracted with CH_2Cl_2 (3 × 20 mL). The combined organic extracts were dried over Na_2SO_4, filtered and concentrated *in vacuo* using a rotatory evaporator to afford sulfone **20m** as a white solid (376 mg, quant.). R_f = 0.27 (60% Et_2O/pentane); mp = 120 °C; IR (film)/cm^{-1} 2949, 2883, 1735 (C=O st), 1494, 1438, 1364, 1307 (SO_2 st as), 1279, 1251,1220, 1178, 1135 (SO_2 st sy), 1097, 1055, 1022, 996, 933, 831, 778, 702, 565, 533, 474; ^1H NMR (400 MHz, $CDCl_3$) δ 7.50–7.45 (m, 3 H, 3 × Ph-CH), 7.33–7.30 (m, 2 H, 2 × Ph-CH), 5.43 (d, *J* = 7.3 Hz, 2 H, C*H*HOC*H*H), 5.17 (d, *J* = 7.3 Hz, 2 H, CH*H*OCH*H*), 3.70 (s, 3 H, CH_3), 3.09 (t, *J* = 7.6 Hz, 2 H, SO_2CH_2), 2.70 (t, *J* = 7.6 Hz, 2 H, CH_2CO_2Me); ^{13}C NMR (101 MHz, $CDCl_3$) δ 170.7 (C_q=O), 133.8 (Ph-C_qC_q), 129.4 (Ph-CH), 129.1 (2 × Ph-CH), 128.1 (2 × Ph-CH), 76.3 (CH_2OCH_2), 68.7 (C_q), 52.4 (OCH_3), 43.3 (CH_2CO_2Me), 25.8 (SO_2CH_2); HRMS (APCI) *m/z* calcd for $C_{13}H_{17}SO_5^+$ $[M+H]^+$: 285.0791; found: 285.0798.

3-Phenyloxetane-3-sulfonyl fluoride (18m)



Sodium methoxide (5.4 M solution in MeOH, 0.13 mL, 0.7 mmol, 1.0 equiv) was added dropwise to a suspension of oxetane sulfone **20m** (200 mg, 0.7 mmol, 1.0 equiv) in anhydrous THF (1.4 mL, 0.5 M) in a 10 mL round bottom flask. Oxetane sulfinate salt **19m** precipitated immediately after addition of base to form a white paste (Figure 86). The reaction mixture was stirred at 25 °C for 20 min, then concentrated *in vacuo* using a rotatory evaporator to afford oxetane sulfinate **19m**, which was subjected directly to the next step without spectroscopical analysis. For the fluorination step, Selectfluor (372 mg, 1.06 mmol, 1.5 equiv) was added to anhydrous MeOH (3.6 mL, 0.2 M) at 0 °C in a 25 mL round bottom flask, then stirred for 5 min. Sulfinate salt **19m** was added portionwise. The reaction mixture was stirred at 0 °C for 1 h, then concentrated *in vacuo* using a rotatory evaporator. The residue was diluted with CH_2Cl_2 (10 mL) and filtered through a plug of Celite, eluting with further CH_2Cl_2. After concentration *in*

vacuo using a rotatory evaporator, purification by flash column chromatography through a very short column (80% CH_2Cl_2/pentane) afforded oxetane sulfonyl fluoride **18m** as white crystals (91.1 mg, 60%). R_f = 0.52 (80% CH_2Cl_2/pentane); mp = 67 °C; IR (film)/cm^{-1} 2967, 2990, 1491, 1400 (SO_2 st as), 1215 (SO_2 st sy), 999, 932, 790, 567, 540; ^{1}H NMR (400 MHz, $CDCl_3$) δ 7.53–7.48 (m, 3 H, 3 × Ph-CH), 7.32–7.28 (m, 2 H, 2 × Ph-CH), 5.46 (d, *J* = 8.0 Hz, 2 H, C*H*HOC*H*H), 5.29 (d, ^2J = 8.0 Hz, J_{HF} = 1.6 Hz, 2 H, CH*H*OCH*H*); ^{13}C NMR (101 MHz, $CDCl_3$) δ 131.7 (Ph-C_qC_q), 130.1 (Ph-CH), 129.2 (2 × Ph-CH), 128.1 (2 × Ph-CH), 77.0 (CH_2OCH_2), 68.3 (d, $^2J_{CF}$ = 15.0 Hz, C_q); ^{19}F NMR (377 MHz, $CDCl_3$) δ 35.1; HRMS (EI) *m/z* calcd for $C_9H_9FSO_3^{\cdot+}$ $[M–e]^{\cdot+}$: 216.0251; found: 216.0287 (error: 17 ppm); also: *m/z* calcd for $C_9H_9O^+$ $[M–SO_2F]^+$: 133.0648; found: 133.0635 (error: 10 ppm).

Notes:

***18m** did not ionise well and a tractable ion could only be found using a hard ionisation technique (EI) with a relatively high error (10 or 17 ppm). Further evidence for the structure of oxetane **18m** was provided by X-ray crystallography (see Figure 28).*

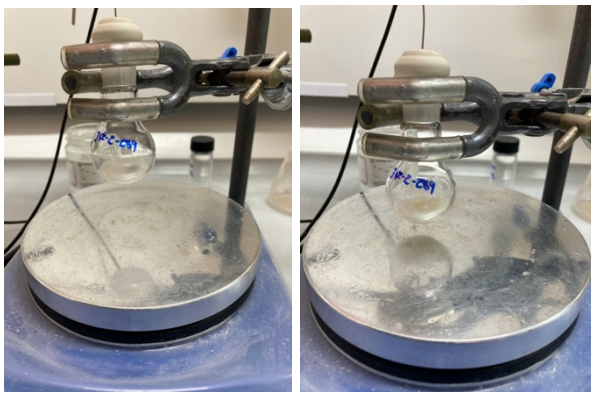


Figure 86. Appearance of reaction mixture before (left) and after (right) addition of base.

7.6.4 Reactions of Oxetane Sulfonyl Fluorides and Related Compounds

General Procedure A

A reaction tube was charged with anhydrous K_2CO_3 (36 mg, 0.26 mmol, 1.3 equiv) and flame-dried under air. The tube was allowed to cool to room temperature (ca. 22 ºC) and the nucleophile (0.24 mmol, 1.2 equiv) and oxetane sulfonyl fluoride (0.20 mmol, 1.0 equiv) were added sequentially. The reaction vessel was sealed, anhydrous acetonitrile (0.66 mL, 0.3 M) was added by syringe and the reaction mixture was stirred at 60 ºC for 2 h. After allowing the tube cool to room temperature (ca. 22 ºC), EtOAc (5 mL) was added and the mixture was filtered through a plug of Celite, eluting with further EtOAc (3 × 10 mL). The solvent was removed *in vacuo* using a rotatory evaporator and purification by flash column chromatography afforded the desired 3,3-disubstituted oxetane.

General Procedure B

As **General Procedure A** but performed under Ar and using 2.0 equiv of nucleophile (0.40 mmol). This procedure was used for hindered nucleophiles such as *t*-$BuNH_2$.

General Procedure C

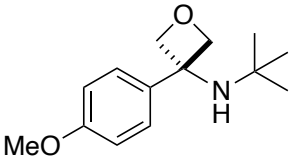
As **General Procedure A** but using 2.6 equiv of K_2CO_3 (72 mg, 0.52 mmol). This procedure was used for ammonium salts as nucleophiles (RNH_3X), typically as the HCl-amine salt.

General Procedure D

A reaction tube was charged with anhydrous K_2CO_3 (18.0 mg, 0.13 mmol, 1.3 equiv) and flame-dried under air. The tube was allowed to cool to room temperature (ca. 22 ºC) and the nucleophile (0.10 mmol, 1.0 equiv) and oxetane sulfonyl fluoride (0.12 mmol, 1.2 equiv) were added sequentially. The reaction vessel was sealed, anhydrous acetonitrile (0.33 mL, 0.3 M) was added by syringe and the reaction mixture was stirred at 60 ºC for 2 h. After allowing the tube cool to room temperature (ca. 22 ºC), EtOAc (5 mL) was added and the mixture was filtered through a plug of Celite, eluting with further EtOAc (3 × 10 mL). The solvent was removed *in vacuo* using a rotatory evaporator and purification by flash column chromatography afforded the desired 3,3-disubstituted oxetane. This procedure was used for the late-stage functionalisation of amine-containing drugs.

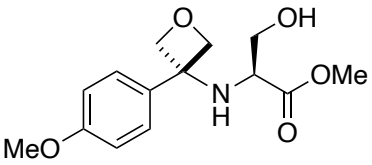
7.6.4.1 Amino-oxetanes

_N_-(_tert_-Butyl)-3-(4-methoxyphenyl)oxetan-3-amine (45)



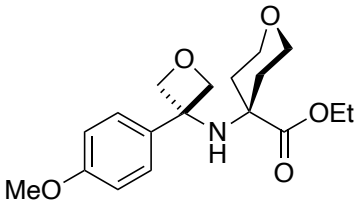
Prepared according to **General Procedure B** and using oxetane sulfonyl fluoride **18a** (49.2 mg) and 2-methylpropan-2-amine (42 μL). Purification by flash-column chromatography (0–35% Et_2O/CH_2Cl_2) afforded oxetane amine **45** as a white solid (38.6 mg, 82%). R_f = 0.08 (10–100% Et_2O/CH_2Cl_2); mp = 51 °C; IR (film)/cm^{-1} 3317 (weak, NH), 2960, 2870, 1614, 1584, 1513, 1461, 1361, 1308, 1245, 1178, 1115, 1036, 984, 910, 835, 809, 734, 675; ^{1}H NMR (400 MHz, $CDCl_3$) δ 7.41–7.37 (m, 2 H, 2 × Ar-CH), 6.92–6.88 (m, 2 H, 2 × Ar-CH), 4.97 (d, *J* = 6.7 Hz, 2 H, C*H*HOC*H*H), 4.75 (d, *J* = 6.7 Hz, 2 H, CH*H*OCH*H*), 3.83 (s, 3 H, OCH_3), 1.87 (br s, 1 H, NH), 0.85 (s, 9 H, 3 × CH_3); ^{13}C NMR (101 MHz, $CDCl_3$) δ 158.6 (Ar-C_qOMe), 135.9 (Ar-C_qC_q), 128.5 (2 × Ar-CH), 113.5 (2 × Ar-CH), 85.8 (CH_2OCH_2), 62.4 (Ar-C_qC_q), 55.2 (OCH_3), 51.9 (HNC_q), 31.2 (3 × CH_3); HRMS (ESI) *m/z* calcd for $C_{14}H_{22}NO_2$ [M+H]: 236.1651; found: 236.1643.

Methyl (3-(4-methoxyphenyl)oxetan-3-yl)-_L_-serinate (46)



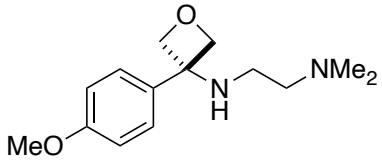
Prepared according to **General Procedure C** and using oxetane sulfonyl fluoride **18a** (49.2 mg) and *L*-serine methyl ester hydrochloride (37.7 mg). Purification by flash-column chromatography (0–5% $MeOH/CH_2Cl_2$) afforded oxetane amine **46** as a light-yellow oil (42.6 mg, 76%). $[a]_D^{16}$ –26.3 (c 1.1, $CHCl_3$); R_f = 0.17 (5% $MeOH/CH_2Cl_2$); IR (film)/cm^{-1} 3429 (OH and NH st, br), 2952, 2878, 1733 (C=O st), 1610, 1517, 1461, 1334, 1297, 1249, 1178, 1029, 980, 910, 835; ^{1}H NMR (400 MHz, $CDCl_3$) δ 7.21–7.17 (m, 2 H, 2 × Ar-CH), 6.93–6.89 (m, 2 H, 2 × Ar-CH), 5.05 (d, *J* = 6.5 Hz, 1 H, C*H*HOCH_2), 4.92 (d, *J* = 6.5 Hz, 1 H, CH_2OC*H*H), 4.75 (d, *J* = 6.5 Hz, 1 H, CH*H*OCH_2), 4.72 (d, *J* = 6.5 Hz, 1 H, CH_2OCH*H*), 3.82 (s, 3 H, Ar-OCH_3), 3.64 (s, 3 H, CO_2CH_3), 3.50 (d, *J* = 5.4 Hz, 2 H, C*H*$_2$OH), 3.36 (t, *J* = 5.5 Hz, 1 H, CH), 2.67 (br s, 2 H, NH + OH); ^{13}C NMR (101 MHz, $CDCl_3$) δ 173.9 (C_q=O), 159.0 (Ar-C_qOMe), 133.9 (Ar-C_qC_q), 127.6 (2 × Ar-CH), 114.1 (2 × Ar-CH), 82.9 (CH_2OCH_2), 81.9 (*C*H_2OCH_2), 63.3 (CH_2OH), 62.7 (Ar-C_qC_q), 57.8 (CH), 55.3 (Ar-OCH_3), 52.4 (CO_2CH_3); HRMS (ESI) *m/z* calcd for $C_{14}H_{20}NO_5$ [M+H]: 282.1341, found: 282.1345.

Ethyl 4-((3-(4-methoxyphenyl)oxetan-3-yl)amino)tetrahydro-2H-pyran-4-carboxylate (47)



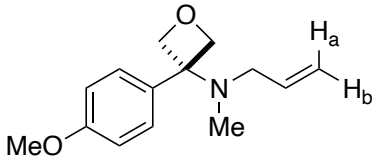
Prepared according to **General Procedure B** using oxetane sulfonyl fluoride **18a** (49.2 mg) and ethyl 4-aminotetrahydro-2H-pyran-4-carboxylate (69.3 mg). Purification by flash column chromatography (50% EtOAc/pentane) afforded oxetane amine **47** as a colourless oil (30.1 mg, 45%). R_f = 0.15 (50% EtOAc/pentane); ^{1}H NMR (400 MHz, $CDCl_3$) δ 7.34–7.27 (m, 2 H, 2 × Ar-CH), 6.93–6.85 (m, 2 H, 2 × Ar-CH), 4.91 (d, *J* = 6.5 Hz, 2 H, C*H*HO$_{(oxetane)}$C*H*H), 4.76 (d, *J* = 6.5 Hz, 2 H, CH*H*O$_{(oxetane)}$CH*H*), 3.97 (q, *J* = 7.2 Hz, 2 H, OC*H*$_2$CH$_3$), 3.82 (s, 3 H, OCH$_3$), 3.76 (ddt, *J* = 15.4, 6.0, 3.0 Hz, 2 H, C*H*HO$_{(THP)}$C*H*H), 3.36 (ddt, *J* = 11.6, 8.5, 3.8 Hz, 2 H, CH*H*O$_{(THP)}$CH*H*), 2.28 (br s, 1 H, NH), 1.86–1.76 (m, 2 H, O$_{(THP)}$(CH$_2$C*H*H)$_2$), 1.47 (ddd, *J* = 13.0, 8.5, 3.8 Hz, 2 H, O$_{(THP)}$(CH$_2$CH*H*)$_2$), 1.25 (t, *J* = 7.1 Hz, 3 H, OCH$_2$C*H*$_3$). The observed characterisation data (R_f, ^{1}H) were consistent with that observed previously in the group.[212]

***N*-(3-(4-Methoxyphenyl)oxetan-3-yl)-*N'*,N'-dimethylethane-1,2-diamine (29)**



Prepared according to **General Procedure A** using oxetane sulfonyl fluoride **18a** (49.2 mg) and *N*,*N*-dimethylethane-1,2-diamine (21.2 mg). Purification by flash column chromatography (90:8:2, CH_2Cl_2: MeOH: Et_3N) afforded oxetane amine **29** as a yellow gum (21.8 mg, 44% [isolated with ca. 20% unknown impurities]). R_f = 0.44 (90:8:2, CH_2Cl_2: MeOH: Et_3N); ^{1}H NMR (400 MHz, $CDCl_3$) δ 7.31–7.28 (m, 2 H, 2 × Ar-CH), 6.93–6.91 (m, 2 H, 2 × Ar-CH), 4.95 (d, *J* = 6.3 Hz, 2 H, C*H*HOC*H*H), 4.75 (d, *J* = 6.3 Hz, 2 H, CH*H*OCH*H*), 3.83 (s, 3 H, OCH$_3$), 2.55 (br s, 4 H, NCH$_2$CH$_2$), 2.36 (s, 6 H, 2 × NCH$_3$). The observed characterisation data (R_f, ^{1}H) were consistent with that observed previously in the group.[210]

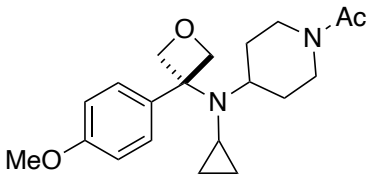
***N*-Allyl-3-(4-methoxyphenyl)-*N*-methyloxetan-3-amine (48)**



Prepared according to **General Procedure A** under air with a Celite workup and using oxetane sulfonyl fluoride **18a** (49.2 mg) and *N*-methylprop-2-en-1-amine (17.1 mg). Purification by flash column chromatography (8–12% acetone/pentane) afforded oxetane amine **48** as a white solid (28.0 mg, 60%). R_f = 0.12 (10% acetone/pentane); mp = 59–61 °C; IR (film)/cm^{-1} 3027, 2941, 2870, 2781, 1610 (C=C st), 1577, 1513, 1446, 1413, 1349, 1297, 1249, 1178, 1118, 1062, 1021, 988, 932, 813, 779, 731, 667; ^{1}H NMR (400 MHz, $CDCl_3$) δ 7.06–7.03 (m, 2 H, 2 × Ar-CH), 6.94–6.90 (m, 2 H, 2 × Ar-CH),

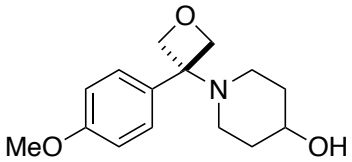
5.85 (ddt, $^3J_{trans}$ = 16.8 Hz, $^3J_{cis}$ = 10.4 Hz, ^3J = 6.4 Hz, 1 H, *H*C=CH$_2$), 5.14–5.11 (br m, 1 H, H$_a$), 5.10–5.09 (br m, 1 H, H$_b$), 4.90 (d, *J* = 5.9 Hz, 2 H, C*H*HOC*H*H), 4.88 (d, *J* = 5.9 Hz, 2 H, CH*H*OCH*H*), 3.84 (s, 3 H, OCH$_3$), 2.71 (br d, *J* = 6.4 Hz, 2 H, CH$_2$N), 2.01 (s, 3 H, NCH$_3$); ^{13}C NMR (101 MHz, CDCl$_3$) δ 158.6 (Ar-C$_q$OMe), 136.1 (H*C*=CH$_2$), 129.3 (Ar-*C*$_q$C$_q$), 128.5 (2 × Ar-CH), 117.4 (HC=*C*H$_2$), 113.1 (2 × Ar-CH), 80.5 (CH$_2$OCH$_2$), 66.6 (C$_q$), 55.3 (OCH$_3$), 54.3 (CH$_2$N), 34.8 (NCH$_3$); HRMS (ESI) *m/z* calcd for C$_{14}$H$_{20}$NO$_2$ [M+H]: 234.1494, found: 234.1497.

1-(4-(Cyclopropyl(3-(4-methoxyphenyl)oxetan-3-yl)amino)piperidin-1-yl)ethan-1-one (49)



Prepared according to **General Procedure B** and using oxetane sulfonyl fluoride **18a** (49.2 mg) and 1-(4-(cyclopropylamino)piperidin-1-yl)ethan-1-one (72.9 mg). Purification by flash chromatography (40% acetone/hexane) afforded oxetane amine **49** as a white solid (25.5 mg, 37%). R$_f$ = 0.24 (40% acetone/hexane); ^{1}H NMR (400 MHz, CDCl$_3$) δ 7.38–7.34 (m, 2 H, 2 × Ar-CH), 6.93–6.91 (m, 2 H, 2 × Ar-CH), 5.09 (d, *J* = 5.4 Hz, 1 H, C*H*HOCH$_2$), 5.08 (d, *J* = 5.4 Hz, 1 H, CH*H*OCH$_2$), 4.81 (d, *J* = 5.7 Hz, 1 H, CH$_2$OC*H*H), 4.78 (d, *J* = 5.7 Hz, 1 H, CH$_2$OCH*H*), 4.56 (ddt, *J* = 13.3, 4.7, 2.6 Hz, 1 H, C*H*HNCH$_2$), 3.84 (s, 3 H, OCH$_3$), 3.72–3.69 (m, 1 H, CH$_2$NC*H*H), 2.87 (td, *J* = 13.1, 2.4 Hz, 1 H, CH*H*NCH$_2$), 2.56–2.46 (m, 1 H, C$_{(piperidine)}$H), 2.33 (td, *J* = 13.1, 2.6 Hz, 1 H, CH$_2$NCH*H*), 2.04 (s, 3 H, C(O)CH$_3$), 1.74–1.67 (m, 1 H, C$_{(cyclopropyl)}$H), 1.59–1.50 (m, 2 H, 2 × C*H*HC$_{(piperidine)}$H), 1.34 (d, *J* = 12.8 Hz, 2 H, 2 × CH*H*C$_{(piperidine)}$H), 0.55–0.48 (m, 4 H, 2 × C$_{(cyclopropyl)}$H$_2$). The observed characterisation data (R$_f$, ^{1}H) were consistent with that observed previously in the group.[285]

1-(3-(4-Methoxyphenyl)oxetan-3-yl)piperidin-4-ol (51)



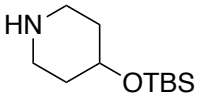
Prepared according to **General Procedure A** and using oxetane sulfonyl fluoride **18a** (49.2 mg) and piperidin-4-ol (24.4 mg). Purification by flash column chromatography (1–5% MeOH/CH$_2$Cl$_2$) afforded oxetane amine **51** as a white solid (26.3 mg, 50%). R$_f$ = 0.28 (10% MeOH/CH$_2$Cl$_2$); mp = 126 °C; IR (film)/cm^{-1} 3399 (OH st, br), 2941, 2837, 1610, 1513, 1465, 1368, 1297, 1245, 1179, 1145, 1118, 1081, 1029, 992, 929, 924, 835, 760, 731; ^{1}H NMR (400 MHz, CDCl$_3$) δ 7.00–6.96 (m, 2 H, 2 × Ar-CH), 6.92–6.88 (m, 2 H, 2 × Ar-CH), 4.89 (d, *J* = 5.8 Hz, 2 H, C*H*HOC*H*H), 4.85 (d, *J* = 5.8 Hz, 2 H, CH*H*OCH*H*), 3.83 (s, 3 H, OCH$_3$), 3.52–3.49 (br m, 1 H, CH), 2.60–2.58 (br m, 2 H, C*H*$_{eq}$HNC*H*$_{eq}$H), 1.94–1.84 (br m, 4 H, CH*H*$_{ax}$NCH*H*$_{ax}$ + C*H*$_{eq}$HCHC*H*$_{eq}$H), 1.66–1.43 (m, 3 H, CH*H*$_{ax}$CHCH*H*$_{ax}$ + OH); ^{13}C NMR

(101 MHz, $CDCl_3$) δ 158.6 (Ar-C_qOMe), 129.1 (Ar-C_qC_q), 128.4 (2 × Ar-CH), 113.1 (2 × Ar-CH), 80.4 (CH_2OCH_2), 67.8 (br and weak, CH), 66.2 (C_q), 55.3 (OCH_3), 43.7 (CH_2NCH_2), 34.6 (CH_2CHCH_2); HRMS (ESI) *m/z* calcd for $C_{15}H_{22}NO_3$ [M+H]: 264.1600, found: 264.1600.

Notes:

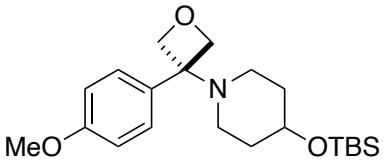
*The multiplet in the ^{1}H NMR spectrum at 1.66–1.43 ppm is a mixture of a broad singlet (1.66–1.43, OH) and a dddd (1.62, ^2J = 13.4 Hz, $^3J_{ax,ax}$ = 10.3 Hz, $^3J_{ax,ax}$ = 9.4 Hz, $^3J_{ax,eq}$ = 4.2 Hz, CH**H**$_{ax}$CHCH**H**$_{ax}$).*

4-((*tert*-Butyldimethylsilyl)oxy)piperidine (S5)[446]



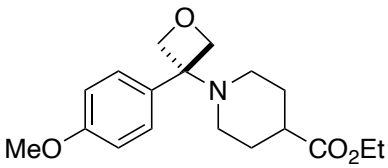
Pyridine (0.4 mL, 4.9 mmol, 1.2 equiv) was added dropwise to a solution of piperidin-4-ol (404.7 mg, 4 mmol, 1.0 equiv) in anhydrous CH_2Cl_2 (4 mL, 1 M) in a 25 mL round bottom flask at 0 °C. After stirring for 5 min, *tert*-butyldimethylsilyl trifluoromethanesulfonate (1.01 mL, 4.4 mmol, 1.1 equiv) was added dropwise at 0 °C. The reaction mixture was stirred at 0 °C for 2.5 h and then quenched with ice-cold (0 °C) distilled water (10 mL). The aqueous layer was extracted with CH_2Cl_2 (3 × 10 mL). The combined organic extracts were dried over Na_2SO_4, filtered and concentrated *in vacuo* using a rotatory evaporator. Purification by flash column chromatography (3–15% MeOH/CH_2Cl_2) afforded a mixture of the free piperidine **S5** with its triflate salt as a light-yellow solid (938 mg; presence of salt detected by ^{13}C and ^{19}F NMR). This mixture was dissolved in CH_2Cl_2 (30 mL) and washed with a saturated aqueous sodium bicarbonate solution (30 mL). The aqueous layer was extracted with CH_2Cl_2 (3 × 20 mL). The organic extracts were combined, dried over Na_2SO_4, filtered and concentrated *in vacuo* using a rotatory evaporator to again afford a mixture of the free piperidine and triflate salt. This residue was dissolved in CH_2Cl_2 (30 mL) and washed with aq. NaOH (1 M, 3 × 30 mL). The organic layer was dried over Na_2SO_4, filtered and concentrated *in vacuo* using a rotatory evaporator to afford piperidine **S5** as a light-yellow oil (470 mg, 55%). R_f = 0.24 (10% MeOH/CH_2Cl_2); IR (film)/cm^{-1} 2930, 2885, 2855, 1468, 1361, 1316, 1252, 1103, 1051, 1178, 1003, 910, 835, 775, 734; ^{1}H NMR (400 MHz, $CDCl_3$) δ 3.74 (tt, $^3J_{ax,ax}$ = 8.8 Hz, $^3J_{ax,eq}$ = 3.9 Hz, 1 H, CH), 3.07 (ddd, ^2J = 12.7 Hz, $^3J_{eq,eq}$ and $^3J_{eq,ax}$ = 3.9 Hz, 2 H, CH_{eq}HNCH_{eq}H), 2.61 (ddd, ^2J = 12.7 Hz, $^3J_{ax,ax}$ = 9.6 Hz, $^3J_{ax,eq}$ = 3.1 Hz, 2 H, CHH_{ax}NCHH_{ax}), 1.80–1.74 (br m, 2 H, CH_{eq}HCHCH_{eq}H), 1.55 (br s, 1 H, NH) 1.43 (dddd, ^2J = 13.0 Hz, $^3J_{ax,ax}$ = 9.6 Hz, $^3J_{ax,ax}$ = 8.8 Hz, $^3J_{ax,eq}$ = 3.9 Hz, 2 H, CHH_{ax}CHCHH_{ax}), 0.90 (s, 9 H, 3 × SiCCH$_3$), 0.06 (s, 6 H, 2 × SiCH$_3$); ^{13}C NMR (101 MHz, $CDCl_3$) δ 68.5 (CH), 44.0 (CH_2NCH_2), 36.3 (CH_2CHCH_2), 25.8 (3 × SiC$_q$CH$_3$), 18.0 (SiC$_q$(CH$_3$)$_3$), -4.7 (2 × SiCH$_3$). The observed characterisation data (^{1}H, ^{13}C) were consistent with that previously reported.[447]

4-((*tert*-Butyldimethylsilyl)oxy)-1-(3-(4-methoxyphenyl)oxetan-3-yl)piperidine (52)



Prepared according to **General Procedure A** and using oxetane sulfonyl fluoride **18a** (49.2 mg) and OTBS-piperidine **S5** (51.7 mg). Purification by flash column chromatography (5–10% acetone/pentane) afforded oxetane amine **52** as a colourless oil (45.3 mg, 60%). R_f = 0.16 (10% acetone/pentane); IR (film)/cm^{-1} 2945, 2855, 1610, 1513, 1469, 1409, 1375, 1297, 1249, 1178, 1103, 1051, 992, 924, 869, 835, 775, 671; ^{1}H NMR (400 MHz, $CDCl_3$) δ 7.01–6.98 (m, 2 H, 2 × Ar-CH), 6.92–6.88 (m, 2 H, 2 × Ar-CH), 4.88 (d, *J* = 5.8 Hz, 2 H, C*H*HOC*H*H), 4.86 (d, *J* = 5.8 Hz, 2 H, CH*H*OCH*H*), 3.83 (s, 3 H, OCH_3), 3.51–3.47 (br m, 1 H, CH), 2.56–2.53 (br m, 2 H, CH_{eq}HNCH_{eq}H), 1.84 (br dd, ^2J and $^3J_{ax,ax}$ = 9.3 Hz, 2 H, CHH_{ax}NCHH_{ax}), 1.80–1.73 (br m, 2 H, CH_{eq}HCHCH_{eq}H) 1.60 (dddd, ^2J = 12.7 Hz, $^3J_{ax,ax}$ = 9.3 Hz, $^3J_{ax,ax}$ = 9.2 Hz, $^3J_{ax,eq}$ = 3.6 Hz, 2 H, CHH_{ax}CHCHH_{ax}), 0.80 (s, 9 H, 3 × SiCCH_3), –0.03 (s, (^{29}Si satellites: d, $^2J_{HSi}$ = 6.1 Hz), 6 H, 2 × SiCH_3); ^{13}C NMR (101 MHz, $CDCl_3$) δ 158.6 (Ar-C_qOMe), 129.4 (Ar-C_qC_q), 128.5 (2 × Ar-CH), 113.0 (2 × Ar-CH), 80.4 (CH_2OCH_2), 68.2 (br and weak, CHOTBS), 66.3 (Ar-C_qC_q), 55.3 (OCH_3), 43.6 (CH_2NCH_2), 35.0 (CH_2CHCH_2), 25.8 (3 × SiC_qCH$_3$), 18.0 (SiC_q(CH$_3$)$_3$), –4.7 (2 × SiCH_3); HRMS (ESI) *m/z* calcd for $C_{21}H_{36}NO_3Si$ [M+H]: 378.2464, found: 378.2468.

Ethyl 1-(3-(4-methoxyphenyl)oxetan-3-yl)piperidine-4-carboxylate (53)

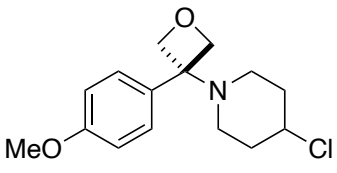


Prepared according to **General Procedure A** and using oxetane sulfonyl fluoride **18a** (49.2 mg) and ethyl piperidine-4-carboxylate (38.5 mg). Purification by flash column chromatography (30–35% EtOAc/pentane) afforded oxetane amine **53** as white crystals (47.1 mg, 74%). R_f = 0.09 (30% EtOAc/pentane); mp = 80 °C; IR (film)/cm^{-1} 2952, 2874, 2810, 1718 (C=O st), 1610, 1510, 1443, 1368, 1297, 1245, 1204, 1178, 1118, 1059, 1021, 988, 928, 816, 760; ^{1}H NMR (400 MHz, $CDCl_3$) δ 7.00–6.96 (m, 2 H, 2 × Ar-CH), 6.92–6.88 (m, 2 H, 2 × Ar-CH), 4.88 (d, *J* = 5.8 Hz, 2 H, C*H*HOC*H*H), 4.85 (d, *J* = 5.8 Hz, 2 H, CH*H*OCH*H*), 4.09 (q, *J* = 7.1 Hz, 2 H, OCH_2CH$_3$), 3.83 (s, 3 H, OCH_3), 2.73 (br d, ^2J = 10.7 Hz, 2 H, CH_{eq}HNCH_{eq}H), 2.12–2.04 (m, 1 H, CH), 1.91–1.87 (m, 2 H, CH_{eq}HCHCH_{eq}H), 1.84–1.78 (m, 2 H, CHH_{ax}CHCHH_{ax}), 1.76–1.67 (m, 2 H, CHH_{ax}NCHH_{ax}), 1.21 (t, *J* = 7.1 Hz, 3 H, OCH$_2$C*H*$_3$); ^{13}C NMR (101 MHz, $CDCl_3$) δ 174.9 (C_q=O), 158.6 (Ar-C_qOMe), 129.1 (Ar-C_qC_q), 128.4 (2 × Ar-CH), 113.0 (2 × Ar-CH), 80.3 (CH_2OCH_2), 66.3 (Ar-C_qC_q), 60.2 (OCH_2CH$_3$), 55.3 (OCH_3), 45.7 (CH_2NCH_2), 41.0 (CH), 28.3 (CH_2CHCH_2), 14.1 (OCH$_2$CH$_3$); HRMS (APCI) *m/z* calcd for $C_{18}H_{26}NO_4^+$ [M+H]$^+$: 320.1856, found: 320.1861.

Notes:

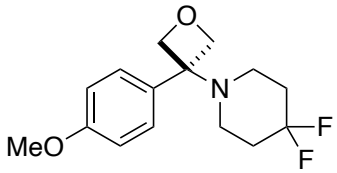
53 *was further characterised by X-ray crystallography (see Figure 34).*

4-Chloro-1-(3-(4-methoxyphenyl)oxetan-3-yl)piperidine (54)



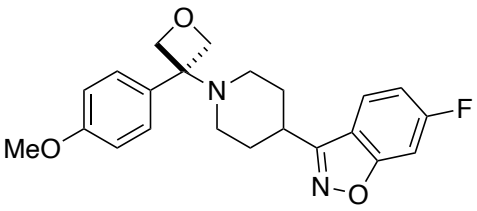
Prepared according to **General Procedure A** and using oxetane sulfonyl fluoride **18a** (49.2 mg) and 4-chloropiperidine (29.0 mg). Purification by flash column chromatography (2–3% MeOH/CH_2Cl_2) afforded oxetane amine **54** as a pale-yellow solid (43.7 mg, 78%). R_f = 0.33 (3% MeOH/ CH_2Cl_2); mp = 91–92 °C; IR (film)/cm^{-1} 2941, 2870, 2833, 2761, 1674, 1607, 1510, 1450, 1383, 1342, 1297, 1245, 1179, 1144, 1025, 988, 929, 869, 842, 734; ^{1}H NMR (400 MHz, $CDCl_3$) δ 6.99–6.96 (m, 2 H, 2 × Ar-CH), 6.93–6.89 (m, 2 H, 2 × Ar-CH), 4.89 (d, *J* = 5.9 Hz, 2 H, C*H*HOC*H*H), 4.84 (d, *J* = 5.9 Hz, 2 H, CH*H*OCH*H*), 3.97–3.73 (br s, 1 H, CH), 3.83 (s, 3 H, OCH_3), 2.59 (br s, 2 H, CH_{eq}HNCH_{eq}H), 2.14–2.09 (br m, 2 H, CH_{eq}HCHCH_{eq}H), 1.97–1.90 (br m, 4 H, CHH_{ax}NCHH_{ax} + CHH_{ax}CHCHH_{ax}); ^{13}C NMR (101 MHz, $CDCl_3$) δ 158.6 (Ar-C_qOMe), 129.0 (Ar-C_qC_q), 128.3 (2 × Ar-CH), 113.1 (2 × Ar-CH), 80.2 (CH_2OCH_2), 66.2 (C_q), 57.1 (CH), 55.3 (OCH_3), 44.4 (br and weak, CH_2NCH_2), 35.8 (CH_2CHCH_2); HRMS (APCI) *m/z* calcd for $C_{15}H_{21}{}^{35}ClNO_2^+$ $[M+H]^+$: 282.1255, found: 282.1255.

4,4-Difluoro-1-(3-(4-methoxyphenyl)oxetan-3-yl)piperidine (55)



Prepared according to **General Procedure A** and using oxetane sulfonyl fluoride **18a** (49.2 mg) and 4,4-difluoropiperidine (29.6 mg). Purification by flash column chromatography (0–10% Et_2O/CH_2Cl_2) afforded oxetane amine **55** as a white solid (46.2 mg, 82%). R_f = 0.32 (10% Et_2O/CH_2Cl_2); mp = 72–75 °C; IR (film)/cm^{-1} 2945, 2878, 2837, 1610, 1513, 1469, 1364, 1297, 1249, 1182, 1118, 1033, 995, 969, 910, 731; ^{1}H NMR (400 MHz, $CDCl_3$) δ 6.99–6.96 (m, 2 H, 2 × Ar-CH), 6.92–6.89 (m, 2 H, 2 × Ar-CH), 4.92 (d, *J* = 5.9 Hz, 2 H, C*H*HOC*H*H), 4.84 (d, *J* = 5.9 Hz, 2 H, CH*H*OCH*H*), 3.83 (s, 3 H, OCH_3), 2.33 (br t, ^3J = 5.6 Hz, 4 H, CH_2NCH_2), 2.03 (tt, $^3J_{HF}$ = 13.3 Hz, ^3J = 5.6 Hz, 4 H, $CH_2CF_2CH_2$); ^{13}C NMR (101 MHz, $CDCl_3$) δ 158.8 (Ar-C_qOMe), 128.9 (Ar-C_qC_q), 128.2 (2 × Ar-CH), 121.6 (t, $^1J_{CF}$ = 241.7 Hz, CF_2), 113.3 (2 × Ar-CH), 80.2 (CH_2OCH_2), 66.1 (Ar-C_qC_q), 55.3 (OCH_3), 43.0 (t, $^3J_{CF}$ = 5.6 Hz, CH_2NCH_2), 34.3 (t, $^2J_{CF}$ = 22.8 Hz, $CH_2CF_2CH_2$); ^{19}F NMR (377 MHz, $CDCl_3$) δ –97.5 (br); HRMS (ESI) *m/z* calcd for $C_{15}H_{20}NO_2F_2$ [M+H]: 284.1462, found: 284.1463.

6-Fluoro-3-(1-(3-(4-methoxyphenyl)oxetan-3-yl)piperidin-4-yl)benzo[*d*]isoxazole (56)

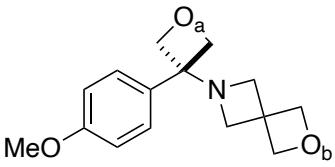


Prepared according to **General Procedure A** and using oxetane sulfonyl fluoride **18a** (49.2 mg) and 6-fluoro-3-(piperidin-4-yl)benzo[*d*]isoxazole (53.2 mg). Purification by flash column chromatography (35–50% EtOAc/pentane) afforded oxetane amine **56** as a white solid (44.3 mg, 58%). R_f = 0.25 (50% EtOAc/pentane); mp = 166 °C; IR (film)/cm^{-1} 2945, 2876, 2810, 1614, 1513, 1446, 1349, 1297, 1245, 1178, 1122, 1066, 1028, 992, 958, 924, 839, 760, 734; ^{1}H NMR (400 MHz, $CDCl_3$) δ 7.66 (dd, ^3J = 8.7 Hz, $^4J_{HF}$ = 5.1 Hz, 1 H, Ar-CFAr-CHAr-C*H*), 7.24 (ddd, $^3J_{HF}$ = 8.5 Hz, ^4J = 2.1 Hz, ^5J = 0.5 Hz, 1 H, Ar-CFAr-CH-Ar-C_q), 7.08–7.01 (m, 3 H, 2 × $Ar_{(PMP)}$-CH + Ar-CFAr-C*H*Ar-CH), 6.96–6.93 (m, 2 H, 2 × $Ar_{(PMP)}$-CH), 4.94 (d, J = 5.9 Hz, 2 H, C*H*HOC*H*H), 4.91 (d, J = 5.9 Hz, 2 H, CH*H*OCH*H*), 3.86 (s, 3 H, OCH_3), 2.94–2.91 (br m, 2 H, CH_{eq}HNCH_{eq}H), 2.90–2.84 (m, 1 H, CH), 2.19–2.09 (m, 2 H, CHH_{ax}CHCHH_{ax}), 2.07–2.03 (br m, 2 H, CH_{eq}HCHCH_{eq}H), 1.87 (ddd, ^2J and $^3J_{ax,ax}$ = 11.4 Hz, $^3J_{ax,eq}$ = 2.4 Hz, 2 H, CHH_{ax}NCHH_{ax}); ^{13}C NMR (101 MHz, $CDCl_3$) δ 164.0 (d, $^1J_{CF}$ = 250.5 Hz, Ar-CF), 163.8 (d, $^3J_{CF}$ = 13.3 Hz, OAr-C_qCH), 160.9 (C_q=N), 158.7 (Ar-C_qOMe), 129.0 ($Ar_{(PMP)}$-C_qC_q), 128.5 (2 × $Ar_{(PMP)}$-CH), 122.5 (d, $^3J_{CF}$ = 11.2 Hz, Ar-CFAr-CHAr-*C*H), 117.2 (OAr-C_qAr-C_q), 113.1 (2 × $Ar_{(PMP)}$-CH), 112.3 (d, $^2J_{CF}$ = 25.2 Hz, Ar-CFAr-*C*HAr-CH), 97.4 (d, $^2J_{CF}$ = 26.5 Hz, Ar-CFAr-*C*HAr-C_q), 80.3 (CH_2OCH_2), 66.4 (C_q), 55.3 (OCH_3), 46.3 (CH_2NCH_2), 34.5 (CH), 30.6 (CH_2CHCH_2); ^{19}F NMR (377 MHz, $CDCl_3$) δ –109.7; HRMS (ESI) *m/z* calcd for $C_{22}H_{24}N_2O_3F$ [M+H]: 383.1771, found: 383.1775.

Notes:

*Amino-oxetane **56** was further characterised by X-ray crystallography (see Figure 34).*

6-(3-(4-Methoxyphenyl)oxetan-3-yl)-2-oxa-6-azaspiro[3.3]heptane (57)



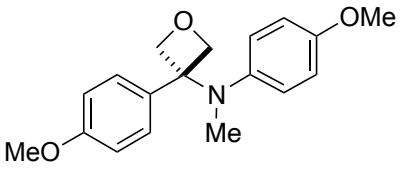
Prepared according to **General Procedure A** and using oxetane sulfonyl fluoride **18a** (49.2 mg) and 2-oxa-6-azaspiro[3.3]heptane (24.0 mg). Purification by flash column chromatography (20–90% Et_2O/CH_2Cl_2, then 1–4% MeOH/Et_2O) afforded oxetane amine **57** as a white solid (33.8 mg, 65%). R_f = 0.10 (1% MeOH/Et_2O); mp = 87–89 °C; IR (film)/cm^{-1} 2945, 2866, 1610, 1513, 1461, 1342, 1301, 1249, 1179, 1143, 1103, 1033, 977, 831; ^{1}H NMR (400 MHz, $CDCl_3$) δ 7.19–7.15 (m, 2 H, 2 × Ar-CH), 6.92–6.89 (m, 2 H, 2 × Ar-CH), 4.86–4.82 (m, 4 H, $CH_2O_aCH_2$), 4.77 (s, 4 H, $CH_2O_bCH_2$), 3.82 (s, 3 H, OCH_3), 3.51 (s, 4 H, CH_2NCH_2); ^{13}C NMR (101 MHz, $CDCl_3$) δ 158.8 (Ar-C_qOMe), 132.6 (Ar-C_qC_q), 127.4 (2 × Ar-CH), 113.7 (2 × Ar-CH), 81.4 ($CH_2O_bCH_2$), 77.6 ($CH_2O_aCH_2$), 65.2 (Ar-C_qC_q), 57.2 (CH_2NCH_2), 55.2

(OCH_3), 37.7 (C_qCH_2N); HRMS (ESI) *m/z* calcd for $C_{15}H_{20}NO_3$ [M+H]: 262.1443, found: 262.1437.

Notes:

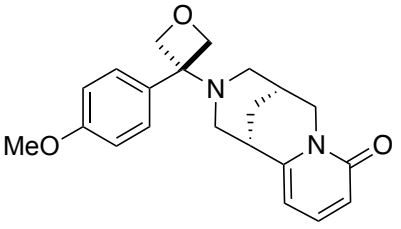
*The multiplet in the ^{1}H NMR spectrum at 4.86–4.82 ppm is likely to be two separate doublets (C**H**HO$_a$C**H**H and CH**H**O$_a$CH**H**) with J = 6.9 Hz.*

_N_,3-bis(4-Methoxyphenyl)-_N_-methyloxetan-3-amine (58)



Prepared according to **General Procedure A** and using oxetane sulfonyl fluoride **18a** (49.2 mg) and 4-methoxy-*N*-methylaniline (33.0 mg). Purification by flash column chromatography (5% acetone/pentane) afforded oxetane amine **58** with 20% of an unknown impurity as a light-yellow gum (55.9 mg). Repurification of the mixture by flash column chromatography (5–10% acetone/pentane) afforded oxetane fluoride **58** as a light-yellow gum (47.0 mg, 78%). R_f = 0.11 (10% acetone/pentane); IR (film)/cm^{-1} 2997, 2952, 2878, 2833, 2248, 1610, 1510, 1461, 1349, 1297, 1241, 1178, 1133, 1070, 1033, 992, 906, 816, 723; ^{1}H NMR (400 MHz, $CDCl_3$) δ 7.45–7.41 (m, 2 × Ar-CH), 6.94–6.90 (m, 2 × Ar-CH), 6.80–6.75 (m, 2 × Ar-CH), 6.29–7.25 (m, 2 × Ar-CH), 5.12 (d, *J* = 6.1 Hz, C*H*HOC*H*H), 4.70 (d, *J* = 6.1 Hz, CH*H*OCH*H*), 3.82 (s, 3 H, OCH_3), 3.75 (s, 3 H, OCH_3), 2.99 (s, 3 H, NCH_3); ^{13}C NMR (101 MHz, $CDCl_3$) δ 158.8 ($Ar_{(PMP)}$-C_qOMe), 151.5 ($Ar_{(Aniline)}$-C_qOMe), 141.4 (Ar-C_qN), 134.1 (Ar-C_qC_q), 126.9 (2 × Ar-CH), 114.6 (2 × Ar-CH), 114.2 (2 × Ar-CH), 114.0 (2 × Ar-CH), 82.8 (CH_2OCH_2), 64.8 (C_q), 55.6 (OCH_3), 55.2 (OCH_3), 35.8 (NCH_3); HRMS (ESI) *m/z* calcd for $C_{18}H_{22}NO_3$ [M+H]: 300.1600, found: 300.1589.

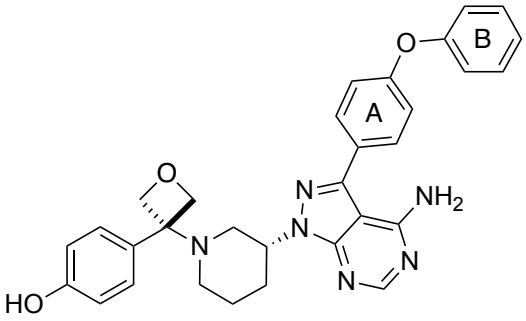
(1_R_,5_S_)-3-(3-(4-Methoxyphenyl)oxetan-3-yl)-1,2,3,4,5,6-hexahydro-8_H_-1,5-methanopyrido[1,2-_a_][1,5]diazocin-8-one (59)



Prepared according to **General Procedure D** and using oxetane sulfonyl fluoride **18a** (29.7 mg) and cytisine (19.2 mg). Purification by flash column chromatography (0–4% MeOH/EtOAc) afforded oxetane amine **59** as a colourless gum (27.1 mg, 77%) which solidified to a pale-yellow solid. $[\alpha]_D^{21}$ –110.0 (c 1, $CDCl_3$); R_f = 0.19 (2% MeOH/EtOAc); mp = 175–180 °C; IR (film)/cm^{-1} 2941, 2870, 2810, 1651 (C=O st), 1610, 1547, 1469, 1357, 1297, 1249, 1178, 1144, 1115, 1059, 1029, 988, 947, 917, 831, 798, 731; ^{1}H NMR (400 MHz, $CDCl_3$) δ 7.31 (dd, *J* = 9.0, 6.8 Hz, 1 H, C*H*CHC$_q$=O), 6.96–6.92 (m, 2 H, 2 × Ar-CH), 6.90–6.85 (m, 2 H, 2 × Ar-CH), 6.50 (dd, ^3J = 9.0 Hz, ^4J = 1.4 Hz, 1 H, CHC$_q$=O), 5.97 (dd, ^3J = 6.8 Hz, ^4J = 1.4 Hz, 1 H,

C*H*CHCHC$_q$=O), 4.76 (d, *J* = 5.9 Hz, 1 H, C*H*HOCH$_2$), 4.70 (d, *J* = 5.9 Hz, 1 H, CH*H*OCH$_2$), 4.68 (d, *J* = 5.8 Hz, 1 H, CH$_2$OC*H*H), 4.44 (d, *J* = 5.8 Hz, 1 H, CH$_2$OCH*H*), 4.07 (d, *J* = 15.3 Hz, 1 H, C*H*HNC$_q$=O), 3.95 (dd, ^2J = 15.3 Hz, ^3J = 6.6 Hz, 1 H, CH*H*NC$_q$=O), 3.81 (s, 3 H, OCH$_3$), 2.92 (br s, 1 H, CHC$_q$N), 2.82 (br d, *J* = 10.9 Hz, 1 H, NC*H*HCHCH$_2$NC$_q$=O), 2.71 (br d, *J* = 10.5 Hz, 1 H, NC*H*HCHC$_q$), 2.42 (br s, 1 H, C*H*CH$_2$NC$_q$=O), 2.08–2.02 (m, 2 H, CH*H*NCH*H*), 1.83 (br d, *J* = 12.8 Hz, 1 H, C$_{(bridge)}$*H*H), 1.60 (br d, *J* = 12.8 Hz, 1 H, C$_{(bridge)}$H*H*); ^{13}C NMR (101 MHz, CDCl$_3$) δ 163.6 (C$_q$=O), 158.7 (Ar-C$_q$OMe), 151.2 (*C*$_q$NC$_q$=O), 138.6 (*C*HCHC$_q$=O), 129.3 (Ar-*C*$_q$C$_q$), 128.1 (2 × Ar-CH), 116.8 (*C*HC$_q$=O), 113.2 (2 × Ar-CH), 104.5 (*C*HCHCHC$_q$=O), 79.7 (*C*H$_2$OCH$_2$), 79.4 (CH$_2$O*C*H$_2$), 65.5 (Ar-C$_q$*C*$_q$), 55.2 (OCH$_3$), 53.7 (N*C*H$_2$CHC$_q$), 52.9 (N*C*H$_2$CHCH$_2$NC$_q$=O), 49.8 (*C*H$_2$NC$_q$=O), 35.1 (*C*HC$_q$N), 27.6 (*C*HCH$_2$NC$_q$=O), 25.6 (C$_{(bridge)}$H$_2$); HRMS (ESI) *m/z* calcd for C$_{21}$H$_{25}$N$_2$O$_3$ [M+H]: 353.1865, found: 353.1877.

(*R*)-4-(3-(3-(4-Amino-3-(4-phenoxyphenyl)-1*H*-pyrazolo[3,4-*d*]pyrimidin-1-yl)piperidin-1-yl)oxetan-3-yl)phenol (60)



Prepared according to **General Procedure D** and using oxetane sulfonyl fluoride **18c** (46.6 mg) and ibrutinib N-1 (38.6 mg). Purification by flash column chromatography (0–10% MeOH/EtOAc) afforded oxetane amine **60** as a white solid (18.9 mg, 35%). $[\alpha]_D^{21}$ +30.0 (c 1, MeOH); R$_f$ = 0.18 (100% EtOAc); mp = 152–156 °C; IR (film)/cm^{-1} 3481, 3321 (OH and NH$_2$ st, br), 3191, 2945, 2878, 2818, 1618, 1521, 1487, 1372, 1312, 1238, 1200, 1141, 1107, 1051, 984, 947, 872, 805, 757, 727, 693; ^{1}H NMR (500 MHz, CDCl$_3$) δ 8.39 (br s, 1 H, NAr-CHN), 7.60–7.58 (m, 2 H, 2 × Ar$_{(A)}$-CH), 7.39–7.35 (m, 2 H, 2 × Ar$_{(B)}$-CH), 7.16 (tt, ^3J = 7.5 Hz, ^4J = 1.1 Hz, 1 H, Ar$_{(B)}$-CH), 7.13–7.10 (m, 2 H, 2 × Ar$_{(A)}$-CH), 7.07–7.04 (m, 2 H, 2 × Ar$_{(B)}$-CH), 6.91 (br d, *J* = 8.5 Hz, 2 H, 2 × Ar$_{(phenol)}$-CH), 6.79 (br d, *J* = 8.5 Hz, 2 H, 2 × Ar$_{(phenol)}$-CH), 5.80 (br s, 3 H, OH and NH$_2$), 5.06 (dddd, $^3J_{ax,ax}$ = 10.5, 10.5 Hz, $^3J_{ax,eq}$ = 4.2, 4.2 Hz, 1 H, CH), 4.94 (d, *J* = 5.9 Hz, 1 H, C*H*HOCHH), 4.90 (d, *J* = 5.9 Hz, 1 H, CHHOC*H*H), 4.88 (d, *J* = 5.9 Hz,1 H, CHHOCH*H*), 4.83 (d, *J* = 5.9 Hz, 1 H, CH*H*OCHH), 3.02 (dd, ^2J = 10.5 Hz, $^3J_{eq,ax}$ = 4.2 Hz, 1 H, NC*H*$_{eq}$HCH), 2.80–2.73 (m, 1 H, NC*H*HCH$_2$), 2.31 (dd, ^2J = 10.5 Hz, $^3J_{ax,ax}$ = 10.5 Hz, 1 H, NCH*H*$_{ax}$CH), 2.06–1.98 (m, 2 H, NCH$_2$C*H*$_2$), 1.87–1.81 (m, 3 H, NCH*H*CH$_2$C*H*$_2$); ^{13}C NMR (126 MHz, CDCl$_3$) δ 158.5 (Ar$_{(A)}$-*C*$_q$OAr$_{(B)}$-C$_q$), 157.6 (br and weak, Ar$_{(het)}$-C), 156.3 (Ar$_{(A)}$-C$_q$OAr$_{(B)}$-*C*$_q$), 155.4 (Ar-C$_q$OH), 154.9 (br and weak, Ar$_{(het)}$-C), 153.7 (Ar$_{(het)}$-C), 143.8 (Ar-*C*$_q$Ar$_{(A)}$-C$_q$), 129.9 (2 × Ar$_{(A)}$-CH and 2 × Ar$_{(B)}$-CH), 128.9 (Ar$_{(phenol)}$-*C*$_q$C$_q$), 128.5 (2 × Ar$_{(phenol)}$-CH), 127.6 (Ar-C$_q$Ar$_{(A)}$-*C*$_q$), 124.0

($Ar_{(B)}$-CH), 119.5 (2 × $Ar_{(B)}$-CH), 119.1 (2 × $Ar_{(A)}$-CH), 114.9 (2 × $Ar_{(phenol)}$-CH), 98.6 (weak, H_2NAr-C_qAr-C_q), 80.4 (CH_2OCH_2), 80.1 (CH_2OCH_2), 66.3 (C_q), 54.5 (CH), 51.1 (NCH_2CH), 45.9 (NCH_2CH_2), 29.6 ($CHCH_2CH_2$), 24.6 (NCH_2CH_2); HRMS (ESI) *m/z* calcd for $C_{31}H_{31}N_6O_3$ [M+H]: 535.2458, found: 535.2451.

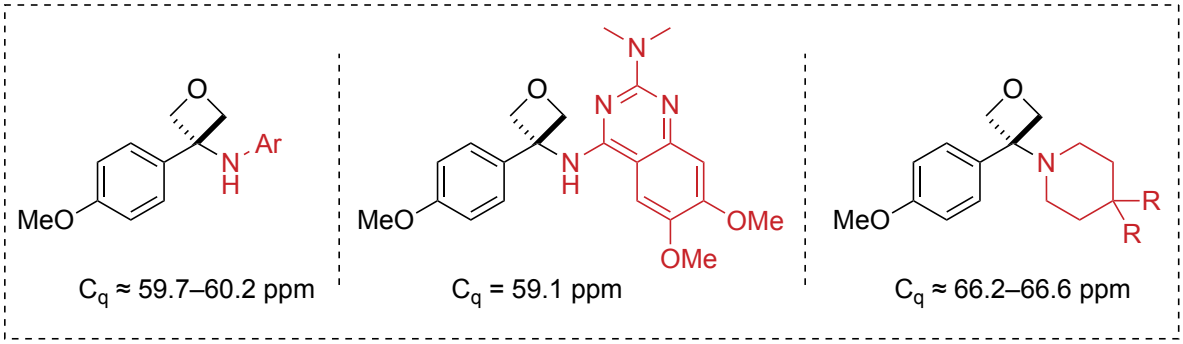
Notes

Due to chemical exchange, the OH and NH_2 signals appeared as one very broad peak with a lower integration (~2.5 H).

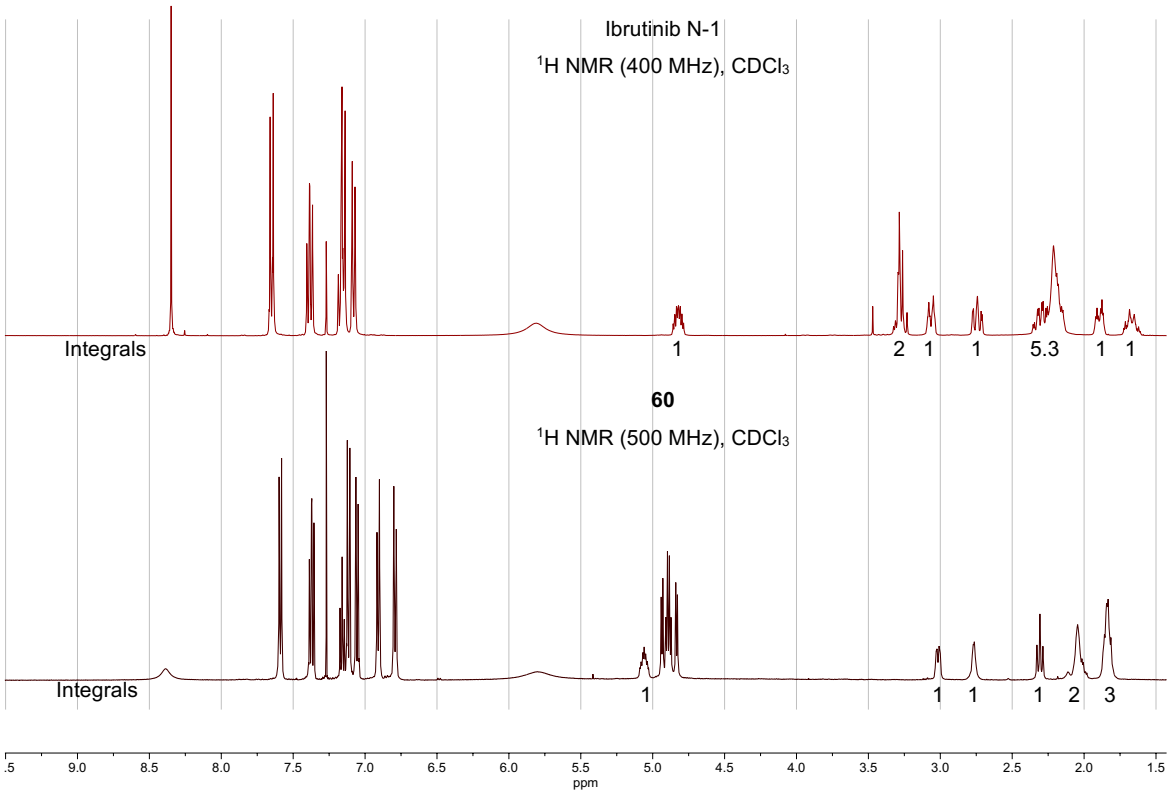
The ^{13}C NMR signal at 98.6 ppm was very weak due to chemical exchange, presumably caused by tautomerism of the pyrazolopyrimidine. A stronger signal could not be obtained even at a very high NMR sample concentration and number of scans (ns = 12'288). The identity of this signal was supported by the presence of a signal at 98.4 ppm in the measured spectrum of ibrutinib N-1 (vide infra).

*The reaction of ibrutinib N-1 with OSF **18c** through the piperidine (as per the suggested structure of oxetane **60**) and not through the heteroaromatic amine is proposed based on the observed analytical data:*

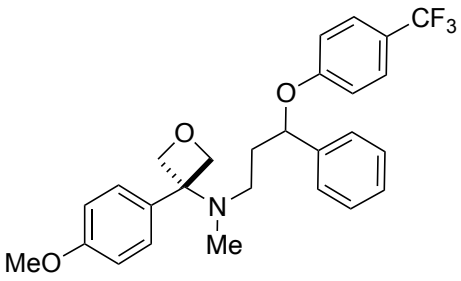
- *The chemical shift of the oxetane C_q (66.3 ppm) is in line with the observed chemical shift of other oxetane-piperidines and is significantly different from the chemical shift of (hetero)aromatic aminooxetanes.*



- *The piperidine region of the ^1H NMR spectrum of **60** is very different from that of ibrutinib N-1 (see stacked spectra below), suggesting that this part of the molecule has undergone significant change, ergo reacted with the oxetane.*



3-(4-Methoxyphenyl)-*N*-methyl-*N*-(3-phenyl-3-(4-(trifluoromethyl)phenoxy)propyl)oxetan-3-amine (61)



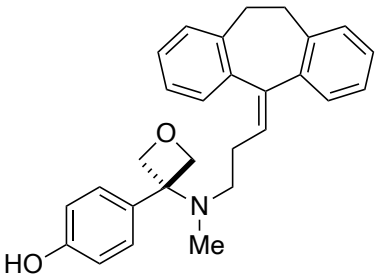
Prepared according to **General Procedure D** and using oxetane sulfonyl fluoride **18a** (29.6 mg) and fluoxetine (31.0 mg). The free-amine form of fluoxetine was acquired by pre-washing a solution of the commercially available hydrochloride salt (100 mg in 20 mL CH_2Cl_2) with 1 M aq. NaOH (3 × 15 mL), drying over Na_2SO_4, filtering and concentrating in vacuo using a rotatory evaporator. [Hydrochloride salts can normally be used in the reaction (see *e.g.* compound **46**) but may lead to a lower yield due to formation of an oxetane chloride as a side product.] Purification by flash column chromatography (10% acetone/pentane) afforded oxetane amine **61** as a colourless gum (29.7 mg, 63%). R_f = 0.30 (15% acetone/pentane); IR (film)/cm^{-1} 3306 (OH st, br), 2952, 2878, 1599, 1517, 1454, 1375, 1275, 1215, 1115, 1066, 1029, 988, 939, 854, 816, 731, 678; ^{1}H NMR (400 MHz, $CDCl_3$) δ 7.45 (d, *J* = 8.6 Hz, 2 H, 2 × $Ar_{(CF_3)}$-CH), 7.38–7.33 (m, 4 H, 4 × $Ar_{(Ph)}$-CH), 7.30–7.25 (m, 1 H, $Ar_{(Ph)}$-CH), 7.02 (d, *J* = 8.7 Hz, 2 H, 2 × $Ar_{(PMP)}$-CH), 6.94 (d, *J* = 8.6 Hz, 2 H, 2 × $Ar_{(CF_3)}$-CH), 6.89 (d, *J* = 8.7 Hz, 2 H, 2 × $Ar_{(PMP)}$-CH), 5.43 (dd, *J* = 8.4, 4.1 Hz, 1 H, CH), 4.85–4.83 (m, 3 H, C*H*$_2$OC*H*H), 4.72 (br d, *J* = 5.8 Hz, 1 H, CH_2OCHH), 3.82 (s, 3 H,

OCH_3), 2.53–2.46 (m, 1 H, NC*H*HCHH), 2.19–2.11 (m, 2 H, NCH*HCH*H), 2.09 (s, 3 H, NCH_3), 2.03–1.92 (m, 1 H, NCHHCH*H*); ^{13}C NMR (101 MHz, $CDCl_3$) δ 160.5 (Ar-C_qOCH), 158.6 (Ar-C_qOMe), 141.1 (Ar-C_qCH), 129.4 (Ar-C_qC_q), 128.8 (2 × $Ar_{(PMP)}$-CH), 128.5 (2 × $Ar_{(Ph)}$-CH), 127.8 (Ar-CH), 126.8 (q, $^3J_{CF}$ = 3.9 Hz, 2 × $Ar_{(CF3)}$-CH), 125.9 (2 × $Ar_{(Ph)}$-CH), 124.3 (q, J_{CF} = 271.1 Hz, CF_3), 122.8 (q, J_{CF} = 32.8 Hz, Ar-C_qCF_3), 115.8 (2 × $Ar_{(CF3)}$-CH), 113.2 (2 × $Ar_{(PMP)}$-CH), 80.4 (CH_2OCH_2), 80.1 (CH_2OCH_2), 77.6 (CH), 67.0 (C_qN), 55.2 (OCH_3), 46.8 (NCH_2), 36.6 (NCH_2CH_2), 34.7 (NCH_3); ^{19}F NMR (377 MHz, $CDCl_3$) δ –61.5; HRMS (ESI) *m/z* calcd for $C_{27}H_{29}NO_3F_3$ [M+H]: 472.2100, found: 472.2098.

Notes:

Only the two central peaks of the quartet ^{13}C signals at 124.3 and 122.8 ppm were observed due to the low intensity of these quaternary signals. The two outer peaks of the quartet at 126.8 ppm were seen as shoulders of the central peaks.

4-(3-((3-(10,11-Dihydro-5*H*-dibenzo[*a*,*d*][7]annulen-5-ylidene)propyl)(methyl)amino)oxetan-3-yl)phenol (62)



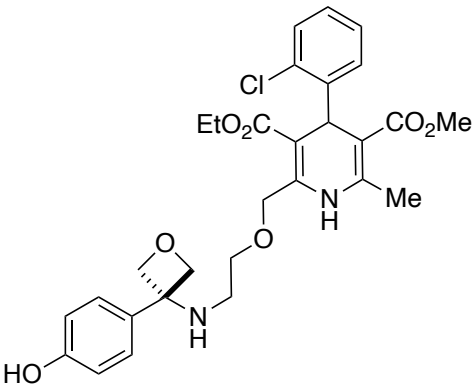
Prepared according to **General Procedure D** and using oxetane sulfonyl fluoride **18c** (46.7 mg) and nortriptyline (26.4 mg). The free-amine form of nortriptyline was acquired by pre-washing a solution of the commercially available hydrochloride salt (100 mg in 20 mL CH_2Cl_2) with 1 M aq. NaOH (3 × 15 mL), drying over Na_2SO_4, filtering and concentrating in vacuo using a rotatory evaporator. [Hydrochloride salts can normally be used in the reaction (see *e.g.* compound **46**) but may lead to a lower yield due to formation of an oxetane chloride as a side product.] Purification by flash column chromatography (35–45% EtOAc/pentane) afforded oxetane amine **62** as a colourless gum (29.6 mg, 72%). R_f = 0.33 (45% EtOAc/pentane); IR (film)/cm^{-1} 3273 (OH st, br), 3060, 3019, 2945, 2878, 2796, 2248, 1730, 1610, 1513, 1484, 1443, 1364, 1234, 1174, 1115, 1059, 1036, 977, 910, 835, 731; ^{1}H NMR (400 MHz, $CDCl_3$) δ 7.30–7.28 (m, 1 H, Ar-CH), 7.22–7.20 (m, 2 H, 2 × Ar-CH), 7.18–7.11 (m, 4 H, 4 × Ar-CH), 6.91 (d, *J* = 8.6 Hz, 2 × $Ar_{(phenol)}$-CH), 6.91 (d, *J* = 8.6 Hz, 2 × $Ar_{(phenol)}$-CH), 5.87 (t, *J* = 7.3 Hz, 1 H, HC=C), 4.87 (br s, 4 H, CH_2OCH_2), 3.42–3.30 (m, 2 H, Ar-C_qC*H*HCHHAr-C_q and Ar-C_qCHHC*H*HAr-C_q), 3.01–2.91 (m, 1 H, Ar-C_qCH*H*CHHAr-C_q), 2.79 (br s, 1 H, Ar-C_qCHHCH*H*Ar-C_q), 2.30 (td, *J* = 7.3, 7.3 Hz, 2 H, NCH_2CH_2), 2.14 (t, *J* = 7.3 Hz, 2 H, NCH_2CH_2), 1.93 (s, 3 H, NCH_3); ^{13}C NMR (101 MHz, $CDCl_3$) δ 155.1 (Ar-C_q-OH), 143.9 (HC=C_q), 141.1 (Ar-C_q), 140.0 (Ar-C_q), 139.3 (Ar-C_q), 137.0 (Ar-C_q), 130.0 (Ar-CH), 128.8 (HC=C_q), 128.6 (2 × $Ar_{(phenol)}$-CH), 128.5 (Ar-CH), 128.1 (Ar-CH), 127.9 (Ar-CH), 126.0 (Ar-

CH), 125.7 (Ar-CH), 114.7 (2 × $Ar_{(phenol)}$-CH), 80.7 (CH_2OCH_2), 66.7 (Ar-C_qC_q), 50.8 (NCH_2), 34.8 (NCH_3), 33.7 (Ar-C_qCH_2), 32.0 (Ar-C_qCH_2), 27.8 (NCH_2CH_2); HRMS (ESI) *m/z* calcd for $C_{28}H_{30}NO_2$ [M+H]: 412.2277, found: 412.2274.

Notes:

*The Ar-**C_qC_q** signal is under the signals at 128.8 & 128.6 ppm and is probably the observed shoulder at 128.7 ppm. This was confirmed by an HMBC 2D correlation spectrum.*

3-Ethyl 5-methyl 4-(2-chlorophenyl)-2-((2-((3-(4-hydroxyphenyl)oxetan-3-yl)amino)ethoxy)methyl)-6-methyl-1,4-dihydropyridine-3,5-dicarboxylate (63)



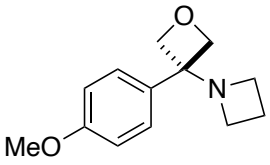
Prepared according to **General Procedure D** with 2.6 equiv K_2CO_3 (36.0 mg, 0.26 mmol) and using oxetane sulfonyl fluoride **18c** (46.6 mg) and amlodipine besylate (56.7 mg). Purification by flash column chromatography (80% EtOAc/pentane) afforded oxetane amine **63** as a colourless gum (55.9 mg, quant.). R_f = 0.30 (80% EtOAc/pentane); IR (film)/cm^{-1} 3317 (OH st, br), 2948, 2870, 1681 (C=O st), 1610, 1517, 1476, 1431, 1368, 1279, 1208, 1096, 1033, 980, 910, 835, 727; ^{1}H NMR (400 MHz, $CDCl_3$) δ 7.37 (dd, ^3J = 7.8 Hz, ^4J = 1.7 Hz, 1 H, CHAr-C_qAr-CH), 7.31 (br s, 1 H, C_qNHC_q), 7.24 (dd, ^3J = 7.9 Hz, ^4J = 1.3 Hz, 1 H, ClAr-C_qAr-CH), 7.22–7.18 (m, 2 H, 2 × $Ar_{(phenol)}$-CH), 7.14 (ddd, ^3J = 7.8, 7.5 Hz, ^4J = 1.3 Hz, 1 H, CHAr-C_qAr-CHAr-C*H*), 7.05 (ddd, ^3J = 7.9, 7.5 Hz, ^4J = 1.7 Hz, 1 H, ClAr-C_qAr-CHAr-C*H*), 6.84–6.80 (m, 2 H, 2 × $Ar_{(phenol)}$-CH), 5.41 (s, 1 H, CH), 4.99 (dd, ^2J = 6.5 Hz, *J* = 1.6 Hz, 2 H, C*H*HOC*H*H), 4.76 (d, *J* = 16.3 Hz, 1 H, OC*H*HC_qNHC_q), 4.75 (d, *J* = 6.5 Hz, 2 H, CH*H*OCH*H*), 4.65 (d, *J* = 16.3 Hz, 1 H, OCH*H*C_qNHC_q), 4.05 (qd, ^3J = 7.1 Hz, *J* = 2.6 Hz, 2 H, OCH_2CH_3), 3.63 (s, 3 H, OCH_3), 3.59 (br t, *J* = 5.2 Hz, 2 H, OCH_2CH_2), 2.70 (t, *J* = 5.2 Hz, 2 H, OCH_2CH_2), 2.33 (s, 3 H, C_qCH_3), 1.18 (t, *J* = 7.1 Hz, 3 H, OCH_2CH_3); ^{13}C NMR (101 MHz, $CDCl_3$) δ 168.2 (CO_2Me), 167.2 (CO_2Et), 155.4 (Ar-C_qOH), 145.6 (Ar-C_qCH), 145.4 ($OCH_2C_qNHC_q$), 144.1 (C_qCH_3), 133.4 (Ar-C_qC_q), 132.3 (Ar-C_qCl), 131.5 (CHAr-C_qAr-CH), 129.3 (ClAr-C_qAr-CH), 127.5 (2 × $Ar_{(phenol)}$-CH), 127.4 (ClAr-C_qAr-CHAr-CH), 126.8 (CHAr-C_qAr-CHAr-CH), 115.6 (2 × $Ar_{(phenol)}$-CH), 103.9 (C_qCO_2Me), 101.5 (C_qCO_2Et), 82.3 (CH_2OCH_2), 71.2 (OCH_2CH_2), 67.8 ($OCH_2C_qNHC_q$), 63.1 (Ar-C_qC_q), 59.9 (OCH_2CH_3), 50.9 (OCH_3), 42.8 (OCH_2CH_2), 37.2 (Ar-C_qCH), 19.5 (C_qCH_3), 14.2 (OCH_2CH_3); HRMS (APCI) *m/z* calcd for $C_{29}H_{34}{}^{35}ClN_2O_7^+$ $[M+H]^+$: 557.2049, found: 557.2047.

Notes:

The doublets at 4.76 (1 H) and 4.75 (2 H) ppm were integrated together to 3 H.

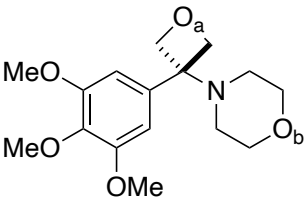
The OH and NH signals (+ H_2O) are probably a very broad peak between 2.79 and 1.46 ppm.

1-(3-(4-Methoxyphenyl)oxetan-3-yl)azetidine (64)



Prepared according to **General Procedure C** and using oxetane sulfonyl fluoride **18a** (49.2 mg) and 3-bromopropanamine hydrobromide (52.5 mg). Purification by flash column chromatography (1–5% MeOH/CH_2Cl_2) afforded oxetane amine **64** as a colourless gum (11.3 mg, 26%). R_f = 0.05 (5% MeOH/CH_2Cl_2); ^{1}H NMR (400 MHz, $CDCl_3$) δ 7.24–7.20 (m, 2 H, 2 × Ar-CH), 6.92–6.89 (m, 2 H, 2 × Ar-CH), 4.99 (d, *J* = 6.7 Hz, 2 H, C*H*HOC*H*H), 4.85 (d, *J* = 6.7 Hz, 2 H, CH*H*OCH*H*), 3.82 (s, 3 H, OCH_3), 3.37 (t, *J* = 7.2 Hz, 4 H, CH_2NCH_2), 2.10 (p, *J* = 7.2 Hz, 2 H, NCH_2CH_2).

4-(3-(3,4,5-Trimethoxyphenyl)oxetan-3-yl)morpholine (65)

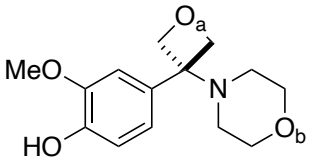


Prepared according to **General Procedure A** for 13 h and using oxetane sulfonyl fluoride **18f** (61.3 mg) and morpholine (21 μL). Purification by flash column chromatography (100% EtOAc) afforded oxetane amine **65** as a white solid (55.6 mg, 90%). R_f = 0.14 (100% EtOAc); mp = 164–170 °C; IR (film)/cm^{-1} 2952, 2878, 2833, 1589, 1510, 1453, 1417, 1331, 1290, 1245, 1185, 1126, 992, 954, 913, 813, 731; ^{1}H NMR (400 MHz, $CDCl_3$) δ 6.28 (s, 2 H, 2 × Ar-CH), 4.89 (br s, 4 H, $CH_2O_aCH_2$), 3.87 (s, 9 H, 3 × OCH_3), 3.76 (br s, 4 H, $CH_2O_bCH_2$), 2.41 (br s, 4 H, CH_2NCH_2); ^{13}C NMR (101 MHz, $CDCl_3$) δ 152.9 (2 × Ar-C_qOMe), 137.5 (weak, Ar-C_qOMe), 133.4 (weak, Ar-C_qC_q), 104.7 (2 × Ar-CH), 78.7 (br, $CH_2O_aCH_2$), 67.1 (br, $CH_2O_bCH_2$ and Ar-C_qC_q), 60.9 (OCH_3), 56.3 (2 × OCH_3), 46.5 (CH_2NCH_2); HRMS (ESI) *m/z* calcd for $C_{16}H_{24}NO_5$ [M+H]: 310.1654, found: 310.1655.

Notes:

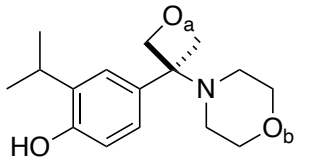
*^{13}C NMR signal at 67.1 ppm: $CH_2O_bCH_2$ was assigned by analogy to other morpholine-containing oxetanes. Ar-C_q**C_q** was assigned by an HMBC correlation spectrum. The signal was also broad and contained a shoulder.*[212]

2-Methoxy-4-(3-morpholinooxetan-3-yl)phenol (66)



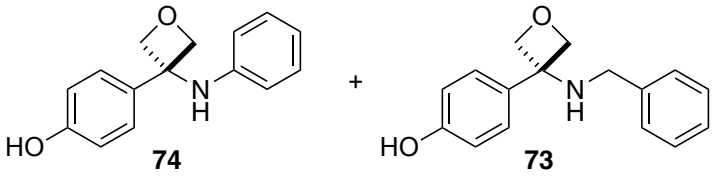
Prepared according to **General Procedure A** and using oxetane sulfonyl fluoride **18g** (83.7 mg; 95:5 mixture of **18g**:**18g'**) and morpholine (20.8 μL). Purification by flash column chromatography (5% MeOH/CH_2Cl_2) afforded oxetane amine **66** as a white solid (44.0 mg, 83%). R_f = 0.14 (5% MeOH/CH_2Cl_2); mp = 135 °C; IR (film)/cm^{-1} 3306 (OH st, br), 2952, 2878, 1599, 1517, 1454, 1375, 1275, 1215, 1115, 1066, 1029, 988, 939, 854, 816, 731, 678; ^{1}H NMR (400 MHz, $CDCl_3$) δ 6.92 (d, *J* = 8.1 Hz, 1 H, HOC_qAr-C*H*), 6.58 (dd, ^3J = 8.1 Hz, ^4J = 1.9 Hz, 1 H, Ar-CH), 6.54 (br s, 1 H, Ar-C_qAr-CHAr-C_q), 5.72 (br s, 1 H, OH), 4.91–4.87 (br m, 4 H, $CH_2O_aCH_2$),3.90 (s, 3 H, OCH_3), 3.75 (br t, *J* = 4.6 Hz, 4 H, $CH_2O_bCH_2$), 2.36 (br s, 4 H, CH_2NCH_2); ^{13}C NMR (101 MHz, $CDCl_3$) δ 146.2 (Ar-C_qOMe), 145.0 (Ar-C_qOH), 129.5 (Ar-*C*$_q$C$_q$), 120.4 (Ar-CH), 113.8 (Ar-C_qOHAr-*C*H), 109.8 (Ar-C_qOMeAr-*C*H), 79.1 ($CH_2O_aCH_2$), 67.1 ($CH_2O_bCH_2$), 66.8 (C_q), 56.0 (OCH_3), 46.4 (CH_2NCH_2); HRMS (APCI) *m/z* calcd for $C_{14}H_{20}NO_4^+$ $[M+H]^+$: 266.1387, found: 266.1389.

2-Isopropyl-4-(3-morpholinooxetan-3-yl)phenol (67)



Prepared according to **General Procedure A** and using oxetane sulfonyl fluoride **18h** (86.1 mg) and morpholine (20.8 μL). Purification by flash column chromatography (80–100% Et_2O/pentane) afforded oxetane amine **67** as a white solid (52.5 mg, 95%). R_f = 0.14 (80% Et_2O/pentane); mp = 172-175 °C; IR (film)/cm^{-1} 3299 (OH st, br), 3027, 2960, 2870, 2740, 1610, 1506, 1454, 1424, 1342, 1267, 1193, 1111, 1066, 980, 939, 910, 857, 813, 731; ^{1}H NMR (400 MHz, $CDCl_3$) δ 6.80 (s, 1 H, Ar-CH), 6.70 (app. d, *J* = 1.3 Hz, 2 H, 2 × Ar-CH), 5.89 (br s, 1 H, OH), 4.93 (d, *J* = 6.0 Hz, 2 H, C*H*HO$_a$C*H*H), 4.89 (d, *J* = 6.0 Hz, 2 H, CH*H*O$_a$CH*H*), 3.76 (br t, *J* = 4.6 Hz, 4 H, $CH_2O_bCH_2$), 3.24 (hept, *J* = 6.9 Hz, 1 H, Ar-C_qCH), 2.30 (br t, *J* = 4.6 Hz, 4 H, CH_2NCH_2), 1.24 (d, *J* = 6.9 Hz, 6 H, 2 × Ar-C_qCHC*H*$_3$); ^{13}C NMR (101 MHz, $CDCl_3$) δ 152.4 (Ar-C_qOH), 134.1 (Ar-C_q), 128.7 (Ar-C_q), 125.5 (Ar-CH), 125.3 (Ar-CH), 114.5 (Ar-CH), 79.6 ($CH_2O_aCH_2$), 67.1 ($CH_2O_bCH_2$), 66.5 (C_q), 46.2 (CH_2NCH_2), 26.9 (Ar-C_q*C*H), 22.5 (2 × Ar-C_qCH*C*H$_3$); HRMS (APCI) *m/z* calcd for $C_{16}H_{24}NO_3^+$ $[M+H]^+$: 278.1751, found: 278.1753.

4-(3-(Phenylamino)oxetan-3-yl)phenol (74) and 4-(3-(benzylamino)oxetan-3-yl)phenol (73)



A reaction tube was charged with anhydrous K_2CO_3 (36 mg, 0.26 mmol, 1.3 equiv) and flame-dried under air. The tube was allowed to cool to room temperature (ca. 22 ºC) and benzylamine (22 μL, 0.20 mmol, 1.0 equiv), aniline (18 μL, 0.20 mmol, 1.0 equiv) and OTIPS oxetane sulfonyl fluoride **18c** (77.7 mg, 0.20 mmol, 1.0 equiv) were added sequentially. The reaction vessel was sealed, anhydrous acetonitrile (0.66 mL, 0.3 M) was added by syringe and the reaction mixture was stirred at 60 ºC for 2 h. After allowing the tube cool to room temperature (ca. 22 ºC), EtOAc (5 mL) was added and the mixture was filtered through a plug of Celite, eluting with further EtOAc (3 × 10 mL). The solvent was removed *in vacuo* using a rotatory evaporator and purification by flash column chromatography (20–60% Et_2O/pentane) afforded phenyl oxetane amine **74** as a white solid (13.9 mg, 29%), followed by benzyl oxetane amine **73** as a white solid (29.1 mg, 57%).

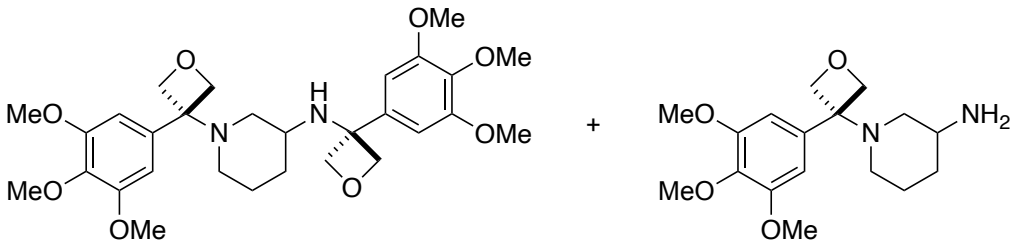
Phenyl oxetane amine **74**: R_f = 0.44 (60% Et_2O/pentane); mp = 172–175 °C; IR (film)/cm^{-1} 3373 (OH and NH st, br), 3049, 2956, 2881, 2494, 1603, 1510, 1439, 1342, 1316, 1252, 1179, 1111, 1051, 977, 898, 835, 753, 693; ^{1}H NMR (400 MHz, CD_3OD) δ 7.47–7.43 (m, 2 H, 2 × Ar-CH), 7.02–6.97 (m, 2 H, 2 × Ar-CH), 6.78–6.75 (m, 2 H, 2 × Ar-CH), 6.56 (tt, *J* = 7.1, 1.0 Hz, 1 H, Ar-CH), 6.26–6.24 (m, 2 H, 2 × Ar-CH), 4.90 (d, *J* = 6.1 Hz, 2 H, C*H*HOC*H*H), 4.88 (d, *J* = 6.1 Hz, 2 H, CH*H*OCH*H*); ^{13}C NMR (101 MHz, CD_3OD) δ 157.6 (Ar-C_qOH), 146.9 (Ar-C_qNH), 134.6 (Ar-C_qC_q), 129.8 (2 × Ar-CH), 127.8 (2 × Ar-CH), 118.1 (Ar-CH), 116.3 (2 × Ar-CH), 115.0 (2 × Ar-CH), 85.2 (CH_2OCH_2), 60.7 (C_q); HRMS (ESI) *m/z* calcd for $C_{15}H_{16}NO_2$ [M+H]: 242.1181, found: 242.1174.

Benzyl oxetane amine **73**: R_f = 0.17 (60% Et_2O/pentane); mp = 105 ºC; IR (film)/cm^{-1} 3247 (OH and NH st, br), 3060, 3027, 2952, 2874, 2602, 2445, 1886, 1610, 1513, 1454, 1361, 1256, 1174, 1111, 1057, 1029, 973, 831, 738, 701; ^{1}H NMR (400 MHz, CD_3OD) δ 7.30–7.19 (m, 7 H, 7 × Ar-CH), 6.87–6.83 (m, 2 H, 2 × Ar-CH), 4.88 (d, *J* = 6.3 Hz, C*H*HOC*H*H), 4.77 (d, *J* = 6.3 Hz, CH*H*OCH*H*), 3.42 (s, 2 H, CH_2Ph); ^{13}C NMR (101 MHz, CD_3OD) δ 157.9 (Ar-C_qOH), 141.1 (Ph-C_q), 133.9 (Ar-C_qC_q), 129.6 (2 × Ar-CH), 129.4 (2 × Ar-CH), 128.9 (2 × Ar-CH), 128.1 (Ph-CH), 116.3 (2 × Ar-CH), 83.8 (CH_2OCH_2), 64.1 (C_q), 48.8 (CH_2Ph); HRMS (ESI) *m/z* calcd for $C_{16}H_{18}NO_2$ [M+H]: 256.1338, found: 256.1330.

Notes:

The CH_2Ph ^{13}C NMR signal at 48.8 ppm was observed as a small shoulder of the CD_3OD solvent peak. Its identity was confirmed by a HSQC 2D correlation spectrum.

_N_,1-bis(3-(3,4,5-Trimethoxyphenyl)oxetan-3-yl)piperidin-3-amine (76) and 1-(3-(3,4,5-trimethoxyphenyl)oxetan-3-yl)piperidin-3-amine (75)



76 **75**

Prepared according to **General Procedure A** for 13 h and using oxetane sulfonyl fluoride **18f** (61.3 mg) and 3-aminopiperidine (24.0 mg). Purification by flash column chromatography (0–20% MeOH/CH_2Cl_2) afforded dimeric oxetane amine **76** as a colourless gum (13.1 mg, 24%), followed by oxetane amine **75** as a colourless gum (13.3 mg, 21%).

Dimeric oxetane amine **76**: R_f = 0.77 (15% MeOH/CH_2Cl_2); IR (film)/cm^{-1} 2937, 1588, 1413, 1241, 1126, 731; ^1H NMR (400 MHz, $CDCl_3$) δ 6.64 (br s, 2 H, 2 × Ar-CH), 6.09 (s, 2 H, 2 × Ar-CH), 5.08 (d, *J* = 6.4 Hz, 1 H, CHO), 4.90 (d, *J* = 5.7 Hz, 2 H, 2 × CHO), 4.80 (d, *J* = 5.8 Hz, 1 H, C*H*HO), 4.77 (d, *J* = 5.8 Hz, 1 H, CH*H*O), 4.73 (br s, 2 H, 2 × CHO), 4.57 (br s, 1 H, CHO), 3.90 (s, 6 H, 2 × OCH_3), 3.89 (s, 3 H, OCH_3), 3.84 (s, 3 H, OCH_3), 3.83 (s, 6 H, 2 × OCH_3), 2.66 (br s, 1 H, CHN), 2.43 (br s, 1 H, CHN), 2.22 (br s, 1 H, CHN), 1.82 (br s, 1 H, CHN), 1.68 (br s, 1 H, CHN), 1.56 (br s, 3 H, 3 × CH), 1.07 (br s, 1 H, CH); ^{13}C NMR (101 MHz, $CDCl_3$) δ 153.5 (2 × Ar-C_qOMe), 152.7 (2 × Ar-C_qOMe), 137.6 (weak, Ar-C_qOMe), 137.4 (weak, Ar-C_qOMe), 132.5 (weak, 2 × Ar-C_qC_q), 104.6 (2 × Ar-CH), 103.8 (2 × Ar-CH), 85.8 (CH_2O), 82.1 (weak, CH_2O), 79.8 (CH_2O), 79.6 (CH_2O), 67.0 (C_q), 63.6 (C_q), 60.9 (OCH_3), 60.8 (OCH_3), 56.4 (2 × OCH_3), 56.3 (2 × OCH_3), 53.2 (weak, CHN), 51.2 (weak, CHN), 46.3 (CHN), 31.9 (weak, CH_2), 23.7 (weak, CH_2); HRMS (APCI) *m/z* calcd for $C_{29}H_{41}N_2O_8^+$ $[M+H]^+$: 545.2857, found: 545.2847.

Notes:

The signals at 4.80, 4.77 and 4.73 ppm in the ^1H NMR spectrum were integrated together to 4 H.

Most signals in the ^{1}H and ^{13}C NMR spectra were broadened and/or weak due to chemical exchange between conformers caused by N and ring-inversion.

Oxetane amine **75**: R_f = 0.03 (15% MeOH/CH_2Cl_2); IR (film)/cm^{-1} 2937, 1588, 1416, 1327, 1126; ^{1}H NMR (400 MHz, $CDCl_3$) δ 6.23 (s, 2 H, 2 × Ar-CH), 4.89 (d, *J* = 5.7 Hz, 1 H, C*H*HOCH$_2$), 4.88 (d, *J* = 5.9 Hz, 1 H, CH$_2$OC*H*H), 4.85 (d, *J* = 5.9 Hz, 1 H, CH$_2$OCH*H*), 4.83 (d, *J* = 5.7 Hz, 1 H, CH*H*OCH$_2$), 3.86 (s, 3 H, OCH$_3$), 3.85 (s, 6 H, 2 × OCH$_3$), 2.99–2.94 (br m, 1 H, CHN), 2.56 (br d, *J* = 7.8 Hz, 1 H, NC*H*HCHNH$_2$), 2.40 (br s, 1 H, NC*H*HCH$_2$), 2.03–1.93 (br m, 3 H, NCH*H*CH$_2$ + NH$_2$ [+ residual H$_2$O peak]), 1.78–1.73 (br m, 3 H, NCH*H*CHNH$_2$ + C*H*HC*H*H), 1.63–1.55 (m, 1 H, CH*H*CH$_2$), 1.14–1.03 (m, 1 H, CH$_2$CH*H*); ^{13}C NMR (101 MHz, $CDCl_3$) δ 152.6 (2 × Ar-C$_q$OMe), 137.2 (Ar-C$_q$OMe), 133.0 (Ar-*C*$_q$C$_q$), 104.7 (2 × Ar-CH), 80.1 (*C*H$_2$OCH$_2$), 80.0 (CH$_2$O*C*H$_2$), 66.9 (C$_q$), 60.8 (OCH$_3$), 56.3 (2 × OCH$_3$), 54.8 (N*C*H$_2$CHNH$_2$), 48.0 (CHNH$_2$), 46.4 (N*C*H$_2$CH$_2$), 33.8 (*C*H$_2$CH$_2$), 23.4 (CH$_2$*C*H$_2$); HRMS (APCI) *m/z* calcd for $C_{17}H_{27}N_2O_4^+$ $[M+H]^+$: 323.1965, found: 323.1963.

Notes:

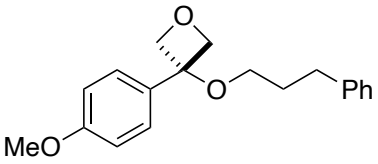
*The ^{1}H and ^{13}C NMR spectra of amino-oxetanes **75** and **93** (troxipide analogue) differed significantly, supporting the proposed structure with oxetane bound to the secondary nitrogen on piperidine.*

The signals at 4.89, 4.88, 4.85 and 4.83 ppm in the ^{1}H NMR spectrum were integrated together to 4 H.

Most signals in the ^{1}H and ^{13}C NMR spectra were broadened and/or weak due to chemical exchange between conformers caused by N and ring-inversion.

7.6.4.2 Oxetane Products From Other Nucleophiles

3-(4-Methoxyphenyl)-3-(3-phenylpropoxy)oxetane (70)

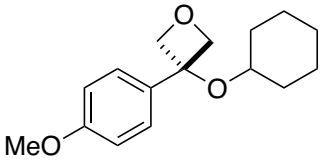


Prepared according to **General Procedure A** and using oxetane sulfonyl fluoride **18a** (49.2 mg) and 3-phenylpropanol (32.7 μL). Purification by flash column chromatography (10% EtOAc/pentane) afforded oxetane ether **70** as a colourless gum that solidified in the freezer to a white solid (35.8 mg, 60%). R_f = 0.14 (15% EtOAc/pentane); mp = 60–62 °C; IR (film)/cm^{-1} 2943, 2873, 1612, 1514, 1455, 1305, 1249, 1178, 1031, 983, 910, 832, 732, 701; ^{1}H NMR (400 MHz, $CDCl_3$) δ 7.35–7.32 (m, 2 H, 2 × Ar$_{(PMP)}$-CH), 7.30–7.25 (m, 2 H, 2 × Ar$_{(Ph)}$-CH), 7.21–7.20 (m, 3 H, 3 × Ar$_{(Ph)}$-CH), 6.96–6.92 (m, 2 H, 2 × Ar$_{(PMP)}$-CH), 4.91 (d, *J* = 6.6 Hz, 2 H, C*H*HOC*H*H), 4.83 (d, *J* = 6.6 Hz, 2 H, CH*H*OCH*H*), 3.84 (s, 3 H, OCH_3), 3.16 (t, *J* = 6.3 Hz, 2 H, OCH_2), 2.71 (t, *J* = 7.6 Hz, 2 H, $PhCH_2$), 1.93–1.86 (m, 2 H, $CH_2CH_2CH_2$); ^{13}C NMR (101 MHz $CDCl_3$) δ 159.2 (Ar-C_qOMe), 141.8 (Ar-$C_q$$CH_2$), 132.3 (Ar-$C_q$$C_q$), 128.4 (2 × Ar-CH), 128.3 (2 × Ar-CH), 127.2 (2 × Ar-CH), 125.8 (Ar-CH), 114.0 (2 × Ar-CH), 81.3 (CH_2OCH_2), 79.9 (C_q), 62.8 (OCH_2), 55.3 (OCH_3), 32.3 ($CH_2CH_2CH_2$), 31.4 ($PhCH_2$); HRMS (ESI) *m/z* calcd for $C_{19}H_{23}O_3$ [M+H]: 299.1647; found: 299.1655.

Notes:

*Oxetane ether **70** was further characterised by X-ray crystallography (see Figure 32).*

3-(Cyclohexyloxy)-3-(4-methoxyphenyl)oxetane (71)



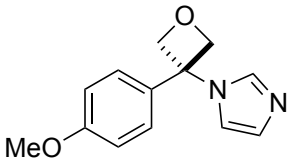
Prepared according to **General Procedure A** and using oxetane sulfonyl fluoride **18a** (49.2 mg) and cyclohexanol (25.4 μL). Purification by flash column chromatography (0–3%Et_2O/CH_2Cl_2) afforded oxetane ether **71** as a yellow gum that solidified in the freezer to a pale-yellow solid (26.4 mg, 50%). R_f = 0.14 (3%Et_2O/CH_2Cl_2); mp = 48 °C; IR (film)/cm^{-1} 2935, 2855, 1612, 1585, 1514, 1453, 1310, 1248, 1180, 1031, 979, 906, 832, 731; ^{1}H NMR (400 MHz, $CDCl_3$) δ 7.38–7.34 (m, 2 H, 2 × Ar-CH), 6.96–6.92 (m, 2 H, 2 × Ar-CH), 4.95 (d, *J* = 7.0 Hz, 2 H, C*H*HOC*H*H), 4.86 (d, *J* = 7.0 Hz, 2 H, CH*H*OCH*H*), 3.85 (s, 3 H, OCH_3), 3.16 (tt, $J_{ax,ax}$ = 9.8 Hz, $J_{ax,eq}$ = 4.0 Hz, 1 H, CH), 1.69–1.63 (m, 2 H, 2 × CH_{eq}HCHO), 1.59–1.56 (m, 2 H, 2 × C$H_{eq}$$HCH_2CHO$), 1.50–1.44 (m, 1 H, C$H_{eq}$$HCH_2CH_2CHO$), 1.31–1.22 (m, 2 H, 2 × CHH_{ax}CHO), 1.16–1.05 (m, 3 H, 2 × CH$H_{ax}$$CH_2CHO$ and CH$H_{ax}$$CH_2CH_2CHO$); ^{13}C NMR (101 MHz $CDCl_3$) δ 159.1 (Ar-C_qOMe), 133.3 (Ar-$C_q$$C_q$), 127.6 (2 × Ar-CH), 113.9 (2 × Ar-CH),

82.6 (CH_2OCH_2), 79.2 (C_q), 73.0 (CH), 55.3 (OCH_3), 33.7 (2 × CH_2), 25.5 (CH_2), 24.3 (2 × CH_2); HRMS (NSI) *m/z* calcd for $C_{16}H_{26}NO_3^+$ $[M+NH_4]^+$: 280.1907; found: 280.1912.

Notes:

*Oxetane ether **71** was further characterised by X-ray crystallography (see Figure 32).*

1-(3-(4-Methoxyphenyl)oxetan-3-yl)-1*H*-imidazole (31)

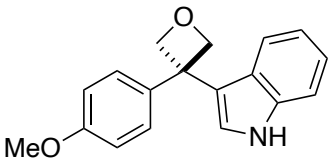


Prepared according to **General Procedure A** and using oxetane sulfonyl fluoride **18a** (49.2 mg) and imidazole (16.3 mg). Purification by flash column chromatography (EtOAc) afforded oxetane-imidazole **31** as a colourless oil (23.9 mg, 52%). R_f = 0.23 (10% MeOH/EtOAc); ^{1}H NMR (400 MHz, $CDCl_3$) δ 7.50 (br s, 1 H, $Ar_{(imidazole)}$-CH), 7.24 (br s, 1 H, $Ar_{(imidazole)}$-CH), 7.15 (br a, 1 H, $Ar_{(imidazole)}$-CH), 7.15–7.09 (m, 2 H, 2 × Ar-CH), 6.98–6.95 (m, 2 H, 2 × Ar-CH), 5.28 (d, *J* = 6.8 Hz, 2 H, C*H*HOC*H*H), 5.24 (d, *J* = 6.8 Hz, 2 H, CH*H*OCH*H*), 3.86 (s, 3 H, OCH_3). The observed characterisation data (R_f, ^{1}H) were consistent with that observed previously in the group.[210]

Notes:

*Imidazole **31** was assigned as the oxetane imidazole and not as the oxetane sulfonate imidazole based on the absence of the SO_2 stretches in the IR spectrum and the absence of sulfur-containing fragments in the mass spectrum.*

3-(3-(4-Methoxyphenyl)oxetan-3-yl)-1*H*-indole (77)



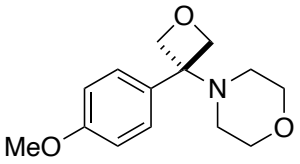
Prepared according to **General Procedure A** and using oxetane sulfonyl fluoride **18a** (49.2 mg) and 1*H*-indole (28.1 mg). Purification by flash-column chromatography (30–90% Et_2O/pentane) afforded diaryl-oxetane **77** as a white solid (47.5 mg, 85%). R_f = 0.54 (40% EtOAc/pentane); mp = 184 °C; IR (film)/cm^{-1} 3244 (NH st, br), 3050, 2987, 2946, 2873, 2829, 1608, 1510, 1456, 1428, 1339, 1299, 1246, 1183, 1152, 1115, 1027, 974, 933, 837, 743, 627, 582, 564; ^{1}H NMR (400 MHz, $CDCl_3$) δ 8.07 (br s, 1 H, NH), 7.69 (d, *J* = 8.0 Hz, $Ar_{(indole)}$-CH), 7.41 (d, *J* = 8.1 Hz, $Ar_{(indole)}$-CH), 7.29–7.22 (m, 3 H, 2 × $Ar_{(PMP)}$-CH + $Ar_{(indole)}$-CH), 7.12 (ddd, ^3J = 8.0, 7.0 Hz, ^4J = 1.0 Hz, $Ar_{(indole)}$-CH), 6.93–6.89 (m, 2 H, 2 × $Ar_{(PMP)}$-CH), 6.69 (d, *J* = 2.5 Hz, HNAr-C*H*), 5.41 (d, *J* = 5.6 Hz, 2 H, C*H*HOC*H*H), 5.30 (d, *J* = 5.6 Hz, 2 H, CH*H*OCH*H*), 3.83 (s, 3 H, OCH_3); ^{13}C NMR (101 MHz, $CDCl_3$) δ 158.1 (Ar-C_qOMe), 137.6 ($Ar_{(PMP)}$-C_qC_q), 136.9 (NHAr-C_q), 127.6 (2 × $Ar_{(PMP)}$-CH), 125.7 (NHAr-C_qAr-C_q), 122.4 (NHAr-CH), 122.3 ($Ar_{(indole)}$-CH), 121.4 ($Ar_{(indole)}$-C_qC_q), 120.0 ($Ar_{(indole)}$-CH), 119.8

($Ar_{(indole)}$-CH), 113.7 (2 × $Ar_{(PMP)}$-CH), 111.4 ($Ar_{(indole)}$-CH), 84.2 (CH_2OCH_2), 55.3 (OCH_3), 46.0 (C_q); HRMS (ESI) *m/z* calcd for $C_{18}H_{18}NO_2$ [M+H]: 280.1338; found: 280.1336.

Notes:

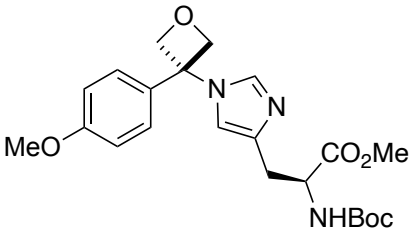
The structure of oxetane indole ***77*** *was confirmed by X-ray crystallography (see Scheme 26).*

4-((3-(4-Methoxyphenyl)oxetan-3-yl)sulfonyl)morpholine (26)



Oxetane sulfonyl fluoride **18a** (24.6 mg, 0.1 mmol, 1.0 equiv) and TMS-morpholine (21.3 μL, 0.12 mmol, 1.2 equiv) were added to a flame-dried reaction tube. The reaction vessel was sealed, anhydrous acetonitrile (0.33 mL, 0.3 M) was added by syringe and the reaction mixture was stirred at 60 ºC for 2 h. After allowing the tube cool to room temperature (ca. 22 ºC), EtOAc (5 mL) was added and the mixture was filtered through a plug of Celite, eluting with further EtOAc (3 × 10 mL). The solvent was removed *in vacuo* using a rotatory evaporator and purification by flash column chromatography (Et_2O) afforded oxetane amine **26** as a colourless gum (20.0 mg, 80%). R_f = 0.14 (Et_2O); ^{1}H NMR (400 MHz, $CDCl_3$) δ 7.00–6.97 (m, 2 H, 2 × Ar-CH), 6.93–6.90 (m, 2 H, 2 × Ar-CH), 4.90 (d, *J* = 6.0 Hz, C*H*HOC*H*H), 4.88 (d, *J* = 6.0 Hz, CH*H*OCH*H*), 3.83 (s, 3 H, OCH_3), 3.74 (br t, *J* = 4.5 Hz, 4 H, $CH_2CH_2OCH_2CH_2$), 2.32 (br s, 4 H, CH_2NCH_2). The observed characterisation data (R_f, ^{1}H) were consistent with that observed previously in the group.[210]

Methyl *N*^{a}-(*tert*-butoxycarbonyl)-*N*^{t}-(3-(4-methoxyphenyl)oxetan-3-yl)-*L*-histidinate (78)



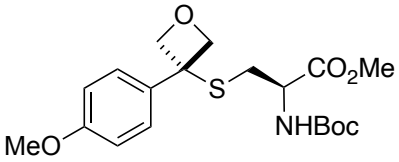
Prepared according to **General Procedure D** and using oxetane sulfonyl fluoride **18a** (29.7 mg) and methyl (*tert*-butoxycarbonyl)-*L*-histidinate (Boc-His-OMe; 26.9 mg). Purification by flash column chromatography (50–80% EtOAc/pentane) afforded oxetane imidazole **78** as a colourless gum (15.1 mg, 35%). Imidazole **78** was also isolated in 37% yield (16.0 mg) using **General Procedure B**. $[\alpha]_D^{21}$ +14.0 (c 1, $CDCl_3$); R_f = 0.10 (80% EtOAc/pentane); IR (film)/cm^{-1} 3357 (br NH), 2969, 2837, 1743 (C=O st), 1708 (C=O st), 1611, 1580, 1513, 1490, 1458, 1437, 1388, 1364, 1299, 1251, 1166, 1093, 1053, 1026, 990, 925, 832, 757, 732, 648, 575, 552; ^{1}H NMR (400 MHz, $CDCl_3$) δ 7.37 (br s, 1 H, $Ar_{(imidazole)}$-CH), 7.08–7.04 (m, 2 H, 2 × $Ar_{(PMP)}$-CH), 6.96–6.93 (m, 2 H, 2 × $Ar_{(PMP)}$-CH), 6.90 (br s, 1 H, $Ar_{(imidazole)}$-CH), 5.91 (d, *J* = 8.3 Hz, 1 H, NH), 5.22 (dd, *J* = 6.8, 1.9 Hz, 2 H, C*H*HOC*H*H), 5.17 (dd, *J* = 10.5, 6.8 Hz, 2 H, CH*H*OCH*H*), 4.60–4.56 (m, 1 H, CH), 3.84 (s, 3 H, Ar-$C_q$$OCH_3$), 3.70 (s, 3 H, CO_2CH_3), 3.17–3.04 (m, 2 H, Ar-$C_q$$CH_2$), 1.43 (s, 9 H, 3 × $C_q$$CH_3$); ^{13}C NMR (101 MHz, $CDCl_3$) δ 172.3

(CO_2Me), 159.9 (Ar-C_qOMe), 155.6 ($NHCO_2t$-Bu), 137.8 (Ar-C_qCH_2), 135.6 ($Ar_{(imidazole)}$-CH), 131.1 (Ar-C_qC_q), 127.0 (2 × $Ar_{(PMP)}$-CH), 115.4 ($Ar_{(imidazole)}$-CH), 114.5 (2 × $Ar_{(PMP)}$-CH), 83.2 (CH_2OCH_2), 79.7 ($C_q(CH_3)_3$), 63.5 (Ar-C_qC_q), 55.4 (Ar-C_qOCH_3), 53.4 (CH), 52.3 (CO_2CH_3), 30.1 (Ar-C_qCH_2), 28.3 (3 × C_qCH_3); HRMS (ESI) *m/z* calcd for $C_{22}H_{30}N_3O_6$ [M+H]: 432.2135, found: 432.2120.

Notes:

*Imidazole **78** was assigned as the oxetane imidazole and not as the oxetane sulfonate imidazole based on the absence of the SO_2 stretches in the IR spectrum and the absence of sulfur-containing fragments in the mass spectrum. The regiochemistry of the imidazole ring was assigned based on the assumption that the sterically less hindered site would react faster.*

Methyl *N*-(*tert*-butoxycarbonyl)-*S*-(3-(4-methoxyphenyl)oxetan-3-yl)-*L*-cysteinate (79)

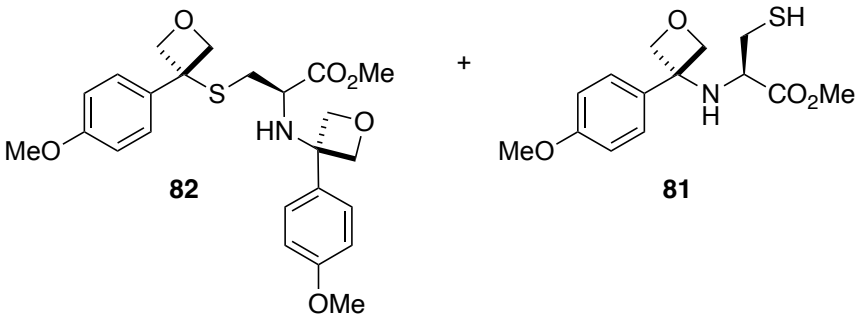


Prepared according to **General Procedure A** and using oxetane sulfonyl fluoride **18a** (49.2 mg) and methyl (*tert*-butoxycarbonyl)-*L*-cysteinate (Boc-Cys-OMe; 49.4 μL). Purification by flash column chromatography (0–6% Et_2O/CH_2Cl_2) afforded impure oxetane sulfide **79** as a colourless gum (38.8 mg). Repurification by flash column chromatography (0–6% Et_2O/CH_2Cl_2) afforded oxetane sulfide **79** as a colourless gum (29.8 mg, 37%). $[\alpha]_D^{22}$ +9.8 (c 1, $CDCl_3$); R_f = 0.22 (6% Et_2O/CH_2Cl_2); IR (film)/cm^{-1} 3357 (br NH), 2953, 1746 (C=O st), 1712 (C=O st), 1512, 1248, 1164; ^{1}H NMR (400 MHz, $CDCl_3$) δ 7.14–7.11 (m, 2 H, 2 × Ar-CH), 6.92–6.88 (m, 2 H, 2 × Ar-CH), 5.20–5.15 (br s, 1 H, NH), 5.18 (d, *J* = 6.4 Hz, 1 H, CHO), 5.16 (d, *J* = 6.4 Hz, 1 H, CHO), 4.87 (d, *J* = 6.4 Hz, 1 H, CHO), 4.86 (d, *J* = 6.4 Hz, 1 H, CHO), 4.44 (br dd, *J* = 5.1, 5.7 Hz, 1 H, CH), 3.82 (s, 3 H, Ar-C_qOCH_3), 3.73 (s, 3 H, CO_2CH_3), 2.84 (dd, *J* = 13.1, 5.1 Hz, 1 H, SC*H*H), 2.79 (dd, *J* = 13.1, 5.7 Hz, 1 H, SCH*H*), 1.45 (s, 9 H, 3 × C_qCH_3); ^{13}C NMR (101 MHz, $CDCl_3$) δ 171.2 (CO_2Me), 158.7 (Ar-C_qOMe), 155.0 ($NHCO_2t$-Bu), 133.8 (Ar-C_qC_q), 127.6 (2 × Ar-CH), 114.0 (2 × Ar-CH), 83.2 (CH_2OCH_2), 83.1 (CH_2OCH_2), 80.2 ($C_q(CH_3)_3$), 55.3 (Ar-C_qOCH_3), 53.0 (CH), 52.6 (CO_2CH_3), 52.1 (Ar-C_qC_q), 32.7 (SCH_2), 28.3 (3 × C_qCH_3); HRMS (ESI) *m/z* calcd for $C_{19}H_{28}NO_6S$ [M+H]: 398.1637, found: 398.1652.

Notes:

The signals at 5.20–5.15, 5.18 and 5.16 ppm in the ^{1}H NMR spectrum were integrated together to 3 H. The signals at 4.87 and 4.86 ppm in the ^{1}H NMR spectrum were integrated together to 2 H.

Methyl *N*,*S*-bis(3-(4-methoxyphenyl)oxetan-3-yl)-*L*-cysteinate (82) and methyl (3-(4-methoxyphenyl)oxetan-3-yl)-*L*-cysteinate (81)



Prepared according to **General Procedure C** and using oxetane sulfonyl fluoride **18a** (49.2 mg) and methyl *L*-cysteinate hydrochloride (Cys-OMe*HCl; 56.5 mg). Purification by flash column chromatography (20–100% EtOAc/pentane) afforded oxetane cysteine dimeric **82** as a colourless gum (10.0 mg, 22% [isolated with ca. 20% unknown impurities]), followed oxetane amine **81** as a colourless gum (3.8 mg, 6% [isolated with ca. 20% unknown impurities]).

Dimer **82**: $[a]_D^{22}$ +22.4 (c 0.43, $CDCl_3$); R_f = 0.55 (40% EtOAc/pentane); IR (film)/cm^{-1} 2950, 1735 (C=O st), 1513, 1248, 1180; ^{1}H NMR (400 MHz, $CDCl_3$) δ 7.21–7.18 (m, 2 H, 2 × Ar-CH), 7.01–6.99 (m, 2 H, 2 × Ar-CH), 6.92–6.90 (m, 2 H, 2 × Ar-CH), 6.88–6.86 (m, 2 H, 2 × Ar-CH), 5.10 (d, *J* = 4.2 Hz, 1 H, CHO), 5.09 (d, *J* = 4.2 Hz, 1 H, CHO), 4.97 (d, *J* = 6.5 Hz, 1 H, CHO), 4.83 (d, *J* = 6.5 Hz, 1 H, CHO), 4.81 (d, *J* = 2.8 Hz, 1 H, CHO), 4.80 (d, *J* = 2.8 Hz, 1 H, CHO), 4.69 (d, *J* = 6.5 Hz, 1 H, CHO), 4.67 (d, *J* = 6.5 Hz, 1 H, CHO), 3.834 (s, 3 H, Ar-C_qOCH$_3$), 3.827 (s, 3 H, Ar-C_qOCH$_3$), 3.59 (s, 3 H, CO_2CH_3), 3.10 (dd, *J* = 6.6, 6.6 Hz, 1 H, CH), 2.57 (dd, *J* = 12.9, 6.6 Hz, 1 H, SC*H*H), 2.49 (dd, *J* = 12.9, 6.6 Hz, 1 H, SCH*H*); ^{13}C NMR (101 MHz, $CDCl_3$) δ 174.2 (CO_2Me), 159.0 (Ar-C_qOMe), 158.6 (Ar-C_qOMe), 134.0 (Ar-C_qC_q), 128.0 (2 × Ar-CH), 127.7 (Ar-C_qC_q), 127.6 (2 × Ar-CH), 113.93 (2 × Ar-CH), 113.88 (2 × Ar-CH), 83.4 (CH_2O), 83.2 (CH_2O), 83.1 (CH_2O), 82.0 (CH_2O), 62.8 (Ar-C_qC_qNH), 56.3 (CH), 55.3 (2 × Ar-C_qOCH$_3$), 52.2 (CO_2CH_3), 52.0 (Ar-C_qC_qS), 34.0 (SCH_2); HRMS (ESI) *m/z* calcd for $C_{24}H_{30}NO_6S$ [M+H]: 460.1794, found: 460.1816.

Notes:

The signals at 5.10 and 5.09 ppm in the ^{1}H NMR spectrum were integrated together to 2 H. The signals at 4.83, 4.81 and 4.80 ppm in the ^{1}H NMR spectrum were integrated together to 3 H. The signals at 4.69 and 4.67 ppm in the ^{1}H NMR spectrum were integrated together to 2 H.

Oxetane amine **81**: $[\alpha]_D^{23}$ +5.1 (c 0.31, $CDCl_3$); R_f = 0.18 (40% EtOAc/pentane); IR (film)/cm^{-1} 2950, 1735 (C=O st), 1514, 1248, 1179; ^{1}H NMR (400 MHz, $CDCl_3$) δ 7.26–7.23 (m, 2 H, 2 × Ar-CH), 6.93–6.91 (m, 2 H, 2 × Ar-CH), 5.02 (d, *J* = 4.2 Hz, 1 H, CHO), 4.90–4.86 (m, 1 H, CHO), 4.78 (d, *J* = 6.5 Hz, 1 H, CHO), 4.75 (d, *J* = 6.5 Hz, 1 H, CHO), 3.83 (s, 3 H, Ar-C_qOCH_3), 3.63–3.58 (m, 3 H, CO_2CH_3), 3.52–3.47 (m, 1 H, CH), 3.13 (m, 2 H, SCH_2); ^{13}C NMR (101 MHz, $CDCl_3$) δ 173.8 (CO_2Me), 159.0 (Ar-C_qOMe), 133.2 (Ar-C_qC_q), 128.0 (2 × Ar-CH), 114.0 (2 × Ar-CH), 83.2 (CH_2OCH_2), 82.1 (CH_2OCH_2), 63.0 (Ar-C_qC_q), 55.6 (CH), 55.3 (Ar-C_qOCH_3), 52.4 (CO_2CH_3), 42.7 (SCH_2); HRMS (ESI) *m/z* calcd for $C_{28}H_{38}N_2O_8S_2$ [2 M]: 594.2070, found: 594.2073.

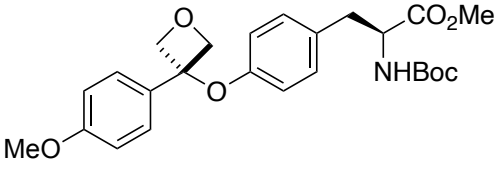
Notes:

*Oxetane **81** was assigned as N-bound and not S-bound based on the diagnostic chemical shift of the oxetane quaternary carbon (Ar-C_q**C_q**, 63.0 ppm) in the ^{13}C NMR spectrum.*

The signals at 5.10 and 5.09 ppm in the ^{1}H NMR spectrum were integrated together to 2 H. The signals at 4.83, 4.81 and 4.80 ppm in the ^{1}H NMR spectrum were integrated together to 3 H. The signals at 4.69 and 4.67 ppm in the ^{1}H NMR spectrum were integrated together to 2 H.

The signals at 173.8, 133.2, 83.2 and 42.7 ppm in the ^{13}C NMR spectrum were assigned with HSQC and HMBC 2D correlation spectra.

Methyl (*S*)-2-((*tert*-butoxycarbonyl)amino)-3-(4-((3-(4-methoxyphenyl)oxetan-3-yl)oxy)phenyl)propanoate (83)



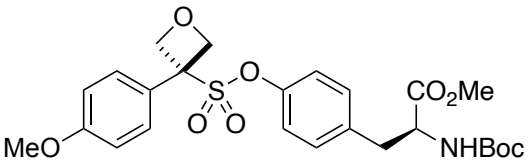
Prepared according to **General Procedure D** and using oxetane sulfonyl fluoride **18a** (29.6 mg) and methyl (*tert*-butoxycarbonyl)-*L*-tyrosinate (Boc-Tyr-OMe; 29.5 mg). Purification by flash column chromatography (0–10% Et_2O/CH_2Cl_2) afforded a mixture of oxetanol **22a**, oxetane ether **83** and oxetane sulfonate ester **84** (37.0 mg). Repurification by flash column chromatography (10–20% acetone/pentane) afforded oxetane ether **83** as a colourless gum (18.8 mg, 41%), followed by oxetane sulfonate ester **84** as a colourless gum (14.5 mg, 28%). Using **General Procedure B**, oxetane ether **83** was isolated in 32% yield (29.0 mg) alongside sulfonate ester **84** in 30% yield (31.4 mg). $[\alpha]_D^{21}$ +38.0 (c 1, $CDCl_3$); R_f = 0.65 (30% acetone/pentane); IR (film)/cm^{-1} 3365 (br NH), 2950, 1743 (C=O st), 1711 (C=O st), 1509, 1247, 1171; ^{1}H NMR (400 MHz, $CDCl_3$) δ 7.49–7.46 (m, 2 H, 2 × $Ar_{(PMP)}$-CH), 6.94–6.89 (m, 4 H, 2 × $Ar_{(Tyr)}$-CH + 2 × $Ar_{(PMP)}$-CH), 6.46–6.43 (m, 2 H, 2 × $Ar_{(Tyr)}$-CH), 5.08 (d, *J* = 6.8 Hz, 1 H, CHO), 5.07 (d, *J* = 6.8

Hz, 1 H, CHO), 4.94 (br d, *J* = 8.5 Hz, 1 H, NH), 4.90 (d, *J* = 6.8 Hz, 1 H, CHO), 4.89 (d, *J* = 6.8 Hz, 1 H, CHO), 4.54–4.49 (m, 1 H, CH), 3.81 (s, 3 H, Ar-C_qOCH_3), 3.68 (s, 3 H, CO_2CH_3), 2.99 (dd, *J* = 14.1, 5.7 Hz, 1 H, Ar-C_qC*H*H), 2.92 (dd, *J* = 14.1, 6.7 Hz, 1 H, Ar-C_qCH*H*), 1.41 (s, 9 H, 3 × C_qCH_3); ^{13}C NMR (101 MHz, $CDCl_3$) δ 172.3 (CO_2Me), 159.1 (Ar-C_qOMe), 155.0 (NHCO_2*t*-Bu), 153.9 (Ar-C_qOC_q), 132.0 (Ar-C_qC_q), 130.2 (2 × $Ar_{(Tyr)}$-CH), 128.4 (Ar-C_qCH_2), 126.0 (2 × $Ar_{(PMP)}$-CH), 116.3 (2 × $Ar_{(Tyr)}$-CH), 114.1 (2 × $Ar_{(PMP)}$-CH), 82.9 (CH_2OCH_2), 82.8 (CH_2OCH_2), 80.1 ($C_q(CH_3)_3$), 79.9 (Ar-C_qC_q), 55.2 (Ar-C_qOCH_3), 54.4 (CH), 52.2 (CO_2CH_3), 37.5 (Ar-C_qCH_2), 28.3 (3 × C_qCH_3); HRMS (ESI) *m/z* calcd for $C_{25}H_{31}NO_7Na$ [M+Na]: 480.1987, found: 480.1998.

Notes:

The signals at 5.08 and 5.07 ppm in the ^{1}H NMR spectrum were integrated together to 2 H. The signals at 4.94, 4.90 and 4.89 ppm in the ^{1}H NMR spectrum were integrated together to 3 H.

Methyl (*S*)-2-((*tert*-butoxycarbonyl)amino)-3-(4-(((3-(4-methoxyphenyl)oxetan-3-yl)sulfonyl)oxy)phenyl) propanoate (84)



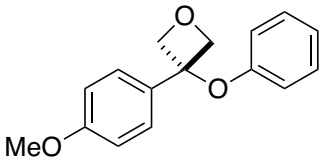
A reaction tube was charged with oven-dried Cs_2CO_3 (84.7 mg, 0.26 mmol, 1.3 equiv), followed by methyl (*tert*-butoxycarbonyl)-*L*-tyrosinate (Boc-Tyr-OMe; 70.9 mg, 0.24 mmol, 1.2 equiv) and oxetane sulfonyl fluoride **18a** (49.2 mg, 0.2 mmol, 1.0 equiv). The reaction vessel was sealed and anhydrous acetonitrile (0.66 mL, 0.3 M) was added by syringe. After stirring the reaction mixture at 60 ºC for 2 h, it was allowed to cool to 25 °C, EtOAc (5 mL) was added and the mixture was filtered through a plug of Celite, eluting with further EtOAc (3 × 10 mL). The solvent was removed *in vacuo* using a rotatory evaporator and purification by flash column chromatography (25% acetone/pentane) afforded oxetane sulfonate ester **84** as a white solid (81.3 mg, 80%). $[\alpha]_D^{21}$ +30.0 (c 1, $CDCl_3$); R_f = 0.42 (30% acetone/pentane); mp = 114 °C; IR (film)/cm^{-1} 3376 (br NH), 2971, 2889, 2839, 1742 (C=O st), 1710 (C=O st), 1609, 1581, 1510, 1441, 1389, 1358 (SO_2 st as), 1301, 1252, 1201, 1165 (SO_2 st sy), 1146, 1105, 1055, 1022, 998, 932, 867, 837, 785, 732, 688, 643, 554; ^{1}H NMR (400 MHz, $CDCl_3$) δ 7.28–7.24 (m, 2 H, 2 × $Ar_{(PMP)}$-CH), 7.11–7.09 (m, 2 H, 2 × $Ar_{(Tyr)}$-CH), 7.03–6.96 (m, 4 H, 2 × $Ar_{(PMP)}$-CH + 2 × $Ar_{(Tyr)}$-CH), 5.50 (d, *J* = 7.4 Hz, 2 H, C*H*HOC*H*H), 5.22 (d, *J* = 7.4 Hz, 2 H, CH*H*OCH*H*), 4.99 (d, *J* = 8.2 Hz, 1 H, NH), 4.56 (br dd, *J* = 6.2, 5.8 Hz, 1 H, CH), 3.86 (s, 3 H, Ar-C_qOCH_3), 3.70 (s, 3 H, CO_2CH_3), 3.11 (dd, *J* = 13.9, 5.8 Hz, 1 H, Ar-C_qC*H*H), 3.01 (dd, *J* = 13.9, 6.2 Hz, 1 H, Ar-C_qCH*H*), 1.42 (s, 9 H, 3 × C_qCH_3); ^{13}C NMR (101 MHz, $CDCl_3$) δ 172.0 (CO_2Me), 160.3

(Ar-C_qOMe), 155.0 (NHCO_2*t*-Bu), 148.0 (Ar-*C*$_q$OSO_2C_q), 135.2 (Ar-*C*$_q$$CH_2$), 130.6 (2 × Ar$_{(Tyr)}$-CH), 129.8 (2 × Ar$_{(PMP)}$-CH), 125.4 (Ar-*C*$_qC_q$), 121.8 (2 × Ar$_{(Tyr)}$-CH), 114.2 (2 × Ar$_{(PMP)}$-CH), 80.1 (*C*$_q$($CH_3$)$_3$), 77.3 ($CH_2OCH_2$), 67.8 (Ar-C$_q$*C*$_q$), 55.4 (Ar-C$_q$O*C*$H_3$), 54.2 (CH), 52.3 ($CO_2$*C*$H_3$), 37.7 (Ar-C$_q$*C*$H_2$), 28.2 (3 × C$_q$*C*$H_3$); HRMS (ESI) *m/z* calcd for $C_{25}H_{31}NO_9NaS$ [M+Na]: 544.1617, found: 544.1596.

Notes:

*The structure of sulfonate ester **84** was confirmed by X-ray crystallography (see Scheme 27).*

3-(4-Methoxyphenyl)-3-phenoxyoxetane (32)



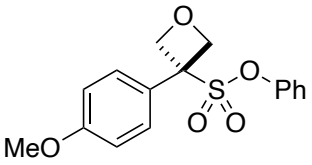
Using TMS-phenol: a reaction tube was charged with trimethyl(phenoxy)silane (43.4 mL, 0.24 mmol, 1.2 equiv) followed by oxetane sulfonyl fluoride **18a** (49.2 mg, 0.2 mmol, 1.0 equiv). The reaction vessel was sealed and anhydrous acetonitrile (0.66 mL, 0.3 M) was added by syringe. After stirring the reaction mixture at 60 ºC for 2 h, it was allowed to cool to room temperature (ca. 22 °C), EtOAc (5 mL) was added and the mixture was filtered through a plug of Celite, eluting with further EtOAc (3 × 10 mL). The solvent was removed *in vacuo* using a rotatory evaporator and purification by flash column chromatography (5–10% Et_2O/pentane) afforded oxetane ether **32** as a colourless gum (31.9 mg, 62%). On one occasion ether **32** crystallised to white crystals (mp = 71–73 °C). R_f = 0.54 (10% EtOAc/pentane); IR (film)/cm^{-1} 2950, 2873, 2834 1585, 1511, 1487, 1458, 1335, 1299, 1280, 1247, 1232, 1176, 1143, 1110, 1072, 1029, 985, 960, 897, 831, 808, 753, 692, 599, 546; ^{1}H NMR (400 MHz, $CDCl_3$) δ 7.52–7.48 (m, 2 H, 2 × Ar-CH), 7.19–7.15 (m, 2 H, 2 × Ar-CH), 6.94–6.88 (m, 3 H, 2 × Ar-CH), 6.55–6.51 (m, 2 H, 2 × Ar-CH), 5.11 (d, *J* = 7.4 Hz, 2 H, C*H*HOC*H*H), 4.91 (d, *J* = 7.4 Hz, 2 H, CH*H*OCH*H*), 3.81 (s, 3 H, OCH_3); ^{13}C NMR (101 MHz, $CDCl_3$) δ 159.1 (Ar-C$_q$OMe), 154.8 (Ar-*C*$_q$OC_q), 132.1 (Ar-*C*$_q$C$_q$), 129.4 (2 × Ar-CH), 126.0 (2 × Ar-CH), 121.0 (Ar-CH), 116.2 (2 × Ar-CH), 114.1 (2 × Ar-CH), 82.9 (CH_2OCH_2), 80.1 (C_q), 55.3 (OCH_3); HRMS (APCI) *m/z* calcd for $C_{10}H_{11}O_2^+$ [M–OPh]$^+$: 163.0754, found: 163.0751.

Using NEt_3 as base: a reaction tube was charged with NEt_3 (36.2 mL, 0.26 mmol, 1.3 equiv) followed by phenol (22.6 mg, 0.24 mmol, 1.2 equiv) and oxetane sulfonyl fluoride **18a** (49.2 mg, 0.2 mmol, 1.0 equiv). The reaction vessel was sealed and anhydrous acetonitrile (0.66 mL, 0.3 M) was added by syringe. After stirring the reaction mixture at 60 ºC for 2 h, it was allowed to cool to 25 °C, EtOAc (5 mL) was added and the mixture was filtered through a plug of Celite, eluting with further EtOAc (3 × 10 mL). The solvent was removed *in vacuo* using a rotatory evaporator and purification by flash column chromatography (5–25% Et_2O/pentane) afforded oxetane ether **32** as a colourless gum (24.9 mg, 49%) followed by oxetane sulfonate ester **85** as a white solid (5.4 mg, 8%).

Notes:

*The structure of oxetane ether **32** was confirmed by the diagnostic chemical shift of the oxetane quaternary carbon (80.1 ppm)[203] and by the synthesis of a genuine sample from oxetanol **22a** using previously developed Lewis acid catalysed conditions (Scheme 27).[203] The structure of **32** was unambiguously confirmed by X-ray crystallography (see Scheme 27).*

Phenyl 3-(4-methoxyphenyl)oxetane-3-sulfonate (85)



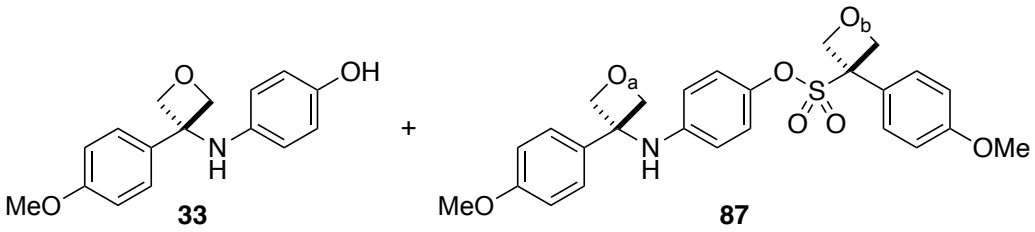
Using NaH: NaH (60 wt% dispersion in mineral oil, 9.6 mg, 0.241 mmol, 1.205 equiv) was added portionwise to a solution of phenol (22.6 mg, 0.24 mmol, 1.20 equiv) in anhydrous acetonitrile (0.66 mL) at 0 °C. The reaction was warmed to 25 °C, oxetane sulfonyl fluoride **18a** (49.2 mg, 0.2 mmol, 1.0 equiv) was added and the reaction vial was sealed. The reaction mixture was warmed up to 60 °C and after stirring the reaction mixture at this temperature for 2 h, it was allowed to cool to room temperature (ca. 22 ºC), EtOAc (5 mL) was added and the mixture was filtered through a plug of Celite, eluting with further EtOAc (3 × 10 mL). The solvent was removed *in vacuo* using a rotatory evaporator and purification by flash column chromatography (20–30% Et_2O/pentane) afforded oxetane sulfonate ester **85** as a white solid (53.1 mg, 83%). R_f = 0.29 (40% Et_2O/pentane); ^{1}H NMR (400 MHz, $CDCl_3$) δ 7.37–7.32 (m, 2 H, 2 × Ar-CH), 7.29–7.25 (m, 3 H, 3 × Ar-CH), 7.11–7.08 (m, 2 H, 2 × Ar-CH), 7.01–6.97 (m, 2 H, 2 × Ar-CH), 5.53 (d, *J* = 7.2 Hz, 2 H, C*H*HOC*H*H), 5.24 (d, *J* = 7.2 Hz, 2 H, CH*H*OCH*H*), 3.86 (s, 3 H, OCH_3); HRMS (APCI) *m/z* calcd for $C_{16}H_{15}O_3^-$ [M–SO_2Ph–H]$^-$: 255.1027, found: 255.1027; also: *m/z* calcd for $C_{10}H_{11}O_5S^-$ [M–Ph]$^-$: 243.0333, found: 243.0332; *m/z* calcd for $C_{10}H_{11}O_4S^-$ [M–OPh]$^-$: 227.0384, found: 227.0381. The observed characterisation data (R_f, ^{1}H) were consistent with that observed previously in the group.[210]

Using Cs_2CO_3: A reaction tube was charged with oven-dried Cs_2CO_3 (84.7 mg, 0.26 mmol, 1.3 equiv), followed by phenol (22.6 mg, 0.24 mmol, 1.2 equiv) and oxetane sulfonyl fluoride **18a** (49.2 mg, 0.2 mmol, 1.0 equiv). The reaction vessel was sealed and anhydrous acetonitrile (0.66 mL, 0.3 M) was added by syringe. After stirring the reaction mixture at 60 ºC for 2 h, it was allowed to cool to room temperature (ca. 22 ºC), EtOAc (5 mL) was added and the mixture was filtered through a plug of Celite, eluting with further EtOAc (3 × 10 mL). The solvent was removed *in vacuo* using a rotatory evaporator and purification by flash column chromatography (5–25% Et_2O/pentane) afforded oxetane ether **32** as a colourless gum (5.2 mg, 10%), followed by oxetane sulfonate ester **85** as a white solid (48.4 mg, 76%).

Notes:

*The structure of oxetane sulfonate ester **85** was confirmed by X-ray crystallography (see Scheme 27).*

4-((3-(4-Methoxyphenyl)oxetan-3-yl)amino)phenol (33) and 4-((3-(4-methoxyphenyl)oxetan-3-yl)amino)phenyl 3-(4-methoxyphenyl)oxetane-3-sulfonate (87)

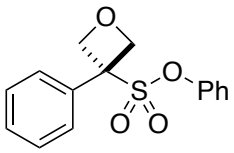


A reaction tube was charged with anhydrous K_2CO_3 (18.0 mg, 0.13 mmol, 1.3 equiv) and flame-dried under air. The tube was allowed to cool to room temperature (ca. 22 ºC) and 4-aminophenol (13.1 mg, 0.12 mmol, 1.2 equiv) and oxetane sulfonyl fluoride **18a** (24.6 mg, 0.10 mmol, 1.0 equiv) were added sequentially. The reaction vessel was sealed, anhydrous acetonitrile (0.33 mL, 0.3 M) was added by syringe and the reaction mixture was stirred at 25 ºC for 24 h. EtOAc (5 mL) was added and the mixture was filtered through a plug of Celite, eluting with further EtOAc (3 × 10 mL). The solvent was removed *in vacuo* using a rotatory evaporator and purification by flash column chromatography (40–100% Et_2O/pentane) afforded oxetane amine **33** as a colourless gum (9.3 mg, 34%), followed by a mixture of oxetane sulfonate ester **86** with dimer **87**. The mixture was repurified by flash column chromatography (0–10% Et_2O/CH_2Cl_2) to afford dimer **87** as a colourless gum (1.8 mg, 1%), followed by a mixture of sulfonate ester **86** and dimer **87** (9.7 mg **86**:**87** = 44:56).

Oxetane amine **33**: R_f = 0.15 (60% Et_2O/pentane); ^1H NMR (400 MHz, $CDCl_3$) δ 7.58–7.56 (m, 2 H, 2 × $Ar_{(PMP)}$-CH), 6.93–6.90 (m, 2 H, 2 × $Ar_{(PMP)}$-CH), 6.63–6.59 (m, 2 H, 2 × $Ar_{(p\text{-}OH)}$-CH), 6.23–6.19 (m, 2 H, 2 × $Ar_{(p\text{-}OH)}$-CH), 4.96 (d, *J* = 6.3 Hz, 2 H C*H*HOC*H*H), 4.85 (d, *J* = 6.3 Hz, 2 H, CH*H*OCH*H*), 4.49 (br s, 1 H, NH or OH), 4.38 (br s, 1 H, NH or OH), 3.82 (s, 3 H, OCH_3). The observed characterisation data (R_f, ^1H) were consistent with that observed previously in the group.[210]

Dimer **87**: R_f = 0.60 (20% Et_2O/CH_2Cl_2); IR (film)/cm^{-1} 3402 (NH st, br), 2956, 1609, 1511, 1344 (SO_2 st as), 1251, 1180 (SO_2 st sy); ^1H NMR (500 MHz, $CDCl_3$) δ 7.54–7.51 (m, 2 H, 2 × Ar-CH), 7.25–7.22 (m, 2 H, 2 × Ar-CH), 6.97–6.94 (m, 2 H, 2 × Ar-CH), 6.93–6.90 (m, 2 H, 2 × Ar-CH), 6.83–6.80 (m, 2 H, 2 × Ar-CH), 6.21–6.18 (m, 2 H, 2 × Ar-CH), 5.48 (d, *J* = 7.5 Hz, 2 H, C*H*HO_bC*H*H), 5.19 (d, *J* = 7.5 Hz, 2 H, CH*H*O_bCH*H*), 4.94 (d, *J* = 6.4 Hz, 2 H, C*H*HO_aC*H*H), 4.83 (d, *J* = 6.4 Hz, 2 H, CH*H*O_aCH*H*), 4.64 (br s, 1 H, NH), 3.84 (s, 3 H, OCH_3), 3.82 (s, 3 H, OCH_3); ^{13}C NMR (126 MHz, $CDCl_3$) δ 160.2 (Ar-C_qOMe), 159.0 (Ar-C_qOMe), 143.6 (Ar-$C_q$$OSO_2$), 140.4 (Ar-$C_q$NH), 133.2 (Ar-$C_q$$C_q$), 129.7 (2 × Ar-CH), 126.6 (2 × Ar-CH), 125.7 (Ar-$C_q$$C_q$), 122.8 (2 × Ar-CH), 114.5 (2 × Ar-CH), 114.18 (2 × Ar-CH), 114.15 (2 × Ar-CH), 84.1 ($CH_2O_aCH_2$), 77.4 ($CH_2O_bCH_2$), 67.4 ($C_qCH_2O_b$), 60.0 ($C_qCH_2O_a$), 55.4 (OCH_3), 55.3 (OCH_3); HRMS (APCI) *m/z* calcd for $C_{26}H_{28}NO_7S^+$ $[M+H]^+$: 498.1581, found: 498.1575.

Phenyl 3-phenyloxetane-3-sulfonate (88)



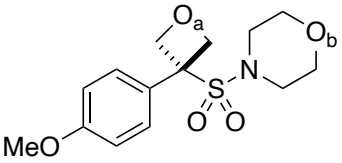
A reaction tube was charged with oven-dried Cs_2CO_3 (49.6 mg, 0.152 mmol, 1.3 equiv), followed by phenol (13.3 mg, 0.141 mmol, 1.2 equiv) and oxetane sulfonyl fluoride **18m** (25.2 mg, 0.117 mmol, 1.0 equiv) were added sequentially. The reaction vessel was sealed and anhydrous acetonitrile (0.39 mL, 0.3 M) was added by syringe. After stirring the reaction mixture at 60 ºC for 2 h, it was allowed to cool to room temperature (ca. 22 ºC), EtOAc (5 mL) was added and the mixture was filtered through a plug of Celite, eluting with further EtOAc (3 × 10 mL). The solvent was removed *in vacuo* using a rotatory evaporator and purification by flash column chromatography (15% Et_2O/pentane) afforded oxetane sulfonate ester **88** as colourless crystals (33.3 mg, 98%).

R_f = 0.17 (15% Et_2O/pentane); mp = 96 °C, IR (film)/cm^{-1} 3059, 2954, 2885, 1584, 1484, 1454, 1352 (SO_2 st as), 1285, 1197, 1167, 1141 (SO_2 st sy), 1107, 1087, 1023, 996, 934, 910, 861, 772, 720, 680, 666, 603, 545, 481; ^{1}H NMR (400 MHz, $CDCl_3$) δ 7.52–7.45 (m, 3 H, 3 × Ph-CH), 7.38–7.32 (m, 4 H, 4 × Ph-CH), 7.29–7.25 (m, 1 H, Ph-CH), 7.07–7.03 (m, 2 H, 2 × Ph-CH), 5.56 (d, *J* = 7.7 Hz, 2 H, C*H*HOC*H*H), 5.29 (d, *J* = 7.7 Hz, 2 H, CH*H*OCH*H*); ^{13}C NMR (101 MHz, $CDCl_3$) δ 149.0 (Ph-C_qOSO$_2$C$_q$), 133.8 (Ph-C_qC$_q$), 129.8 (2 × Ph-CH), 129.4 (Ph-CH), 128.8 (2 × Ph-CH), 128.5 (2 × Ph-CH), 127.1 (Ph-CH), 121.7 (2 × Ph-CH), 77.3 (CH_2OCH_2), 68.2 (C_q); mass ion not found by HRMS (APCI).

Notes:

*The structure of sulfonate ester **88** was confirmed by X-ray crystallography (see Scheme 28).*

4-((3-(4-Methoxyphenyl)oxetan-3-yl)sulfonyl)morpholine (25)



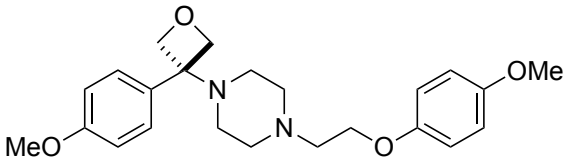
n-BuLi (1.54 M in hexanes, 0.065 mL, 0.1 mmol, 2.0 equiv) was added to a solution of morpholine (8.7 μL, 0.1 mmol, 2.0 equiv) in anhydrous THF (0.5 mL, 0.1 M) at –78 ºC in a reaction tube. After stirring for 15 min, oxetane sulfonyl fluoride **18a** (12.3 mg, 0.05 mmol, 1.0 equiv) was added in one portion and the reaction was allowed to warm to 0 ºC over 1 h. The reaction was quenched with methanol (1.0 mL) and concentrated *in vacuo* using a rotatory evaporator. Purification by flash column chromatography (60–80% Et_2O/pentane) afforded oxetane sulfonamide **25** as colourless crystals (10.5 mg, 67%). R_f = 0.21 (80% Et_2O/pentane); mp = 149 °C; IR (film)/cm^{-1} 2959, 1610, 1514, 1335, 1322 (SO_2 st as), 1252, 1149 (SO_2 st sy), 1113, 954; ^{1}H NMR (400 MHz, $CDCl_3$) δ 7.22–7.19 (m, 2 H, 2 × Ar-CH), 6.98–6.94 (m, 2 H, 2 × Ar-CH), 5.35 (d, *J* = 7.0 Hz, 2 H, C*H*HO$_a$C*H*H), 5.10 (d, *J* = 7.0 Hz, 2 H, CH*H*O$_a$CH*H*), 3.85 (s, 3 H, OCH_3), 3.56 (br t, *J* = 4.7 Hz, 4 H, $CH_2O_bCH_2$), 2.98 (br t, *J* = 4.7 Hz, 4 H, CH_2NCH_2); ^{13}C NMR (101 MHz, $CDCl_3$) δ 160.0 (Ar-C_qOMe), 129.4 (2 × Ar-CH), 126.8 (Ar-C_qC$_q$), 114.0 (2 × Ar-CH), 78.0 ($CH_2O_aCH_2$), 68.5 (C_q), 66.9 ($CH_2O_bCH_2$), 55.4 (OCH_3), 47.0 (CH_2NCH_2); HRMS (APCI) *m/z* calcd for $C_{14}H_{19}NO_5S^{35}Cl^-$ [M+Cl]$^-$: 348.0678, found: 348.0670.

Notes:

*The structure of oxetane sulfonamide **25** was confirmed by X-ray crystallography (see Scheme 28).*

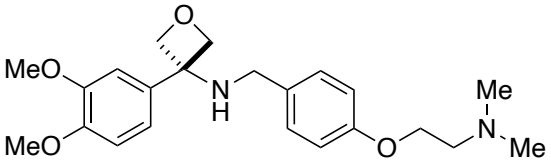
7.6.4.3 Oxetane Analogues of Drugs

1-(2-(4-Methoxyphenoxy)ethyl)-4-(3-(4-methoxyphenyl)oxetan-3-yl)piperazine (89)



Prepared according to **General Procedure A** and using oxetane sulfonyl fluoride **18a** (49.2 mg) and 1-(2-(4-methoxyphenoxy)ethyl)-piperazine (56.7 mg). Purification by flash column chromatography (20–50% Et_2O/CH_2Cl_2) afforded oxetane amine **89** as a light-yellow gum (53.5 mg, 67%). R_f = 0.13 (20% Et_2O/CH_2Cl_2); IR (film)/cm^{-1} 3001, 2945, 2878, 2833, 1610, 1510, 1461, 1353, 1297, 1230, 1178, 1122, 1036, 910, 828, 731; ^{1}H NMR (400 MHz, $CDCl_3$) δ 6.99–6.95 (m, 2 H, 2 × Ar-CH), 6.90–6.87 (m, 2 H, 2 × Ar-CH), 6.81 (s, 4 H, 4 × Ar-CH), 4.90 (d, *J* = 5.9 Hz, 2 H, C*H*HOC*H*H), 4.86 (d, *J* = 5.9 Hz, 2 H, CH*H*OCH*H*), 4.01 (t, *J* = 5.8 Hz, 2 H, OC$H_2$$CH_2$), 3.81 (s, 3 H, OCH_3), 3.76 (s, 3 H, OCH_3), 2.78 (t, *J* = 5.8 Hz, 2 H, $OCH_2C$$H_2$), 2.67 (br s, 4 H, CH_2NCH_2), 2.35 (br s, 4 H, CH_2NCH_2); ^{13}C NMR (101 MHz, $CDCl_3$) δ 158.7 (Ar-C_qO), 153.8 (Ar-C_qO), 152.8 (Ar-C_qO), 129.2 (Ar-$C_q$$C_q$), 128.4 (2 × Ar-CH), 115.5 (2 × Ar-CH), 114.5 (2 × Ar-CH), 113.2 (2 × Ar-CH), 79.8 (CH_2OCH_2), 66.3 (O$C$$H_2$$CH_2$), 66.2 ($C_q$), 57.2 ($OCH_2$$CH_2$), 55.7 ($OCH_3$), 55.3 ($OCH_3$), 53.7 ($CH_2NCH_2$), 45.5 ($CH_2NCH_2$); HRMS (ESI) *m/z* calcd for $C_{23}H_{31}N_2O_4^+$ $[M+H]^+$: 399.2278, found: 399.2273.

3-(3,4-Dimethoxyphenyl)-*N*-(4-(2-(dimethylamino)ethoxy)benzyl)oxetan-3-amine (90)



Prepared according to **General Procedure A** under air with a Celite workup and using oxetane sulfonyl fluoride **18n** (55.3 mg)[ii] and 2-(4-(aminomethyl)phenoxy)-*N*,*N*-dimethylethan-1-amine (47.0 mg). Purification by flash column chromatography (2–15% $MeOH/CH_2Cl_2$) afforded oxetane amine **90** as a light-yellow solid (37.5 mg, 49%). R_f = 0.12 (10% $MeOH/CH_2Cl_2$); mp = 93–96 °C; IR (film)/cm^{-1} 2941, 2870, 2825, 2773,1685, 1610, 1513, 1461, 1409, 1334, 1297, 1249, 1170, 1029, 984, 913, 813, 764, 731; ^{1}H NMR (400 MHz, $CDCl_3$) δ 7.22–7.18 (m, 2 H, 2 × Ar-CH), 7.04–7.01 (m, 2 H, Ar-C_qOMeAr-CHAr-C_qAr-CH), 6.90 (d, *J* = 8.6 Hz, 1 H, Ar-C_qOMeC*H*CH), 6.88–6.85 (m, 2 H, 2 × Ar-CH), 4.94 (d, *J* = 6.4 Hz, 2 H, C*H*HOC*H*H), 4.73 (d, *J* = 6.4 Hz, 2 H, CH*H*OCH*H*), 4.08 (t, *J* = 5.7 Hz, 2 H, OC$H_2$$CH_2$), 3.91 (s, 3 H, OCH_3), 3.90 (s, 3 H, OCH_3), 3.47 (s, 2 H, NCH_2Ar-C_q), 2.78 (t, *J* = 5.7 Hz, 2 H, $OCH_2C$$H_2$), 2.38 (s, 6 H, 2 × NCH_3); ^{13}C NMR (101 MHz, $CDCl_3$) δ 157.8 (Ar-C_qO), 149.2 (Ar-C_qO), 148.2 (Ar-C_qO), 134.5 (Ar-$C_q$$C_q$), 132.3 (Ar-$C_q$$C_q$), 129.2 (2 × Ar-CH), 118.5 (Ar-CH),

[ii] Prepared by E. Briggs.[212]

114.5 (2 × Ar-CH), 110.8 (Ar-CH), 109.3 (Ar-CH), 82.7 (CH_2OCH_2), 65.7 (OCH_2CH_2), 63.4 (C_q), 58.1 (OCH_2CH_2), 55.91 (OCH_3), 55.87 (OCH_3), 47.3 ($NCH_2Ar\text{-}C_q$), 45.7 (2 × NCH_3); HRMS (APCI) *m/z* calcd for $C_{22}H_{31}N_2O_4^+$ $[M+H]^+$: 387.2278, found: 387.2276.

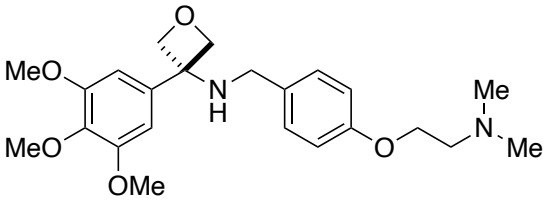
Notes:

The multiplet at 7.04–7.01 was composed of a dd and a singlet. The ^3J coupling was obscured by the singlet, but ^4J = 2.1 Hz.

The doublet at 6.90 (1 H) and the multiplet at 6.88–6.85 (2 H) ppm were integrated together to 3 H. The singlets at 3.91 (3 H) and 3.90 (3 H) ppm were integrated together to 6 H.

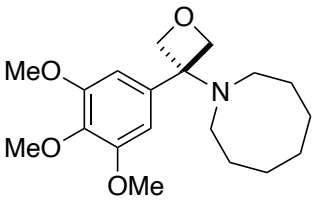
There was a very broad singlet under the triplet at 2.78 ppm which was assigned to NH + H_2O.

_N_-(4-(2-(Dimethylamino)ethoxy)benzyl)-3-(3,4,5-trimethoxyphenyl)oxetan-3-amine (91)



Prepared according to **General Procedure A** for 13 h and using oxetane sulfonyl fluoride **18f** (61.6 mg) and 2-(4-(aminomethyl)phenoxy)-*N*,*N*-dimethylethan-1-amine (47.0 mg). Purification by flash column chromatography (5–10% MeOH/CH_2Cl_2) afforded oxetane amine **91** as a colourless oil (26.5 mg, 32%). The product was somewhat unstable on silica. Column chromatography was performed in the shortest time possible (<30 min) with the shortest possible column. A benzaldehyde side product which was not present in the crude reaction mixture, was observed in some of the collected fractions after the purification. The aldehyde was presumably formed by oxidation at the non-oxetanyl aminobenzylic position. R_f = 0.21 (10% MeOH/CH_2Cl_2); IR (film)/cm^{-1} 2941, 2870, 2825, 2773, 1588, 1510, 1461, 1413, 1334, 1297, 1238, 1175, 1126, 1036, 828, 775, 731; ^{1}H NMR (400 MHz, $CDCl_3$) δ 7.23–7.20 (m, 2 H, 2 × Ar-CH), 6.89–6.85 (m, 2 H, 2 × Ar-CH), 6.72 (s, 2 H, 2 × Ar-CH), 4.93 (d, *J* = 6.5 Hz, 2 H, C*H*HOC*H*H), 4.73 (d, *J* = 6.5 Hz, 2 H, CH*H*OCH*H*), 4.08 (t, *J* = 5.6 Hz, 2 H, OCH_2CH_2), 3.89 (s, 6 H, 2 × OCH_3), 3.87 (s, 3 H, OCH_3), 3.50 (s, 2 H, NCH_2Ph), 2.78 (t, *J* = 5.6 Hz, 2 H, OCH_2CH_2), 2.59 (br s, 1 H, NH), 2.38 (s, 6 H, 2 × NCH_3); ^{13}C NMR (101 MHz, $CDCl_3$) δ 157.9 ($Ar\text{-}C_qOCH_2$), 153.3 (2 × $Ar\text{-}C_qOMe$), 137.7 ($Ar\text{-}C_qOMe$), 137.0 ($Ar\text{-}C_qC_q$), 132.2 ($Ar\text{-}C_qCH_2$), 129.2 (2 × $Ar\text{-}CHC_qCH_2$), 114.5 (2 × $Ar\text{-}CHC_qOCH_2$), 103.3 (2 × $Ar\text{-}CHC_qC_q$), 82.7 (CH_2OCH_2), 65.7 (OCH_2CH_2), 63.7 ($Ar\text{-}C_qC_q$), 60.8 (OCH_3), 58.1 (OCH_2CH_2), 56.2 (2 × OCH_3), 47.3 (NCH_2Ph), 45.7 (2 × NCH_3); HRMS (ESI) *m/z* calcd for $C_{23}H_{33}N_2O_5$ [M+H]: 417.2389, found: 417.2389.

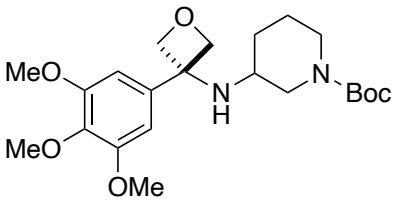
1-(3-(3,4,5-Trimethoxyphenyl)oxetan-3-yl)azocane (92)



Prepared according to **General Procedure A** for 13 h and using oxetane sulfonyl fluoride **18f** (61.3 mg) and azocane (31 μL). Purification by automated column chromatography afforded oxetane amine **92** as a colourless gum with unknown impurities (45.1 mg). Repurification by flash column chromatography (40% Et_2O/pentane) afforded oxetane amine **92** as a colourless gum (30.8 mg, 46%). R_f = 0.38 (40% Et_2O/pentane); IR (film)/cm^{-1} 2919, 1584, 1510, 1454, 1413, 1327, 1245, 1170, 1126, 987, 958, 869, 835, 772, 739, 708; ^{1}H NMR (400 MHz, $CDCl_3$) δ 6.49 (s, 2 H, 2 × Ar-CH), 4.88 (d, *J* = 6.0 Hz, 2 H, C*H*HOC*H*H), 4.84 (d, *J* = 6.0 Hz, 2 H, CH*H*OCH*H*), 3.87 (s, 6 H, 2 × OCH_3), 3.86 (s, 3 H, OCH_3), 2.50 (t, *J* = 5.9 Hz, 4 H, CH_2NCH_2), 1.73–1.58 (m, 10 H, 5 × CH_2); ^{13}C NMR (101 MHz, $CDCl_3$) δ 152.8 (2 × Ar-C_qOMe), 137.4 (Ar-C_qOMe), 136.9 (Ar-C_q), 104.1 (2 × Ar-CH), 80.8 (CH_2OCH_2), 68.0 (C_q), 60.9 (OCH_3), 56.2 (2 × OCH_3), 49.0 (CH_2NCH_2), 28.8 (2 × CH_2), 28.4 (CH_2), 25.3 (2 × CH_2); HRMS (ESI) *m/z* calcd for $C_{19}H_{30}NO_4$ [M+H]: 336.2175, found: 336.2175.

Automated column conditions: Column Type: Biotage® Sfär HC 10 g. Flow rate: 40 mL/min. 14 column volumes (CV) 0–4% MeOH/CH_2Cl_2, 2 CV 4–100% MeOH/CH_2Cl_2. Fractions 5–21: impure oxetane amine **92**.

***tert*-Butyl 3-((3-(3,4,5-trimethoxyphenyl)oxetan-3-yl)amino)piperidine-1-carboxylate (93')**



Prepared according to **General Procedure** for 13 h and using oxetane sulfonyl fluoride **18f** (61.3 mg) and *tert*-butyl 3-aminopiperidine-1-carboxylate (48.3 mg). Purification by flash column chromatography (25% acetone/pentane) afforded oxetane amine **93'** as a yellow gum (62.8 mg, 74%). R_f = 0.24 (30% acetone/pentane); IR (film)/cm^{-1} 2937, 2864, 1685 (C=O st), 1588, 1510, 1465, 1416, 1364, 1241, 1126, 1007, 980, 924, 857, 768, 734; ^{1}H NMR (400 MHz, $CDCl_3$) δ 6.65 (br s, 2 H, 2 × Ar-CH), 5.08 (br s, 1 H, C*H*HO), 4.93 (d, *J* = 6.3 Hz, 1 H, C*H*HO), 4.74 (br s, 2 H, 2 × C*H*HO), 3.89 (s, 6 H, 2 × OCH_3), 3.86 (s, 3 H, OCH_3), 2.79 (ddd, $^3J_{ax,ax}$ = 13.5, 10.6 Hz, $^3J_{ax,eq}$ = 3.1 Hz, CH), 2.59 (br s, 1 H, C*H*HN), 2.38 (br s, 1 H, C*H*HN), 1.97–1.50 (br m, 5 H, 5 × C*H*H), 1.46–1.24 (br m, 10 H, 3 × C_qCH_3 + C*H*H); ^{13}C NMR (101 MHz, $CDCl_3$) δ 154.6 (C_q=O), 153.3 (2 × Ar-C_qOMe), 137.2 (weak, Ar-C_qOMe), 103.6 (2 × Ar-CH), 83.7 (br and weak, CH_2OCH_2), 79.5 ($C_q(CH_3)_3$), 63.2 (Ar-C_qC_q), 60.8 (OCH_3), 56.2 (2 × OCH_3), 49.9

(N*C*H$_2$CH), 43.8 (br and weak, CH), 32.5 (br and weak, CH$_2$), 28.3 (3 × C$_q$*C*H$_3$), 23.8 (CH$_2$); HRMS (APCI) *m/z* calcd for $C_{22}H_{35}N_2O_6^+$ [M+H]$^+$: 423.2490, found: 423.2480.

Notes:

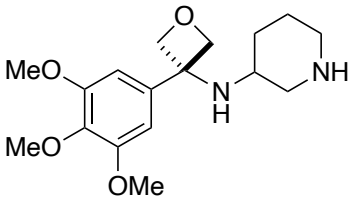
The singlet for the tert-butyl group was located at 1.40 ppm under the broad multiplet between 1.46–1.24.

Most signals in the ^{1}H and ^{13}C NMR spectra were broadened and/or weak due to chemical exchange between conformers caused by N and ring-inversion and carbamate rotation.

*The weak ^{13}C signals were assigned by HSQC and HMBC 2D correlation spectra. The Ar**C**$_q$C$_q$ and one CH$_2$ signal were not found in the ^{13}C NMR spectrum nor 2D correlation spectra. There seemed to be a weak HMBC correlation between C$_{(oxetane)}$H$_2$'s and a very weak and broad peak at 138.0 ppm which could be the Ar**C**$_q$C$_q$ signal.*[212]

*The identity of Boc-protected **93'** was confirmed by HRMS and the assignment of its Boc-deprotected derivative **93**.*

N-(3-(3,4,5-Trimethoxyphenyl)oxetan-3-yl)piperidin-3-amine (93)



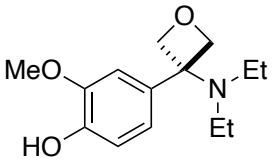
Trifluoroacetic acid (0.11 mL, 1.44 mmol, 10 equiv) was added dropwise to a solution of oxetane amine **18f** (62.6 mg, 0.148 mmol, 1.0 equiv) in anhydrous CH_2Cl_2 (0.74 mL, 0.2 M) at 0 °C. After stirring for 5 min at 0 °C, the reaction mixture was warmed to 25 °C and stirred for further 16 h. Sat. aq. $NaHCO_3$ (5 mL) was added and the aqueous layer was extracted with EtOAc (6 × 10 mL). The organic layers were combined and dried over Na_2SO_4, filtered and concentrated *in vacuo* using a rotatory evaporator to yield oxetane di-amine **93** as a light-yellow gum (32.7 mg). Brine (5 mL) and aq. NaOH (1 M, 2 mL) were added to the aqueous phase and it was reextracted with EtOAc (2 × 10 mL), CH_2Cl_2 (2 × 10 mL) and a mixture of $CHCl_3$:isopropanol (3:1, 2 × 10 mL). The organic layers were combined and dried over Na_2SO_4, filtered and concentrated *in vacuo* using a rotatory evaporator to yield further oxetane di-amine **93** as a light-yellow gum (15.0 mg). A total of 47.7 mg (quant.) were obtained. R_f = 0.17 (10% MeOH/CH_2Cl_2); IR (film)/cm^{-1} 2945, 2870, 1677, 1592, 1510, 1465, 1416, 1334, 1241, 1200, 1126, 1006, 910, 835, 768, 731; ^{1}H NMR (400 MHz, $CDCl_3$) δ 6.58 (s, 2 H, 2 × Ar-CH), 4.99 (d, *J* = 6.3 Hz, 1 H, C*H*HOCHH), 4.90 (d, *J* = 6.3 Hz, 1 H, CHHOC*H*H), 4.69 (d, *J* = 6.3 Hz, 1 H, CH*H*OCHH), 4.68 (d, *J* = 6.3 Hz, 1 H, CHHOCH*H*), 3.87 (s, 6 H, 2 × OCH_3), 3.85 (s, 3 H, OCH_3), 3.25 (br s, 2 H, 2 × NH), 2.92–2.87 (m, 1 H, NC*H*HCH$_2$), 2.76 (dd, ^2J = 11.8 Hz, $^3J_{eq,ax}$ = 3.8 Hz, 1 H, NCH_{eq}HCH), 2.64–2.53 (m, 2 H, CH + NCH*H*CH$_2$), 2.34 (dd, ^2J = 11.8 Hz, $^3J_{ax,ax}$ = 8.7 Hz, NCHH_{ax}CH), 1.76–1.69 (m, 2 H, CHC*H*HC*H*H), 1.53–1.42 (m, 1 H, CHCH$_2$CH*H*), 1.31–1.21

(m, 1 H, CHCH*H*CH_2); ^{13}C NMR (101 MHz, $CDCl_3$) δ 153.4 (2 × Ar-C_qOMe), 138.3 (Ar-C_qC_q), 137.2 (Ar-C_qOMe), 103.5 (2 × Ar-CH), 83.9 (CH_2OCH_2), 83.1 (CH_2OCH_2), 63.4 (C_q), 60.9 (OCH_3), 56.2 (2 × OCH_3), 52.4 (NCH_2CH), 49.7 (CH), 45.4 (NCH_2CH_2), 32.5 ($CHCH_2$), 23.7 ($CHCH_2CH_2$); HRMS (APCI) *m/z* calcd for $C_{17}H_{27}N_2O_4^+$ $[M+H]^+$: 323.1965, found: 323.1965.

Notes:

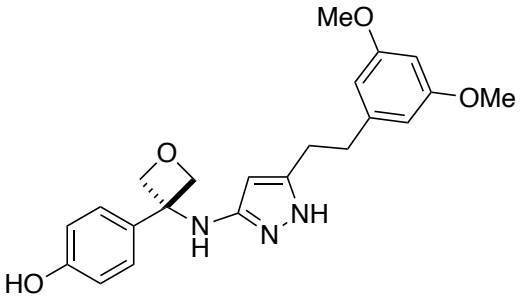
The signals at 4.69 and 4.68 ppm were integrated together to 2 H.

4-(3-(Diethylamino)oxetan-3-yl)-2-methoxyphenol (94)



A reaction tube was charged with anhydrous K_2CO_3 (18.0 mg, 0.13 mmol, 1.3 equiv) and flame-dried under air. The tube was allowed to cool to room temperature (ca. 22 ºC) and diethylamine (12.4 μL) and oxetane sulfonyl fluoride **18g** (41.9 mg, 0.10 mmol, 1.0 equiv; 95:5 mixture of **18g**:**18g'**) were added sequentially. The reaction vessel was sealed and acetonitrile (0.33 mL, 0.3 M) was added by syringe. Addition of OSF **18g** and sealing of the reaction tube was done as quickly as possible to avoid evaporation of volatile diethylamine. The reaction mixture was stirred at 60 ºC for 2 h, allowed to cool to room temperature (ca. 22 ºC), EtOAc (5 mL) was added and the mixture was filtered through a plug of Celite, eluting with further EtOAc (3 × 10 mL). The solvent was removed *in vacuo* using a rotatory evaporator and purification by flash column chromatography (80% Et_2O/pentane) afforded oxetane amine **94** as a colourless gum (20.1 mg, 80%). Phenol-oxetane **94** was also obtained in 87% yield (21.8 mg) using 3.0 equivalents of diethylamine. R_f = 0.18 (80% Et_2O/pentane); IR (film)/cm^{-1} 3291 (OH st, br), 2967, 2874, 2837, 1599, 1513, 1461, 1420, 1375, 1271, 1219, 1126, 1074, 1033, 984, 921, 883, 787, 738; ^{1}H NMR (400 MHz, $CDCl_3$) δ 6.91 (d, *J* = 8.2 Hz, 1 H, HOC_qAr-C*H*), 6.80 (dd, ^3J = 8.2 Hz, ^4J = 2.1 Hz, 1 H, Ar-CH), 6.77 (br s, 1 H, Ar-C_qAr-CHAr-C_q), 5.70 (br s, 1 H, OH), 4.92 (d, *J* = 5.9 Hz, 2 H, C*H*HOC*H*H), 4.86 (d, *J* = 5.9 Hz, 2 H, CH*H*OCH*H*), 3.90 (s, 3 H, OCH_3), 2.40 (q, *J* = 7.2 Hz, 4 H, 2 × NCH_2), 1.06 (t, *J* = 7.2 Hz, 6 H, 2 × NCH_2CH_3); ^{13}C NMR (101 MHz, $CDCl_3$) δ 146.2 (Ar-C_qOMe), 144.7 (Ar-C_qOH), 132.7 (Ar-C_qC_q), 120.1 (Ar-CH), 113.7 (Ar-C_qOHAr-*C*H), 109.7 (Ar-C_qOMeAr-*C*H), 81.5 (CH_2OCH_2), 67.4 (C_q), 56.0 (OCH_3), 43.6 (2 × NCH_2), 15.4 (2 × CH_2CH_3); HRMS (APCI) *m/z* calcd for $C_{14}H_{20}NO_3^-$ $[M–H]^-$: 250.1449, found: 266.1446.

4-(3-((5-(3,5-Dimethoxyphenethyl)-1*H*-pyrazol-3-yl)amino)oxetan-3-yl)phenol (95)



Prepared according to **General Procedure A** and using oxetane sulfonyl fluoride **18c** (77.6 mg) and 5-(3,5-dimethoxyphenethyl)-1*H*-pyrazol-3-amine (59.4 mg). Purification by flash column chromatography (2–5% MeOH/CH_2Cl_2) afforded oxetane amine **95** as a white solid (71.4 mg, 90%). R_f = 0.25 (10% MeOH/CH_2Cl_2); mp = 192 °C; IR (film)/cm^{-1} 3224 (OH st, br), 2997, 2956, 2885, 2833, 2673, 2479, 2378, 2184, 2113, 1987, 1908, 1610, 1588, 1551, 1510, 1476, 1458, 1372, 1316, 1260, 1200, 1159, 1107, 1066, 1018, 932, 876, 835, 746, 719, 682; ^{1}H NMR (400 MHz, $(CD_3)_2SO$) δ 11.18 (br s, 1 H, $N_{(pyrazole)}H$), 9.25 (br s, 1 H, OH), 7.33–7.31 (m, 2 H, 2 × Ar-CH), 6.70–6.68 (m, 2 H, 2 × Ar-CH), 6.34 (d, *J* = 2.3 Hz, 2 H, 2 × Ar-CH), 6.30 (t, *J* = 2.3 Hz, 1 H, Ar-CH), 6.16 (br s, 1 H, $N_{(amine)}H$), 5.03 (br s, 1 H, $C_{(pyrazole)}H$), 4.78 (d, *J* = 6.0 Hz, 2 H, C*H*HOC*H*H), 4.65 (d, *J* = 6.0 Hz, 2 H, CH*H*OCH*H*), 3.69 (s, 6 H, 2 × OCH_3), 2.76–2.69 (m, 2 H, $C_{(pyrazole)}CH_2$), 2.67–2.60 (m, 2 H, $C_{(pyrazole)}CH_2CH_2$); ^{13}C NMR (101 MHz, $(CD_3)_2SO$) δ 160.3 (2 × Ar-C_qOMe), 155.8 (Ar-C_qOH), 153.9 (weak, $C_{q(pyrazole)}CH_2$), 143.5 (Ar-$C_q$$CH_2$), 142.3 (weak, $C_{q(pyrazole)}NH$), 134.6 (weak, Ar-C_qC_q), 126.7 (2 × $Ar_{(phenol)}$-CH), 114.6 (Ar-*C*HAr-C_qOHAr-*C*H), 106.2 (2 × $Ar_{(di\text{-}OMe)}$-CH), 97.8 (Ar-CH), 90.1 (weak, $C_{(pyrazole)}H$), 82.5 (CH_2OCH_2), 59.5 (Ar-C_qC_q), 55.0 (2 × OCH_3), 34.8 ($C_{(pyrazole)}CH_2CH_2$), 26.9 ($C_{(pyrazole)}CH_2CH_2$); HRMS (APCI) *m/z* calcd for $C_{22}H_{26}N_3O_4^+$ $[M+H]^+$: 396.1918, found: 396.1913.

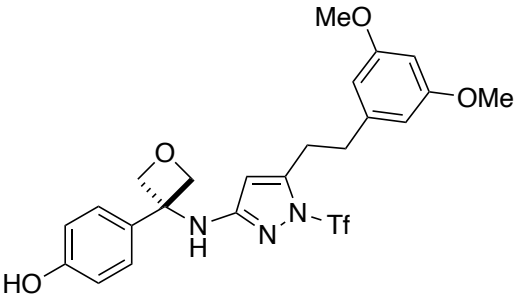
Notes:

The OH and NH signals were of broad and of lower intensity due to chemical exchange.

In this example, both the H_2O (3.35 ppm) and HDO (3.32 ppm) peaks were visible in the ^{1}H NMR spectrum.

*Some peaks (Ar-C_qOH, Ar-**C**HAr-C_qOHAr-**C**H and Ar-C_q**C_q**) in the ^{13}C NMR spectrum appeared as two signals and some peaks (**$C_{q(pyrazole)}$**CH_2, $C_{q(pyrazole)}$NH, Ar-**C_q**C_q and $C_{(pyrazole)}$H) were very broad and weak due to chemical exchange caused by an equilibrium between pyrazole tautomers. In the former case, the chemical shift was given as the average of both signals.*

4-(3-((5-(3,5-Dimethoxyphenethyl)-1-((trifluoromethyl)sulfonyl)-1*H*-pyrazol-3-yl)amino)oxetan-3-yl)phenol (96)



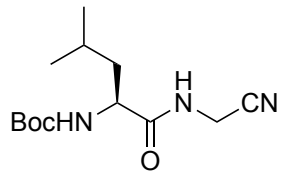
Triflic anhydride (16.8 μL, 0.1 mmol, 1.2 equiv) was added to a solution of phenol oxetane **95** (31.6 mg, 0.08 mmol, 1.0 equiv) and pyridine (12.9 μL, 0.16 mmol, 2.0 equiv) in anhydrous CH_2Cl_2 (0.8 mL, 0.1 M) at 0 °C in a 10 mL round bottom flask. After stirring the reaction mixture for 3 h at 0 ºC, distilled water (2 mL) was added. The aqueous layer was extracted with EtOAc (3 × 5 mL). The combined organic extracts were dried over Na_2SO_4, filtered and concentrated *in vacuo* using a rotatory evaporator. Purification by flash column chromatography (0–10% MeOH/CH_2Cl_2) afforded impure triflate **96** (28.4 mg), followed by phenol starting material **95** (12.6 mg, 40% RSM). Repurification by flash column chromatography (30–100% Et_2O/pentane) afforded triflate **96** as a white solid (2.5 mg, 6%). R_f = 0.14 (60% Et_2O/pentane); mp = 170 °C; IR (film)/cm^{-1} 3407 (OH st, br), 2933, 1592, 1513, 1424, 1226, 1148, 1088; ^{1}H NMR (400 MHz, CD_3Cl_3) δ 7.37–7.33 (m, 2 H, 2 × Ar-CH), 6.89–6.86 (m, 2 H, 2 × Ar-CH), 6.30 (t, *J* = 2.3 Hz, 1 H, $Ar_{(di\text{-}OMe)}$-CH), 6.26 (d, *J* = 2.3 Hz, 2 H, 2 × $Ar_{(di\text{-}OMe)}$-CH), 6.23 (br s, 1 H, NH), 4.90 (d, *J* = 6.7 Hz, 2 H, C*H*HOC*H*H), 4.85 (d, *J* = 6.7 Hz, 2 H, CH*H*OCH*H*), 4.57 (br s, 1 H, $C_{(pyrazole)}$H), 3.75 (s, 6 H, 2 × OCH_3), 2.76–2.69 (m, 4 H, CH_2CH_2); ^{13}C NMR (101 MHz, $CDCl_3$) δ 161.6 (Ar-C_qNTf), 160.7 (2 × Ar-C_qOMe), 155.5 (Ar-C_qOH), 149.5 (Ar-C_qNH), 142.7 (Ar-$C_q$$CH_2$), 131.2 (Ar-$C_q$$C_q$), 126.6 (2 × $Ar_{(phenol)}$-CH), 116.0 (2 × $Ar_{(phenol)}$-CH), 106.4 (2 × $Ar_{(di\text{-}OMe)}$-CH), 98.2 (Ar-CH), 89.9 (Ar-$C_{(pyrazole)}$H), 82.5 (CH_2OCH_2), 60.9 (C_q), 55.2 (2 × OCH_3), 34.5 (CH_2), 30.0 (CH_2); ^{19}F NMR (377 MHz, $CDCl_3$) δ –73.6; HRMS (APCI) *m/z* calcd for $C_{23}H_{25}F_3N_3O_6S^+$ $[M+H]^+$: 528.1411, found: 528.1404.

Notes:

The CF_3 peak was not observed in the ^{13}C NMR spectrum.

*The structure of oxetane triflate **96** was confirmed by X-ray crystallography (see Scheme 30).*

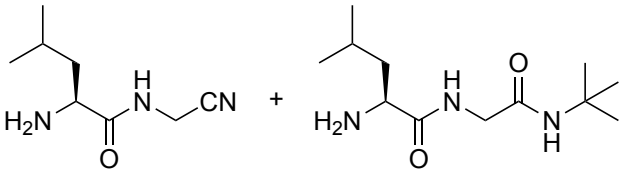
***tert*-Butyl (*S*)-(1-((cyanomethyl)amino)-4-methyl-1-oxopentan-2-yl)carbamate (98)[278]**



Prepared in a 5.0 mmol scale from *N*-Boc-leucine using a literature procedure.[278] Concentration *in vacuo* using a rotatory evaporator afforded nitrile-Boc-leucine **98** as white solid (1.16 g, 86%). $[\alpha]_D^{21}$ –32.0 (c 1, $CDCl_3$) (Lit.: $[\alpha]_D^{20}$ –23.4 (c 2.11, MeOH));[448] R_f = 0.42 (10% MeOH/CH_2Cl_2); mp = 103–110 °C (Lit.: mp = 114–116 °C);[448] IR (film)/cm^{-1} 3302 (br NH), 2960, 2874, 2255 (weak, C≡N st), 1670 (C=O st), 1521, 1368, 1249, 1163,

1126, 1047, 913, 872, 783, 734; ^{1}H NMR (400 MHz, $CDCl_3$) δ 7.65 (br s, 1 H, NH), 5.36–5.10 (br m, 1 H, NH), 4.20 (br s, 1 H, NCH), 4.15 (d, *J* = 5.7 Hz, 2 H, CH_2CN), 1.72–1.52 (m, 3 H, NCHC*H*$_2$C*H*), 1.45 (s, 9 H, 3 × C_qCH_3), 0.95 (d, *J* = 6.4 Hz, 3 H, CHC*H*$_3$), 0.92 (d, *J* = 6.4 Hz, 3 H, CHC*H*$_3$); ^{13}C NMR (101 MHz, $CDCl_3$) δ 173.4 (C_q=$O_{(amide)}$), 156.2 (C_q=$O_{(carbamate)}$), 116.0 (C≡N), 80.6 (*C*$_q$(CH$_3$)$_3$), 52.7 (NCH), 40.8 (*C*H$_2$CH), 28.3 (3 × C_q(*C*H$_3$)), 27.3 (*C*H$_2$CN), 24.6 (*C*H(CH$_3$)$_2$), 22.9 (CH*C*H$_3$), 21.8 (CH*C*H$_3$). The observed characterisation data (mp, $[\alpha]_D$, ^{1}H, ^{13}C) were consistent with that previously reported.[448]

(*S*)-2-Amino-*N*-(cyanomethyl)-4-methylpentanamide (97) and (*S*)-2-amino-*N*-(2-(*tert*-butylamino)-2-oxoethyl)-4-methylpentanamide (99)[280]



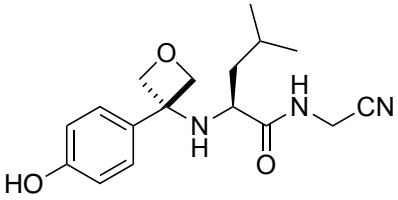
97 **99**

Methane sulfonic acid (1.42 mL, 21.9 mmol, 5.0 equiv) was added dropwise to a solution of nitrile-Boc-leucine **98** in anhydrous THF (8.8 mL, 0.5 M) at 0 °C under a flow of N_2. Then, a light vacuum (~500 mbar) was applied to the reaction using a water jet pump while keeping the flow of N_2. After stirring the reaction for further 30 min at 0 °C, THF was removed *in vacuo* using a rotatory evaporator. Aq. NaOH (1 M) was added to the residue until a pH of ~10 was reached and the resulting aqueous solution was extracted with EtOAc (3 × 20 mL). The combined organic extracts were washed with sat. aq. $NaHCO_3$ (20 mL) and brine (20 mL), dried over Na_2SO_4, filtered and concentrated *in vacuo* using a rotatory evaporator. Purification by flash column chromatography (0–10% MeOH/MeCN) afforded nitrile-leucine **97** as a yellow gum (384.3 mg, 52%), followed by *tert*-butyl leucine **99** as a white solid (79.2 mg, 7%).

97: $[a]_D^{20}$ +14.0 (c 1, MeOH) (Lit.: $[a]_D^{18}$ +4.5 (c 1.569, H_2O));[449] R_f = 0.29 (10% MeOH/CH_2Cl_2); IR (film)/cm^{-1} 3314 (br NH), 2956, 2870, 2255 (weak, C≡N st), 1659 (C=O st), 1506, 1413, 1342, 1256, 1141, 1115, 1029, 962, 902, 824; ^{1}H NMR (400 MHz, CD_3OD) δ 4.17 (d, *J* = 2.7 Hz, 2 H, CH_2CN), 3.38 (dd, *J* = 8.2, 6.1 Hz, 1 H, NCH), 1.70 (dh, *J* = 13.1, 6.6 Hz, 1 H, C*H*(CH$_3$)$_2$), 1.54 (ddd, *J* = 13.6, 7.8, 6.1 Hz, 1 H, C*H*HCH), 1.41 (ddd, *J* = 13.6, 8.2, 6.4 Hz, 1 H, CH*H*CH), 0.96 (d, *J* = 6.6 Hz, 3 H, CHC*H*$_3$), 0.94 (d, *J* = 6.6 Hz, 3 H, CHC*H*$_3$); ^{13}C NMR (101 MHz, CD_3OD) δ 178.5 (C_q=O), 117.6 (C≡N), 54.3 (NCH), 45.4 (*C*H$_2$CH), 27.9 (*C*H$_2$CN), 25.7 (*C*H(CH$_3$)$_2$), 23.4 (CH*C*H$_3$), 22.4 (CH*C*H$_3$); HRMS (ESI) *m/z* calcd for $C_8H_{16}N_3O$ [M+H]: 170.1293, found: 170.1290. The observed characterisation data ($[\alpha]_D$, ^{1}H, ^{13}C) were consistent with that previously reported.[280,449]

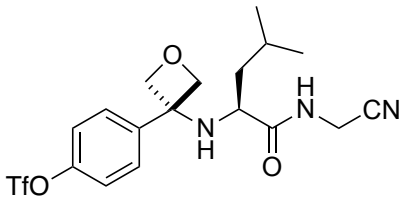
99: $[a]_D^{20}$ +8.0 (c 1, MeOH); R_f = 0.09 (10% MeOH/CH_2Cl_2); mp = 164–167 °C; IR (film)/cm^{-1} 3325 (br NH), 3086, 2960, 2870, 2475, 2400, 1640 (C=O st), 1517, 1435, 1390, 1327, 1275, 1226, 1074, 1044, 999, 928, 891, 828, 790, 697; ^{1}H NMR (400 MHz, CD_3OD) δ 3.77 (d, *J* = 3.7 Hz, 2 H, NCH_2), 3.37 (dd, *J* = 8.3, 6.1 Hz, 1 H, NCH), 1.78–1.67 (m, 1 H, C*H*$(CH_3)_2$), 1.55 (ddd, *J* = 13.6, 7.9, 6.1 Hz, 1 H, C*H*HCH), 1.39 (ddd, *J* = 13.6, 8.3, 6.4 Hz, 1 H, CH*H*CH), 1.33 (s, 9 H, 3 × C_qCH_3), 0.96 (d, *J* = 6.6 Hz, 3 H, CHC*H*$_3$), 0.94 (d, *J* = 6.6 Hz, 3 H, CHC*H*$_3$); ^{13}C NMR (101 MHz, CD_3OD) δ 178.2 (C_q=O), 170.4 (C_q=O), 54.4 (NCH), 52.1 ($C_q(CH_3)_3$), 45.1 (CH_2CH), 43.7 (NCH_2), 28.9 (3 × C_qCH_3), 25.8 ($CH(CH_3)_2$), 23.4 ($CHCH_3$), 22.4 ($CHCH_3$); HRMS (APCI) *m/z* calcd for $C_{12}H_{26}N_3O_2^+$ $[M+H]^+$: 244.2020, found: 244.2018.

(*S*)-*N*-(Cyanomethyl)-2-((3-(4-hydroxyphenyl)oxetan-3-yl)amino)-4-methylpentanamide (100)



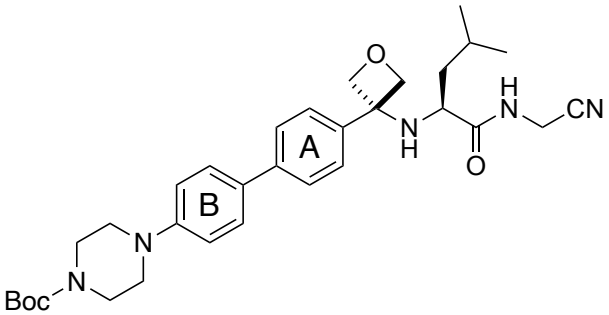
A reaction tube was charged with anhydrous K_2CO_3 (103.3 mg, 0.748 mmol, 1.3 equiv) and flame-dried under air. The tube was allowed to cool to room temperature (ca. 22 ºC) and amine **97** (116.9 mg, 0.691 mmol, 1.2 equiv) and sulfonyl fluoride **18c** (223.5 mg, 0.575 mmol, 1.0 equiv) were added sequentially. The reaction vessel was sealed and anhydrous acetonitrile (1.9 mL, 0.3 M) was added by syringe. After stirring the reaction mixture at 60 ºC for 2 h, it was allowed to cool to room temperature (ca. 22 ºC), EtOAc (5 mL) was added and the mixture was filtered through a plug of Celite, eluting with further EtOAc (3 × 10 mL). The solvent was removed *in vacuo* using a rotatory evaporator and purification by flash column chromatography (20–30% MeCN/CH_2Cl_2) afforded oxetane amine **100** as a colourless, solid foam (146.2 mg, 80%). $[a]_D^{20}$ –32.0 (c 1, MeOH); R_f = 0.21 (30% MeCN/CH_2Cl_2); mp = 65–70 °C; IR (film)/cm^{-1} 3317 (OH and NH st, br), 2956, 2870, 2468, 1655 (C=O st), 1614, 1517, 1469, 1342, 1264, 1234, 1174, 1115, 1036, 977, 902, 835, 686; ^{1}H NMR (400 MHz, CD_3OD) δ 7.17–7.14 (m, 2 H, 2 × Ar-CH), 6.81–6.78 (m, 2 H, 2 × Ar-CH), 4.94 (d, *J* = 6.4 Hz, 1 H, C*H*HOCH_2), 4.84 (d, *J* = 6.0 Hz, 1 H, CH_2OCHH), 4.76 (d, *J* = 6.4 Hz, 1 H, CH*H*OCH_2), 4.73 (d, *J* = 6.0 Hz, 1 H, CH_2OCHH), 3.96 (d, *J* = 2.8 Hz, 2 H, CH_2CN), 2.92 (dd, *J* = 8.6, 5.6 Hz, 1 H, NCH), 1.71–1.58 (m, 1 H, C*H*$(CH_3)_2$), 1.38 (ddd, *J* = 13.7, 8.6, 5.7 Hz, 1 H, C*H*HCH), 1.28 (ddd, *J* = 13.7, 8.3, 5.6 Hz, 1 H, CH*H*CH), 0.85 (d, *J* = 6.6 Hz, 3 H, CHC*H*$_3$), 0.72 (d, *J* = 6.6 Hz, 3 H, CHC*H*$_3$); ^{13}C NMR (101 MHz, CD_3OD) 178.9 (C_q=O), 157.9 (Ar-C_qOH), 134.0 (Ar-C_qC_q), 129.3 (2 × Ar-CH), 117.3 (C≡N), 116.3 (2 × Ar-CH), 85.0 (CH_2OCH_2), 83.2 (CH_2OCH_2), 64.1 (Ar-C_qC_q), 57.1 (NCH), 44.8 (CH_2CH), 27.8 (CH_2CN), 25.6 ($CH(CH_3)_2$), 23.4 ($CHCH_3$), 22.3 ($CHCH_3$); HRMS (ESI) *m/z* calcd for $C_{17}H_{24}N_3O_3$ [M+H]: 318.1818, found: 318.1806.

(*S*)-4-(3-((1-((Cyanomethyl)amino)-4-methyl-1-oxopentan-2-yl)amino)oxetan-3-yl)phenyl trifluoromethanesulfonate (101)



Triethylamine (0.15 mL, 1.07 mmol, 3 equiv), 4-dimethylaminopyridine (DMAP, 4.3 mg, 0.0355 mmol, 0.1 equiv) and *N*,*N*-bis(Trifluoromethylsulfonyl)aniline (NTf_2Ph, 190.3 mg, 0.53 mmol, 1.5 equiv) were added sequentially to a solution of phenol oxetane amine **100** (112.7 mg, 0.355 mmol, 1.0 equiv) in anhydrous CH_2Cl_2 (1.8 mL, 0.2 M) at 0 °C. After stirring for 5 min at 0 °C, the ice bath was removed and the reaction mixture was stirred for further 4 h at 25 °C. Then, the reaction mixture was concentrated *in vacuo* using a rotatory evaporator. Purification by flash column chromatography (10% Et_2O/CH_2Cl_2) afforded triflate **101** as colourless crystals (137.1 mg, 86%). The reaction was monitored by TLC and stopped as soon as all starting material was consumed (4 h). A lower yield was observed when the reaction was stirred for 13 h. $[\alpha]_D^{20}$ –42.0 (c 1, $CDCl_3$); R_f = 0.23 (25% acetone/pentane); mp = 116 °C; IR (film)/cm^{-1} 3321 (br NH), 3038, 2956, 2878, 2363 (weak, C≡N st), 1670 (C=O st), 1599, 1506, 1424, 1346, 1215, 1141, 1018, 984, 947, 891, 846, 783, 757; ^{1}H NMR (400 MHz, $CDCl_3$) δ 7.34–7.29 (m, 4 H, 4 × Ar-CH), 7.16 (br app. t, *J* = 6.0 Hz, 1 H, N*H*CH_2), 4.98 (app. t, *J* = 6.3 Hz, 2 H, C*H*HOC*H*H), 4.70 (d, *J* = 7.0 Hz, 1 H, CH*H*OCH_2), 4.68 (d, *J* = 7.0 Hz, 1 H, CH_2OCH*H*), 4.03 (dd, *J* = 17.5, 6.1 Hz, 1 H, C*H*HCN), 3.82 (dd, *J* = 17.5, 5.7 Hz, 1 H, CH*H*CN), 3.14 (dd, *J* = 8.9, 4.8 Hz, 1 H, NCH), 2.33 (br s, 1 H, N*H*CH), 1.64–1.54 (m, 1 H, C*H*$(CH_3)_2$), 1.49 (ddd, *J* = 13.5, 8.6, 4.8 Hz, 1 H, C*H*HCH), 1.44–1.36 (m, 1 H, CH*H*CH), 0.90 (d, *J* = 6.5 Hz, 3 H, CHC*H*$_3$), 0.77 (d, *J* = 6.5 Hz, 3 H, CHC*H*$_3$); ^{13}C NMR (101 MHz, $CDCl_3$) 174.7 (C_q=O), 148.9 (Ar-C_qOTf), 142.0 (Ar-C_qC_q), 128.4 (2 × Ar-CH), 122.1 (2 × Ar-CH), 118.7 (q, J_{CF} = 320.8 Hz, CF_3), 115.7 (C≡N), 81.5 (CH_2OCH_2), 81.0 (CH_2OCH_2), 63.4 (Ar-C_qC_q), 56.4 (NCH), 43.8 (CH_2CH), 26.9 (CH_2CN), 24.7 (CH$(CH_3)_2$), 23.1 (CHCH_3), 21.8 (CHCH_3); ^{19}F NMR (377 MHz, $CDCl_3$) δ –72.8; HRMS (ESI) *m/z* calcd for $C_{18}H_{23}N_3O_5SF_3$ [M+H]: 450.1311, found: 450.1306.

***tert*-Butyl (*S*)-4-(4'-(3-((1-((cyanomethyl)amino)-4-methyl-1-oxopentan-2-yl)amino)oxetan-3-yl)-[1,1'-biphenyl]-4-yl)piperazine-1-carboxylate (102)**



A reaction tube was charged sequentially with triflate **101** (89.1 mg, 0.198 mmol, 1.0 equiv), *tert*-butyl 4-(4-(4,4,5,5-tetramethyl-1,3,2-dioxaborolan-2-yl)phenyl) piperazine-1-carboxylate (100.1 mg, 0.258 mmol, 1.3 equiv), [1,1′-bis(diphenylphosphino)ferrocene]dichloropalladium(II) ($PdCl_2$(dppf), 7.2 mg, 0.0099 mmol, 0.05 equiv) and sodium carbonate (63.0 mg, 0.594 mmol, 3.0 equiv). The reaction vessel was sealed and evacuated and refilled with argon (× 3). In a separate flask, anhydrous DMF was sparged with argon for 15 min. The same procedure was performed with distilled water. Sparged DMF (1.65 mL, DMF:H_2O = 2:1, 0.08 M) and sparged water (0.83 mL) were added to the reaction mixture by syringe. After stirring the reaction mixture at 90 ºC for 1.5 h, it was allowed to cool to room temperature (ca. 22 °C) and EtOAc (10 mL) and water (10 mL) were added. The phases were separated and the aqueous phase was extracted with EtOAc (6 × 20 mL). The combined organic extracts were dried over Na_2SO_4, filtered and concentrated *in vacuo* using a rotatory evaporator. Purification by flash column chromatography (15–25% acetone/pentane) afforded biaryl oxetane **102** as a white solid (82.5 mg, 74%). $[\alpha]_D^{21}$ –46.0 (c 1, $CDCl_3$); R_f = 0.27 (25% acetone/pentane); mp = 176–180 °C; IR (film)/cm^{-1} 3314 (br NH), 2960, 2870, 2822, 2095 (weak, C≡N st), 1689 (C=O st), 1607, 1528, 1502, 1457, 1424, 1234, 1167, 1126, 1085, 1051, 999, 917, 820, 772, 731; ^{1}H NMR (400 MHz, $CDCl_3$) δ 7.58 (br d, *J* = 8.2 Hz, 2 H, 2 × $Ar_{(A)}$-CH), 7.52 (br d, *J* = 8.7 Hz, 2 H, 2 × $Ar_{(B)}$-CH), 7.30 (br app. t, *J* = 5.5 Hz, 1 H, N*H*CH_2), 7.20 (br d, *J* = 8.2 Hz, 2 H, 2 × $Ar_{(A)}$-CH), 7.02 (br d, *J* = 8.2 Hz, 2 H, 2 × $Ar_{(B)}$-CH), 5.08 (d, *J* = 6.4 Hz, 1 H, C*H*HOCH_2), 5.05 (d, *J* = 6.7 Hz, 1 H, CH_2OC*H*H), 4.69 (app. t, *J* = 7.2 Hz, 2 H, CH*H*OCH*H*), 3.98 (dd, *J* = 17.5, 6.2 Hz, 1 H, C*H*HCN), 3.67 (dd, *J* = 17.5, 5.5 Hz, 1 H, CH*H*CN), 3.62 (br app. t, *J* = 4.7 Hz, 4 H, CH_2N-ArCH_2), 3.24–3.20 (m, 5 H, NCH + CH_2NBocCH_2), 2.34 (br s, N*H*CH), 1.70–1.60 (m, 1 H, C*H*$(CH_3)_2$), 1.56–1.48 (m, 1 H, C*H*HCH), 1.50 (s, 9 H, 3 × C_qCH_3), 1.41 (ddd, *J* = 14.0, 9.0, 5.4 Hz, 1 H, CH*H*CH), 0.92 (d, *J* = 6.5 Hz, 3 H, CHC*H*$_3$), 0.81 (d, *J* = 6.5 Hz, 3 H, CHC*H*$_3$); ^{13}C NMR (101 MHz, $CDCl_3$) 174.7 (br and weak, C_q=$O_{(amide)}$), 154.7 (C_q=$O_{(carbamate)}$), 150.5 (br and weak, Ar-C_qN) 140.5 ($Ar_{(A)}$-*C*$_q$Ar-C_q), 139.2 (br and weak, Ar-*C*$_q$$C_q$), 131.8 (br and weak, $Ar_{(B)}$-*C*$_q$Ar-C_q), 127.8 (2 × $Ar_{(B)}$-CH), 126.9 (2 × $Ar_{(A)}$-CH), 126.7 (2 × $Ar_{(A)}$-CH), 116.8 (br and weak, 2 × $Ar_{(B)}$-CH), 115.7 (C≡N), 81.5 (CH_2O*C*H_2), 81.4 (*C*H_2OCH_2), 80.0 (*C*$_q$$(CH_3)_3$), 63.7 (Ar-$C_q$*C*$_q$), 56.5 (NCH), 49.3 (br and weak, CH_2NBocCH_2), 43.6 (*C*H_2CH), 43.1 (br and weak,

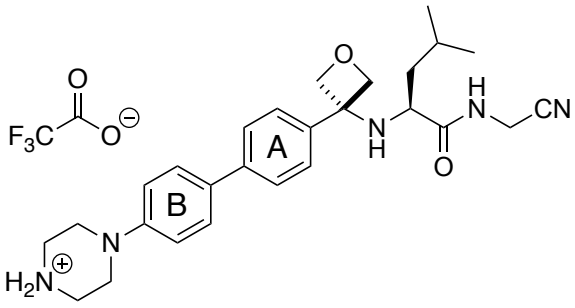
CH_2N-ArCH_2), 28.4 (3 × C_qCH_3), 26.9 (CH_2CN), 24.7 ($CH(CH_3)_2$), 23.1 ($CHCH_3$), 21.8 ($CHCH_3$); HRMS (ESI) *m/z* calcd for $C_{32}H_{44}N_5O_4$ [M+H]: 562.3393, found: 562.3406.

Notes:

In the ^{1}H NMR spectrum, the dd at 3.67 ppm and the br app. t at 3.62 ppm were integrated together to 5 H. Also, the m at 1.56–1.48 ppm and the s at 1.50 ppm were integrated together to 10 H.

Some signals in the ^{13}C NMR spectrum appeared very weak and broad due to chemical exchange caused by the presence of conformers. The signals were identified and assigned with HSQC and HMBC 2D correlation spectra.[212]

(*S*)-*N*-(Cyanomethyl)-4-methyl-2-((3-(4'-(piperazin-1-yl)-[1,1'-biphenyl]-4-yl)oxetan-3-yl)amino)pentanamide 2,2,2-trifluoroacetic acid salt (103)



Methane sulfonic acid (72 μL, 1.11 mmol, 10.0 equiv) was added dropwise to a solution of biaryl oxetane **102** in anhydrous THF (1.1 mL, 0.1 M) at 0 °C under a flow of N_2. Then, a light vacuum (~500 mbar) was applied to the reaction using a water jet pump while keeping the flow of N_2. After stirring the reaction for further 30 min at 0 °C, THF was removed *in vacuo* using a rotatory evaporator. Aq. NaOH (1 M) was added to the residue until a pH of ~10 was reached and the resulting aqueous solution was extracted with EtOAc (6 × 10 mL). The combined organic extracts were dried over Na_2SO_4, filtered and concentrated *in vacuo* using a rotatory evaporator. Purification by flash column chromatography (20:1:79 MeOH:NEt_3:MeCN) afforded impure oxetane amine **103** as a light-yellow gum (29.3 mg). Repurification by automated column chromatography afforded impure oxetane amine **103** as a colourless gum (23.8 mg). Repurification by automated reversed-phase column chromatography afforded oxetane amine **103** as the TFA salt as a colourless gum (21.0 mg, 33%). $[\alpha]_D^{21}$ –8.0 (c 0.5, MeOH); R_f = 0.31 (20% MeOH/CH_2Cl_2); IR (film)/cm^{-1} 3347 (br NH), 3060, 2363 (weak, C≡N st), 2028, 1670 (C=O st), 1610, 1532, 1506, 1461, 1200, 1137, 928, 820, 723; ^{1}H NMR (400 MHz, CD_3OD) δ 7.79–7.76 (m, 2 H, 2 × $Ar_{(A)}$-CH), 7.67–7.63 (m, 2 H, 2 × $Ar_{(B)}$-CH), 7.53–7.49 (m, 2 H, 2 × $Ar_{(A)}$-CH), 7.16–7.12 (m, 2 H, 2 × $Ar_{(B)}$-CH), 5.23 (d, *J* = 8.0 Hz, 1 H, C*H*HOCH_2), 5.14–5.08 (m, 3 H, CH*H*OC*H*$_2$), 4.00 (d, *J* = 8.3, Hz, 2 H, CH_2CN), 3.51–3.48 (m, 4 H, CH_2N-ArCH_2), 3.41–3.36 (m, 5 H, NCH + C*H*$_2$NHC*H*$_2$), 1.74–1.54 (m, 3 H, C*H*$(CH_3)_2$ + C*H*$_2$CH), 0.88 (d, *J* = 6.2 Hz, 3 H, CHC*H*$_3$), 0.85 (d, *J* = 6.2 Hz, 3 H, CHC*H*$_3$); ^{13}C NMR (101 MHz, CD_3OD) 170.6 (C_q=O), 151.5

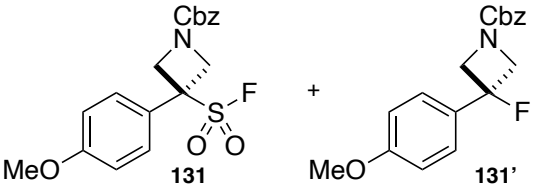
(Ar-C_qN) 143.6 ($Ar_{(A)}$-C_qAr-C_q), 134.1 (Ar-C_qC_q), 133.2 ($Ar_{(B)}$-C_qAr-C_q), 129.5 (2 × $Ar_{(A)}$-CH), 128.9 (2 × $Ar_{(B)}$-CH), 128.3 (2 × $Ar_{(A)}$-CH), 118.1 (2 × $Ar_{(B)}$-CH), 116.8 (C≡N), 80.6 (CH_2OCH_2), 79.8 (CH_2OCH_2), 65.6 (Ar-C_qC_q), 58.0 (NCH), 47.5 (CH_2N-ArCH_2), 44.7 (CH_2NHCH_2), 42.0 (CH_2CH), 28.0 (CH_2CN), 25.5 ($CH(CH_3)_2$), 22.9 ($CHCH_3$), 22.4 ($CHCH_3$); HRMS (ESI) *m/z* calcd for $C_{27}H_{36}N_5O_2$ [M–$C_2F_3O_2$]: 462.2869, found: 462.2859.

Automated column conditions: Column Type: Biotage® Sfär HC 5 g. Flow rate: 18 mL/min. 1 column volumes (CV) 10% MeOH/CH_2Cl_2, 10 CV 10–40% MeOH/CH_2Cl_2, 15 CV 40% MeOH/CH_2Cl_2. Fractions 8–26: impure oxetane amine **103**.

Automated reversed-phase column conditions: Column Type: Biotage® Sfär C18 D Duo 6 g. Flow rate: 6 mL/min. Modifier: 0.1% 2,2,2-trifluoroacetic acid. 8 column volumes (CV) 0–50% MeCN/H_2O, 5 CV 50–100% MeCN/H_2O, 5 CV 100% MeCN/H_2O. Fractions 9–11: oxetane amine **103**. Fractions 12–14: impure oxetane amine **103** (not collected). There was no visual difference between fractions 9–14 by TLC (normal phase). The fractions were separated on the basis of the UV trace measured by the Biotage instrument.

7.6.4.4 Azetidine Sulfonyl Fluoride 131 and Amino-azetidine 132

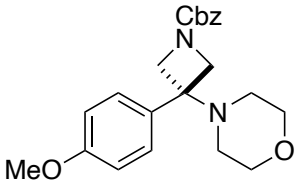
Benzyl 3-(fluorosulfonyl)-3-(4-methoxyphenyl)azetidine-1-carboxylate (131) and benzyl 3-fluoro-3-(4-methoxyphenyl)azetidine-1-carboxylate (131')



Sodium methoxide (5.4 M solution in MeOH, 93 μL, 0.5 mmol, 1.0 equiv) was added dropwise to a solution of azetidine sulfone **130** (223.9 mg, 0.5 mmol, 1.0 equiv)[ji] in anhydrous THF (1.0 mL, 0.5 M) in a 5 mL round bottom flask. Azetidine sulfone **130** was not very soluble in THF and the reaction mixture was sonicated before addition of base. The azetidine sulfinate salt did not precipitate after addition of base, but the reaction mixture turned from light-yellow to orange. The reaction mixture was stirred at 25 °C for 20 min, then concentrated *in vacuo* using a rotatory evaporator to afford an azetidine sulfinate, which was subjected directly to the next step without spectroscopical analysis. For the fluorination step, Selectfluor (266 mg, 0.75 mmol, 1.5 equiv) was added to pre-cooled (0 °C) anhydrous MeOH (2.5 mL, 0.2 M) in a 10 mL round bottom flask. After 5 min of stirring at 0 °C, the azetidine sulfinate was added portion-wise. The reaction mixture was stirred for 1 h at 0 °C, then concentrated *in vacuo* using a rotatory evaporator, re-dissolved in CH_2Cl_2 and filtered through a pad of Celite, eluting with further CH_2Cl_2. After concentration *in vacuo* using a rotatory evaporator, purification by flash column chromatography through a very short column (0–2% Et_2O/CH_2Cl_2) afforded an 89:11 mixture of azetidine sulfonyl fluoride **131** and azetidine fluoride **131'** as a white solid (46.9 mg, 23%). R_f = 0.55 (**131**) and 0.52 (**131'**) (2% Et_2O/CH_2Cl_2); ^{1}H NMR (400 MHz, $CDCl_3$) δ 7.40–7.34 (m, 5.69 H, 5 × $Ar_{(Cbz)}$-CH, **131** + **131'**), 7.27–7.24 (m, 2.48 H, 2 × $Ar_{(PMP)}$-CH, **131** + **131'** [with $CDCl_3$]), 7.01–6.96 (m, 2 H, 2 × $Ar_{(PMP)}$-CH, **131**), 6.95–6.93 (m, 0.23 H, 2 × $Ar_{(PMP)}$-CH, **131'**), 5.16 (s, 0.32 H, OCH_2Ph, **131'**), 5.13 (s, 2 H, OCH_2Ph, **131**), 4.91 (d, J = 9.8 Hz, 2 H, C*H*HNC*H*H, **131**), 4.63 (d, J = 9.8 Hz, 2 H, CH*H*NCH*H*, **131**), 4.47 (ddd, $^3J_{HF}$ = 21.7 Hz, ^2J = 10.2 Hz, J = 1.2 Hz, 0.24 H, C*H*HNC*H*H, **131'**), 4.36 (ddd, $^3J_{HF}$ = 19.4 Hz, ^2J = 10.2 Hz, J = 1.0 Hz, 0.23 H, CH*H*NCH*H*, **131'**), 3.85 (s, 3 H, OCH_3, **131**), 3.84 (s, 0.39 H, OCH_3, **131'**); ^{19}F NMR (377 MHz, $CDCl_3$) δ 33.5 (**131**), –143.8 (**131'**); HRMS (APCI) *m/z* calcd for $C_{18}H_{18}NO_3^+$ [M_{131}–SO_2F or $M_{131'}$–F]$^+$: 296.1281, found: 296.1282; also: *m/z* calcd for $C_{10}H_{13}FNO_3S^+$ [M_{131}–Cbz+H+H]$^+$: 246.0595; found: 246.0595; *m/z* calcd for $C_{18}H_{19}FNO_3^+$ [$M_{131'}$+H]$^+$: 316.1343; found: 316.1344.

[ji] Synthesised by A. Lazaridou.[207]

Benzyl 3-(4-methoxyphenyl)-3-morpholinoazetidine-1-carboxylate (132)



A reaction tube was charged with anhydrous K_2CO_3 (19.2 mg, 0.139 mmol, 1.3 equiv) and flame-dried under air. The tube was allowed to cool to room temperature (ca. 22 ºC) and morpholine (11 μL, 0.691 mmol, 1.2 equiv) and azetidine sulfonyl fluoride **131** (45.0 mg, 0.107 mmol, 1.0 equiv; 99:11 mixture of **131**:**131'**) were added sequentially. The reaction vessel was sealed and anhydrous acetonitrile (0.36 mL, 0.3 M) was added by syringe. After stirring the reaction mixture at 60 ºC for 2 h, it was allowed to cool to 25 °C, EtOAc (5 mL) was added and the mixture was filtered through a plug of Celite, eluting with further EtOAc (3 × 10 mL). The solvent was removed *in vacuo* using a rotatory evaporator and purification by flash column chromatography (70% EtOAc/pentane) afforded impure azetidine amine **132** (33.5 mg). Repurification by flash column chromatography (0–100% CH_2Cl_2/hexane, then 0–100% Et_2O/CH_2Cl_2) afforded azetidine amine **132** as a white gum (26.6 mg, 65%). R_f = 0.28 (70% EtOAc/pentane); IR (film)/cm^{-1} 2952, 2855, 1703 (C=O st), 1610, 1513, 1453, 1416, 1359, 1297, 1245, 1178, 1115, 1021, 947, 910, 831, 731, 697; ^{1}H NMR (400 MHz, $CDCl_3$) δ 7.36–7.29 (m, 5 H, 5 × Ph-CH), 7.04–6.99 (m, 2 H, 2 × Ar-CH), 6.93–6.90 (m, 2 H, 2 × Ar-CH), 5.10 (s, 2 H, OCH_2Ph), 4.25 (br s, 4 H, $CH_2N_{(Cbz)}CH_2$), 3.83 (s, 3 H, OCH_3), 3.70 (br s, 4 H, CH_2OCH_2), 2.30 (br s, 4 H, $CH_2N_{(morpholine)}CH_2$); ^{13}C NMR (101 MHz, $CDCl_3$) δ 158.9 (Ar-C_qOMe), 156.4 (C=O), 136.5 (Ph-C_q), 128.6 (2 × Ar-CH), 128.4 (Ph-CH), 128.03 (2 × Ar-CH), 128.00 (2 × Ar-CH), 113.3 (2 × Ar-CH), 66.9 (CH_2OCH_2 or CH_2Ph), 66.7 (CH_2OCH_2 or CH_2Ph), 62.3 (Ar-C_qC_q), 58.4 and 57.5 (weak and broad, $CH_2N_{(Cbz)}CH_2$), 55.3 (OCH_3), 46.3 ($CH_2N_{(morpholine)}CH_2$); HRMS (ESI) *m/z* calcd for $C_{22}H_{27}N_2O_4$ [M+H]: 383.1971, found: 383.1971.

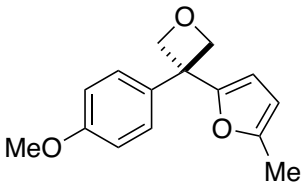
Notes:

The ^{13}C signals at 58.4 and 57.5 ppm were weak due to a chemical exchange between two rotamers caused by the presence of a carbamate with a high rotational barrier.

*The Ar-**C_q**C_q signal could not be found in the spectrum. Presumably, it was obscured by the signals between 128.6 and 128.0 ppm.*

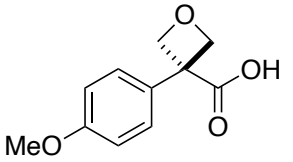
7.6.5 Oxetane Carboxylic Acids and Precursors

2-(3-(4-Methoxyphenyl)oxetan-3-yl)-5-methylfuran (156)[352]



Lithium bis(trifluoromethanesulfonimide) (1.26 g, 4.40 mmol, 0.11 equiv), tetrabutylammonium hexafluorophosphate (852 mg, 2.20 mmol, 0.055 equiv), oxetanol **22a** (7.21 g, 40.0 mmol, 1.0 equiv), 2-methylfuran (18.0 mL, 200 mmol, 5.0 equiv) and by toluene (80 mL, 0.5 M) were added sequentially to a 500 mL round bottom flask. After stirring the reaction mixture at 40 °C for 2 h, sat. aq. $NaHCO_3$ (150 mL) was added followed by Et_2O (80 mL). The layers were separated and the aqueous phase was extracted with Et_2O (3 × 80 mL). The combined organic extracts were dried over Na_2SO_4, filtered and concentrated *in vacuo* using a rotatory evaporator. Purification by flash column chromatography (5–10% Et_2O/pentane) afforded oxetane furan **156** as a white solid (4.96 g, 51%). R_f = 0.55 (20% Et_2O/pentane); ^{1}H NMR (400 MHz, $CDCl_3$) δ 7.18–7.14 (m, 2 H, 2 × Ar-CH), 6.94–6.90 (m, 2 H, 2 × Ar-CH), 5.87 (dq, *J* = 3.1, 1.1 Hz, 1 H, $Ar_{(furan)}$-CH), 5.68 (d, *J* = 3.1 Hz, 1 H, $Ar_{(furan)}$-CH), 5.22 (d, *J* = 5.6 Hz, 2 H, C*H*HOC*H*H), 5.12 (d, *J* = 5.6 Hz, 2 H, CH*H*OCH*H*), 3.83 (s, 3 H, OCH_3), 2.31 (d, *J* = 1.1 Hz, 3 H, CH_3). The observed characterisation data (R_f, ^{1}H) were consistent with that observed previously in the group.[352]

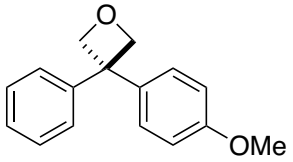
3-(4-Methoxyphenyl)oxetane-3-carboxylic acid (148a)[352]



$NaIO_4$ (24.03 g, 112.35 mmol, 7.0 equiv) was added to a solution of oxetane furan **156** (3.92 g, 16.05 mmol) in heptane/EtOAc/H_2O (100 mL/100 mL/200 mL, 0.04 M) in a 1000 mL round bottom flask. The reaction mixture was stirred for 5 min, cooled to 0 °C and $RuCl_3$ (16.6 mg, 0.825 mmol, 0.005 equiv) was added, upon which the reaction mixture immediately turned orange and then black (after 15 min). After stirring the reaction mixture for 18 h at 25 °C, distilled water was added (170 mL) followed by EtOAc (170 mL) and the layers were separated. The aqueous phase was extracted with EtOAc (3 × 250 mL). The combined organic extracts were dried over Na_2SO_4, filtered through Celite and concentrated *in vacuo* using a rotatory evaporator and a high-vacuum pump to afford carboxylic acid **148a** as a brown solid (2.95 g, 88%). The purity of the sample described above was determined to be 98.9% by quantitative ^{1}H NMR. ^{1}H NMR (400 MHz, $CDCl_3$) δ 7.21–7.17 (m, 2 H, 2 × Ar-CH), 6.94–6.91 (m, 2 H, 2 × Ar-CH), 5.26 (d, *J* = 6.2 Hz, 2 H, C*H*HOC*H*H), 5.02 (d, *J* = 6.2 Hz, 2 H, CH*H*OCH*H*), 3.82 (s, 3 H, OCH_3). The observed characterisation data (^{1}H) were consistent with that observed previously in the group.[352] Another sample of acid **148a** was further purified to 99.9% purity by trituration from CH_2Cl_2/pentane by the following procedure (also see Scheme 43): oxetane acid **148a** ('batch 2'; 1.5 g; 81.0% purity) was dissolved in CH_2Cl_2

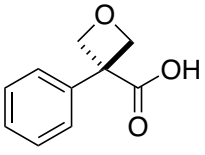
(30 mL) and pentane was added (30 mL) until a solid precipitated. The solid was filtered and washed with pentane (10 mL) to afford acid **148a** in 99.9% purity as a crystalline beige solid (784 mg, Scheme 43c). The filtrate was filtered and washed with pentane (10 mL) a second time to afford further **148a** in 96.2% purity as a beige solid (291 mg). The filtrate was filtered and washed with pentane (10 mL) a third time to afford further **148a** in 93.2% purity as a white solid (134 mg). The remaining filtrate was concentrated in vacuo using a rotatory evaporator to afford **148a** as a dark brown solid in 52.6% purity (328 mg).

3-(4-Methoxyphenyl)-3-phenyloxetane (158)



Following a modified procedure developed by M. Dubois,[211] $FeCl_3$ (64.8 mg, 0.4 mmol, 0.1 equiv) was weighed under argon in a J Young's ampoule. 3-Phenyloxetan-3-ol **22m** (600.8 mg, 4.0 mmol, 1.0 equiv)[kk] and anisole (0.74 mL, 6.8 mmol, 1.7 equiv) were added, followed by HFIP (40.0 mL, 0.1 M). The ampoule was sealed and the reaction mixture was stirred for 18 h at 80 °C (see Scheme 44c for a picture of the reaction set-up). After allowing the ampoule cool to room temperature (ca. 22 ºC), sat. aq. $NaHCO_3$ (10 mL) was added and the aqueous phase was extracted with Et_2O (3 × 80 mL). The combined organic extracts were dried over Na_2SO_4, filtered and concentrated *in vacuo* using a rotatory evaporator. Purification by flash chromatography (6–10% Et_2O/pentane) afforded diaryl-oxetane **158** as a light-yellow solid (319 mg, 37%). R_f = 0.15 (10% Et_2O/pentane); ^1H NMR (400 MHz, $CDCl_3$) δ 7.40–7.35 (m, 2 H, 2 × Ph-CH), 7.30–7.25 (m, 1 H, Ph-CH), 7.24–7.21 (m, 2 H, 2 × Ph-CH), 7.18–7.14 (m, 2 H, 2 × Ar-CH), 6.92–6.88 (m, 2 H, 2 × Ar-CH), 5.27 (d, *J* = 5.6 Hz, 2 H, C*H*HOC*H*H), 5.23 (d, *J* = 5.6 Hz, 2 H, CH*H*OCH*H*), 3.82 (s, 3 H, OCH_3). The observed characterisation data (R_f, ^1H) were consistent with that observed previously in the group.[211]

3-Phenyloxetane-3-carboxylic acid (148m)



Following a modified procedure developed by Maulide,[356c] oxetane **158** (334 mg, 1.40 mmol, 1.0 equiv), $RuCl_3$ (29.0 mg, 0.14 mmol, 0.1 equiv) and $NaIO_4$ (7.19 g, 33.6 mmol, 24.0 equiv) were added to a 100 mL round bottom flask. Then, distilled H_2O (18.7 mL), EtOAc (4.67 mL) and MeCN (4.67 mL) (H_2O:EtOAc:MeCN = 4:1:1, 0.05 M) were added sequentially and the reaction mixture was stirred at 25 ºC for 18 h (see Figure 87 for a picture of the reaction set-up). Distilled water was added (50 mL) followed by EtOAc (50 mL) and the layers were separated. The aqueous phase was extracted with EtOAc (3 × 50 mL). The combined organic extracts were dried over

[kk] Provided by Pfizer.

Na_2SO_4, filtered through Celite and concentrated *in vacuo* using a rotatory evaporator. Purification by flash column chromatography (30% EtOAc/pentane + 0.5% AcOH) afforded phenyloxetane acid **148m** as colourless crystals (64.0 mg, 26%). R_f = 0.25 (30% EtOAc/pentane + 0.5% AcOH). ^{1}H NMR (400 MHz, $CDCl_3$) δ 7.43–7.33 (m, 3 H, 3 × Ph-CH), 7.28–7.26 (m, 2 H, 2 × Ph-CH), 5.28 (d, *J* = 6.2 Hz, 2 H, C*H*HOC*H*H), 5.06 (d, *J* = 6.2 Hz, 2 H, CH*H*OCH*H*). The observed characterisation data (R_f, ^{1}H) were consistent with that observed previously in the group.[352]

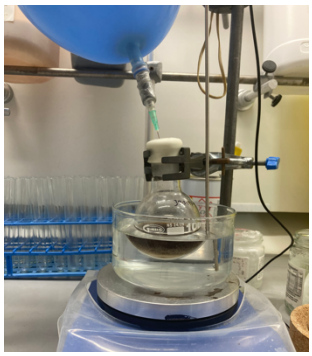


Figure 87. Reaction mixture of the oxidative cleavage of diaryl-oxetane 158.

7.6.6 3-Aryl-3-alkyl-oxetanes and Related Compounds

General Procedure E

For liquid acceptors

An oven-dried 4 mL vial was charged with carboxylic acid (0.20 mmol, 1.0 equiv), oven-dried Cs_2CO_3 (78.2 mg, 0.24 mmol, 1.2 equiv) and [Ir{dF(CF_3)ppy}$_2$(dtbbpy)]PF_6 ([Ir] **133**; 2.2 mg, 0.002 mmol, 1.0 mol%). The vial was sealed with a screwcap equipped with a PTFE/silicon septum and anhydrous DMF (1.0 mL, 0.2 M) was added by syringe. Argon was bubbled through the mixture for 5 min and liquid acceptor (0.30 mmol, 1.5 equiv) was added by syringe under argon. After sealing the cap with parafilm on top, the reaction mixture was stirred at 1000 rpm using the set-up shown in Figure 89 and irradiated with two 467 nm Kessel lamps at 36 °C (heat generated by the lamps).[211] After 18 h the lights were switched off and the reaction mixture was transferred into a separating funnel. Distilled water (10 mL) and Et_2O or EtOAc (10 mL) were added, the layers were separated and the aqueous portion was extracted with Et_2O or EtOAc (2 × 10 mL). The combined organic extracts were dried over Na_2SO_4, filtered and concentrated *in vacuo* using a rotatory evaporator. The crude reaction mixture was purified by flash column chromatography.

General Procedure F

For solid acceptors

An oven-dried 4 mL vial was charged with carboxylic acid (0.20 mmol, 1.0 equiv), oven-dried Cs_2CO_3 (78.2 mg, 0.24 mmol, 1.2 equiv), [Ir{dF(CF_3)ppy}$_2$(dtbbpy)]PF_6 ([Ir] **133**; 2.2 mg, 0.002 mmol, 1.0 mol%) and solid acceptor (0.30 mmol, 1.5 equiv). The vial was sealed with a screwcap equipped with a PTFE/silicon septum and anhydrous DMF (1.0 mL, 0.2 M) was added by syringe. Argon was then bubbled through the mixture for 5 min. After sealing the cap with parafilm on top, the reaction mixture was stirred at 1000 rpm using the set-up shown in Figure 89 and irradiated with two 467 nm Kessel lamps at 36 °C (heat generated by the lamps).[211] After 18 h the lights were switched off and the reaction mixture was transferred into a separating funnel. Distilled water (10 mL) and Et_2O or EtOAc (10 mL) were added, the layers were separated and the aqueous portion was extracted with Et_2O or EtOAc (2 × 10 mL). The combined organic extracts were dried over Na_2SO_4, filtered and concentrated *in vacuo* using a rotatory evaporator. The crude reaction mixture was purified by flash column chromatography.

Further remarks:

Unless otherwise stated, all purifications by flash chromatography were performed on a basic alumina (IV) stationary phase (see Section **7.1** for preparation). Silica can also be used as stationary phase, but basic alumina (IV) was found to provide a time advantage and higher yields.

Radical scavengers used as stabilisers in many commercial alkenes must be removed before using the alkene. This was typically done by distillation (see Section **7.1**).

If a toxic and volatile alkene was used as radical acceptor (*e.g.* ethyl acrylate), a rotatory evaporator in a ventilated space was used during workup. Excess acceptor in the syringe was quenched with a dilute bleach bath (bleach:H_2O = 1:1) and the syringe was left to stand in the bleach bath for 24 h before disposal.

LED lamps emit potentially high-intensity blue/visible-light which is not generally considered harmful unless the eye is exposed for a long period of time. Care should be taken not to look directly at the light. Transparent-orange covered safety glasses were worn and a transparent-orange covered safety screen was placed in front of the set up.

In productive reactions, the colour of the reaction mixture typically turned from light yellow to dark brown (Figure 88).



Figure 88. Typical end colour of the reaction mixture in productive reactions.

Photoredox apparatus

Photoredox reactions were performed in oven-dried 4 mL vials (product code: 854190, Sigma-Aldrich) with a thickness of 1 mm which were sealed with screwcaps with PTFE/silicon septa (product code: SU860078, Sigma-Aldrich). Reactions were run in batches of one or two vials (Figure 89). The vials were attached together using two elastic bands positioned over the screw-caps. Irradiation was provided by two 40 W Kessil PR160 LED lamps with intensity dials set to maximum and placed 4 cm away from the center of the vials.

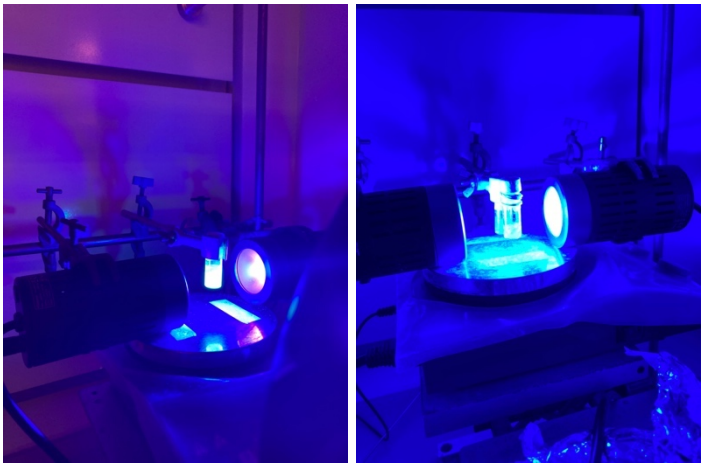
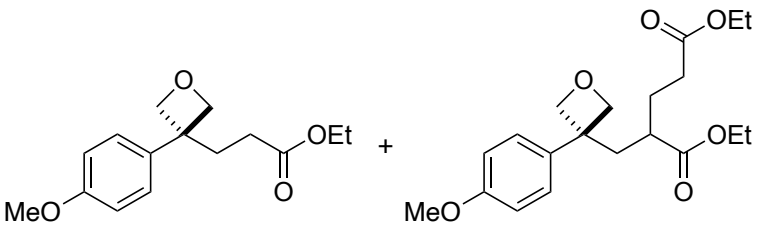


Figure 89. Picture of a photoredox reaction run as a single- (left) or two parallel reactions (right).

Ethyl 3-(3-(4-methoxyphenyl)oxetan-3-yl)propanoate (149, III-A) and diethyl 2-((3-(4-methoxyphenyl)oxetan-3-yl)methyl)pentanedioate (149', III-A')



149, **III-A** **149'**, **III-A'**

Following **General Procedure E** and using oxetane carboxylic acid **148a** ('batch 1', 41.6 mg) and ethyl acrylate (33 μL). Purification by basic alumina (IV) column chromatography (20–50% Et_2O/pentane) afforded oxetane **149** as colourless crystals (28.0 mg, 53%), followed by di addition product **149'** as a colourless gum (7.0 mg, 10%; [isolated with 3% of dimer **154**; **III-B**]). Oxetane **149** was obtained in 67% yield (35.2 mg) when using repurified oxetane acid **148a** (repurified 'batch 2'; 99.9% instead of 98.9% purity).

149 (**III-A**): R_f = 0.27 (50% Et_2O/pentane); ^{1}H NMR (400 MHz, $CDCl_3$) δ 6.97–6.93 (m, 2 H, 2 × Ar-CH), 6.90–6.87 (m, 2 H, 2 × Ar-CH), 4.95 (d, *J* = 5.7 Hz, 2 H, C*H*HOC*H*H), 4.64 (d, *J* = 5.7 Hz, 2 H, CH*H*OCH*H*), 4.06 (q, *J* = 7.2 Hz, 2 H, CH_2CH$_3$), 3.81 (s, 3 H, OCH$_3$), 2.43–

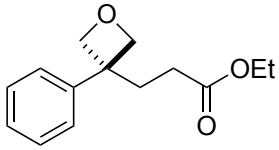
2.38 (m, 2 H, CH_2), 2.14–2.10 (m, 2 H, CH_2), 1.22 (t, *J* = 7.2 Hz, 3 H, CH_2CH_3). The observed characterisation data (R_f, ^1H) were consistent with that observed previously in the group.[211]

Notes:

***149** was further characterised by X-ray crystallography (Figure 58).*

149' (**III-A'**): R_f = 0.15 (50% Et_2O/pentane); IR (film)/cm^{-1} 2937, 1730 (C=O st), 1513, 1249, 1182, 731; ^1H NMR (400 MHz, $CDCl_3$) δ 7.00–6.96 (m, 2 H, 2 × Ar-CH), 6.90–6.86 (m, 2 H, 2 × Ar-CH), 4.95 (d, *J* = 5.7 Hz, 1 H, C*H*HO), 4.89 (d, *J* = 5.7 Hz, 1 H, C*H*HO), 4.64 (d, *J* = 5.7 Hz, 1 H, CH*H*O), 4.63 (d, *J* = 5.7 Hz, 1 H, CH*H*O), 4.08 (q, *J* = 7.1 Hz, 2 H, CH_2CH_3), 3.96–3.83 (m, 2 H, CH_2CH_3), 3.81 (s, 3 H, OCH_3), 2.66–2.60 (m, 1 H, C_qCHH), 2.21–2.16 (m, 2 H, $CHCH_2CH_2$), 2.15–2.11 (m, 2 H, CH + C_qCHH), 1.90–1.80 (m, 1 H, $CHCHHCH_2$), 1.74–1.65 (m, 1 H, $CHCHHCH_2$), 1.22 (t, *J* = 7.1 Hz, 3 H, CH_2CH_3), 1.18 (t, *J* = 7.1 Hz, 3 H, CH_2CH_3); ^{13}C NMR (101 MHz, $CDCl_3$) δ 175.1 (C_q=O), 172.6 (C_q=O), 158.1 (Ar-C_qOMe), 135.8 (Ar-C_qC_q), 127.1 (2 × Ar-CH), 113.8 (2 × Ar-CH), 82.2 (CH_2OCH_2), 81.8 (CH_2OCH_2), 60.5 (CH_2CH_3), 60.4 (CH_2CH_3), 55.3 (OCH_3), 46.5 (C_q), 43.3 (C_qCH_2), 41.3 (CH), 31.7 ($CHCH_2CH_2$), 28.6 ($CHCH_2CH_2$), 14.1 (CH_2CH_3), 14.0 (CH_2CH_3); HRMS (ESI) *m/z* calcd for $C_{20}H_{29}O_6$ 365.1964 $[M+H]^+$, found 365.1967.

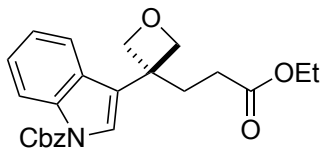
Ethyl 3-(3-phenyloxetan-3-yl)propanoate (152)



An oven-dried 4 mL vial was charged with 3-phenyloxetane-3-carboxylic acid **148m** (17.8 mg, 0.10 mmol, 1.0 equiv), oven-dried Cs_2CO_3 (39.1 mg, 0.12 mmol, 1.2 equiv) and $[Ir\{dF(CF_3)ppy\}_2(dtbbpy)]PF_6$ ([Ir] **133**; 1.1 mg, 0.001 mmol, 1.0 mol%). The vial was sealed with a screwcap equipped with a PTFE/silicon septum and anhydrous DMF (0.5 mL, 0.2 M) was added by syringe. Argon was bubbled through the mixture for 5 min and ethyl acrylate (18 μL, 0.15 mmol, 1.5 equiv) was added by syringe under argon. After sealing the cap with parafilm on top, the reaction mixture was stirred at 1000 rpm using the set-up shown in Figure 89 and irradiated with two 467 nm Kessel lamps at 36 °C (heat generated by the lamps).[211] After 14 h the lights were switched off and the reaction mixture was transferred into a separating funnel. Distilled water (10 mL) and Et_2O (10 mL) were added, the layers were separated and the aqueous portion was extracted with Et_2O (2 × 10 mL). The combined organic extracts were dried over Na_2SO_4, filtered and concentrated *in vacuo* using a rotatory evaporator. Purification by basic alumina (IV) column chromatography (10–20% Et_2O/pentane) afforded oxetane **152** as a colourless oil (11.4 mg, 49%). R_f = 0.35 (30% Et_2O/pentane); ^1H NMR (400 MHz, $CDCl_3$) δ 7.38–7.33 (m, 2 H, 2 × Ph-CH), 7.28–7.23 (m, 1 H, Ph-CH), 7.04–7.01 (m, 2 H, 2 × Ph-CH), 5.00 (d, *J* = 5.8 Hz, 2 H, C*H*HOC*H*H), 4.67 (d,

J = 5.8 Hz, 2 H, CH*H*OCH*H*), 4.06 (q, *J* = 7.2 Hz, 2 H, C*H*$_2$CH$_3$), 2.46–2.42 (m, 2 H, C*H*$_2$CH$_2$), 2.16–2.12 (m, 2 H, CH$_2$C*H*$_2$), 1.22 (t, *J* = 7.2 Hz, 3 H, CH$_2$C*H*$_3$). The observed characterisation data (R_f, ^{1}H) were consistent with that observed previously in the group.[211]

Benzyl 3-(3-(3-ethoxy-3-oxopropyl)oxetan-3-yl)-1*H*-indole-1-carboxylate (160)



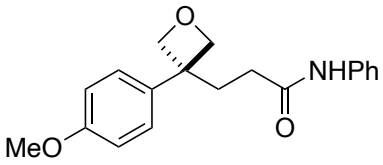
An oven-dried 4 mL vial was charged with 3-(1-((benzyloxy)carbonyl)-1*H*-indol-3-yl)oxetane-3-carboxylic acid (35.1 mg, 0.10 mmol, 1.0 equiv),[‖] oven-dried Cs_2CO_3 (39.1 mg, 0.12 mmol, 1.2 equiv) and [Ir{dF(CF$_3$)ppy}$_2$(dtbbpy)]PF$_6$ ([Ir] **133**; 1.1 mg, 0.001 mmol, 1.0 mol%). The vial was sealed with a screwcap equipped with a PTFE/silicon septum and anhydrous DMF (0.5 mL, 0.2 M) was added by syringe. Argon was bubbled through the mixture for 5 min and ethyl acrylate (18 μL, 0.15 mmol, 1.5 equiv) was added by syringe under argon. After sealing the cap with parafilm on top, the reaction mixture was stirred at 1000 rpm using the set-up shown in Figure 89 and irradiated with two 467 nm Kessel lamps at 36 °C (heat generated by the lamps).[211] After 18 h the lights were switched off and the reaction mixture was transferred into a separating funnel. Distilled water (10 mL) and EtOAc (10 mL) were added, the layers were separated and the aqueous portion was extracted with EtOAc (2 × 10 mL). The combined organic extracts were dried over Na_2SO_4, filtered and concentrated *in vacuo* using a rotatory evaporator. Purification by basic alumina (IV) column chromatography (30–50% Et_2O/pentane) afforded oxetane **160** as a colourless gum (15.4 mg, 38%). R_f = 0.28 (50% Et_2O/pentane); IR (film)/cm^{-1} 2951, 1730 (C=O st), 1453, 1396, 1237; ^{1}H NMR (400 MHz, $CDCl_3$) δ 8.22 (br s, 1 H, Ar$_{(indole)}$–CH), 7.52–7.50 (m, 2 H, 2 × Ar-CH), 7.47–7.31 (m, 6 H, 6 × Ar-CH), 7.27–7.23 (m, 1 H, Ar$_{(indole)}$-CH), 5.47 (s, 2 H, CH$_2$Ph), 5.00 (d, *J* = 5.8 Hz, 2 H, C*H*HOC*H*H), 4.78 (d, *J* = 5.8 Hz, 2 H, CH*H*OCH*H*), 4.02 (q, *J* = 7.2 Hz, 2 H, C*H*$_2$CH$_3$), 2.58–2.54 (m, 2 H, C*H*$_2$CH$_2$), 2.19–2.15 (m, 2 H, CH$_2$C*H*$_2$), 1.17 (t, *J* = 7.2 Hz, 3 H, CH$_2$C*H*$_3$); ^{13}C NMR (101 MHz, $CDCl_3$) δ 172.9 (C$_q$=O$_{(ester)}$), 150.7 (C$_q$=O$_{(carbamate)}$), 136.0 (Ar-C$_q$), 134.9 (Ph-C$_q$), 128.82 (Ar-CH), 128.80 (2 × Ar-CH), 128.6 (2 × Ar-CH), 128.2 (Ar-C$_q$), 125.0 (Ar-CH), 123.5 (Ar-*C*$_q$C$_q$), 123.0 (Ar-CH), 122.1 (Ar-CH), 119.5 (Ar-CH), 115.7 (Ar$_{(indole)}$-CH), 81.2 (CH$_2$OCH$_2$), 68.9 (CH$_2$Ph), 60.5 (*C*H$_2$CH$_3$), 41.9 (C$_q$), 32.9 (*C*H$_2$CH$_2$), 30.1 (CH$_2$*C*H$_2$), 14.1 (CH$_2$*C*H$_3$); HRMS (ESI) *m/z* calcd for $C_{24}H_{26}NO_5$ [M+H]$^+$: 408.1811, found 408.1818.

[‖] Synthesised by M. Dubois.[352]

Notes:

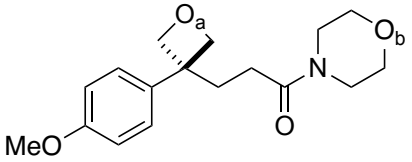
The signals at 150.7 and 136.0 ppm in the ^{13}C NMR spectrum were very weak due to chemical exchange between carbamate rotamers. They were assigned based on HMBC 2D correlation peaks.[311]

3-(3-(4-Methoxyphenyl)oxetan-3-yl)-*N*-phenylpropanamide (161)



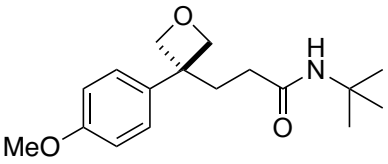
Following **General Procedure F** and using oxetane carboxylic acid **148a** (41.6 mg) and *N*-phenylacrylamide (44.2 mg). Purification by basic alumina (IV) column chromatography (50–80% Et_2O/pentane) afforded oxetane **161** as a colourless gum (42.5 mg, 68%). R_f = 0.11 (20% Et_2O/pentane); IR (film)/cm^{-1} 3306 (NH st, br), 2939, 1665 (C=O st), 1605, 1545, 1510, 1443, 1244, 1184, 980, 757; ^1H NMR (400 MHz, $CDCl_3$) δ 7.45–7.42 (m, 2 H, 2 × Ar-CH), 7.32–7.28 (m, 2 H, 2 × Ar-CH), 7.17 (br s, 1 H, NH), 7.11–7.08 (m, 1 H, Ph-CH), 7.00–6.97 (m, 2 H, 2 × Ar-CH), 6.91–6.89 (m, 2 H, 2 × Ar-CH), 4.96 (d, *J* = 5.7 Hz, 2 H, C*H*HOC*H*H), 4.68 (d, *J* = 5.7 Hz, 2 H, CH*H*OCH*H*), 3.80 (s, 3 H, OCH_3), 2.52–2.48 (m, 2 H, C$H_2$$CH_2$), 2.19–2.15 (m, 2 H, CH_2CH_2); ^{13}C NMR (101 MHz, $CDCl_3$) δ 170.4 (C_q=O), 158.2 (Ar-C_qOMe), 137.7 (Ar-C_q), 136.0 (Ar-C_q), 129.0 (2 × Ar-CH), 126.8 (2 × Ar-CH), 124.2 (Ph-CH), 119.7 (2 × Ar-CH), 114.0 (2 × Ar-CH), 81.5 (CH_2OCH_2), 55.3 (OCH_3), 46.3 (C_q), 36.3 (*C*$H_2$$CH_2$), 33.0 ($CH_2$*C*$H_2$); HRMS (EI) *m/z* calcd for $C_{19}H_{22}NO_3^+$ $[M+H]^+$: 312.1594, found 312.1595.

3-(3-(4-Methoxyphenyl)oxetan-3-yl)-1-morpholinopropan-1-one (162)



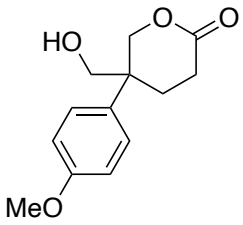
Following **General Procedure E** and using oxetane carboxylic acid **148a** (41.6 mg) and 1-morpholinoprop-2-en-1-one (38 μL). Purification by silica column chromatography (30–50% acetone/pentane) afforded oxetane **162** as a colourless gum (32.6 mg, 53%). This compound slowly degraded on basic alumina (IV) but was still isolated in 51% yield (31.2 mg) when purified on this stationary phase. R_f = 0.10 (30% acetone/pentane); IR (film)/cm^{-1} 2858, 1636 (C=O st), 1512, 1432, 1245, 1113, 1029, 979, 832; ^{1}H NMR (400 MHz, $CDCl_3$) δ 7.00–6.96 (m, 2 H, 2 × Ar-CH), 6.90–6.87 (m, 2 H, 2 × Ar-CH), 4.94 (d, *J* = 5.7 Hz, 2 H, C*H*HO$_a$C*H*H), 4.66 (d, *J* = 5.7 Hz, 2 H, CH*H*O$_a$CH*H*), 3.81 (s, 3 H, OCH_3), 3.64–3.61 (m, 2 H, C*H*HO$_b$C*H*H), 3.59–3.55 (m, 4 H, CH*H*O$_b$CH*H* + C*H*HNC*H*H), 3.26 (br t, *J* = 4.9 Hz, 2 H, CH*H*NCH*H*), 2.43–2.38 (m, 2 H, CH_2CH$_2$), 2.12–2.08 (m, 2 H, CH$_2$CH_2); ^{13}C NMR (101 MHz, $CDCl_3$) δ 170.9 (C$_q$=O), 158.1 (Ar-C$_q$OMe), 136.1 (Ar-*C*$_q$C$_q$), 126.7 (2 × Ar-CH), 114.0 (2 × Ar-CH), 81.5 (CH$_2$O$_a$CH$_2$), 66.8 (*C*H$_2$O$_b$CH$_2$), 66.4 (CH$_2$O$_b$*C*H$_2$), 55.2 (OCH_3), 46.2 (C$_q$), 45.7 (*C*H$_2$NCH$_2$), 41.8 (CH$_2$N*C*H$_2$), 36.0 (*C*H$_2$CH$_2$), 28.2 (CH$_2$*C*H$_2$); HRMS (ESI) *m/z* calcd for $C_{17}H_{24}NO_4$ [M+H]$^+$: 306.1705, found 306.1691.

***N*-(*tert*-Butyl)-3-(3-(4-methoxyphenyl)oxetan-3-yl)propanamide (163)**



Following **General Procedure F** and using oxetane carboxylic acid **148a** (41.6 mg) and *N*-(*tert*-butyl)acrylamide (38.2 mg). Purification by basic alumina (IV) column chromatography (70–80% Et_2O/pentane) afforded oxetane **163** as a white solid (21.9 mg, 38%). R_f = 0.17 (80% Et_2O/pentane); mp = 69–70 °C; IR (film)/cm^{-1} 3313 (NH st, br), 2958, 1646 (C=O st), 1512, 1246, 1031, 980; ^{1}H NMR (400 MHz, $CDCl_3$) δ 6.98–6.95 (m, 2 H, 2 × Ar-CH), 6.90–6.87 (m, 2 H, 2 × Ar-CH), 5.15 (br s, 1 H, NH), 4.93 (d, *J* = 5.7 Hz, 2 H, C*H*HOC*H*H), 4.65 (d, *J* = 5.7 Hz, 2 H, CH*H*OCH*H*), 3.81 (s, 3 H, OCH_3), 2.39–2.35 (m, 2 H, CH_2CH$_2$), 1.92–1.88 (m, 2 H, CH$_2$CH_2), 1.30 (s, 9 H, 3 × CH_3); ^{13}C NMR (101 MHz, $CDCl_3$) δ 171.4 (C$_q$=O), 158.1 (Ar-C$_q$OMe), 136.3 (Ar-*C*$_q$C$_q$), 126.8 (2 × Ar-CH), 113.9 (2 × Ar-CH), 81.6 (CH$_2$OCH$_2$), 55.3 (OCH_3), 46.3 (C$_q$), 36.5 (*C*H$_2$CH$_2$), 32.8 (CH$_2$*C*H$_2$), 30.3 (*C*$_q$(CH$_3$)$_3$), 28.7 (C$_q$(*C*H$_3$)$_3$); HRMS (ESI) *m/z* calcd for $C_{17}H_{26}NO_3$ [M+H]$^+$: 292.1913, found 292.1908.

5-(Hydroxymethyl)-5-(4-methoxyphenyl)tetrahydro-2H-pyran-2-one (164)

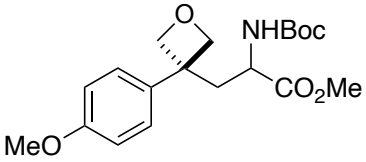


Trifluoroacetic acid (44 μL, 0.58 mmol, 10 equiv) was added to a solution of oxetane amide **163** (16.8 mg, 0.058 mmol, 1.0 equiv) in anhydrous CH_2Cl_2 (0.60 mL, 0.2 M) at 0 °C. After stirring for 5 min at 0 °C, the reaction mixture was warmed to 25 °C and stirred for further 18 h. Sat. aq. $NaHCO_3$ (5 mL) was added and the aqueous layer was extracted with EtOAc (6 × 10 mL). The combined organic extracts were dried over Na_2SO_4, filtered and concentrated *in vacuo* using a rotatory evaporator. Purification by flash column chromatography (80% EtOAc/pentane) afforded pyranone **164** as colourless gum (7.5 mg, 55%). R_f = 0.31 (80% EtOAc/pentane); IR (film)/cm^{-1} 3430 (OH st, br), 2925, 2362, 1728 (C=O st), 1515, 1251, 1189, 1032; ^{1}H NMR (400 MHz, $CDCl_3$) δ 7.34–7.30 (m, 2 H, 2 × Ar-CH), 6.97–6.93 (m, 2 H, 2 × Ar-CH), 4.80 (dd, ^2J = 11.8 Hz, ^4J = 2.1 Hz, 1 H, (C=O)OC*H*H), 4.53 (d, *J* = 11.8 Hz, 1 H, (C=O)OCH*H*)), 3.82 (s, 3 H, OCH_3), 3.78 (d, *J* = 11.2 Hz, 1 H, HOC*H*H), 3.70 (d, *J* = 11.2 Hz, 1 H, HOCH*H*), 2.62 (ddd, ^2J = 18.0 Hz, $^3J_{eq,ax}$ = 6.5 Hz, $^3J_{eq,eq}$ = 4.3 Hz, 1 H, C*H*HCH$_2$), 2.39 (ddd, ^2J = 18.0 Hz, $^3J_{ax,ax}$ = 10.4 Hz, $^3J_{ax,eq}$ = 7.3 Hz, 1 H, CH*H*CH$_2$), 2.24–2.10 (m, 2 H, CH$_2$C*H*$_2$); ^{13}C NMR (101 MHz, $CDCl_3$) δ 170.8 (C_q=O), 158.9 (Ar-C_qOMe), 130.8 (Ar-$C_q$$C_q$), 127.8 (2 × Ar-CH), 114.6 (2 × Ar-CH), 73.3 (*C*H$_2$O(C=O)), 68.7 (CH$_2$OH), 55.3 (OCH_3) 42.1 (Ar-$C_q$$C_q$), 28.0 (*C*H$_2CH_2$), 27.2 (CH$_2$*C*H$_2$); mass ion not found by HRMS (APCI).

Notes:

The observed characterisation data (IR, ^{1}H, ^{13}C) were consistent with that observed previously in the group for a related pyranone.[311]

Methyl 2-((*tert*-butoxycarbonyl)amino)-3-(3-(4-methoxyphenyl)oxetan-3-yl)propanoate (165)



Following **General Procedure E** and using oxetane carboxylic acid **148a** (41.6 mg) and methyl 2-((*tert*-butoxycarbonyl)amino)acrylate (60.4 mg). Purification by basic alumina (IV) column chromatography (10–60% Et_2O/pentane) afforded oxetane **165** as a colourless gum which was crystallised by slow evaporation using acetone to form colourless crystals (44.2 mg, 60%). R_f = 0.31 (80% Et_2O/pentane); mp = 103–106 °C; IR (film)/cm^{-1} 3355 (NH st, br), 2956, 1720 (C=O st), 1715 (C=O st), 1513, 1252, 1163; ^{1}H NMR (400 MHz, $CDCl_3$) δ 7.08–7.04 (m, 2 H, 2 × Ar-CH), 6.92–6.89 (m, 2 H, 2 × Ar-CH), 4.96–4.93 (m, 2 H, C*H*HOC*H*H), 4.75–4.68 (br s, 1 H, NH), 4.75 (d, *J* = 5.7 Hz, 1 H, CH*H*OCH$_2$), 4.68 (d, *J* = 5.7 Hz, 1 H, CH$_2$OCH*H*), 4.05–4.04 (br m, 1 H, CH), 3.81 (s, 3 H, Ar-$C_q$$OCH_3$), 3.60 (s,

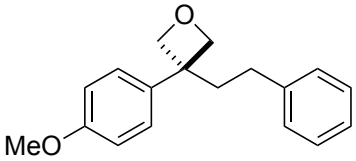
3 H, CO_2CH_3), 2.60 (br dd, ^2J = 14.1 Hz, ^3J = 4.0 Hz, 1 H, C*H*HCH), 2.47 (dd, ^2J = 14.1 Hz, ^3J = 8.1 Hz, 1 H, CH*H*CH), 1.40 (s, 9 H, $C_q(CH_3)_3$); ^{13}C NMR (101 MHz, $CDCl_3$) δ 172.8 (C_q=O_{ester}), 158.2 (Ar-C_qOMe), 154.8 (C_q=$O_{carbamate}$), 135.2 (Ar-$C_q$$C_q$), 127.0 (2 × Ar-CH), 114.0 (2 × Ar-CH), 82.1 (CH_2OCH_2), 81.9 (CH_2OCH_2), 79.9 ($C_q(CH_3)_3$), 55.2 (Ar-C_qOCH_3), 52.3 (CO_2CH_3), 51.1 (CH), 45.8 (C_q), 42.8 (CH_2CH), 28.2 ($C_q(CH_3)_3$); HRMS (APCI) *m/z* calcd for $C_{19}H_{28}NO_6^+$ $[M+H]^+$: 366.1911, found 366.1912.

Notes:

*Oxetane amino acid **165** was further characterised by X-ray crystallography (see Figure 58).*

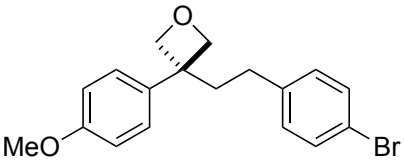
*The NH, CH**H**OCH$_2$ and CH$_2$OCH**H** signals in the ^{1}H NMR spectrum were integrated together to 3 H.*

3-(4-Methoxyphenyl)-3-phenethyloxetane (166)



Following **General Procedure E** and using oxetane carboxylic acid **148a** (41.6 mg) and styrene (35 μL). Purification by basic alumina (IV) column chromatography (0–50% Et_2O/pentane) afforded oxetane **166** as a colourless oil (5.5 mg, 10%). R_f = 0.24 (10% Et_2O/pentane); ^{1}H NMR (400 MHz, $CDCl_3$) δ 7.31–7.27 (m, 2 H, 2 × Ar-CH), 7.22–7.14 (m, 3 H, 3 × Ar-CH), 7.07–7.05 (m, 2 H, 2 × Ar-CH), 6.99–6.95 (m, 2 H, 2 × Ar-CH), 5.00 (d, *J* = 5.5 Hz, 2 H, C*H*HOC*H*H), 4.71 (d, *J* = 5.5 Hz, 2 H, CH*H*OCH*H*), 3.87 (s, 3 H, OCH_3), 2.42 (br s, 4 H, CH_2CH_2). The observed characterisation data (R_f, ^{1}H) were consistent with that observed previously in the group.[211]

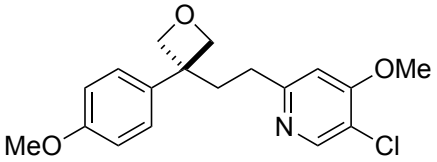
3-(4-Bromophenethyl)-3-(4-methoxyphenyl)oxetane (167)



Following **General Procedure E** and using oxetane carboxylic acid **148a** (41.6 mg) and 1-bromo-4-vinylbenzene (39 μL). Purification by basic alumina (IV) column chromatography (0–20% Et_2O/pentane) afforded oxetane **167** as a colourless oil (20.1 mg). The aqueous phase from the reaction workup was left to evaporate, EtOAc was added (10 mL) and then filtered sequentially through celite and basic alumina (IV) to yield further 30.7 mg of oxetane **167** (total of 50.8 mg, 73%). R_f = 0.11 (20% Et_2O/pentane); IR (film)/cm^{-1} 2933, 1515, 1244, 829; ^{1}H NMR (400 MHz, $CDCl_3$) δ 7.39–7.36 (m, 2 H, 2 × Ar-CH), 7.03–6.97 (m, 4 H, 2 × Ar-CH), 6.94–6.91 (m, 2 H, 2 × Ar-CH), 4.97 (d, *J* = 5.7 Hz, 2 H, C*H*HOC*H*H), 4.66 (d, *J* = 5.7 Hz, 2 H, CH*H*OCH*H*), 3.84 (s, 3 H, OCH_3), 2.35 (s, 4 H, CH_2CH_2); ^{13}C NMR (101 MHz, $CDCl_3$) δ 158.1 (Ar-C_qOMe), 140.7 (Ar-$C_q$$CH_2$), 136.4 (Ar-$C_q$$C_q$), 131.4 (2 × Ar-CH), 130.0 (2 × Ar-CH), 126.8 (2 × Ar-CH), 119.6 (Ar-C_qBr), 114.0

(2 × Ar-CH), 81.8 (CH_2OCH_2), 55.3 (OCH_3), 46.8 (C_q), 43.0 (CH_2CH_2), 30.4 (CH_2CH_2); mass ion not found by HRMS (APCI nor EI).

5-Chloro-4-methoxy-2-(2-(3-(4-methoxyphenyl)oxetan-3-yl)ethyl)pyridine (168)



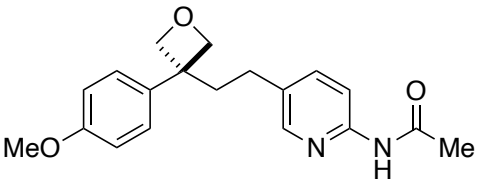
Following **General Procedure F** and using oxetane carboxylic acid **148a** (41.6 mg) and 5-chloro-4-methoxy-2-vinylpyridine (50.9 mg). Purification by basic alumina (IV) column chromatography (80–100% Et_2O/pentane) afforded oxetane **168** as a colourless gum (28.9 mg, 40%). R_f = 0.14 (Et_2O); IR (film)/cm^{-1} 2931, 2224, 1589, 1513, 1245, 1024, 979, 831; ^{1}H NMR (400 MHz, $CDCl_3$) δ 8.55 (s, 1 H, Pyr-CH), 7.01–6.98 (m, 2 H, 2 × Ar-CH), 6.91–6.88 (m, 2 H, 2 × Ar-CH), 6.62 (s, 1 H, Pyr-CH), 4.99 (d, *J* = 5.7 Hz, 2 H, C*H*HOC*H*H), 4.69 (d, *J* = 5.7 Hz, 2 H, CH*H*OCH*H*), 3.94 (s, 3 H, OCH_3), 3.81 (s, 3 H, OCH_3), 2.65–2.61 (m, 2 H, CH_2CH_2), 2.52–2.48 (m, 2 H, CH_2CH_2); ^{13}C NMR (101 MHz, $CDCl_3$) δ 168.1 ($Ar_{(pyridine)}$-C_qCH_2), 166.7 (Pyr-C_qOMe), 158.1 ($Ar_{(PMP)}$-C_qOMe), 153.6 (Pyr-CH), 136.1 (Ar-C_qC_q), 126.8 (2 × Ar-CH), 114.0 (2 × Ar-CH), 105.4 (Pyr-CH), 97.7 (Pyr-C_qCl), 81.6 (CH_2OCH_2), 56.1 (OCH_3), 55.3 (OCH_3), 46.7 (C_q), 40.3 (CH_2CH_2), 34.4 (CH_2CH_2); mass ion not found by HRMS (APCI nor EI).

Notes:

There was an additional signal in the ^{13}C NMR spectrum at 114.5 ppm which showed clear HMBC correlation signals with the pyridine protons.[311] Presumably this was due to chemical exchange between two different pyridine species in equilibrium (for example pyridine–pyridinium).

Presumably strong intramolecular fragmentation, known for 2-alkylpyridines,[267] led to intractable ion fragments in the mass spectrum.

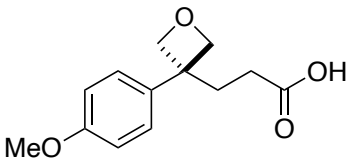
***N*-(5-(2-(3-(4-Methoxyphenyl)oxetan-3-yl)ethyl)pyridin-2-yl)acetamide (169)**



Following **General Procedure F** and using oxetane carboxylic acid **148a** (41.6 mg) and *N*-(5-vinylpyridin-2-yl)acetamide (97.3 mg, 0.6 mmol, 3.0 equiv). Purification by basic alumina (IV) column chromatography (100% CH_2Cl_2) afforded oxetane **169** as a colourless oil (15.0 mg, 23%). Using oxetane acid **148a** in excess (3.0 equiv; 1.0 equiv vinylpyridine) did not increase the yield of acetamide **169** (24% yield by quantitative NMR). R_f = 0.14 (50% Et_2O/CH_2Cl_2); ^{1}H NMR (400 MHz, $CDCl_3$) δ 8.19 (s, 1 H, NH), 8.09 (d, *J* = 8.5 Hz, 1 H, Pyr-CH), 8.00 (br s, 1 H, Pyr-CH), 7.46 (dd, *J* = 8.5, 2.4 Hz, 1 H, Pyr-CH), 7.01 (br d, *J* = 8.5 Hz, 2 H, 2 × Ar-CH), 6.93

(br d, *J* = 8.5 Hz, 2 H, 2 × Ar-CH), 4.98 (d, *J* = 5.7 Hz, 2 H, C*H*HOC*H*H), 4.67 (d, *J* = 5.7 Hz, 2 H, CH*H*OCH*H*), 3.83 (s, 3 H, OCH_3), 2.36 (s, 4 H, CH_2CH_2), 2.19 (s, 3 H, $C(O)CH_3$). The observed characterisation data (R_f, ^1H) were consistent with that observed previously in the group.[311]

3-(3-(4-Methoxyphenyl)oxetan-3-yl)propanoic acid (178)

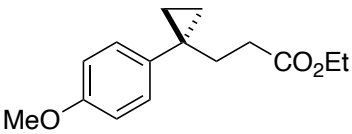


LiOH (7.2 mg, 0.3 mmol, 3.0 equiv) was added to a solution of PMP oxetane ethyl ester **149** (26.4 mg, 0.1 mmol, 1.0 equiv) in a THF (0.2 mL) / MeOH (0.2 mL) / H_2O (0.6 mL) mixture (THF:MeOH:H_2O = 1:1:3, 0.1 M) at 25 °C under air. After stirring the reaction mixture at 25 °C for 24 h, distilled water (15 mL) was added. The aqueous solution was extracted with Et_2O (2 × 10 mL), acidified to pH 1 with 1 M aq. HCl and re-extracted with EtOAc (3 × 15 mL). The EtOAc layers were combined, dried over Na_2SO_4, filtered and concentrated *in vacuo* using a rotatory evaporator to afford oxetane acid **178** as colourless crystals (23.4 mg, 99%). R_f = 0.09 (50% EtOAc/pentane); mp = 104 °C; IR (film)/cm^{-1} 3029 (COOH st, H-bonded, br), 2935, 1729 (C=O st, H-bonded), 1708, 1514, 1248, 831; ^1H NMR (400 MHz, $CDCl_3$) δ 6.95 (d, *J* = 8.2 Hz, 2 H, 2 × Ar-CH), 6.88 (d, *J* = 8.2 Hz, 2 H, 2 × Ar-CH), 4.97 (d, *J* = 5.7 Hz, 2 H, C*H*HOC*H*H), 4.65 (d, *J* = 5.7 Hz, 2 H, CH*H*OCH*H*), 3.80 (s, 3 H, OCH_3), 2.41 (t, *J* = 8.0 Hz, 2 H, C*H*$_2$CH$_2$), 2.17 (t, *J* = 8.0 Hz, 2 H, CH$_2$C*H*$_2$); ^{13}C NMR (101 MHz, $CDCl_3$) δ 178.7 (C_q=O), 158.2 (Ar-C_qOMe), 135.5 (Ar-$C_q$$C_q$), 126.8 (2 × Ar-CH), 114.0 (2 × Ar-CH), 81.5 (CH_2OCH_2), 55.3 (OCH_3), 46.1 (C_q), 35.6 (*C*H_2CH_2), 29.5 (CH_2CH_2); HRMS (ESI) *m/z* calcd for $C_{15}H_{20}NO_4$ $[M+MeCN+H]^+$: 278.1392, found 278.1400.

Notes:

*Oxetane acid **178** was further characterised by X-ray crystallography (see Figure 58).*

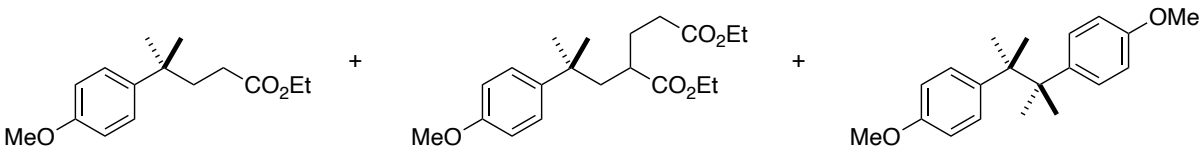
Ethyl 3-(1-(4-methoxyphenyl)cyclopropyl)propanoate (II-A)



Following **General Procedure A** and using 1-(4-methoxyphenyl)cyclopropane-1-carboxylic acid (38.4 mg) and ethyl acrylate (33 μL). Purification by basic alumina (IV) column chromatography (0–5% Et_2O/pentane) afforded cyclopropane **II-A** as a colourless gum (9.2 mg, 19%). R_f = 0.31 (10% Et_2O/pentane); IR (film)/cm^{-1} 2982, 1730 (C=O st), 1513, 1245, 1178, 1036; ^1H NMR (400 MHz, $CDCl_3$) δ 7.24–7.20 (m, 2 H, 2 × Ar-CH), 6.84–6.81 (m, 2 H, 2 × Ar-CH), 4.06 (q, *J* = 7.1 Hz, 2 H, C*H*$_2$CH$_3$), 3.79 (s, 3 H, OCH_3), 2.29–2.25 (m, 2 H, C*H*$_2$CH$_2$), 1.87–1.83 (m, 2 H, CH$_2$C*H*$_2$), 1.22 (t, *J* = 7.1 Hz, 3 H, CH$_2$C*H*$_3$), 0.78–0.75 (m, 2 H, $CH_{2(cyclopropane)}$), 0.69–0.66 (m, 2 H, $CH_{2(cyclopropane)}$); ^{13}C NMR (101 MHz, $CDCl_3$) δ 173.8

(C_q=O), 158.0 (Ar-C_qOMe), 136.2 (Ar-C_qC_q), 130.3 (2 × Ar-CH), 113.5 (2 × Ar-CH), 60.2 (CH_2CH_3), 55.3 and 55.2 (OCH_3), 35.9 (CH_2CH_2), 32.4 (CH_2CH_2), 24.6 (C_q), 14.2 (CH_2CH_3), 12.8 (2 × $CH_{2(cyclopropane)}$); HRMS (ESI) *m/z* calcd for $C_{15}H_{21}O_3$ $[M+H]^+$: 249.1491, found 249.1500.

Ethyl 4-(4-methoxyphenyl)-4-methylpentanoate (VII-A), **diethyl 2-(2-(4-methoxyphenyl)-2-methylpropyl)pentanedioate (VII-A') and 4,4'-(2,3-dimethylbutane-2,3-diyl)bis(methoxybenzene) (VII-B)**



VII-A **VII-A'** **VII-B**

Following **General Procedure A** and using 2-(4-methoxyphenyl)-2-methylpropanoic acid (38.8 mg) and ethyl acrylate (33 μL). Purification by silica flash column chromatography (2–15% Et_2O/pentane) afforded dimer **VII-B** as a white solid (11.8 mg, 40%), followed by alkane **VII-A** as a colourless oil (22.5 mg, 45%) and alkane **VII-A'** as a colourless oil (8.1 mg, 12%).

Dimer **VII-B:** R_f = 0.25 (4% Et_2O/pentane); ^{1}H NMR (400 MHz, $CDCl_3$) δ 6.98–6.94 (m, 4 H, 4 × Ar-CH), 6.75–6.71 (m, 4 H, 4 × Ar-CH), 3.80 (s, 6 H, 2 × OCH_3), 1.28 (s, 12 H, 4 × CH_3). The observed characterisation data (R_f and ^{1}H) were consistent with that previously reported in the group.[211]

Notes:

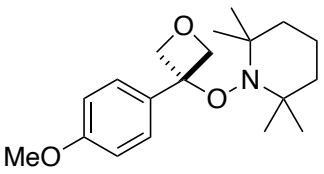
VII-B *was further characterised by X-ray crystallography (see Figure 60).*

gem-Dimethyl **VII-A**: R_f = 0.14 (4% Et_2O/pentane); ^{1}H NMR (400 MHz, $CDCl_3$) δ 7.27–7.23 (m, 2 H, 2 × Ar-CH), 6.87–6.84 (m, 2 H, 2 × Ar-CH), 4.06 (q, *J* = 7.0 Hz, 2 H, C*H*$_2$CH$_3$), 3.80 (s, 3 H, OCH_3), 2.08–2.03 (m, 2 H, C*H*$_2$CH$_2$), 1.96–1.92 (m, 2 H, CH$_2$C*H*$_2$), 1.30 (s, 6 H, 2 × CH_3), 1.21 (t, *J* = 7.0 Hz, 3 H, CH$_2$C*H*$_3$); The observed characterisation data (R_f, ^{1}H) were consistent with that observed previously in the group.[211]

gem-Dimethyl **VII-A'**: R_f = 0.22 (20% Et_2O/pentane); ^{1}H NMR (400 MHz, $CDCl_3$) δ 7.25–7.21 (m, 2 H, 2 × Ar-CH), 6.85–6.81 (m, 2 H, 2 × Ar-CH), 4.09 (q, *J* = 7.1 Hz, 2 H, C*H*$_2$CH$_3$), 3.93–3.82 (m, 2 H, C*H*$_2$CH$_3$), 3.79 (s, 3 H, OCH_3), 2.28–2.13 (m, 4 H, C_qC*H*HCH + CH + CHC*H*$_2$CH$_2$), 1.82–1.63 (m, 3 H, C_qCH*H*CH + CH$_2$C*H*$_2$CO$_2$), 1.29 (s, 3 H, CH_3), 1.26 (s, 3 H,

CH_3), 1.22 (t, *J* = 7.1 Hz, 3 H, CH_2CH_3), 1.16 (t, *J* = 7.2 Hz, 3 H, CH_2CH_3); The observed characterisation data (R_f, ^1H) were consistent with that observed previously in the group.[211]

1-((3-(4-Methoxyphenyl)oxetan-3-yl)oxy)-2,2,6,6-tetramethylpiperidine (182)



An oven-dried 4 mL vial was charged with oxetane carboxylic acid **148a** (41.6 mg, 0.20 mmol, 1.0 equiv), oven-dried Cs_2CO_3 (78.2 mg, 0.24 mmol, 1.2 equiv), (2,2,6,6-tetramethylpiperidin-1-yl)oxyl (TEMPO, 62.5 mg, 0.40 mmol, 2.0 equiv) and [Ir{dF(CF_3)ppy}$_2$(dtbbpy)]PF_6 ([Ir] **133**; 2.2 mg, 0.002 mmol, 1.0 mol%). The vial was sealed with a screwcap equipped with a PTFE/silicon septum and anhydrous DMF (1.0 mL, 0.2 M) was added by syringe. Argon was bubbled through the mixture for 5 min and ethyl acrylate (33 μL, 0.30 mmol, 1.5 equiv) was added by syringe under argon. After sealing the cap with parafilm on top, the reaction mixture was stirred at 1000 rpm using the set-up shown in Figure 89 and irradiated with two 467 nm Kessel lamps at 36 °C (heat generated by the lamps).[211] After 18 h the lights were switched off and the reaction mixture was transferred into a separating funnel. Distilled water (10 mL) and Et_2O (10 mL) were added, the layers were separated and the aqueous portion was extracted with Et_2O (2 × 10 mL). The combined organic extracts were dried over Na_2SO_4, filtered and concentrated *in vacuo* using a rotatory evaporator. Purification by basic alumina (IV) column chromatography (10–100% Et_2O/pentane) afforded impure oxetane **182** as a colourless gum (27.5 mg). Repurification by basic alumina (IV) column chromatography (80% CH_2Cl_2/pentane) afforded oxetane **182** as colourless crystals (13.6 mg, 21%). R_f = 0.22 (80% CH_2Cl_2/pentane); mp = 207 °C; IR (film)/cm^{-1} 2927, 1511, 1245, 1178; ^1H NMR (400 MHz, $CDCl_3$) δ 7.66–7.63 (m, 2 H, 2 × Ar-CH), 6.96–6.92 (m, 2 H, 2 × Ar-CH), 5.57 (d, *J* = 7.0 Hz, 2 H, C*H*HOC*H*H), 4.52 (d, *J* = 7.0 Hz, 2 H, CH*H*OCH*H*), 3.84 (s, 3 H, OCH_3), 1.66–1.49 (m, 5 H, CH_2CHHCH_2), 1.38–1.33 (m, 1 H, CH_2CHCH_2), 1.18 (s, 6 H, 2 × CH_3), 0.99 (s, 6 H, 2 × CH_3); ^{13}C NMR (101 MHz, $CDCl_3$) δ 158.5 (Ar-C_qOMe), 136.9 (Ar-C_qC_q), 125.8 (2 × Ar-CH), 113.6 (2 × Ar-CH), 82.1 (C_q), 81.3 (CH_2OCH_2), 59.5 (C_qNC_q), 55.2 (OCH_3), 40.4 ($CH_2CH_2CH_2$), 33.3 (2 × CH_3), 21.0 (2 × CH_3), 17.1 ($CH_2CH_2CH_2$); HRMS (ESI) *m/z* calcd for $C_{19}H_{30}NO_3$ $[M+H]^+$: 320.2226, found 320.2223.

Notes:

*Oxetane hydroxylamine **182** was further characterised by X-ray crystallography (see Scheme 47).*

[1.1.1]propellane (solution in Et_2O) (185)

Using modified procedures from Baran,[302] Bräse,[249] Anderson[450] and Leonori,[376a] 1,1-dibromo-2,2-bis(chloromethyl)cyclopropane (1.48 g, 5.0 mmol, 1.0 equiv) was added to a 25 mL round bottom flash and evacuated and refilled with argon (× 3). Anhydrous Et_2O was added (7.2 mL, 0.7 M) and the reaction mixture was cooled to –40 ºC with a cryostat. PhLi (1.79 M in Bu_2O, 5.59 mL, 10.0 mmol, 2.0 equiv) was added dropwise over 10 min, after which the reaction mixture turned from cloudy/colourless to clear/light-yellow. The reaction mixture was warmed to 0 ºC and stirred for further 2 h at 0 ºC, upon which the reaction mixture turned cloudy/light-yellow. The reaction mixture was allowed to warm to room temperature (ca. 22 ºC), attached to a short path distillation apparatus under Ar and the pressure was slowly reduced from 1000 mbar to ca. 10 mbar whilst cooling the condensing section and receiving flask with dry ice and not connected to water (see Figure 90 for the set-up used throughout the reaction and during distillation). Purification by distillation afforded propellane **185** as a solution in Et_2O (0.447 M and ca. 7 mL, 63%). The concentration of propellane **185** in Et_2O was determined by quantitative ^{1}H NMR using 1,2-dichloroethane as internal standard (0.20 mL propellane in Et_2O solution and 64.0 mg 1,2-dichloroethane used).[450] ^{1}H NMR (400 MHz, $CDCl_3$) δ 1.96 (s, 6 H, 3 × CH_2). The observed characterisation data (^{1}H NMR) were consistent with that previously reported.[451] Propellane **185** was stored under Ar, in the dark at –20 ºC.

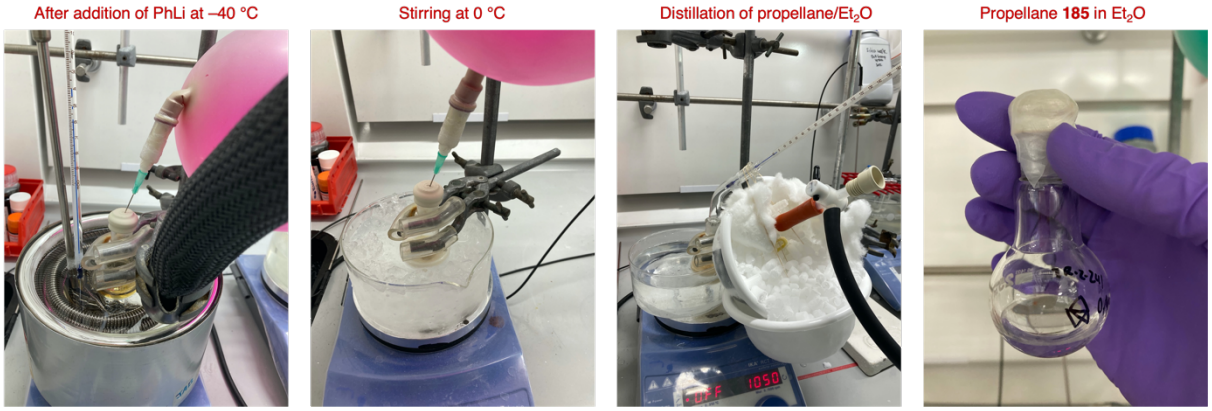
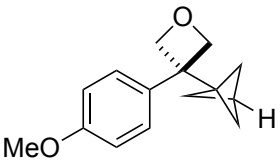


Figure 90. Synthesis of propellane 185 in Et_2O solution.

3-(Bicyclo[1.1.1]pentan-1-yl)-3-(4-methoxyphenyl)oxetane (186)



Following **General Procedure E** and using oxetane carboxylic acid **148a** (41.6 mg) and propellane **185** (0.447 M in Et_2O, 0.68 mL).[mm] Purification by basic alumina (IV) column chromatography (10% Et_2O/pentane) afforded a mixture of oxetane bicyclopentane **186** with staffanes (24.4 mg, ca. 75% pure **186**). Repurification by basic alumina (IV) column chromatography (Et_2O:CH_2Cl_2:pentane = 5:25:70) afforded oxetane bicyclopentane **186** as white crystals (3.9 mg, 8%). R_f = 0.47 (8% acetone/pentane); IR (film)/cm^{-1} 2960, 2867, 1512, 1245; ^1H NMR (400 MHz, $CDCl_3$) δ 6.89–6.84 (m, 2 H, 2 × Ar-CH), 6.81–6.77 (m, 2 H, 2 × Ar-CH), 4.89 (d, *J* = 5.4 Hz, 2 H, C*H*HOC*H*H), 4.78 (d, *J* = 5.4 Hz, 2 H, CH*H*OCH*H*), 3.81 (s, 3 H, OCH_3), 2.58 (s, 1 H, CH), 1.68 (s, 6 H, 3 × CHCH_2); ^{13}C NMR (101 MHz, $CDCl_3$) δ 157.8 (Ar-C_qOMe), 135.1 (Ar-C_qC_q), 126.8 (2 × Ar-CH), 113.6 (2 × Ar-CH), 78.7 (CH_2OCH_2), 55.2 (OCH_3), 49.6 (C_q), 47.2 (C_q), 46.8 (3 × CH_2CH), 26.9 (CH); HRMS (APCI) *m/z* calcd for $C_{15}H_{19}O_2^+$ $[M+H]^+$: 231.1380, found 231.1377.

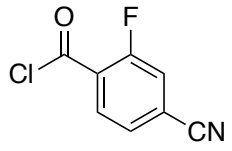
Notes:

*Oxetane bicyclopentane **186** was further characterised by X-ray crystallography (see Scheme 48).*

[mm] Amount of DMF adjusted (0.32 mL) for an overall concentration of 0.3 M (0.32 mL DMF + 0.68 mL **185** in Et_2O = 1.0 mL).

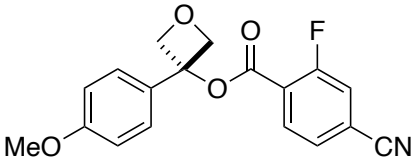
7.6.7 Redox-Active Oxetane Esters

4-Cyano-2-fluorobenzoyl chloride (187)[391e]



Oxalyl chloride (0.31 mL, 3.6 mmol, 1.44 equiv) was added dropwise to a suspension of 4-cyano-2-fluorobenzoic acid (495 mg, 3.0 mmol, 1.2 equiv) in anhydrous CH_2Cl_2 (7.5 mL, 0.40 M) at 25 ºC in a 25 mL round bottom flask. 5 drops of anhydrous DMF were added at the same temperature to the reaction mixture upon which vigorous gas evolution occurred (CO_2). The septum of the flask was pierced with an out needle before addition of DMF to allow for release of pressure. The out needle was removed after the vigorous gas evolution stopped (ca. 2 min). After stirring for 1 h (reaction became homogenous upon complete conversion), the reaction mixture was concentrated *in vacuo* using a rotatory evaporator to afford crude acyl chloride **187**.

3-(4-Methoxyphenyl)oxetan-3-yl 4-cyano-2-fluorobenzoate (188)



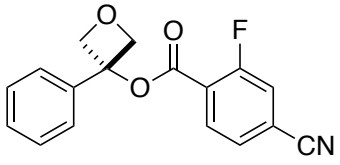
4-(Dimethylamino)pyridine (153 mg, 1.25 mmol, 0.5 equiv) and triethylamine (0.42 mL, 3.0 mmol, 1.2 equiv) were added sequentially to a solution of oxetanol **22a** (451 mg, 2.5 mmol, 1.0 equiv) in anhydrous CH_2Cl_2 (6.6 mL, 0.38 M) at 25 ºC in a 25 mL round bottom flask. A solution of the freshly prepared crude acyl chloride **187** in anhydrous CH_2Cl_2 (ca. 3.0 mmol, 1.2 equiv) was added dropwise in two portions (2 × 1 mL) to the reaction mixture at 0 ºC. After stirring the reaction mixture for 24 h at 25 ºC, CH_2Cl_2 (20 mL) and distilled water (15 mL) were added. The phases were separated, the organic layer was washed with brine (15 mL), dried over Na_2SO_4, filtered and concentrated *in vacuo* using a rotatory evaporator. Purification by flash column chromatography (40% Et_2O/pentane) afforded oxetane ester **188** as light yellow crystals (760 mg, 93%). R_f = 0.58 (60% Et_2O/pentane); mp = 115–117 °C; IR (film)/cm^{-1} 2959, 1727 (C=O st), 1515, 1415, 1282, 1250; ^{1}H NMR (400 MHz, $CDCl_3$) δ 8.05 (dd, *J* = 7.6, 7.6 Hz, 1 H, Ar-C*H*Ar-CHAr-CCN), 7.54 (d, *J* = 7.6 Hz, 1 H, Ar-CHAr-C*H*Ar-CCN), 7.49 (d, *J* = 8.9 Hz, 1 H, Ar-CFAr-CH), 7.46 (d, *J* = 8.7 Hz, 2 H, 2 × Ar-CH), 6.94 (d, *J* = 8.7 Hz, 2 H, 2 × Ar-CH), 5.19 (d, *J* = 7.6 Hz, 2 H, C*H*HOC*H*H), 5.09 (d, *J* = 7.6 Hz, 2 H, CH*H*OCH*H*), 3.82 (s, 3 H, OCH_3); ^{13}C NMR (101 MHz, $CDCl_3$) δ 161.34 (d, J_{C-F} = 264.6 Hz, Ar-C_qF), 161.26 (d, J_{C-F} = 3.8 Hz, C_q=O), 159.6 (Ar-C_qOMe), 133.3 (Ar-CHAr-*C*HAr-CCN), 130.5 (Ar-C_qC_qCH$_2$), 127.8 (d, J_{C-F} = 4.4 Hz, Ar-*C*HAr-CHAr-CCN), 126.8 (2 × Ar-CH), 122.6 (d, J_{C-F} = 10.5 Hz, Ar-C_qC=O), 121.0 (d, J_{C-F} = 26.1 Hz, Ar-*C*HAr-CF), 118.0 (d, J_{C-F} = 9.8 Hz, Ar-C_qCN), 116.5 (d, J_{C-F} = 1.8 Hz, CN), 114.1 (2 × Ar-CH), 81.9 (Ar-C_qC_qCH$_2$), 81.6 (CH_2OCH_2), 55.3 (OCH_3); ^{19}F NMR (377 MHz, $CDCl_3$) δ –105.4; HRMS (ESI) *m/z* calcd for $C_{10}H_{11}O$ [M+AcO]: 386.1040, found: 386.0797 (error: 62.9 ppm).

Notes:

*Oxetane ester **188** was further characterised by X-ray crystallography (see Scheme 51).*

The three doublets between 7.54 and 7.46 ppm were integrated together to 4 H.

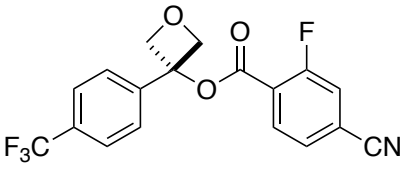
3-Phenyloxetan-3-yl 4-cyano-2-fluorobenzoate (189)



4-(Dimethylamino)pyridine (153 mg, 1.25 mmol, 0.5 equiv) and triethylamine (0.42 mL, 3.0 mmol, 1.2 equiv) were added sequentially to a solution of oxetanol **22m** (375 mg, 2.5 mmol, 1.0 equiv)[nn] in anhydrous CH_2Cl_2 (6.6 mL, 0.38 M) at 25 ºC in a 25 mL round bottom flask. A solution of the freshly prepared crude acyl chloride **187** in anhydrous CH_2Cl_2 (ca. 3.0 mmol, 1.2 equiv) was added dropwise in two portions (2 × 1 mL) to the reaction mixture at 0 ºC. After stirring the reaction mixture for 24 h at 25 ºC, CH_2Cl_2 (20 mL) and distilled water (15 mL) were added. The phases were separated, the organic layer was washed with brine (15 mL), dried over Na_2SO_4, filtered and concentrated *in vacuo* using a rotatory evaporator. Purification by flash column chromatography (20–40% Et_2O/pentane) afforded oxetane ester **189** as light-yellow crystals (651 mg, 88%). R_f = 0.32 (40% Et_2O/pentane); mp = 95 °C; IR (film)/cm^{-1} 2957, 1729 (C=O st), 1415, 1301, 1280, 1251, 1139; ^{1}H NMR (400 MHz, $CDCl_3$) δ 8.08 (dd, *J* = 8.0, 7.0 Hz, 1 H, Ar-C*H*Ar-CHArC-CN), 7.57–7.53 (m, 3 H, 3 × Ar-CH), 7.51 (dd, *J* = 9.7, 1.5 Hz, 1 H, Ar-CH), 7.46–7.41 (m, 2 H, 2 × Ar-CH), 7.39–7.34 (m, 1 H, Ar-CH), 5.21 (d, *J* = 8.3 Hz, 2 H, C*H*HOC*H*H), 5.09 (d, *J* = 8.3 Hz, 2 H, CH*H*OCH*H*); ^{13}C NMR (101 MHz, $CDCl_3$) δ 161.4 (d, J_{C-F} = 264.6 Hz, Ar-C_qF), 161.3 (d, J_{C-F} = 3.7 Hz, C_q=O), 138.4 (Ph-C_q), 133.3 (Ar-CHAr-*C*HAr-CCN), 128.8 (2 × Ph-CH), 128.5 (Ph-CH), 127.8 (d, J_{C-F} = 4.5 Hz, Ar-*C*HAr-CHAr-CCN), 124.9 (2 × Ph-CH), 122.5 (d, J_{C-F} = 10.6 Hz, Ar-C_qC=O), 121.1 (d, J_{C-F} = 26.0 Hz, Ar-*C*HAr-CF), 118.1 (d, J_{C-F} = 9.6 Hz, Ar-C_qCN), 116.5 (d, J_{C-F} = 2.3 Hz, CN), 81.9 (Ph-C_qC_q), 81.7 (CH_2OCH_2); ^{19}F NMR (377 MHz, $CDCl_3$) δ –105.2; mass ion not found by HRMS (ESI).

[nn] Provided by Pfizer.

3-(4-(Trifluoromethyl)phenyl)oxetan-3-yl 4-cyano-2-fluorobenzoate (190)



4-(Dimethylamino)pyridine (153 mg, 1.25 mmol, 0.5 equiv) and triethylamine (0.42 mL, 3.0 mmol, 1.2 equiv) were added sequentially to a solution of 3-(4-(trifluoromethyl)phenyl)oxetan-3-ol (545.5 mg, 2.5 mmol, 1.0 equiv)[oo] in anhydrous CH_2Cl_2 (6.6 mL, 0.38 M) at 25 ºC in a 25 mL round bottom flask. A solution of the freshly prepared crude acyl chloride **187** in anhydrous CH_2Cl_2 (ca. 3.0 mmol, 1.2 equiv) was added dropwise in two portions (2 × 1 mL) to the reaction mixture at 0 ºC. After stirring the reaction mixture for 24 h at 25 ºC, CH_2Cl_2 (20 mL) and distilled water (15 mL) were added. The phases were separated, the organic layer was washed with brine (15 mL), dried over Na_2SO_4, filtered and concentrated *in vacuo* using a rotatory evaporator. Purification by flash column chromatography (10–30% Et_2O/pentane) afforded oxetane ester **190** as light yellow crystals (835 mg, 91%). R_f = 0.39 (40% Et_2O/pentane); mp = 97 °C; IR (film)/cm^{-1} 2885, 1725 (C=O st), 1414, 1325, 1279, 1247, 1113, 1074; ^{1}H NMR (400 MHz, $CDCl_3$) δ 8.09 (dd, *J* = 7.5, 7.5 Hz, 1 H, Ar-C*H*Ar-CHArC-CN), 7.71 (d, *J* = 8.9 Hz, 2 × Ar-CH), 7.68 (d, *J* = 8.9 Hz, 2 × Ar-CH), 7.53 (dd, *J* = 7.5, 1.5 Hz, 1 H, Ar-CHAr-C*H*ArC-CN), 7.53 (dd, *J* = 9.8, 1.5 Hz, 1 H, Ar-CFAr-CH), 5.22 (d, *J* = 8.0 Hz, 2 H, C*H*HOC*H*H), 5.05 (d, *J* = 8.0 Hz, 2 H, CH*H*OCH*H*); ^{13}C NMR (101 MHz, $CDCl_3$) δ 161.4 (d, $J_{C–F}$ = 264.8 Hz, Ar-C_qF), 161.3 (d, $J_{C–F}$ = 3.9 Hz, C_q=O), 142.4 (Ar-$C_q$$C_q$$CH_2$), 133.4 (Ar-CHAr-*C*HAr-CCN), 130.8 (q, $J_{C–F}$ = 32.7 Hz, Ar-$C_q$$CF_3$), 127.9 (d, $J_{C–F}$ = 4.6 Hz, Ar-*C*HAr-CHAr-CCN), 126.0 (q, $J_{C–F}$ = 3.8 Hz, 2 × Ar-CH), 125.2 (2 × Ar-CH), 123.8 (q, $J_{C–F}$ = 272.1 Hz, CF_3), 122.0 (d, $J_{C–F}$ = 10.1 Hz, Ar-C_qC=O), 121.1 (d, $J_{C–F}$ = 26.0 Hz, Ar-*C*HAr-CF), 118.5 (d, $J_{C–F}$ = 9.9 Hz, Ar-C_qCN), 116.4 (d, $J_{C–F}$ = 2.6 Hz, CN), 81.4 (CH_2OCH_2), 81.2 (Ar-$C_q$$C_q$$CH_2$); ^{19}F NMR (377 MHz, $CDCl_3$) δ –62.8 (CF_3), –105.2 (Ar-CF); HRMS (ESI) *m/z* calcd for $C_{10}H_8F_3O_2^-$ [M–C_8H_3FNO]$^-$: 217.0482, found: 217.0473.

Notes:

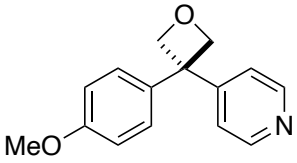
The two doublets between 7.71 and 7.68 ppm were integrated together to 4 H.

The mass of the corresponding oxetane alkoxide was found.

[oo] Synthesised by M. Dubois.

7.6.8 4-Pyridyl Diaryl Oxetanes and Related Structures

4-(3-(4-Methoxyphenyl)oxetan-3-yl)pyridine (191)

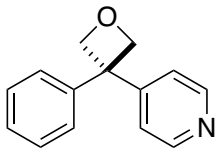


A flame-dried reaction tube was charged with oxetane ester **188** (32.7 mg, 0.1 mmol, 1.0 equiv), 4-cyanopyridine (15.6 mg, 0.15 mmol, 1.5 equiv), Hantzsch ester (50.7 mg, 0.2 mmol, 2.0 equiv) and sodium acetate (16.4 mg, 0.2 mmol, 2.0 equiv). The reaction vessel was sealed and evacuated and refilled with argon (× 3). Anhydrous DMSO (2.0 mL, 0.05 M) was added to the reaction mixture and argon was bubbled through the reaction for 10 min. The reaction mixture was stirred at 1000 rpm and irradiated with two broad spectrum blue lights at full intensity placed 3 cm away from the vial and with a fan placed in front of the vial (20 cm distance). After 17 h the lights were switched off and the reaction mixture was transferred into a separating funnel. CH_2Cl_2 (10 mL) and 5% aq. Na_2CO_3 (2 mL) were added, the layers were separated and the aqueous portion was extracted with CH_2Cl_2 (10 mL). The combined organic extracts were washed with brine (2 × 20 mL), dried over Na_2SO_4, filtered and concentrated *in vacuo* using a rotatory evaporator. NaCN is a by-product of the reaction. The aq. phase was kept basic at all times and quenched with diluted bleach at the end of the reaction. Purification by flash column chromatography (80–100% Et_2O/pentane) afforded diaryl-oxetane **191** as colourless crystals (15.1 mg, 63%). R_f = 0.13 (Et_2O); mp = 78 °C; IR (film)/cm^{-1} 2955, 1596, 1513, 1249; ^{1}H NMR (400 MHz, $CDCl_3$) δ 8.59 (d, *J* = 5.5 Hz, 2 H, 2 × Pyr-CH), 7.19 (d, *J* = 5.5 Hz, 2 H, 2 × Pyr-CH), 7.08 (d, *J* = 8.3 Hz, 2 H, 2 × Ar-CH), 6.93 (d, *J* = 8.3 Hz, 2 H, 2 × Ar-CH), 5.27 (d, *J* = 5.8 Hz, 2 H, C*H*HOC*H*H), 5.14 (d, *J* = 5.8 Hz, 2 H, CH*H*OCH*H*), 3.83 (s, 3 H, OCH_3); ^{13}C NMR (101 MHz, $CDCl_3$) δ 158.6 (Ar-C_qOMe), 154.9 (Pyr-C_qC_q), 150.1 (2 × Pyr-CH), 135.6 (Ar-C_qC_q), 127.6 (2 × Ar-CH), 121.5 (2 × Pyr-CH), 114.2 (2 × Ar-CH), 83.8 (CH_2OCH_2), 55.3 (OCH_3), 50.5 (C_q); HRMS (ESI) *m/z* calcd for $C_{15}H_{16}NO_2$ [M+H]: 242.1181, found: 242.1181.

Notes:

*Diaryloxetane **191** was further characterised by X-ray crystallography (see Scheme 52).*

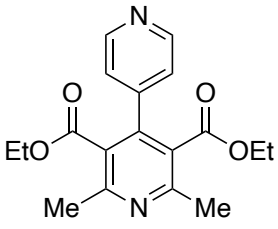
4-(3-Phenyloxetan-3-yl)pyridine (192)



A flame-dried reaction tube was charged with oxetane ester **189** (29.7 mg, 0.1 mmol, 1.0 equiv), 4-cyanopyridine (15.6 mg, 0.15 mmol, 1.5 equiv), Hantzsch ester (50.7 mg, 0.2 mmol, 2.0 equiv) and sodium acetate (16.4 mg, 0.2 mmol, 2.0 equiv). The reaction vessel was sealed and evacuated and refilled with argon (× 3). Anhydrous DMSO (2.0 mL, 0.05 M) was added to the reaction mixture and argon was bubbled through the reaction for 10 min. The reaction mixture was stirred at

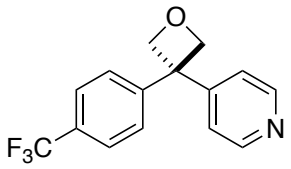
1000 rpm and irradiated with two broad spectrum blue lights at full intensity placed 3 cm away from the vial and with a fan placed in front of the vial (20 cm distance). After 17 h the lights were switched off and the reaction mixture was transferred into a separating funnel. CH_2Cl_2 (10 mL) and 5% aq. Na_2CO_3 (2 mL) were added, the layers were separated and the aqueous portion was extracted with CH_2Cl_2 (10 mL). The combined organic extracts were washed with brine (2 × 20 mL), dried over Na_2SO_4, filtered and concentrated *in vacuo* using a rotatory evaporator. Purification by flash column chromatography (80–100% Et_2O/pentane) afforded diaryl-oxetane **192** as colourless crystals (11.2 mg, 53%). R_f = 0.23 (Et_2O); mp = 91–93 ºC; IR (film)/cm^{-1} 2957, 1597, 1413, 985, 705; ^{1}H NMR (400 MHz, $CDCl_3$) δ 8.59 (d, *J* = 6.0 Hz, 2 H, 2 × Pyr-CH), 7.43–7.39 (m, 2 H, 2 × Ph-CH), 7.34–7.30 (m, 1 H, Ph-CH), 7.20 (d, *J* = 6.0 Hz, 2 H, 2 × Pyr-CH), 7.16 (d, *J* = 7.3 Hz, 2 H, 2 × Ph-CH), 5.32 (d, *J* = 5.9 Hz, 2 H, C*H*HOC*H*H), 5.16 (d, *J* = 5.9 Hz, 2 H, CH*H*OCH*H*); ^{13}C NMR (101 MHz, $CDCl_3$) δ 154.6 (Pyr-C_qC_q), 150.1 (2 × Pyr-CH), 143.5 (Ph-C_qC_q), 128.9 (2 × Ph-CH), 127.2 (Ph-CH), 126.4 (2 × Ph-CH), 121.5 (2 × Pyr-CH), 83.6 (CH_2OCH_2), 51.1 (C_q); HRMS (ESI) *m/z* calcd for $C_{14}H_{14}NO$ [M+H]: 212.1075, found: 212.1073.

Diethyl 2,6-dimethyl-[4,4'-bipyridine]-3,5-dicarboxylate (193') and 4-(3-(4-(trifluoromethyl)phenyl)oxetan-3-yl)pyridine (193)



193'

+



193

A flame-dried reaction tube was charged with oxetane ester **190** (36.5 mg, 0.1 mmol, 1.0 equiv), 4-cyanopyridine (15.6 mg, 0.15 mmol, 1.5 equiv), Hantzsch ester (50.7 mg, 0.2 mmol, 2.0 equiv) and sodium acetate (16.4 mg, 0.2 mmol, 2.0 equiv). The reaction vessel was sealed and evacuated and refilled with argon (× 3). Anhydrous DMSO (2.0 mL, 0.05 M) was added to the reaction mixture and argon was bubbled through the reaction for 10 min. The reaction mixture was stirred at 1000 rpm and irradiated with two broad spectrum blue lights at full intensity placed 3 cm away from the vial and with a fan placed in front of the vial (20 cm distance). After 17 h the lights were switched off and the reaction mixture was transferred into a separating funnel. CH_2Cl_2 (10 mL) and 5% aq. Na_2CO_3 (2 mL) were added, the layers were separated and the aqueous portion was extracted with CH_2Cl_2 (10 mL). The combined organic extracts were washed with brine (2 × 20 mL), dried over Na_2SO_4, filtered and concentrated *in vacuo* using a rotatory evaporator. Purification by flash column chromatography (60–100% Et_2O/pentane) afforded bipyridyl **193'** as a white solid (5.9 mg, 12%), followed by diaryl-oxetane **193** as a white solid (8.3 mg, 30%).

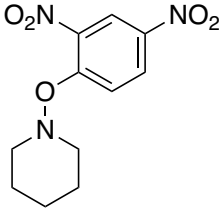
Bipyridyl **193'**: R_f = 0.32 (Et_2O); mp = 100 ºC; IR (film)/cm^{-1} 2981, 1762 (C=O st), 1561, 1233; ^1H NMR (400 MHz, $CDCl_3$) δ 8.65–8.64 (m, 2 H, 2 × Pyr-CH), 7.22–7.20 (m, 2 H, 2 × Pyr-CH), 4.03 (q, *J* = 7.2 Hz, 4 H, 2 × OC*H*$_2$CH$_3$), 2.63 (s, 6 H, 2 × CH_3), 0.94 (t, *J* = 7.2 Hz, 6 H, 2 × OCH_2C*H*$_3$); ^{13}C NMR (101 MHz, $CDCl_3$) δ 167.1 (2 × C_q=O), 156.2 (Pyr-C_qNPyr-C_q), 149.6 (2 × Pyr-CH), 144.8 (Pyr-*C*$_q$Pyr-C_q), 143.4 (Pyr-C_qPyr-*C*$_q$), 126.0 (2 × Pyr-*C*$_q$C=O), 123.0 (2 × Pyr-CH), 61.6 (2 × O*C*H_2CH_3), 23.1 (2 × CH_3), 13.5 (2 × OCH_2*C*H_3); HRMS (ESI) *m/z* calcd for $C_{18}H_{21}N_2O_4$ [M+H]: 329.1501, found: 329.1485.

Diaryl oxetane **193**: R_f = 0.11 (Et_2O); mp = 81 ºC; IR (film)/cm^{-1} 2958, 1326, 1166, 1121; ^1H NMR (400 MHz, $CDCl_3$) δ 8.63–8.62 (m, 2 H, 2 × Pyr-CH), 7.67 (d, *J* = 8.2 Hz, 2 H, 2 × Ar-CH), 7.32 (d, *J* = 8.2 Hz, 2 H, 2 × Ar-CH), 7.18–7.17 (m, 2 H, 2 × Pyr-CH), 5.28 (d, *J* = 6.0 Hz, 2 H, C*H*HOC*H*H), 5.20 (d, *J* = 6.0 Hz, 2 H, CH*H*OCH*H*); ^{13}C NMR (101 MHz, $CDCl_3$) δ 153.4 (Pyr-*C*$_q$C$_q$), 150.4 (2 × Pyr-CH), 147.5 (Ar-*C*$_q$C$_q$), 129.7 (q, $J_{C–F}$ = 32.8 Hz, Ar-*C*$_q$$CF_3$), 126.9 (2 × Ar-CH), 125.9 (q, $J_{C–F}$ = 3.7 Hz, 2 × Ar-CH), 122.3 (CF_3), 121.4 (2 × Pyr-CH), 83.2 (CH_2OCH_2), 51.1 (C_q); ^{19}F NMR (377 MHz, $CDCl_3$) δ –62.6; HRMS (ESI) *m/z* calcd for $C_{15}H_{13}F_3NO$ [M+H]: 280.0949, found: 280.0943.

Notes:

*The CF_3 peak in the ^{13}C NMR spectrum was not observed, but it was confirmed by an HMBC 2D correlation. The frequency of the J coupling of the expected quartet could not be determined. The **C_q**CF_3 peak was also confirmed by HMBC.*

1-(2,4-Dinitrophenoxy)piperidine (194)[396a]

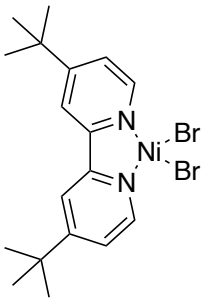


Benzoyl peroxide (75% [rest water]; 4.55 g, 14.09 mmol, 1.2 equiv) was added to a solution of piperidine (1.16 mL, 11.74 mmol, 1.0 equiv) and K_2HPO_4 (4.09 g, 23.48 mmol, 2.0 equiv) in DMF (59 mL, 0.2 M) in a 250 mL round bottom flask and the reaction mixture was stirred at 25 ºC for 18 h. Distilled water was added (50 mL) and the aqueous phase extracted with EtOAc (2 × 50 mL). The combined organic extracts were washed with brine (3 × 50 mL) and aq. NH_4Cl (50 mL), dried over Na_2SO_4, filtered and concentrated *in vacuo* using a rotatory evaporator to afford piperidin-1-yl benzoate, which was taken to the next step without further purification.

K_2CO_3 (3.25 g, 23.48 mmol, 2.0 equiv) was added to a solution of crude piperidin-1-yl benzoate (1.0 equiv) in MeOH (23.5 mL, 0.5 M) in a 100 mL round bottom flask and stirred at 25 ºC for 3 h. The reaction mixture was concentrated *in vacuo* using a rotatory evaporator and distilled water was added (50 mL). The aqueous solution was extracted with EtOAc (4 × 50 mL) and the combined organic extracts were dried over Na_2SO_4, filtered and concentrated *in vacuo* using a rotatory evaporator to afford piperidin-1-ol, which was taken to the next step without further purification.

1-Fluoro-2,4-dinitrobenzene (1.77 mL, 14.09 mmol, 1.2 equiv) and NEt_3 (3.27 mL, 23.48 mmol, 2.0 equiv) were added sequentially to a solution of crude piperidin-1-ol (1.0 equiv) in CH_2Cl_2 (59 mL, 0.2 M) at 0 ºC in a 250 mL round bottom flask. The reaction mixture was allowed to warm to room temperature (ca. 22 ºC) and stirred at 25 ºC for 14 h. Distilled water (50 mL) and CH_2Cl_2 (50 mL) were added, the layers separated and the aqueous layer extracted with EtOAc (3 × 50 mL). The combined organic extracts were dried over Na_2SO_4, filtered and concentrated *in vacuo* using a rotatory evaporator. Purification by flash column chromatography (0–15% Et_2O/pentane) afforded substituted hydroxylamine **194** as yellow crystals (1.12 g, 36%). R_f = 0.26 (10% Et_2O/pentane); mp = 77 ºC; IR (film)/cm^{-1} 2942, 2851, 1600, 1521, 1337, 1275; ^{1}H NMR (400 MHz, $CDCl_3$) δ 8.80 (d, *J* = 2.8 Hz, 1 H, Ar-CH), 8.39 (dd, *J* = 9.4, 2.8 Hz, 1 H, Ar-CH), 7.90 (d, *J* = 9.4 Hz, 1 H, Ar-CH), 3.40–3.36 (m, 2 H, C*H*HNC*H*H), 2.93–2.87 (m, 2 H, CH*H*NCH*H*), 1.95–1.88 (m, 2 H, 2 × CH), 1.77–1.66 (m, 3 H, 3 × CH), 1.38–1.28 (m, 1 H, CH); ^{13}C NMR (101 MHz, $CDCl_3$) δ 157.9 (Ar-C_qON), 140.1 (Ar-$C_q$$NO_2$), 136.3 (Ar-$C_q$$NO_2$), 129.3 (Ar-CH), 122.0 (Ar-CH), 116.9 (Ar-CH), 57.0 (CH_2NCH_2), 25.2 ($CH_2CH_2CH_2$), 22.9 ($CH_2CH_2CH_2$). The observed characterisation data (R_f, IR, ^{1}H, ^{13}C) were consistent with that previously reported.[396a]

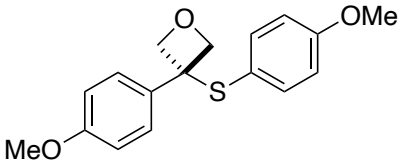
[4,4′-Bis(1,1-dimethylethyl)-2,2′-bipyridine] nickel (II) dibromide ($NiBr_2$•dtbbpy, 195)[452]



$NiBr_2$•DME (1.00 g, 3.24 mmol, 1.0 equiv) was added to a solution of 4,4'-di-*tert*-butyl-2,2'-bipyridyl (dtbbpy; 957 mg, 3.56 mmol, 1.1 equiv) in anhydrous THF (16.2 mL, 0.2 M) and the reaction mixture was stirred at room temperature (ca. 22 ºC) for 24 h. Then, the mixture was filtered and washed with anhydrous THF (5 × 2 mL) to afford a green/yellow solid which was grounded to a fine powder and dried *in vacuo* for 15 h using a high-vacuum pump and a drying pistol at 140 ºC to afford $NiBr_2$•dtbbpy (**195**) as a green/yellow solid (1.10 g, 70%). ^{1}H NMR (400 MHz, $(CD_3)_2SO$) δ 1.51 (br s, 18 H, 6 × CH_3), 0.87 (br s, 6 H, 6 × Ar-CH).

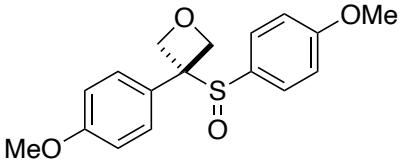
7.6.9 Oxetane Sulfoxides and Precursors

3-(4-Methoxyphenyl)-3-[(4-methoxyphenyl)sulfanyl]oxetane (216)



Lithium bis(trifluoromethanesulfonimide) (316 mg, 1.1 mmol, 0.11 equiv) and tetrabutylammonium hexafluorophosphate (213 mg, 0.55 mmol, 0.055 equiv) were added sequentially to a solution of oxetanol **22a** (1.80 g, 10.0 mmol, 1.0 equiv) and 4-methoxybenzenethiol (2.46 mL, 20.0 mmol, 2.0 equiv) in non-anhydrous chloroform (20 mL, 0.5 M) in a 100 mL round bottom flask. The reaction flask was placed into a preheated oil bath at 40 °C and then heated to 65 °C over 50 min. At 65 °C there was a change in colour from light-yellow to orange. From the moment of the colour change, the reaction was stirred for further 25 min and quenched with sat. aq. $NaHCO_3$ (25 mL). The aqueous layer was extracted with CH_2Cl_2 (3 × 25 mL). The combined organic extracts were washed with aq. NaOH (1 M, 35 mL), dried over Na_2SO_4, filtered and concentrated *in vacuo* using a rotatory evaporator. Purification by flash column chromatography (5–30% Et_2O/pentane) afforded oxetane **216** as a white solid (1.82 g, 60%). R_f = 0.21 (25% Et_2O/pentane); mp = 118–120 °C; IR (film)/cm^{-1} 2955, 1584, 1511, 1491, 1244, 1023, 833, 811; ^{1}H NMR (400 MHz, $CDCl_3$) δ 7.19–7.15 (m, 2 H, 2 × Ar-CH), 6.89–6.85 (m, 2 H, 2 × Ar-CH), 6.83–6.76 (m, 4 H, 4 × Ar-CH), 5.11 (d, *J* = 6.5 Hz, 2 H, C*H*HOC*H*H), 4.94 (d, *J* = 6.5 Hz, 2 H, CH*H*OCH*H*), 3.81 (s, 3 H, OCH_3), 3.80 (s, 3 H, OCH_3); ^{13}C NMR (101 MHz, $CDCl_3$) δ 160.6 (Ar-C_qOMe), 158.4 (Ar-C_qOMe), 137.8 (2 × Ar-CH), 135.0 (Ar-C_qC_q), 127.6 (2 × Ar-CH), 122.5 (Ar-C_qS), 114.2 (2 × Ar-CH), 113.5 (2 × Ar-CH), 82.2 (CH_2OCH_2), 55.3 (2 × OCH_3), 54.9 (C_q). The observed characterisation data (R_f, mp, IR, ^{1}H, ^{13}C) were consistent with that previously reported in the group.[110]

3-(4-Methoxybenzenesulfinyl)-3-(4-methoxyphenyl)oxetane (217)[110]



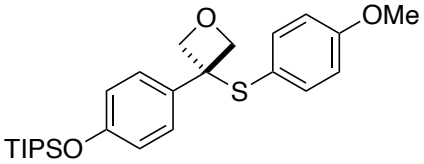
*m*CPBA (959 mg, 5.56 mmol, 1.05 equiv) was added in 3 portions over 30 minutes to a solution of oxetane sulfide **216** (1.60 g, 5.29 mmol, 1.0 equiv) in anhydrous CH_2Cl_2 (53 mL, 0.1 M) at 0 ºC in a 250 mL round bottom flask. After stirring the reaction mixture at 0 ºC for 2.5 h, 3 M aq. KOH (100 mL) was added and the phases separated. The aqueous layer was extracted with EtOAc (4 × 100 mL). The combined organic extracts were dried over Na_2SO_4, filtered and concentrated *in vacuo* using a rotatory evaporator. Purification by flash column chromatography (50–70% EtOAc/pentane) afforded sulfoxide **217** as a white solid (1.40 g, 83%). R_f = 0.31 (70% EtO/pentane); mp = 130–132 ºC; IR (film)/cm^{-1} 2938, 1590, 1507, 1250, 1020 (S=O st), 823, 541; ^{1}H NMR (400 MHz, $CDCl_3$) δ

6.95–6.92 (m, 2 H, 2 × Ar-CH), 6.83–6.79 (m, 4 H, 4 × Ar-CH), 6.61–6.57 (m, 2 H, 2 × Ar-CH), 5.35 (d, *J* = 7.2 Hz, 1 H, C*H*HOCH$_2$), 5.27 (d, *J* = 7.0 Hz, 1 H, CH$_2$OC*H*H), 4.98 (d, *J* = 7.0 Hz, 1 H, CH$_2$OCH*H*), 4.88 (d, *J* = 7.2 Hz, 1 H, CH*H*OCH$_2$), 3.82 (s, 3 H, OCH$_3$), 3.81 (s, 3 H, OCH$_3$); ^{13}C NMR (101 MHz, CDCl$_3$) δ 162.3 (Ar-C$_q$OMe), 159.6 (Ar-C$_q$OMe), 129.4 (Ar-C$_q$SO), 129.0 (2 × Ar-CH), 127.2 (2 × Ar-CH), 126.3 (Ar-*C*$_q$C$_q$), 113.8 (2 × Ar-CH), 113.6 (2 × Ar-CH), 77.2 (CH$_2$O), 73.7 (CH$_2$O), 67.2 (C$_q$), 55.4 (OCH$_3$), 55.3 (OCH$_3$). The observed characterisation data (R$_f$, mp, IR, ^{1}H, ^{13}C) were consistent with that previously reported in the group.[110]

Notes:

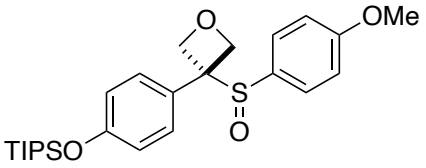
*Oxetane sulfoxide **217** was further characterised by X-ray crystallography (see Scheme 57).*

Triisopropyl(4-(3-((4-methoxyphenyl)thio)oxetan-3-yl)phenoxy)silane (227)



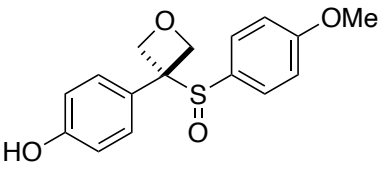
Lithium bis(trifluoromethanesulfonimide) (316 mg, 1.1 mmol, 0.11 equiv) and tetrabutylammonium hexafluorophosphate (213 mg, 0.55 mmol, 0.055 equiv) were added sequentially to a solution of oxetanol **22c** (3.23 g, 10.0 mmol, 1.0 equiv) and 4-methoxybenzenethiol (2.46 mL, 20.0 mmol, 2.0 equiv) in non-anhydrous chloroform (20 mL, 0.5 M) in a 100 mL round bottom flask. The reaction flask was placed into a preheated oil bath at 40 °C and then heated to 65 °C in 20 min. At 65 °C there was a change in appearance from clear to cloudy. From the moment of the colour change, the reaction was stirred for further 25 min and quenched with sat. aq. NaHCO$_3$ (25 mL). The aqueous layer was extracted with CH$_2$Cl$_2$ (3 × 25 mL). The combined organic extracts were washed with aq. NaOH (1 M, 35 mL), dried over Na$_2$SO$_4$, filtered and concentrated *in vacuo* using a rotatory evaporator. Purification by flash column chromatography (5–20% Et$_2$O/pentane) afforded oxetane sulfide **227** as a colourless oil (3.88 g, 87%). R$_f$ = 0.43 (20% Et$_2$O/pentane); IR (film)/cm^{-1} 2942, 2865, 1592, 1510, 1491, 1245, 910, 829; ^{1}H NMR (400 MHz, CDCl$_3$) δ 7.14–7.10 (m, 2 H, 2 × Ar-CH), 6.79–6.73 (m, 6 H, 6 × Ar-CH), 5.12 (d, *J* = 6.4 Hz, 2 H, C*H*HOC*H*H), 4.93 (d, *J* = 6.4 Hz, 2 H, CH*H*OCH*H*), 3.79 (s, 3 H, OCH$_3$), 1.30–1.21 (m, 3 H, 3 × SiCH), 1.11 (d, *J* = 7.3 Hz, 18 H, 6 × SiCHC*H*$_3$); ^{13}C NMR (101 MHz, CDCl$_3$) δ 160.5 (Ar-C$_q$OMe), 154.9 (Ar-C$_q$OTIPS), 137.9 (2 × Ar-CH), 135.3 (Ar-*C*$_q$C$_q$), 127.5 (2 × Ar-CH), 122.5 (Ar-C$_q$S), 119.5 (2 × Ar-CH), 114.1 (2 × Ar-CH), 82.3 (CH$_2$OCH$_2$), 55.2 (OCH$_3$), 17.9 (6 × SiCH*C*H$_3$), 12.6 (3 × SiCH); HRMS (ESI) *m/z* calcd for C$_{25}$H$_{37}$O$_3$SiS [M+H]: 445.2233, found: 445.2234.

Triisopropyl(4-(3-((4-methoxyphenyl)sulfinyl)oxetan-3-yl)phenoxy)silane (228)



*m*CPBA (1.09 g, 6.3 mmol, 1.05 equiv) was added in 3 portions over 30 minutes to a solution of oxetane sulfide **227** (2.67 g, 6.0 mmol, 1.0 equiv) in anhydrous CH_2Cl_2 (60 mL, 0.1 M) at 0 ºC in a 250 mL round bottom flask. After stirring the reaction mixture at 0 ºC for 2.5 h, 3 M aq. KOH (100 mL) was added and the phases separated. The aqueous layer was extracted with EtOAc (4 × 100 mL). The combined organic extracts were dried over Na_2SO_4, filtered and concentrated *in vacuo* using a rotatory evaporator. Purification by flash column chromatography (20–40% EtOAc/pentane) afforded sulfoxide **228** as a colourless gum (2.14 g, 77%). R_f = 0.41 (40% EtOAc/pentane); IR (film)/cm^{-1} 2942, 2866, 1595, 1511, 1255, 1053 (S=O st), 910; ^{1}H NMR (400 MHz, $CDCl_3$) δ 6.94–6.91 (m, 2 H, 2 × Ar-CH), 6.80–6.75 (m, 4 H, 4 × Ar-CH), 6.52–6.51 (m, 2 H, 2 × Ar-CH), 5.36 (d, *J* = 7.2 Hz, 1 H, C*H*HOCH$_2$), 5.28 (d, *J* = 6.9 Hz, 1 H, CH$_2$OC*H*H), 4.99 (d, *J* = 6.9 Hz, 1 H, CH$_2$OCH*H*), 4.87 (d, *J* = 7.2 Hz, 1 H, CH*H*OCH$_2$), 3.80 (s, 3 H, OCH$_3$), 1.31–1.21 (m, 3 H, 3 × SiCH), 1.11 (d, *J* = 7.3 Hz, 18 H, 6 × SiCHC*H*$_3$); ^{13}C NMR (101 MHz, $CDCl_3$) δ 162.2 (Ar-C$_q$OMe), 156.3 (Ar-C$_q$OTIPS), 129.4 (Ar-C$_q$SO), 128.9 (2 × Ar-CH), 127.1 (2 × Ar-CH), 126.6 (Ar-*C*$_q$C$_q$), 119.7 (2 × Ar-CH), 113.7 (2 × Ar-CH), 77.3 (CH$_2$O), 73.4 (CH$_2$O), 67.2 (C$_q$), 55.4 (OCH$_3$), 17.9 (6 × SiCH*C*H$_3$), 12.6 (3 × SiCH); HRMS (ESI) *m/z* calcd for $C_{25}H_{37}O_4SiS$ [M+H]: 461.2182, found: 461.2177.

4-(3-((4-Methoxyphenyl)sulfinyl)oxetan-3-yl)phenol (229)



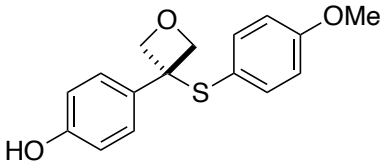
TBAF (1.0 M in THF, 1.5 mL, 1.5 mmol, 1.5 equiv) was added dropwise to a solution of OTIPS oxetane sulfoxide **228** (460 mg, 1.0 mmol, 1.0 equiv) in anhydrous THF (3.4 mL, 0.3 M) at 0 °C in a 25 mL round bottom flask. The reaction mixture was warmed to 25 °C and stirred for further 3 h. The reaction was then quenched with sat. aq. NH_4Cl (15 mL). The aqueous layer was extracted with EtOAc (4 × 20 mL). The combined organic extracts were dried over Na_2SO_4, filtered and concentrated *in vacuo* using a rotatory evaporator. Purification by flash column chromatography (20–100% EtOAc/pentane) afforded phenol sulfoxide **229** as a colourless gum (36.7 mg, 12%). R_f = 0.77 (70% EtOAc/pentane); IR (film)/cm^{-1} 3150 (OH st, br), 2949, 1592, 1512, 1258, 1140, 1021 (S=O st), 993; ^{1}H NMR (400 MHz, $(CD_3)_2SO$) δ 9.70 (s, 1 H, OH), 7.35 (d, *J* = 8.7 Hz, 2 H, 2 × Ar–CH), 7.02 (d, *J* = 8.7 Hz, 2 H, 2 × Ar–CH), 6.69 (d, *J* = 9.0 Hz, 2 H, 2 × Ar–CH), 6.67 (d, *J* = 9.0 Hz, 2 H, 2 × Ar–CH), 5.26 (d, *J* = 7.3 Hz, 2 H, C*H*HOC*H*H), 4.92 (d, *J* = 7.3 Hz, 2 H, CH*H*OCH*H*), 3.82 (s, 3 H, OCH$_3$); ^{13}C NMR (101 MHz, $(CD_3)_2SO$) δ 163.7 (Ar-C$_q$OMe), 157.6 (Ar-C$_q$OH), 131.6 (2 × Ar-CH), 129.8 (2 × Ar-CH), 125.9 (Ar-C$_q$), 124.6 (Ar-C$_q$),

114.8 (2 × Ar-CH), 114.2 (2 × Ar-CH), 75.9 (CH_2OCH_2), 68.4 (C_q), 55.8 (OCH_3); mass ion not found by HRMS (APCI).

Notes:

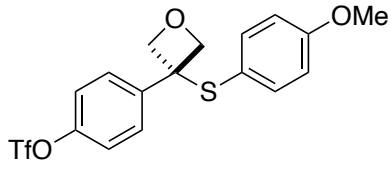
The signals at 6.69 and 6.67 ppm in the ^{1}H NMR spectrum were integrated together to 4 H.

4-(3-((4-Methoxyphenyl)thio)oxetan-3-yl)phenol (230)



TBAF (1.0 M in THF, 3.67 mL, 3.67 mmol, 1.5 equiv) was added dropwise to a solution of OTIPS oxetane sulfide **227** (1.09 g, 2.44 mmol, 1.0 equiv) in anhydrous THF (8.1 mL, 0.3 M) at 0 °C in a 50 mL round bottom flask. The reaction mixture was warmed to 25 °C and stirred for further 3 h. The reaction was then quenched with sat. aq. NH_4Cl (40 mL). The aqueous layer was extracted with EtOAc (4 × 50 mL). The combined organic extracts were dried over Na_2SO_4, filtered and concentrated *in vacuo* using a rotatory evaporator. Purification by flash chromatography (0–6% Et_2O/CH_2Cl_2) afforded phenol oxetanol sulfide **230** as a white solid (539 mg, 77%). R_f = 0.29 (6% Et_2O/ CH_2Cl_2); mp = 223 °C; IR (film)/cm^{-1} 3226 (OH st, br), 2958, 2404, 1587, 1513, 1242, 830; ^{1}H NMR (400 MHz, $(CD_3)_2SO$) δ 9.48 (s, 1 H, OH), 7.26–7.22 (m, 2 H, 2 × Ar-CH), 6.90–6.85 (m, 4 H, 4 × Ar-CH), 6.70–6.67 (m, 2 H, 2 × Ar-CH), 4.96 (d, *J* = 6.7 Hz, 2 H, C*H*HOC*H*H), 4.80 (d, *J* = 6.7 Hz, 2 H, CH*H*OCH*H*), 3.75 (s, 3 H, OCH_3); ^{13}C NMR (101 MHz, $(CD_3)_2SO$) δ 160.2 (Ar-C_qOMe), 156.3 (Ar-C_qOH), 137.6 (2 × Ar-CH), 132.7 (Ar-$C_q$$C_q$), 127.7 (2 × Ar-CH), 122.3 (Ar-C_qS), 114.9 (2 × Ar-CH), 114.5 (2 × Ar-CH), 81.2 (CH_2OCH_2), 55.2 (OCH_3), 54.6 (C_q); HRMS (APCI) *m/z* calcd for $C_{16}H_{15}O_3S^-$ $[M–H]^-$: 287.0747, found: 287.0753.

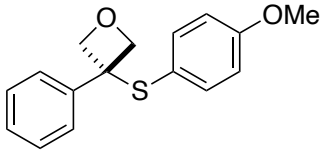
4-(3-((4-Methoxyphenyl)thio)oxetan-3-yl)phenyl trifluoromethanesulfonate (231)



Pyridine (0.25 mL, 3.04 mmol, 2.0 equiv) and triflic anhydride (0.30 mL, 1.82 mmol, 1.2 equiv) were added sequentially to a solution of phenol oxetane sulfide **230** (438 mg, 1.52 mmol, 1.0 equiv) in anhydrous CH_2Cl_2 (19 mL, 0.08 M) at 0 °C in a 50 mL round bottom flask. The reaction mixture was warmed to 25 °C and stirred for 1 h. The reaction was then quenched with distilled water (25 mL). The aqueous layer was extracted with CH_2Cl_2 (3 × 40 mL). The combined organic extracts were dried over Na_2SO_4, filtered and concentrated *in vacuo* using a rotatory evaporator. Purification by flash column chromatography (40–60% CH_2Cl_2/pentane) afforded oxetane triflate **231** as a white solid (558 mg, 97%). R_f = 0.56 (60% CH_2Cl_2/pentane); mp = 73 °C; IR (film)/cm^{-1} 2949, 1592, 1496, 1424, 1249, 1140, 889; ^{1}H NMR (400 MHz, $CDCl_3$) δ 7.19–7.15 (m, 2 H, 2 × Ar-CH), 7.08–7.05 (m, 2 H, 2 × Ar-CH), 6.95–6.91 (m, 2 H, 2 × Ar-CH), 6.77–6.73 (m, 2 H, 2 × Ar-CH), 5.12

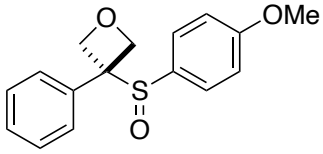
(d, *J* = 6.5 Hz, 2 H, C*H*HOC*H*H), 4.98 (d, *J* = 6.5 Hz, 2 H, CH*H*OCH*H*), 3.79 (s, 3 H, OCH_3); ^{13}C NMR (101 MHz, $CDCl_3$) δ 160.9 (Ar-C_qOMe), 148.1 (Ar-C_qOTf), 143.5 (Ar-C_qC_q), 137.8 (2 × Ar-CH), 128.3 (2 × Ar-CH), 121.5 (Ar-C_qS), 121.1 (2 × Ar-CH), 118.7 (q, J_{C-F} = 320.8 Hz, CF_3), 114.4 (2 × Ar-CH), 81.8 (CH_2OCH_2), 55.3 (OCH_3), 54.7 (C_q); ^{19}F NMR (377 MHz, $CDCl_3$) δ –72.7; HRMS (APCI) *m/z* calcd for $C_{17}H_{16}F_3S_2O_5^+$ $[M+H]^+$: 421.0386; found: 421.0378.

3-((4-Methoxyphenyl)thio)-3-phenyloxetane (232)



Following adapted conditions developed by Ortar,[253] triethyl amine (0.58 mL, 4.14 mmol, 3.0 equiv) and formic acid (104 μL, 2.76 mmol, 2.0 equiv) were added sequentially to a solution of oxetane triflate **231** (580 mg, 1.38 mmol, 1.0 equiv), $Pd(OAc)_2$ (6.2 mg, 0.028 mmol, 0.02 equiv) and (ferrocene-1,1′-diyl) bis(diphenylphosphane) (dppf; 15.3 mg, 0.028 mmol, 0.02 equiv) in anhydrous DMF (13.8 mL, 0.1 M) in a 50 mL round bottom flask. The reaction mixture was warmed to 60 °C and stirred for 1 h. The reaction was cooled down to 25 °C, then brine was added (50 mL). The aqueous layer was extracted with EtOAc (3 × 50 mL). The combined organic extracts were washed with brine (2 × 50 mL), dried over Na_2SO_4, filtered and concentrated *in vacuo* using a rotatory evaporator. Purification by flash column chromatography (20% Et_2O/pentane) afforded phenyl oxetane sulfide **232** as a white solid (356 mg, 95%). R_f = 0.39 (20% Et_2O/pentane); IR (film)/cm^{-1} 2945, 1590, 1491, 1286, 1246, 1028, 983, 830; ^1H NMR (400 MHz, $CDCl_3$) δ 7.31–7.24 (m, 3 H, 3 × Ph-CH), 7.15 (d, *J* = 8.2 Hz, 2 H, 2 × Ar-CH), 6.92 (d, *J* = 7.3 Hz, 2 H, 2 × Ph-CH), 6.77 (d, *J* = 8.2 Hz, 2 H, 2 × Ar-CH), 5.16 (d, *J* = 6.4 Hz, 2 H, C*H*HOC*H*H), 4.97 (d, *J* = 6.4 Hz, 2 H, CH*H*OCH*H*), 3.80 (s, 3 H, OCH_3); ^{13}C NMR (101 MHz, $CDCl_3$) δ 160.6 (Ar-C_qOMe) 142.8 (Ph-C_qC_q), 137.9 (2 × Ar-CH), 128.2 (2 × Ar-CH), 127.0 (Ph-CH), 126.4 (2 × Ar-CH), 122.3 (Ar-C_qS), 114.2 (2 × Ar-CH), 82.0 (CH_2OCH_2), 55.3 (OCH_3); HRMS (ESI) *m/z* calcd for $C_{16}H_{17}O_2S^+$ $[M+H]^+$: 273.0944, found: 273.0900 [error: 16.1 ppm].

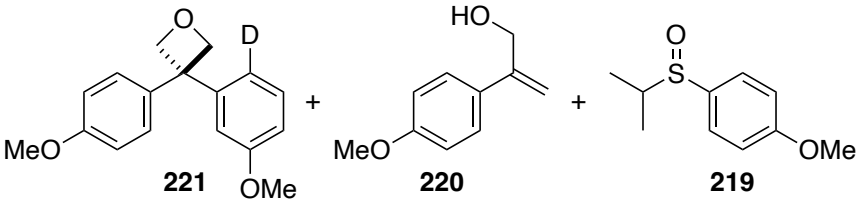
3-((4-Methoxyphenyl)sulfinyl)-3-phenyloxetane (233)



*m*CPBA (263 mg, 1.523 mmol, 1.05 equiv) was added in 3 portions over 30 minutes to a solution of oxetane sulfide **232** (396 mg, 1.45 mmol, 1.0 equiv) in anhydrous CH_2Cl_2 (14.5 mL, 0.1 M) at 0 ºC in a 50 mL round bottom flask. After stirring the reaction mixture at 0 ºC for 2.5 h, 3 M aq. KOH (25 mL) was added and the phases separated. The aqueous layer was extracted with EtOAc (4 × 25 mL). The combined organic extracts were dried over Na_2SO_4, filtered and concentrated *in vacuo* using a rotatory evaporator. Purification by flash column chromatography (30–50% EtOAc/pentane) afforded sulfoxide **233** as a colourless gum (396 mg, 95%). R_f = 0.43 (40% EtO/pentane); IR (film)/cm^{-1} 2937, 1591, 1492, 1249, 1049 (S=O st), 829, 698; ^{1}H NMR (400 MHz, $CDCl_3$) δ 7.36–7.26 (m, 3 H, 3 × Ar-CH), 6.92–6.89 (m, 2 H, 2 × Ar-CH), 6.80–6.77 (m, 2 H, 2 × Ar-CH), 6.68–6.66 (m, 2 H, 2 × Ar-CH), 5.38 (d, *J* = 7.2 Hz, 1 H, C*H*HOCH$_2$), 5.31 (d, *J* = 7.0 Hz, 1 H, CH$_2$OC*H*H), 5.03 (d, *J* = 7.0 Hz, 1 H, CH$_2$OCH*H*), 4.93 (d, *J* = 7.2 Hz, 1 H, CH*H*OCH$_2$), 3.80 (s, 3 H, OCH$_3$); ^{13}C NMR (101 MHz, $CDCl_3$) δ 162.4 (Ar-C_qOMe), 134.4 (Ph-C_qC_q), 129.3 (Ar-C_qSO), 128.3 (Ph-CH), 128.2 (2 × Ar-CH), 127.7 (2 × Ar-CH), 127.0 (2 × Ar-CH), 113.8 (2 × Ar-CH), 77.2 (CH$_2$O), 73.4 (CH$_2$O), 67.7 (C_q), 55.4 (OCH$_3$); HRMS (ESI) *m/z* calcd for $C_{16}H_{17}O_3S$ [M+H]: 289.0898, found: 289.0889.

7.6.10 Products of Ligand Exchange

3-(3-Methoxyphenyl-6-*d*)-3-(4-methoxyphenyl)oxetane (221) 2-(4-methoxyphenyl)prop-2-en-1-ol (220) and 1-(isopropylsulfinyl)-4-methoxybenzene (219)



i-PrMgCl (1.94 M in Et_2O, 0.155 mL, 0.3 mmol, 1.5 equiv) was added over 1 min to a solution of oxetane sulfoxide **217** (63.6 mg, 0.20 mmol, 1.0 equiv) in anhydrous THF (2.0 mL, 0.1 M) at –60 ºC (cooled using a cryostat) in a reaction tube, upon which the reaction turned from colourless to bright yellow (Figure 74d). After stirring the reaction mixture for 20 min at –60 ºC, anhydrous CD_3CO_2D (0.2 mL) was added (change of colour back to colourless) and the reaction mixture was stirred for further 10 min at –60 ºC. The reaction mixture was allowed to warm to room temperature (ca. 22 ºC) and concentrated *in vacuo* using a rotatory evaporator. Purification by flash column chromatography (10–90% EtOAc/pentane) afforded diaryl-oxetane **221** as a light-yellow gum (6.0 mg, 11%), followed by allylic alcohol **220** as a white solid (16.2 mg, 49%) and sulfoxide **219** as a colourless gum (16.9 mg, 43%).

Diaryloxetane **221**: R_f = 0.36 (25% EtOAc/pentane); IR (film)/cm^{-1} 2945, 2361, 1512, 1248; ^{1}H NMR (400 MHz, $CDCl_3$) δ 7.35–7.28 (m, 1 H, Ar-CH), 7.18–7.15 (m, 2 H, 2 × Ar-CH), 6.90–6.88 (m, 2 H, 2 × Ar-CH), 6.81 (dd, *J* = 8.2, 2.5 Hz, Ar-CH), 6.74 (d, *J* = 2.5 Hz, Ar-CH), 5.25 (d, *J* = 5.6 Hz, 2 H, C*H*HOC*H*H), 5.20 (d, *J* = 5.6 Hz, 2 H, CH*H*OCH*H*), 3.81 (s, 3 H, OCH_3), 3.80 (s, 3 H, OCH_3); ^{13}C NMR (101 MHz, $CDCl_3$) δ 159.8 (Ar-C_qOMe), 158.6 (Ar-C_qOMe), 147.3 (Ar-C_qC_q), 138.1 (Ar-C_qC_q), 129.5 (Ar-CH), 127.6 (2 × Ar-CH), 113.9 (2 × Ar-CH), 112.8 (Ar-CH), 111.5 (Ar-CH), 84.7 (CH_2OCH_2), 55.3 (OCH_3), 55.2 (OCH_3). The observed characterisation data (R_f, IR, ^{1}H, ^{13}C) were consistent with that previously reported in the group.[211]

Notes:

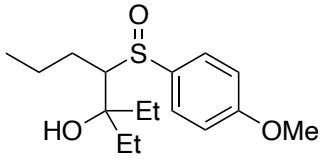
The Ar-CD and C_q signals were not observed in the ^{13}C NMR spectrum.

The signals at 159.8 (Ar-C_qOMe), 158.6 (Ar-C_qOMe), 147.3 (Ar-C_qC_q) and 138.1 ppm (Ar-C_qC_q) were assigned with an HMBC 2D correlation spectrum.

Allylic alcohol **220**: R_f = 0.31 (25% EtOAc/pentane); ^{1}H NMR (400 MHz, $CDCl_3$) δ 7.43–7.40 (m, 2 H, 2 × Ar-CH), 6.92–6.89 (m, 2 H, 2 × Ar-CH), 5.41 (br s, 1 H, C=C*H*H), 5.27 (d, *J* = 1.3 Hz, 1 H, C=CH*H*), 4.53 (s, 2 H, CH_2), 3.83 (s, 3 H, OCH_3). The observed characterisation data (^{1}H) were consistent with that previously reported.[453] Alcohol **220** degraded in $CDCl_3$ solution before any further characterisation data could be recorded.

Sulfoxide **219**: R_f = 0.24 (70% EtOAc/pentane); IR (film)/cm^{-1} 2966, 1593, 1495, 1248, 1024 (S=O st); ^{1}H NMR (400 MHz, $CDCl_3$) δ 7.55–7.51 (m, 2 H, 2 × Ar-CH), 7.04–7.00 (m, 2 H, 2 × Ar-CH), 3.86 (s, 3 H, OCH_3), 2.81 (qq, *J* = 6.5, 6.5 Hz, 1 H, SCH), 1.17 (d, *J* = 6.5 Hz, 3 H, CHC*H*$_3$), 1.16 (d, *J* = 6.5 Hz, 3 H, CHC*H*$_3$); ^{13}C NMR (101 MHz, $CDCl_3$) δ 161.9 (Ar-C_qOMe), 132.5 (Ar-C_qS), 126.8 (2 × Ar-CH), 114.4 (2 × Ar-CH), 55.5 (OCH_3), 54.6 (SCH), 15.5 (CH*C*H$_3$), 14.4 (CH*C*H$_3$). The observed characterisation data (^{1}H, ^{13}C) were consistent with that previously reported.[454]

3-Ethyl-4-((4-methoxyphenyl)sulfinyl)heptan-3-ol (224)

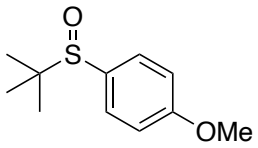


A solution of oxetane sulfoxide **217** (63.6 mg, 0.20 mmol, 1.0 equiv) in anhydrous THF (0.5 mL) was added by syringe over 1 min to a solution of *n*-BuLi (1.48 M in hexanes, 0.34 mL, 0.5 mmol, 2.5 equiv) in anhydrous THF (2 mL, 0.1 M) at –100 ºC (Et_2O/N_2(l) bath) in a 10 mL round bottom flask. After stirring the reaction mixture at –100 ºC for 5 s, pentan-3-one (64 μL, 0.6 mmol, 3.0 equiv) was added and the reaction mixture was stirred for further 10 min at –100 ºC. CD_3CO_2D (0.2 mL) was added, the reaction mixture was stirred for 10 min at –100 ºC, and then allowed to warm to room temperature (ca. 22 ºC). Sat. aq. NH_4Cl (10 mL) was added, followed by CH_2Cl_2 (10 mL) and the layers were separated. The aqueous layer was extracted with CH_2Cl_2 (2 × 10 mL), the organic extracts were combined, dried over Na_2SO_4, filtered and concentrated *in vacuo* using a rotatory evaporator. Purification by flash column chromatography (30% EtOAc/pentane) afforded alcohol **224** as a colourless gum (16.8 mg, 28%). R_f = 0.31 (50% EtOAc/pentane); IR (film)/cm^{-1} 3386 (OH st, br), 2962, 1594, 1495, 1251, 1026 (S=O st); ^{1}H NMR (400 MHz, $CDCl_3$) δ 7.49–7.46 (m, 2 H, 2 × Ar-CH), 7.05–7.02 (m, 2 H, 2 × Ar-CH), 3.87 (s, 3 H, OCH_3), 2.73 (s, 1 H, OH), 2.43 (dd, *J* = 5.7, 3.2 Hz, 1 H, CH), 2.05–1.94 (m, 2 H, $C_qCH_2CH_3$), 1.90–1.82 (m, 1 H, C*H*HCH), 1.80–1.73 (m, 1 H, C_qCHHCH_3), 1.62–1.49 (m, 2 H, CH*H*CH + C_qCHHCH_3), 1.01 (t, *J* = 7.4 Hz, 3 H, $C_qCH_2CH_3$), 0.97–0.89 (br m, 1 H, CH_2CHHCH_3), 0.93 (t, *J* = 7.5 Hz, 3 H, $C_qCH_2CH_3$), 0.61 (t, *J* = 7.1 Hz, 3 H, $CH_2CH_2CH_3$), 0.57–0.46 (m, 1 H, CH_2CHHCH_3); ^{13}C NMR (101 MHz, $CDCl_3$) δ 161.5 (Ar-C_qOMe), 132.9 (Ar-C_qS), 125.7 (2 × Ar-CH), 114.5 (2 × Ar-CH), 77.2 (C_qOH), 70.1 (CH), 55.5 (OCH_3), 29.7 ($C_qCH_2CH_3$), 28.5 ($C_qCH_2CH_3$), 23.6 ($CH_2CH_2CH_3$), 22.3 ($CHCH_2$), 14.0 ($CH_2CH_2CH_3$), 8.0 ($C_qCH_2CH_3$), 7.6 ($C_qCH_2CH_3$); mass ion not found by HRMS (APCI).

Notes:

The multiplet at 0.97–0.89 ppm and the triplet at 0.93 ppm in the ^{1}H NMR spectrum were integrated together to 4 H.

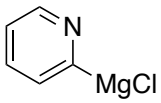
1-(*tert*-Butylsulfinyl)-4-methoxybenzene (226)



A solution of oxetane sulfoxide **217** (63.6 mg, 0.20 mmol, 1.0 equiv) in anhydrous THF (0.5 mL) was added by syringe over 1 min to a solution of *t*-BuLi (1.70 M in pentanes, 0.29 mL, 0.5 mmol, 2.5 equiv) in anhydrous THF (2 mL, 0.1 M) at –100 ºC (Et_2O/N_2(l) bath) in a 10 mL round bottom flask. Immediately after the addition of sulfoxide **217**, pentan-3-one (0.21 mL, 2.0 mmol, 10.0 equiv) was added and the reaction mixture was stirred for further 30 min at –100 ºC. CD_3CO_2D (0.2 mL) was added and the reaction mixture was allowed to warm to room temperature (ca. 22 ºC). Sat. aq. NH_4Cl (10 mL) was added, followed by CH_2Cl_2 (10 mL) and the layers were separated. The aqueous layer was extracted with CH_2Cl_2 (2 × 10 mL), the organic extracts were combined, dried over Na_2SO_4, filtered and concentrated *in vacuo* using a rotatory evaporator. Purification by flash column chromatography (40–100% EtOAc/pentane) afforded sulfoxide **226** as a light-yellow gum (25.1 mg, 59% [isolated with ca. 22% of unknown impurities]). R_f = 0.26 (60% EtOAc/pentane); IR (film)/cm^{-1} 2958, 1725, 1594, 1495, 1252, 1038 (S=O st); ^{1}H NMR (400 MHz, $CDCl_3$) δ 7.55–7.51 (m, 2 H, 2 × Ar-CH), 7.01–6.99 (m, 2 H, 2 × Ar-CH), 3.86 (s, 3 H, OCH_3), 1.16 (s, 9 H, 3 × C_qCH_3); ^{13}C NMR (101 MHz, $CDCl_3$) δ 162.0 (Ar-C_qOMe), 130.8 (Ar-C_qS), 127.9 (2 × Ar-CH), 113.9 (2 × Ar-CH), 55.6 (C_q), 55.4 (OCH_3), 22.7 (3 × C_qCH_3). The observed characterisation data (^{1}H, ^{13}C) were consistent with that previously reported.[455]

7.6.11 2-Pyridyl Diaryl Oxetanes

Pyridin-2-ylmagnesium chloride (solution in THF) (243)[403a]



i-PrMgCl.LiCl ('Turbo Grignard', 1.25 M in THF, 4.2 mL, 5.25 mmol, 1.05 equiv) was added dropwise to a solution of 2-bromopyridine (0.48 mL, 5.0 mmol, 1.0 equiv) in anhydrous THF (5.3 mL) at 25 ºC in a 25 mL round bottom flask. The reaction mixture was stirred at 25 ºC for 3 h to afford 2-pyridylmagnesium chloride **243** as a dark brown solution in THF (Figure 91), whose concentration was determined by titration using salicylaldehyde phenylhydrazone as indicator (concentration ranged from 0.51–0.52 M).[435]

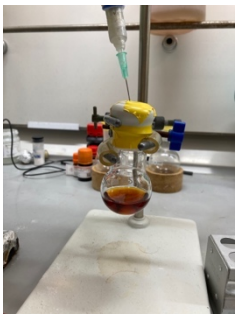
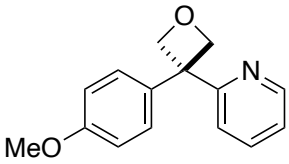


Figure 91. Solution of pyridin-2-ylmagnesium chloride (243) in THF.

2-(3-(4-Methoxyphenyl)oxetan-3-yl)pyridine (242)



2-Pyridylmagnesium chloride **243** (0.52 M in THF, 0.425 mL, 0.22 mmol, 1.1 equiv) was added dropwise to a solution of oxetane sulfoxide **217** (63.6 mg, 0.20 mmol, 1.0 equiv) in anhydrous THF (2.0 mL, 0.1 M) at room temperature (ca. 22 ºC) in a 10 mL round bottom flask, upon which the reaction mixture turned red (Figure 92). After stirring the reaction mixture for 1 h at room temperature (reaction mixture turned black; Figure 92), sat. aq. NH_4Cl (10 mL) was added, followed by EtOAc (10 mL) and the phases were separated. The aqueous layer was extracted with EtOAc (2 × 10 mL), the organic extracts were combined, dried over Na_2SO_4, filtered and concentrated *in vacuo* using a rotatory evaporator. Purification by flash column chromatography (10–100% Et_2O/pentane) afforded diaryl-oxetane **242** as a colourless gum (11.4 mg, 24%). R_f = 0.29 (60% Et_2O/pentane); IR (film)/cm^{-1} 2953, 1512, 1247, 1030, 984; ^{1}H NMR (400 MHz, $CDCl_3$) δ 8.66 (ddd, *J* = 4.9, 1.9, 1.0 Hz, 1 H, Pyr-CHN), 7.62 (ddd, *J* = 7.8, 7.8, 1.9 Hz, 1 H, Pyr-CH), 7.20–7.15 (m, 3 H, 2 × Ar-CH + Pyr-CH), 7.02 (ddd, *J* = 7.8, 1.0, 1.0 Hz, 1 H, Pyr-CH), 6.91–6.88 (m, 2 H, 2 × Ar-CH), 5.45 (d, *J* = 5.7 Hz, 2 H, C*H*HOC*H*H), 5.23 (d, *J* = 5.7 Hz, 2 H, CH*H*OCH*H*), 3.80 (s, 3 H, OCH_3); ^{13}C NMR (101 MHz, $CDCl_3$) δ 164.2 (Pyr-C_q), 158.3 (Ar-C_qOMe), 149.3 (Pyr-CH), 136.8 (Ar-$C_q$$C_q$), 136.5 (Pyr-CH), 127.4 (2 × Ar-CH), 121.5 (Pyr-CH), 121.2 (Pyr-CH), 114.0 (2 × Ar-CH), 82.7 (CH_2OCH_2), 55.3 (OCH_3), 51.1 (C_q); HRMS (ESI) *m/z* calcd for $C_{15}H_{16}NO_2$ [M+H]: 242.1181, found: 242.1177.

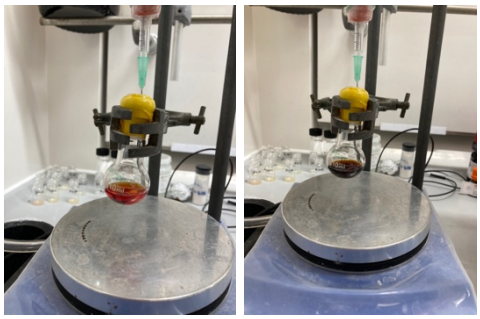
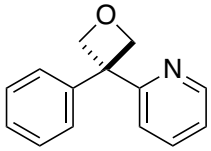


Figure 92. Reaction mixture after addition of 2-pyridylmagnesium chloride 243 (left) and after stirring for 1 h at room temperature (right).

2-(3-Phenyloxetan-3-yl)pyridine (244)



2-Pyridylmagnesium chloride **243** (0.51 M in THF, 0.43 mL, 0.22 mmol, 1.1 equiv) was added dropwise to a solution of oxetane sulfoxide **233** (57.6 mg, 0.20 mmol, 1.0 equiv) in anhydrous THF (2.0 mL, 0.1 M) at room temperature (ca. 22 ºC) in a 10 mL round bottom flask. After stirring the reaction mixture for 2 h at room temperature, sat. aq. NH_4Cl (10 mL) was added, followed by EtOAc (10 mL) and the phases were separated. The aqueous layer was extracted with EtOAc (2 × 10 mL), the organic extracts were combined, dried over Na_2SO_4, filtered and concentrated *in vacuo* using a rotatory evaporator. Purification by flash column chromatography (20–60% Et_2O/pentane) afforded diaryl-oxetane **244** as a yellow gum (9.6 mg, 23%). R_f = 0.10 (40% Et_2O/pentane); IR (film)/cm^{-1} 2921, 1586, 1468, 1423, 983, 751, 700; ^{1}H NMR (400 MHz, $CDCl_3$) δ 8.67 (ddd, *J* = 4.9, 1.9, 1.0 Hz, 1 H, Pyr-CHN), 7.63 (ddd, *J* = 7.8, 7.8, 1.9 Hz, 1 H, Pyr-CH), 7.39–7.34 (m, 2 H, 2 × Ph-CH), 7.29–7.25 (m, 3 H, 3 × Ph-CH), 7.18 (ddd, *J* = 7.8, 4.9, 1.0 Hz, 1 H, Pyr-CH), 7.03 (ddd, *J* = 7.8, 1.0, 1.0 Hz, 1 H, Pyr-CH), 5.47 (d, *J* = 5.7 Hz, 2 H, C*H*HOC*H*H), 5.28 (d, *J* = 5.7 Hz, 2 H, CH*H*OCH*H*); ^{13}C NMR (101 MHz, $CDCl_3$) δ 163.9 (Pyr-C_q), 149.3 (Pyr-CH), 144.7 (Ph-C_q), 136.6 (Pyr-CH), 128.7 (2 × Ph-CH), 126.8 (Ph-CH), 126.3 (2 × Ph-CH), 121.6 (Pyr-CH), 121.3 (Pyr-CH), 82.6 (CH_2OCH_2), 53.3 (C_q); HRMS (ESI) *m/z* calcd for $C_{14}H_{14}NO$ [M+H]: 212.1075, found: 212.1076.

8 References

1 (a) Campos, K. R.; Coleman, P. J.; Alvarez, J. C.; Dreher, S. D.; Garbaccio, R. M.; Terrett, N. K.; Tillyer, R. D.; Truppo, M. D.; Parmee, E. R. *Science* **2019**, *363*, eaat0805. (b) Blakemore, D. C.; Castro, L.; Churcher, I.; Rees, D. C.; Thomas, A. W.; Wilson, D. M.; Wood, A. *Nat. Chem.* **2018**, *10*, 383–394. (c) Grygorenko, O. O.; Volochnyuk, D. M.; Ryabukhin, S. V.; Judd, D. B. *Chem. Eur. J.* **2020**, *26*, 1196–1237.

2 (a) Li, J.; Eastgate, M. D. *Org. Biomol. Chem.* **2015**, *13*, 7164–7176. (b) Caille, S.; Cui, S.; Faul, M. M.; Mennen, S. M.; Tedrow, J. S.; Walker, S. D. *J. Org. Chem.* **2019**, *84*, 4583–4603. (c) Ivanenkov, Y. A.; Zagribelnyy, B. A.; Aladinskiy, V. A. *J. Med. Chem.* **2019**, *62*, 10026–10043.

3 Méndez-Lucio, O.; Medina-Franco, J. L. *Drug Discov. Today* **2017**, *22*, 120–126.

4 Lovering, F.; Bikker, J.; Humblet, C. *J. Med. Chem.* **2009**, *52*, 6752–6756.

5 (a) Hann, M. M.; Leach, A. R.; Harper, G. *J. Chem. Inf. Comput. Sci.* **2001**, *41*, 856–864. (b) Clemons, P. A.; Bodycombe, N. E.; Carrinski, H. A.; Wilson, J. A.; Shamji, A. F.; Wagner, B. K.; Koehler, A. N.; Schreiber, S. L. *Proc. Natl. Acad. Sci.* **2010**, *107*, 18787–18792. (c) Lovering, F. *Medchemcomm* **2013**, *4*, 515–519.

6 González-Medina, M.; Prieto-Martínez, F. D.; Naveja, J. J.; Méndez-Lucio, O.; El-Elimat, T.; Pearce, C. J.; Oberlies, N. H.; Figueroa, M.; Medina-Franco, J. L. *Future Med. Chem.* **2016**, *8*, 1399–1412.

7 (a) Halford, G. M.; Lordkipanidzé, M.; Watson, S. P. *Platelets* **2012**, *23*, 415–422. (b) Fischer, J.; Ganellin, C. R. In *Analogue-based Drug Discovery*; John Wiley & Sons, Hoboken New Jersey, USA; 2006; p. 453. (c) Foote, K. M.; Nissink, J. W. M.; McGuire, T.; Turner, P.; Guichard, S.; Yates, J. W. T.; Lau, A.; Blades, K.; Heathcote, D.; Odedra, R.; Wilkinson, G.; Wilson, Z.; Wood, C. M.; Jewsbury, P. J. *J. Med. Chem.* **2018**, *61*, 9889–9907. (d) Bacon, E. M.; Chin, E.; Cottell, J. J.; Katana, A. A.; Kato, D.; Link, J. O.; Shapiro, N.; Trejo Martin, T. A.; Yang, Z.-Y (Gilead Sciences Inc.) *Atazanavir (ATV) Analogues for Treating HIV Infections*, WO Patent Appl. No WO2018145021A1, **2018**.

8 Brown, D. G.; Boström, J. *J. Med. Chem.* **2016**, *59*, 4443–4458.

9 Walters, W. P.; Green, J.; Weiss, J. R.; Murcko, M. A. *J. Med. Chem.* **2011**, *54*, 6405–6416.

10 Prosser, K. E.; Stokes, R. W.; Cohen, S. M. *ACS Med. Chem. Lett.* **2020**, *11*, 1292–1298.

11 Wu, G.; Zhao, T.; Kang, D.; Zhang, J.; Song, Y.; Namasivayam, V.; Kongsted, J.; Pannecouque, C.; De Clercq, E.; Poongavanam, V.; Liu, X.; Zhan, P. *J. Med. Chem.* **2019**, *62*, 9375–9414.

12 Szymkuć, S.; Badowski, T.; Grzybowski, B. A. *Angew. Chem. Int. Ed.* **2021**, *60*, 26226–26232.

13 (a) Foley, D. J.; Nelson, A.; Marsden, S. P. *Angew. Chem. Int. Ed.* **2016**, *55*, 13650–13657. (b) Silvestri, I. P.; Colbon, P. J. J. *ACS Med. Chem. Lett.* **2021**, *12*, 1220–1229.

14 Grygorenko, O. O.; Volochnyuk, D. M.; Vashchenko, B. V. *Eur. J. Org. Chem.* **2021**, *2021*, 6478–6510.

15 (a) Klein, H. F.; Hamilton, D. J.; de Esch, I. J. P.; Wijtmans, M.; O'Brien, P. *Drug Discov. Today* **2022**, *27*, 2484–2496. (b) Cox, B.; Zdorichenko, V.; Cox, P. B.; Booker-Milburn, K. I.; Paumier, R.; Elliott, L. D.; Robertson-Ralph, M.; Bloomfield, G. *ACS Med. Chem. Lett.* **2020**, *11*, 1185–1190.

16 (a) Moir, M.; Danon, J. J.; Reekie, T. A.; Kassiou, M. *Expert Opin. Drug Discov.* **2019**, *14*, 1137–1149. (b) Börgel, J.; Ritter, T. *Chem* **2020**, *6*, 1877–1887. (c) Kim, K. E.; Kim, A. N.; McCormick, C. J.; Stoltz, B. M. *J. Am. Chem. Soc.* **2021**, *143*, 16890–16901. (d) Guillemard, L.; Kaplaneris, N.; Ackermann, L.; Johansson, M. J. *Nat. Rev. Chem.* **2021**, *5*, 522–545.

17 (a) Malone, M. L.; Paegel, B. M. *ACS Comb. Sci.* **2016**, *18*, 182–187. (b) Flood, D. T.; Kingston, C.; Vantourout, J. C.; Dawson, P. E.; Baran, P. S. *Isr. J. Chem.* **2020**, *60*, 268–280. (c) Shi, Y.; Wu, Y.; Yu, J.; Zhang, W.; Zhuang, C. *RSC Adv.* **2021**, *11*, 2359–2376. (d) Fitzgerald, P. R.; Paegel, B. M. *Chem. Rev.* **2021**, *121*, 7155–7177.

18 (a) Qi, S.-M.; Dong, J.; Xu, Z.-Y.; Cheng, X.-D.; Zhang, W.-D.; Qin, J.-J. *Front. Pharmacol.* **2021**, *12*, 692574. (b) Li, K.; Crews, C. M. *Chem. Soc. Rev.* **2022**, *51*, 5214–5236. (c) Békés, M.; Langley, D. R.; Crews, C. M. *Nat. Rev. Drug Discov.* **2022**, *21*, 181–200.

19 (a) Ghosh, A. K.; Samanta, I.; Mondal, A.; Liu, W. R. *ChemMedChem* **2019**, *14*, 889–906. (b) Sutanto, F.; Konstantinidou, M.; Dömling, A. *RSC Med. Chem.* **2020**, *11*, 876–884. (c) Boike, L.; Henning, N. J.; Nomura, D. K. *Nat. Rev. Drug Discov.* **2022**, *21*, 881–898.

20 (a) Kolb, H. C.; Finn, M. G.; Sharpless, K. B. *Angew. Chem. Int. Ed.* **2001**, *40*, 2004–2021. (b) Dong, J.; Krasnova, L.; Finn, M. G.; Sharpless, K. B. *Angew. Chem. Int. Ed.* **2014**, *53*, 9430–9448. (c) Devaraj, N. K.; Finn, M. G. *Chem. Rev.* **2021**, *121*, 6697–6698. (d) Ed. Chandrasekaran, S. In *Click Reactions in Organic Synthesis*; Wiley-VCH Verlag GmbH & Co. KGaA: Weinheim, Germany, 2016.

21 (a) Smith, J. M.; Harwood, S. J.; Baran, P. S. *Acc. Chem. Res.* **2018**, *51*, 1807–1817. (b) Yan, M.; Lo, J. C.; Edwards, J. T.; Baran, P. S. *J. Am. Chem. Soc.* **2016**, *138*, 12692–12714.

22 (a) Marzo, L.; Pagire, S. K.; Reiser, O.; König, B. *Angew. Chem. Int. Ed.* **2018**, *57*, 10034–10072. (b) McAtee, R. C.; McClain, E. J.; Stephenson, C. R. J. *Trends Chem.* **2019**, *1*, 111–125. (c) Li, P.; Terrett, J. A.; Zbieg, J. R. *ACS Med. Chem. Lett.* **2020**, *11*, 2120–2130. (d) Douglas, J. J. The Application of Visible-Light-Mediated Reactions to the Synthesis of Pharmaceutical Compounds. In *Visible Light Photocatalysis in Organic Chemistry*; Wiley-VCH Verlag GmbH & Co. KGaA: Weinheim, Germany, 2018; pp 415–430.

23 (a) Yan, M.; Kawamata, Y.; Baran, P. S. *Chem. Rev.* **2017**, *117*, 13230–13319. (b) Wiebe, A.; Gieshoff, T.; Möhle, S.; Rodrigo, E.; Zirbes, M.; Waldvogel, S. R. *Angew. Chem. Int. Ed.* **2018**, *57*, 5594–5619. (c) Pollok, D.; Waldvogel, S. R. *Chem. Sci.* **2020**, *11*, 12386–12400.

24 (a) Moses, J. E.; Moorhouse, A. D. *Chem. Soc. Rev.* **2007**, *36*, 1249–1262. (b) Thirumurugan, P.; Matosiuk, D.; Jozwiak, K. *Chem. Rev.* **2013**, *113*, 4905–4979. (c) Sletten, E. M.; Bertozzi, C. R. *Angew. Chem. Int. Ed.* **2009**, *48*, 6974–6998. (d) Thirumurugan, P.; Matosiuk, D.; Jozwiak, K. *Chem. Rev.* **2013**, *113*, 4905–4979. (e) Devaraj, N. K. *ACS Cent. Sci.* **2018**, *4*, 952–959. (f) Bird, R. E.; Lemmel, S. A.; Yu, X.; Zhou, Q. A. *Bioconjug. Chem.* **2021**, *32*, 2457–2479.

25 (a) Geri, J. B.; Oakley, J. V.; Reyes-Robles, T.; Wang, T.; McCarver, S. J.; White, C. H.; Rodriguez-Rivera, F. P.; Parker, D. L.; Hett, E. C.; Fadeyi, O. O.; Oslund, R. C.; MacMillan, D. W. C. *Science* **2020**, *367*, 1091–1097. (b) Seath, C. P.; Trowbridge, A. D.; Muir, T. W.; MacMillan, D. W. C. *Chem. Soc. Rev.* **2021**, *50*, 2911–2926. (c) Li, B. X.; Kim, D. K.; Bloom, S.; Huang, R. Y. C.; Qiao, J. X.; Ewing, W. R.; Oblinsky, D. G.; Scholes, G. D.; MacMillan, D. W. C. *Nat. Chem.* **2021**, *13*, 902–908. (d) Kawamata, Y.; Ryu, K. A.; Hermann, G. N.; Sandahl, A.; Vantourout, J. C.; Olow, A. K.; Adams, L. A.; Rivera-Chao, E.; Roberts, L. R.; Oslund, R. C.; Fadeyi, O. O.; Baran, P. S. *Electroaffinity Labeling: A New Platform for Chemoproteomic-based Target Identification* [preprint] **2022**; 10.26434/chemrxiv-2022-s2m8f. (e) Laudadio, G.; Palkowitz, M. D.; El-Hayek Ewing, T.; Baran, P. S. *ACS Med. Chem. Lett.* **2022**, *13*, 1413–1420.

26 (a) Gray, N. S. *Nat. Chem. Biol.* **2006**, *2*, 649–653. (b) Nicolaou, K. C. *Angew. Chem. Int. Ed.* **2014**, *53*, 4730–4730. (c) Michaudel, Q.; Ishihara, Y.; Baran, P. S. *Acc. Chem. Res.* **2015**, *48*, 712–721.

27 (a) Rogers-Evans, M.; Knust, H.; Plancher, J.-M.; Carreira, E. M.; Wuitschik, G.; Burkhard, J.; Li, D. B.; Guérot, C. *Chimia* **2014**, *68*, 492–499. (b) Carreira, E. M.; Fessard, T. C. *Chem. Rev.* **2014**, *114*, 8257–8322.

28 (a) Zheng, X.; Gao, L.; Wang, L.; Liang, C.; Wang, B.; Liu, Y.; Feng, S.; Zhang, B.; Zhou, M.; Yu, X.; Xiang, K.; Chen, L.; Guo, T.; Shen, H. C.; Zou, G.; Wu, J. Z.; Yun, H. *J. Med.*

Chem. **2019**, *62*, 6003–6014. (b) White, C.; McGowan, M. A.; Zhou, H.; Sciammetta, N.; Fradera, X.; Lim, J.; Joshi, E. M.; Andrews, C.; Nickbarg, E. B.; Cowley, P.; Trewick, S.; Augustin, M.; von Köenig, K.; Lesburg, C. A.; Otte, K.; Knemeyer, I.; Woo, H.; Yu, W.; Cheng, M.; Spacciapoli, P.; Geda, P.; Song, X.; Smotrov, N.; Curran, P.; Heo, M. R.; Abeywickrema, P.; Miller, J. R.; Bennett, D. J.; Han, Y. *ACS Med. Chem. Lett.* **2020**, *11*, 550–557. (c) Wellington, K.; Scott, L. J. *Drugs* **2003**, *63*, 2613–2621. (d) Graham, T. H.; Shu, M.; Verras, A.; Chen, Q.; Garcia-Calvo, M.; Li, X.; Lisnock, J.; Tong, X.; Tung, E. C.; Wiltsie, J.; Hale, J. J.; Pinto, S.; Shen, D.-M. *Bioorg. Med. Chem. Lett.* **2014**, *24*, 1657–1660. (e) Grosse, S.; Tahri, A.; Raboisson, P.; Houpis, Y.; Stoops, B.; Jacoby, E.; Neefs, J.-M.; Van Loock, M.; Goethals, O.; Geluykens, P.; Bonfanti, J.-F.; Jonckers, T. H. M. *ACS Med. Chem. Lett.* **2022**, *13*, 1879–1884. (f) Myriem, E. Q.; Cassayre, J. Y. (Syngenta Crop Protection) *Methods of pest control in soybean*, WO Patent Appl. No. WO2014019957A2, **2014**.

29 (a) Malarney, K. P.; KC, S.; Schmidt, V. A. *Org. Biomol. Chem.* **2021**, *19*, 8425–8441. (b) Bull, J. A.; Croft, R. A.; Davis, O. A.; Doran, R.; Morgan, K. F. *Chem. Rev.* **2016**, *116*, 12150–12233. (c) Mughal, H.; Szostak, M. *Org. Biomol. Chem.* **2021**, *19*, 3274–3286. (d) Xu, J. *Beilstein J. Org. Chem.* **2020**, *16*, 1357–1410.

30 (a) Jenkinson, S. F.; Fleet, G. W. J. *Chimia* **2011**, *65*, 71–75. (b) Davis, O.; Bull, J. *Synlett* **2015**, *26*, 1283–1288.

31 (a) Abe, M. *J. Chinese Chem. Soc.* **2008**, *55*, 479–486. (b) D'Auria, M.; Racioppi, R. *Molecules* **2013**, *18*, 11384–11428. (c) Fréneau, M.; Hoffmann, N. *J. Photochem. Photobiol. C Photochem. Rev.* **2017**, *33*, 83–108. (d) D'Auria, M. *Photochem. Photobiol. Sci.* **2019**, *18*, 2297–2362. (e) Franceschi, P.; Cuadros, S.; Goti, G.; Dell'Amico, L. *Angew. Chem. Int. Ed.* **2023**, e202217210.

32 (a) Mack, D. J.; Njardarson, J. T. *ACS Catal.* **2013**, *3*, 272–286. (b) Njardarson, J. *Synlett* **2013**, *24*, 787–803. (c) Ilardi, E. A.; Njardarson, J. T. *J. Org. Chem.* **2013**, *78*, 9533–9540. (d) Wang, Z.; Chen, Z.; Sun, J. *Org. Biomol. Chem.* **2014**, *12*, 6028–6032. (e) Malapit, C. A.; Howell, A. R. *J. Org. Chem.* **2015**, *80*, 8489–8495. (f) Mahal, A. *Eur. J. Chem.* **2015**, *6*, 357–366. (g) Ahmad, S.; Yousaf, M.; Mansha, A.; Rasool, N.; Zahoor, A. F.; Hafeez, F.; Rizvi, S. M. A. *Synth. Commun.* **2016**, *46*, 1397–1416. (h) Wang, C. *Synthesis* **2017**, *49*, 5307–5319. (i) An, J.; Riel, L. P.; Howell, A. R. *Acc. Chem. Res.* **2021**, *54*, 3850–3862. (j) Sandvoß, A.; Wahl, J. M. *Chem. Eur. J.* **2021**, *27*, 5871–5879.

33 (a) Burkhard, J. A.; Wuitschik, G.; Rogers-Evans, M.; Müller, K.; Carreira, E. M. *Angew. Chem. Int. Ed.* **2010**, *49*, 9052–9067. (b) Alves, F. R. de S.; Couñago, R. M.; Laufer, S. *Int. J. Mol. Sci.* **2020**, *21*, 8199. (c) Bauer, M. R.; Di Fruscia, P.; Lucas, S. C. C.;

Michaelides, I. N.; Nelson, J. E.; Storer, R. I.; Whitehurst, B. C. *RSC Med. Chem.* **2021**, *12*, 448–471.

34 Rojas, J. J.; Bull, J. A. Oxetanes and Oxetenes: Monocyclic. In *Comprehensive Heterocyclic Chemistry IV*; Black, D. S., Cossy, J., Stevens, C. V., Eds.; Elsevier, 2022; Vol. 1, pp 212.

35 For selected examples, see: (a) Harrane, A.; Naar, N.; Belbachir, M. *Mater. Lett.* **2007**, *61*, 3555–3558. (b) Darensbourg, D. J.; Moncada, A. I.; Choi, W.; Reibenspies, J. H. *J. Am. Chem. Soc.* **2008**, *130*, 6523–6533. (c) Rahm, M.; Westlund, R.; Eldsäter, C.; Malmström, E. *J. Polym. Sci. Part A Polym. Chem.* **2009**, *47*, 6191–6200. (d) Yang, Q.; Pan, X.; Huang, F.; Li, K. *Cellulose* **2011**, *18*, 1611–1621. (e) Crivello, J. V. *J. Polym. Sci. Part A Polym. Chem.* **2014**, *52*, 2934–2946.

36 For selected examples, see: (a) Guo, K.; Luo, Y.; Chen, J.; Li, X.; Huang, L. *Propellants, Explos. Pyrotech.* **2010**, *35*, 423–424. (b) Zhang, C.; Li, J.; Luo, Y. *Propellants, Explos. Pyrotech.* **2012**, *37*, 235–240. (c) Wang, G.; Ge, Z.; Luo, Y. *Propellants, Explos. Pyrotech.* **2015**, *40*, 920–926. (d) Zhao, J.; Jin, B.; Peng, R.; Deng, N.; Gong, W.; Liu, Q.; Chu, S. *RSC Adv.* **2015**, *5*, 90422–90427. (e) Zhang, C.; Zheng, X.; Li, Z.; Cao, G.; Zhang, X.; Zhai, B. *Propellants, Explos. Pyrotech.* **2017**, *42*, 1037–1043. (f) Mukhametshin, T. I.; Petrov, A. I.; Kuznetsova, N. V.; Petrov, V. A.; Averianova, N. V.; Garaev, I. K.; Kostochko, A. V.; Gubaidullin, A. T.; Vinogradov, D. B.; Bulatov, P. V. *Chem. Heterocycl. Compd.* **2017**, *53*, 811–821.

37 For selected examples, see: (a) Chen, Z.; Wang, B.; Wang, Z.; Zhu, G.; Sun, J. *Angew. Chem. Int. Ed.* **2013**, *52*, 2027–2031. (b) White, A. R.; Kozlowski, R. A.; Tsai, S.-C.; Vanderwal, C. D. *Angew. Chem. Int. Ed.* **2017**, *56*, 10525–10529. (c) Wang, G.; Huang, H.; Guo, W.; Qian, C.; Sun, J. *Angew. Chem. Int. Ed.* **2020**, *59*, 11245–11249. (d) Strassfeld, D. A.; Wickens, Z. K.; Picazo, E.; Jacobsen, E. N. *J. Am. Chem. Soc.* **2020**, *142*, 9175–9180. (e) Zhang, R.; Sun, M.; Yan, Q.; Lin, X.; Li, X.; Fang, X.; Sung, H. H. Y.; Williams, I. D.; Sun, J. *Org. Lett.* **2022**, *24*, 2359–2364. (f) Also see Figure 6 and associated discussion.

38 Wani, M. C.; Taylor, H. L.; Wall, M. E.; Coggon, P.; McPhail, A. T. *J. Am. Chem. Soc.* **1971**, *93*, 2325–2327.

39 World Health Organisation, **2019**. World Health Organisation model list of essential medicines: 21st list 2019. World Health Organisation. https://apps.who.int/iris/handle/10665/325771.

40 Ganem, B.; Franke, R. R. *J. Org. Chem.* **2007**, *72*, 3981–3987.

41 (a) Holton, R. A.; Somoza, C.; Kim, H. B.; Liang, F.; Biediger, R. J.; Boatman, P. D.; Shindo, M.; Smith, C. C.; Kim, S. *J. Am. Chem. Soc.* **1994**, *116*, 1597–1598. (b) Holton,

R. A.; Kim, H. B.; Somoza, C.; Liang, F.; Biediger, R. J.; Boatman, P. D.; Shindo, M.; Smith, C. C.; Kim, S. *J. Am. Chem. Soc.* **1994**, *116*, 1599–1600. (c) Nicolaou, K. C.; Yang, Z.; Liu, J. J.; Ueno, H.; Nantermet, P. G.; Guy, R. K.; Claiborne, C. F.; Renaud, J.; Couladouros, E. A.; Paulvannan, K.; Sorensen, E. J. *Nature* **1994**, *367*, 630–634. (d) Danishefsky, S. J.; Masters, J. J.; Young, W. B.; Link, J. T.; Snyder, L. B.; Magee, T. V.; Jung, D. K.; Isaacs, R. C. A.; Bornmann, W. G.; Alaimo, C. A.; Coburn, C. A.; Di Grandi, M. J. *J. Am. Chem. Soc.* **1996**, *118*, 2843–2859. (e) Wender, P. A.; Badham, N. F.; Conway, S. P.; Floreancig, P. E.; Glass, T. E.; Gränicher, C.; Houze, J. B.; Jänichen, J.; Lee, D.; Marquess, D. G.; McGrane, P. L.; Meng, W.; Mucciaro, T. P.; Mühlebach, M.; Natchus, M. G.; Paulsen, H.; Rawlins, D. B.; Satkofsky, J.; Shuker, A. J.; Sutton, J. C.; Taylor, R. E.; Tomooka, K. *J. Am. Chem. Soc.* **1997**, *119*, 2755–2756. (f) Wender, P. A.; Badham, N. F.; Conway, S. P.; Floreancig, P. E.; Glass, T. E.; Houze, J. B.; Krauss, N. E.; Lee, D.; Marquess, D. G.; McGrane, P. L.; Meng, W.; Natchus, M. G.; Shuker, A. J.; Sutton, J. C.; Taylor, R. E. *J. Am. Chem. Soc.* **1997**, *119*, 2757–2758. (g) Shiina, I.; Iwadare, H.; Sakoh, H.; Hasegawa, M.; Tani, Y.; Mukaiyama, T. *Chem. Lett.* **1998**, *27*, 1–2. (h) Morihira, K.; Hara, R.; Kawahara, S.; Nishimori, T.; Nakamura, N.; Kusama, H.; Kuwajima, I. *J. Am. Chem. Soc.* **1998**, *120*, 12980–12981. (i) Kusama, H.; Hara, R.; Kawahara, S.; Nishimori, T.; Kashima, H.; Nakamura, N.; Morihira, K.; Kuwajima, I. *J. Am. Chem. Soc.* **2000**, *122*, 3811–3820. (j) Doi, T.; Fuse, S.; Miyamoto, S.; Nakai, K.; Sasuga, D.; Takahashi, T. *Chem. Asian J.* **2006**, *1*, 370–383. (k) Hirai, S.; Utsugi, M.; Iwamoto, M.; Nakada, M. *Chem. Eur. J.* **2015**, *21*, 355–359. (l) Fukaya, K.; Tanaka, Y.; Sato, A. C.; Kodama, K.; Yamazaki, H.; Ishimoto, T.; Nozaki, Y.; Iwaki, Y. M.; Yuki, Y.; Umei, K.; Sugai, T.; Yamaguchi, Y.; Watanabe, A.; Oishi, T.; Sato, T.; Chida, N. *Org. Lett.* **2015**, *17*, 2570–2573. (m) Fukaya, K.; Kodama, K.; Tanaka, Y.; Yamazaki, H.; Sugai, T.; Yamaguchi, Y.; Watanabe, A.; Oishi, T.; Sato, T.; Chida, N. *Org. Lett.* **2015**, *17*, 2574–2577. (n) Kanda, Y.; Nakamura, H.; Umemiya, S.; Puthukanoori, R. K.; Murthy Appala, V. R.; Gaddamanugu, G. K.; Paraselli, B. R.; Baran, P. S. *J. Am. Chem. Soc.* **2020**, *142*, 10526–10533. (o) Hu, Y.-J.; Gu, C.-C.; Wang, X.-F.; Min, L.; Li, C.-C. *J. Am. Chem. Soc.* **2021**, *143*, 17862–17870. (p) Iiyama, S.; Fukaya, K.; Yamaguchi, Y.; Watanabe, A.; Yamamoto, H.; Mochizuki, S.; Saio, R.; Noguchi, T.; Oishi, T.; Sato, T.; Chida, N. *Org. Lett.* **2022**, *24*, 202–206. (q) Imamura, Y.; Takaoka, K.; Komori, Y.; Nagatomo, M.; Inoue, M. *Angew. Chem. Int. Ed.* **2023**, *62*, e202219114.

42 Min, L.; Han, J.-C.; Zhang, W.; Gu, C.-C.; Zou, Y.-P.; Li, C.-C. *Chem. Rev.* **2023**, DOI: 10.1021/acs.chemrev.2c00763.

43 Wang, S.-R.; Yang, C.-G.; Sánchez-Murcia, P. A.; Snyder, J. P.; Yan, N.; Sáez-Calvo, G.; Díaz, J. F.; Gago, F.; Fang, W.-S. *Org. Lett.* **2015**, *17*, 6098–6101.

44 Shimada, N.; Hasegawa, S.; Harada, T.; Tomisawa, T.; Fujii, A.; Taktia, T. *J. Antibiot.* **1986**, *39*, 1623–1625.

45 Hamberg, M.; Svensson, J.; Samuelsson, B. *Proc. Natl. Acad. Sci.* **1975**, *72*, 2994–2998.

46 Li, C.; Lee, D.; Graf, T. N.; Phifer, S. S.; Nakanishi, Y.; Burgess, J. P.; Riswan, S.; Setyowati, F. M.; Saribi, A. M.; Soejarto, D. D.; Farnsworth, N. R.; Falkinham, J. O.; Kroll, D. J.; Kinghorn, A. D.; Wani, M. C.; Oberlies, N. H. *Org. Lett.* **2005**, *7*, 5709–5712.

47 Huang, J.; Yokoyama, R.; Yang, C.; Fukuyama, Y. *Tetrahedron Lett.* **2000**, *41*, 6111–6114.

48 (a) Schneider, M.; Richter, M. J. R.; Carreira, E. M. *J. Am. Chem. Soc.* **2020**, *142*, 17802–17809. (b) Wein, L. A.; Wurst, K.; Angyal, P.; Weisheit, L.; Magauer, T. *J. Am. Chem. Soc.* **2019**, *141*, 19589–19593.

49 Shen, Y.; Li, L.; Xiao, X.; Yang, S.; Hua, Y.; Wang, Y.; Zhang, Y.; Zhang, Y. *J. Am. Chem. Soc.* **2021**, *143*, 3256–3263.

50 Fan, P.-H.; Geng, Y.; Romo, A. J.; Zhong, A.; Zhang, J.; Yeh, Y.-C.; Lee, Y.-H.; Liu, H. *Angew. Chem. Int. Ed.* **2022**, *61*, e202210362.

51 Sulaiman, S. N.; Zahari, A.; Liew, S. Y.; Litaudon, M.; Issam, A. M.; Wahab, H. A.; Awang, K. *Phytochem. Lett.* **2018**, *25*, 22–26.

52 Wang, J.; Shu, Y.; Liu, S.; Hu, J.; Sun, C.; Zhou, H.; Gan, D.; Cai, X.-Y.; Pu, W.; Cai, L.; Ding, Z. *Org. Chem. Front.* **2019**, *6*, 3839–3846.

53 Kutateladze, A. G.; Holt, T.; Reddy, D. S. *J. Org. Chem.* **2019**, *84*, 7575–7586.

54 Lucas, S. D.; Fischer, H.; Alker, A.; Rauter, A. P.; Wessel, H. P. *J. Carbohydr. Chem.* **2011**, *30*, 498–548.

55 Gleeson, M. P. *J. Med. Chem.* **2008**, *51*, 817–834.

56 (a) Johnson, T. W.; Dress, K. R.; Edwards, M. *Bioorg. Med. Chem. Lett.* **2009**, *19*, 5560–5564. (b) Waring, M. J. *Expert Opin. Drug Discov.* **2010**, *5*, 235–248.

57 For an example, see: Waring, M. J.; Johnstone, C. *Bioorg. Med. Chem. Lett.* **2007**, *17*, 1759–1764.

58 van de Waterbeemd, H.; Smith, D. A.; Beaumont, K.; Walker, D. K. *J. Med. Chem.* **2001**, *44*, 1313–1333.

59 Hitchcock, S. A.; Pennington, L. D. *J. Med. Chem.* **2006**, *49*, 7559–7583.

60 Ishikawa, M.; Hashimoto, Y. *J. Med. Chem.* **2011**, *54*, 1539–1554.

61 Skoda, E. M.; Sacher, J. R.; Kazancioglu, M. Z.; Saha, J.; Wipf, P. *ACS Med. Chem. Lett.* **2014**, *5*, 900–904.

62 Luger, P.; Buschmann, J. *J. Am. Chem. Soc.* **1984**, *106*, 7118–7121.

63 Holan, G.; Kowala, C.; Wunderlich, J. A. *J. Chem. Soc. Chem. Commun.* **1973**, *12*, 34.

64 Walsh, A. D. *Trans. Faraday Soc.* **1949**, *45*, 179–190.

65 (a) Hoffmann, R.; Davidson, R. B. *J. Am. Chem. Soc.* **1971**, *93*, 5699–5705. (b) Mollere, P. D. *Tetrahedron Lett.* **1973**, *14*, 2791–2794. (a) Mollere, P. D.; Houk, K. N. *J. Am. Chem. Soc.* **1977**, *99*, 3226–3233.

66 Berthelot, M.; Besseau, F.; Laurence, C. *Eur. J. Org. Chem.* **1998**, *1998*, 925–931.

67 Bellon, L.; Taft, R. W.; Abboud, J.-L. M. *J. Org. Chem.* **1980**, *45*, 1166–1168.

68 West, R.; Powell, D. L.; Lee, M. K. T.; Whatley, L. S. *J. Am. Chem. Soc.* **1964**, *86*, 3227–3229.

69 (a) Le Questel, J.-Y.; Laurence, C.; Lachkar, A.; Helbert, M.; Berthelot, M. *J. Chem. Soc. Perkin Trans. 2* **1992**, 2091–2094. (b) Besseau, F.; Laurence, C.; Berthelot, M. *J. Chem. Soc. Perkin Trans. 2* **1994**, 485–489. (c) Besseau, F.; Luçon, M.; Laurence, C.; Berthelot, M. *J. Chem. Soc. Perkin Trans. 2* **1998**, 101–108.

70 Wuitschik, G.; Carreira, E. M.; Wagner, B.; Fischer, H.; Parrilla, I.; Schuler, F.; Rogers-Evans, M.; Müller, K. *J. Med. Chem.* **2010**, *53*, 3227–3246.

71 (a) Fletcher, R. A.; Pilcher, G. *Trans. Faraday Soc.* **1970**, *66*, 794–799. (b) Eigenmann, H. K.; Golden, D. M.; Benson, S. W. *J. Phys. Chem.* **1973**, *77*, 1687–1691.

72 Rojas, J. J.; Torrisi, E.; Dubois, M. A. J.; Hossain, R.; White, A. J. P.; Zappia, G.; Mousseau, J. J.; Choi, C.; Bull, J. A. *Org. Lett.* **2022**, *24*, 2365–2370.

73 For other representative examples, see: (a) Loy, R. N.; Jacobsen, E. N. *J. Am. Chem. Soc.* **2009**, *131*, 2786–2787. (b) Yang, W.; Sun, J. *Angew. Chem. Int. Ed.* **2016**, *55*, 1868–1871. (c) Zou, X.; Sun, G.; Huang, H.; Wang, J.; Yang, W.; Sun, J. *Org. Lett.* **2020**, *22*, 249–252.

74 Chalyk, B.; Grynyova, A.; Filimonova, K.; Rudenko, T. V; Dibchak, D.; Mykhailiuk, P. K. *Org. Lett.* **2022**, *24*, 4722–4728.

75 Duncton, M. A. J.; Estiarte, M. A.; Tan, D.; Kaub, C.; O'Mahony, D. J. R.; Johnson, R. J.; Cox, M.; Edwards, W. T.; Wan, M.; Kincaid, J.; Kelly, M. G. *Org. Lett.* **2008**, *10*, 3259–3262.

76 Stepan, A. F.; Karki, K.; McDonald, W. S.; Dorff, P. H.; Dutra, J. K.; DiRico, K. J.; Won, A.; Subramanyam, C.; Efremov, I. V.; O'Donnell, C. J.; Nolan, C. E.; Becker, S. L.; Pustilnik, L. R.; Sneed, B.; Sun, H.; Lu, Y.; Robshaw, A. E.; Riddell, D.; O'Sullivan, T. J.; Sibley, E.; Capetta, S.; Atchison, K.; Hallgren, A. J.; Miller, E.; Wood, A.; Obach, R. S. *J. Med. Chem.* **2011**, *54*, 7772–7783.

77 Stepan, A. F.; Kauffman, G. W.; Keefer, C. E.; Verhoest, P. R.; Edwards, M. *J. Med. Chem.* **2013**, *56*, 6985–6990.

78 Dowling, J. E.; Alimzhanov, M.; Bao, L.; Block, M. H.; Chuaqui, C.; Cooke, E. L.; Denz, C. R.; Hird, A.; Huang, S.; Larsen, N. A.; Peng, B.; Pontz, T. W.; Rivard-Costa, C.; Saeh,

J. C.; Thakur, K.; Ye, Q.; Zhang, T.; Lyne, P. D. *ACS Med. Chem. Lett.* **2013**, *4*, 800–805.

79 Li, X. Q.; Grönberg, G.; Bangur, E. H.; Hayes, M. A.; Castagnoli, N.; Weidolf, L. *Drug Metab. Dispos.* **2019**, *47*, 1247–1256.

80 Li, X.-Q.; Hayes, M. A.; Gronberg, G.; Berggren, K.; Castagnoli, N.; Weidolf, L. *Drug Metab. Dispos.* **2016**, *44*, 1341–1348.

81 (a) Toselli, F.; Fredenwall, M.; Svensson, P.; Li, X.-Q.; Johansson, A.; Weidolf, L.; Hayes, M. A. *Drug Metab. Dispos.* **2017**, *45*, 966–973. (b) Raffa, R. B.; Pergolizzi, J. V. *Pharmacol. & Pharm.* **2019**, *10*, 465–473. (c) Barnych, B.; Singh, N.; Negrel, S.; Zhang, Y.; Magis, D.; Roux, C.; Hua, X.; Ding, Z.; Morisseau, C.; Tantillo, D. J.; Siegel, J. B.; Hammock, B. D. *Eur. J. Med. Chem.* **2020**, *193*, 112206.

82 Rioux, N.; Duncan, K. W.; Lantz, R. J.; Miao, X.; Chan-Penebre, E.; Moyer, M. P.; Munchhof, M. J.; Copeland, R. A.; Chesworth, R.; Waters, N. J. *Xenobiotica* **2016**, *46*, 268–277.

83 (a) Khanna, A.; Côté, A.; Arora, S.; Moine, L.; Gehling, V. S.; Brenneman, J.; Cantone, N.; Stuckey, J. I.; Apte, S.; Ramakrishnan, A.; Bruderek, K.; Bradley, W. D.; Audia, J. E.; Cummings, R. T.; Sims, R. J.; Trojer, P.; Levell, J. R. *ACS Med. Chem. Lett.* **2020**, *11*, 1205–1212. (b) Driscoll, J. P.; Sadlowski, C. M.; Shah, N. R.; Feula, A. *J. Med. Chem.* **2020**, *63*, 6303–6314. (c) Hall, A.; Chanteux, H.; Ménochet, K.; Ledecq, M.; Schulze, M.-S. E. D. *J. Med. Chem.* **2021**, *64*, 6413–6522.

84 Raffa, R. B.; Pergolizzi, J. V. *Pharmacol. & Pharm.* **2019**, *10*, 465–473.

85 Wermuth, C. G.; Ganellin, C. R.; Lindberg, P.; Mitscher, L. A. *Pure Appl. Chem.* **1998**, *70*, 1129–1143.

86 Meanwell, N. A. *J. Agric. Food Chem.* **2023**, DOI: 10.1021/acs.jafc.3c00765.

87 Langmuir, I. *J. Am. Chem. Soc.* **1919**, *41*, 1543–1559.

88 Meanwell, N. A. *J. Med. Chem.* **2011**, *54*, 2529–2591.

89 (a) Sun, S.; Jia, Q.; Zhang, Z. *Bioorg. Med. Chem. Lett.* **2019**, *29*, 2535–2550. (b) Kumari, S.; Carmona, A. V.; Tiwari, A. K.; Trippier, P. C. *J. Med. Chem.* **2020**, *63*, 12290–12358. (c) Kleebauer, L.; Zborovsky, L.; Hommernick, K.; Seidel, M.; Weston, J. B.; Süssmuth, R. D. *Org. Lett.* **2021**, *23*, 7023–7027.

90 Ertl, P.; Altmann, E.; McKenna, J. M. *J. Med. Chem.* **2020**, *63*, 8408–8418.

91 (a) Pattabiraman, V. R.; Bode, J. W. *Nature* **2011**, *480*, 471–479. (b) Sabatini, M. T.; Boulton, L. T.; Sneddon, H. F.; Sheppard, T. D. *Nat. Catal.* **2019**, *2*, 10–17.

92 Wuitschik, G.; Rogers-Evans, M.; Müller, K.; Fischer, H.; Wagner, B.; Schuler, F.; Polonchuk, L.; Carreira, E. M. *Angew. Chem. Int. Ed.* **2006**, *45*, 7736–7739.

93 Cavalli, A.; Poluzzi, E.; De Ponti, F.; Recanatini, M. *J. Med. Chem.* **2002**, *45*, 3844–3853.

94 Barnes-Seeman, D.; Jain, M.; Bell, L.; Ferreira, S.; Cohen, S.; Chen, X.-H.; Amin, J.; Snodgrass, B.; Hatsis, P. *ACS Med. Chem. Lett.* **2013**, *4*, 514–516.

95 Mukherjee, P.; Pettersson, M.; Dutra, J. K.; Xie, L.; am Ende, C. W. *ChemMedChem* **2017**, *12*, 1574–1577.

96 Davis, B. J.; Erlanson, D. A. *Bioorg. Med. Chem. Lett.* **2013**, *23*, 2844–2852.

97 Wuitschik, G.; Rogers-Evans, M.; Buckl, A.; Bernasconi, M.; Märki, M.; Godel, T.; Fischer, H.; Wagner, B.; Parrilla, I.; Schuler, F.; Schneider, J.; Alker, A.; Schweizer, W. B.; Müller, K.; Carreira, E. M. *Angew. Chem. Int. Ed.* **2008**, *47*, 4512–4515.

98 Carreira, E. M.; Fessard, T. C. *Chem. Rev.* **2014**, *114*, 8257–8322.

99 Degorce, S. L.; Bodnarchuk, M. S.; Scott, J. S. *ACS Med. Chem. Lett.* **2019**, *10*, 1198–1204.

100 Burkhard, J. A.; Wuitschik, G.; Plancher, J.-M.; Rogers-Evans, M.; Carreira, E. M. *Org. Lett.* **2013**, *15*, 4312–4315.

101 Eriksson, T.; Bjöurkman, S.; Roth, B.; Fyge, Å.; Höuglund, P. *Chirality* **1995**, *7*, 44–52.

102 (a) Smith, S. W. *Toxicol. Sci.* **2009**, *110*, 4–30. (b) Kim, J. H.; Scialli, A. R. *Toxicol. Sci.* **2011**, *122*, 1–6.

103 Dubois, M. A. J.; Croft, R. A.; Ding, Y.; Choi, C.; Owen, D. R.; Bull, J. A.; Mousseau, J. J. *RSC Med. Chem.* **2021**, *12*, 2045–2052.

104 (a) Pettit, G. R.; Toki, B.; Herald, D. L.; Verdier-Pinard, P.; Boyd, M. R.; Hamel, E.; Pettit, R. K. *J. Med. Chem.* **1998**, *41*, 1688–1695. (b) Bernardi, A. P. M.; Ferraz, A. B. F.; Albring, D. V.; Bordignon, S. A. L.; Schripsema, J.; Bridi, R.; Dutra-Filho, C. S.; Henriques, A. T.; von Poser, G. L. *J. Nat. Prod.* **2005**, *68*, 784–786. (c) Wu, S.-B.; Long, C.; Kennelly, E. J. *Nat. Prod. Rep.* **2014**, *31*, 1158–1174.

105 (a) Brandes, L. J.; Hermonat, M. W. *Biochem. Biophys. Res. Commun.* **1984**, *123*, 724–728. (b) Reyno, L.; Seymour, L.; Tu, D.; Dent, S.; Gelmon, K.; Walley, B.; Pluzanska, A.; Gorbunova, V.; Garin, A.; Jassem, J.; Pienkowski, T.; Dancey, J.; Pearce, L.; MacNeil, M.; Marlin, S.; Lebwohl, D.; Voi, M.; Pritchard, K. *J. Clin. Oncol.* **2004**, *22*, 269–276. (c) Mondal, S.; Panda, G. *RSC Adv.* **2014**, *4*, 28317–28358. (d) Walter, F. R.; Veszelka, S.; Pásztói, M.; Péterfi, Z. A.; Tóth, A.; Rákhely, G.; Cervenak, L.; Ábrahám, C. S.; Deli, M. A. *J. Neurochem.* **2015**, *134*, 1040–1054.

106 (a) Boscá, F.; Miranda, M. A. *J. Photochem. Photobiol. B Biol.* **1998**, *43*, 1–26. (b) Cuquerella, M. C.; Lhiaubet-Vallet, V.; Cadet, J.; Miranda, M. A. *Acc. Chem. Res.* **2012**, *45*, 1558–1570.

107 Sterckx, H.; De Houwer, J.; Mensch, C.; Caretti, I.; Tehrani, K. A.; Herrebout, W. A.; Van Doorslaer, S.; Maes, B. U. W. *Chem. Sci.* **2016**, *7*, 346–357.

108 Lassalas, P.; Oukoloff, K.; Makani, V.; James, M.; Tran, V.; Yao, Y.; Huang, L.; Vijayendran, K.; Monti, L.; Trojanowski, J. Q.; Lee, V. M. Y.; Kozlowski, M. C.; Smith, A. B.; Brunden, K. R.; Ballatore, C. *ACS Med. Chem. Lett.* **2017**, *8*, 864–868.

109 Horgan, C.; O'Sullivan, T. P. *Curr. Med. Chem.* **2022**, *29*, 2203–2234.

110 Croft, R. A.; Mousseau, J. J.; Choi, C.; Bull, J. A. *Chem. Eur. J.* **2018**, *24*, 818–821.

111 Ellis, B. D.; Milligan, J. C.; White, A. R.; Duong, V.; Altman, P. X.; Mohammed, L. Y.; Crump, M. P.; Crosby, J.; Luo, R.; Vanderwal, C. D.; Tsai, S.-C. *J. Am. Chem. Soc.* **2018**, *140*, 4961–4964.

112 Francisco, K. R.; Varricchio, C.; Paniak, T. J.; Kozlowski, M. C.; Brancale, A.; Ballatore, C. *Eur. J. Med. Chem.* **2021**, *218*, 113399.

113 Kobayakawa, T. *J. Synth. Org. Chem. Japan* **2019**, *77*, 720–721.

114 Ecker, A. K.; Levorse, D. A.; Victor, D. A.; Mitcheltree, M. J. *ACS Med. Chem. Lett.* **2022**, *13*, 964–971.

115 (a) McLaughlin, M.; Yazaki, R.; Fessard, T. C.; Carreira, E. M. *Org. Lett.* **2014**, *16*, 4070–4073. (b) Powell, N. H.; Clarkson, G. J.; Notman, R.; Raubo, P.; Martin, N. G.; Shipman, M. *Chem. Commun.* **2014**, *50*, 8797–8800.

116 Gudelis, E.; Krikštolaitytė, S.; Stančiauskaitė, M.; Šachlevičiūtė, U.; Bieliauskas, A.; Milišiūnaitė, V.; Jankauskas, R.; Kleizienė, N.; Sløk, F. A.; Šačkus, A. *Molecules* **2023**, *28*, 1091.

117 Möller, G. P.; Müller, S.; Wolfstädter, B. T.; Wolfrum, S.; Schepmann, D.; Wünsch, B.; Carreira, E. M. *Org. Lett.* **2017**, *19*, 2510–2513.

118 Beadle, J. D.; Knuhtsen, A.; Hoose, A.; Raubo, P.; Jamieson, A. G.; Shipman, M. *Org. Lett.* **2017**, *19*, 3303–3306.

119 Roesner, S.; Saunders, G. J.; Wilkening, I.; Jayawant, E.; Geden, J. V.; Kerby, P.; Dixon, A. M.; Notman, R.; Shipman, M. *Chem. Sci.* **2019**, *10*, 2465–2472.

120 Roesner, S.; Beadle, J. D.; Tam, L. K. B.; Wilkening, I.; Clarkson, G. J.; Raubo, P.; Shipman, M. *Org. Biomol. Chem.* **2020**, *18*, 5400–5405.

121 McDougall, L.; Draper, E. R.; Beadle, J. D.; Shipman, M.; Raubo, P.; Jamieson, A. G.; Adams, D. J. *Chem. Commun.* **2018**, *54*, 1793–1796.

122 Jayawant, E. S.; Beadle, J. D.; Wilkening, I.; Raubo, P.; Shipman, M.; Notman, R.; Dixon, A. M. *Phys. Chem. Chem. Phys.* **2020**, *22*, 25075–25083.

123 (a) Fujishima, T.; Nozaki, T.; Suenaga, T. *Bioorg. Med. Chem.* **2013**, *21*, 5209–5217. (b) Fujishima, T.; Suenaga, T.; Nozaki, T. *Tetrahedron Lett.* **2014**, *55*, 3805–3808.

124 Shearer, J.; Castro, J. L.; Lawson, A. D. G.; MacCoss, M.; Taylor, R. D. *J. Med. Chem.* **2022**, *65*, 8699–8712.

125 (a) Lewis, N. L.; Lewis, L. D.; Eder, J. P.; Reddy, N. J.; Guo, F.; Pierce, K. J.; Olszanski, A. J.; Cohen, R. B. *J. Clin. Oncol.* **2009**, *27*, 5262–5269. (b) Smith, C. C.; Lasater, E. A.; Lin, K. C.; Wang, Q.; McCreery, M. Q.; Stewart, W. K.; Damon, L. E.; Perl, A. E.; Jeschke, G. R.; Sugita, M.; Carroll, M.; Kogan, S. C.; Kuriyan, J.; Shah, N. P. *Proc. Natl. Acad. Sci.* **2014**, *111*, 5319–5324. (c) For an overview of all clinical trials and further investigations, see: *Drug Bank*. https://go.drugbank.com/drugs/DB11832. (Accessed on 26.01.2023).

126 (a) Crawford, J. J.; Zhang, H. In *ACS Symposium Series*; American Chemical Society, 2019; Vol. 1332, pp 239–266. (b) Wang, X.; Barbosa, J.; Blomgren, P.; Bremer, M. C.; Chen, J.; Crawford, J. J.; Deng, W.; Dong, L.; Eigenbrot, C.; Gallion, S.; Hau, J.; Hu, H.; Johnson, A. R.; Katewa, A.; Kropf, J. E.; Lee, S. H.; Liu, L.; Lubach, J. W.; Macaluso, J.; Maciejewski, P.; Mitchell, S. A.; Ortwine, D. F.; DiPaolo, J.; Reif, K.; Scheerens, H.; Schmitt, A.; Wong, H.; Xiong, J.-M.; Xu, J.; Zhao, Z.; Zhou, F.; Currie, K. S.; Young, W. B. *ACS Med. Chem. Lett.* **2017**, *8*, 608–613. (c) For an overview of all clinical trials and further investigations, see: *Drug Bank*. https://go.drugbank.com/drugs/DB14785. (Accessed on 26.01.2023).

127 (a) Zheng, X.; Liang, C.; Wang, L.; Wang, B.; Liu, Y.; Feng, S.; Wu, J. Z.; Gao, L.; Feng, L.; Chen, L.; Guo, T.; Shen, H. C.; Yun, H. *J. Med. Chem.* **2018**, *61*, 10228–10241. (b) For an overview of all clinical trials and further investigations, see: *Drug Bank*. https://go.drugbank.com/drugs/DB15145. (Accessed on 26.01.2023).

128 (a) Blomgren, P.; Chandrasekhar, J.; Di Paolo, J. A.; Fung, W.; Geng, G.; Ip, C.; Jones, R.; Kropf, J. E.; Lansdon, E. B.; Lee, S.; Lo, J. R.; Mitchell, S. A.; Murray, B.; Pohlmeyer, C.; Schmitt, A.; Suekawa-Pirrone, K.; Wise, S.; Xiong, J.-M.; Xu, J.; Yu, H.; Zhao, Z.; Currie, K. S. *ACS Med. Chem. Lett.* **2020**, *11*, 506–513. (b) For an overview of all clinical trials and further investigations, see: *Drug Bank*. https://go.drugbank.com/drugs/DB14770. (Accessed on 26.01.2023).

129 (a) Griffith, D. A.; Edmonds, D. J.; Fortin, J.-P.; Kalgutkar, A. S.; Kuzmiski, J. B.; Loria, P. M.; Saxena, A. R.; Bagley, S. W.; Buckeridge, C.; Curto, J. M.; Derksen, D. R.; Dias, J. M.; Griffor, M. C.; Han, S.; Jackson, V. M.; Landis, M. S.; Lettiere, D.; Limberakis, C.; Liu, Y.; Mathiowetz, A. M.; Patel, J. C.; Piotrowski, D. W.; Price, D. A.; Ruggeri, R. B.; Tess, D. A. *J. Med. Chem.* **2022**, *65*, 8208–8226. (b) For an overview of all clinical trials and further investigations, see: *Drug Bank*. https://go.drugbank.com/drugs/DB16043. (Accessed on 26.01.2023).

130 (a) Pei, Z.; Blackwood, E.; Liu, L.; Malek, S.; Belvin, M.; Koehler, M. F. T.; Ortwine, D. F.; Chen, H.; Cohen, F.; Kenny, J. R.; Bergeron, P.; Lau, K.; Ly, C.; Zhao, X.; Estrada, A. A.; Truong, T.; Epler, J. A.; Nonomiya, J.; Trinh, L.; Sideris, S.; Lesnick, J.; Bao, L.; Vijapurkar, U.; Mukadam, S.; Tay, S.; Deshmukh, G.; Chen, Y.-H.; Ding, X.; Friedman, L. S.; Lyssikatos, J. P. *ACS Med. Chem. Lett.* **2013**, *4*, 103–107. (b) For an overview of all clinical trials and further investigations, see: *Drug Bank*. https://go.drugbank.com/drugs/DB13072. (Accessed on 26.01.2023).

131 (a) Kung, P.-P.; Bingham, P.; Brooun, A.; Collins, M.; Deng, Y.-L.; Dinh, D.; Fan, C.; Gajiwala, K. S.; Grantner, R.; Gukasyan, H. J.; Hu, W.; Huang, B.; Kania, R.; Kephart, S. E.; Krivacic, C.; Kumpf, R. A.; Khamphavong, P.; Kraus, M.; Liu, W.; Maegley, K. A.; Nguyen, L.; Ren, S.; Richter, D.; Rollins, R. A.; Sach, N.; Sharma, S.; Sherrill, J.; Spangler, J.; Stewart, A. E.; Sutton, S.; Uryu, S.; Verhelle, D.; Wang, H.; Wang, S.; Wythes, M.; Xin, S.; Yamazaki, S.; Zhu, H.; Zhu, J.; Zehnder, L.; Edwards, M. *J. Med. Chem.* **2018**, *61*, 650–665. (b) For an overview of all clinical trials and further investigations, see: *Drug Bank*. https://go.drugbank.com/drugs/DB14799. (Accessed on 26.01.2023).

132 (a) Liang, J.; Jakalian, A.; Lambrecht, M. J.; Larouche-Gauthier, R.; Huestis, M.; Ung, M. U.; Wang, X.; Yadav, A.; Zbieg, J. R.; Broccatelli, F. (Genentech Inc.) *Lactams as Cbl-b Inhibitors*, WO Patent Appl. No WO2022169997A1, **2022**. (b) Dorsch, D.; Blum, A.; Buchstaller, H.-P. (Merck Patent GmbH) *4-(Imidazo[1,2-a]pyridin-3-yl)-pyrimidine derivatives*, WO Patent Appl. No WO2021013864A1, **2021**. (c) Dai, X.; Dore, M.; Gu, X. J.; Li, L.; Liu, K. K. C.; Mak, S. Y. F.; Mi, Y.; Oyang, C.; Papillon, J.; Qi, W.; Yan, X.; Yu, Z.; Zhang, J. Y.; Zhao, K. (Novartis AG) *Quinoline Compounds and Compositions for Inhibiting EZH2*, WO Patent Appl. No WO2022033492A1, **2022**. (d) Acton, J. J., III; Chau, R.; Fuller, P. H.; Gulati, A.; Johnson, R. E.; Kattar, S.; Keylor, M. H.; Li, D. Margrey, K. A.; Morriello, G. J.; Yan, X. (Merck Sharp & Dome Corp.) *2-Aminoquinazolines as LRRK2 Inhibitors, Pharmaceutical Compositions, and Uses Thereof*, WO Patent Appl. No WO2022051337A1, **2022**. (e) Bernardelli, P.; Deprets, S.; Dubois, L.; Macor, J.; Petit, F.; Terrier, C. Bianciotto, M. (Sanofi) *Substituted Pyrrolo[2,3-D]Pyrimidines, Their Preparation and Their Therapeutic Application*, WO Patent Appl. No WO2022263472A1, **2022**. (f) Bachman, J. L.; Byun, D. H.; Clark, C. T.; Jansa, P.; Kaplan, J.; Kasun, Z. A.; Lo, J. R.; Neubig, M. E.; Stanley, N. H.; Stevens, K. L. (Gilead Sciences Inc.) *KHK Inhibitors*, WO Patent Appl. No WO2022212194A1, **2022**. (g) Bobinski, T. P.; Smith, C. R.; Marx, M. A.; Ketcham, J. M.; Burns, A. C.; Lawson, J. D.; Kulyk, S.; Kuehler, J.; Ivetac, A. (Mirati Therapuetics Inc.) *MTA-Cooperative PRMT5 Inhibitors*, WO Patent Appl. No WO2022192745A1, **2022**. (h) Kim, J. L.; Dineen, T. A.;

Guzi, T. (Blueprint Medicines Corporation) *Pyrrolotriazine Derivatives for Treating KIT- and PDGFRA-Mediated Diseases*, WO Patent Appl. No WO2020210293A1, **2020**. (i) Blom, P. M.; Housseman, C. G.; Daugan, D. A.; Dumoulin, A.; Laugeois, M.; Denis, A.; Faucher, N.; Botez, I.; Le Tiran, A.; Christense, K.; Lamotte, Y. (Les Laboratoires Servier) *New Macrocyclic LRRK2 Kinase Inhibitors*, WO Patent Appl. No WO2021224320A1, **2021**.

133 (a) Cheong, J. E.; Zaffagni, M.; Chung, I.; Xu, Y.; Wang, Y.; Jernigan, F. E.; Zetter, B. R.; Sun, L. *Eur. J. Med. Chem.* **2018**, *144*, 372–385. (b) Huddle, B. C.; Grimley, E.; Chtcherbinine, M.; Buchman, C. D.; Takahashi, C.; Debnath, B.; McGonigal, S. C.; Mao, S.; Li, S.; Felton, J.; Pan, S.; Wen, B.; Sun, D.; Neamati, N.; Buckanovich, R. J.; Hurley, T. D.; Larsen, S. D. *Eur. J. Med. Chem.* **2021**, *211*, 113060. (c) Knapinska, A. M.; Singh, C.; Drotleff, G.; Blanco, D.; Chai, C.; Schwab, J.; Herd, A.; Fields, G. B. *ChemMedChem* **2021**, *16*, 1133–1142. (d) Owens, T. D.; Brameld, K. A.; Verner, E. J.; Ton, T.; Li, X.; Zhu, J.; Masjedizadeh, M. R.; Bradshaw, J. M.; Hill, R. J.; Tam, D.; Bisconte, A.; Kim, E. O.; Francesco, M.; Xing, Y.; Shu, J.; Karr, D.; LaStant, J.; Finkle, D.; Loewenstein, N.; Haberstock-Debic, H.; Taylor, M. J.; Nunn, P.; Langrish, C. L.; Goldstein, D. M. *J. Med. Chem.* **2022**, *65*, 5300–5316. (e) Xue, D.; Xu, Y.; Kyani, A.; Roy, J.; Dai, L.; Sun, D.; Neamati, N. *J. Med. Chem.* **2022**, *65*, 3404–3419.

134 (a) Collier, P. N.; Twin, H. C.; Knegtel, R. M. A.; Boyall, D.; Brenchley, G.; Davis, C. J.; Keily, S.; Mak, C.; Miller, A.; Pierard, F.; Settimo, L.; Bolton, C. M.; Chiu, P.; Curnock, A.; Doyle, E.; Tanner, A. J.; Jimenez, J.-M. *ACS Med. Chem. Lett.* **2019**, *10*, 1134–1139. (b) Zhu, C.; Li, X.; Zhao, B.; Peng, W.; Li, W.; Fu, W. *Eur. J. Med. Chem.* **2020**, *193*, 112214.

135 Kawahata, W.; Asami, T.; Kiyoi, T.; Irie, T.; Kashimoto, S.; Furuichi, H.; Sawa, M. *J. Med. Chem.* **2021**, *64*, 14129–14141.

136 (a) Hopkins, B. T.; Bame, E.; Bajrami, B.; Black, C.; Bohnert, T.; Boiselle, C.; Burdette, D.; Burns, J. C.; Delva, L.; Donaldson, D.; Grater, R.; Gu, C.; Hoemberger, M.; Johnson, J.; Kapadnis, S.; King, K.; Lulla, M.; Ma, B.; Marx, I.; Magee, T.; Meissner, R.; Metrick, C. M.; Mingueneau, M.; Murugan, P.; Otipoby, K. L.; Polack, E.; Poreci, U.; Prince, R.; Roach, A. M.; Rowbottom, C.; Santoro, J. C.; Schroeder, P.; Tang, H.; Tien, E.; Zhang, F.; Lyssikatos, J. *J. Med. Chem.* **2022**, *65*, 1206–1224. (b) Wilson, C.; Ray, P.; Zuccotto, F.; Hernandez, J.; Aggarwal, A.; Mackenzie, C.; Caldwell, N.; Taylor, M.; Huggett, M.; Mathieson, M.; Murugesan, D.; Smith, A.; Davis, S.; Cocco, M.; Parai, M. K.; Acharya, A.; Tamaki, F.; Scullion, P.; Epemolu, O.; Riley, J.; Stojanovski, L.; Lopez-Román, E. M.; Torres-Gómez, P. A.; Toledo, A. M.; Guijarro-Lopez, L.; Camino, I.; Engelhart, C. A.; Schnappinger, D.; Massoudi, L. M.; Lenaerts, A.; Robertson, G. T.; Walpole, C.;

Matthews, D.; Floyd, D.; Sacchettini, J. C.; Read, K. D.; Encinas, L.; Bates, R. H.; Green, S. R.; Wyatt, P. G. *J. Med. Chem.* **2022**, *65*, 409–423.

137 (a) Li, D.; Sloman, D. L.; Achab, A.; Zhou, H.; McGowan, M. A.; White, C.; Gibeau, C.; Zhang, H.; Pu, Q.; Bharathan, I.; Hopkins, B.; Liu, K.; Ferguson, H.; Fradera, X.; Lesburg, C. A.; Martinot, T. A.; Qi, J.; Song, Z. J.; Yin, J.; Zhang, H.; Song, L.; Wan, B.; DAddio, S.; Solban, N.; Miller, J. R.; Zamlynny, B.; Bass, A.; Freeland, E.; Ykoruk, B.; Hilliard, C.; Ferraro, J.; Zhai, J.; Knemeyer, I.; Otte, K. M.; Vincent, S.; Sciammetta, N.; Pasternak, A.; Bennett, D. J.; Han, Y. *J. Med. Chem.* **2022**, *65*, 6001–6016. (b) Henley, Z. A.; Amour, A.; Barton, N.; Bantscheff, M.; Bergamini, G.; Bertrand, S. M.; Convery, M.; Down, K.; Dümpelfeld, B.; Edwards, C. D.; Grandi, P.; Gore, P. M.; Keeling, S.; Livia, S.; Mallett, D.; Maxwell, A.; Price, M.; Rau, C.; Reinhard, F. B. M.; Rowedder, J.; Rowland, P.; Taylor, J. A.; Thomas, D. A.; Hessel, E. M.; Hamblin, J. N. *J. Med. Chem.* **2020**, *63*, 638–655. (c) Huff, S.; Kummetha, I. R.; Zhang, L.; Wang, L.; Bray, W.; Yin, J.; Kelley, V.; Wang, Y.; Rana, T. M. *J. Med. Chem.* **2022**, *65*, 10920–10937.

138 (a) Feng, S.; Li, C.; Chen, D.; Zheng, X.; Yun, H.; Gao, L.; Shen, H. C. *Eur. J. Med. Chem.* **2017**, *138*, 1147–1157. (b) Huddle, B. C.; Grimley, E.; Buchman, C. D.; Chtcherbinine, M.; Debnath, B.; Mehta, P.; Yang, K.; Morgan, C. A.; Li, S.; Felton, J.; Sun, D.; Mehta, G.; Neamati, N.; Buckanovich, R. J.; Hurley, T. D.; Larsen, S. D. *J. Med. Chem.* **2018**, *61*, 8754–8773. (c) Lin, S.; Jin, J.; Liu, Y.; Tian, H.; Zhang, Y.; Fu, R.; Zhang, J.; Wang, M.; Du, T.; Ji, M.; Wu, D.; Zhang, K.; Sheng, L.; Li, Y.; Chen, X.; Xu, H. *J. Med. Chem.* **2019**, *62*, 8873–8879. (d) Mullarky, E.; Xu, J.; Robin, A. D.; Huggins, D. J.; Jennings, A.; Noguchi, N.; Olland, A.; Lakshminarasimhan, D.; Miller, M.; Tomita, D.; Michino, M.; Su, T.; Zhang, G.; Stamford, A. W.; Meinke, P. T.; Kargman, S.; Cantley, L. C. *Bioorg. Med. Chem. Lett.* **2019**, *29*, 2503–2510. (e) Yaragani, M.; Yadlapalli, P.; Raghavan, S.; Ayyadurai, N.; Chinnusamy, S.; Mandava, V. B. R.; Kottapalli, R. P. *J. Chem. Sci.* **2020**, *132*, 136. (f) Mlakar, L.; Lane, J.; Takihara, T.; Lim, C.; Sprachman, M. M.; Lloyd, K. R.; Wipf, P.; Feghali-Bostwick, C. *ACS Med. Chem. Lett.* **2020**, *11*, 2312–2317. (g) Jo, U.; Senatorov, I. S.; Zimmermann, A.; Saha, L. K.; Murai, Y.; Kim, S. H.; Rajapakse, V. N.; Elloumi, F.; Takahashi, N.; Schultz, C. W.; Thomas, A.; Zenke, F. T.; Pommier, Y. *Mol. Cancer Ther.* **2021**, *20*, 1431–1441. (h) Du, L.; Wang, X.; Cui, G.; Xu, B. *Bioorg. Med. Chem.* **2021**, *29*, 115878. (i) Feng, Y.; Park, H.; Bauer, L.; Ryu, J. C.; Yoon, S. O. K. *ACS Med. Chem. Lett.* **2021**, *12*, 24–29. (j) Fuerst, R.; Choi, J. Y.; Knapinska, A. M.; Cameron, M. D.; Ruiz, C.; Delmas, A.; Sundrud, M. S.; Fields, G. B.; Roush, W. R. *Bioorg. Med. Chem. Lett.* **2022**, *76*, 129014. (k) Shinde, A.; Ugale, S. R.; Nandurkar, Y.; Modak, M.; Chavan, A. P.; Mhaske, P. C. *ACS Omega* **2022**, *7*, 47096–47107.

139 For selected examples, see: (a) Vazquez, M. L.; Kaila, N.; Strohbach, J. W.; Trzupek, J. D.; Brown, M. F.; Flanagan, M. E.; Mitton-Fry, M. J.; Johnson, T. A.; TenBrink, R. E.; Arnold, E. P.; Basak, A.; Heasley, S. E.; Kwon, S.; Langille, J.; Parikh, M. D.; Griffin, S. H.; Casavant, J. M.; Duclos, B. A.; Fenwick, A. E.; Harris, T. M.; Han, S.; Caspers, N.; Dowty, M. E.; Yang, X.; Banker, M. E.; Hegen, M.; Symanowicz, P. T.; Li, L.; Wang, L.; Lin, T. H.; Jussif, J.; Clark, J. D.; Telliez, J.-B.; Robinson, R. P.; Unwalla, R. *J. Med. Chem.* **2018**, *61*, 1130–1152. (b) Guerrero, M.; Urbano, M.; Kim, E.-K.; Gamo, A. M.; Riley, S.; Abgaryan, L.; Leaf, N.; Van Orden, L. J.; Brown, S. J.; Xie, J. Y.; Porreca, F.; Cameron, M. D.; Rosen, H.; Roberts, E. *J. Med. Chem.* **2019**, *62*, 1761–1780. (c) Wellaway, C. R.; Amans, D.; Bamborough, P.; Barnett, H.; Bit, R. A.; Brown, J. A.; Carlson, N. R.; Chung, C.; Cooper, A. W. J.; Craggs, P. D.; Davis, R. P.; Dean, T. W.; Evans, J. P.; Gordon, L.; Harada, I. L.; Hirst, D. J.; Humphreys, P. G.; Jones, K. L.; Lewis, A. J.; Lindon, M. J.; Lugo, D.; Mahmood, M.; McCleary, S.; Medeiros, P.; Mitchell, D. J.; O'Sullivan, M.; Le Gall, A.; Patel, V. K.; Patten, C.; Poole, D. L.; Shah, R. R.; Smith, J. E.; Stafford, K. A. J.; Thomas, P. J.; Vimal, M.; Wall, I. D.; Watson, R. J.; Wellaway, N.; Yao, G.; Prinjha, R. K. *J. Med. Chem.* **2020**, *63*, 714–746.

140 (a) Millan, D. S.; Kayser-Bricker, K. J.; Martin, M. W.; Talbot, A. C.; Schiller, S. E. R.; Herbertz, T.; Williams, G. L.; Luke, G. P.; Hubbs, S.; Alvarez Morales, M. A.; Cardillo, D.; Troccolo, P.; Mendes, R. L.; McKinnon, C. *ACS Med. Chem. Lett.* **2017**, *8*, 847–852. (b) Bagal, S. K.; Omoto, K.; Blakemore, D. C.; Bungay, P. J.; Bilsland, J. G.; Clarke, P. J.; Corbett, M. S.; Cronin, C. N.; Cui, J. J.; Dias, R.; Flanagan, N. J.; Greasley, S. E.; Grimley, R.; Johnson, E.; Fengas, D.; Kitching, L.; Kraus, M. L.; McAlpine, I.; Nagata, A.; Waldron, G. J.; Warmus, J. S. *J. Med. Chem.* **2019**, *62*, 247–265.

141 (a) Hugelshofer, C. L.; Magauer, T. *Chem. Eur. J.* **2016**, *22*, 15125–15136. (b) Guo, Y.-A.; Lee, W.; Krische, M. J. *Chem. Eur. J.* **2017**, *23*, 2557–2559.

142 Reboul, M. *Ann. Chim.* **1878**, *14*, 495–497.

143 (a) Searles, S.; Gortatowski, M. J. *J. Am. Chem. Soc.* **1953**, *75*, 3030–3031. (b) Searles, S.; Nickerson, R. G.; Witsiepe, W. K. *J. Org. Chem.* **1959**, *24*, 1839–1844.

144 Wuitschik, G. Oxetanes in drug discovery, PhD Thesis, ETH Zürich, Switzerland, 2008.

145 (a) Vigo, D.; Stasi, L.; Gagliardi, S. *Tetrahedron Lett.* **2011**, *52*, 565–567. (b) Boyd, S.; Davies, C. D. *Tetrahedron Lett.* **2014**, *55*, 4117–4119.

146 (a) Chang, W.; Du, J.; Rachakonda, S.; Ross, B. S.; Convers-Reignier, S.; Yau, W. T.; Pons, J.-F.; Murakami, E.; Bao, H.; Steuer, H. M.; Furman, P. A.; Otto, M. J.; Sofia, M. J. *Bioorg. Med. Chem. Lett.* **2010**, *20*, 4539–4543. (b) Jonckers, T. H. M.; Vandyck, K.; Vandekerckhove, L.; Hu, L.; Tahri, A.; Van Hoof, S.; Lin, T.-I.; Vijgen, L.; Berke, J. M.; Lachau-Durand, S.; Stoops, B.; Leclercq, L.; Fanning, G.; Samuelsson, B.; Nilsson, M.;

Rosenquist, Å.; Simmen, K.; Raboisson, P. *J. Med. Chem.* **2014**, *57*, 1836–1844. (c) Komsta, Z.; Mayes, B.; Moussa, A.; Shelbourne, M.; Stewart, A.; Tyrrell, A. J.; Wallis, L. L.; Weymouth-Wilson, A. C.; Yurek-George, A. *Tetrahedron Lett.* **2014**, *55*, 6216–6219. (d) Jonckers, T. H. M.; Tahri, A.; Vijgen, L.; Berke, J. M.; Lachau-Durand, S.; Stoops, B.; Snoeys, J.; Leclercq, L.; Tambuyzer, L.; Lin, T.-I.; Simmen, K.; Raboisson, P. *J. Med. Chem.* **2016**, *59*, 5790–5798. (e) Hazelard, D.; Compain, P. *Org. Biomol. Chem.* **2017**, *15*, 3806–3827.

147 (a) Geary, G. C.; Nortcliffe, A.; Pearce, C. A.; Hamza, D.; Jones, G.; Moody, C. J. *Bioorg. Med. Chem.* **2018**, *26*, 791–797. (b) Feskov, I. O.; Chernykh, A. V.; Kuchkovska, Y. O.; Daniliuc, C. G.; Kondratov, I. S.; Grygorenko, O. O. *J. Org. Chem.* **2019**, *84*, 1363–1371. (c) Rulev, A. Y.; Romanov, A. R.; Kondrashov, E. V.; Ushakov, I. A.; Muzalevskiy, V. M.; Nenajdenko, V. G. *J. Fluor. Chem.* **2019**, *227*, 109366. (d) Zhang, X.; Zhang, Q.; Li, L.; Cao, S.; Liu, Z.; Zanoni, G.; Ning, Y.; Wu, Y. *Org. Lett.* **2021**, *23*, 3674–3679. (e) Roberts, D. D.; McLaughlin, M. G. *Chem. Commun.* **2022**, *58*, 8376–8379.

148 Huang, S.; Pink, M.; Ngendahimana, T.; Rajca, S.; Eaton, G. R.; Eaton, S. S.; Rajca, A. *J. Org. Chem.* **2021**, *86*, 13636–13643.

149 Ye, L.; He, W.; Zhang, L. *J. Am. Chem. Soc.* **2010**, *132*, 8550–8551.

150 Thompson, S. J.; Thach, D. Q.; Dong, G. *J. Am. Chem. Soc.* **2015**, *137*, 11586–11589.

151 Li, J.; Hu, W.; Li, C.; Yang, S.; Wu, W.; Jiang, H. *Org. Chem. Front.* **2017**, *4*, 373–376.

152 Willand-Charnley, R.; Puffer, B. W.; Dussault, P. H. *J. Am. Chem. Soc.* **2014**, *136*, 5821–5823.

153 (a) Ye, Y.; Zheng, C.; Fan, R. *Org. Lett.* **2009**, *11*, 3156–3159. (b) Miao, C.-B.; Zhang, M.; Tian, Z.-Y.; Xi, H.-T.; Sun, X.-Q.; Yang, H.-T. *J. Org. Chem.* **2011**, *76*, 9809–9816.

154 Kerschgens, I.; Rovira, A. R.; Sarpong, R. *J. Am. Chem. Soc.* **2018**, *140*, 9810–9813.

155 Demoret, R. M.; Baker, M. A.; Ohtawa, M.; Chen, S.; Lam, C. C.; Khom, S.; Roberto, M.; Forli, S.; Houk, K. N.; Shenvi, R. A. *J. Am. Chem. Soc.* **2020**, *142*, 18599–18618.

156 Gersbach, P.; Jantsch, A.; Feyen, F.; Scherr, N.; Dangy, J.-P.; Pluschke, G.; Altmann, K.-H. *Chem. Eur. J.* **2011**, *17*, 13017–13031.

157 Yadav, J. S.; Gyanchander, E.; Das, S. *Tetrahedron Lett.* **2014**, *55*, 3996–3998.

158 (a) Morgan, K. F.; Hollingsworth, I. A.; Bull, J. A. *Chem. Commun.* **2014**, *50*, 5203–5205. (b) Morgan, K. F.; Hollingsworth, I. A.; Bull, J. A. *Org. Biomol. Chem.* **2015**, *13*, 5265–5272. (c) Morgan, K.; Doran, R.; Croft, R.; Hollingsworth, I.; Bull, J. *Synlett* **2015**, *27*, 106–110.

159 (a) Davis, O. A.; Bull, J. A. *Angew. Chem. Int. Ed.* **2014**, *53*, 14230–14234. (b) Davis, O. A.; Croft, R. A.; Bull, J. A. *Chem. Commun.* **2015**, *51*, 15446–15449.

160 Nicolle, S. M.; Nortcliffe, A.; Bartrum, H. E.; Lewis, W.; Hayes, C. J.; Moody, C. J. *Chem. Eur. J.* **2017**, *23*, 13623–13627.

161 E. Paternò, G. Chieffi, *Gazz. Chim. Ital.* **1909**, *39*, 341–361.

162 (a) Pangaribowo, D. A.; Abe, M. *Org. Biomol. Chem.* **2020**, *18*, 4962–4970. (b) Michalska, W. Z.; Halcovitch, N. R.; Coote, S. C. *Chem. Commun.* **2023**, *59*, 784–787.

163 For applications to total synthesis research programs, see: (a) Boxall, R.; Grainger, R.; Aricò, C.; Ferris, L. *Synlett* **2008**, *2008*, 25–28. (b) Valiulin, R. A.; Kutateladze, A. G. *Org. Lett.* **2009**, *11*, 3886–3889. (c) Huang, C.; Yu, H.; Miao, Z.; Zhou, J.; Wang, S.; Fun, H.-K.; Xu, J.; Zhang, Y. *Org. Biomol. Chem.* **2011**, *9*, 3629–3631. (d) Pepper, H. P.; Kuan, K. K. W.; George, J. H. *Org. Lett.* **2012**, *14*, 1524–1527.

164 (a) Gomez Fernandez, M. A.; Lefebvre, C.; Sudau, A.; Genix, P.; Vors, J.; Abe, M.; Hoffmann, N. *Chem. Eur. J.* **2021**, *27*, 15722–15729. (b) Zhang, Y.; Niu, Y.; Guo, Y.; Wang, J.; Zhang, Y.; Liu, S.; Shen, X. *Angew. Chem. Int. Ed.* **2022**, *61*, e202212201.

165 (a) Rykaczewski, K. A.; Schindler, C. S. *Org. Lett.* **2020**, *22*, 6516–6519. (b) Zheng, J.; Dong, X.; Yoon, T. P. *Org. Lett.* **2020**, *22*, 6520–6525.

166 D'Annibale, A.; D'Auria, M.; Prati, F.; Romagnoli, C.; Stoia, S.; Racioppi, R.; Viggiani, L. *Tetrahedron* **2013**, *69*, 3782–3795.

167 (a) Vogt, F.; Jödicke, K.; Schröder, J.; Bach, T. *Synthesis* **2009**, 4268–4273. (b) Kassir, A. F.; Ragab, S. S.; Nguyen, T. A. M.; Charnay-Pouget, F.; Guillot, R.; Scherrmann, M.-C.; Boddaert, T.; Aitken, D. J. *J. Org. Chem.* **2016**, *81*, 9983–9991.

168 (a) Fukuyama, T.; Kajihara, Y.; Hino, Y.; Ryu, I. *J. Flow Chem.* **2012**, *1*, 40–45. (b) Terao, K.; Nishiyama, Y.; Kakiuchi, K. *J. Flow Chem.* **2015**, *4*, 35–39. (c) Ralph, M.; Ng, S.; Booker-Milburn, K. I. *Org. Lett.* **2016**, *18*, 968–971. (d) Franceschi, P.; Mateos, J.; Vega-Peñaloza, A.; Dell'Amico, L. *Eur. J. Org. Chem.* **2020**, *2020*, 6718–6722.

169 (a) Ma, X.; Xia, Y. *Angew. Chem. Int. Ed.* **2014**, *53*, 2592–2596. (b) Bechtella, L.; Kirschbaum, C.; Cosset, M.; Clodic, G.; Matheron, L.; Bolbach, G.; Sagan, S.; Walrant, A.; Sachon, E. *Anal. Chem.* **2019**, *91*, 9102–9110. (c) Li, H.; Cao, W.; Ma, X.; Xie, X.; Xia, Y.; Ouyang, Z. *J. Am. Chem. Soc.* **2020**, *142*, 3499–3505. (d) Feng, G.; Hao, Y.; Wu, L.; Chen, S. *Chem. Sci.* **2020**, *11*, 7244–7251. (e) Ma, X.; Zhang, W.; Li, Z.; Xia, Y.; Ouyang, Z. *Acc. Chem. Res.* **2021**, *54*, 3873–3882.

170 (a) Brogaard, R. Y.; Schalk, O.; Boguslavskiy, A. E.; Enright, G. D.; Hopf, H.; Raev, V.; Tarcoveanu, E.; Sølling, T. I.; Stolow, A. *Phys. Chem. Chem. Phys.* **2012**, *14*, 8572–8580. (b) Harris, S. J.; Murdock, D.; Grubb, M. P.; Clark, I. P.; Greetham, G. M.; Towrie, M.; Ashfold, M. N. R. *J. Phys. Chem. A* **2014**, *118*, 10240–10245. (c) Mateos, J.;

Rigodanza, F.; Costa, P.; Natali, M.; Vega-Peñaloza, A.; Fresch, E.; Collini, E.; Bonchio, M.; Sartorel, A.; Dell'Amico, L. *Nat. Synth.* **2022**, *2*, 26–36.

171 For representative examples, see: (a) Ludwig, J. R.; Zimmerman, P. M.; Gianino, J. B.; Schindler, C. S. *Nature* **2016**, *533*, 374–379. (b) McAtee, C. C.; Riehl, P. S.; Schindler, C. S. *J. Am. Chem. Soc.* **2017**, *139*, 2960–2963. (c) Ludwig, J. R.; Watson, R. B.; Nasrallah, D. J.; Gianino, J. B.; Zimmerman, P. M.; Wiscons, R. A.; Schindler, C. S. *Science* **2018**, *361*, 1363–1369. (d) Albright, H.; Riehl, P. S.; McAtee, C. C.; Reid, J. P.; Ludwig, J. R.; Karp, L. A.; Zimmerman, P. M.; Sigman, M. S.; Schindler, C. S. *J. Am. Chem. Soc.* **2019**, *141*, 1690–1700.

172 Flores, D. M.; Schmidt, V. A. *J. Am. Chem. Soc.* **2019**, *141*, 8741–8745.

173 (a) Saunders, L. B.; Miller, S. J. *ACS Catal.* **2011**, *1*, 1347–1350. (b) Wang, T.; Chen, X.-Y.; Ye, S. *Tetrahedron Lett.* **2011**, *52*, 5488–5490. (c) Zhao, Q.-Y.; Huang, L.; Wei, Y.; Shi, M. *Adv. Synth. Catal.* **2012**, *354*, 1926–1932.

174 For recent examples, see: (a) Burkhard, J. A.; Guérot, C.; Knust, H.; Rogers-Evans, M.; Carreira, E. M. *Org. Lett.* **2010**, *12*, 1944–1947. (b) Cai, Y.; Liu, C.; Liu, G.; Li, C.; Jiang, H.; Zhu, C. *Org. Biomol. Chem.* **2022**, *20*, 1500–1509. (c) Ref. 95.

175 Butova, E. D.; Barabash, A. V.; Petrova, A. A.; Kleiner, C. M.; Schreiner, P. R.; Fokin, A. A. *J. Org. Chem.* **2010**, *75*, 6229–6235.

176 Sone, T.; Lu, G.; Matsunaga, S.; Shibasaki, M. *Angew. Chem. Int. Ed.* **2009**, *48*, 1677–1680.

177 Sun, S.-Q.; Chen, S.-L. *J. Phys. Chem. Lett.* **2020**, *11*, 6812–6818.

178 (a) Rodina, L. L.; Malashikhin, S. A.; Galkina, O. S.; Nikolaev, V. A. *Helv. Chim. Acta* **2009**, *92*, 1990–1998. (b) Nikolaev, V. A.; Galkina, O. S.; Sieler, J.; Rodina, L. L. *Tetrahedron Lett.* **2010**, *51*, 2713–2716. (c) Rodina, L. L.; Baranovskii, V. I.; Galkina, O. S.; Nikolaev, V. A.; Tonogina, N. L.; Povolotskiy, A. V. *J. Org. Chem.* **2017**, *82*, 11399–11405.

179 Qi, D.; Bai, J.; Zhang, H.; Li, B.; Song, Z.; Ma, N.; Guo, L.; Song, L.; Xia, W. *Green Chem.* **2022**, *24*, 5046–5051.

180 (a) Coppi, D. I.; Salomone, A.; Perna, F. M.; Capriati, V. *Chem. Commun.* **2011**, *47*, 9918–9920. (b) Degennaro, L.; Nagaki, A.; Moriwaki, Y.; Romanazzi, G.; Dell'Anna, M. M.; Yoshida, J.; Luisi, R. *Open Chem.* **2016**, *14*, 377–382.

181 Capriati, V.; Florio, S.; Luisi, R. *Eur. J. Org. Chem.* **2014**, *2014*, 5397–5417.

182 (a) Coppi, D. I.; Salomone, A.; Perna, F. M.; Capriati, V. *Angew. Chem. Int. Ed.* **2012**, *51*, 7532–7536. (b) Rouquet, G.; Blakemore, D. C.; Ley, S. V. *Chem. Commun.* **2014**, *50*, 8908–8911.

183 Zhang, C.; Pei, H.; He, J.; Zhu, J.; Li, W.; Niu, T.; Xiang, M.; Chen, L. *Eur. J. Med. Chem.* **2019**, *169*, 121–143.

184 Estrada, A. A.; Chan, B. K.; Baker-Glenn, C.; Beresford, A.; Burdick, D. J.; Chambers, M.; Chen, H.; Dominguez, S. L.; Dotson, J.; Drummond, J.; Flagella, M.; Fuji, R.; Gill, A.; Halladay, J.; Harris, S. F.; Heffron, T. P.; Kleinheinz, T.; Lee, D. W.; Pichon, C. E. Le; Liu, X.; Lyssikatos, J. P.; Medhurst, A. D.; Moffat, J. G.; Nash, K.; Scearce-Levie, K.; Sheng, Z.; Shore, D. G.; Wong, S.; Zhang, S.; Zhang, X.; Zhu, H.; Sweeney, Z. K. *J. Med. Chem.* **2014**, *57*, 921–936.

185 Nassoy, A.-C. M. A.; Raubo, P.; Harrity, J. P. A. *Chem. Commun.* **2015**, *51*, 5914–5916.

186 DeRatt, L. G.; Lawson, E. C.; Kumar, K.; Hwang, S. S.; DesJarlais, R. L.; Kuduk, S. D. *Org. Lett.* **2020**, *22*, 5828–5832.

187 Boutureira, O.; Martínez-Sáez, N.; Brindle, K. M.; Neves, A. A.; Corzana, F.; Bernardes, G. J. L. *Chem. Eur. J.* **2017**, *23*, 6483–6489.

188 Zhang, X.; Yang, C. *Adv. Synth. Catal.* **2015**, *357*, 2721–2727.

189 Molander, G. A.; Traister, K. M.; O'Neill, B. T. *J. Org. Chem.* **2015**, *80*, 2907–2911.

190 Bhonde, V. R.; O'Neill, B. T.; Buchwald, S. L. *Angew. Chem. Int. Ed.* **2016**, *55*, 1849–1853.

191 (a) Ludwig, J. R.; Simmons, E. M.; Wisniewski, S. R.; Chirik, P. J. *Org. Lett.* **2021**, *23*, 625–630. (b) Mills, L. R.; Gygi, D.; Ludwig, J. R.; Simmons, E. M.; Wisniewski, S. R.; Kim, J.; Chirik, P. J. *ACS Catal.* **2022**, *12*, 1905–1918.

192 Geden, J. V.; Beasley, B. O.; Clarkson, G. J.; Shipman, M. *J. Org. Chem.* **2013**, *78*, 12243–12250.

193 Ding, R.; Wolf, C. *Org. Lett.* **2018**, *20*, 892–895.

194 Phelan, J. P.; Ellman, J. A. *Adv. Synth. Catal.* **2016**, *358*, 1713–1718.

195 Phelan, J. P.; Patel, E. J.; Ellman, J. A. *Angew. Chem. Int. Ed.* **2014**, *53*, 11329–11332.

196 Kang, T.; Erbay, T. G.; Xu, K. L.; Gallego, G. M.; Burtea, A.; Nair, S. K.; Patman, R. L.; Zhou, R.; Sutton, S. C.; McAlpine, I. J.; Liu, P.; Engle, K. M. *ACS Catal.* **2020**, *10*, 13075–13083.

197 Jones, B.; Proud, M.; Sridharan, V. *Tetrahedron Lett.* **2016**, *57*, 2811–2813.

198 Deng, H.; Jia, R.; Yang, W.-L.; Yu, X.; Deng, W.-P. *Chem. Commun.* **2019**, *55*, 7346–7349.

199 Chalyk, B. A.; Butko, M. V.; Yanshyna, O. O.; Gavrilenko, K. S.; Druzhenko, T. V.; Mykhailiuk, P. K. *Chem. Eur. J.* **2017**, *23*, 16782–16786.

200 Monleón, A.; Glaus, F.; Vergura, S.; Jørgensen, K. A. *Angew. Chem. Int. Ed.* **2016**, *55*, 2478–2482.

201 For recent selected examples from the patent literature, see: (a) Billen, S.; Curtis, M.; Ewin, R. A.; Goodwin, R. M.; Johnson, P. D.; Johnson, T. A.; Kyne, G. M.; Maddux, T. M.; Sheehan, S. M. K.; Vairagoundar, R. (Zoetis LLC) *Phenicol Antibacterial Agents*, US Patent Appl. No US2014088046A1, **2014**. (b) Heimann, A.; Dahmann, G.; Grundl, M.; Mueller, S. G.; Wellenzohn, B. (Boehringer Ingelheim Int.) *Piperazine Derivatives and their use as Positive Allosteric Modulators of MGLU5 Receptors*, WO Patent Appl. No WO2013087805 A1, **2013**. (c) Luo, G.; Chem, L.; Dubowchik, G. M.; Jacutin-Porte, S. E.; Vrudhula, V. M.; Pan, S.; Sivaprakasam, P.; Macor, J. E. (Bristol-Myers Squibb) *GSK-3 Inhibitors*, WO Patent Appl. No WO201569594A1, **2015**. (d) Skerratt, A. E.; Bagal, S. K.; Swain, N. A.; Omoto, K.; Andrews, M. D. (Pfizer Ltd.) *N-Acylpiperidine Ether Tropomyosin-Related Kinase Inhibitors*, WO Patent Appl. No WO2015092610A1, **2015**.

202 Croft, R. A.; Mousseau, J. J.; Choi, C.; Bull, J. A. *Chem. Eur. J.* **2016**, *22*, 16271–16276.

203 Croft, R. A.; Mousseau, J. J.; Choi, C.; Bull, J. A. *Tetrahedron* **2018**, *74*, 5427–5435.

204 Rojas, J. J. Exploiting Brønsted Acid Catalysis on Oxetan-3-ols as Versatile Substrates, MRes Thesis, Imperial College London, **2018**.

205 Saejong, P; Rojas, J. J.; Denis, C.; White, A. J. P.; Voisin-Chiret, A. S.; Choi, C.; Bull, J. A. *manuscript submitted* **2023**.

206 Denis, C.; Dubois, M. A. J.; Voisin-Chiret, A. S.; Bureau, R.; Choi, C.; Mousseau, J. J.; Bull, J. A. *Org. Lett.* **2019**, *21*, 300–304.

207 Dubois, M. A. J.; Lazaridou, A.; Choi, C.; Mousseau, J. J.; Bull, J. A. *J. Org. Chem.* **2019**, *84*, 5943–5956.

208 Croft, R. A.; Dubois, M. A. J.; Boddy, A. J.; Denis, C.; Lazaridou, A.; Voisin-Chiret, A. S.; Bureau, R.; Choi, C.; Mousseau, J. J.; Bull, J. A. *Eur. J. Org. Chem.* **2019**, *2019*, 5385–5395.

209 Li, P.; Zbieg, J. R.; Terrett, J. A. *ACS Catal.* **2021**, *11*, 10997–11004.

210 Croft, R. A. Exploring Oxetane Isosteres for Drug Discovery through the Catalytic Generation of Oxetanyl Carbocations, PhD Thesis, Imperial College London, **2018**.

211 Dubois, M. A. J. New 3,3-disubstituted oxetanes and azetidines: Synthesis, evaluation and new opportunities for drug discovery, PhD Thesis, Imperial College London, **2020**.

212 Rojas, J. J.; Croft, R. A.; Sterling, A. J.; Briggs, E. L.; Antermite, D.; Schmitt, D. C.; Blagojevic, L.; Haycock, P.; White, A. J. P.; Duarte, F.; Choi, C.; Mousseau, J. J.; Bull, J. A. *Nat. Chem.* **2022**, *14*, 160–169.

213 Rojas, J. J.; Bull, J. A. 3-(4-Methoxyphenyl)-3-oxetanesulfonyl Fluoride. In *Encyclopedia of Reagents for Organic Synthesis*; Wiley, 2023; pp 1–3.

214 Rojas, J. J.; Bull, J. A. *Chimia* **2023**, DOI: 10.2533/chimia.2023.192.

215 (a) Steinkopf, W. *J. für Prakt. Chemie* **1927**, *117*, 1–82. (b) Steinkopf, W.; Jaeger, P. *J. für Prakt. Chemie* **1930**, *128*, 63–88. (c) Lange, W.; Müller, E. *Chem. Ber.* **1930**, *63*, 2653–2657. (d) Davies, W.; Dick, J. H. *J. Chem. Soc.* **1932**, 2042–2046. (e) Davies, W.; Dick, J. H. *J. Chem. Soc.* **1932**, 483–486.

216 Dong, J.; Krasnova, L.; Finn, M. G.; Sharpless, K. B. *Angew. Chem. Int. Ed.* **2014**, *53*, 9430–9448.

217 Measured in SO_2F_2 and SO_2Cl_2, respectively: Wray, K. L.; Feldman, E. V. *J. Chem. Phys.* **1971**, *54*, 3445–3449.

218 For representative examples, see: (a) Gahtory, D.; Sen, R.; Pujari, S.; Li, S.; Zheng, Q.; Moses, J. E.; Sharpless, K. B.; Zuilhof, H. *Chem. Eur. J.* **2018**, *24*, 10550–10556. (b) Randall, J. D.; Eyckens, D. J.; Stojcevski, F.; Francis, P. S.; Doeven, E. H.; Barlow, A. J.; Barrow, A. S.; Arnold, C. L.; Moses, J. E.; Henderson, L. C. *ChemPhysChem* **2018**, *19*, 3176–3181. (c) Li, S.; Li, G.; Gao, B.; Pujari, S. P.; Chen, X.; Kim, H.; Zhou, F.; Klivansky, L. M.; Liu, Y.; Driss, H.; Liang, D.-D.; Lu, J.; Wu, P.; Zuilhof, H.; Moses, J.; Sharpless, K. B. *Nat. Chem.* **2021**, *13*, 858–867.

219 (a) Abdul Fattah, T.; Saeed, A.; Albericio, F. *J. Fluor. Chem.* **2018**, *213*, 87–112. (b) Chinthakindi, P. K.; Arvidsson, P. I. *Eur. J. Org. Chem.* **2018**, *2018*, 3648–3666. (c) Barrow, A. S.; Smedley, C. J.; Zheng, Q.; Li, S.; Dong, J.; Moses, J. E. *Chem. Soc. Rev.* **2019**, *48*, 4731–4758.

220 (a) Zhong, T.; Chen, Z.; Yi, J.; Lu, G.; Weng, J. *Chinese Chem. Lett.* **2021**, *32*, 2736–2750. (b) Lou, T. S.-B.; Willis, M. C. *Nat. Rev. Chem.* **2022**, *6*, 146–162. (c) He, F.-S.; Li, Y.; Wu, J. *Org. Chem. Front.* **2022**, *9*, 5299–5305. (d) Zeng, D.; Deng, W.; Jiang, X. *Chem. Eur. J.* **2023**, *13*, 287–288.

221 (a) Baker, B. R. *Acc. Chem. Res.* **1969**, *2*, 129–136. (b) Narayanan, A.; Jones, L. H. *Chem. Sci.* **2015**, *6*, 2650–2659. (c) Pascali, G.; Matesic, L.; Zhang, B.; King, A. T.; Robinson, A. J.; Ung, A. T.; Fraser, B. H. *EJNMMI Radiopharm. Chem.* **2017**, *2*, 9. (d) Carneiro, S. N.; Khasnavis, S. R.; Lee, J.; Butler, T. W.; Majmudar, J. D.; am Ende, C. W.; Ball, N. D. *Org. Biomol. Chem.* **2023**, *21*, 1356–1372.

222 Lee, C.; Cook, A. J.; Elisabeth, J. E.; Friede, N. C.; Sammis, G. M.; Ball, N. D. *ACS Catal.* **2021**, *11*, 6578–6589.

223 C. M. Suter, *The Organic Chemistry of Sulfur*, Wiley, New York, 1944, pp. 453–572.

224 Nambo, M.; Maekawa, Y.; Crudden, C. M. *ACS Catal.* **2022**, *12*, 3013–3032.

225 (a) Smith, J. M.; Dixon, J. A.; DeGruyter, J. N.; Baran, P. S. *J. Med. Chem.* **2019**, *62*, 2256–2264. (b) Aziz, J.; Hamze, A. *Org. Biomol. Chem.* **2020**, *18*, 9136–9159.

226 Chatelain, P.; Muller, C.; Sau, A.; Brykczyńska, D.; Bahadori, M.; Rowley, C. N.; Moran, J. *Angew. Chem. Int. Ed.* **2021**, *60*, 25307–25312.

227 Zhang, G.; Guan, C.; Zhao, Y.; Miao, H.; Ding, C. *New J. Chem.* **2022**, *46*, 3560–3564.

228 In accordance with the Suzuki–Miyaura coupling of aryl sulfones: Chatelain, P.; Sau, A.; Rowley, C. N.; Moran, J. *Angew. Chem. Int. Ed.* **2019**, *58*, 14959–14963.

229 (a) Giel, M.; Smedley, C. J.; Mackie, E. R. R.; Guo, T.; Dong, J.; Soares da Costa, T. P.; Moses, J. E. *Angew. Chem. Int. Ed.* **2020**, *59*, 1181–1186. (b) Yang, W.-F.; Shu, T.; Chen, H.-R.; Qin, H.-L.; Tang, H. *Org. Biomol. Chem.* **2022**, *20*, 3506–3510. (c) Sandeep, K.; Sanjeeva Kumar, A.; Kumara Swamy, K. C. *Eur. J. Org. Chem.* **2022**, *2022*, e202201037. (d) Sandeep, K.; Sanjeeva Kumar, A.; Qureshi, A. A.; Kumara Swamy, K. C. *Synthesis* **2022**, *54*, 4111–4119.

230 (a) Kagabu, S.; Hara, K.; Takahashi, J. *J. Chem. Soc. Chem. Commun.* **1991**, 408–410. (b) Jiang, Y.; Fang, W.-Y.; Rakesh, K. P.; Qin, H.-L. *Org. Chem. Front.* **2020**, *7*, 1696–1702.

231 (a) Van der Puy, M. *J. Org. Chem.* **1988**, *53*, 4398–4401. (b) Yazawa, N.; Suzuki, H.; Yoshida, Y.; Furusawa, O.; Kimura, Y. *Chem. Lett.* **1989**, *18*, 2213–2216.

232 (a) Chen, Q.; Wu, S. *J. Org. Chem.* **1989**, *54*, 6140–6140. (b) Tian, F.; Kruger, V.; Bautista, O.; Duan, J.-X.; Li, A.-R.; Dolbier, W. R.; Chen, Q.-Y. *Org. Lett.* **2000**, *2*, 563–564. (c) Zhang, C.-P.; Chen, Q.-Y.; Guo, Y.; Xiao, J.-C.; Gu, Y.-C. *Coord. Chem. Rev.* **2014**, *261*, 28–72.

233 Kielbasinski, P.; Drabowicz, J.; Mikolajczyk, M. *J. Org. Chem.* **1982**, *47*, 4806–4808.

234 Olah, G. A.; Narang, S. C.; Field, L. D.; Karpeles, R. *J. Org. Chem.* **1981**, *46*, 2408–2410.

235 (a) Shimizu, M.; Nakahara, Y.; Yoshioka, H. *Tetrahedron Lett.* **1985**, *26*, 4207–4210. (b) Bennua-Skalmowski, B.; Vorbrüggen, H. *Tetrahedron Lett.* **1995**, *36*, 2611–2614. (c) Nielsen, M. K.; Ugaz, C. R.; Li, W.; Doyle, A. G. *J. Am. Chem. Soc.* **2015**, *137*, 9571–9574. (d) Nielsen, M. K.; Ahneman, D. T.; Riera, O.; Doyle, A. G. *J. Am. Chem. Soc.* **2018**, *140*, 5004–5008. (e) Shields, B. J.; Stevens, J.; Li, J.; Parasram, M.; Damani, F.; Alvarado, J. I. M.; Janey, J. M.; Adams, R. P.; Doyle, A. G. *Nature* **2021**, *590*, 89–96. (f) Żurański, A. M.; Gandhi, S. S.; Doyle, A. G. *J. Am. Chem. Soc.* **2023**, DOI: 10.1021/jacs.2c13093.

236 Meng, G.; Guo, T.; Ma, T.; Zhang, J.; Shen, Y.; Sharpless, K. B.; Dong, J. *Nature* **2019**, *574*, 86–89.

237 (a) Krasheninina, O. A.; Thaler, J.; Erlacher, M. D.; Micura, R. *Angew. Chem. Int. Ed.* **2021**, *60*, 6970–6974. (b) Kofsky, J. M.; Daskhan, G. C.; Macauley, M. S.; Capicciotti, C. J. *Eur. J. Org. Chem.* **2022**, e202200108.

238 Pandiakumar, A. K.; Sarma, S. P.; Samuelson, A. G. *Tetrahedron Lett.* **2014**, *55*, 2917–2920.

239 Smedley, C. J.; Barrow, A. S.; Spiteri, C.; Giel, M.-C.; Sharma, P.; Moses, J. E. *Chem. Eur. J.* **2017**, *23*, 9990–9995.

240 For the use of sulfuryl fluoride as amide coupling agent, see: Wang, S.-M.; Zhao, C.; Zhang, X.; Qin, H.-L. *Org. Biomol. Chem.* **2019**, *17*, 4087–4101.

241 (a) Davies, A. T.; Curto, J. M.; Bagley, S. W.; Willis, M. C. *Chem. Sci.* **2017**, *8*, 1233–1237. (b) Tribby, A. L.; Rodríguez, I.; Shariffudin, S.; Ball, N. D. *J. Org. Chem.* **2017**, *82*, 2294–2299. (c) Lo, P. K. T.; Chen, Y.; Willis, M. C. *ACS Catal.* **2019**, *9*, 10668–10673. (d) Lou, T. S.-B.; Bagley, S. W.; Willis, M. C. *Angew. Chem. Int. Ed.* **2019**, *58*, 18859–18863.

242 (a) Pu, Y.-M.; Christesen, A.; Ku, Y.-Y. *Tetrahedron Lett.* **2010**, *51*, 418–421. (b) Veisi, H. *Bull Korean Chem. Soc.* **2012**, *33*, 383–386.

243 Fahrney, D. E.; Gold, A. M. *J. Am. Chem. Soc.* **1963**, *85*, 997–1000.

244 According to the Drug Bank database (https://go.drugbank.com). Wishart, D. S. *Nucleic Acids Res.* **2006**, *34*, D668–D672.

245 Hamzik, P. J.; Brubaker, J. D. *Org. Lett.* **2010**, *12*, 1116–1119.

246 Jung, H. H.; Buesking, A. W.; Ellman, J. A. *Org. Lett.* **2011**, *13*, 3912–3915.

247 Kolahdouzan, K.; Khalaf, R.; Grandner, J. M.; Chen, Y.; Terrett, J. A.; Huestis, M. P. *ACS Catal.* **2020**, *10*, 405–411.

248 (a) Mukherjee, P.; Woroch, C. P.; Cleary, L.; Rusznak, M.; Franzese, R. W.; Reese, M. R.; Tucker, J. W.; Humphrey, J. M.; Etuk, S. M.; Kwan, S. C.; am Ende, C. W.; Ball, N. D. *Org. Lett.* **2018**, *20*, 3943–3947. (b) Mahapatra, S.; Woroch, C. P.; Butler, T. W.; Carneiro, S. N.; Kwan, S. C.; Khasnavis, S. R.; Gu, J.; Dutra, J. K.; Vetelino, B. C.; Bellenger, J.; am Ende, C. W.; Ball, N. D. *Org. Lett.* **2020**, *22*, 4389–4394.

249 Bär, R. M.; Gross, P. J.; Nieger, M.; Bräse, S. *Chem. Eur. J.* **2020**, *26*, 4242–4245.

250 Leech, M. C.; Lam, K. *Nat. Rev. Chem.* **2022**, *6*, 275–286.

251 Gagne, R. R.; Koval, C. A.; Lisensky, G. C. *Inorganic Chemistry*. **1980**, *19*, 2854–2855.

252 Pavlishchuk, V. V.; Addison, A. W. *Inorganica Chim. Acta* **2000**, *298*, 97–102.

253 Cacchi, S.; Ciattini, P. G.; Morera, E.; Ortar, G. *Tetrahedron Lett.* **1986**, *27*, 5541–5544.

254 Meister, E. In *Grundpraktikum Physikalische Chemie*, 2nd ed., vdf UTB, Zürich, 2012.

255 Han, B.; Khasnavis, S. R.; Nwerem, M.; Bertagna, M.; Ball, N. D.; Ogba, O. M. *Inorg. Chem.* **2022**, *61*, 9746–9755.

256 Wei, M.; Liang, D.; Cao, X.; Luo, W.; Ma, G.; Liu, Z.; Li, L. *Angew. Chem. Int. Ed.* **2021**, *60*, 7397–7404.

257 Smedley, C. J.; Homer, J. A.; Gialelis, T. L.; Barrow, A. S.; Koelln, R. A.; Moses, J. E. *Angew. Chem. Int. Ed.* **2022**, *61*, 2–10.

258 Short, M. A.; Shehata, M. F.; Sanders, M. A.; Roizen, J. L. *Chem. Sci.* **2020**, *11*, 217–223.

259 Rakesh, K. P.; Shantharam, C. S.; Sridhara, M. B.; Manukumar, H. M.; Qin, H.-L. *Medchemcomm* **2017**, *8*, 2023–2039.

260 Colomer, I.; Chamberlain, A. E. R.; Haughey, M. B.; Donohoe, T. J. *Nat. Rev. Chem.* **2017**, *1*, 0088.

261 For representative examples, see: (a) Mo, X.; Yakiwchuk, J.; Dansereau, J.; McCubbin, J. A.; Hall, D. G. *J. Am. Chem. Soc.* **2015**, *137*, 9694–9703. (b) Vuković, V. D.; Richmond, E.; Wolf, E.; Moran, J. *Angew. Chem. Int. Ed.* **2017**, *56*, 3085–3089. (c) Qi, C.; Gandon, V.; Lebœuf, D. *Angew. Chem. Int. Ed.* **2018**, *57*, 14245–14249.

262 Huestis, M. P.; Terrett, J. A. *Nat. Chem.* **2022**, *14*, 120–121.

263 Manchester, J.; Walkup, G.; Rivin, O.; You, Z. *J. Chem. Inf. Model.* **2010**, *50*, 565–571.

264 Mayer, R. J.; Breugst, M.; Hampel, N.; Ofial, A. R.; Mayr, H. *J. Org. Chem.* **2019**, *84*, 8837–8858.

265 Kanzian, T.; Nigst, T. A.; Maier, A.; Pichl, S.; Mayr, H. *Eur. J. Org. Chem.* **2009**, *2009*, 6379–6385.

266 Greed, S.; Briggs, E. L.; Idiris, F. I. M.; White, A. J. P.; Lücking, U.; Bull, J. A. *Chem. Eur. J.* **2020**, *26*, 12533–12538.

267 Pretsch, E.; Bühlmann, P.; Badertscher, M. In *Spektroskopische Daten zur Strukturaufklärung organischer Verbindungen*, 5th ed.; Springer, Berlin Heidelberg, 2010.

268 Moritz, A. E.; Free, R. B.; Weiner, W. S.; Akano, E. O.; Gandhi, D.; Abramyan, A.; Keck, T. M.; Ferrer, M.; Hu, X.; Southall, N.; Steiner, J.; Aubé, J.; Shi, L.; Frankowski, K. J.; Sibley, D. R. *J. Med. Chem.* **2020**, *63*, 5526–5567.

269 Iwanaga, Y.; Miyashita, N.; Morikawa, K.; Mizumoto, A.; Kondo, Y.; Itoh, Z. *Gastroenterology* **1990**, *99*, 401–408.

270 Skinner, W. A.; Kennedy, J.; DeGraw, J. I.; Johnson, H. *J. Med. Chem.* **1969**, *12*, 715–717.

271 Dalbeth, N.; Lauterio, T. J.; Wolfe, H. R. *Clin. Ther.* **2014**, *36*, 1465–1479.

272 (a) Trimethobenzamide: Hurley, J. D.; Eshelman, F. N. *J. Clin. Pharmacol.* **1980**, *20*, 352–356. (b) Trimetozine: *Index Nominum 2000: International Drug Directory*, Medpharm Scientific, 2000. (c) Triithiozine: Pellegrini, R. *J. Int. Med. Res.* **1979**, *7*, 452–458. (d) Trocimine: Luts, H. A.; Zucarello, W. A.; Nobles, W. L.; Grattan, J. F. *J. Pharm. Sci.* **1966**, *55*, 1459–1461. (e) Troxipide: Irikura, T.; Kasuga, K. *J. Med. Chem.* **1971**, *14*, 357–361.

273 Hirsh, K.; Wang, S. C. *J. Pharmacol. Exp. Ther.* **1975**, *193*, 657–663.

274 (a) Gavine, P. R.; Mooney, L.; Kilgour, E.; Thomas, A. P.; Al-Kadhimi, K.; Beck, S.; Rooney, C.; Coleman, T.; Baker, D.; Mellor, M. J.; Brooks, A. N.; Klinowska, T. *Cancer Res.* **2012**, *72*, 2045–2056. (b) Kang, J.; Choi, Y. J.; Seo, B. Y.; Jo, U.; Park, S. I.; Kim, Y. H.; Park, K. H. *Sci. Rep.* **2019**, *9*, 8726.

275 Tucker, J. A.; Klein, T.; Breed, J.; Breeze, A. L.; Overman, R.; Phillips, C.; Norman, R. A. *Structure* **2014**, *22*, 1764–1774.

276 Black, W. C.; Bayly, C. I.; Davis, D. E.; Desmarais, S.; Falgueyret, J.-P.; Léger, S.; Li, C. S.; Massé, F.; McKay, D. J.; Palmer, J. T.; Percival, M. D.; Robichaud, J.; Tsou, N.; Zamboni, R. *Bioorg. Med. Chem. Lett.* **2005**, *15*, 4741–4744.

277 Lanigan, R. M.; Karaluka, V.; Sabatini, M. T.; Starkov, P.; Badland, M.; Boulton, L.; Sheppard, T. D. *Chem. Commun.* **2016**, *52*, 8846–8849.

278 Frizler, M.; Lohr, F.; Furtmann, N.; Kläs, J.; Gütschow, M. *J. Med. Chem.* **2011**, *54*, 396–400.

279 Wammes, A. E. M.; Hendriks, T. G.; Amatdjais-Groenen, H. I. V.; Wijdeven, M. A.; van Hest, J. C. M.; van Delft, F. L.; Ritschel, T.; Rutjes, F. P. J. T. *Bioorg. Med. Chem.* **2014**, *22*, 5593–5603.

280 Zwicker, J. D.; Diaz, N. A.; Guerra, A. J.; Kirchhoff, P. D.; Wen, B.; Sun, D.; Carruthers, V. B.; Larsen, S. D. *Bioorg. Med. Chem. Lett.* **2018**, *28*, 1972–1980.

281 Tan, J. Q.; Kim, R. M.; Mirc, J. W. (Merck Sharp and Dohme LLC) *Soluble Guanylate Cyclase Activators*, US Patent Appl. No US2013/210798, **2013**.

282 (a) Jin, C.; Zhang, Y. (Guangdong HEC Pharmaceutical) *Substituted piperazine compound as well as application method and application thereof*, China Patent Appl. No CN104725363, **2014**.

283 For example: (a) Shen, X.; Hyde, A. M.; Buchwald, S. L. *J. Am. Chem. Soc.* **2010**, *132*, 14076–14078. (b) Pan, J.; Wang, X.; Zhang, Y.; Buchwald, S. L. *Org. Lett.* **2011**, *13*, 4974–4976.

284 (a) Griffen, E.; Leach, A. G.; Robb, G. R.; Warner, D. J. *J. Med. Chem.* **2011**, *54*, 7739–7750. (b) Yang, Z.; Shi, S.; Fu, L.; Lu, A.; Hou, T.; Cao, D. *J. Med. Chem.* **2023**, DOI: 10.1021/acs.jmedchem.2c01787.

285 Blagojevic, L. Synthesis and Evaluation of 3-Aryl-3-Aminooxetanes as Potential Bioisosteres of N-Substituted Benzamides, MRes Thesis, Imperial College London, **2019**.

286 Luk, J. Computational Studies on the Conformation of Amino Oxetanes and the Carbocation Stability of Four-Membered Rings, MSci Thesis, Imperial College London, **2021**.

287 Bordwell, F. G. *Acc. Chem. Res.* **1988**, *21*, 456–463.

288 Trummal, A.; Lipping, L.; Kaljurand, I.; Koppel, I. A.; Leito, I. *J. Phys. Chem. A* **2016**, *120*, 3663–3669.

289 Christ, P.; Lindsay, A. G.; Vormittag, S. S.; Neudörfl, J.-M.; Berkessel, A.; O'Donoghue, A. C. *Chem. Eur. J.* **2011**, *17*, 8524–8528.

290 Yalkowsky, S. H.; Valvani, S. C. *J. Pharm. Sci.* **1980**, *69*, 912–922.

291 Lipinski, C. A.; Lombardo, F.; Dominy, B. W.; Feeney, P. J. *Adv. Drug Deliv. Rev.* **1997**, *23*, 3–25.

292 Ghose, A. K.; Viswanadhan, V. N.; Wendoloski, J. J. *J. Comb. Chem.* **1999**, *1*, 55–68.

293 Landry, M. L.; Crawford, J. J. *ACS Med. Chem. Lett.* **2020**, *11*, 72–76.

294 Diaz, G. J.; Daniell, K.; Leitza, S. T.; Martin, R. L.; Su, Z.; McDermott, J. S.; Cox, B. F.; Gintant, G. A. *J. Pharmacol. Toxicol. Methods* **2004**, *50*, 187–199.

295 Davies, H. M. L.; Dai, X. *J. Org. Chem.* **2005**, *70*, 6680–6684.

296 (a) Burés, J. *Angew. Chem. Int. Ed.* **2016**, *55*, 2028–2031. (b) Burés, J. *Angew. Chem. Int. Ed.* **2016**, *55*, 16084–16087. (c) Nielsen, C. D. T.; Burés, J. *Chem. Sci.* **2019**, *10*, 348–353.

297 McConnell, H. M. *J. Chem. Phys.* **1958**, *28*, 430–431.

298 (a) Arrhenius, S. *Zeitschrift für Phys. Chemie* **1889**, *4*, 96–116. (b) Arrhenius, S. *Zeitschrift für Phys. Chemie* **1889**, *4*, 226–248.

299 Press, W. H.; Flannery, B. P.; Teukolsky, S. A.; Vetterling, W. T. In *Numerical Recipes in Pascal, The Art of Scientific Computing*; Cambridge University Press, Cambridge, 1989.

300 Neese, F. *WIREs Comput. Mol. Sci.* **2018**, 8:e1327.

301 Rojas, J. J.; Croft, R. A.; Sterling, A. J.; Briggs, E. L.; Antermite, D.; Schmitt, D. C.; Blagojevic, L.; Haycock, P.; White, A. J. P.; Duarte, F.; Choi, C.; Mousseau, J. J.; Bull, J. A. *Imperial College London Research Data Repository* **2021**, https://doi.org/10.14469/hpc/8380.

302 Gianatassio, R.; Lopchuk, J. M.; Wang, J.; Pan, C.-M.; Malins, L. R.; Prieto, L.; Brandt, T. A.; Collins, M. R.; Gallego, G. M.; Sach, N. W.; Spangler, J. E.; Zhu, H.; Zhu, J.; Baran, P. S. *Science* **2016**, *351*, 241–246.

303 Marenich, A. V.; Cramer, C. J.; Truhlar, D. G. *J. Phys. Chem. B* **2009**, *113*, 6378–6396.

304 Grimme, S. *J. Chem. Phys.* **2003**, *118*, 9095–9102.

305 Weigend, F.; Ahlrichs, R. *Phys. Chem. Chem. Phys.* **2005**, *7*, 3297–3305.

306 Riplinger, C.; Neese, F. *J. Chem. Phys.* **2013**, *138*, 034106.

307 Chai, J.-D.; Head-Gordon, M. *Phys. Chem. Chem. Phys.* **2008**, *10*, 6615–6620.

308 Young, T. A.; Silcock, J. J.; Sterling, A. J.; Duarte, F. *Angew. Chem. Int. Ed.* **2021**, *60*, 4266–4274.

309 Lee, I.; Kang, H. K. *Tetrahedron Lett.* **1987**, *28*, 1183–1186.

310 Leffler, J. E.; Grunwald, E. In *Rates and Equilibria of Organic Reactions as Treated by Statistical, Thermodynamic, and Extrathermodynamic Methods*; Dover Publications, New York, 1963.

311 Dubois, M. A. J.; Rojas, J. J.; Sterling, A. J.; Broderick, H. C.; Smith, M. A.; White, A. J. P.; Miller, P. W.; Choi, C.; Mousseau, J. J.; Duarte, F.; Bull, J. A. *J. Org. Chem.* **2023**, DOI: 10.1021/acs.joc.3c00083.

312 Stephenson, C. R. J.; Studer, A.; Curran, D. P. *Beilstein J. Org. Chem.* **2013**, *9*, 2778–2780.

313 (a) Yoshida, J.; Kataoka, K.; Horcajada, R.; Nagaki, A. *Chem. Rev.* **2008**, *108*, 2265–2299. (b) Waldvogel, S. R.; Janza, B. *Angew. Chem. Int. Ed.* **2014**, *53*, 7122–7123. (c) Rosen, B. R.; Werner, E. W.; O'Brien, A. G.; Baran, P. S. *J. Am. Chem. Soc.* **2014**, *136*, 5571–5574. (d) Yan, M.; Kawamata, Y.; Baran, P. S. *Chem. Rev.* **2017**, *117*, 13230–13319. (e) Wiebe, A.; Gieshoff, T.; Möhle, S.; Rodrigo, E.; Zirbes, M.; Waldvogel, S. R. *Angew. Chem. Int. Ed.* **2018**, *57*, 5594–5619. (f) Pollok, D.; Waldvogel, S. R. *Chem. Sci.* **2020**, *11*, 12386–12400.

314 (a) Prier, C. K.; Rankic, D. A.; MacMillan, D. W. C. *Chem. Rev.* **2013**, *113*, 5322–5363. (b) Roslin, S.; Odell, L. R. *Eur. J. Org. Chem.* **2017**, *2017*, 1993–2007. (c) Marzo, L.; Pagire, S. K.; Reiser, O.; König, B. *Angew. Chem. Int. Ed.* **2018**, *57*, 10034–10072. (d) McAtee, R. C.; McClain, E. J.; Stephenson, C. R. J. *Trends Chem.* **2019**, *1*, 111–125. (e) Petzold, D.; Giedyk, M.; Chatterjee, A.; König, B. *Eur. J. Org. Chem.* **2020**, *2020*, 1193–1244.

315 Pitre, S. P.; Overman, L. E. *Chem. Rev.* **2022**, *122*, 1717–1751.

316 (a) Cannalire, R.; Pelliccia, S.; Sancineto, L.; Novellino, E.; Tron, G. C.; Giustiniano, M. *Chem. Soc. Rev.* **2021**, *50*, 766–897. (b) Zhang, R.; Li, G.; Wismer, M.; Vachal, P.; Colletti, S. L.; Shi, Z.-C. *ACS Med. Chem. Lett.* **2018**, *9*, 773–777.

317 Shaw, M. H.; Twilton, J.; MacMillan, D. W. C. *J. Org. Chem.* **2016**, *81*, 6898–6926.

318 Giese: Chu, L.; Ohta, C.; Zuo, Z.; MacMillan, D. W. C. *J. Am. Chem. Soc.* **2014**, *136*, 10886–10889.

319 Minisci: Pitre, S. P.; Muuronen, M.; Fishman, D. A.; Overman, L. E. *ACS Catal.* **2019**, *9*, 3413–3418.

320 (a) Gant Kanegusuku, A. L.; Roizen, J. L. *Angew. Chem., Int. Ed.* **2021**, *60*, 21116−21149. (b) Kitcatt, D. M.; Nicolle, S.; Lee, A.-L. *Chem. Soc. Rev.* **2022**, *51*, 1415−1453.

321 (a) Duncton, M. A. J. *Medchemcomm* **2011**, *2*, 1135–1161. (b) Proctor, R. S. J.; Phipps, R. J. *Angew. Chem. Int. Ed.* **2019**, *58*, 13666–13699. (c) Colgan, A. C.; Phipps, R. J. *Trends Chem.* **2021**, *3*, 332–333.

322 For representative examples, see: (a) Narayanam, J. M. R.; Tucker, J. W.; Stephenson, C. R. J. *J. Am. Chem. Soc.* **2009**, *131*, 8756–8757. (b) Nguyen, J. D.; D'Amato, E. M.; Narayanam, J. M. R.; Stephenson, C. R. J. *Nat. Chem.* **2012**, *4*, 854–859.

323 Giese, B. *Angew. Chem. Int. Ed.* **1983**, *22*, 753–764.

324 Minisci, F.; Bernardi, R.; Bertini, F.; Galli, R.; Perchinummo, M. *Tetrahedron* **1971**, *27*, 3575–3579.

325 (a) Tabaei, S. H.; Pittman, C. U.; Mead, K. T. *Tetrahedron Lett.* **1991**, *32*, 2727–2730. (b) Corey, E. J.; Choi, S. *Tetrahedron Lett.* **1991**, *32*, 2857–2860.

326 For reviews, see: (a) Twilton, J.; Le, C.; Zhang, P.; Shaw, M. H.; Evans, R. W.; MacMillan, D. W. C. *Nat. Rev. Chem.* **2017**, *1*, 0052. (b) Milligan, J. A.; Phelan, J. P.; Badir, S. O.; Molander, G. A. *Angew. Chem. Int. Ed.* **2019**, *58*, 6152–6163. (c) Chan, A. Y.; Perry, I. B.; Bissonnette, N. B.; Buksh, B. F.; Edwards, G. A.; Frye, L. I.; Garry, O. L.; Lavagnino, M. N.; Li, B. X.; Liang, Y.; Mao, E.; Millet, A.; Oakley, J. V.; Reed, N. L.; Sakai, H. A.; Seath, C. P.; MacMillan, D. W. C. *Chem. Rev.* **2022**, *122*, 1485–1542.

327 For seminal reports, see: (a) Tellis, J. C.; Primer, D. N.; Molander, G. A. *Science* **2014**, *345*, 433–436. (b) Zuo, Z.; Ahneman, D. T.; Chu, L.; Terrett, J. A.; Doyle, A. G.; MacMillan, D. W. C. *Science* **2014**, *345*, 437–440.

328 For selected examples, see: (a) Zuo, Z.; MacMillan, D. W. C. *J. Am. Chem. Soc.* **2014**, *136*, 5257–5260. (b) Noble, A.; McCarver, S. J.; MacMillan, D. W. C. *J. Am. Chem. Soc.* **2015**, *137*, 624–627. (c) Karmakar, S.; Silamkoti, A.; Meanwell, N. A.; Mathur, A.; Gupta, A. K. *Adv. Synth. Catal.* **2021**, *363*, 3693–3736.

329 For selected examples, see: (a) Nawrat, C. C.; Jamison, C. R.; Slutskyy, Y.; MacMillan, D. W. C.; Overman, L. E. *J. Am. Chem. Soc.* **2015**, *137*, 11270–11273. (b) Fu, M.-C.; Shang, R.; Zhao, B.; Wang, B.; Fu, Y. *Science* **2019**, *363*, 1429–1434. (c) Wu, J.; Bär, R. M.; Guo, L.; Noble, A.; Aggarwal, V. K. *Angew. Chem. Int. Ed.* **2019**, *58*, 18830–18834. (d) Dong, Z.; MacMillan, D. W. C. *Nature* **2021**, *598*, 451–456. (e) Williams, O. P.; Chmiel, A. F.; Mikhael, M.; Bates, D. F.; Yeung, C. S.; Wickens, Z. *Angew. Chem. Int. Ed.* **2023**, e202300178.

330 For a review, see: Anwar, K.; Merkens, K.; Aguilar Troyano, F. J.; Gómez-Suárez, A. *Eur. J. Org. Chem.* **2022**, *2022*, e202200330.

331 For selected examples, see: (a) Gutierrez, O.; Tellis, J. C.; Primer, D. N.; Molander, G. A.; Kozlowski, M. C. *J. Am. Chem. Soc.* **2015**, *137*, 4896–4899. (b) Primer, D. N.;

Karakaya, I.; Tellis, J. C.; Molander, G. A. *J. Am. Chem. Soc.* **2015**, *137*, 2195–2198. (c) Yamashita, Y.; Tellis, J. C.; Molander, G. A. *Proc. Natl. Acad. Sci.* **2015**, *112*, 12026–12029. (d) Amani, J.; Molander, G. A. *J. Org. Chem.* **2017**, *82*, 1856–1863. (e) Primer, D. N.; Molander, G. A. *J. Am. Chem. Soc.* **2017**, *139*, 9847–9850.

332 For selected examples, see: (a) Kohls, P.; Jadhav, D.; Pandey, G.; Reiser, O. *Org. Lett.* **2012**, *14*, 672–675. (b) Noble, A.; MacMillan, D. W. C. *J. Am. Chem. Soc.* **2014**, *136*, 11602–11605. (c) Shaw, M. H.; Shurtleff, V. W.; Terrett, J. A.; Cuthbertson, J. D.; MacMillan, D. W. C. *Science* **2016**, *352*, 1304–1308. (d) Leitch, J. A.; Fuentes de Arriba, A. L.; Tan, J.; Hoff, O.; Martínez, C. M.; Dixon, D. J. *Chem. Sci.* **2018**, *9*, 6653–6658. (e) Leitch, J. A.; Rogova, T.; Duarte, F.; Dixon, D. J. *Angew. Chem. Int. Ed.* **2020**, *59*, 4121–4130. (f) Leitch, J. A.; Rossolini, T.; Rogova, T.; Maitland, J. A. P.; Dixon, D. J. *ACS Catal.* **2020**, *10*, 2009–2025. (g) Rogova, T.; Gabriel, P.; Zavitsanou, S.; Leitch, J. A.; Duarte, F.; Dixon, D. J. *ACS Catal.* **2020**, *10*, 11438–11447. (h) Maitland, J. A. P.; Leitch, J. A.; Yamazaki, K.; Christensen, K. E.; Cassar, D. J.; Hamlin, T. A.; Dixon, D. J. *Angew. Chem. Int. Ed.* **2021**, *60*, 24116–24123. (i) Mao, E.; MacMillan, D. W. C. *J. Am. Chem. Soc.* **2023**, *145*, 2787–2793.

333 For selected examples, see: (a) Jin, J.; MacMillan, D. W. C. *Angew. Chem. Int. Ed.* **2015**, *54*, 1565–1569. (b) Rossolini, T.; Ferko, B.; Dixon, D. J. *Org. Lett.* **2019**, *21*, 6668–6673. (c) Jiang, S.; Tian, X.-J.; Feng, S.-Y.; Li, J.-S.; Li, Z.-W.; Lu, C.-H.; Li, C.-J.; Liu, W.-D. *Org. Lett.* **2021**, *23*, 692–696. (d) Tao, J.-Y.; Wang, Y.-X.; Zhang, Q.-H.; Ni, K.; Zhu, T.-H.; Zhao, K. *Green Chem.* **2022**, *24*, 4004–4011.

334 (a) Griller, D.; Lossing, F. P. *J. Am. Chem. Soc.* **1981**, *103*, 1586–1587. (b) Burkey, T. J.; Castelhano, A. L.; Griller, D.; Lossing, F. P. *J. Am. Chem. Soc.* **1983**, *105*, 4701–4703. (c) Wayner, D. D. M.; Clark, K. B.; Rauk, A.; Yu, D.; Armstrong, D. A. *J. Am. Chem. Soc.* **1997**, *119*, 8925–8932.

335 Blanksby, S. J.; Ellison, G. B. *Acc. Chem. Res.* **2003**, *36*, 255–263.

336 Ravelli, D.; Zoccolillo, M.; Mella, M.; Fagnoni, M. *Adv. Synth. Catal.* **2014**, *356*, 2781–2786.

337 (a) Le, C.; Liang, Y.; Evans, R. W.; Li, X.; MacMillan, D. W. C. *Nature* **2017**, *547*, 79–83. (b) Xu, S.; Ping, Y.; Li, W.; Guo, H.; Su, Y.; Li, Z.; Wang, M.; Kong, W. *J. Am. Chem. Soc.* **2023**, *145*, 5231–5241.

338 Duncton, M. A. J.; Estiarte, M. A.; Johnson, R. J.; Cox, M.; O'Mahony, D. J. R.; Edwards, W. T.; Kelly, M. G. *J. Org. Chem.* **2009**, *74*, 6354–6357.

339 Minisci, F.; Vismara, E.; Fontana, F. *J. Org. Chem.* **1989**, *54*, 5224–5227.

340 Nuhant, P.; Oderinde, M. S.; Genovino, J.; Juneau, A.; Gagné, Y.; Allais, C.; Chinigo, G. M.; Choi, C.; Sach, N. W.; Bernier, L.; Fobian, Y. M.; Bundesmann, M. W.; Khunte, B.; Frenette, M.; Fadeyi, O. O. *Angew. Chem. Int. Ed.* **2017**, *56*, 15309–15313.

341 (a) Constantin, T.; Zanini, M.; Regni, A.; Sheikh, N. S.; Juliá, F.; Leonori, D. *Science* **2020**, *367*, 1021–1026. (b) Górski, B.; Barthelemy, A.; Douglas, J. J.; Juliá, F.; Leonori, D. *Nat. Catal.* **2021**, *4*, 623–630.

342 ElMarrouni, A.; Ritts, C. B.; Balsells, J. *Chem. Sci.* **2018**, *9*, 6639–6646.

343 Dow, N. W.; Cabré, A.; MacMillan, D. W. C. *Chem* **2021**, *7*, 1827–1842.

344 Genovino, J.; Lian, Y.; Zhang, Y.; Hope, T. O.; Juneau, A.; Gagné, Y.; Ingle, G.; Frenette, M. *Org. Lett.* **2018**, *20*, 3229–3232.

345 Green, S. A.; Vásquez-Céspedes, S.; Shenvi, R. A. *J. Am. Chem. Soc.* **2018**, *140*, 11317–11324.

346 Murray, P. R. D.; Bussink, W. M. M.; Davies, G. H. M.; van der Mei, F. W.; Antropow, A. H.; Edwards, J. T.; D'Agostino, L. A.; Ellis, J. M.; Hamann, L. G.; Romanov-Michailidis, F.; Knowles, R. R. *J. Am. Chem. Soc.* **2021**, *143*, 4055–4063.

347 Zhang, Y.; Zhang, Y.; Shen, X. *Chem Catal.* **2021**, *1*, 423–436.

348 Li, Z.; Wang, X.; Xia, S.; Jin, J. *Org. Lett.* **2019**, *21*, 4259–4265.

349 (a) Capaldo, L.; Buzzetti, L.; Merli, D.; Fagnoni, M.; Ravelli, D. *J. Org. Chem.* **2016**, *81*, 7102–7109. (b) Manley, D. W.; Walton, J. C. *Org. Lett.* **2014**, *16*, 5394–5397. (c) McLean, E. B.; Mooney, D. T.; Burns, D. J.; Lee, A.-L. *Org. Lett.* **2022**, *24*, 686–691.

350 For examples of benzylic substrates showing decreased or alternative reactivity in radical reactions, see: (a) Suga, T.; Shimazu, S.; Ukaji, Y. *Org. Lett.* **2018**, *20*, 5389–5392. (b) Ryder, A. S. H.; Cunningham, W. B.; Ballantyne, G.; Mules, T.; Kinsella, A. G.; Turner-Dore, J.; Alder, C. M.; Edwards, L. J.; McKay, B. S. J.; Grayson, M. N.; Cresswell, A. J. *Angew. Chem. Int. Ed.* **2020**, *59*, 14986–14991. (c) Ma, G.; Chen, C.; Talukdar, S.; Zhao, X.; Lei, C.-H.; Gong, H. *Chem. Commun.* **2020**, *56*, 10219–10222. (d) Askey, H. E.; Grayson, J. D.; Tibbetts, J. D.; Turner-Dore, J. C.; Holmes, J. M.; Kociok-Kohn, G.; Wrigley, G. L.; Cresswell, A. J. *J. Am. Chem. Soc.* **2021**, *143*, 15936–15945. (e) Suga, T.; Takahashi, Y.; Miki, C.; Ukaji, Y. *Angew. Chem. Int. Ed.* **2022**, *61*, e202112533.

351 Li, P.; Zbieg, J. R.; Terrett, J. A. *Org. Lett.* **2021**, *23*, 9563–9568.

352 Dubois, M. A. J.; Smith, M. A.; White, A. J. P.; Lee Wei Jie, A.; Mousseau, J. J.; Choi, C.; Bull, J. A. *Org. Lett.* **2020**, *22*, 5279–5283.

353 For other methods to synthesise aryloxetane carboxylic acids, see: (a) Buckman, B. O.; Nicholas, J. B.; Emayan, K.; Seiwert, S. D. (Intermune Inc.) *Lysophosphatidic Acid Receptor Antagonists*. WO Patent Appl. No WO2013025733A1, **2013**. (b) see ref. 137b.

354 Ye, Y.; Sanford, M. S. *J. Am. Chem. Soc.* **2012**, *134*, 9034–9037.

355 (a) Lowry, M. S.; Goldsmith, J. I.; Slinker, J. D.; Rohl, R.; Pascal, R. A.; Malliaras, G. G.; Bernhard, S. *Chem. Mater.* **2005**, *17*, 5712–5719. (b) Miyake, Y.; Nakajima, K.; Nishibayashi, Y. *Chem. Commun.* **2013**, *49*, 7854–7856. (c) Merkens, K.; Aguilar Troyano, F. J.; Djossou, J.; Gómez-Suárez, A. *Adv. Synth. Catal.* **2020**, *362*, 2354–2359. (d) Fernandez-Rodriguez, P.; Legros, F.; Maier, T.; Weber, A.; Méndez, M.; Derdau, V.; Hessler, G.; Kurz, M.; Villar-Garea, A.; Ruf, S. *Eur. J. Org. Chem.* **2021**, *2021*, 782–787.

356 (a) Carlsen, P. H. J.; Katsuki, T.; Martin, V. S.; Sharpless, K. B. *J. Org. Chem.* **1981**, *46*, 3936–3938. (b) Miranda, L.; Vasconcellos, M. *Synthesis* **2004**, *2004*, 1767–1770. (c) O' Donovan, D. H.; Aillard, P.; Berger, M.; de la Torre, A.; Petkova, D.; Knittl-Frank, C.; Geerdink, D.; Kaiser, M.; Maulide, N. *Angew. Chem. Int. Ed.* **2018**, *57*, 10737–10741.

357 Dubois, M. A. J.; Rojas, J. J.; Sterling, A. J.; Broderick, H. C.; Smith, M. A.; White, A. J. P.; Miller, P. W.; Choi, C.; Mousseau, J. J.; Duarte, F.; Bull, J. A. *Imperial College London Research Data Repository* **2023**, https://doi.org/10.14469/hpc/10668.

358 Truong, T. N.; Stefanovich, E. V. *Chem. Phys. Lett.* **1995**, *240*, 253–260.

359 Lin, Y.-S.; Li, G.-D.; Mao, S.-P.; Chai, J.-D. *J. Chem. Theory Comput.* **2013**, *9*, 263–272.

360 Weigend, F.; Ahlrichs, R. *Phys. Chem. Chem. Phys.* **2005**, *7*, 3297–3305.

361 Walsh, R. *Int. J. Chem. Kinet.* **1970**, *2*, 71–74.

362 Lewis, G. N. *Proc. Natl. Acad. Sci.* **1925**, *11*, 179–183.

363 Costentin, C.; Savéant, J. M. *J. Phys. Chem. A* **2005**, *109*, 4125–4132.

364 (a) Foster, J. P.; Weinhold, F. *J. Am. Chem. Soc.* **1980**, *102*, 7211–7218. (b) Glendening, E. D.; Weinhold, F. *J. Comput. Chem.* **1998**, *19*, 593–609.

365 Bent, H. A. *Chem. Rev.* **1961**, *61*, 275–311.

366 Elgrishi, N.; Rountree, K. J.; McCarthy, B. D.; Rountree, E. S.; Eisenhart, T. T.; Dempsey, J. L. *J. Chem. Educ.* **2018**, *95*, 197–206.

367 Gagne, R. R.; Koval, C. A.; Lisensky, G. C. *Inorganic Chemistry*. **1980**, *19*, 2854–2855.

368 Pavlishchuk, V. V.; Addison, A. W. *Inorganica Chim. Acta* **2000**, *298*, 97–102.

369 Schmittel, M.; Lal, M.; Lal, R.; Röck, M.; Langels, A.; Rappoport, Z.; Basheer, A.; Schlirf, J.; Deiseroth, H.-J.; Flörke, U.; Gescheidt, G. *Tetrahedron* **2009**, *65*, 10842–10855.

370 (a) Salamone, M.; Milan, M.; DiLabio, G. A.; Bietti, M. *J. Org. Chem.* **2013**, *78*, 5909–5917. (b) Tam, C. M.; To, C. T.; Chan, K. S. *Organometallics* **2016**, *35*, 2174–2177. (c) Samai, S.; Rouichi, S.; Ferhati, A.; Chakir, A. *Arab. J. Chem.* **2019**, *12*, 4957–4970.

371 (a) Huynh, M. H. V; Meyer, T. J. *Chem. Rev.* **2007**, *107*, 5004–5064. (b) Weinberg, D. R.; Gagliardi, C. J.; Hull, J. F.; Murphy, C. F.; Kent, C. A.; Westlake, B. C.; Paul, A.; Ess,

D. H.; McCafferty, D. G.; Meyer, T. J. *Chem. Rev.* **2012**, *112*, 4016–4093. (c) Miller, D. C.; Tarantino, K. T.; Knowles, R. R. *Top. Curr. Chem.* **2016**, *374*, 30. (d) Gentry, E. C.; Knowles, R. R. *Acc. Chem. Res.* **2016**, *49*, 1546–1556. (e) Murray, P. R. D.; Cox, J. H.; Chiappini, N. D.; Roos, C. B.; McLoughlin, E. A.; Hejna, B. G.; Nguyen, S. T.; Ripberger, H. H.; Ganley, J. M.; Tsui, E.; Shin, N. Y.; Koronkiewicz, B.; Qiu, G.; Knowles, R. R. *Chem. Rev.* **2022**, *122*, 2017–2291.

372 Tyssee, D. A.; Baizer, M. M. *J. Org. Chem.* **1974**, *39*, 2819–2823.

373 Arnold, D. R.; Borg, R. M.; Albini, A. *J. Chem. Soc. Chem. Commun.* **1981**, 138–139.

374 Potrząsaj, A.; Ociepa, M.; Chaładaj, W.; Gryko, D. *Org. Lett.* **2022**, *24*, 2469–2473.

375 Abel, B.; Assmann, J.; Buback, M.; Grimm, C.; Kling, M.; Schmatz, S.; Schroeder, J.; Witte, T. *J. Phys. Chem. A* **2003**, *107*, 9499–9510.

376 For selected recent examples of radical reactivity, see (for more examples, see references therein): (a) Kim, J. H.; Ruffoni, A.; Al-Faiyz, Y. S. S.; Sheikh, N. S.; Leonori, D. *Angew. Chem. Int. Ed.* **2020**, *59*, 8225–8231. (b) Shin, S.; Lee, S.; Choi, W.; Kim, N.; Hong, S. *Angew. Chem. Int. Ed.* **2021**, *60*, 7873–7879. (c) Wong, M. L. J.; Sterling, A. J.; Mousseau, J. J.; Duarte, F.; Anderson, E. A. *Nat. Commun.* **2021**, *12*, 1644. (d) Pickford, H. D.; Nugent, J.; Owen, B.; Mousseau, J. J.; Smith, R. C.; Anderson, E. A. *J. Am. Chem. Soc.* **2021**, *143*, 9729–9736. (e) Nugent, J.; Sterling, A. J.; Frank, N.; Mousseau, J. J.; Anderson, E. A. *Org. Lett.* **2021**, *23*, 8628–8633.

377 (a) Stepan, A. F.; Subramanyam, C.; Efremov, I. V.; Dutra, J. K.; O'Sullivan, T. J.; DiRico, K. J.; McDonald, W. S.; Won, A.; Dorff, P. H.; Nolan, C. E.; Becker, S. L.; Pustilnik, L. R.; Riddell, D. R.; Kauffman, G. W.; Kormos, B. L.; Zhang, L.; Lu, Y.; Capetta, S. H.; Green, M. E.; Karki, K.; Sibley, E.; Atchison, K. P.; Hallgren, A. J.; Oborski, C. E.; Robshaw, A. E.; Sneed, B.; O'Donnell, C. J. *J. Med. Chem.* **2012**, *55*, 3414–3424. (b) Auberson, Y. P.; Brocklehurst, C.; Furegati, M.; Fessard, T. C.; Koch, G.; Decker, A.; La Vecchia, L.; Briard, E. *ChemMedChem* **2017**, *12*, 590–598. (c) Mykhailiuk, P. K. *Org. Biomol. Chem.* **2019**, *17*, 2839–2849.

378 (a) Zhang, X.; Smith, R. T.; Le, C.; McCarver, S. J.; Shireman, B. T.; Carruthers, N. I.; MacMillan, D. W. C. *Nature* **2020**, *580*, 220–226. (b) Dong, W.; Yen-Pon, E.; Li, L.; Bhattacharjee, A.; Jolit, A.; Molander, G. A. *Nat. Chem.* **2022**, *14*, 1068–1077. (c) Mousseau, J. J.; Perry, M. A.; Bundesmann, M. W.; Chinigo, G. M.; Choi, C.; Gallego, G.; Hicklin, R. W.; Hoy, S.; Limburg, D. C.; Sach, N. W.; Zhang, Y. *ACS Catal.* **2022**, *12*, 600–606.

379 Li, Q. Y.; Gockel, S. N.; Lutovsky, G. A.; DeGlopper, K. S.; Baldwin, N. J.; Bundesmann, M. W.; Tucker, J. W.; Bagley, S. W.; Yoon, T. P. *Nat. Chem.* **2022**, *14*, 94–99.

380 Nguyen, V. T.; Haug, G. C.; Nguyen, V. D.; Vuong, N. T. H.; Arman, H. D.; Larionov, O. V. *Chem. Sci.* **2021**, *12*, 6429–6436.

381 Shatskiy, A.; Axelsson, A.; Stepanova, E. V.; Liu, J.-Q.; Temerdashev, A. Z.; Kore, B. P.; Blomkvist, B.; Gardner, J. M.; Dinér, P.; Kärkäs, M. D. *Chem. Sci.* **2021**, *12*, 5430–5437.

382 Kerr, J. A. *Chem. Rev.* **1966**, *66*, 465–500.

383 Roth, H.; Romero, N.; Nicewicz, D. *Synlett* **2015**, *27*, 714–723.

384 For a review, see: Tsui, E.; Wang, H.; Knowles, R. R. *Chem. Sci.* **2020**, *11*, 11124–11141.

385 Selected examples: (a) Yayla, H. G.; Wang, H.; Tarantino, K. T.; Orbe, H. S.; Knowles, R. R. *J. Am. Chem. Soc.* **2016**, *138*, 10794–10797. (b) Hu, A.; Guo, J.-J.; Pan, H.; Tang, H.; Gao, Z.; Zuo, Z. *J. Am. Chem. Soc.* **2018**, *140*, 1612–1616. (c) Hu, A.; Chen, Y.; Guo, J.-J.; Yu, N.; An, Q.; Zuo, Z. *J. Am. Chem. Soc.* **2018**, *140*, 13580–13585. (d) Shi, J.-L.; Wang, Y.; Wang, Z.; Dou, B.; Wang, J. *Chem. Commun.* **2020**, *56*, 5002–5005. (e) Ji, T.; Chen, X.; Huang, L.; Rueping, M. *Org. Lett.* **2020**, *22*, 2579–2583. (f) Gao, Y.; Liu, J.; Wei, C.; Li, Y.; Zhang, K.; Song, L.; Cai, L. *Nat. Commun.* **2022**, *13*, 7450.

386 Selected examples: (a) Lam, K.; Markó, I. E. *Org. Lett.* **2011**, *13*, 406–409. (b) Stache, E. E.; Ertel, A. B.; Rovis, T.; Doyle, A. G. *ACS Catal.* **2018**, *8*, 11134–11139. (c) Tian, X.; Karl, T. A.; Reiter, S.; Yakubov, S.; Vivie-Riedle, R.; König, B.; Barham, J. P. *Angew. Chem. Int. Ed.* **2021**, *60*, 20817–20825.

387 Selected examples: (a) Zhu, L.; Liu, S.; Douglas, J. T.; Altman, R. A. *Chem. Eur. J.* **2013**, *19*, 12800–12805. (b) Vara, B. A.; Patel, N. R.; Molander, G. A. *ACS Catal.* **2017**, *7*, 3955–3959. (c) Mills, L. R.; Monteith, J. J.; dos Passos Gomes, G.; Aspuru-Guzik, A.; Rousseaux, S. A. L. *J. Am. Chem. Soc.* **2020**, *142*, 13246–13254. (d) Guo, H.-M.; Wu, X. *Nat. Commun.* **2021**, *12*, 5365. (e) Cai, A.; Yan, W.; Liu, W. *J. Am. Chem. Soc.* **2021**, *143*, 9952–9960. (f) Nanjo, T.; Matsugasako, T.; Maruo, Y.; Takemoto, Y. *Org. Lett.* **2022**, *24*, 359–363.

388 Selected examples: (a) Lackner, G. L.; Quasdorf, K. W.; Overman, L. E. *J. Am. Chem. Soc.* **2013**, *135*, 15342–15345. (b) Zhang, X.; MacMillan, D. W. C. *J. Am. Chem. Soc.* **2016**, *138*, 13862–13865. (c) Guo, L.; Tu, H.-Y.; Zhu, S.; Chu, L. *Org. Lett.* **2019**, *21*, 4771–4776. (d) Friese, F. W.; Studer, A. *Angew. Chem. Int. Ed.* **2019**, *58*, 9561–9564. (e) Ma, G.; Chen, C.; Talukdar, S.; Zhao, X.; Lei, C.; Gong, H. *Chem. Commun.* **2020**, *56*, 10219–10222.

389 Selected examples: (a) Suga, T.; Shimazu, S.; Ukaji, Y. *Org. Lett.* **2018**, *20*, 5389–5392. (b) Xie, H.; Guo, J.; Wang, Y.-Q.; Wang, K.; Guo, P.; Su, P.-F.; Wang, X.; Shu, X.-Z. *J.*

Am. Chem. Soc. **2020**, *142*, 16787–16794. (c) Suga, T.; Takahashi, Y.; Miki, C.; Ukaji, Y. *Angew. Chem. Int. Ed.* **2022**, *61*, e202112533. (d) Tian, H.; Zhang, R.; Shi, L.; Zhao, C.; Wang, X. *Chinese J. Chem.* **2023**, DOI:10.1002/cjoc.202300096.

390 Selected examples: (a) Wang, J. Z.; Sakai, H. A.; MacMillan, D. W. C. *Angew. Chem. Int. Ed.* **2022**, *61*, e202207150. (b) Intermaggio, N. E.; Millet, A.; Davis, D. L.; MacMillan, D. W. C. *J. Am. Chem. Soc.* **2022**, *144*, 11961–11968. (c) Sakai, H. A.; MacMillan, D. W. C. *J. Am. Chem. Soc.* **2022**, *144*, 6185–6192.

391 Selected examples: (a) Lam, K.; Markó, I. E. *Org. Lett.* **2008**, *10*, 2773–2776. (b) Rackl, D.; Kais, V.; Kreitmeier, P.; Reiser, O. *Beilstein J. Org. Chem.* **2014**, *10*, 2157–2165. (c) Rackl, D.; Kais, V.; Lutsker, E.; Reiser, and O. *Eur. J. Org. Chem.* **2017**, *2017*, 2130–2138. (d) Chen, H.; Lu, F.; Cheng, Y.; Jia, Y.; Lu, L.; Xiao, W. *Chinese J. Chem.* **2020**, *38*, 1671–1675. (e) Kolusu, S. R. N.; Nappi, M. *Chem. Sci.* **2022**, *13*, 6982–6989.

392 Mcdevitt, P.; Vittimberga, B. M. *J. Heterocycl. Chem.* **1990**, *27*, 1903–1908.

393 Jung, J.; Kim, J.; Park, G.; You, Y.; Cho, E. J. *Adv. Synth. Catal.* **2016**, *358*, 74–80.

394 For an example, see: Elgrishi, N.; Kurtz, D. A.; Dempsey, J. L. *J. Am. Chem. Soc.* **2017**, *139*, 239–244.

395 For recent reviews, see: (a) Murarka, S. *Adv. Synth. Catal.* **2018**, *360*, 1735–1753. (b) Niu, P.; Li, J.; Zhang, Y.; Huo, C. *Eur. J. Org. Chem.* **2020**, *2020*, 5801–5814. (c) Karmakar, S.; Silamkoti, A.; Meanwell, N. A.; Mathur, A.; Gupta, A. K. *Adv. Synth. Catal.* **2021**, *363*, 3693–3736. (d) Chen, H.; Liu, Y. A.; Liao, X. *Synthesis* **2021**, *53*, 1–29.

396 (a) Svejstrup, T. D.; Ruffoni, A.; Juliá, F.; Aubert, V. M.; Leonori, D. *Angew. Chem. Int. Ed.* **2017**, *56*, 14948–14952. (b) Davies, J.; Morcillo, S. P.; Douglas, J. J.; Leonori, D. *Chem. Eur. J.* **2018**, *24*, 12154–12163. (c) Angelini, L.; Davies, J.; Simonetti, M.; Malet Sanz, L.; Sheikh, N. S.; Leonori, D. *Angew. Chem. Int. Ed.* **2019**, *58*, 5003–5007.

397 Fawcett, A.; Pradeilles, J.; Wang, Y.; Mutsuga, T.; Myers, E. L.; Aggarwal, V. K. *Science* **2017**, *357*, 283–286.

398 Kammer, L. M.; Badir, S. O.; Hu, R.; Molander, G. A. *Chem. Sci.* **2021**, *12*, 5450–5457.

399 Tong, S.; Li, K.; Ouyang, X.; Song, R.; Li, J. *Green Synth. Catal.* **2021**, *2*, 145–155.

400 Noury, S.; Silvi, B.; Gillespie, R. J. *Inorg. Chem.* **2002**, *41*, 2164–2172.

401 Kaiser, D.; Klose, I.; Oost, R.; Neuhaus, J.; Maulide, N. *Chem. Rev.* **2019**, *119*, 8701–8780.

402 (a) Oae, S.; Furukawa, N. In *Advances in Heterocyclic Chemistry*; 1990; Vol. 48, pp 1–63. (b) Oae, S.; Uchida, Y. *Acc. Chem. Res.* **1991**, *24*, 202–208.

403 (a) Zhou, M.; Tsien, J.; Qin, T. *Angew. Chem. Int. Ed.* **2020**, *59*, 7372–7376. (b) Zhou, M.; Tsien, J.; Qin, T. *Synlett* **2020**, *31*, 1962–1966.

404 (a) Tang, R.; Mislow, K. *J. Am. Chem. Soc.* **1969**, *91*, 5644–5645. (b) Durst, T.; LeBelle, M. J.; Elzen, R. Van den; Tin, K.-C. *Can. J. Chem.* **1974**, *52*, 761–766.

405 (a) Martin, J. C.; Arhart, R. J. *J. Am. Chem. Soc.* **1971**, *93*, 2341–2342. (b) Perozzi, E. F.; Martin, J. C. *J. Am. Chem. Soc.* **1972**, *94*, 5519–5520.

406 For example: (a) Oae, S.; Inubushi, Y.; Yoshihara, M. *Heteroat. Chem.* **1993**, *4*, 185–188. (b) Inubushi, Y.; Yoshihara, M.; Oae, S. *Heteroat. Chem.* **1996**, *7*, 299–306.

407 Moc, J.; Dorigo, A. E.; Morokuma, K. *Chem. Phys. Lett.* **1993**, *204*, 65–72.

408 Calculated low barrier for pseudorotation: Cameron, D. R.; Thatcher, G. R. J. *J. Org. Chem.* **1996**, *61*, 5986–5997.

409 Oae, S.; Takeda, T.; Kawai, T.; Furukawa, N. *Phosphorous Sulfur Relat. Elem.* **1987**, *34*, 133–137.

410 Andersen, K. K.; A. Yeager, S.; Peynircioglu, N. B. *Tetrahedron Lett.* **1970**, *11*, 2485–2488.

411 (a) Kawai, T.; Kodera, Y.; Oae, S.; Ishida, M.; Takeda, T.; Wakabayashi, S.; Furukawa, N. *Phosphorous Sulfur Relat. Elem.* **1987**, *34*, 139–148. (b) Shibutani, T.; Fujihara, H.; Furukawa, N.; Oae, S. *Heteroat. Chem.* **1991**, *2*, 521–531.

412 Fuchs, K. *Monatshefte für Chemie* **1929**, *53*, 438–444.

413 For selected examples, see: (a) Mislow, K.; Green, M. M.; Laur, P.; Melillo, J. T.; Simmons, T.; Ternay, A. L. *J. Am. Chem. Soc.* **1965**, *87*, 1958–1976. (b) Lockard, J.; Schroeck, C.; Johnson, C. *Synthesis* **2002**, *1973*, 485–486. (c) Sekiguchi, K.; Kimura, T. *Use of 1-Chlorovinyl p-Tolyl Sulfoxides as Alkynylmagnesium Chloride Sources* [preprint] **2023**; 10.26434/chemrxiv-2023-xbgkd.

414 (a) Satoh, T.; Sato, T.; Oohara, T.; Yamakawa, K. *J. Org. Chem.* **1989**, *54*, 3973–3978. (b) Satoh, T.; Oohara, T.; Ueda, Y.; Yamakawa, K. *J. Org. Chem.* **1989**, *54*, 3130–3136. (c) Satoh, T.; Horiguchi, K. *Tetrahedron Lett.* **1995**, *36*, 8235–8238. (d) Kopp, F.; Sklute, G.; Polborn, K.; Marek, I.; Knochel, P. *Org. Lett.* **2005**, *7*, 3789–3791. (e) Chawner, S. J.; Cases-Thomas, M. J.; Bull, J. A. *Eur. J. Org. Chem.* **2017**, *2017*, 5015–5024. (f) Fawcett, A.; Biberger, T.; Aggarwal, V. K. *Nat. Chem.* **2019**, *11*, 117–122.

415 (a) Rauhut, C. B.; Melzig, L.; Knochel, P. *Org. Lett.* **2008**, *10*, 3891–3894. (b) Melzig, L.; Rauhut, C.; Knochel, P. *Synthesis* **2009**, *2009*, 1041–1048. (c) Melzig, L.; Rauhut, C. B.; Knochel, P. *Chem. Commun.* **2009**, *24*, 3536–3538. (d) Melzig, L.; Rauhut, C. B.; Naredi-Rainer, N.; Knochel, P. *Chem. Eur. J.* **2011**, *17*, 5362–5372.

416 Rayner, P. J.; O'Brien, P.; Horan, R. A. J. *J. Am. Chem. Soc.* **2013**, *135*, 8071–8077.

417 Hughes, M.; Boultwood, T.; Zeppetelli, G.; Bull, J. A. *J. Org. Chem.* **2013**, *78*, 844–854.

418 For a recent review, see: Morofuji, T.; Kano, N. *Synthesis* **2022**, *54*, 5186–5191.

419 (a) Oae, S.; Kawai, T.; Furukawa, N. *Tetrahedron Lett.* **1984**, *25*, 69–72. (b) Oae, S.; Kawai, T.; Furukawa, N.; Iwasaki, F. *J. Chem. Soc., Perkin Trans. 2* **1987**, 405–411.

420 Wakabayashi, S.; Ishida, M.; Takeda, T.; Oae, S. *Tetrahedron Lett.* **1988**, *29*, 4441–4444.

421 (a) Kawai, T.; Furukawa, N.; Oae, S. *Tetrahedron Lett.* **1984**, *25*, 2549–2552. (b) Furukawa, N.; Shibutani, T.; Fujihara, H. *Tetrahedron Lett.* **1987**, *28*, 5845–5848. (c) Oae, S.; Kawai, T.; Furukawa, N. *Phosphorous Sulfur Relat. Elem.* **1987**, *34*, 123–132. (d) Oae, S.; Takeda, T.; Wakabayashi, S. *Tetrahedron Lett.* **1988**, *29*, 4445–4448. (e) Oae, S.; Inubushi, Y.; Yoshihara, M. *Phosphorus. Sulfur. Silicon Relat. Elem.* **1995**, *103*, 101–110. (f) Oae, S. *Pure Appl. Chem.* **1996**, *68*, 805–812. (g) Oae, S.; Takeda, T.; Uenishi, J.; Wakabayashi, S. *Phosphorus. Sulfur. Silicon Relat. Elem.* **1996**, *115*, 179–182.

422 Dean, W. M.; Šiaučiulis, M.; Storr, T. E.; Lewis, W.; Stockman, R. A. *Angew. Chem. Int. Ed.* **2016**, *55*, 10013–10016.

423 Zhou, M.; Tsien, J.; Dykstra, R.; Hughes, J. M. E.; Peters, B. K.; Merchant, R. R.; Gutierrez, O.; Qin, T. *Nat. Chem.* **2023**, DOI: 10.1038/s41557-023-01150-z.

424 Chen, D.-L.; Sun, Y.; Chen, M.; Li, X.; Zhang, L.; Huang, X.; Bai, Y.; Luo, F.; Peng, B. *Org. Lett.* **2019**, *21*, 3986–3989.

425 Saito, F. *Angew. Chem. Int. Ed*. **2022**, *61*, e202213872.

426 Krasovskiy, A.; Kopp, F.; Knochel, P. *Angew. Chem. Int. Ed.* **2006**, *45*, 497–500.

427 Ziegler, D. S.; Wei, B.; Knochel, P. *Chem. Eur. J.* **2019**, *25*, 2695–2703.

428 (a) Kremsmair, A.; Harenberg, J. H.; Schwärzer, K.; Hess, A.; Knochel, P. *Chem. Sci.* **2021**, *12*, 6011–6019. (b) Kremsmair, A.; Wilke, H. R.; Harenberg, J. H.; Bissinger, B. R. G.; Simon, M. M.; Alandini, N.; Knochel, P. *Angew. Chem. Int. Ed.* **2023**, *62*, e202214377.

429 For selected examples, see: (a) Metzger, A.; Gavryushin, A.; Knochel, P. *Synlett* **2009**, *2009*, 1433–1436. (b) Richter, M. J. R.; Schneider, M.; Brandstätter, M.; Krautwald, S.; Carreira, E. M. *J. Am. Chem. Soc.* **2018**, *140*, 16704–16710. (c) Péter, Á.; Crisenza, G. E. M.; Procter, D. J. *J. Am. Chem. Soc.* **2022**, *144*, 7457–7464. (d) Qin, H.; Jin, C.; Odilov, A.; Mintah Bonku, E.; Zhu, F.; Liu, Q.; Shen, J.; Aisa, H. A. *Org. Process Res. Dev.* **2023**, *27*, 78–83.

430 For selected examples, see: (a) Imamoto, T.; Kusumoto, T.; Tawarayama, Y.; Sugiura, Y.; Mita, T.; Hatanaka, Y.; Yokoyama, M. *J. Org. Chem.* **1984**, *49*, 3904–3912. (b) Imamoto, T.; Sugiura, Y.; Takiyama, N. *Tetrahedron Lett.* **1984**, *25*, 4233–4236. (c) Imamoto, T.; Takiyama, N.; Nakamura, K.; Hatajima, T.; Kamiya, Y. *J. Am. Chem. Soc.*

1989, *111*, 4392–4398. (d) Liu, H.-J.; Shia, K.-S.; Shang, X.; Zhu, B.-Y. *Tetrahedron* **1999**, *55*, 3803–3830.

431 For selected examples, see: (a) Hatano, M.; Suzuki, S.; Ishihara, K. *Synlett* **2010**, *2010*, 321–324. (b) Hatano, M.; Ito, O.; Suzuki, S.; Ishihara, K. *Chem. Commun.* **2010**, *46*, 2674–2676. (c) Hatano, M.; Ito, O.; Suzuki, S.; Ishihara, K. *J. Org. Chem.* **2010**, *75*, 5008–5016. (d) Hatano, M.; Mizuno, M.; Ishihara, K. *Org. Lett.* **2016**, *18*, 4462–4465. (e) Shiomi, S.; Shennan, B. D. A.; Yamazaki, K.; Fuentes de Arriba, Á. L.; Vasu, D.; Hamlin, T. A.; Dixon, D. J. *J. Am. Chem. Soc.* **2022**, *144*, 1407–1415.

432 For reviews and concept articles, see: (a) Yoshida, J.; Nagaki, A.; Yamada, T. *Chem. Eur. J.* **2008**, *14*, 7450–7459. (b) Yoshida, J.; Takahashi, Y.; Nagaki, A. *Chem. Commun.* **2013**, *49*, 9896–9904. (c) Colella, M.; Nagaki, A.; Luisi, R. *Chem. Eur. J.* **2020**, *26*, 19–32.

433 For selected examples by Luisi, see: (a) Musci, P.; Colella, M.; Sivo, A.; Romanazzi, G.; Luisi, R.; Degennaro, L. *Org. Lett.* **2020**, *22*, 3623–3627. (b) Colella, M.; Tota, A.; Takahashi, Y.; Higuma, R.; Ishikawa, S.; Degennaro, L.; Luisi, R.; Nagaki, A. *Angew. Chem. Int. Ed.* **2020**, *59*, 10924–10928. (c) Musci, P.; Keutz, T.; Belaj, F.; Degennaro, L.; Cantillo, D.; Kappe, C. O.; Luisi, R. *Angew. Chem. Int. Ed.* **2021**, *60*, 6395–6399. (d) Musci, P.; Colella, M.; Andresini, M.; Aramini, A.; Degennaro, L.; Luisi, R. *Chem. Commun.* **2022**, *58*, 6356–6359.

434 For selected examples by Yoshida, see: (a) Kim, H.; Nagaki, A.; Yoshida, J. *Nat. Commun.* **2011**, *2*, 264. (b) Tomida, Y.; Nagaki, A.; Yoshida, J. *J. Am. Chem. Soc.* **2011**, *133*, 3744–3747. (c) Nagaki, A.; Ichinari, D.; Yoshida, J. *J. Am. Chem. Soc.* **2014**, *136*, 12245–12248. (d) Nagaki, A.; Imai, K.; Ishiuchi, S.; Yoshida, J. *Angew. Chem. Int. Ed.* **2015**, *54*, 1914–1918. (e) Kim, H.; Min, K.-I.; Inoue, K.; Im, D. J.; Kim, D.-P.; Yoshida, J. *Science* **2016**, *352*, 691–694.

435 Love, B. E.; Jones, E. G. *J. Org. Chem.* **1999**, *64*, 3755–3756.

436 Lombardo, F.; Shalaeva, M. Y.; Tupper, K. A.; Gao, F. *J. Med. Chem.* **2001**, *44*, 2490–2497.

437 Finlayson, K.; Turnbull, L.; January, C. T.; Sharkey, J.; Kelly, J. S. *Eur. J. Pharmacol.* **2001**, *430*, 147–148.

438 R Core Team. *R: A language and environment for statistical computing*, version 3.2.2; R Foundation for Statistical Computing: Vienna, Austria, 2015.

439 Gagne, R. R.; Koval, C. A.; Lisensky, G. C. *Inorganic Chemistry*. **1980**, *19*, 2854–2855.

440 Pavlishchuk, V. V.; Addison, A. W. *Inorganica Chim. Acta* **2000**, *298*, 97–102.

441 Han, Y. T. *Nat. Prod. Commun.* **2017**, *12*, 95–98.

442 Takahashi, N.; Maeda, K.; Asano, Y.; Watanabe, N. *Bioorg. Med. Chem.* **2014**, *22*, 488–498.

443 Pirali, T.; Zhang, F.; Miller, A. H.; Head, J. L.; McAusland, D.; Greaney, M. F. *Angew. Chem. Int. Ed.* **2012**, *51*, 1006–1009.

444 Park, K.-Y.; Song, H.-J.; Heo, J.-N. *Adv. Synth. Catal.* **2015**, *357*, 3197–3205.

445 Kim, B.; Park, H.; Lee, S. K.; Park, S. J.; Koo, T.-S.; Kang, N. S.; Hong, K. B.; Choi, S. *Eur. J. Med. Chem.* **2016**, *123*, 777–787.

446 Burrows, J. N.; Tucker, H. (AstraZeneca UK Ltd.) *N-Sulfonylpiperidines as Metalloproteinase Inhibitors (TACE)*, WO Patent Appl. No WO2004006925A1, **2004**.

447 Ankner, T.; Said Stålsmeden, A.; Hilmersson, G. *Chem. Commun.* **2013**, *49*, 6867–6889.

448 Löser, R.; Schilling, K.; Dimmig, E.; Gütschow, M. *J. Med. Chem.* **2005**, *48*, 7688–7707.

449 Suzue, S.; Irikura, T. *Chem. Pharm. Bull.* **1968**, *16*, 1417–1432.

450 Nugent, J.; Arroniz, C.; Shire, B. R.; Sterling, A. J.; Pickford, H. D.; Wong, M. L. J.; Mansfield, S. J.; Caputo, D. F. J.; Owen, B.; Mousseau, J. J.; Duarte, F.; Anderson, E. A. *ACS Catal.* **2019**, *9*, 9568–9574.

451 Bunker, K. D.; Sach, N. W.; Huang, Q.; Richardson, P. F. *Org. Lett.* **2011**, *13*, 4746–4748.

452 Yahata, K.; Ye, N.; Ai, Y.; Iso, K.; Kishi, Y. *Angew. Chem. Int. Ed.* **2017**, *56*, 10796–10800.

453 Loison, A.; Hanquet, G.; Toulgoat, F.; Billard, T.; Panossian, A.; Leroux, F. R. *Org. Lett.* **2022**, *24*, 8316–8321.

454 Hampel, T.; Ruppenthal, S.; Sälinger, D.; Brückner, R. *Chem. Eur. J.* **2012**, *18*, 3136–3140.

455 Xu, F.; Chen, Y.; Fan, E.; Sun, Z. *Org. Lett.* **2016**, *18*, 2777–2779.

9 Appendix

9.1 Appearance of Thietane Rings in the Literature

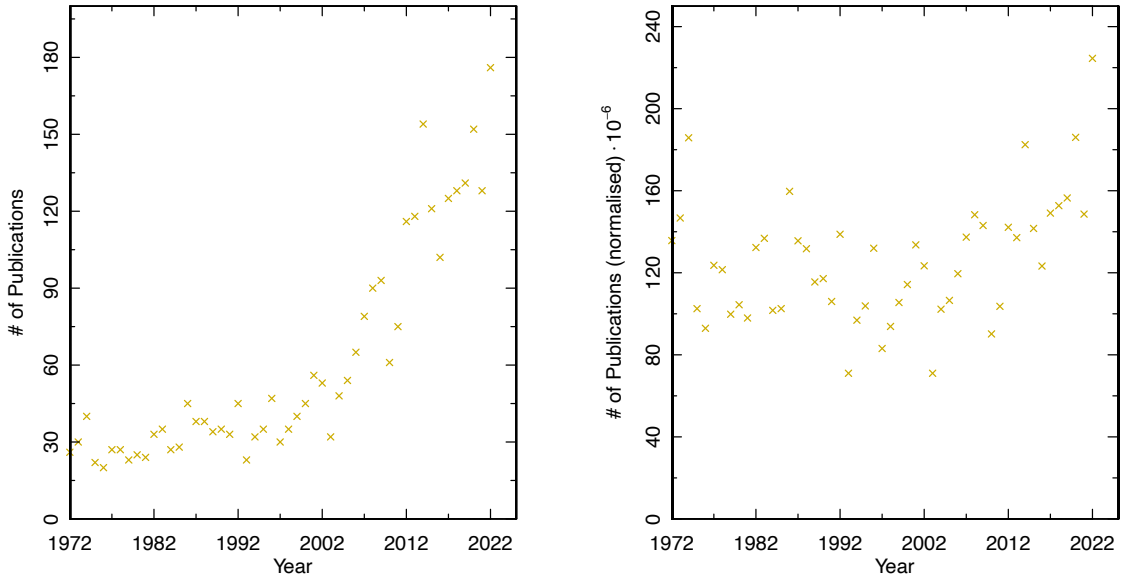


Figure 93. Number of publications that include a thietane ring between 1972 and 2022.[pp] Left: Absolute number of publications. Right: normalised against the total number of publications recorded per year.

9.2 Complete List of References for the Application of Oxetanes in Medicinal Chemistry Campaigns

A comprehensive list of references of all medicinal chemistry campaigns that included an oxetane structure between 2017–2022 in scientific articles is listed below ordered by year:

2017

Low, J. D.; Bartberger, M. D.; Chen, K.; Cheng, Y.; Fielden, M. R.; Gore, V.; Hickman, D.; Liu, Q.; Allen Sickmier, E.; Vargas, H. M.; Werner, J.; White, R. D.; Whittington, D. A.; Wood, S.; Minatti, A. E. *Medchemcomm* **2017**, *8*, 1196–1206. Eastman, K. J.; Parcella, K.; Yeung, K.-S.; Grant-Young, K. A.; Zhu, J.; Wang, T.; Zhang, Z.; Yin, Z.; Beno, B. R.; Sheriff, S.; Kish, K.; Tredup, J.; Jardel, A. G.; Halan, V.; Ghosh, K.; Parker, D.; Mosure, K.; Fang, H.; Wang, Y.-K.; Lemm, J.; Zhuo, X.; Hanumegowda, U.; Rigat, K.; Donoso, M.; Tuttle, M.; Zvyaga, T.; Haarhoff, Z.; Meanwell, N. A.; Soars, M. G.; Roberts, S. B.; Kadow, J. F. *Medchemcomm* **2017**, *8*, 796–806. Feng, S.; Li, C.; Chen, D.; Zheng, X.; Yun, H.; Gao, L.; Shen, H. C. *Eur. J.*

[pp] Values obtained from a Scifinder search on 19.01.2023. Only publications that include: biological study, therapeutic use, pharmacological activity, preparation, synthetic preparation, biological study (unclassified), pharmacokinetics, biological use (unclassified), agricultural use, biosynthetic preparation and natural product occurrence.

Med. Chem. **2017**, *138*, 1147–1157. Wang, X.; Barbosa, J.; Blomgren, P.; Bremer, M. C.; Chen, J.; Crawford, J. J.; Deng, W.; Dong, L.; Eigenbrot, C.; Gallion, S.; Hau, J.; Hu, H.; Johnson, A. R.; Katewa, A.; Kropf, J. E.; Lee, S. H.; Liu, L.; Lubach, J. W.; Macaluso, J.; Maciejewski, P.; Mitchell, S. A.; Ortwine, D. F.; DiPaolo, J.; Reif, K.; Scheerens, H.; Schmitt, A.; Wong, H.; Xiong, J.-M.; Xu, J.; Zhao, Z.; Zhou, F.; Currie, K. S.; Young, W. B. *ACS Med. Chem. Lett.* **2017**, *8*, 608–613. Millan, D. S.; Kayser-Bricker, K. J.; Martin, M. W.; Talbot, A. C.; Schiller, S. E. R.; Herbertz, T.; Williams, G. L.; Luke, G. P.; Hubbs, S.; Alvarez Morales, M. A.; Cardillo, D.; Troccolo, P.; Mendes, R. L.; McKinnon, C. *ACS Med. Chem. Lett.* **2017**, *8*, 847–852. Llona-Minguez, S.; Höglund, A.; Ghassemian, A.; Desroses, M.; Calderón-Montaño, J. M.; Burgos Morón, E.; Valerie, N. C. K.; Wiita, E.; Almlöf, I.; Koolmeister, T.; Mateus, A.; Cazares-Körner, C.; Sanjiv, K.; Homan, E.; Loseva, O.; Baranczewski, P.; Darabi, M.; Mehdizadeh, A.; Fayezi, S.; Jemth, A.-S.; Warpman Berglund, U.; Sigmundsson, K.; Lundbäck, T.; Jenmalm Jensen, A.; Artursson, P.; Scobie, M.; Helleday, T. *J. Med. Chem.* **2017**, *60*, 4279–4292. Burks, H. E.; Abrams, T.; Kirby, C. A.; Baird, J.; Fekete, A.; Hamann, L. G.; Kim, S.; Lombardo, F.; Loo, A.; Lubicka, D.; Macchi, K.; McDonnell, D. P.; Mishina, Y.; Norris, J. D.; Nunez, J.; Saran, C.; Sun, Y.; Thomsen, N. M.; Wang, C.; Wang, J.; Peukert, S. *J. Med. Chem.* **2017**, *60*, 2790–2818. Nordqvist, A.; O'Mahony, G.; Fridén-Saxin, M.; Fredenwall, M.; Hogner, A.; Granberg, K. L.; Aagaard, A.; Bäckström, S.; Gunnarsson, A.; Kaminski, T.; Xue, Y.; Dellsén, A.; Hansson, E.; Hansson, P.; Ivarsson, I.; Karlsson, U.; Bamberg, K.; Hermansson, M.; Georgsson, J.; Lindmark, B.; Edman, K. *ChemMedChem* **2017**, *12*, 50–65. Gibson, T. S.; Johnson, B.; Fanjul, A.; Halkowycz, P.; Dougan, D. R.; Cole, D.; Swann, S. *Bioorg. Med. Chem. Lett.* **2017**, *27*, 1709–1713. Wang, L.; Pratt, J. K.; Soltwedel, T.; Sheppard, G. S.; Fidanze, S. D.; Liu, D.; Hasvold, L. A.; Mantei, R. A.; Holms, J. H.; McClellan, W. J.; Wendt, M. D.; Wada, C.; Frey, R.; Hansen, T. M.; Hubbard, R.; Park, C. H.; Li, L.; Magoc, T. J.; Albert, D. H.; Lin, X.; Warder, S. E.; Kovar, P.; Huang, X.; Wilcox, D.; Wang, R.; Rajaraman, G.; Petros, A. M.; Hutchins, C. W.; Panchal, S. C.; Sun, C.; Elmore, S. W.; Shen, Y.; Kati, W. M.; McDaniel, K. F. *J. Med. Chem.* **2017**, *60*, 3828–3850. Riggs, J. R.; Nagy, M.; Elsner, J.; Erdman, P.; Cashion, D.; Robinson, D.; Harris, R.; Huang, D.; Tehrani, L.; Deyanat-Yazdi, G.; Narla, R. K.; Peng, X.; Tran, T.; Barnes, L.; Miller, T.; Katz, J.; Tang, Y.; Chen, M.; Moghaddam, M. F.; Bahmanyar, S.; Pagarigan, B.; Delker, S.; LeBrun, L.; Chamberlain, P. P.; Calabrese, A.; Canan, S. S.; Leftheris, K.; Zhu, D.; Boylan, J. F. *J. Med. Chem.* **2017**, *60*, 8989–9002. Siu, T.; Brubaker, J.; Fuller, P.; Torres, L.; Zeng, H.; Close, J.; Mampreian, D. M.; Shi, F.; Liu, D.; Fradera, X.; Johnson, K.; Bays, N.; Kadic, E.; He, F.; Goldenblatt, P.; Shaffer, L.; Patel, S. B.; Lesburg, C. A.; Alpert, C.; Dorosh, L.; Deshmukh, S. V.; Yu, H.; Klappenbach, J.; Elwood, F.; Dinsmore, C. J.; Fernandez, R.; Moy, L.; Young, J. R. *J. Med. Chem.* **2017**, *60*, 9676–9690. Bezençon, O.; Heidmann, B.; Siegrist, R.; Stamm, S.; Richard, S.; Pozzi, D.; Corminboeuf, O.; Roch, C.; Kessler, M.; Ertel, E. A.; Reymond, I.;

Pfeifer, T.; de Kanter, R.; Toeroek-Schafroth, M.; Moccia, L. G.; Mawet, J.; Moon, R.; Rey, M.; Capeleto, B.; Fournier, E. *J. Med. Chem.* **2017**, *60*, 9769–9789. Boga, S. B.; Alhassan, A.-B.; Liu, J.; Guiadeen, D.; Krikorian, A.; Gao, X.; Wang, J.; Yu, Y.; Anand, R.; Liu, S.; Yang, C.; Wu, H.; Cai, J.; Zhu, H.; Desai, J.; Maloney, K.; Gao, Y.-D.; Fischmann, T. O.; Presland, J.; Mansueto, M.; Xu, Z.; Leccese, E.; Knemeyer, I.; Garlisi, C. G.; Bays, N.; Stivers, P.; Brandish, P. E.; Hicks, A.; Cooper, A.; Kim, R. M.; Kozlowski, J. A. *Bioorg. Med. Chem. Lett.* **2017**, *27*, 3939–3943. Patel, S.; Meilandt, W. J.; Erickson, R. I.; Chen, J.; Deshmukh, G.; Estrada, A. A.; Fuji, R. N.; Gibbons, P.; Gustafson, A.; Harris, S. F.; Imperio, J.; Liu, W.; Liu, X.; Liu, Y.; Lyssikatos, J. P.; Ma, C.; Yin, J.; Lewcock, J. W.; Siu, M. *J. Med. Chem.* **2017**, *60*, 8083–8102.

2018

Poce, G.; Cocozza, M.; Alfonso, S.; Consalvi, S.; Venditti, G.; Fernandez-Menendez, R.; Bates, R. H.; Barros Aguirre, D.; Ballell, L.; De Logu, A.; Vistoli, G.; Biava, M. *Eur. J. Med. Chem.* **2018**, *145*, 539–550. Cheong, J. E.; Zaffagni, M.; Chung, I.; Xu, Y.; Wang, Y.; Jernigan, F. E.; Zetter, B. R.; Sun, L. *Eur. J. Med. Chem.* **2018**, *144*, 372–385. Vazquez, M. L.; Kaila, N.; Strohbach, J. W.; Trzupek, J. D.; Brown, M. F.; Flanagan, M. E.; Mitton-Fry, M. J.; Johnson, T. A.; TenBrink, R. E.; Arnold, E. P.; Basak, A.; Heasley, S. E.; Kwon, S.; Langille, J.; Parikh, M. D.; Griffin, S. H.; Casavant, J. M.; Duclos, B. A.; Fenwick, A. E.; Harris, T. M.; Han, S.; Caspers, N.; Dowty, M. E.; Yang, X.; Banker, M. E.; Hegen, M.; Symanowicz, P. T.; Li, L.; Wang, L.; Lin, T. H.; Jussif, J.; Clark, J. D.; Telliez, J.-B.; Robinson, R. P.; Unwalla, R. *J. Med. Chem.* **2018**, *61*, 1130–1152. Kung, P.-P.; Bingham, P.; Brooun, A.; Collins, M.; Deng, Y.-L.; Dinh, D.; Fan, C.; Gajiwala, K. S.; Grantner, R.; Gukasyan, H. J.; Hu, W.; Huang, B.; Kania, R.; Kephart, S. E.; Krivacic, C.; Kumpf, R. A.; Khamphavong, P.; Kraus, M.; Liu, W.; Maegley, K. A.; Nguyen, L.; Ren, S.; Richter, D.; Rollins, R. A.; Sach, N.; Sharma, S.; Sherrill, J.; Spangler, J.; Stewart, A. E.; Sutton, S.; Uryu, S.; Verhelle, D.; Wang, H.; Wang, S.; Wythes, M.; Xin, S.; Yamazaki, S.; Zhu, H.; Zhu, J.; Zehnder, L.; Edwards, M. *J. Med. Chem.* **2018**, *61*, 650–665. Soares, P.; Gadd, M. S.; Frost, J.; Galdeano, C.; Ellis, L.; Epemolu, O.; Rocha, S.; Read, K. D.; Ciulli, A. *J. Med. Chem.* **2018**, *61*, 599–618. Crawford, J. J.; Johnson, A. R.; Misner, D. L.; Belmont, L. D.; Castanedo, G.; Choy, R.; Coraggio, M.; Dong, L.; Eigenbrot, C.; Erickson, R.; Ghilardi, N.; Hau, J.; Katewa, A.; Kohli, P. B.; Lee, W.; Lubach, J. W.; McKenzie, B. S.; Ortwine, D. F.; Schutt, L.; Tay, S.; Wei, B.; Reif, K.; Liu, L.; Wong, H.; Young, W. B. *J. Med. Chem.* **2018**, *61*, 2227–2245. Pu, S.-Y.; Wouters, R.; Schor, S.; Rozenski, J.; Barouch-Bentov, R.; Prugar, L. I.; O'Brien, C. M.; Brannan, J. M.; Dye, J. M.; Herdewijn, P.; De Jonghe, S.; Einav, S. *J. Med. Chem.* **2018**, *61*, 6178–6192. Procopiou, P. A.; Anderson, N. A.; Barrett, J.; Barrett, T. N.; Crawford, M. H. J.; Fallon, B. J.; Hancock, A. P.; Le, J.; Lemma, S.; Marshall, R. P.; Morrell, J.; Pritchard, J. M.; Rowedder, J. E.; Saklatvala, P.; Slack, R. J.; Sollis, S. L.; Suckling, C. J.; Thorp, L. R.; Vitulli, G.; Macdonald, S. J. F. *J. Med. Chem.* **2018**, *61*, 8417–8443. Rogacki, M. K.; Pitta, E.; Balabon, O.; Huss, S.; Lopez-Roman, E. M.; Argyrou, A.;

Blanco-Ruano, D.; Cacho, M.; Vande Velde, C. M. L.; Augustyns, K.; Ballell, L.; Barros, D.; Bates, R. H.; Cunningham, F.; Van der Veken, P. *J. Med. Chem.* **2018**, *61*, 11221–11249. LaPorte, M. G.; Burnett, J. C.; Colombo, R.; Bulfer, S. L.; Alverez, C.; Chou, T.-F.; Neitz, R. J.; Green, N.; Moore, W. J.; Yue, Z.; Li, S.; Arkin, M. R.; Wipf, P.; Huryn, D. M. *ACS Med. Chem. Lett.* **2018**, *9*, 1075–1081. Akama, T.; Zhang, Y.-K.; Freund, Y. R.; Berry, P.; Lee, J.; Easom, E. E.; Jacobs, R. T.; Plattner, J. J.; Witty, M. J.; Peter, R.; Rowan, T. G.; Gillingwater, K.; Brun, R.; Nare, B.; Mercer, L.; Xu, M.; Wang, J.; Liang, H. *Bioorg. Med. Chem. Lett.* **2018**, *28*, 6–10. Chowdhury, S.; Owens, K. N.; Herr, R. J.; Jiang, Q.; Chen, X.; Johnson, G.; Groppi, V. E.; Raible, D. W.; Rubel, E. W.; Simon, J. A. *J. Med. Chem.* **2018**, *61*, 84–97. Chevillard, F.; Rimmer, H.; Betti, C.; Pardon, E.; Ballet, S.; van Hilten, N.; Steyaert, J.; Diederich, W. E.; Kolb, P. *J. Med. Chem.* **2018**, *61*, 1118–1129. Rahm, F.; Viklund, J.; Trésaugues, L.; Ellermann, M.; Giese, A.; Ericsson, U.; Forsblom, R.; Ginman, T.; Günther, J.; Hallberg, K.; Lindström, J.; Persson, L. B.; Silvander, C.; Talagas, A.; Díaz-Sáez, L.; Fedorov, O.; Huber, K. V. M.; Panagakou, I.; Siejka, P.; Gorjánácz, M.; Bauser, M.; Andersson, M. *J. Med. Chem.* **2018**, *61*, 2533–2551. Lu, H.; Yang, T.; Xu, Z.; Lin, X.; Ding, Q.; Zhang, Y.; Cai, X.; Dong, K.; Gong, S.; Zhang, W.; Patel, M.; Copley, R. C. B.; Xiang, J.; Guan, X.; Wren, P.; Ren, F. *J. Med. Chem.* **2018**, *61*, 2518–2532. Amato, G. S.; Manke, A.; Vasukuttan, V.; Wiethe, R. W.; Snyder, R. W.; Runyon, S. P.; Maitra, R. *Bioorg. Med. Chem.* **2018**, *26*, 4518–4531. Vandyck, K.; Rombouts, G.; Stoops, B.; Tahri, A.; Vos, A.; Verschueren, W.; Wu, Y.; Yang, J.; Hou, F.; Huang, B.; Vergauwen, K.; Dehertogh, P.; Berke, J. M.; Raboisson, P. *J. Med. Chem.* **2018**, *61*, 6247–6260. Pike, K. G.; Barlaam, B.; Cadogan, E.; Campbell, A.; Chen, Y.; Colclough, N.; Davies, N. L.; De-Almeida, C.; Degorce, S. L.; Didelot, M.; Dishington, A.; Ducray, R.; Durant, S. T.; Hassall, L. A.; Holmes, J.; Hughes, G. D.; MacFaul, P. A.; Mulholland, K. R.; McGuire, T. M.; Ouvry, G.; Pass, M.; Robb, G.; Stratton, N.; Wang, Z.; Wilson, J.; Zhai, B.; Zhao, K.; Al-Huniti, N. *J. Med. Chem.* **2018**, *61*, 3823–3841. Giroud, M.; Kuhn, B.; Saint-Auret, S.; Kuratli, C.; Martin, R. E.; Schuler, F.; Diederich, F.; Kaiser, M.; Brun, R.; Schirmeister, T.; Haap, W. *J. Med. Chem.* **2018**, *61*, 3370–3388. Huddle, B. C.; Grimley, E.; Buchman, C. D.; Chtcherbinine, M.; Debnath, B.; Mehta, P.; Yang, K.; Morgan, C. A.; Li, S.; Felton, J.; Sun, D.; Mehta, G.; Neamati, N.; Buckanovich, R. J.; Hurley, T. D.; Larsen, S. D. *J. Med. Chem.* **2018**, *61*, 8754–8773. Liu, X.; Zhang, Y.; Huang, W.; Tan, W.; Zhang, A. *Bioorg. Med. Chem.* **2018**, *26*, 443–454.

2019

Cao, H.; Zhu, G.; Sun, L.; Chen, G.; Ma, X.; Luo, X.; Zhu, J. *Eur. J. Med. Chem.* **2019**, *183*, 111694. Chen, P.; Zhang, D.; Li, M.; Wu, Q.; Lam, Y. P. Y.; Guo, Y.; Chen, C.; Bai, N.; Malhotra, S.; Li, W.; O'Connor, P. B.; Fu, H. *Eur. J. Med. Chem.* **2019**, *183*, 111722. Zhu, Y.; Sun, N.; Yu, M.; Guo, H.; Xie, Q.; Wang, Y. *Eur. J. Med. Chem.* **2019**, *182*, 111589. Chen, S.; Guo, W.; Liu, X.; Sun, P.; Wang, Y.; Ding, C.; Meng, L.; Zhang, A. *Eur. J. Med. Chem.* **2019**,

179, 38–55. Zhang, C.; Pei, H.; He, J.; Zhu, J.; Li, W.; Niu, T.; Xiang, M.; Chen, L. *Eur. J. Med. Chem.* **2019**, *169*, 121–143. Bagal, S. K.; Omoto, K.; Blakemore, D. C.; Bungay, P. J.; Bilsland, J. G.; Clarke, P. J.; Corbett, M. S.; Cronin, C. N.; Cui, J. J.; Dias, R.; Flanagan, N. J.; Greasley, S. E.; Grimley, R.; Johnson, E.; Fengas, D.; Kitching, L.; Kraus, M. L.; McAlpine, I.; Nagata, A.; Waldron, G. J.; Warmus, J. S. *J. Med. Chem.* **2019**, *62*, 247–265. Guerrero, M.; Urbano, M.; Kim, E.-K.; Gamo, A. M.; Riley, S.; Abgaryan, L.; Leaf, N.; Van Orden, L. J.; Brown, S. J.; Xie, J. Y.; Porreca, F.; Cameron, M. D.; Rosen, H.; Roberts, E. *J. Med. Chem.* **2019**, *62*, 1761–1780. Caille, S.; Cui, S.; Faul, M. M.; Mennen, S. M.; Tedrow, J. S.; Walker, S. D. *J. Org. Chem.* **2019**, *84*, 4583–4603. Kong, D.; Guo, S.; Yang, Y.; Guo, B.; Xie, X.; Hu, W. *Bioorg. Med. Chem. Lett.* **2019**, *29*, 848–852. Wang, H.-L.; Andrews, K. L.; Booker, S. K.; Canon, J.; Cee, V. J.; Chavez, F.; Chen, Y.; Eastwood, H.; Guerrero, N.; Herberich, B.; Hickman, D.; Lanman, B. A.; Laszlo, J.; Lee, M. R.; Lipford, J. R.; Mattson, B.; Mohr, C.; Nguyen, Y.; Norman, M. H.; Pettus, L. H.; Powers, D.; Reed, A. B.; Rex, K.; Sastri, C.; Tamayo, N.; Wang, P.; Winston, J. T.; Wu, B.; Wu, Q.; Wu, T.; Wurz, R. P.; Xu, Y.; Zhou, Y.; Tasker, A. S. *J. Med. Chem.* **2019**, *62*, 1523–1540. Shi, C.; Zhang, Y.; Wang, T.; Lu, W.; Zhang, S.; Guo, B.; Chen, Q.; Luo, C.; Zhou, X.; Yang, Y. *J. Med. Chem.* **2019**, *62*, 2950–2973. Aguilar, A.; Zheng, K.; Xu, T.; Xu, S.; Huang, L.; Fernandez-Salas, E.; Liu, L.; Bernard, D.; Harvey, K. P.; Foster, C.; McEachern, D.; Stuckey, J.; Chinnaswamy, K.; Delproposto, J.; Kampf, J. W.; Wang, S. *J. Med. Chem.* **2019**, *62*, 6015–6034. Alen, J.; Schade, M.; Wagener, M.; Christian, F.; Nordhoff, S.; Merla, B.; Dunkern, T. R.; Bahrenberg, G.; Ratcliffe, P. *J. Med. Chem.* **2019**, *62*, 6391–6397. Fleau, C.; Padilla, A.; Miguel-Siles, J.; Quesada-Campos, M. T.; Saiz-Nicolas, I.; Cotillo, I.; Cantizani Perez, J.; Tarleton, R. L.; Marco, M.; Courtemanche, G. *J. Med. Chem.* **2019**, *62*, 10362–10375. Werner, S.; Mesch, S.; Hillig, R. C.; ter Laak, A.; Klint, J.; Neagoe, I.; Laux-Biehlmann, A.; Dahllöf, H.; Bräuer, N.; Puetter, V.; Nubbemeyer, R.; Schulz, S.; Bairlein, M.; Zollner, T. M.; Steinmeyer, A. *J. Med. Chem.* **2019**, *62*, 11194–11217. Dai, W.; Samanta, S.; Xue, D.; Petrunak, E. M.; Stuckey, J. A.; Han, Y.; Sun, D.; Wu, Y.; Neamati, N. *J. Med. Chem.* **2019**, *62*, 3068–3087. Toledo-Sherman, L.; Breccia, P.; Cachope, R.; Bate, J. R.; Angulo-Herrera, I.; Wishart, G.; Matthews, K. L.; Martin, S. L.; Cox, H. C.; McAllister, G.; Penrose, S. D.; Vater, H.; Esmieu, W.; Van de Poël, A.; Van de Bospoort, R.; Strijbosch, A.; Lamers, M.; Leonard, P.; Jarvis, R. E.; Blackaby, W.; Barnes, K.; Eznarriaga, M.; Dowler, S.; Smith, G. D.; Fischer, D. F.; Lazari, O.; Yates, D.; Rose, M.; Jang, S.-W.; Muñoz-Sanjuan, I.; Dominguez, C. *J. Med. Chem.* **2019**, *62*, 2988–3008. Bell, M.; Foley, D.; Naylor, C.; Wood, G.; Robinson, C.; Riley, J.; Epemolu, O.; Ellis, L.; Scullion, P.; Shishikura, Y.; Osuna-Cabello, M.; Ferguson, L.; Pinto, E.; Fletcher, D.; Katz, E.; McLean, W. H. I.; Wyatt, P.; Read, K. D.; Woodland, A. *ACS Med. Chem. Lett.* **2019**, *10*, 341–347. Meinig, J. M.; Ferrara, S. J.; Banerji, T.; Banerji, T.; Sanford-Crane, H. S.; Bourdette, D.; Scanlan, T. S. *ACS Med. Chem. Lett.* **2019**, *10*, 111–116. Felts, A. S.; Bollinger, K. A.; Brassard, C. J.; Rodriguez, A. L.; Morrison, R. D.; Scott

Daniels, J.; Blobaum, A. L.; Niswender, C. M.; Jones, C. K.; Jeffrey Conn, P.; Emmitte, K. A.; Lindsley, C. W. *Bioorg. Med. Chem. Lett.* **2019**, *29*, 47–50. Kaieda, A.; Takahashi, M.; Fukuda, H.; Okamoto, R.; Morimoto, S.; Gotoh, M.; Miyazaki, T.; Hori, Y.; Unno, S.; Kawamoto, T.; Tanaka, T.; Itono, S.; Takagi, T.; Sugimoto, H.; Okada, K.; Lane, W.; Sang, B.; Saikatendu, K.; Matsunaga, S.; Miwatashi, S. *ChemMedChem* **2019**, *14*, 2093–2101. Meng, W.; Adam, L. P.; Behnia, K.; Zhao, L.; Yang, R.; Kopcho, L. M.; Locke, G. A.; Taylor, D. S.; Yin, X.; Wexler, R. R.; Finlay, H. *Bioorg. Med. Chem. Lett.* **2019**, *29*, 126673. Amato, G.; Wiethe, R.; Manke, A.; Vasukuttan, V.; Snyder, R.; Runyon, S.; Maitra, R. *Bioorg. Med. Chem.* **2019**, *27*, 3632–3649. Mazur, M.; Dymek, B.; Koralewski, R.; Sklepkiewicz, P.; Olejniczak, S.; Mazurkiewicz, M.; Piotrowicz, M.; Salamon, M.; Jędrzejczak, K.; Zagozdzon, A.; Czestkowski, W.; Matyszewski, K.; Borek, B.; Bartoszewicz, A.; Pluta, E.; Rymaszewska, A.; Mozga, W.; Stefaniak, F.; Dobrzański, P.; Dzwonek, K.; Golab, J.; Golebiowski, A.; Olczak, J. *J. Med. Chem.* **2019**, *62*, 7126–7145. Owen, R. M.; Blakemore, D. C.; Cao, L.; Flanagan, N.; Fish, R.; Gibson, K. R.; Gurrell, R.; Huh, C. W.; Kammonen, J.; Mortimer-Cassen, E.; Nickolls, S.; Omoto, K.; Owen, D. R.; Pike, A.; Pryde, D. C.; Reynolds, D.; Roeloffs, R.; Rose, C. R.; Stead, C.; Takeuchi, M.; Warmus, J. S.; Watson, C. *J. Med. Chem.* **2019**, *62*, 5773–5796. Velcicky, J.; Mathison, C. J. N.; Nikulin, V.; Pflieger, D.; Epple, R.; Azimioara, M.; Cow, C.; Michellys, P.-Y.; Rigollier, P.; Beisner, D. R.; Bodendorf, U.; Guerini, D.; Liu, B.; Wen, B.; Zaharevitz, S.; Brandl, T. *ACS Med. Chem. Lett.* **2019**, *10*, 887–892. Cioffi, C. L.; Racz, B.; Varadi, A.; Freeman, E. E.; Conlon, M. P.; Chen, P.; Zhu, L.; Kitchen, D. B.; Barnes, K. D.; Martin, W. H.; Pearson, P. G.; Johnson, G.; Blaner, W. S.; Petrukhin, K. *J. Med. Chem.* **2019**, *62*, 5470–5500. Fushimi, M.; Fujimori, I.; Wakabayashi, T.; Hasui, T.; Kawakita, Y.; Imamura, K.; Kato, T.; Murakami, M.; Ishii, T.; Kikko, Y.; Kasahara, M.; Nakatani, A.; Hiura, Y.; Miyamoto, M.; Saikatendu, K.; Zou, H.; Lane, S. W.; Lawson, J. D.; Imoto, H. *J. Med. Chem.* **2019**, *62*, 4915–4935. Kahl, D. J.; Hutchings, K. M.; Lisabeth, E. M.; Haak, A. J.; Leipprandt, J. R.; Dexheimer, T.; Khanna, D.; Tsou, P.-S.; Campbell, P. L.; Fox, D. A.; Wen, B.; Sun, D.; Bailie, M.; Neubig, R. R.; Larsen, S. D. *J. Med. Chem.* **2019**, *62*, 4350–4369. Riggs, J. R.; Elsner, J.; Cashion, D.; Robinson, D.; Tehrani, L.; Nagy, M.; Fultz, K. E.; Krishna Narla, R.; Peng, X.; Tran, T.; Kulkarni, A.; Bahmanyar, S.; Condroski, K.; Pagarigan, B.; Fenalti, G.; LeBrun, L.; Leftheris, K.; Zhu, D.; Boylan, J. F. *J. Med. Chem.* **2019**, *62*, 4401–4410. Lin, S.; Jin, J.; Liu, Y.; Tian, H.; Zhang, Y.; Fu, R.; Zhang, J.; Wang, M.; Du, T.; Ji, M.; Wu, D.; Zhang, K.; Sheng, L.; Li, Y.; Chen, X.; Xu, H. *J. Med. Chem.* **2019**, *62*, 8873–8879. Mullarky, E.; Xu, J.; Robin, A. D.; Huggins, D. J.; Jennings, A.; Noguchi, N.; Olland, A.; Lakshminarasimhan, D.; Miller, M.; Tomita, D.; Michino, M.; Su, T.; Zhang, G.; Stamford, A. W.; Meinke, P. T.; Kargman, S.; Cantley, L. C. *Bioorg. Med. Chem. Lett.* **2019**, *29*, 2503–2510. Collier, P. N.; Twin, H. C.; Knegtel, R. M. A.; Boyall, D.; Brenchley, G.; Davis, C. J.; Keily, S.; Mak, C.; Miller, A.; Pierard,

F.; Settimo, L.; Bolton, C. M.; Chiu, P.; Curnock, A.; Doyle, E.; Tanner, A. J.; Jimenez, J.-M. *ACS Med. Chem. Lett.* **2019**, *10*, 1134–1139.

2020

Xu, G.; Zhang, Y.; Wang, H.; Guo, Z.; Wang, X.; Li, X.; Chang, S.; Sun, T.; Yu, Z.; Xu, T.; Zhao, L.; Wang, Y.; Yu, W. *Eur. J. Med. Chem.* **2020**, *198*, 112354. Zhu, F.; Wang, Y.; Du, Q.; Ge, W.; Li, Z.; Wang, X.; Fu, C.; Luo, L.; Tian, S.; Ma, H.; Zheng, J.; Zhang, Y.; Sun, X.; He, S.; Zhang, X. *Eur. J. Med. Chem.* **2020**, *187*, 111914. Zhu, C.; Li, X.; Zhao, B.; Peng, W.; Li, W.; Fu, W. *Eur. J. Med. Chem.* **2020**, *193*, 112214.Khanna, A.; Côté, A.; Arora, S.; Moine, L.; Gehling, V. S.; Brenneman, J.; Cantone, N.; Stuckey, J. I.; Apte, S.; Ramakrishnan, A.; Bruderek, K.; Bradley, W. D.; Audia, J. E.; Cummings, R. T.; Sims, R. J.; Trojer, P.; Levell, J. R. *ACS Med. Chem. Lett.* **2020**, *11*, 1205–1212. Wellaway, C. R.; Amans, D.; Bamborough, P.; Barnett, H.; Bit, R. A.; Brown, J. A.; Carlson, N. R.; Chung, C.; Cooper, A. W. J.; Craggs, P. D.; Davis, R. P.; Dean, T. W.; Evans, J. P.; Gordon, L.; Harada, I. L.; Hirst, D. J.; Humphreys, P. G.; Jones, K. L.; Lewis, A. J.; Lindon, M. J.; Lugo, D.; Mahmood, M.; McCleary, S.; Medeiros, P.; Mitchell, D. J.; O'Sullivan, M.; Le Gall, A.; Patel, V. K.; Patten, C.; Poole, D. L.; Shah, R. R.; Smith, J. E.; Stafford, K. A. J.; Thomas, P. J.; Vimal, M.; Wall, I. D.; Watson, R. J.; Wellaway, N.; Yao, G.; Prinjha, R. K. *J. Med. Chem.* **2020**, *63*, 714–746. Blomgren, P.; Chandrasekhar, J.; Di Paolo, J. A.; Fung, W.; Geng, G.; Ip, C.; Jones, R.; Kropf, J. E.; Lansdon, E. B.; Lee, S.; Lo, J. R.; Mitchell, S. A.; Murray, B.; Pohlmeyer, C.; Schmitt, A.; Suekawa-Pirrone, K.; Wise, S.; Xiong, J.-M.; Xu, J.; Yu, H.; Zhao, Z.; Currie, K. S. *ACS Med. Chem. Lett.* **2020**, *11*, 506–513. Panchaud, P.; Surivet, J.-P.; Diethelm, S.; Blumstein, A.-C.; Gauvin, J.-C.; Jacob, L.; Masse, F.; Mathieu, G.; Mirre, A.; Schmitt, C.; Enderlin-Paput, M.; Lange, R.; Gnerre, C.; Seeland, S.; Herrmann, C.; Locher, H. H.; Seiler, P.; Ritz, D.; Rueedi, G. *J. Med. Chem.* **2020**, *63*, 88–102. Kwiatkowski, J.; Liu, B.; Pang, S.; Ahmad, N. H. B.; Wang, G.; Poulsen, A.; Yang, H.; Poh, Y. R.; Tee, D. H. Y.; Ong, E.; Retna, P.; Dinie, N.; Kwek, P.; Wee, J. L. K.; Manoharan, V.; Low, C. B.; Seah, P. G.; Pendharkar, V.; Sangthongpitag, K.; Joy, J.; Baburajendran, N.; Jansson, A. E.; Nacro, K.; Hill, J.; Keller, T. H.; Hung, A. W. *J. Med. Chem.* **2020**, *63*, 621–637. Shirai, F.; Mizutani, A.; Yashiroda, Y.; Tsumura, T.; Kano, Y.; Muramatsu, Y.; Chikada, T.; Yuki, H.; Niwa, H.; Sato, S.; Washizuka, K.; Koda, Y.; Mazaki, Y.; Jang, M.-K.; Yoshida, H.; Nagamori, A.; Okue, M.; Watanabe, T.; Kitamura, K.; Shitara, E.; Honma, T.; Umehara, T.; Shirouzu, M.; Fukami, T.; Seimiya, H.; Yoshida, M.; Koyama, H. *J. Med. Chem.* **2020**, *63*, 4183–4204. Leger, P. R.; Hu, D. X.; Biannic, B.; Bui, M.; Han, X.; Karbarz, E.; Maung, J.; Okano, A.; Osipov, M.; Shibuya, G. M.; Young, K.; Higgs, C.; Abraham, B.; Bradford, D.; Cho, C.; Colas, C.; Jacobson, S.; Ohol, Y. M.; Pookot, D.; Rana, P.; Sanchez, J.; Shah, N.; Sun, M.; Wong, S.; Brockstedt, D. G.; Kassner, P. D.; Schwarz, J. B.; Wustrow, D. J. *J. Med. Chem.* **2020**, *63*, 5398–5420. Vendeville, S.; Tahri, A.; Hu, L.; Demin, S.; Cooymans, L.; Vos, A.; Kwanten, L.; Van den Berg, J.; Battles, M. B.; McLellan, J. S.; Koul,

A.; Raboisson, P.; Roymans, D.; Jonckers, T. H. M. *J. Med. Chem.* **2020**, *63*, 8046–8058. Wang, C.; Pei, Y.; Wang, L.; Li, S.; Jiang, C.; Tan, X.; Dong, Y.; Xiang, Y.; Ma, Y.; Liu, G. *J. Med. Chem.* **2020**, *63*, 6066–6089. Li, Y.; Zhao, J.; Gutgesell, L. M.; Shen, Z.; Ratia, K.; Dye, K.; Dubrovskyi, O.; Zhao, H.; Huang, F.; Tonetti, D. A.; Thatcher, G. R. J.; Xiong, R. *J. Med. Chem.* **2020**, *63*, 7186–7210. Rodríguez Sarmiento, R. M.; Bissantz, C.; Bylund, J.; Limberg, A.; Neidhart, W.; Jakob-Roetne, R.; Wang, L.; Baumann, K. *J. Med. Chem.* **2020**, *63*, 8534–8553. Shen, Y.; Gao, G.; Yu, X.; Kim, H.; Wang, L.; Xie, L.; Schwarz, M.; Chen, X.; Guccione, E.; Liu, J.; Bedford, M. T.; Jin, J. *J. Med. Chem.* **2020**, *63*, 9977–9989. Furukawa, H.; Miyamoto, Y.; Hirata, Y.; Watanabe, K.; Hitomi, Y.; Yoshitomi, Y.; Aida, J.; Noguchi, N.; Takakura, N.; Takami, K.; Miwatashi, S.; Hirozane, Y.; Hamada, T.; Ito, R.; Ookawara, M.; Moritoh, Y.; Watanabe, M.; Maekawa, T. *J. Med. Chem.* **2020**, *63*, 10352–10379. Chen, J.; Zhou, Y.; Dong, X.; Liu, L.; Bai, L.; McEachern, D.; Przybranowski, S.; Yang, C.-Y.; Stuckey, J.; Li, X.; Wen, B.; Zhao, T.; Sun, S.; Sun, D.; Jiao, L.; Jing, Y.; Guo, M.; Yang, D.; Wang, S. *J. Med. Chem.* **2020**, *63*, 13994–14016. Hügle, M.; Regenass, P.; Warstat, R.; Hau, M.; Schmidtkunz, K.; Lucas, X.; Wohlwend, D.; Einsle, O.; Jung, M.; Breit, B.; Günther, S. *J. Med. Chem.* **2020**, *63*, 15603–15620. Martin, M. C.; Zeng, G.; Yu, J.; Schiltz, G. E. *J. Med. Chem.* **2020**, *63*, 15344–15370. Crawford, J. J.; Lee, W.; Johnson, A. R.; Delatorre, K. J.; Chen, J.; Eigenbrot, C.; Heidmann, J.; Kakiuchi-Kiyota, S.; Katewa, A.; Kiefer, J. R.; Liu, L.; Lubach, J. W.; Misner, D.; Purkey, H.; Reif, K.; Vogt, J.; Wong, H.; Yu, C.; Young, W. B. *ACS Med. Chem. Lett.* **2020**, *11*, 1588–1597. Gehling, V. S.; McGrath, J. P.; Duplessis, M.; Khanna, A.; Brucelle, F.; Vaswani, R. G.; Côté, A.; Stuckey, J.; Watson, V.; Cummings, R. T.; Balasubramanian, S.; Iyer, P.; Sawant, P.; Good, A. C.; Albrecht, B. K.; Harmange, J.-C.; Audia, J. E.; Bellon, S. F.; Trojer, P.; Levell, J. R. *ACS Med. Chem. Lett.* **2020**, *11*, 1213–1220. Grandjean, J.-M. M.; Jiu, A. Y.; West, J. W.; Aoyagi, A.; Droege, D. G.; Elepano, M.; Hirasawa, M.; Hirouchi, M.; Murakami, R.; Lee, J.; Sasaki, K.; Hirano, S.; Ohyama, T.; Tang, B. C.; Vaz, R. J.; Inoue, M.; Olson, S. H.; Prusiner, S. B.; Conrad, J.; Paras, N. A. *ACS Med. Chem. Lett.* **2020**, *11*, 127–132. Methot, J. L.; Achab, A.; Christopher, M.; Zhou, H.; McGowan, M. A.; Trotter, B. W.; Fradera, X.; Lesburg, C. A.; Goldenblatt, P.; Hill, A.; Chen, D.; Otte, K. M.; Augustin, M.; Shah, S.; Katz, J. D. *ACS Med. Chem. Lett.* **2020**, *11*, 2461–2469. Yamada, Y.; Takashima, H.; Walmsley, D. L.; Ushiyama, F.; Matsuda, Y.; Kanazawa, H.; Yamaguchi-Sasaki, T.; Tanaka-Yamamoto, N.; Yamagishi, J.; Kurimoto-Tsuruta, R.; Ogata, Y.; Ohtake, N.; Angove, H.; Baker, L.; Harris, R.; Macias, A.; Robertson, A.; Surgenor, A.; Watanabe, H.; Nakano, K.; Mima, M.; Iwamoto, K.; Okada, A.; Takata, I.; Hitaka, K.; Tanaka, A.; Fujita, K.; Sugiyama, H.; Hubbard, R. E. *J. Med. Chem.* **2020**, *63*, 14805–14820. Larsen, J.; Lambert, M.; Pettersson, H.; Vifian, T.; Larsen, M.; Ollerstam, A.; Hegardt, P.; Eskilsson, C.; Laursen, S.; Soehoel, A.; Skak-Nielsen, T.; Hansen, L. M.; Knudsen, N. Ø.; Eirefelt, S.; Sørensen, M. D.; Stilou, T. G.; Nielsen, S. F. *J. Med. Chem.* **2020**, *63*, 14502–14521. Degorce, S. L.; Aagaard, A.; Anjum, R.;

Cumming, I. A.; Diène, C. R.; Fallan, C.; Johnson, T.; Leuchowius, K.-J.; Orton, A. L.; Pearson, S.; Robb, G. R.; Rosen, A.; Scarfe, G. B.; Scott, J. S.; Smith, J. M.; Steward, O. R.; Terstiege, I.; Tucker, M. J.; Turner, P.; Wilkinson, S. D.; Wrigley, G. L.; Xue, Y. *Bioorg. Med. Chem.* **2020**, *28*, 115815. Durand-Réville, T. F.; Comita-Prevoir, J.; Zhang, J.; Wu, X.; May-Dracka, T. L.; Romero, J. A. C.; Wu, F.; Chen, A.; Shapiro, A. B.; Carter, N. M.; McLeod, S. M.; Giacobbe, R. A.; Verheijen, J. C.; Lahiri, S. D.; Sacco, M. D.; Chen, Y.; O'Donnell, J. P.; Miller, A. A.; Mueller, J. P.; Tommasi, R. A. *J. Med. Chem.* **2020**, *63*, 12511–12525. Zhan, W.; Singh, P. K.; Ban, Y.; Qing, X.; Ah Kioon, M. D.; Fan, H.; Zhao, Q.; Wang, R.; Sukenick, G.; Salmon, J.; Warren, J. D.; Ma, X.; Barrat, F. J.; Nathan, C. F.; Lin, G. *J. Med. Chem.* **2020**, *63*, 13103–13123. Dong, J.; Huang, J.; Zhou, J.; Tan, Y.; Jin, J.; Tan, X.; Wang, B.; Yu, T.; Wu, C.; Chen, S.; Wang, T.-L. *ACS Med. Chem. Lett.* **2020**, *11*, 1463–1469. Klug, D. M.; Tschiegg, L.; Diaz, R.; Rojas-Barros, D.; Perez-Moreno, G.; Ceballos, G.; García-Hernández, R.; Martinez-Martinez, M. S.; Manzano, P.; Ruiz, L. M.; Caffrey, C. R.; Gamarro, F.; Pacanowska, D. G.; Ferrins, L.; Navarro, M.; Pollastri, M. P. *J. Med. Chem.* **2020**, *63*, 2527–2546. Zhu, C.; Li, X.; Peng, W.; Fu, W. *Molecules* **2020**, *25*, 5078. Yaragani, M.; Yadlapalli, P.; Raghavan, S.; Ayyadurai, N.; Chinnusamy, S.; Mandava, V. B. R.; Kottapalli, R. P. *J. Chem. Sci.* **2020**, *132*, 136. Mlakar, L.; Lane, J.; Takihara, T.; Lim, C.; Sprachman, M. M.; Lloyd, K. R.; Wipf, P.; Feghali-Bostwick, C. *ACS Med. Chem. Lett.* **2020**, *11*, 2312–2317. Henley, Z. A.; Amour, A.; Barton, N.; Bantscheff, M.; Bergamini, G.; Bertrand, S. M.; Convery, M.; Down, K.; Dümpelfeld, B.; Edwards, C. D.; Grandi, P.; Gore, P. M.; Keeling, S.; Livia, S.; Mallett, D.; Maxwell, A.; Price, M.; Rau, C.; Reinhard, F. B. M.; Rowedder, J.; Rowland, P.; Taylor, J. A.; Thomas, D. A.; Hessel, E. M.; Hamblin, J. N. *J. Med. Chem.* **2020**, *63*, 638–655. White, C.; McGowan, M. A.; Zhou, H.; Sciammetta, N.; Fradera, X.; Lim, J.; Joshi, E. M.; Andrews, C.; Nickbarg, E. B.; Cowley, P.; Trewick, S.; Augustin, M.; von Köenig, K.; Lesburg, C. A.; Otte, K.; Knemeyer, I.; Woo, H.; Yu, W.; Cheng, M.; Spacciapoli, P.; Geda, P.; Song, X.; Smotrov, N.; Curran, P.; Heo, M. R.; Abeywickrema, P.; Miller, J. R.; Bennett, D. J.; Han, Y. *ACS Med. Chem. Lett.* **2020**, *11*, 550–557.

2021

Pan, C.; Nie, W.; Wang, J.; Du, J.; Pan, Z.; Gao, J.; Lu, Y.; Che, J.; Zhu, H.; Dai, H.; Chen, B.; He, Q.; Dong, X. *Eur. J. Med. Chem.* **2021**, *225*, 113794. Zhao, L.; Yin, W.; Sun, Y.; Sun, N.; Tian, L.; Zheng, Y.; Zhang, C.; Zhao, S.; Su, X.; Zhao, D.; Cheng, M. *Eur. J. Med. Chem.* **2021**, *224*, 113715. Wu, C.-J.; Wu, J.-Q.; Hu, Y.; Pu, S.; Lin, Y.; Zeng, Z.; Hu, J.; Chen, W.-H. *Eur. J. Med. Chem.* **2021**, *223*, 113629. Ran, K.; Zeng, J.; Wan, G.; He, X.; Feng, Z.; Xiang, W.; Wei, W.; Hu, X.; Wang, N.; Liu, Z.; Yu, L. *Eur. J. Med. Chem.* **2021**, *220*, 113499. Wu, S.; Xu, C.; Xia, K.; Lin, Y.; Tian, S.; Ma, H.; Ji, Y.; Zhu, F.; He, S.; Zhang, X. *Eur. J. Med. Chem.* **2021**, *217*, 113327. Maciuszek, M.; Ortega-Gomez, A.; Maas, S. L.; Perretti, M.; Merritt, A.; Soehnlein, O.; Chapman, T. M. *Eur. J. Med. Chem.* **2021**, *214*, 113194. Xia, Y.; Yu, M.; Zhao,

Y.; Xia, L.; Huang, Y.; Sun, N.; Song, M.; Guo, H.; Zhang, Y.; Zhu, D.; Xie, Q.; Wang, Y. *Eur. J. Med. Chem.* **2021**, *211*, 113013. Gulati, A.; Yeung, C. S.; Lapointe, B.; Kattar, S. D.; Gunaydin, H.; Scott, J. D.; Childers, K. K.; Methot, J. L.; Simov, V.; Kurukulasuriya, R.; Pio, B.; Morriello, G. J.; Liu, P.; Tang, H.; Neelamkavil, S.; Wood, H. B.; Rada, V. L.; Ardolino, M. J.; Yan, X. C.; Palte, R.; Otte, K.; Faltus, R.; Woodhouse, J.; Hegde, L. G.; Ciaccio, P.; Minnihan, E. C.; DiMauro, E. F.; Fell, M. J.; Fuller, P. H.; Ellis, J. M. *RSC Med. Chem.* **2021**, *12*, 1164–1173. Akao, Y.; Canan, S.; Cao, Y.; Condroski, K.; Engkvist, O.; Itono, S.; Kaki, R.; Kimura, C.; Kogej, T.; Nagaoka, K.; Naito, A.; Nakai, H.; Pairaudeau, G.; Radu, C.; Roberts, I.; Shimada, M.; Shum, D.; Watanabe, N.; Xie, H.; Yonezawa, S.; Yoshida, O.; Yoshida, R.; Mowbray, C.; Perry, B. *RSC Med. Chem.* **2021**, *12*, 384–393. Zhang, G.; Sheng, L.; Hegde, P.; Li, Y.; Aldrich, C. C. *Med. Chem. Res.* **2021**, *30*, 449–458. Huddle, B. C.; Grimley, E.; Chtcherbinine, M.; Buchman, C. D.; Takahashi, C.; Debnath, B.; McGonigal, S. C.; Mao, S.; Li, S.; Felton, J.; Pan, S.; Wen, B.; Sun, D.; Neamati, N.; Buckanovich, R. J.; Hurley, T. D.; Larsen, S. D. *Eur. J. Med. Chem.* **2021**, *211*, 113060. Jung, Y.-H.; Salmaso, V.; Wen, Z.; Bennett, J. M.; Phung, N. B.; Lieberman, D. I.; Gopinatth, V.; Randle, J. C. R.; Chen, Z.; Salvemini, D.; Karcz, T. P.; Cook, D. N.; Jacobson, K. A. *J. Med. Chem.* **2021**, *64*, 5099–5122. Safina, B. S.; McKerrall, S. J.; Sun, S.; Chen, C. A.; Chowdhury, S.; Jia, Q.; Li, J.; Zenova, A. Y.; Andrez, J. C.; Bankar, G.; Bergeron, P.; Chang, J. H.; Chang, E.; Chen, J.; Dean, R.; Decker, S. M.; Dipasquale, A.; Focken, T.; Hemeon, I.; Khakh, K.; Kim, A.; Kwan, R.; Lindgren, A.; Lin, S.; Maher, J.; Mezeyova, J.; Misner, D.; Nelkenbrecher, K.; Pang, J.; Reese, R.; Shields, S. D.; Sojo, L.; Sheng, T.; Verschoof, H.; Waldbrook, M.; Wilson, M. S.; Xie, Z.; Young, C.; Zabka, T. S.; Hackos, D. H.; Ortwine, D. F.; White, A. D.; Johnson, J. P.; Robinette, C. L.; Dehnhardt, C. M.; Cohen, C. J.; Sutherlin, D. P. *J. Med. Chem.* **2021**, *64*, 2953–2966. Safina, B. S.; McKerrall, S. J.; Sun, S.; Chen, C.-A.; Chowdhury, S.; Jia, Q.; Li, J.; Zenova, A. Y.; Andrez, J.-C.; Bankar, G.; Bergeron, P.; Chang, J. H.; Chang, E.; Chen, J.; Dean, R.; Decker, S. M.; DiPasquale, A.; Focken, T.; Hemeon, I.; Khakh, K.; Kim, A.; Kwan, R.; Lindgren, A.; Lin, S.; Maher, J.; Mezeyova, J.; Misner, D.; Nelkenbrecher, K.; Pang, J.; Reese, R.; Shields, S. D.; Sojo, L.; Sheng, T.; Verschoof, H.; Waldbrook, M.; Wilson, M. S.; Xie, Z.; Young, C.; Zabka, T. S.; Hackos, D. H.; Ortwine, D. F.; White, A. D.; Johnson, J. P.; Robinette, C. L.; Dehnhardt, C. M.; Cohen, C. J.; Sutherlin, D. P. *J. Med. Chem.* **2021**, *64*, 2953–2966. Wu, Y.; Wang, Q.; Jiang, M.-Y.; Huang, Y.-Y.; Zhu, Z.; Han, C.; Tian, Y.-J.; Zhang, B.; Luo, H.-B. *J. Med. Chem.* **2021**, *64*, 9537–9549. Liang, J.; Zbieg, J. R.; Blake, R. A.; Chang, J. H.; Daly, S.; DiPasquale, A. G.; Friedman, L. S.; Gelzleichter, T.; Gill, M.; Giltnane, J. M.; Goodacre, S.; Guan, J.; Hartman, S. J.; Ingalla, E. R.; Kategaya, L.; Kiefer, J. R.; Kleinheinz, T.; Labadie, S. S.; Lai, T.; Li, J.; Liao, J.; Liu, Z.; Mody, V.; McLean, N.; Metcalfe, C.; Nannini, M. A.; Oeh, J.; O'Rourke, M. G.; Ortwine, D. F.; Ran, Y.; Ray, N. C.; Roussel, F.; Sambrone, A.; Sampath, D.; Schutt, L. K.; Vinogradova, M.; Wai, J.; Wang, T.; Wertz, I. E.; White, J. R.; Yeap, S. K.;

Young, A.; Zhang, B.; Zheng, X.; Zhou, W.; Zhong, Y.; Wang, X. *J. Med. Chem.* **2021**, *64*, 11841–11856. Rianjongdee, F.; Atkinson, S. J.; Chung, C.; Grandi, P.; Gray, J. R. J.; Kaushansky, L. J.; Medeiros, P.; Messenger, C.; Phillipou, A.; Preston, A.; Prinjha, R. K.; Rioja, I.; Satz, A. L.; Taylor, S.; Wall, I. D.; Watson, R. J.; Yao, G.; Demont, E. H. *J. Med. Chem.* **2021**, *64*, 10806–10833. Zhang, Z.; Ghosh, A.; Connolly, P. J.; King, P.; Wilde, T.; Wang, J.; Dong, Y.; Li, X.; Liao, D.; Chen, H.; Tian, G.; Suarez, J.; Bonnette, W. G.; Pande, V.; Diloreto, K. A.; Shi, Y.; Patel, S.; Pietrak, B.; Szewczuk, L.; Sensenhauser, C.; Dallas, S.; Edwards, J. P.; Bachman, K. E.; Evans, D. C. *J. Med. Chem.* **2021**, *64*, 11570–11596. Aicher, T. D.; Van Huis, C. A.; Hurd, A. R.; Skalitzky, D. J.; Taylor, C. B.; Beleh, O. M.; Glick, G.; Toogood, P. L.; Yang, B.; Zheng, T.; Huo, C.; Gao, J.; Qiao, C.; Tian, X.; Zhang, J.; Demock, K.; Hao, L.-Y.; Lesch, C. A.; Morgan, R. W.; Moisan, J.; Wang, Y.; Scatina, J.; Paulos, C. M.; Zou, W.; Carter, L. L.; Hu, X. *J. Med. Chem.* **2021**, *64*, 13410–13428. Röhm, S.; Berger, B.-T.; Schröder, M.; Chatterjee, D.; Mathea, S.; Joerger, A. C.; Pinkas, D. M.; Bufton, J. C.; Tjaden, A.; Kovooru, L.; Kudolo, M.; Pohl, C.; Bullock, A. N.; Müller, S.; Laufer, S.; Knapp, S. *J. Med. Chem.* **2021**, *64*, 13451–13474. Chen, L.; Su, M.; Jin, Q.; Wang, W.; Wang, C.-G.; Assani, I.; Wang, M.-X.; Zhao, S.-F.; Lv, S.-M.; Wang, J.-W.; Sun, B.; Li, Y.; Liao, Z.-X. *J. Med. Chem.* **2021**, *64*, 16106–16131. Come, J. H.; Senter, T. J.; Clark, M. P.; Court, J. J.; Gale-Day, Z.; Gu, W.; Krueger, E.; Liang, J.; Morris, M.; Nanthakumar, S.; O'Dowd, H.; Maltais, F.; Iyer, G.; Andreassi, J.; Boucher, C.; Considine, T.; Moody, C. S.; Taylor, W.; Mohanty, A. K.; Huang, Y.; Zuccola, H.; Coll, J.; Bonanno, K. C.; Gagnon, K. J.; Gan, L.; Lu, F.; Gao, H.; Chakilam, A.; Engtrakul, J.; Song, B.; Crawford, D.; Doyle, E.; Kramer, T.; Vought, B.; Phillips, J.; Kemper, R.; Sanders, M.; Swett, R.; Furey, B.; Winquist, R.; Bunnage, M. E.; Jackson, K. L.; Charifson, P. S.; Magavi, S. S. *J. Med. Chem.* **2021**, *64*, 17753–17776. Lillich, F. F.; Willems, S.; Ni, X.; Kilu, W.; Borkowsky, C.; Brodsky, M.; Kramer, J. S.; Brunst, S.; Hernandez-Olmos, V.; Heering, J.; Schierle, S.; Kestner, R.-I.; Mayser, F. M.; Helmstädter, M.; Göbel, T.; Weizel, L.; Namgaladze, D.; Kaiser, A.; Steinhilber, D.; Pfeilschifter, W.; Kahnt, A. S.; Proschak, A.; Chaikuad, A.; Knapp, S.; Merk, D.; Proschak, E. *J. Med. Chem.* **2021**, *64*, 17259–17276. Li, D.; Deng, Y.; Achab, A.; Bharathan, I.; Hopkins, B. A.; Yu, W.; Zhang, H.; Sanyal, S.; Pu, Q.; Zhou, H.; Liu, K.; Lim, J.; Fradera, X.; Lesburg, C. A.; Lammens, A.; Martinot, T. A.; Cohen, R. D.; Doty, A. C.; Ferguson, H.; Nickbarg, E. B.; Cheng, M.; Spacciapoli, P.; Geda, P.; Song, X.; Smotrov, N.; Abeywickrema, P.; Andrews, C.; Chamberlin, C.; Mabrouk, O.; Curran, P.; Richards, M.; Saradjian, P.; Miller, J. R.; Knemeyer, I.; Otte, K. M.; Vincent, S.; Sciammetta, N.; Pasternak, A.; Bennett, D. J.; Han, Y. *ACS Med. Chem. Lett.* **2021**, *12*, 389–396. Narayanan, S.; Wang, S.; Vasukuttan, V.; Vyas Devambatla, R. K.; Dai, D.; Jin, C.; Snyder, R.; Laudermilk, L.; Runyon, S. P.; Maitra, R. *J. Med. Chem.* **2021**, *64*, 3006–3025. Josa-Culleré, L.; Cogswell, T.; Georgiou, I.; Jay-Smith, M.; Jackson, T.; Bataille, C.; Davies, S.; Vyas, P.; Milne, T.; Wynne, G.; Russell, A. *Molecules* **2021**, *26*, 6648. Liu, Q.;

Luo, Y.; Li, Z.; Chen, C.; Fang, L. *Bioorg. Med. Chem.* **2021**, *36*, 116094. Palmer, M. J.; Deng, X.; Watts, S.; Krilov, G.; Gerasyuto, A.; Kokkonda, S.; El Mazouni, F.; White, J.; White, K. L.; Striepen, J.; Bath, J.; Schindler, K. A.; Yeo, T.; Shackleford, D. M.; Mok, S.; Deni, I.; Lawong, A.; Huang, A.; Chen, G.; Wang, W.; Jayaseelan, J.; Katneni, K.; Patil, R.; Saunders, J.; Shahi, S. P.; Chittimalla, R.; Angulo-Barturen, I.; Jiménez-Díaz, M. B.; Wittlin, S.; Tumwebaze, P. K.; Rosenthal, P. J.; Cooper, R. A.; Aguiar, A. C. C.; Guido, R. V. C.; Pereira, D. B.; Mittal, N.; Winzeler, E. A.; Tomchick, D. R.; Laleu, B.; Burrows, J. N.; Rathod, P. K.; Fidock, D. A.; Charman, S. A.; Phillips, M. A. *J. Med. Chem.* **2021**, *64*, 6085–6136. Perry, M. W. D.; Björhall, K.; Bold, P.; Brűlls, M.; Börjesson, U.; Carlsson, J.; Chang, H.-F. A.; Chen, Y.; Eriksson, A.; Fihn, B.-M.; Fransson, R.; Fredlund, L.; Ge, H.; Huang, H.; Karabelas, K.; Lamm Bergström, E.; Lever, S.; Lindmark, H.; Mogemark, M.; Nikitidis, A.; Palmgren, A.-P.; Pemberton, N.; Petersen, J.; Rodrigo Blomqvist, M.; Smith, R. W.; Thomas, M. J.; Ullah, V.; Tyrchan, C.; Wennberg, T.; Westin Eriksson, A.; Yang, W.; Zhao, S.; Öster, L. *J. Med. Chem.* **2021**, *64*, 8053–8075. Williamson, D. S.; Smith, G. P.; Mikkelsen, G. K.; Jensen, T.; Acheson-Dossang, P.; Badolo, L.; Bedford, S. T.; Chell, V.; Chen, I.-J.; Dokurno, P.; Hentzer, M.; Newland, S.; Ray, S. C.; Shaw, T.; Surgenor, A. E.; Terry, L.; Wang, Y.; Christensen, K. V. *J. Med. Chem.* **2021**, *64*, 10312–10332. Harrison, L. A.; Atkinson, S. J.; Bassil, A.; Chung, C.; Grandi, P.; Gray, J. R. J.; Levernier, E.; Lewis, A.; Lugo, D.; Messenger, C.; Michon, A.-M.; Mitchell, D. J.; Preston, A.; Prinjha, R. K.; Rioja, I.; Seal, J. T.; Taylor, S.; Wall, I. D.; Watson, R. J.; Woolven, J. M.; Demont, E. H. *J. Med. Chem.* **2021**, *64*, 10742–10771. Heightman, T. D.; Berdini, V.; Bevan, L.; Buck, I. M.; Carr, M. G.; Courtin, A.; Coyle, J. E.; Day, J. E. H.; East, C.; Fazal, L.; Griffiths-Jones, C. M.; Howard, S.; Kucia-Tran, J.; Martins, V.; Muench, S.; Munck, J. M.; Norton, D.; O'Reilly, M.; Palmer, N.; Pathuri, P.; Peakman, T. M.; Reader, M.; Rees, D. C.; Rich, S. J.; Shah, A.; Wallis, N. G.; Walton, H.; Wilsher, N. E.; Woolford, A. J. A.; Cooke, M.; Cousin, D.; Onions, S.; Shannon, J.; Watts, J.; Murray, C. W. *J. Med. Chem.* **2021**, *64*, 12286–12303. Ryan, M. D.; Parkes, A. L.; Corbett, D.; Dickie, A. P.; Southey, M.; Andersen, O. A.; Stein, D. B.; Barbeau, O. R.; Sanzone, A.; Thommes, P.; Barker, J.; Cain, R.; Compper, C.; Dejob, M.; Dorali, A.; Etheridge, D.; Evans, S.; Faulkner, A.; Gadouleau, E.; Gorman, T.; Haase, D.; Holbrow-Wilshaw, M.; Krulle, T.; Li, X.; Lumley, C.; Mertins, B.; Napier, S.; Odedra, R.; Papadopoulos, K.; Roumpelakis, V.; Spear, K.; Trimby, E.; Williams, J.; Zahn, M.; Keefe, A. D.; Zhang, Y.; Soutter, H. T.; Centrella, P. A.; Clark, M. A.; Cuozzo, J. W.; Deng, B.; Hunt, A.; Sigel, E. A.; Troast, D. M.; Dejonge, B. L. M. *J. Med. Chem.* **2021**, *64*, 14377–14425. Du, L.; Wang, X.; Cui, G.; Xu, B. *Bioorg. Med. Chem.* **2021**, *29*, 115878. Long, M. F.; Capstick, R. A.; Spearing, P. K.; Engers, J. L.; Gregro, A. R.; Bollinger, S. R.; Chang, S.; Luscombe, V. B.; Rodriguez, A. L.; Cho, H. P.; Niswender, C. M.; Bridges, T. M.; Conn, P. J.; Lindsley, C. W.; Engers, D. W.; Temple, K. J. *Bioorg. Med. Chem. Lett.* **2021**, *53*, 128416. Feng, Y.; Park, H.; Bauer, L.; Ryu, J. C.; Yoon, S. O. K. *ACS Med. Chem. Lett.* **2021**, *12*, 24–

29. Jo, U.; Senatorov, I. S.; Zimmermann, A.; Saha, L. K.; Murai, Y.; Kim, S. H.; Rajapakse, V. N.; Elloumi, F.; Takahashi, N.; Schultz, C. W.; Thomas, A.; Zenke, F. T.; Pommier, Y. *Mol. Cancer Ther.* **2021**, *20*, 1431–1441. Kawahata, W.; Asami, T.; Kiyoi, T.; Irie, T.; Kashimoto, S.; Furuichi, H.; Sawa, M. *J. Med. Chem.* **2021**, *64*, 14129–14141.

2022

Li, H.; Ouyang, S.; Zhang, Y.; Peng, K.; Fang, W.; Liu, Z.; Wang, C.-Y.; Zhang, X.; Wang, Y. *Eur. J. Med. Chem.* **2022**, *244*, 114858. Leśniak, R. K.; Nichols, R. J.; Schonemann, M.; Zhao, J.; Gajera, C. R.; Lam, G.; Nguyen, K. C.; Langston, J. W.; Smith, M.; Montine, T. J. *Eur. J. Med. Chem.* **2022**, *242*, 114693. Gong, Y.; Wu, F.-X.; Wang, M.-S.; Xu, H.-C.; Zhuo, L.-S.; Yang, G.-F.; Huang, W. *Eur. J. Med. Chem.* **2022**, *241*, 114654. Niu, J.; Bai, H.; Li, Z.; Gao, Y.; Zhang, Y.; Wang, X.; Yang, Y.; Xu, Y.; Geng, M.; Xie, Z.; Zhou, B. *Eur. J. Med. Chem.* **2022**, *238*, 114482. Mei, L.-C.; Zhuo, L.-S.; Xu, H.-C.; Huang, W.; Hao, G.-F.; Yang, G.-F. *Eur. J. Med. Chem.* **2022**, *237*, 114406. Grychowska, K.; Olejarz-Maciej, A.; Blicharz, K.; Pietruś, W.; Karcz, T.; Kurczab, R.; Koczurkiewicz, P.; Doroz-Płonka, A.; Latacz, G.; Keeri, A. R.; Piska, K.; Satała, G.; Pęgiel, J.; Trybała, W.; Jastrzębska-Więsek, M.; Bojarski, A. J.; Lamaty, F.; Partyka, A.; Walczak, M.; Krawczyk, M.; Malikowska-Racia, N.; Popik, P.; Zajdel, P. *Eur. J. Med. Chem.* **2022**, *236*, 114329. Chen, L.; Su, M.; Wu, X.-Z.; Wang, D.-Z.; Kang, Y.; Wang, C.-G.; Assani, I.; Wang, M.-X.; Zhao, S.-F.; Lv, S.-M.; Wang, J.-W.; Sun, B.; Li, Y.; Jin, Q.; Huang, R.-Z.; Liao, Z.-X. *Eur. J. Med. Chem.* **2022**, *229*, 114065. Yan, Y.-H.; Li, W.; Chen, W.; Li, C.; Zhu, K.-R.; Deng, J.; Dai, Q.-Q.; Yang, L.-L.; Wang, Z.; Li, G.-B. *Eur. J. Med. Chem.* **2022**, *228*, 113965. Wei, W.; Feng, Z.; Liu, Z.; Li, X.; He, H.; Ran, K.; Shi, Y.; Zhu, Y.; Ye, T.; Gao, C.; Wang, N.; Yu, L. *Eur. J. Med. Chem.* **2022**, *228*, 113978. Lu, Y.; Feng, Y.; Li, Z.; Li, J.; Zhang, H.; Hu, X.; Jiang, W.; Shi, T.; Wang, Z. *Eur. J. Med. Chem.* **2022**, *227*, 113908. Griffith, D. A.; Edmonds, D. J.; Fortin, J.-P.; Kalgutkar, A. S.; Kuzmiski, J. B.; Loria, P. M.; Saxena, A. R.; Bagley, S. W.; Buckeridge, C.; Curto, J. M.; Derksen, D. R.; Dias, J. M.; Griffor, M. C.; Han, S.; Jackson, V. M.; Landis, M. S.; Lettiere, D.; Limberakis, C.; Liu, Y.; Mathiowetz, A. M.; Patel, J. C.; Piotrowski, D. W.; Price, D. A.; Ruggeri, R. B.; Tess, D. A. *J. Med. Chem.* **2022**, *65*, 8208–8226. Shearer, J.; Castro, J. L.; Lawson, A. D. G.; MacCoss, M.; Taylor, R. D. *J. Med. Chem.* **2022**, *65*, 8699–8712. Shinde, A.; Ugale, S. R.; Nandurkar, Y.; Modak, M.; Chavan, A. P.; Mhaske, P. C. *ACS Omega* **2022**, *7*, 47096–47107. Hopkins, B. T.; Bame, E.; Bajrami, B.; Black, C.; Bohnert, T.; Boiselle, C.; Burdette, D.; Burns, J. C.; Delva, L.; Donaldson, D.; Grater, R.; Gu, C.; Hoemberger, M.; Johnson, J.; Kapadnis, S.; King, K.; Lulla, M.; Ma, B.; Marx, I.; Magee, T.; Meissner, R.; Metrick, C. M.; Mingueneau, M.; Murugan, P.; Otipoby, K. L.; Polack, E.; Poreci, U.; Prince, R.; Roach, A. M.; Rowbottom, C.; Santoro, J. C.; Schroeder, P.; Tang, H.; Tien, E.; Zhang, F.; Lyssikatos, J. *J. Med. Chem.* **2022**, *65*, 1206–1224. Keylor, M. H.; Gulati, A.; Kattar, S. D.; Johnson, R. E.; Chau, R. W.; Margrey, K. A.; Ardolino, M. J.; Zarate, C.; Poremba, K. E.; Simov, V.; Morriello, G. J.; Acton, J. J.; Pio, B.;

Yan, X.; Palte, R. L.; McMinn, S. E.; Nogle, L.; Lesburg, C. A.; Adpressa, D.; Lin, S.; Neelamkavil, S.; Liu, P.; Su, J.; Hegde, L. G.; Woodhouse, J. D.; Faltus, R.; Xiong, T.; Ciaccio, P. J.; Piesvaux, J.; Otte, K. M.; Wood, H. B.; Kennedy, M. E.; Bennett, D. J.; DiMauro, E. F.; Fell, M. J.; Fuller, P. H. *J. Med. Chem.* **2022**, *65*, 838–856. Casimiro-Garcia, A.; Allais, C.; Brennan, A.; Choi, C.; Dower, G.; Farley, K. A.; Fleming, M.; Flick, A.; Frisbie, R. K.; Hall, J.; Hepworth, D.; Jones, H.; Knafels, J. D.; Kortum, S.; Lovering, F. E.; Mathias, J. P.; Mohan, S.; Morgan, P. M.; Parng, C.; Parris, K.; Pullen, N.; Schlerman, F.; Stansfield, J.; Strohbach, J. W.; Vajdos, F. F.; Vincent, F.; Wang, H.; Wang, X.; Webster, R.; Wright, S. W. *J. Med. Chem.* **2022**, *65*, 757–784. Jecs, E.; Tahirovic, Y. A.; Wilson, R. J.; Miller, E. J.; Kim, M.; Truax, V.; Nguyen, H. H.; Akins, N. S.; Saindane, M.; Wang, T.; Sum, C. S.; Cvijic, M. E.; Schroeder, G. M.; Burton, S. L.; Derdeyn, C. A.; Xu, L.; Jiang, Y.; Wilson, L. J.; Liotta, D. C. *J. Med. Chem.* **2022**, *65*, 4058–4084. Frankowski, K. J.; Patnaik, S.; Wang, C.; Southall, N.; Dutta, D.; De, S.; Li, D.; Dextras, C.; Lin, Y.-H.; Bryant-Connah, M.; Davis, D.; Wang, F.; Wachsmuth, L. M.; Shah, P.; Williams, J.; Kabir, M.; Zhu, E.; Baljinnyam, B.; Wang, A.; Xu, X.; Norton, J.; Ferrer, M.; Titus, S.; Simeonov, A.; Zheng, W.; Mathews Griner, L. A.; Jadhav, A.; Aubé, J.; Henderson, M. J.; Rudloff, U.; Schoenen, F. J.; Huang, S.; Marugan, J. J. *J. Med. Chem.* **2022**, *65*, 8303–8331. Hartz, R. A.; Xu, L.; Sit, S.-Y.; Chen, J.; Venables, B. L.; Lin, Z.; Zhang, S.; Li, Z.; Parker, D.; Simmons, T. S.; Jenkins, S.; Hanumegowda, U. M.; Dicker, I.; Krystal, M.; Meanwell, N. A.; Regueiro-Ren, A. *J. Med. Chem.* **2022**, *65*, 15935–15966. Meibom, D.; Micus, S.; Andreevski, A. L.; Anlauf, S.; Bogner, P.; von Buehler, C.-J.; Dieskau, A. P.; Dreher, J.; Eitner, F.; Fliegner, D.; Follmann, M.; Gericke, K. M.; Maassen, S.; Meyer, J.; Schlemmer, K.-H.; Steuber, H.; Tersteegen, A.; Wunder, F. *J. Med. Chem.* **2022**, *65*, 16420–16431. Goldberg, F. W.; Ting, A. K. T.; Beattie, D.; Lamont, G. M.; Fallan, C.; Finlay, M. R. V.; Williamson, B.; Schimpl, M.; Harmer, A. R.; Adeyemi, O. B.; Nordell, P.; Cronin, A. S.; Vazquez-Chantada, M.; Barratt, D.; Ramos-Montoya, A.; Cadogan, E. B.; Davies, B. R. *ACS Med. Chem. Lett.* **2022**, *13*, 1295–1301. Xue, D.; Xu, Y.; Kyani, A.; Roy, J.; Dai, L.; Sun, D.; Neamati, N. *J. Med. Chem.* **2022**, *65*, 343–368. Mata, G.; Miles, D. H.; Drew, S. L.; Fournier, J.; Lawson, K. V.; Mailyan, A. K.; Sharif, E. U.; Yan, X.; Beatty, J. W.; Banuelos, J.; Chen, J.; Ginn, E.; Chen, A.; Gerrick, K. Y.; Pham, A. T.; Wong, K.; Soni, D.; Dhanota, P.; Shaqfeh, S. G.; Meleza, C.; Narasappa, N.; Singh, H.; Zhao, X.; Jin, L.; Schindler, U.; Walters, M. J.; Young, S. W.; Walker, N. P.; Leleti, M. R.; Powers, J. P.; Jeffrey, J. L. *J. Med. Chem.* **2022**, *65*, 1418–1444. Xue, D.; Xu, Y.; Kyani, A.; Roy, J.; Dai, L.; Sun, D.; Neamati, N. *J. Med. Chem.* **2022**, *65*, 3404–3419. Li, X.; Zhang, Z.; Chen, Y.; Wang, B.; Yang, G.; Xu, X.; Yechao, B.; Bai, D.; Feng, B.; Mao, Y.; Feng, J.; Bai, C.; He, F.; Tao, W. *ACS Med. Chem. Lett.* **2022**, *13*, 507–512. Verma, V. A.; Wang, L.; Labadie, S. S.; Liang, J.; Sellers, B. D.; Wang, J.; Dong, L.; Wang, Q.; Zhang, S.; Xu, Z.; Zhang, Y.; Niu, Y.; Wang, X.; Wai, J.; Koehler, M. F. T.; Hu, H.; Alexander, M. K.; Nishiyama, M.; Miu, A.; Xu, Y.; Pang, J.; Katakam, A. K.; Reichelt, M.; Austin,

C. D.; Ho, H.; Payandeh, J.; Koth, C. M. *J. Med. Chem.* **2022**, *65*, 4085–4120. Tamayo, N. A.; Bourbeau, M. P.; Allen, J. R.; Ashton, K. S.; Chen, J. J.; Kaller, M. R.; Nguyen, T. T.; Nishimura, N.; Pettus, L. H.; Walton, M.; Belmontes, B.; Moriguchi, J.; Chen, K.; McCarter, J. D.; Hanestad, K.; Chung, G.; Ninniri, M. S. S.; Sun, J.; Poppe, L.; Spahr, C.; Hui, J.; Jia, L.; Wu, T.; Dahal, U. P.; Edson, K. Z.; Payton, M. *J. Med. Chem.* **2022**, *65*, 4972–4990. Yin, W.; Wu, T.; Liu, L.; Jiang, H.; Zhang, Y.; Cui, H.; Sun, Y.; Qin, Q.; Sun, Y.; Gao, Z.; Zhao, L.; Su, X.; Zhao, D.; Cheng, M. *J. Med. Chem.* **2022**, *65*, 5539–5564. Chen, P.; Bin, H.; Jiao, Y.; Lin, G.; Zhang, Y.; Xia, A.; Pan, Z.; Qiao, J.; Guo, Y.; Liu, J.; Zhou, Y.; Li, L. *Bioorg. Med. Chem. Lett.* **2022**, *63*, 128651. Caroff, E.; Meyer, E. A.; Äänismaa, P.; Froidevaux, S.; Keller, M.; Piali, L. *J. Med. Chem.* **2022**, *65*, 11533–11549. Gao, Y.; Wang, H.; Shen, L.; Xu, H.; Deng, M.; Cheng, M.; Wang, J. *Bioorg. Chem.* **2022**, *123*, 105769. Chen, D.; Tan, X.; Chen, W.; Liu, Y.; Li, C.; Wu, J.; Zheng, J.; Shen, H. C.; Zhang, M.; Wu, W.; Wang, L.; Xiong, J.; Dai, J.; Sun, K.; Zhang, J. D.; Xiang, K.; Li, B.; Ni, X.; Zhu, Q.; Gao, L.; Wang, L.; Feng, S. *J. Med. Chem.* **2022**, *65*, 10938–10955. Pandit, N.; Yoo, M.; Hyun Park, T.; Kim, J.; Mi Kim, S.; Myung Lee, K.; Kim, Y.; Min Bong, S.; Il Lee, B.; Jung, K.-Y.; Hoon Park, C. *Bioorg. Med. Chem.* **2022**, *72*, 116967. Pujala, B.; Ramachandran, S. A.; Sonawane, M.; Kamble, M. M.; Panpatil, D.; Adhikari, S.; Soni, S.; Subbareddy, V.; Shinde, B. U.; Nayak, A. K.; Bansal, C.; Gupta, A.; Mukherjee, K.; Agarwal, A. K.; Guerrero, J.; Herrera, F. J.; Bernales, S.; Guha, M.; Chakravarty, S.; Pham, S. M.; Rai, R. *Bioorg. Med. Chem. Lett.* **2022**, *75*, 128979. Shvartsbart, A.; Roach, J. J.; Witten, M. R.; Koblish, H.; Harris, J. J.; Covington, M.; Hess, R.; Lin, L.; Frascella, M.; Truong, L.; Leffet, L.; Conlen, P.; Beshad, E.; Klabe, R.; Katiyar, K.; Kaldon, L.; Young-Sciame, R.; He, X.; Petusky, S.; Chen, K.-J.; Horsey, A.; Lei, H.-T.; Epling, L. B.; Deller, M. C.; Vechorkin, O.; Yao, W. *J. Med. Chem.* **2022**, *65*, 15433–15442. Li, D.; Sloman, D. L.; Achab, A.; Zhou, H.; McGowan, M. A.; White, C.; Gibeau, C.; Zhang, H.; Pu, Q.; Bharathan, I.; Hopkins, B.; Liu, K.; Ferguson, H.; Fradera, X.; Lesburg, C. A.; Martinot, T. A.; Qi, J.; Song, Z. J.; Yin, J.; Zhang, H.; Song, L.; Wan, B.; DAddio, S.; Solban, N.; Miller, J. R.; Zamlynny, B.; Bass, A.; Freeland, E.; Ykoruk, B.; Hilliard, C.; Ferraro, J.; Zhai, J.; Knemeyer, I.; Otte, K. M.; Vincent, S.; Sciammetta, N.; Pasternak, A.; Bennett, D. J.; Han, Y. *J. Med. Chem.* **2022**, *65*, 6001–6016. Fuerst, R.; Choi, J. Y.; Knapinska, A. M.; Cameron, M. D.; Ruiz, C.; Delmas, A.; Sundrud, M. S.; Fields, G. B.; Roush, W. R. *Bioorg. Med. Chem. Lett.* **2022**, *76*, 129014. Huff, S.; Kummetha, I. R.; Zhang, L.; Wang, L.; Bray, W.; Yin, J.; Kelley, V.; Wang, Y.; Rana, T. M. *J. Med. Chem.* **2022**, *65*, 10920–10937. Wilson, C.; Ray, P.; Zuccotto, F.; Hernandez, J.; Aggarwal, A.; Mackenzie, C.; Caldwell, N.; Taylor, M.; Huggett, M.; Mathieson, M.; Murugesan, D.; Smith, A.; Davis, S.; Cocco, M.; Parai, M. K.; Acharya, A.; Tamaki, F.; Scullion, P.; Epemolu, O.; Riley, J.; Stojanovski, L.; Lopez-Román, E. M.; Torres-Gómez, P. A.; Toledo, A. M.; Guijarro-Lopez, L.; Camino, I.; Engelhart, C. A.; Schnappinger, D.; Massoudi, L. M.; Lenaerts, A.; Robertson, G. T.; Walpole, C.; Matthews, D.; Floyd, D.; Sacchettini, J. C.; Read,

K. D.; Encinas, L.; Bates, R. H.; Green, S. R.; Wyatt, P. G. *J. Med. Chem.* **2022**, *65*, 409–423.
Owens, T. D.; Brameld, K. A.; Verner, E. J.; Ton, T.; Li, X.; Zhu, J.; Masjedizadeh, M. R.; Bradshaw, J. M.; Hill, R. J.; Tam, D.; Bisconte, A.; Kim, E. O.; Francesco, M.; Xing, Y.; Shu, J.; Karr, D.; LaStant, J.; Finkle, D.; Loewenstein, N.; Haberstock-Debic, H.; Taylor, M. J.; Nunn, P.; Langrish, C. L.; Goldstein, D. M. *J. Med. Chem.* **2022**, *65*, 5300–5316.

9.3 Reactivity and Applications of Sulfonyl Fluorides

Recent years have seen a surge in sulfonyl fluoride research and publications, sparked by Sharpless' influential paper in *Angewandte Chemie* in 2014. Advances have been made in the synthesis of sulfonyl fluorides, including new sulfonyl-fluorination reagents, enhancing the reactivity and improving the mechanistic understanding of SuFEx reactions, and applications to drug discovery and chemical biology.

Improved conditions for the oxidative fluorination of sulfonic acids and salts were recently reported,[456] as well as new sulfonyl fluoride precursors such as Grignard reagents,[457] aryl hydrazines,[458] aryl diazonium salts[459] and thiols.[460] The Willis and Ball labs have published valuable contributions for the synthesis of aryl and alkenyl sulfonyl fluorides *via* transition metal-catalysis, using DABSO as an SO_2 source and electrophilic fluoride sources such as NFSI.[241c] Modern avant-garde methods in organic chemistry such as electrochemical- and decarboxylative processes have also found application towards the synthesis of sulfonyl fluorides.[461,462] Notably, Baran reported the Ni-catalysed 'e-sulfinylation' of aryl halides, followed by *in situ* fluorination (Figure 94a). Cathodic electrochemical reduction of dissolved SO_2 generated an $SO_2^{\bullet-}$ radical anion which reductively added into an arylnickel(III) species. SO_2 migratory insertion, followed by ligand exchange and electrophilic fluorination yielded the sulfonyl fluoride product.[461c] The photoredox/copper dually catalysed decarboxylative fluorosulfonylation of aliphatic carboxylic acids was demonstrated by Lu and Weng (Figure 94b). Hydrogen atom transfer (HAT) from carboxylic acid to an excited acridinium catalyst generated an alkyl radical which added into SO_2 (from DABSO) to give a sulfonyl radical intermediate to which a fluoride atom was transferred from a catalytically generated Cu^{II}–F complex to yield sulfonyl fluorides.[462d] Further, novel reagents to install –SO_2F motifs have been developed (Figure 94c). Most of these are fluorosulfonylation reagents (*i.e.* install an –SO_2F group) *via* the generation of a fluorosulfonyl radical,[463] others fluorinate sulfonyl derivatives,[464] or install a larger SO_2F-containing organic fragment.[465]

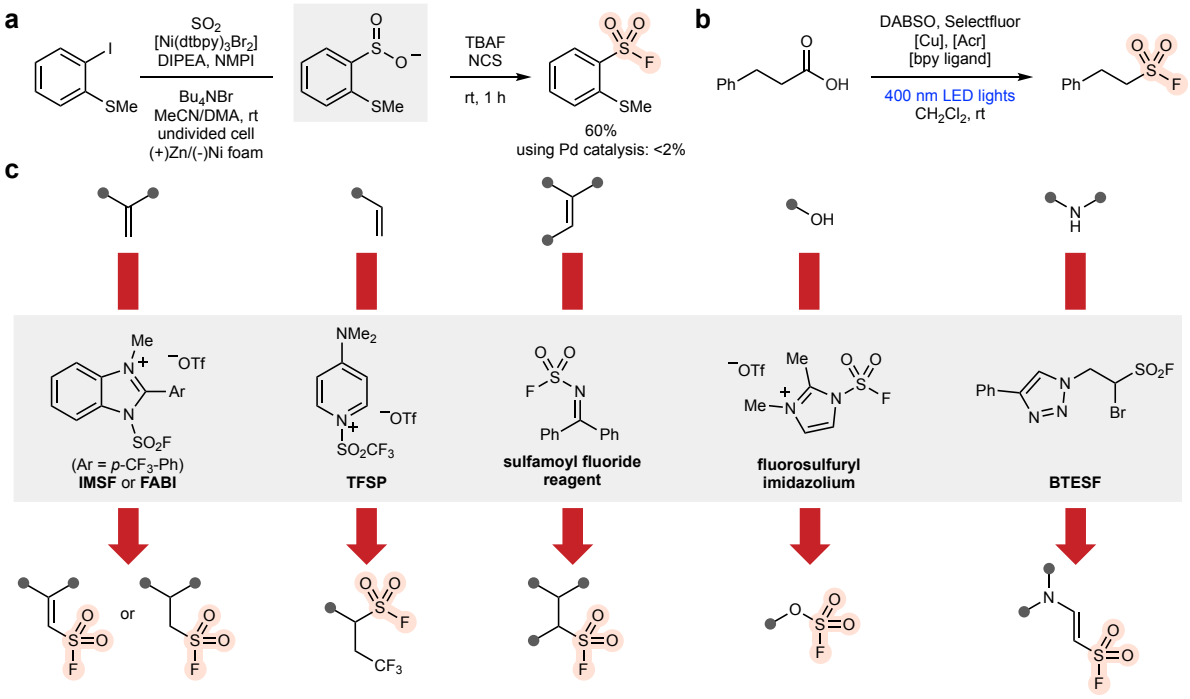


Figure 94. Selected advances in the synthesis of sulfonyl fluorides. **a**, Electrochemical coupling.[461c] **b**, Decarboxylative photoredox fluorosulfonylation.[462d] **c**, New sulfonyl fluoride reagents.[463a,d,f,464c,465]

SuFEx reactions themselves, although in theory 'clickable', often suffer from sluggish reactivity, ironically, due to the inertness and stability of sulfonyl fluoride substrates. It is hence of value to end users to develop chemical systems that accelerate SuFEx reactions, to reduce reaction times and avoid elevated temperatures, which could degrade sensitive chemical matter. To this purpose, catalytic and stoichiometric additives have been developed to accelerate SuFEx couplings, broadening the scope of both less reactive sulfonyl fluoride substrates and nucleophiles. Lewis acidic and Lewis basic (*i.e.* nucleophilic) additives have been discovered that significantly expedite SuFEx reactions *via* distinctive mechanisms (Figure 95).

Lewis acidic stoichiometric additives such as $Ca(NTf_2)_2$ were believed to coordinate to fluoride and oxygen atoms, increasing the electrophilicity of the sulfur centre.[248a] The addition of DABCO as a second additive unlocked a lower energy reaction pathway, allowing for overall milder reaction conditions.[248b] An in-depth mechanistic analysis revealed DABCO to serve as Brønsted base, involved in the SuFEx TS to deprotonate the amine nucleophile synchronous to attack of the amine on the sulfur centre.[255] A strong post-SuFEx Ca–F bond, which was proposed to impede catalytic turnover of Ca^{2+}, was disrupted by the addition of TMDS as a third additive. TMDS was suggested to serve as fluoride scavenger, which increased the efficiency of the SuFEx reaction and allowed for third generation conditions using catalytic amounts of $Ca(NTf_2)_2$ (20 mol%).

Li reported on the use of catalytic amounts of HOBt as nucleophilic catalyst in combination with super-stoichiometric quantities of TMDS as fluoride scavenger.[256] This set of conditions was particularly efficient for hindered substrates such as *ortho*-substituted aryl-sulfonyl fluorides and *t*-butyl-amine. HOBt was proposed to substitute fluoride and form a reactive OBt-sulfonate intermediate which then reacted with the amine nucleophile to form the desired sulfonamide product. TMDS was shown to be crucial to promote the first HOBt substitution step. A related NHC or NHC-HOBt catalysed system was reported, the NHC proposedly acting as a Brønsted base.[466] Catalytic amounts of Barton's base (BTMG) in combination with one equivalent of HMDS was also shown by Moses to accelerate SuFEx processes with phenol nucleophiles. NMR titration experiments supported the intermediacy of a phenolate–guanidinium complex and an accelerating effect of the silicon additive. A six-membered TS was proposed, whereby the fluoride is torn away from the S^{VI} centre by HMDS with the synchronous attack of phenolate onto sulfur.[257]

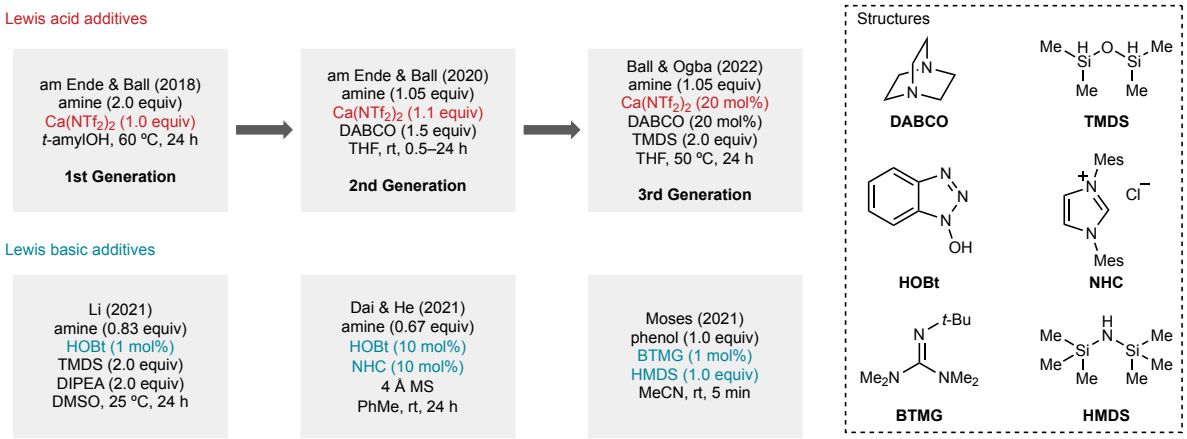


Figure 95. Additive-accelerated SuFEx reactions.[248,255-257]

Further, small and functional sulfonyl fluoride building blocks have been reported such as triflating agent **CF_3SO_2F**,[467] bicyclo[1.1.1]pentane sulfonyl fluoride **BCP-SF**,[468] fluorosulfuryl isocyanate **FSI** for the synthesis of sulfamoyl fluorides,[469] and alkyne sulfonyl fluoride **SASF** for the diversity oriented synthesis (DOS) of lead-like compounds (Figure 96).[470] Notable advances in new reagents[471] and reactivity[472,473] of important substituted ethane sulfonyl fluorides electrophiles (**ESF**) have also been developed.

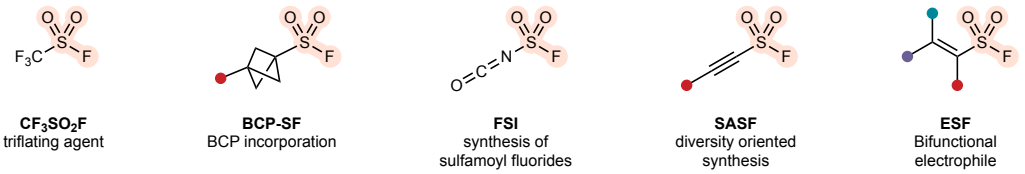


Figure 96. Developed sulfonyl fluoride building blocks.

The attractive combination of stability and selective activation ascribed to sulfonyl fluorides has found growing interest as biocompatible chemical probes. Applications have been reported as tools in chemical biology,[474,475] reactive fragments for ligand discovery,[476] radiolabelling[477] and as covalent inhibitors.[478] The 'clickability' of SuFEx reactions have also allowed their use in high-throughput hit-to-lead processes.[479]

9.4 Raw Cyclic Voltammograms

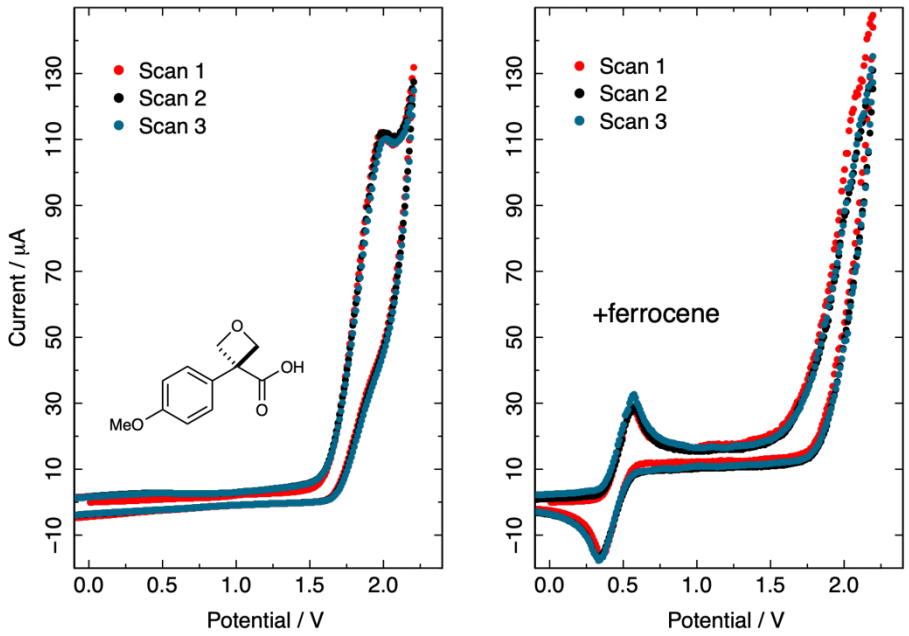


Figure 97. Measured cyclic voltammogram of PMP-oxetane carboxylic acid 148a without (*left*) and with (*right*) ferrocene.

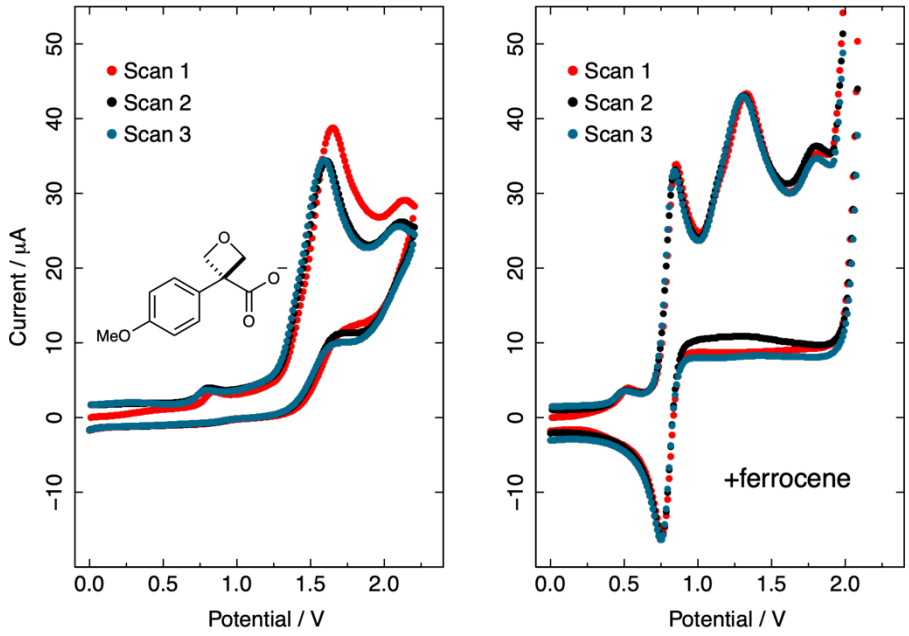


Figure 98. Measured cyclic voltammogram of PMP-oxetane carboxylate 148a⁻ without (left) and with (right) ferrocene.

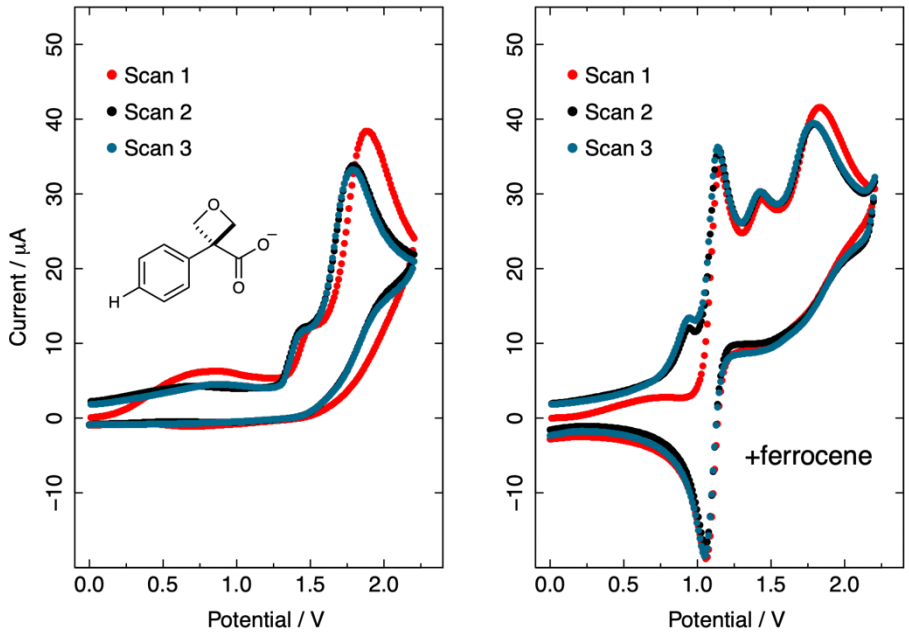


Figure 99. Measured cyclic voltammogram of Ph-oxetane carboxylate 148m⁻ without (*left*) and with (*right*) ferrocene.

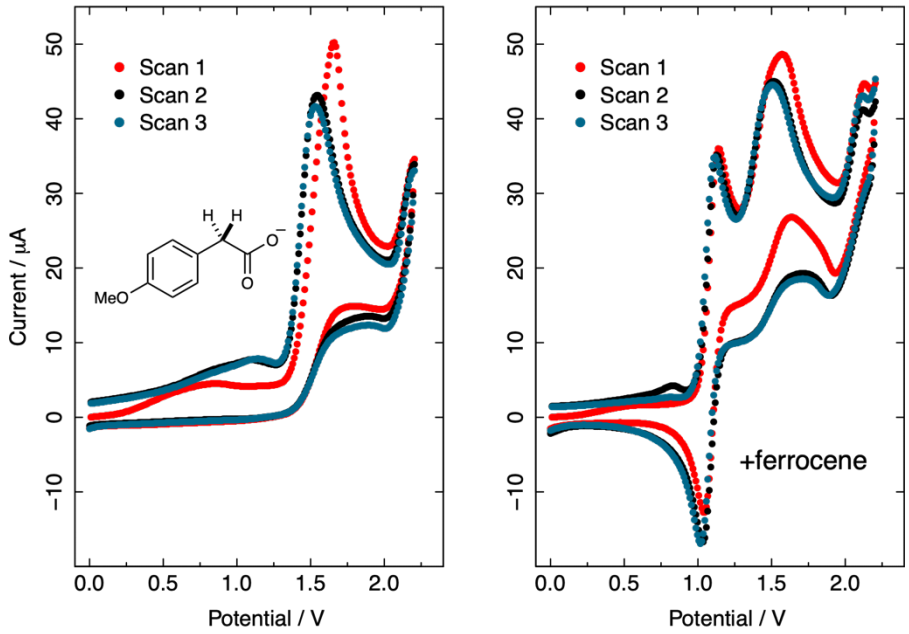


Figure 100. Measured cyclic voltammogram of PMP-methylene carboxylate without (left) and with (right) ferrocene.

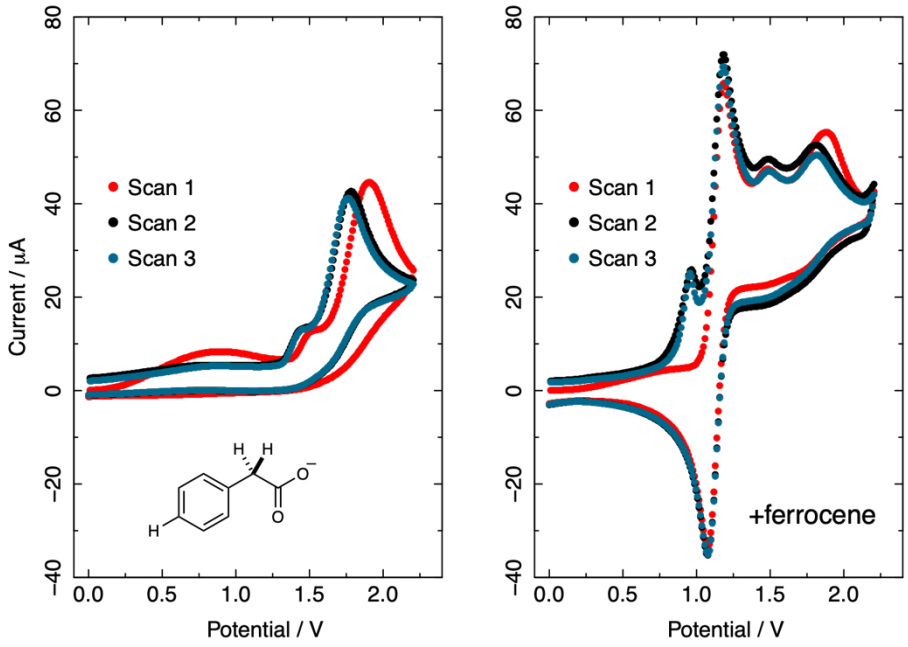


Figure 101. Measured cyclic voltammogram of Ph-methylene carboxylate without (*left*) and with (*right*) ferrocene.

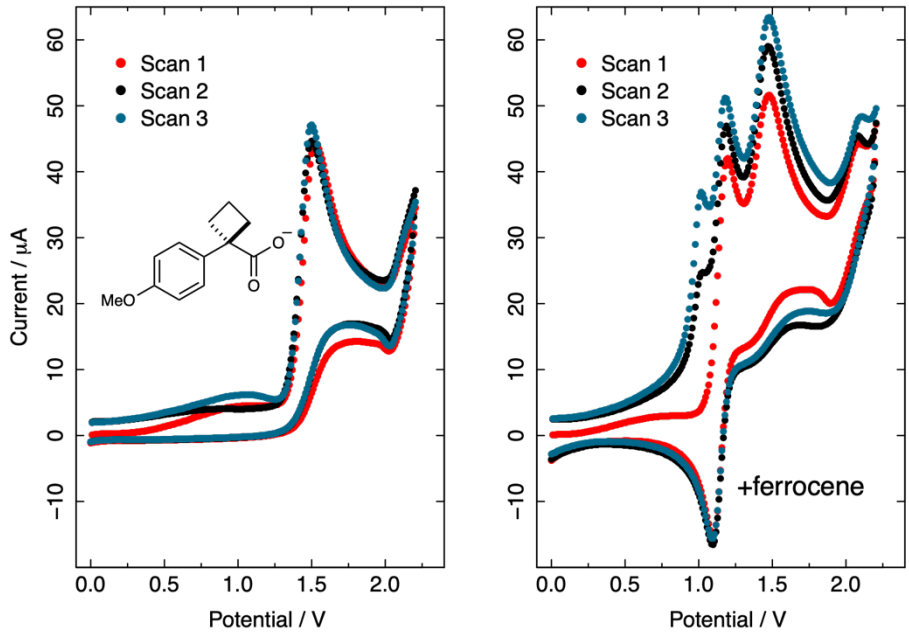


Figure 102. Measured cyclic voltammogram of PMP-cyclobutane carboxylate without (*left*) and with (*right*) ferrocene.

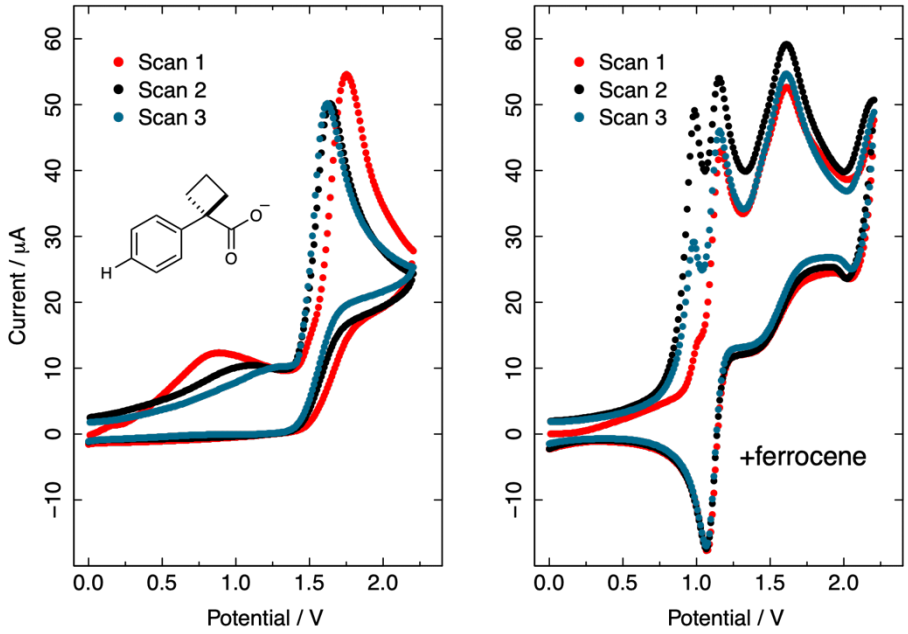


Figure 103. Measured cyclic voltammogram of Ph-cyclobutane carboxylate without (*left*) and with (*right*) ferrocene.

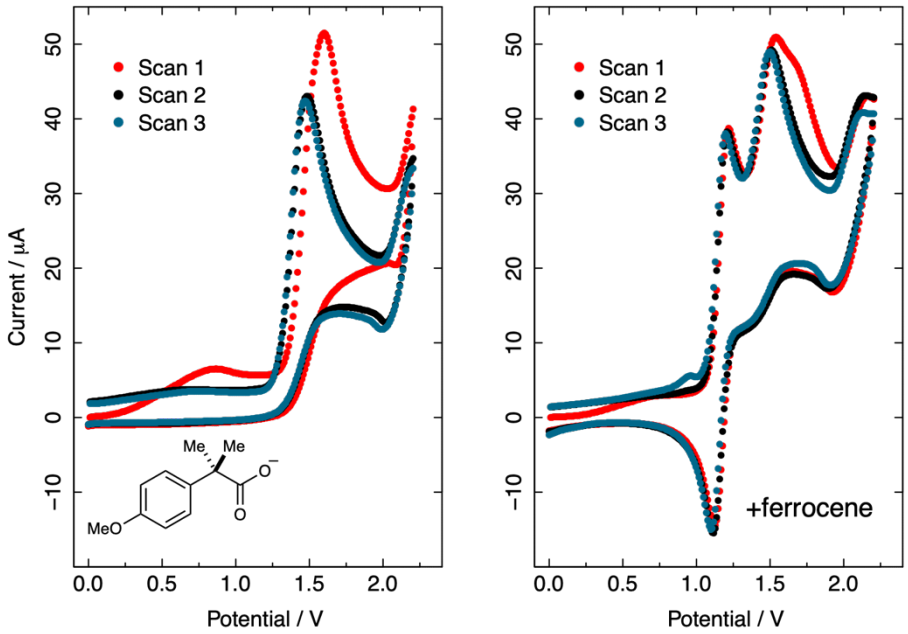


Figure 104. Measured cyclic voltammogram of PMP-*gem*-dimethyl carboxylate without (*left*) and with (*right*) ferrocene.

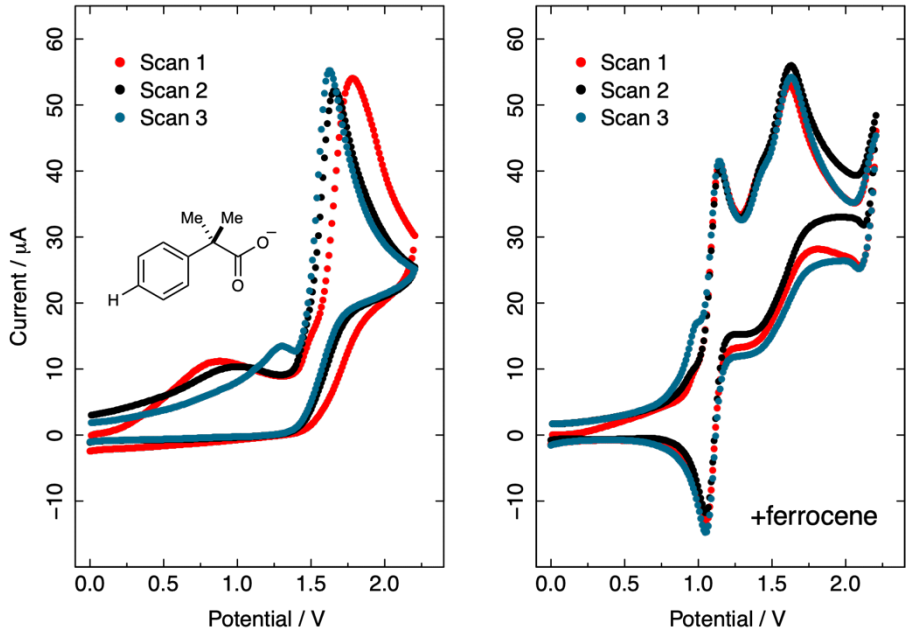


Figure 105. Measured cyclic voltammogram of Ph-*gem*-dimethyl carboxylate without (*left*) and with (*right*) ferrocene.

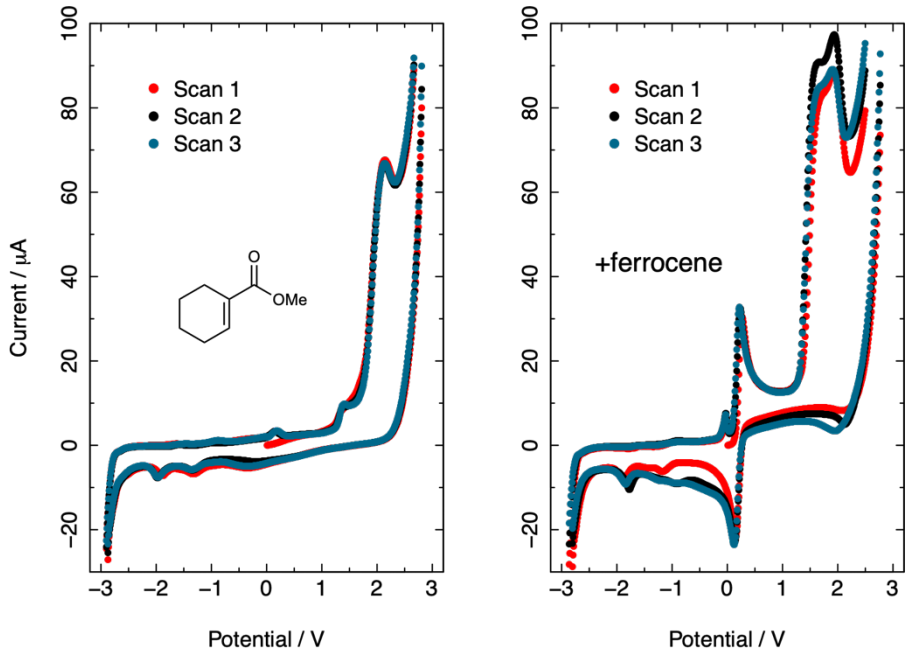


Figure 106. Measured cyclic voltammogram of cyclohexene methyl carboxylate without (*left*) and with (*right*) ferrocene.

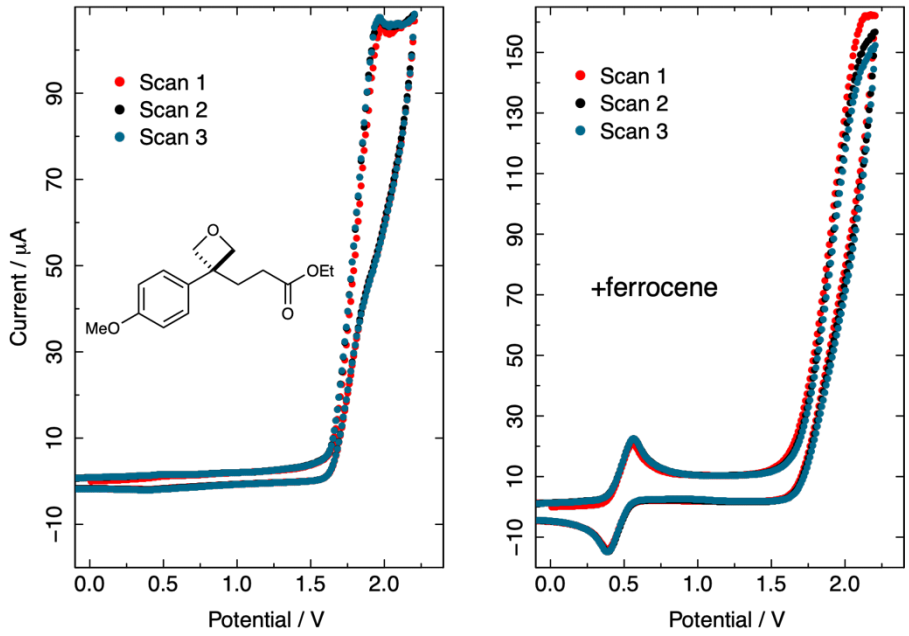


Figure 107. Measured cyclic voltammogram of aryl-alkyl-oxetane 149 without (*left*) and with (*right*) ferrocene.

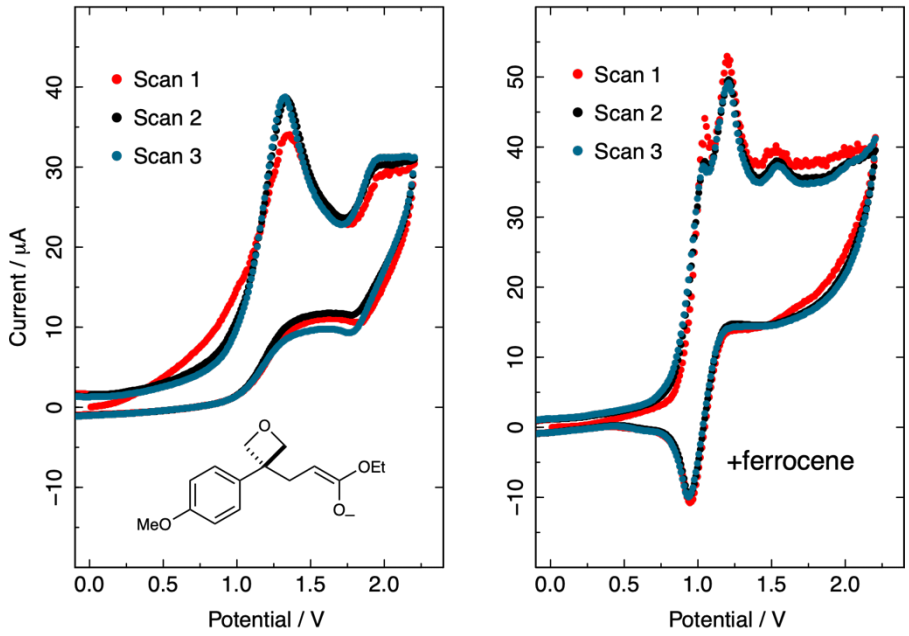


Figure 108. Measured cyclic voltammogram of aryl-alkyl-oxetane enolate 149⁻ without (*left*) and with (*right*) ferrocene.

9.5 ^{1}H NMR Spectra of Deuteration Studies

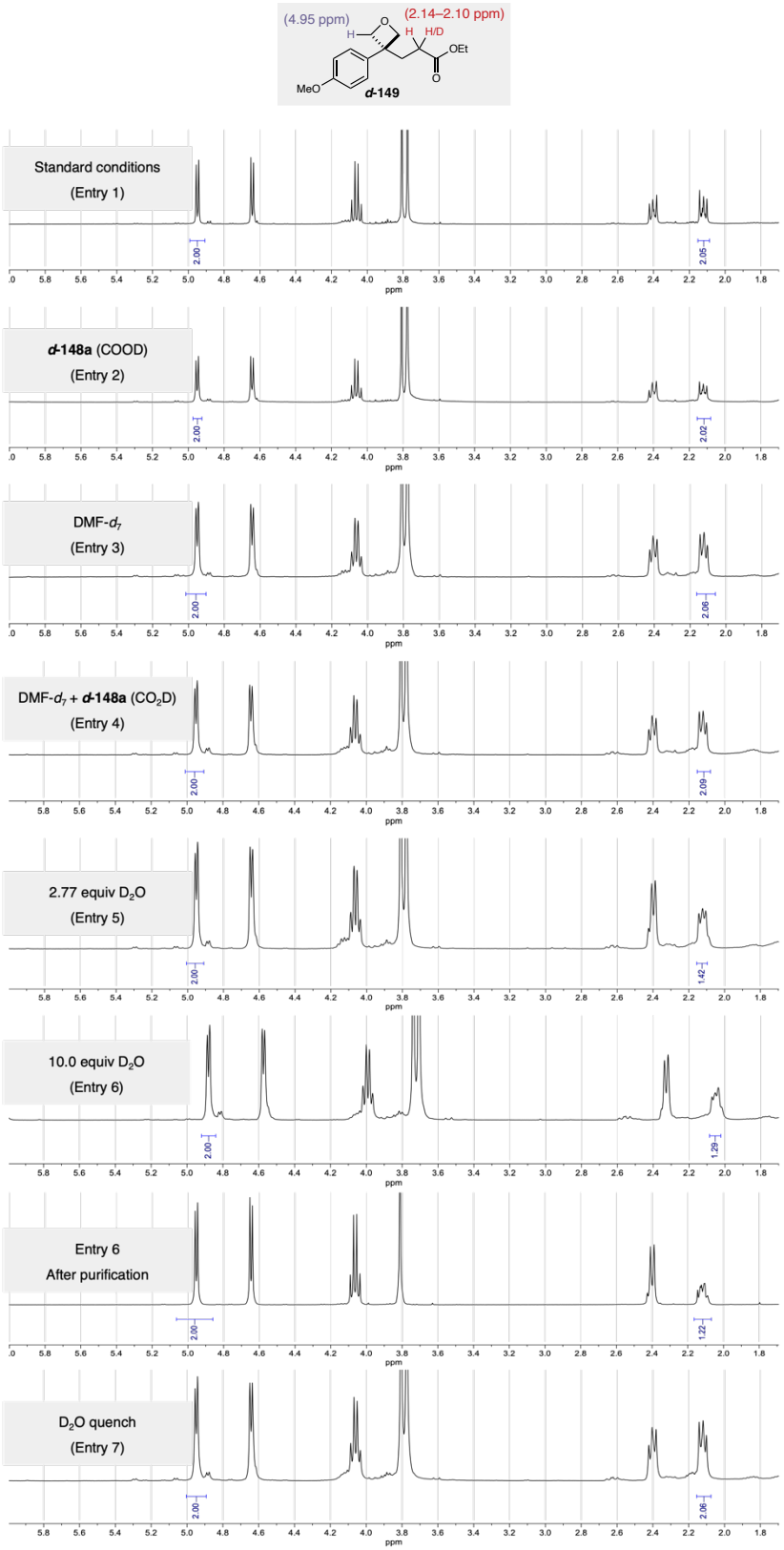


Figure 109. ^{1}H NMR spectra of entries in Table 20. HMBC allowed unambiguous assignment of the proton a to the ester.[311]

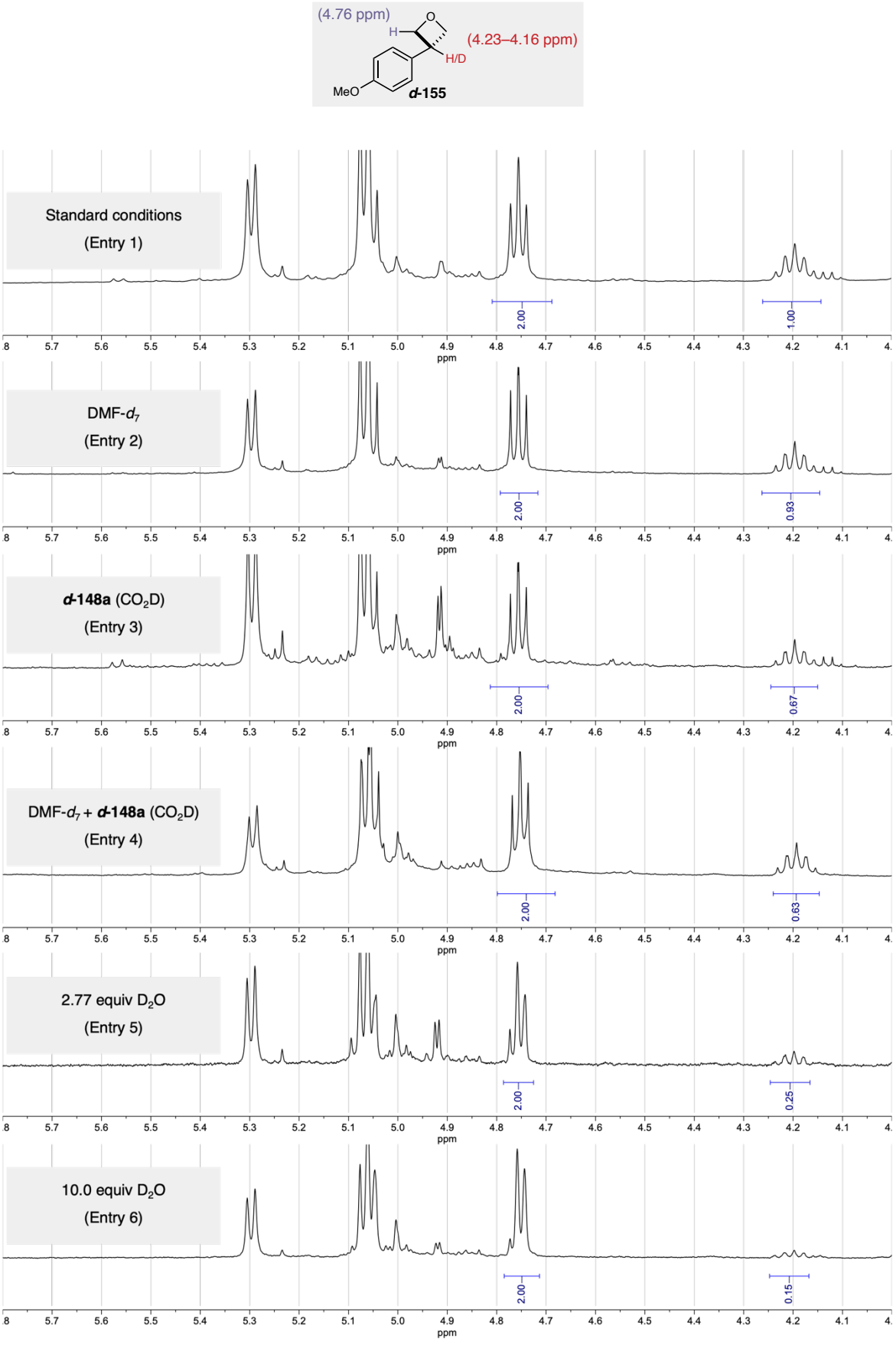


Figure 110. ^{1}H NMR spectra of entries in Table 22.

9.6 References Appendix

456 Thomson, B. J.; Khasnavis, S. R.; Grigorian, E. C.; Krishnan, R.; Yassa, T. D.; Lee, K.; Sammis, G. M.; Ball, N. D. *Chem. Commun.* **2023**, *59*, 555–558.

457 Lee, C.; Ball, N. D.; Sammis, G. M. *Chem. Commun.* **2019**, *55*, 14753–14756.

458 Tran, V. H.; Kim, H. *Asian J. Org. Chem.* **2022**, *11*, e202200004.

459 Liu, Y.; Yu, D.; Guo, Y.; Xiao, J.-C.; Chen, Q.-Y.; Liu, C. *Org. Lett.* **2020**, *22*, 2281–2286.

460 (a) Kirihara, M.; Naito, S.; Ishizuka, Y.; Hanai, H.; Noguchi, T. *Tetrahedron Lett.* **2011**, *52*, 3086–3089. (b) Kirihara, M.; Naito, S.; Nishimura, Y.; Ishizuka, Y.; Iwai, T.; Takeuchi, H.; Ogata, T.; Hanai, H.; Kinoshita, Y.; Kishida, M.; Yamazaki, K.; Noguchi, T.; Yamashoji, S. *Tetrahedron* **2014**, *70*, 2464 2471. (c) Laudadio, G.; Bartolomeu, A. de A.; Verwijlen, L. M. H. M.; Cao, Y.; de Oliveira, K. T.; Noël, T. *J. Am. Chem. Soc.* **2019**, *141*, 11832–11836.

461 Electrochemical methods: (a) Park, J. K.; Oh, J.; Lee, S. *Org. Chem. Front.* **2022**, *9*, 3407–3413. (b) Feng, Q.; Fu, Y.; Zheng, Y.; Liao, S.; Huang, S. *Org. Lett.* **2022**, *24*, 3702–3706. (c) Lou, T. S.; Kawamata, Y.; Ewing, T.; Correa-Otero, G. A.; Collins, M. R.; Baran, P. S. *Angew. Chem. Int. Ed.* **2022**, *61*, e202208080.

462 Decarboxylative methods: (a) Xu, T.; Cao, T.; Yang, M.; Xu, R.; Nie, X.; Liao, S. *Org. Lett.* **2020**, *22*, 3692–3696. (b) Ma, Z.; Liu, Y.; Ma, X.; Hu, X.; Guo, Y.; Chen, Q.-Y.; Liu, C. *Org. Chem. Front.* **2022**, *9*, 1115–1120. (c) Chen, Z.-D.; Zhou, X.; Yi, J.-T.; Diao, H.-J.; Chen, Q.-L.; Lu, G.; Weng, J. *Org. Lett.* **2022**, *24*, 2474–2478. (d) Yi, J.; Zhou, X.; Chen, Q.-L.; Chen, Z.; Lu, G.; Weng, J. *Chem. Commun.* **2022**, *58*, 9409–9412.

463 (a) Guo, T.; Meng, G.; Zhan, X.; Yang, Q.; Ma, T.; Xu, L.; Sharpless, K. B.; Dong, J. *Angew. Chem. Int. Ed.* **2018**, *57*, 2605–2610. (b) Wang, P.; Zhang, H.; Nie, X.; Xu, T.; Liao, S. *Nat. Commun.* **2022**, *13*, 3370. (c) Wang, P.; Zhang, H.; Zhao, M.; Ji, S.; Lin, L.; Yang, N.; Nie, X.; Song, J.; Liao, S. *Angew. Chem. Int. Ed.* **2022**, *61*, e202207684. (d) Zhang, W.; Li, H.; Li, X.; Zou, Z.; Huang, M.; Liu, J.; Wang, X.; Ni, S.; Pan, Y.; Wang, Y. *Nat. Commun.* **2022**, *13*, 3515. (e) Tryniszewski, M.; Basiak, D.; Barbasiewicz, M. *Org. Lett.* **2022**, *24*, 4270–4274. (f) Erchinger, J. E.; Hoogesteger, R.; Laskar, R.; Dutta, S.; Hümpel, C.; Rana, D.; Daniliuc, C. G.; Glorius, F. *J. Am. Chem. Soc.* **2023**, *145*, 2364–2374.

464 (a) Kwon, Y.-D.; Jeon, M. H.; Park, N. K.; Seo, J. K.; Son, J.; Ryu, Y. H.; Hong, S. Y.; Chun, J.-H. *Org. Lett.* **2020**, *22*, 5511–5516. (b) Passia, M. T.; Demaerel, J.; Amer, M. M.; Drichel, A.; Zimmer, S.; Bolm, C. *Org. Lett.* **2022**, *24*, 8802–8805. (c) Yang, Y.; Xiao, F.; Lin, J.; Xiao, J. *Adv. Synth. Catal.* **2023**, *365*, 301–306.

465 Leng, J.; Tang, W.; Fang, W.; Zhao, C.; Qin, H. *Org. Lett.* **2020**, *22*, 4316–4321.

466 Lin, M.; Luo, J.; Xie, Y.; Du, G.; Cai, Z.; Dai, B.; He; L. *Organocatalytic Silicon-Free SuFEx reactions for modular synthesis of sulfonates and sulfonamides* [preprint] **2021**; 10.26434/chemrxiv-2021-kw8xx.

467 Li, B.-Y.; Voets, L.; Van Lommel, R.; Hoppenbrouwers, F.; Alonso, M.; Verhelst, S. H. L.; De Borggraeve, W. M.; Demaerel, J. *Chem. Sci.* **2022**, *13*, 2270–2279.

468 Kokhan, S. O.; Valter, Y. B.; Tymtsunik, A. V.; Komarov, I. V.; Grygorenko, O. O. *Eur. J. Org. Chem.* **2020**, *2020*, 2210–2216.

469 Sun, S.; Gao, B.; Chen, J.; Sharpless, K. B.; Dong, J. *Angew. Chem. Int. Ed.* **2021**, *60*, 21195–21199.

470 Smedley, C. J.; Li, G.; Barrow, A. S.; Gialelis, T. L.; Giel, M.; Ottonello, A.; Cheng, Y.; Kitamura, S.; Wolan, D. W.; Sharpless, K. B.; Moses, J. E. *Angew. Chem. Int. Ed.* **2020**, *59*, 12460–12469.

471 (a) Zhang, X.; Qin, H.-L. *Org. Lett.* **2022**, *24*, 9311–9315. (b) Liu, M.; Tang, W.; Qin, H.-L. *J. Org. Chem.* **2023**, *88*, 1909–1917. (c) Chen, L.-Y.; Rakesh, K. P.; Qin, H.-L. *Org. Chem. Front.* **2023**, *10*, 951–956.

472 For a recent review, see: Meng, Y.-P.; Wang, S.-M.; Fang, W.-Y.; Xie, Z.-Z.; Leng, J.; Alsulami, H.; Qin, H.-L. *Synthesis* **2020**, *52*, 673–687.

473 (a) Xu, R.; Xu, T.; Yang, M.; Cao, T.; Liao, S. *Nat. Commun.* **2019**, *10*, 3752. (b) Zhang, Z.-W.; Rakesh, K. P.; Liu, J.; Qin, H.-L.; Tang, H. *Org. Biomol. Chem.* **2021**, *19*, 6021–6024. (c) Yamanushkin, P.; Kaya, K.; Feliciano, M. A. M.; Gold, B. *J. Org. Chem.* **2022**, *87*, 3868–3873. (d) Chen, J.; Zhang, Y.; Zhu, D.; Zhang, X.; Yan, M. *Asian J. Org. Chem.* **2022**, *11*, 11–14. (e) Zhu, D.; Chen, Y.; Zhang, X.; Yan, M. *Org. Biomol. Chem.* **2022**, *20*, 4714–4718. (f) Xiong, H.; Wu, J.; Qin, H.-L. *Org. Chem. Front.* **2023**, *10*, 342–347. (g) Park, J. H.; González-Montiel, G. A.; Cheong, P. H.-Y.; Bae, H. Y. *Org. Lett.* **2023**, *25*, 1056–1060.

474 For a review, see: Jones, L. H.; Kelly, J. W. *RSC Med. Chem.* **2020**, *11*, 10–17.

475 (a) Fadeyi, O.; Parikh, M. D.; Chen, M. Z.; Kyne, R. E.; Taylor, A. P.; O'Doherty, I.; Kaiser, S. E.; Barbas, S.; Niessen, S.; Shi, M.; Weinrich, S. L.; Kath, J. C.; Jones, L. H.; Robinson, R. P. *ChemBioChem* **2016**, *17*, 1925–1930. (b) Suto, N.; Kamoshita, S.; Hosoya, S.; Sakurai, K. *Angew. Chem. Int. Ed.* **2021**, *60*, 17080–17087. (c) Gilbert, K. E.; Vuorinen, A.; Aatkar, A.; Pogány, P.; Pettinger, J.; Grant, E. K.; Kirkpatrick, J. M.; Rittinger, K.; House, D.; Burley, G. A.; Bush, J. T. *ACS Chem. Biol.* **2023**, *18*, 285–295.

476 Aatkar, A.; Vuorinen, A.; Longfield, O. E.; Gilbert, K.; Peltier-Heap, R.; Wagner, C. D.; Zappacosta, F.; Rittinger, K.; Chung, C.-W.; House, D.; Tomkinson, N. C. O.; Bush, J. T. *ACS Chem. Biol.* **2023**, DOI: 10.1021/acschembio.3c00034.

477 (a) Zheng, Q.; Xu, H.; Wang, H.; Du, W. H.; Wang, N.; Xiong, H.; Gu, Y.; Noodleman, L.; Sharpless, K. B.; Yang, G.; Wu, P. *J. Am. Chem. Soc.* **2021**, *143*, 3753–3763. (b) Zhang, W.; Deng, X.; Zhang, F.-X.; Lin, J.-H.; Xiao, J.-C.; Liang, S. H. *Org. Lett.* **2022**, *24*, 4992–4997. (c) King, A. T.; Matesic, L.; Keaveney, S. T.; Jamie, J. F. *Mol. Pharm.* **2023**, *20*, 1061–1071.

478 (a) Zheng, Q.; Woehl, J. L.; Kitamura, S.; Santos-Martins, D.; Smedley, C. J.; Li, G.; Forli, S.; Moses, J. E.; Wolan, D. W.; Sharpless, K. B. *Proc. Natl. Acad. Sci.* **2019**, *116*, 18808–18814. (b) Shishido, Y.; Tomoike, F.; Kuwata, K.; Fujikawa, H.; Sekido, Y.; Murakami-Tonami, Y.; Kameda, T.; Abe, N.; Kimura, Y.; Shuto, S.; Abe, H. *ChemBioChem* **2019**, *20*, 900–905. (c) Teng, M.; Ficarro, S. B.; Yoon, H.; Che, J.; Zhou, J.; Fischer, E. S.; Marto, J. A.; Zhang, T.; Gray, N. S. *ACS Med. Chem. Lett.* **2020**, *11*, 1269–1273. (d) Cruite, J. T.; Dann, G. P.; Che, J.; Donovan, K. A.; Ferrao, S.; Ficarro, S. B.; Fischer, E. S.; Gray, N. S.; Huerta, F.; Kong, N. R.; Liu, H.; Marto, J. A.; Metivier, R. J.; Nowak, R. P.; Zerfas, B. L.; Jones, L. H. *RSC Chem. Biol.* **2022**, *3*, 1105–1110. (e) Cheng, Y.; Li, G.; Smedley, C. J.; Giel, M.-C.; Kitamura, S.; Woehl, J. L.; Bianco, G.; Forli, S.; Homer, J. A.; Cappiello, J. R.; Wolan, D. W.; Moses, J. E.; Sharpless, K. B. *Proc. Natl. Acad. Sci.* **2022**, *119*, e2208540119.

479 (a) Kitamura, S.; Zheng, Q.; Woehl, J. L.; Solania, A.; Chen, E.; Dillon, N.; Hull, M. V; Kotaniguchi, M.; Cappiello, J. R.; Kitamura, S.; Nizet, V.; Sharpless, K. B.; Wolan, D. W. *J. Am. Chem. Soc.* **2020**, *142*, 10899–10904. (b) Ghosh, J.; Mendoza, J.; Cooks, R. G. *Angew. Chem. Int. Ed.* **2022**, *61*, e202214090.